Electrophilic Phosphonothiolates for Cysteine-selective Bioconjugations

Dissertation zur Erlangung des akademischen Grades doctor rerum naturalium (Dr. rer. nat.)

im Fach: Chemie
Spezialisierung: Organische und Bioorganische Chemie

eingereicht an der
Mathematisch-Naturwissenschaftlichen Fakultät der Humboldt-Universität zu Berlin
von

M. Sc. Alice Leonie Baumann

Präsidentin der Humboldt-Universität zu Berlin
Prof. Dr.-Ing. Dr. Sabine Kunst

Dekan der Mathematisch-Naturwissenschaftlichen Fakultät
Prof. Dr. Elmar Kulke

Berlin, Juli 2020

---

1. Gutachter: Prof. Dr. Christian P. R. Hackenberger
2. Gutachter: Prof. Dr. Joseph M. Fox
3. Gutachter: Prof. Dr. Christoph Arenz

Tag der Dissertationsverteidigung: 19.11.2020

Declaration

The present work has been accomplished in the time between the 4th of January 2016 until the 14th of July 2020 under the supervision of Prof. Dr. Christian P. R. Hackenberger at the Institut für Chemie of the Humboldt-Universität zu Berlin and the Leibniz–Forschungsinstitut für Molekulare Pharmakologie.
I hereby declare, that I have authored the present dissertation independently and only by means of the stated resources in accordance to §7 paragraph 3 of the doctoral degree regulations of the faculty of mathematics and natural sciences, published in the official gazette of the Humboldt–Universität zu Berlin AMB No. 42/2018 from the 11th of July 2018. I have not applied for a doctors degree elsewhere and do not hold a corresponding doctors degree.

Berlin,

Alice Leonie Baumann

Die vorliegende Arbeit wurde in der Zeit vom 4.1.2016 bis zum 14. Juli 2020 unter der Leitung von Prof. Dr. Christian P. R. Hackenberger am Institut für Chemie der Humboldt-Universität zu Berlin sowie am Leibniz-Forschungsinstitut für Molekulare Pharmakologie angefertigt. Hiermit erkläre ich, die vorliegende Dissertation selbstständig und nur unter Verwendung der angegebenen Hilfsmittel, gemäß §7 Absatz 3 der Promotionsordnung der Mathematisch–Naturwissenschaftlichen Fakultät, veröffentlicht im Amtlichen Mitteilungsblatt Nr. 42/2018 vom 11. Juli 2018, angefertigt zu haben. Ich habe mich nicht anderweitig um einen Doktorgrad in dem Promotionsfach beworben und besitze keinen entsprechenden Doktorgrad.

Berlin,

Alice Leonie Baumann

Publications, patent, talks, posters

The work that has been performed during the doctoral studies of the author resulted so far in the following publications, patent, talks and posters:

Publications

1. Alice Leonie Baumann*, Sergej Schwagerus*, Kevin Broi, Kristin Kemnitz-Hassanin, Christian Ewald Stieger, Nils Trieloff, Peter Schmieder, Christian Peter Richard Hackenberger. Chemically Induced Vinylphosphonothiolate Electrophiles for Thiol–Thiol Bioconjugations. *J. Am. Chem. Soc.* **2020**, *142*, 9544-9552. (* shared first authorship)

2. Alice Leonie Baumann, Christian Peter Richard Hackenberger. Tag and release: strategies for the intracellular cleavage of protein conjugates. *Current Opinion in Chemical Biology* **2019**, *52*, 39-46. (Review)

3. Alice Leonie Baumann, Christian Peter Richard Hackenberger. Modern Ligation Methods to Access Natural and Modified Proteins. *CHIMIA* **2018**, *72*, 802-808. (Review)

Patent

Alice Leonie Baumann, Marc-André Kasper, Stephen Byrne, Jonas Helma, Heinrich Leonhardt, Tina Stoschek, Marcus Gerlach, Jonas Helma, Dominik Schumacher, Christian P. R. Hackenberger. Chemoselective Thiol-Conjugation with Alkene or Alkyne-Phosphonothiolates and -Phosphonates. PCT/EP2019/055509.

Talks

1. Alice Baumann, Manuel Iburg. PhD workshop from the priority program SPP1623, Nürnberg, Germany, 27th–29th March **2017**. *Functionalization of antibodies to analyze proteostasis in C. elegans.*

2. Alice Baumann. Doktorandenforum der Deutschen Studienstiftung, Münster, Germany, 8th–11th of March **2018**. *Cystein-selektive Biokonjugation.*

Posters

1. Alice Leonie Baumann, Marc-André Kasper, Jordi Bertran-Vicente, Christian P. R Hackenberger. 7th Chemical Protein Synthesis (CPS) Meeting, Haifa, Israel, 4th–7th of September **2017**. *Development of New Cysteine-Selective Bioconjugation Methods Based on Electrophilic Phosphorus(V) Compounds.*

2. Alice Baumann, Manuel Iburg, Janine Kirstein, Christian Hackenberger. 12th GDCh Scientific Forum Chemistry 2017 – Anniversary Congress GDCh – 150 Years, Berlin, Germany, 10th–14th of September **2017** *Functionalization of antibodies to study proteostasis in C. elegans.*

3. Alice Baumann, Manuel Iburg, Janine Kirstein, Christian Hackenberger. 4th Joint-meeting and 6th Phd-workshop of the SPP1623 priority program, Darmstadt, Germany, 19th–22nd of June, **2018**. *Functionalization of antigen binding proteins to study proteostasis in C. elegans.*

4. Alice Baumann, Marc-André Kasper, Maria Glanz, Sergej Schwagerus, Andreas Stengl, Jonas Helma, Dominik Schumacher, Heinrich Leonhardt, Christian P. R. Hackenberger. ArmChemFront 2018 Frontiers in Chemistry, Yerevan, Armenia, 21th–25th of October **2018**. *A cysteine-selective bioconjugation method based on electrophilic phosphorus(V) compounds.*

5. Alice Baumann*, Maria Glanz*, Marc-André Kasper*, Sergej Schwagerus*, Christian Hackenberger. 8th Chemical Protein Synthesis (CPS) Meeting, Berlin, Germany, 16th-19th of June **2019**. *Cysteine-selective bioconjugations based on electrophilic phosphorus(V) reagents.* (* authors contributed equally, shared poster prize award)

Acknowledgements

First of all, I would like to thank Prof. Dr. Christian Hackenberger for his guidance and constant support over the last years in supervising my PhD project. I appreciated the fruitful scientific discussions and most importantly, Christian's trust in my decisions. I am truly grateful for the opportunities Christian gave me during my time as a PhD student in his group, both in developing my project as well as in trusting me with the co-organisation of some of the meetings within the SPP1623 priority program. Moreover, I would like to express my gratitude for the great chances I had to present our work outside and within the FMP.

I would like to thank Prof. Dr. Joseph Fox and Prof. Dr. Christoph Arenz for taking their precious time to review this thesis.
Moreover, I thank Prof. Dr. Christian Limberg and Prof. Dr. Kallol Ray for being part of my PhD committee.

Over the last years I had the chance to collaborate with and be supported by outstanding researchers. First, I would like to thank Manuel Iburg from Prof. Dr. Janine Kirsteins group for his collaboration efforts on the chaperone crosslinking project. Furthermore, I am grateful to Songwhan Hwang from the group of Dr. Han Sun for the generation of the electrostatic potential maps of unsaturated phosphorus(V) electrophiles. I am grateful to Fabian Müller for his time and efforts to help me understand reactivity differences between P(V) electrophiles. A big thanks goes to the whole Tubulis team for their evaluation of the phosphonothiolate-linked ADCs. I would also like to thank Lee Armstrong and Prof. Dr. Yogesh Kulathu for inspiring discussions about DUBs and I am looking forward to our on-going collaboration. Moreover, I would like to thank Yerin Park and Hyejin Moon from the group of Prof. Dr. Mookie Baik for their on-going collaboration efforts in modelling thiol-additions to unsaturated P(V) electrophiles.
A special thanks goes to Peter Schmieder, Nils Trieloff, Brigitte Schlegel and Monika Beerbaum from the NMR group at the FMP for their support in interpreting NMR spectra, setting up experiments and maintaining the instruments. Another big thanks goes to the MS facility, especially to Heike Stephanowitz, Dr. Michal Nadler-Holly and Dr. Fan Liu for setting up MS experiments and for valuable discussions.
For MS/MS data analysis I thank Christian Stieger from our group for his very kind support. Moreover, I am truly thankful to our technical assistants Kristin Kemnitz-Hassanin, Beate Kindt and Dagmar Krause for their support with protein expression and HPLC purification and for always offering their help wherever needed. I further would like to thank Ines Kretzschmar and Dr. Rudolf Volkmer from the peptide synthesis group for their support with SPPS.

Many thanks go to the students I had the chance to supervise. Thank you, Jahaziel Jazerah, Stephen Byrne, Kevin Broi, Kevin Schiefelbein and Eleftheria Poulou for the great time and for your help and inspiration for my projects.

I was really blessed with great colleagues that were always helpful and supportive and made working much more fun. Very special thanks go to all current and former members of our group: Alec Michels, Anett Hauser, Anselm Schneider, Antoine Wallabregue, Beate Kindt, Bingjia Yan, Christian Stieger, Dagmar Krause, Debasish Bhowmick, Dominik Schumacher, Don Shenal Munasinghe, Eleftheria Poulou, Ines Kretzschmar, Jacob Gorenflos, Jennifer Trümpler, Jordi Bertran-Vicente, Katrin Wittig, Kristin Kemnitz-Hassanin, Kristina Siebertz, Luise Franz, Lutz Adam, Marc-André Kasper, Maria Glanz, Marianne Dreißigacker, Martin Penkert, Olaia Nieto García, Oliver Reimann, Philipp Ochtrop, Reihaneh Safavi-Sohi, Sebastián Florez Rueda, Sergej Schwagerus, Simon Klenk, Simon Reiske and Wenyi Li. And many thanks in particular to my B3.02 lab colleagues Anett, Sergej, Reihaneh, Bingjia and Elef for creating an enjoyable working atmosphere. Thank you Marc, Anett, Philipp and Sergej very much for highly valuable discussions about my projects.

Thank you Philipp, Kevin, Elef, Manuel, Marc, Alec, Mark and Janine for proofreading parts of this thesis.

Finally, I would like to thank the Studienstiftung des Deutschen Volkes for financial support as well as the priority program SPP1623. Within the SPP1623, I would like to thank Christian and Katta for building up a great network between chemical biology groups in Germany and Jan Bierlmeier for being a fantastic co-doctoral speaker to work together.

Am allerimeischte möcht ich mine Fründe und minere Familie Danke säge für üchi Unterstützig. Öpis isch immer.

Abstract

Chemoselective reactions enable the transformation of distinct functional groups in the presence of others. As such, these transformations are a powerful class of chemical reactions avoiding cumbersome protecting group manipulations in organic molecules and importantly, facilitate the modification of complex biomolecules at predefined sites, yielding homogenous products. The latter is essential for a wide range of applications in life sciences, in particular for the investigation of protein function and for the development of biopharmaceuticals.

In this thesis, a chemoselective transformation for the synthesis of unsaturated vinyl- and ethynylphosphonothiolates was developed. We were able to show that these types of compounds are efficiently synthesised from unsaturated phosphonites and electrophilic disulfides in the presence of other functional groups. A key step in the development of this chemoselective transformation was to prevent formation of an unwanted addition product, which resulted from the nucleophilic attack of a thiolate leaving group to the desired unsaturated phosphonothiolates. Efficient suppression of this side reaction was achieved when the disulfide-phosphonite reaction was performed under acidic conditions. We demonstrated the scope and chemoselectivity of the disulfide-phosphonite reaction for the synthesis of a number of small molecule derivatives as well as for the installation of vinylphosphonothiolates on unprotected peptides and small proteins, with ubiquitin as the most complex substrate. Furthermore, we showed that vinyl- and ethynylphosphonothiolates react chemoselectively with thiols and in particular with cysteine residues on proteins to form thiol-phosphonothiolate conjugates. Comparing the reactivity of vinyl- and ethynylphosphonothiolates in thiol additions with glutathione, we found that ethynyl-derivatives are significantly more reactive with a bimolecular rate constant of $1.32\,M^{-1}s^{-1}$ at pH 7.4, as opposed to $2.0\,mM^{-1}s^{-1}$ for the glutathione addition to the respective vinyl-derivatives. However, the enhanced reactivity of ethynylphosphonothiolates is compromised by the stability of these reagents and their thiol-conjugates.

The versatility of the herein developed method was demonstrated in three applications. First, site-selectively ubiquitinated protein conjugates were generated by employing the vinylphosphonothiolate-ubiquitin probe for conjugation with proteins carrying a single cysteine. In particular, this strategy was used to generate a non-hydrolysable diubiquitin as well as a ubiquitin-α-Synuclein conjugate. This study emphasises the conceptual value of the disulfide-phosphonite reaction, as it enables the chemoselective installation of electrophilic groups onto proteins, inducing thereby reactivity towards nucleophilic additions and consequently allowing protein-protein conjugations via canonical nucleophilic amino acids.

In a second application, unsaturated phosphonothiolates were evaluated as cysteine-selective linkers for the generation of antibody-drug conjugates (ADCs). Using ethynylphosphonothiolates, the efficient generation of brentuximab-MMAE ADCs with high average drug to antibody ratios (DARs) was possible, however these ADCs were not stable at neutral pH. On the other hand, using the less reactive vinylphosphonothiolate derivatives, the generation of ADCs with decent DARs was more challenging but the resulting ADCs proved to be more stable. In fact, the ADCs generated with vinylphosphonothiolates appeared to be more stable in rat serum than the maleimide-linked, clinically approved ADC Adcetris®.
In a last application, vinylphosphonothiolates were used as linkers to equip distinct proteins with photo-reactive crosslinkers to study dynamic protein-protein interactions. To this end, specific antibodies against molecular chaperones as well as deubiquitinating enzymes were chosen as model substrates. While the attempt to identify specific interaction partners of chaperones was not fruitful, promising preliminary results for the covalent crosslinking between DUB-photocrosslinker conjugates and ubiquitin substrates were obtained.
Taken together, the herein developed method enables the chemoselective transformation of electrophilic disulfides into electrophilic vinyl- and ethynylphosphonothiolates, thereby inducing reactivity for subsequent cysteine-selective thiol additions. This formal conjugation of two complex thiol-containing molecules forms a promising platform for the generation of homogenous peptide and protein conjugates without the need for non-canonical amino acids.

Zusammenfassung

Chemoselektive Reaktionen ermöglichen die selektive Umwandlung einer bestimmten funktionellen Gruppe innerhalb eines Moleküls in Gegenwart anderer funktioneller Gruppen und sind somit eine wichtige Klasse von Reaktionen für die Herstellung von homogen modifizierten Biomolekülen. Letztere sind für eine Reihe von Anwendungen in den Biowissenschaften wichtig, insbesondere für die Untersuchung von Proteinfunktionen, sowie für die Herstellung von Biopharmazeutika.
In der vorliegenden Arbeit wurde eine chemoselektive Synthese für die Herstellung von ungesättigten Vinyl- und Ethynylphosphonothiolaten entwickelt. Es konnte gezeigt werden, dass diese Verbindungen effizient aus ungesättigten Phosphoniten und elektrophilen Disulfiden in Gegenwart anderer funktioneller Gruppen synthetisiert werden können. Ein wichtiger Schritt dabei war die Unterdrückung eines Nebenprodukts, welches aus der Addition einer Thiolat-Abgangsgruppe an die ungesättigten Phosphonothiolate resultierte. Die effiziente Unterdrückung dieser Nebenreaktion konnte erreicht werden, indem die Disulfid-Phosphonit-Reaktion unter sauren Bedingungen durchgeführt wurde. Die hohe Chemoselektivität der Disulfid-Phosphonit-Reaktion wurde anhand der Einführung von Vinylphosphonothiolaten auf ungeschützten Modellpeptiden und dem Protein Ubiquitin demonstriert. Ungesättigte Phosphonothiolate reagieren in einer zweiten, ebenfalls chemoselektiven Reaktion mit Thiolen und insbesondere mit Cysteinen von Proteinen unter Bildung von Thiol-Phosphonothiolat-Konjugaten. Beim Vergleich von Vinyl- und Ethynylphosphonothiolaten hinsichtlich ihrer Reaktivität mit Thiolen wurde festgestellt, dass Ethynylderivate Geschwindigkeitskonstanten zweiter Ordnung im niedrigen $M^{-1}s^{-1}$ aufweisen und somit signifikant reaktiver sind als die Vinylphosphonothiolate mit Geschwindigkeitskonstanten im $mM^{-1}s^{-1}$ Bereich. Der hohen Reaktivität von Ethynylphosphonothiolaten steht jedoch die suboptimale Stabilität dieser Reagenzien an sich als auch ihrer Thiolkonjugate gegenüber.
Die Vielseitigkeit des hier entwickelten Verfahrens wurde in drei Anwendungen demonstriert. Ausgehend von einem elektrophilen Vinylphoshonothiolat-modifizierten Ubiquitin gelang es uns, homogene Ubiquitin-Protein-Konjugate zu erzeugen, insbesondere ein nicht hydrolysierbares Diubiqutin-Konjugat und ein Ubiquitin-α–Synuclein-Konjugat. In einer zweiten Anwendung wurden ungesättigte Phosphonothiolate als Linker in Antikörper-Wirkstoff-Konjugaten (ADCs) untersucht. Unter Verwendung von Ethynylphosphonothiolaten konnten Brentuximab-MMAE-ADCs mit hohen Antikörper zu Wirkstoff Verhältnissen (DARs) hergestellt werden, doch diese ADCs waren selbst unter neutralen Bedingungen nicht stabil. Im Gegenzug dazu war es schwieriger, ADCs mit hohen DARs herzustellen, wenn die weniger reaktiven Vinylphosphonothiolat-Derivate verwendet wurden. Diese ADCs erwiesen sich jedoch als deutlich stabiler und wiesen sogar eine höhere Serumstabilität auf als das klinisch zugelassene ADC Adcetris®.
Schliesslich wurden Vinylphosphonothiolate als Linker verwendet, um sowohl spezifische Antikörper gegen molekulare Chaperone als auch Deubiquitinasen (DUB) mit photoreaktiven Crosslinkern auszustatten, um mit diesen Konjugaten dynamische Protein-Protein Interaktionen zu untersuchen. Versuche, mit Hilfe von Antikörper-Photocrosslinker Konjugaten spezifische Interaktionspartner von Chaperonen zu

identifizieren, waren nicht erfolgreich. Hingegen konnten vielversprechende Ergebnisse für die kovalente Verknüpfung zwischen DUB-Photocrosslinker-Konjugaten und Ubiquitin-Substraten erzielt werden.
Insgesamt ermöglicht das hier entwickelte Verfahren die chemoselektive Umwandlung von elektrophilen Disulfiden in elektrophile Vinyl- und Ethynylphosphonothiolate, wodurch Reaktivität für Cystein-selektive Thioladditionen induziert wird. Wir glauben, dass diese formale Konjugation von zwei komplexen thiolhaltigen Molekülen beruhend auf kanonischen Aminosäuren Anwendung finden wird, um homogen modifizierte Peptid- und Proteinkonjugate herzustellen.

List of Abbreviations

ADC	antibody-drug conjugate
Ar	aryl
Boc	*tert*-butyloxycarbonyl
°C	degrees Celsius
C. elegans	*Caenorhabditis elegans*
CoA	coenzyme A
CPP	cell penetrating peptide
δ	chemical shifts in ppm for NMR analysis
DAR	drug to antibody ratio
DCC	*N,N*-dicyclohexylcarbodiimide
DCM	dichloromethane
DIPEA	*N,N*-diisopropylethylamine (Hünig base)
DiUb	diubiquitin
DMF	*N,N*-dimethylformamide
DMSO	dimethyl sulfoxide
DNA	deoxyribonucleic acid
DTNP	2,2′-dithiobis(5-nitropyridine)
DTT	dithiothreitol
DUB	deubiquitinating enzyme
E. coli	*Escherichia coli*
EDANS	5-((2-aminoethyl)amino)naphthalene-1-sulfonic acid
EDTA	ethylenediaminetetraacetic acid
eGFP	enhanced green fluorescent protein
El	electrophile
ESI	electrospray ionization
Et	ethyl
EtOAc	ethyl acetate
EtOH	ethanol
Et_3N	triethylamine
eq.	equivalents
EWG	electron-withdrawing group
Fig.	figure
Fmoc	fluorenylmethyloxycarbonyl

FRET	förster resonance energy transfer
g	gram
GSH	glutathione (reduced form)
HC and LC	heavy chain and light chain of IgG antibody
h	hour
HOBt	hydroxybenzotriazole
HPLC	high-performance liquid chromatography
HR-MS	high resolution-mass spectrometry
HSP	heat shock protein
Hz	Hertz
IEDDA	inverse electron demand Diels-Alder reaction
IgG	immunoglobulin G
J	coupling constant in ppm (for NMR analysis)
LC-MS	liquid chromatography-mass spectrometry
LR-MS	low resolution-mass spectrometry
m	multiplet, NMR analysis
M	molar
mbar	millibar
Me	methyl
MeCN	acetonitrile
MeOH	methanol
μg	microgram
MHz	megahertz
min	minutes
mL	milliliter
μL	microliter
mM	millimolar
MMAE	monomethyl auristatin E
mmol	millimole
MS	mass spectrometry
MWCO	molecular weight cut-off
NHC	*N*-heterocyclic carbene
NHS	*N*-hydroxysuccinimide
nm	nanometer
nM	nanomolar
NMR	nuclear magnetic resonance
Nu	nucleophile
o/n	overnight

PAB	para-amino-benzyl
PBS	phosphate-buffered saline
PEG	poly ethylene glycol
Ph	phenyl
POI	protein of interest
PTM	post-translational modification
rDA	retro-Diels-Alder reaction
r.t.	room temperature
sat.	saturated
SDS-PAGE	sodium dodecyl sulfate-polyacrylamide gel electrophoresis
SEC	size-exclusion chromatography
SPhR	Staudinger-phosphonite reaction
SPPS	solid-phase peptide synthesis
TCEP	tris(2-carboxyethyl)phosphine
TCO	*trans*-cyclooctene
TFA	trifluoroacetic acid
THF	tetrahydrofuran
TIS	triisopropylsilane
TLC	thin layer chromatography
Tris	tris(hydroxymethyl)aminomethane
Ub	ubiquitin
UV	ultraviolet

"The need still exists for additional orthogonal functional groups and improvements in the kinetics and selectivities of the reactions already at hand. Mining of the periodic table and classic organic literature are two avenues that are likely to bear interesting fruit. Group 15 has been particularly lucrative in terms of bioorthogonal reactions, and perhaps the larger elements within this group, bismuth and antimony, could be similarly beneficial. **In addition, novel combinations of phosphorus and sulfur have yet to be explored.**"

Ellen M. Sletten and Carolyn R. Bertozzi, Bioorthogonal Chemistry: Fishing for Selectivity in a Sea of Functionality, *Angew. Chem. Int. Ed.* **2009**, *48*, 6974-6998.

Contents

1 Introduction

1.1 Motivation: The need for protein modification methods

Proteins are among the most abundant biomolecules within a cell and are involved in all cellular processes ranging from the maintenance of metabolism to the control of signalling pathways, allowing differentiation and cell-cell communication. Gaining insight into these processes, both in health and disease, is tightly connected to the understanding of the function and interactions of the involved proteins on a molecular level. Consequently, the investigation of proteins is a major goal in natural life sciences. To this end, modifying proteins with functional moieties provides a powerful tool to study and manipulate their function (Fig. 1) [1, 2, 3, 4, 5]. For instance, cellular localisation of a protein can be visualised through fluorescent labelling. Alternatively, proteins can be equipped with reactive crosslinkers to study protein-protein interactions [6] or with cell-penetrating peptides (CPPs) to facilitate intracellular delivery [7]. Furthermore, proteins can be converted into therapeutic agents by attaching pharmacophores as exemplified with antibody-drug conjugates (ADCs) [8]. Moreover, the installation of post-translational modifications (PTMs) allows to study their effects on protein function.

Given the molecular complexity of proteins, the selective modification with functional handles is a challenging endeavour. Despite tremendous advances in the last years and decades, the challenge of modifying proteins with precise control still prevails.

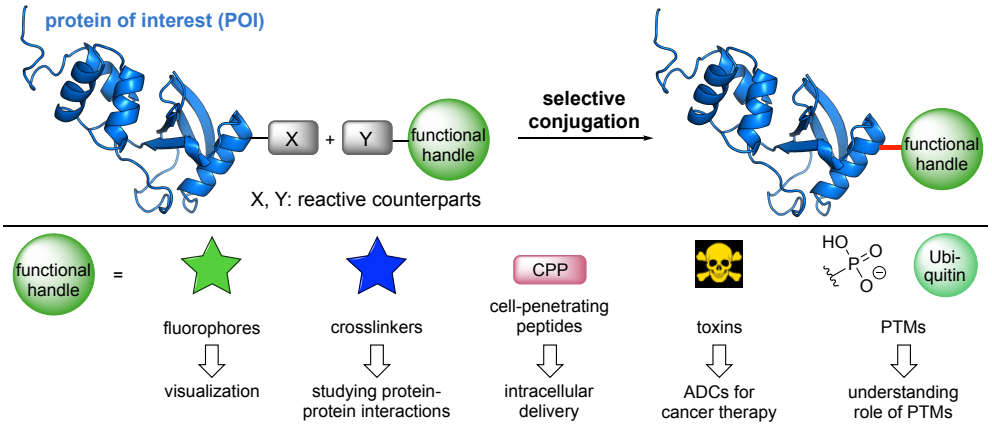

Fig. 1 The controlled modification of proteins with functional handles can be achieved by means of selective conjugation strategies. The resulting protein conjugates find application in basic research, diagnostics and therapy.

1.2 Protein modification strategies

Tackling the challenge of modifying proteins in a selective manner, a number of strategies have been developed as depicted in Fig. 2.

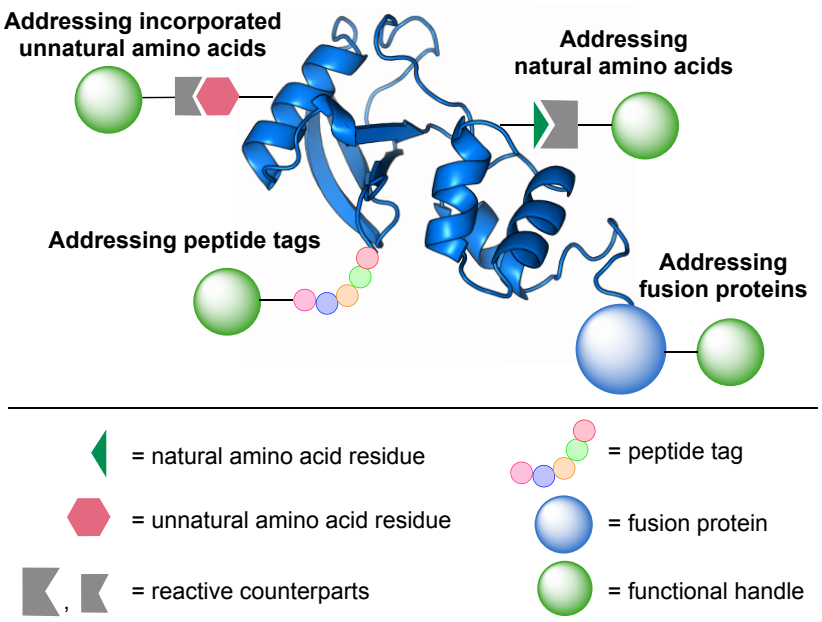

Fig. 2 Strategies for the selective modification of proteins with functional handles.

1.2.1 Protein modification via fusion proteins

For the selective modification of proteins within complex environments such as living cells, the use of genetically fused proteins has proven a particularly powerful strategy. For example, fluorescent fusion proteins have become indispensable tools to study the localisation and interactions of proteins inside living cells by fluorescent microscopy or FRET-based assays [9]. The best known example of a fluorescent protein is the green fluorescent protein (GFP) from the jellyfish *Aequorea victoria* [10]. Genetic engineering of the amino acids that contribute to its chromophore, along with the discovery of new fluorescent protein scaffolds has produced an array of available fluorescent proteins with different colours [9]. Fluorescently labelled proteins can be generated by genetically fusing the gene of the protein of interest and the fluorescent protein (Fig. 3A). To minimise interference with protein function, the modifier protein is usually fused at either the N- or the C-terminus. Nevertheless, since GFP and its derivatives are relatively large proteins (27 kDa), their attachment can still cause perturbations of the structure and function of the protein of interest.

In a different strategy, so-called self-labelling proteins are fused to the protein of interest and can subsequently be covalently modified with functional handles equipped with specific recognition substrates (Fig. 3B) [11]. Well-known examples following this strategy include the self-labelling enzymes SNAP- and CLIP-tag, which can be selectively modified at their active site cysteine with nucleobase-derivatives carrying fluorophores or other reporter compounds [12, 13, 14]. Another example is the HaloTag, an engineered variant of the bacterial enzyme haloalkane dehalogenase, which recognises functionalised alkyl halides as substrates and thereby gets labelled at a nucleophilic aspartate residue [15, 16]. All of these tags are well suited for the specific labelling of proteins within

cells. Given their orthogonality, they can also be used in combination, allowing for the versatile multi-labelling of proteins within the same system [13]. Nevertheless, also these self-labelling proteins are relatively big and may perturb protein function.

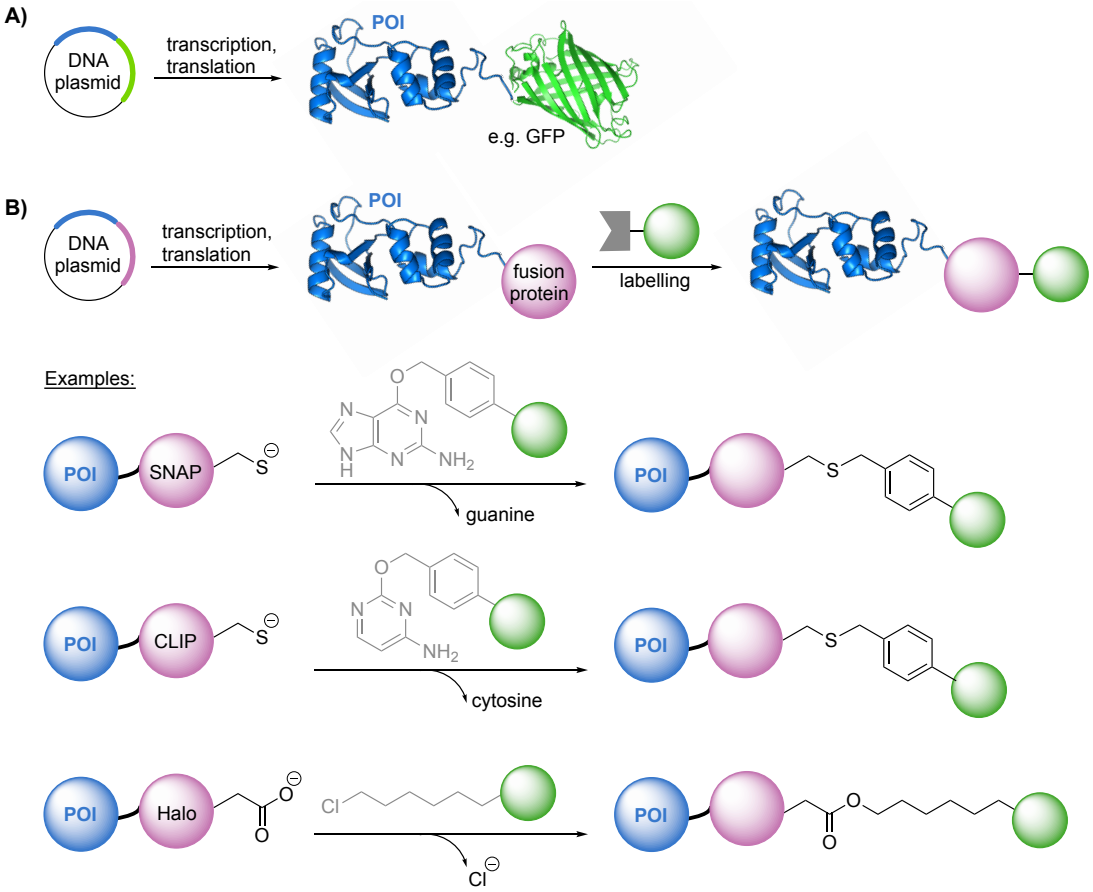

Fig. 3 Selective protein labelling via fusion proteins. A) The fusion protein itself can be the reporter tag, such as the green fluorescent proteins (GFP). B) The self-labelling proteins SNAP-, CLIP- and Halo-tag recognise *O*-6-benzylguanine, *O*-6-benzylcytosine or 1-chloro-hexyl derivatives, respectively, thereby getting covalently modified at either cysteine residues (SNAP- and CLIP-tag) or at a nucleophilic aspartate residue (Halo-tag).

1.2.2 Protein modification via peptide tags

An attractive alternative to the large protein tags described above are short peptide-based recognition tags [17]. These tags, which are only a few amino acids long, are genetically fused to a protein of interest and can for instance recognise and bind a small-molecule probe (Fig. 4). One of the shortest peptide-tag employed for this labelling strategy is a tetra-cysteine motif (Fig. 4A). As shown by Tsien and co-workers in 1998, this tag exploits the high affinity of the CCxxCC sequence (xx are most commonly the amino acids Gly, Pro) towards organobiarsenical compounds [18]. The latter can be derivatised with fluorescent dyes, such as fluorescein and other dyes with the xanthene backbone [19, 20, 21]. The resulting masked dye-arsenical-helix-binders enable the intracellular labelling of proteins containing the CCxxCC motif. Upon thiol-exchange with the cysteines of the peptide tag, the fluorescence drastically increases. Drawbacks of this labelling method are the cytotoxicity of arsenic-containing compounds as well as the need for extensive washing steps to remove hydrophobic dyes that are non-specifically

bound to membranes or off-target cellular proteins. Furthermore, micromolar concentrations of 1,2-ethanediol have to be added to the cells in order to reduce non-specific binding to endogenous cysteine pairs [18, 19].

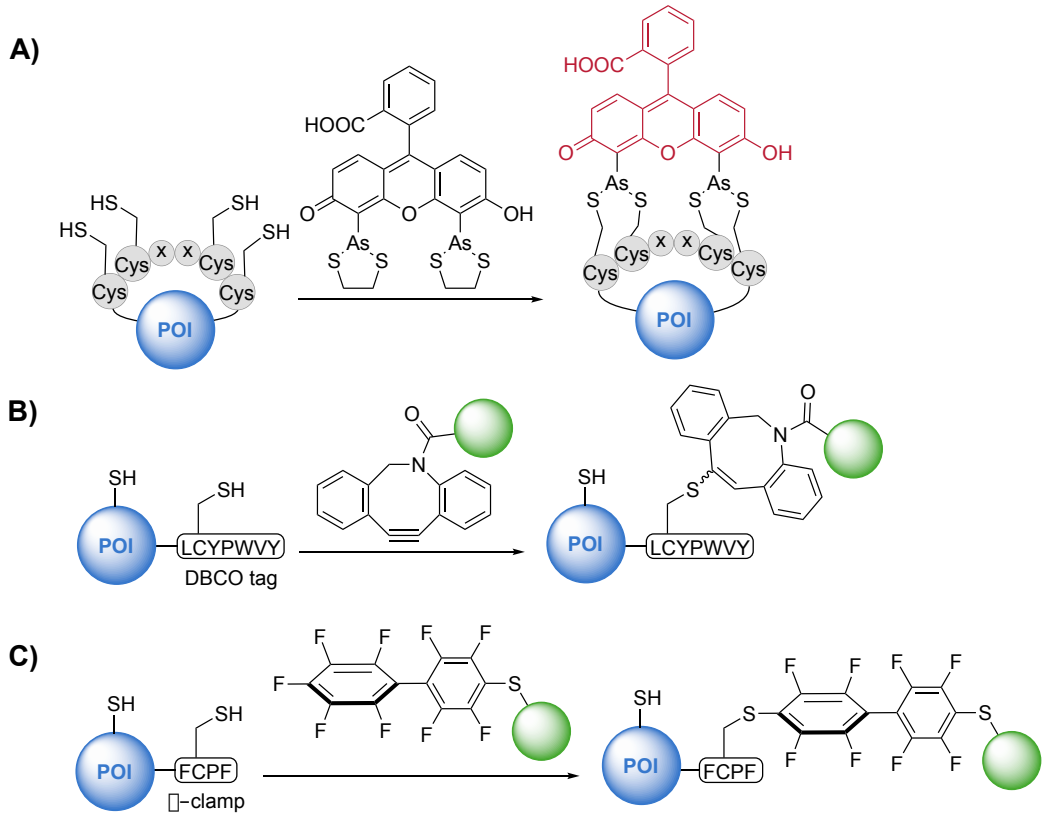

Fig. 4 Examples for methods making use of peptide tags to enable site-selective protein labelling. A) Biarsenical-functionalised fluorescent dyes react selectively with a tetracysteine motif. B) The DBCO-tag increases the rate of thiol-yne reactions. C) The π-clamp tag promotes nucleophilic aromatic substitution of perfluoroaromatic compounds with cysteine.

A further limitation of this method can be that the introduced tetra-cysteine tag gives rise to the formation of incorrect disulfide bonds within the protein of interest. Some of these problems were overcome by the development of the tetraserine motif SSPGSS, which can be labelled with bisboronic acid dyes instead [22]. Nevertheless, a limitation to this strategy is the relative high abundance of the SSPGSS sequence in human proteins, giving rise to background labelling.

Pentelute and co-workers developed two other short peptide sequences, which can be used for site-selective protein labelling. The DBCO-tag, a seven residue peptide tag, increases the rate of the thiol-yne reaction between a cysteine in the tag sequence and cyclooctyne derivatives more than 200-fold, thereby enabling regioselective labelling of the tag in the presence of other cysteines (Fig. 4B) [23]. Similarly, they found that the nucleophilic aromatic substitution between cysteine residues and perfluoroaromatic molecules can be promoted efficiently in aqueous solutions by the π-clamp, a four-residue peptide sequence (Fig. 4C) [24].

In order to further improve the binding affinity of a peptide tag for a given labelling agent, peptide-binding peptide tags have been employed [17]. High-affinity peptide-pairs characterised by nM binding affinities are for instance found in coiled-coil motifs

[25]. In 2008, Matsuzaki and co-workers have used such a high-affinity coiled-coil peptide-pair for the labelling of cell surface receptors of living cells [26]. Those systems have been refined further to drive covalent bond formation between a protein and a labelling tag of interest. Thereby, reactive groups on both peptide tags (e.g. a nucleophilic amino acid on one peptide tag and an electrophilic moiety on the other peptide tag) are brought in proximity, inducing reactivity for covalent bond formation. For example, the Seitz group made use of a system relying on transthioesterification of a cysteine-containing a peptide tag and a thioester-containing functional handle, thereby liberating the reporter tag peptide (Fig. 5) [27].

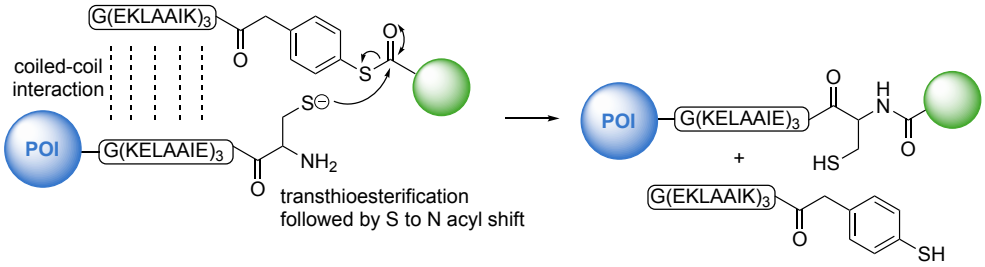

Fig. 5 Example for peptide-peptide interaction-mediated protein labelling.

Next to the above described systems, the inherent chemoselectivity of enzymes has been used a lot for the site-selective labelling of proteins at short peptide recognition sequences[1]. These enzymes recognise a specific peptide sequence and selectively transfer the desired label onto a specific amino acid within the peptide tag (Fig. 6).
For instance, the Wells group introduced the enzyme subtiligase, which is an engineered peptide ligase derived from the bacterial serine protease subtilisin (BPN) [29, 30]. The two point mutations S221C P225A alter the mechanism of BPN to favour aminolysis over peptidase activity, thereby facilitating the ligation of a C-terminal ester-containing peptide to an acceptor peptide containing an amine. Subtiligase accepts a wide scope of substrate amino acid sequences on both peptide ends, including non-natural amino acids, which can be further reacted with orthogonal groups to introduce functional handles site-selectively. To overcome the initial restriction of this labelling method to proteins C-termini, Weeks and Wells recently reported a library of subtiligase variants with defined specificities that allow for site-specific modification of proteins also at their N-termini [31]. These recent findings, along with the high efficiency of subtiligase and the mild reaction conditions make subtiligase-catalysed ligation a very powerful tool for peptide ligation.

[1] *Parts of the text on enzymatic labelling methods was taken and adapted from Baumann et al. (Ref. [28]).*

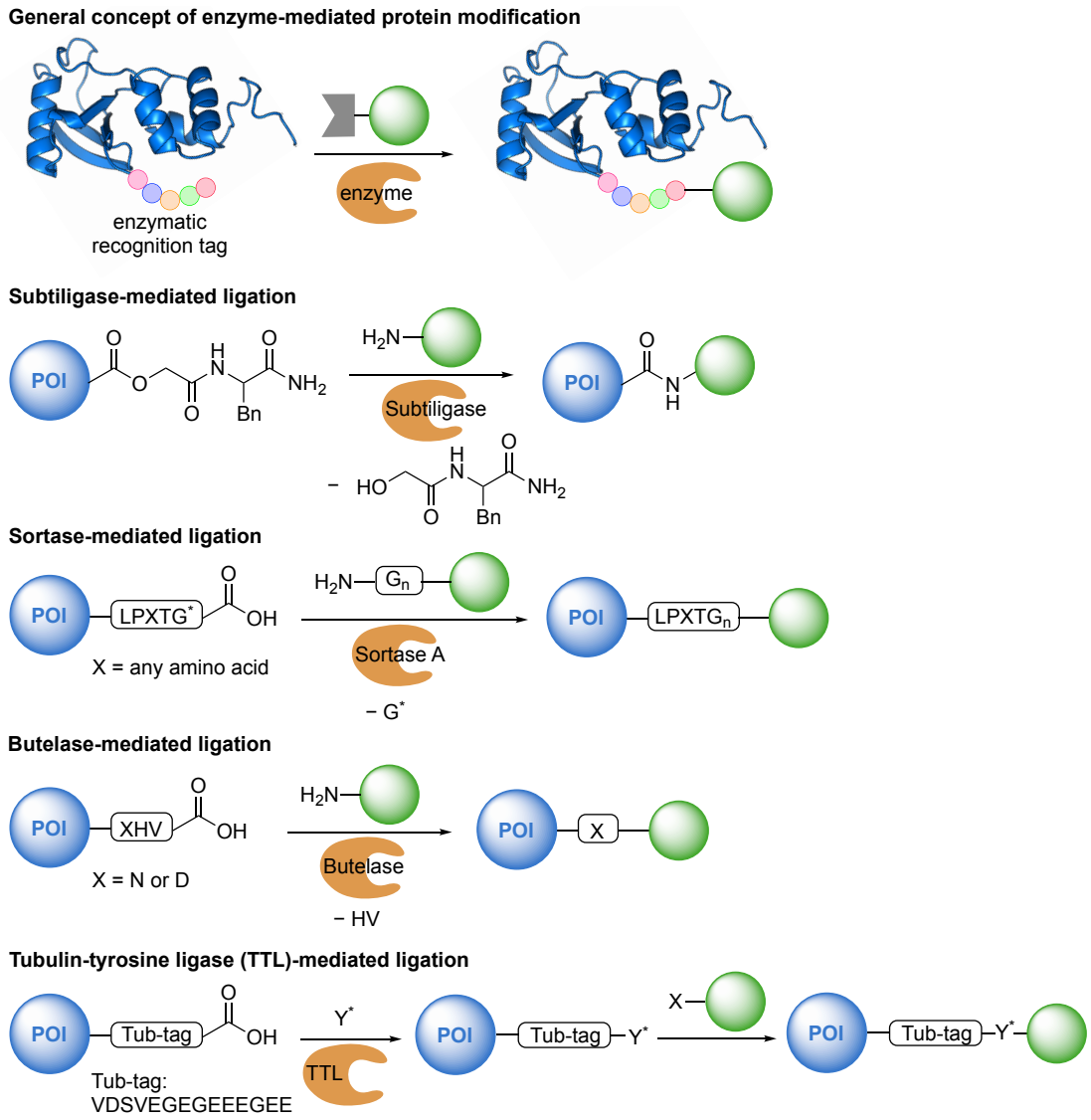

Fig. 6 Examples for enzyme-mediated protein labelling methods.

Another enzyme widely used for protein labelling is sortase A, a transpeptidase naturally catalysing the ligation of surface proteins to the cell wall of Gram-positive bacteria [32]. Sortase A recognises the C-terminal amino acid sequence LPXTG and cleaves it at the threonine residue. The resulting enzyme-substrate intermediate can then be conjugated to a second peptide fragment, bearing at least one glycine residue at the N-terminus [33, 34]. Recently, the Lang group developed a sortase-mediated ligation of an engineered ubiquitin to a protein of interest, giving rise to non-hydrolysable, site-specifically ubiquitinated proteins in living cells [35].
Butelase 1, another peptide ligase, was recently discovered by Nguyen *et al.* [36]. This enzyme was isolated from *C. ternatea*, a tropical cyclotide-producing plant. Butelase 1 recognises a C-terminal tripeptide motif Asn/Asp-His-Val and cleaves after Asn/Asp to ligate it to the N-terminal residue of a substrate peptide. Catalytic efficiencies are as high as 1.34 x 10^6 $M^{-1}s^{-1}$ [37]. Consequently, butelase 1 mediated ligation reactions are generally completed within minutes and give excellent yields. Moreover, butelase 1 is particularly useful for the efficient cyclisation of peptides [38].

In our group, yet a different enzymatic method has been developed, employing the enzyme tubulin tyrosine ligase (TTL). In nature, TTL recognises a 14-mer amino acid C-terminal sequence of a protein and attaches the amino acid tyrosine to it [39]. TTL also tolerates tyrosine-derivatives, e.g. equipped with an azide or an aldehyde functionality. This allows for the subsequent, chemoselective modification with functional handles containing alkyne or hydroxylamine groups [40, 41].

Given the size of the peptide and protein tags discussed above, the general challenge with these strategies is to maintain the integrity of the engineered protein with respect to correct folding and activity. Introducing extra amino acids into a protein can influence the correct three dimensional fold by disrupting covalent or non-covalent interactions between amino acids. Also the solubility of the protein of interest can be changed upon adding amino acids to the sequence. Furthermore, attached polypeptide tags may hamper protein-protein interactions by blocking substrate recognition sites. In order to minimise disruptions in the protein folding and activity, the polypeptide recognition tags are commonly attached at the N- or C-termini. Site-selective labelling at other sites is often prohibited or limited to unstructured areas of the protein. Further reducing the size of the recognition tag is thus a valuable strategy toward low-invasive labelling of proteins also at other sites than the termini.

1.2.3 Protein modification via unnatural amino acids

A strategy to reduce the size of the introduced tag in proteins is the incorporation of non-canonical amino acids. The power of this approach lies in the ability to site-selectively introduce unnatural functional groups into proteins, which can then be addressed with excellent chemoselectivity by orthogonal counterparts, also within complex environments (Fig. 7) [42].

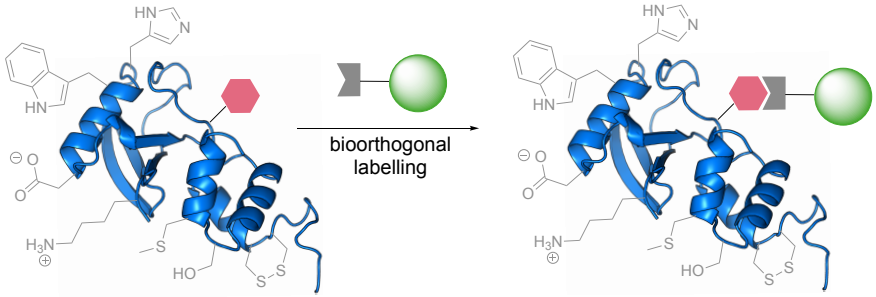

Fig. 7 The site-selective incorporation of unnatural amino acids into proteins allows for bioorthogonal labelling in biological systems.

Suitable chemical reactions for such selective labelling in biological environments have to fulfil several criteria [2]. Most importantly, bioorthognal reactions should not cross-react with any functional groups present in biomolecules to avoid background labelling and ensure specific labelling of the protein of interest. Furthermore, these reactions have to proceed under physiological conditions (ambient temperatures, pH around 6-8). Moreover, it is often desirable that the generated product as well as the reaction partners are stable under these physiological conditions and non-toxic to living systems. In recent years, considerable effort has driven the development of bioorthognal reactions that fulfil most of these criteria.

Ketones and aldehydes were among the first functionalities explored for bioorthogonal labelling of proteins [43] (scheme 1A). Their carbonyl group can be addressed with strong nucleophiles such as alkoxyamines [44], hydrazides [45] or hydrazines [46] under slightly acidic conditions (pH 4-6). However, with bimolecular rate constants in the range of 10^{-4} to 10^{-3} $M^{-1}s^{-1}$, these types of reactions are rather slow and must thus typically be carried out at high concentrations [47]. With the need for acidic conditions as well as observed cross-reactivity with other carbonyl-bearing metabolites [48], these transformations can not be regarded as fully bioorthogonal.

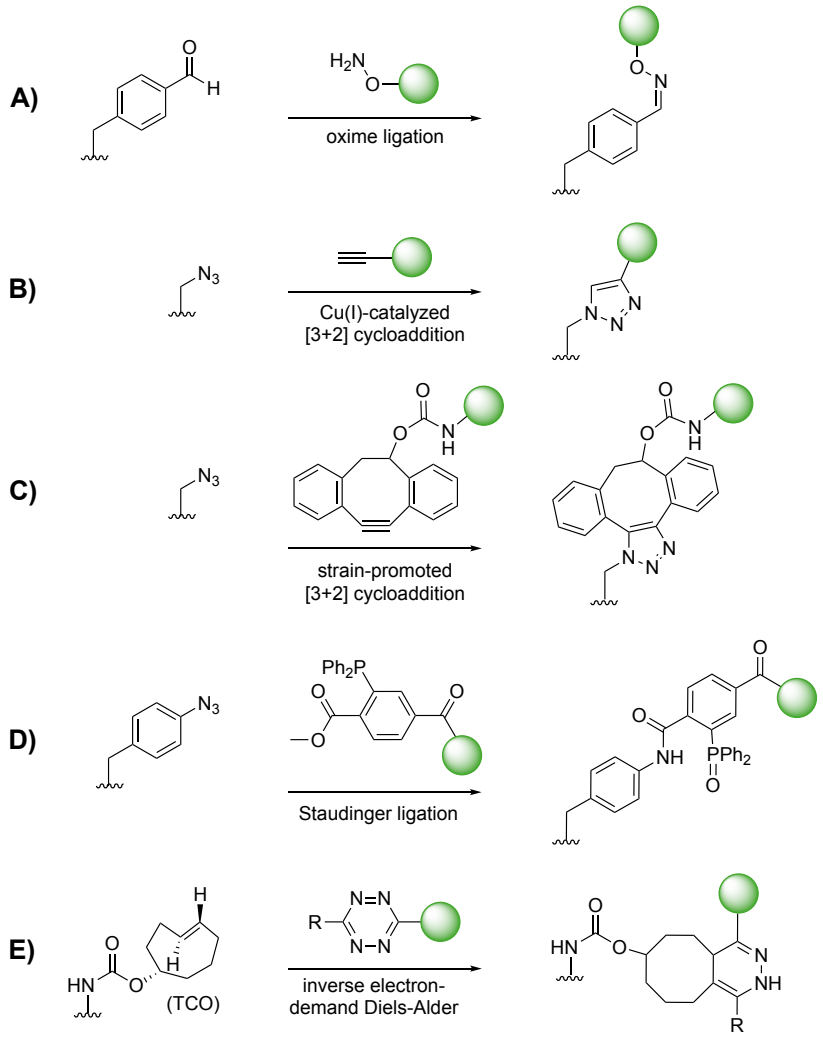

Scheme 1 Examples for bioorthogonal reactions.

Azides on the other hand are absent in biological systems and have therefore been widely employed for bioorthogonal labelling reactions [47]. Azides are relatively stable under physiological conditions and they are small and thus easy to incorporate into various biomolecules. They can undergo [3+2]-cycloadditions with alkynes to form stable triazoles [48, 49, 50] (scheme 1B). This reaction can be catalysed by copper (I) [51, 52], which made it applicable for bioorthogonal labelling. To avoid cell-toxic Cu(I)-salts [53], strain-promoted alkyne-azide-cycloadditions (typically using strained cyclooctynes) have been developed [54, 55] (scheme 1C). Limitations of these types of molecules can be their hydrophobicity [56] as well as cross-reactivity with thiols

of cysteines in thiol-yne reactions [57]. In addition to alkyne substrates, azides can also undergo chemoselective reactions in complex mixtures with triarylphosphines in the so-called Staudinger ligation, which is discussed in detail in chapter 1.4 (scheme 1D).

A major limitation of the bioorthogonal reactions discussed above are their slow reaction rates, necessitating long reaction times or high excess of reagents to achieve sufficient labelling [47]. In contrast, the bioorthogonal inverse-electron demand Diels-Alder (IEDDA) reaction between tetrazines and strained alkenes or alkynes exhibits extraordinary fast reaction rates [58]. Gaseous nitrogen is the only by-product in these irreversible reactions. Based on earlier work by Boger and others [59, 60], the groups of Fox and Hilderbrand simultaneously reported the application of IEDDA reactions for bioorthogonal labelling [61, 62]. The rates of IEDDA reactions have been further increased by introducing ring strain to the dienophile or by changing the electron deficiency of the tetrazines. For bioorthogonal reactions, the Fox group developed *trans*-cyclooctenes (TCO) (scheme 1E) as highly reactive dienophiles with bimolecular rate constants in the range of $10^6\,M^{-1}s^{-1}$ [63]. Even more reactive dienophiles could be generated by further increasing the ring-strain of TCOs [64, 65]. High selectivity and rapid kinetics of IEDDA reactions makes them one of the most promising class of reactions for bioorthognal protein modification in biological systems.

One way to incorporate the unnatural amino acid into a protein is to employ an enzymatic ligation method (compare chapter 1.2.2). Alternatively, unnatural amino acids can be incorporated by means of protein semi-synthesis [66, 28]. A further, more straight-forward, strategy is to supplement the medium of expressing cells with an unnatural amino acid structurally similar to a canonical amino acid. Given the translational machinery and in particular the aminoacyl-tRNA synthetase tolerates the unnatural amino acid, the latter gets incorporated in place of its structural natural analogue. In a seminal study by Cowie and Cohen in 1957, this concept has been demonstrated for the incorporation of selenomethionine in methionine-depleted growth-medium [67]. Increased yields can be obtained using auxotrophic expression systems, meaning cells or bacteria, which themselves are unable to synthesise the natural amino acid to be replaced. This method has been expanded for the incorporation of several bioorthogonal functional groups like homopropargylglycine, homoallylglycine [68] and azidohomoalanine [69], which can be further functionalised by means of bioorthogonal chemistry. In a very recent report, Lauster *et al.* have used this strategy to introduce homopropargylglycine into Qβ-phage capsids for subsequent functionalisation with azide-containing sialic acid derivatives by means of copper-catalysed azide-alkyne cycloadditions (CuAAC) [70]. Thereby, they generated a multivalent binder for the viral spike protein haemagglutinin of the influenza A virus, shown to inhibit influenza virus entry. While auxotrophic expression usually gives high yields, drawbacks of this method are the limited scope of amino acids tolerated by the translational machinery as well as the residue-specific, global incorporation of the non-canonical amino acid.
Genetic code expansion on the other hand enables the incorporation of non-canonical amino acids in a site-selective manner, while at the same time offers more structural diversity [71]. In this concept, aminoacyl-tRNA synthetase/tRNA-pairs are employed, which are orthogonal to natural occurring pairs. The promiscous synthetase transfers the non-canonical amino acid onto a tRNA complementary to a blank codon. For example, in the amber suppression technique, the stop codon UAG is repurposed for the incorporation of the desired unnatural amino acid [72]. The catalogue of non-canonical amino acids that can be incorporated into proteins by this method has been steadily

expanded over the last years by the evolution of several orthogonal aminoacyl-tRNA synthetases [73, 74]. Out of these, the pyrrolysyl-tRNA synthetase (PylRS)/$tRNA_{CUA}$ pairs have proven particularly useful as they are orthogonal not only in bacteria but also in eukaryotic cells [75, 76, 77] and in animals [78, 79, 80, 81]. Examples for unnatural functional groups that were incorporated into proteins by means of genetic code expansion include azides and alkynes [82, 83], tetrazines [84], bicyclononynes and *trans*-cyclooctenes [85] (Fig. 7). Despite its excellent site-specificity, a drawback of amber suppression is the competition with the termination of the protein, which gives rise to truncated proteins at the modification side [86].

1.2.4 Protein modification via natural amino acids

Although the protein modification strategies outlined in the three previous chapters are undoubtedly indispensable for the selective labelling of proteins in complex environments, they all rely on genetical engineering, which may perturb protein function or result in low yields of the expressed proteins. Therefore, whenever possible, directly addressing the natural amino acids with chemoselective methods is often more straight-forward. This strategy mainly finds application for the modification of purified proteins *in vitro*, although in certain cases, there are also ways to achieve selective modification of natural amino acids within complex mixtures, as discussed below. To date, a plethora of methods exist for the selective modification of many of the natural amino acids [3]. The primary amine groups of lysines can for instance be selectively addressed with *N*-hydroxysuccinimide esters (NHS), isocyanates and isothiocyanates or via reductive amination [3]. Given though that proteins are large and usually contain multiple addressable lysines, these strategies typically lead to a heterogeneous mixture of modified proteins carrying different numbers of modifications. For applications, in which the site of modifications is important, other labelling strategies must be pursued. One strategy to improve site-selective labelling of natural amino acids relies on affinity-induced labelling [87]. Here, high-affinity ligands are employed, which direct a latent electrophile to a distinct area of a protein, thereby inducing reactivity to nucleophilic residues in proximity. Electrophilic warheads that have been employed in this strategy include phenyl esters [88], tosyl groups [89] and acyl imidazoles [90]. Impressively, this strategy enabled the selective labelling of endogenous proteins even *in vivo* [91, 92]. Nevertheless, the scope of this methods is limited to proteins with an identified ligand. Furthermore, within the binding region of the ligand, it is difficult to steer which exact residue is getting labelled when several nuleophilic functional groups are in close proximity.
Another, more general strategy towards homogenous protein labelling is to target low-abundant natural amino acids, such as cysteine (see chapter 1.3). This approach is complemented by site-directed mutagenesis, which provides a means to either remove amino acids that should not be labelled or introduce a single addressable copy of a given amino acid to ensure site-selectivity.

1.3 Methods for selective protein modification via cysteine

Within the natural amino acids, cysteine has seen the most attention for selective protein modification [93, 94]. This is partly due to its low natural abundance, which facilitates site-selective labelling. Depending on the literature source, the natural abundance of cysteine is approximately 1.1% [95]. For comparison, lysine is much more abundant with about 6.3% (Fig. 8B). Furthermore, cysteines are often bound in disulfide bridges, which reduce their abundance as addressable nucleophiles even further. Thus often only one free cysteine is available for functionalisation or can be introduced by means of site-directed mutagenesis, allowing site-selective functionalisation. Alternatively, disulfide bridges can be reduced to two free cysteines, thereby making them accessible for modification with electrophiles.
The other reason why cysteine is an attractive target for selective protein modification lies in its distinct, yet diverse reactivity profile. Compared to other nucleophilic amino acids, cysteine has a unique nucleophilicity. With a pKa value of around[2] 8 it has a high tendency to form the nucleophilic thiolate under physiological conditions and can thus be addressed with various electrophiles. For comparison, lysine has a pKa value of approximately 10 and is thus mainly protonated under physiological conditions. Consequently, at neutral or slightly basic pH (ca. 7-8.5), cysteine can usually be addressed with high selectivity over lysine. However, cross-reactivity is sometimes observed with the nucleophilic groups of tyrosine, histidine, serine/threonine or the N-terminus.

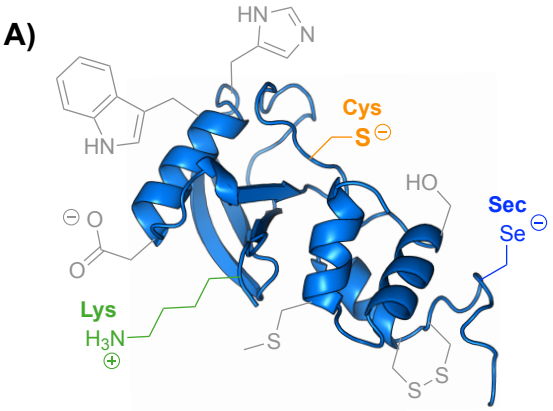

B)

	Lys	Cys	Sec
natural abundance	~6.3%	~1.1%	<< 1%
pKa	~10	~8	~5
redox potential E_0		−220 mV	−388 mV
atomic radius		105 pm	120 pm

Fig. 8 Comparison of the nucleophilic amino acids lysine (Lys), cysteine (Cys) and selenocysteine (Sec).

A close analogue to cysteine is selenocysteine (Sec), also referred to as the 21st proteinogenic amino acid [98]. Sec is very low abundant in proteins, nevertheless plays an important role in several enzymes with redox functions [99]. Cys and Sec only differ by one atom, sulphur versus selenium. This seemingly small difference distinguishes though the properties of cysteine and selenocysteine distinctly. The pKa value of Sec (around 5) is much lower than that of Cys. As a consequence, under physiological conditions, most of the selenol (R-SeH) side chains in Sec are present in the deprotonated selenolate (R-Se-) form. Compared to thiolates, the negative charge on selenolates is better stabilized due to the larger size of selenium versus sulphur [100] and its lower

[2]The pKa value of amino acids varies depending on the local environment with respect to buffer exposure and the neighbouring residues [96, 97].

redox potential (Fig. 8B) [98]. This makes selenolates much better nucleophiles than the respective thiolates of deprotonated cysteines. However, the larger atomic size and higher polarisability of selenium also make the chemical bonds with selenium generally weaker than the corresponding bonds with sulphur. This feature of selenium has been employed in the development of rapid ligation methods using peptide selenoesters [66]. Although selenocysteine is a better nucleophile at physiological pH than cysteine and could thus interfere when addressing cysteine, this is mostly not a problem given the very low abundance of cysteine in natural proteins. The distinct chemical properties of cysteine has been an inspiration for researchers for decades, illustrated by the plethora of cysteine-selective methods available to date [93, 94]. The bulk of existing methods rely on addressing cysteine with electrophilic reagents (Fig. 2A), while others engage cysteine in radical reactions (Fig. 2B). Some methods also make use of the high affinity of cysteine to metals [101, 102, 103, 104]. Yet another approach to employ cysteine for protein modification is by selectively transforming it first selectively into an electrophilic handle, to allow subsequent modification with nucleophiles (Fig. 2C).

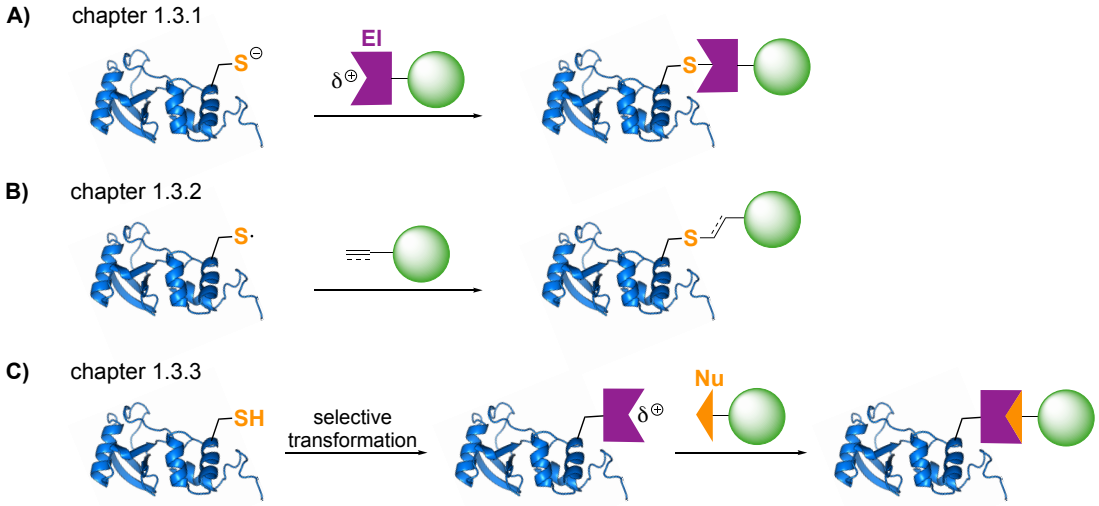

Scheme 2 Different strategies to selectively modify cysteine on proteins: A) With electrophiles (El), B) through radical transformations, C) via intermediary conversion into an electrophile, inducing reactivity for subsequent labelling with nucleophiles (Nu).

1.3.1 Selective modification of cysteine with electrophiles

The majority of cysteine-selective labelling methods rely on electrophilic reagents (Fig. 9). Next to their synthetic accessibility and their selectivity for cysteine-labelling, other important aspects are high reactivity to allow labelling under dilute conditions as well as good stability of the labelling reagents as well as the conjugation products.

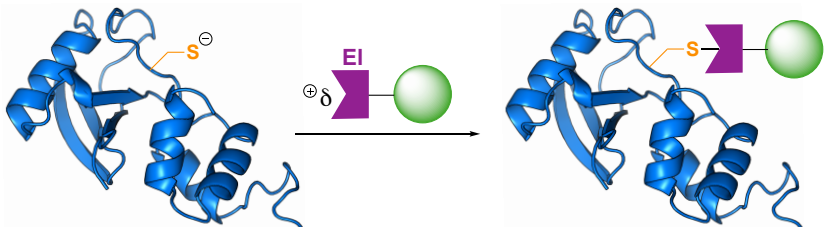

Fig. 9 Cysteines can selectively be addressed with a variety of electrophilic reagents (El).

Maleimides and related compounds

In the toolbox for cysteine-selective modification, maleimides stand out owing to their excellent reactivity. Thiol-Michael additions to maleimides are characterised by bimolecular rate constants in the range from 10^2-10^4 $M^{-1}s^{-1}$ dependent on the pH and the reagent structure [105, 106]. Due to their excellent reactivity, maleimides have been widely applied in various bioconjugation applications. Also most of the currently approved antibody-drug conjugates were generated using maleimides [8]. Nonetheless, there are several drawbacks for classical maleimides like the observed cross-reactivity with lysine and histidine, particularly under basic conditions when using the maleimide reagent in excess [107]. Another drawback of classical maleimides is the reactivity of the thiosuccinimide adducts towards retro-Michael addition and subsequent thiol-exchange reactions (scheme 3A) [108, 109]. The latter ones are particularly critical in the context of ADC therapeutics, in which premature release of the cytotoxic payload can compromise efficacy or lead to off-target toxicity. To overcome this issue, Lyon *et al.* developed self-hydrolysing maleimides that accelerate the hydrolysis of the thiosuccinimide adducts to succinamic acid thioethers by installing an adjacent basic amino group, thereby stabilising the thiol-adducts (scheme 3B) [110].

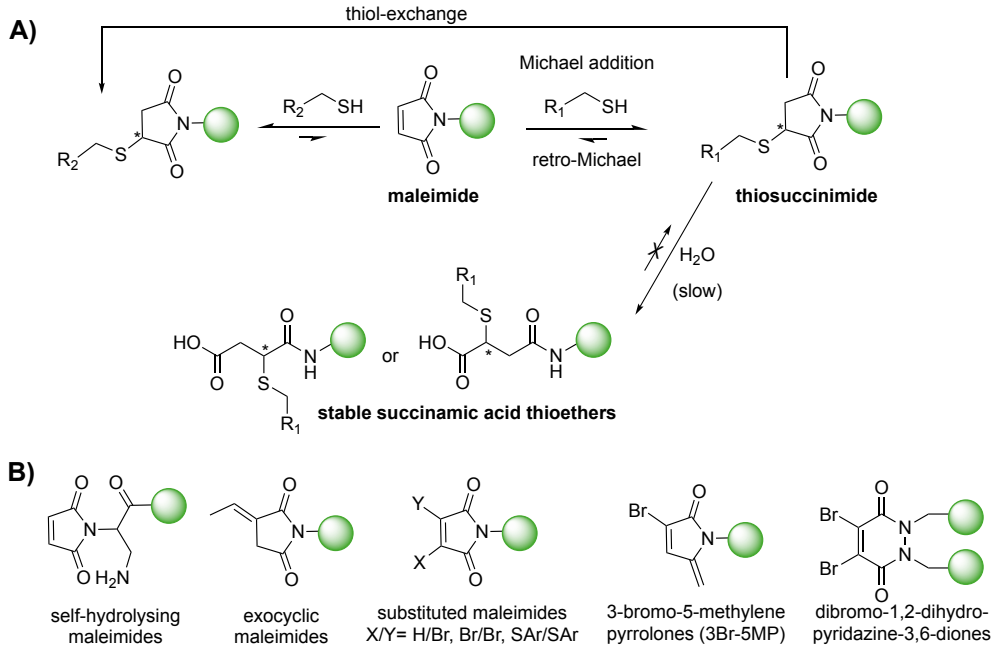

Scheme 3 A) Problems associated with classical maleimides. B) Structures of next-generation maleimide-derivatives and related compounds.

In a different approach, Kalia and co-workers tackled retro-Michael degradation using 3-substituted exocyclic maleimides, which give rise to more stable thiosuccinimide adducts [111]. Other next-generation maleimides include mono- and dihalogen- or thioaryl-substituted derivatives that possess advanced reactivity allowing multiple thiol additions. For example, monobromomaleimides, developed by Tedaldi *et al.* rapidly react with cysteines [112], and allow a second Michael addition to the resulting thiomaleimide [113]. Alternatively, the first addition reaction can be reverted by the addition of TCEP [112]. Similarly to this approach, dibromomaleimides introduced by Smith *et al.* [114] allow for the addition of two thiols to a maleimide scaffold, thus enabling the rebridging of disulfides in a protein of interest [115]. The resulting bioconjugates can further be

stabilised by hydrolysis or are reversible by the addition of external thiols [116]. As an alternative to dibromomaleimides, diarylthiomaleimides (scheme 3B), which do not show cross-reactivity with TCEP allow for one-pot TCEP reduction and rebridging of disulfides [117]. Yet other reagents for disulfide double functionalisation of cysteine-peptides and disulfide rebridging are 3-bromo-5-methylene-pyrrolones, recently introduced by Zhang *et al.* [118]. Thiol additions to these reagents are however reversible and the thiol-conjugates must be stabilised by reduction-mediated ring-openings. As a last example of maleimide-related reagents for cysteine-labelling, dibromopyridazinediones developed by Chudasama *et al.* are to be mentioned [119]. Thiol-conjugates to these reagents employ excellent hydrolytic stability but are reversible in the presence of excess thiols.

While the development of next-generation maleimides and maleimide-related compounds has led to significant improvements of classical maleimides, another important aspect for cysteine-labelling reagents is their synthetic accessibility. From a users perspective, the question of how easily these cysteine-reactive handles can be synthesised and incorporated into a certain functional moiety for labelling is highly relevant.

As for the synthesis of *N*-functionalised maleimides, there are two routes that prevail in the literature, employing either succinic anhydride or maleimide as starting materials (scheme 4A/B).

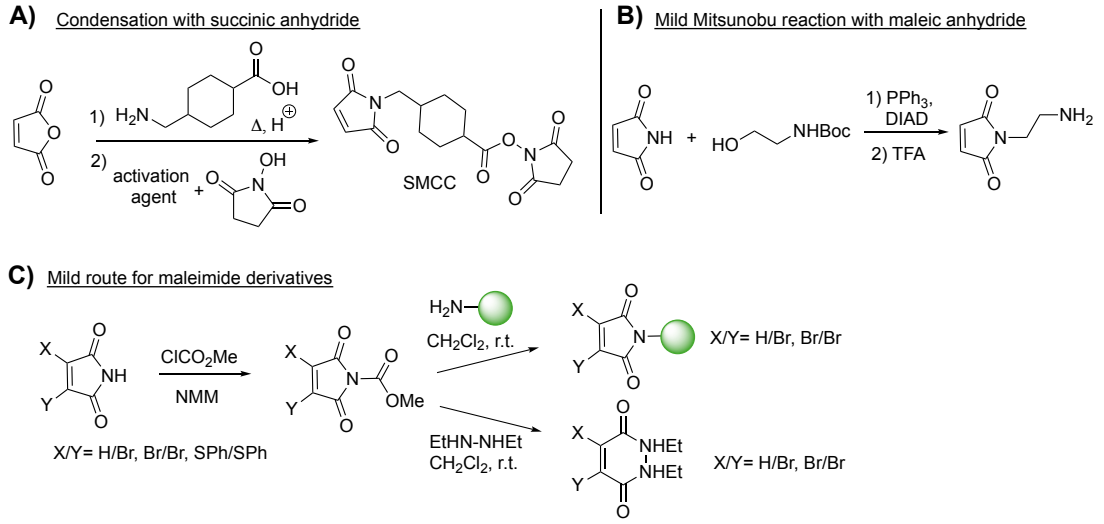

Scheme 4 Synthesis of maleimide derivatives. A) Commonly used synthetic route to generate *N*-functionalised maleimides from the condensation of succinic anhydride with amines. B) Alternative, mild route to access maleimide derivatives via the Mitsunobu reaction with maleic anhydrides. Both routes can be used to generate bifunctional linkers. C) Mild synthetic route to access substituted maleimide derivatives. PPh_3=triphenylphosphine, DIPEA=*N,N*-diisopropylethylamine, $ClCO_2Me$= methyl chloroformate, NMM=*N*-methylmorpholine.

In the first route, the amine opens the succinic anhydride and the resulting maleic acid condensates under elevated temperatures and acidic conditions (scheme 4A) [120]. In the second route, direct *N*-alkylation of maleimides can be accomplished under milder conditions by means of a Mitsunobu reaction, using alcohols as alkyl group donors (scheme 4B) [121]. Another mild approach for the synthesis of *N*-derivatised substituted maleimides and bromopyridazinediones has been reported by Castañeda *et al.* using *N*-methoxycarbonyl activated maleimide intermediates (scheme 4C) [122]. All of these synthetic routes enable the synthesis of general building blocks [123, 124] (e.g.

the SMCC linker, scheme 4A), which can be used in subsequent amide couplings for further functionalisation. To date, a wide selection of such bifunctional maleimide linkers are commercially available, which still promotes the use of classical maleimides for bioconjugations, despite suboptimal selectivity and stability of these compounds.
While the site-selective incorporation of maleimides using bifunctional linkers is straightforward for functional handles that contain only one reactive group (e.g. an amine or carboxylic acid), more complex biomolecules like peptides or oligonucleotides often require more selective chemistry or protecting group manipulations. Even though installing a maleimide group on an unprotected peptide can in principle be accomplished with the SMCC linker, this process would lead to a mixture of products when several amino groups are present in the sequence. Thus, the site-selective incorporation of a maleimide group into a peptide or a protein requires either the installation of an unnatural amino acid, which can be addressed with an orthogonal bifunctional linker, or a suitable protecting-group strategy. The latter approach has been used for instance by Marburg *et al.* [125] as depicted in scheme 5A. They employed an orthogonally-removable lysine-protecting group and introduced the maleimide functionality via an *N*-hydroxysuccinimide ester in the last step of a standard Fmoc-SPPS. An example for the incorporation of a maleimide group into oligonucleotides has been accomplished by Sanchez *et al.* (scheme 5B) [126]. They incorporated a 2,5-dimethylfuran protected maleimide at the 5′-end through a phosphoramidite building block, which is inert against the ammonia treatment during oligonucleotide synthesis. Deprotection is achieved in the final step by means of a retro-Diels-Alder (rDA) reaction at elevated temperature.

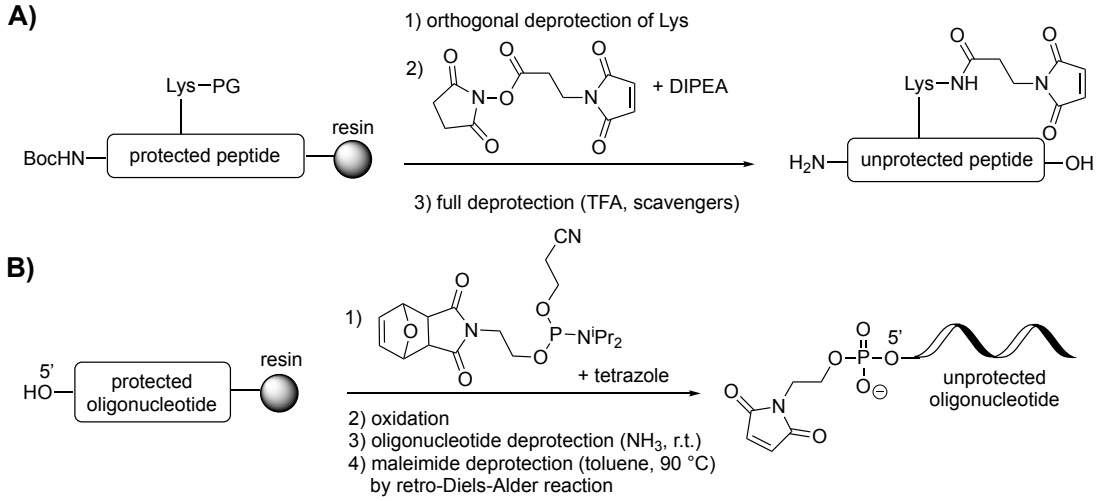

Scheme 5 A) Example for the incorporation of a maleimide group into a protected peptide [125]. B) Example for the installation of a protected maleimide precursor into a protected oligonucleotide [126].

α-halocarbonyl reagents

Next to maleimides, α-halocarbonyl reagents have been used to functionalise cysteines (scheme 6A) [127]. Owing to the excellent stability of the formed thioether bond, these reagents are extensively used in MS sample preparation of digested proteins [128] and have also been applied for the construction of stable immunoconjugates [129]. The reactivity of α-halocarbonyl reagents increases in the order of chlorine, bromine and iodine derivatives. Reported rate constants for thiol-additions to chloroacetamides at physiological pH are in the low $M^{-1}s^{-1}$ range [130]. Cysteine-selectivity in turn is best for the least reactive chlorines derivatives [131].
α-halocarbonyl reagents are often synthesised from substitution of activated carbonyls with amines (scheme 6B). Chloro- and bromoacetamides can be accessed from chloro- and bromo-acetylchlorides/bromides with amines under cooled conditions by the aid of a base. Thereby, selective substitution occurs at the more electrophilic carbonyl position. This conversion tolerates alcohols [132], carboxyclic acids and Boc-protected amines, thus allowing the synthesis of bifunctional linkers (scheme 6D) that for instance have been used to conjugate cytotoxins to antibodies [133, 129]. Treatment of chloro- or bromoacetamides with potassium- or sodiumiodide gives rise to *N*-derivatised iodoacetamides (scheme 6B). Alternatively, α-haloacetamides can be accessed from haloacetic anhydrides (scheme 6C). The latter strategy was used to synthesise a diazirine iodoacetamide derivative for photocrosslinking studies [134]. The incorporation of haloacetamides into biomolecules like peptides and oligonucleotides has not seen a lot attention, most likely due to the incompatibility of the available synthetic methods with complex biological substrates.

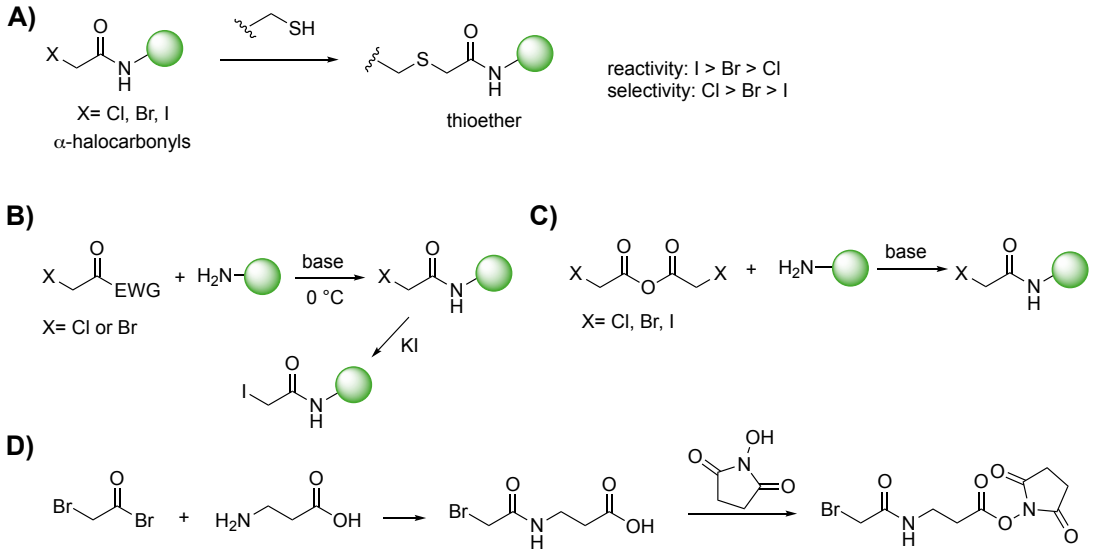

Scheme 6 A) Modification of cysteine with α-halocarbonyl reagents. B/C) Synthetic approaches for the synthesis of α-halocarbonyl reagents. D) Example for the synthesis of a bifunctional linker.

α/β-unsaturated carbonyl reagents

Another class of cysteine-selective, electrophilic reagents are α/β-unsaturated carbonyls, some of which are depicted in scheme 7. Bernardes and co-workers introduced carbonyl-acrylic reagents as Michael-acceptors for thiol-addition, with benzoyl acrylamide as the best-performing derivative (scheme 7A) [135]. They were able to show that cysteine addition to these compounds is highly selective and proceeds with rapid kinetics (k_2= 10.9 $M^{-1}s^{-1}$ at pH 8.0), enabling the labelling of various proteins under stoichiometric conditions, including the therapeutic antibody trastuzumab. *N*-derivatised benzoyl acrylamides are easily accessible from amide couplings between amines and the commercially available 3-benzoylacrylic acid [136, 135].
2-azidoacrylates, which were introduced by Ariyasu *et al.* are reactive, cysteine-selective Michael-acceptors (k_2 (for glutathione addition) of about 0.51 $M^{-1}s^{-1}$) at pH 7.4 (scheme 7B) [137]. Furthermore, these reagents allow for dual functionalisation through successive alkyne-azide cycloadditions. The authors synthesised the amino 2-azidoacrylate precursors, which are amenable for couplings at the amino group, from *N*-Boc-protected acrylates via bromination and transformation with NaN_3.

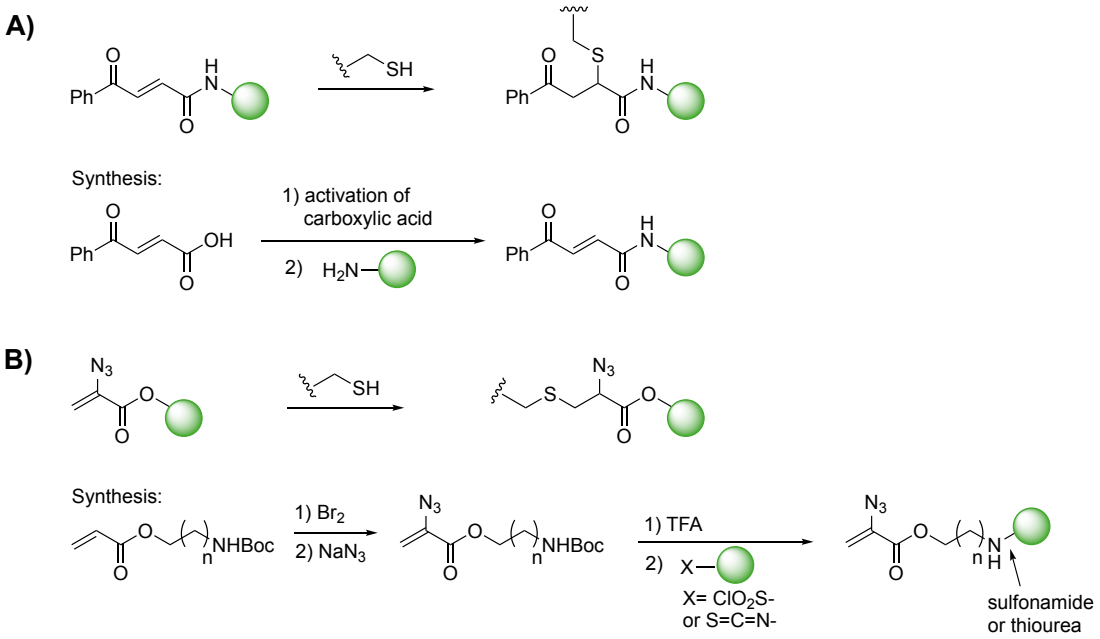

Scheme 7 Cysteine-selective α/β-unsaturated carbonyl reagents and examples for their synthesis: A) Carbonylacrylic reagents, B) 2-azidoacrylates.

Based on unsaturated bissulfones [138], Wang *et al.* introduced water-soluble α,β-unsaturated ketones for cysteine-selective bioconjugation (scheme 8) [139]. These reagents allow for disulfide-rebridging, while at the same time introducing a functional handle at the bridged site. A PEG amine allyl sulfone derivative, which serves as substrate to introduce functional handles via amide couplings, was synthesised in a lengthy synthetic procedure sequence starting from *N*-Boc-protected alcohols.

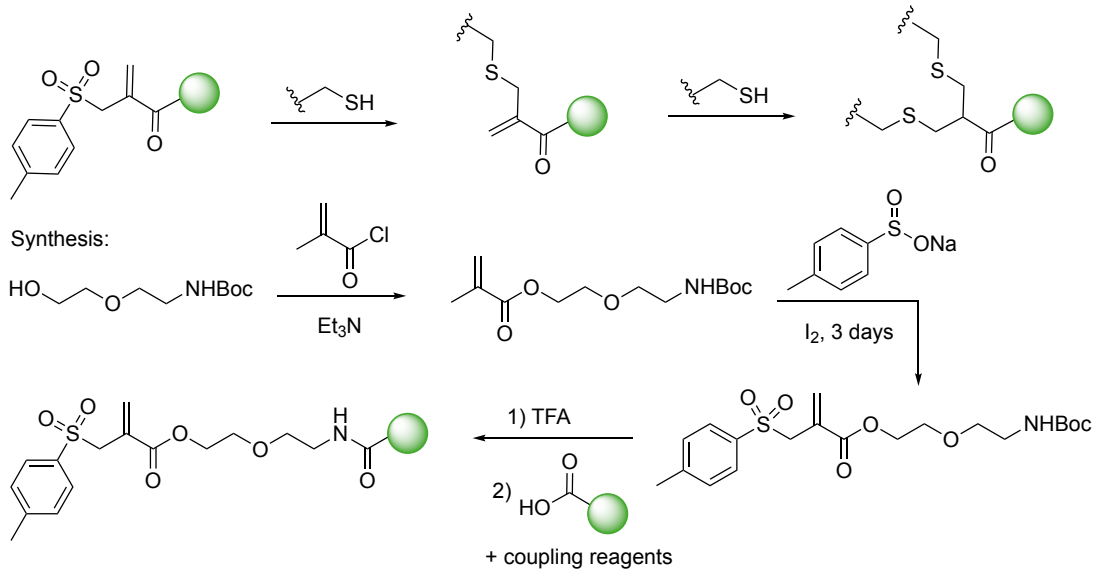

Scheme 8 Cysteine-selective α,β-unsaturated ketones and an example for their synthesis.

Finally, Fox and co-workers introduced cyclopropenyl ketones as a new class of irreversible cysteine alkylators (scheme 9) [140]. Thiol additions to the strained cyclopropenyl exhibit extraordinary fast kinetics (k_2= 595 $M^{-1}s^{-1}$ for glutathione addition in PBS at pH 7.4), thus allowing excellent conversions at low protein concentrations in short time. As opposed to maleimides, here the products are stable towards retro-Michael addition in the presence of excess external thiol in PBS and human plasma. The authors synthesised amide-derivatised cyclopropenyl ketones from 2-methylcycloprop-2-enecarboxylic acid and propanal, followed by NHS-mediated amide coupling and oxidation using Dess-Martins reagent [141, 140].

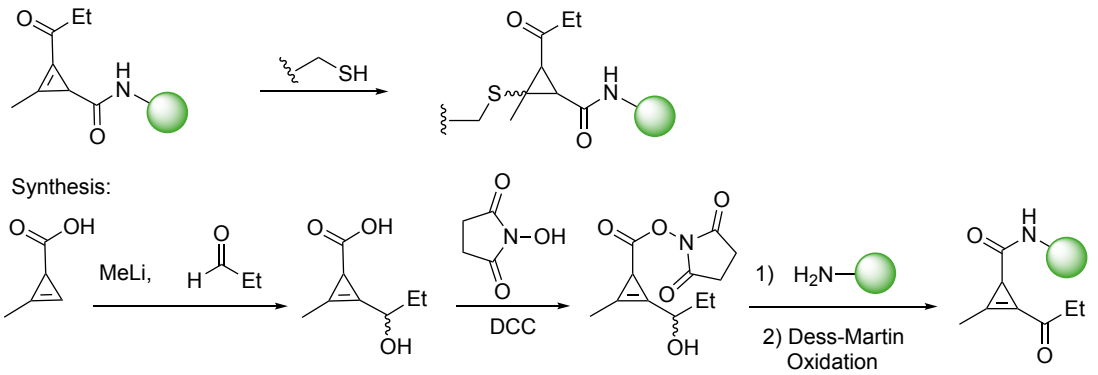

Scheme 9 Reaction of cyclopropenyl ketones with cysteine and synthetic route to access these reagents.

Other unsaturated electrophiles

Next to the above discussed Michael-acceptors, other unsaturated electrophiles serve as good cysteine-selective reagents. Luo *et al.* for instance have recently introduced 1,4-dinitroimidazoles (1,4-DNIms) as highly efficient cysteine-selective bioconjugation reagents (scheme 10) [142]. Under aqueous acidic or neutral conditions, 1,4-DNIms react exclusively with thiols and modify cysteine on proteins quantitatively in seconds. The authors used a carboxylic acid derivative to install the 1,4-dinitroimidazole group on a fluorophore and peptides via amide couplings. The synthesis of this general building block required several steps including protecting group manipulations (scheme 10), thus the direct formation of the 1,4-dinitroimidazole group on complex biomolecules is not feasible with this route.

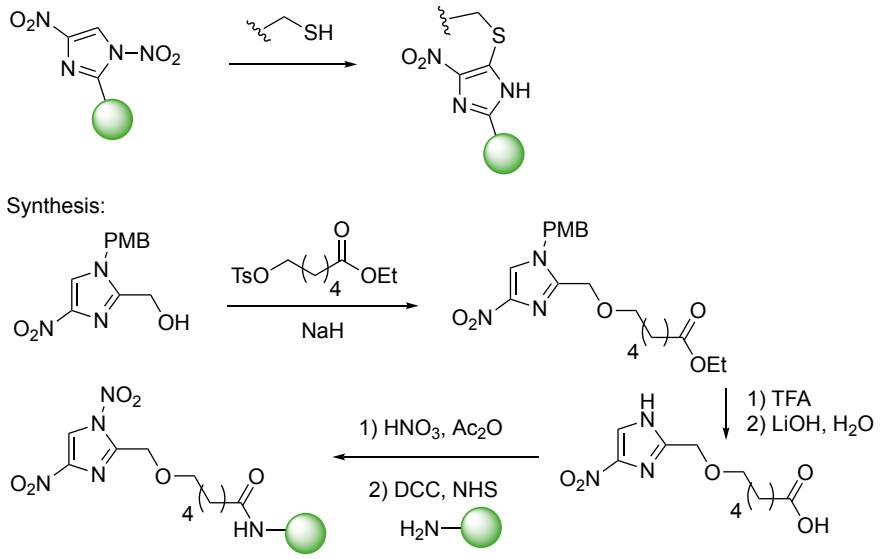

Scheme 10 Reaction of 1,4-dinitroimidazole with cysteine and synthetic route to access these unsaturated electrophiles. PMB= *para*-methoxybenzyl.

Another class of unsaturated electrophiles, azabicyclic vinyl sulfones, has been developed by Bernardes and co-workers (scheme 11) [143]. Excellent conversions were obtained for the modification of a cysteine-ubiquitin mutant at pH 7.0 with as little as 1-5 eq. after only 30 min. The formed thiol conjugates proved to be stable against thiol exchange and retro-Michael addition but can undergo slow cleavage through a rDA reaction. However, the introduced azabicyclic dienophile can be stabilised against this pathway via a second bioorthogonal derivatisation by means of an inverse electron demand Diels-Alder reaction (IEDDA) with tetrazines. This system was further refined by introduction of norbornadiene bromovinyl sulfones that also react selectively with cysteines on proteins [144]. Subsequent modification with tetrazines, followed by a double rDA gives rise to pyrrole-linked protein conjugates that are stable in the presence of high amounts of glutathione. *N*-derivatisation of these reagents can be achieved via amide coupling to the bridging nitrogen, as demonstrated in the coupling with biotin and a fluorophore.

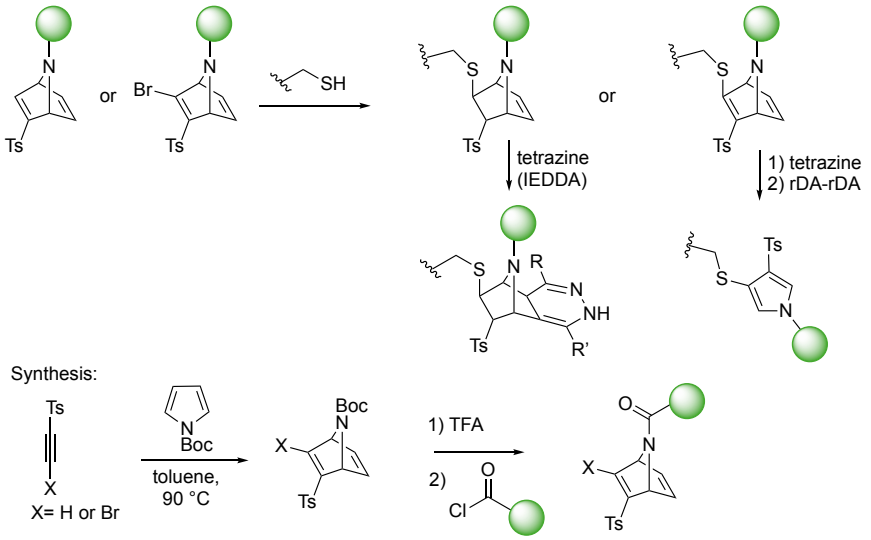

Scheme 11 Top: Reaction of azabicyclic vinyl sulfones with cysteine and further derivatisations with tetrazine. Bottom: Synthetic route to access azabicyclic vinyl sulfones. Ts=4-toluenesulfonyl.

Yet another thiol-reactive motif are unsaturated phosphonates. On a small molecule level, thiol-addition to unsaturated phosphonates has for instance been demonstrated by Khusainova *et al.* (scheme 12) [145]. As reagents for protein modification however, those compounds have not seen a lot of attention, likely due to their low reactivity. Nevertheless, Gao *et al.* have installed electrophilic vinylphosphonates on aminoglycosides for the conjugation to coenzyme A (CoA) via a sulfhydril group [146]. They have synthesised the vinylphosphonate from a phosphonochloridate intermediate, adapting protocols from Fourgeaud *et al.* and others [147, 148].

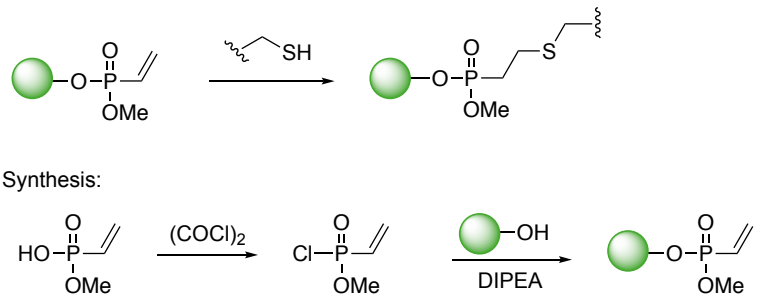

Scheme 12 Reaction of vinylphosphonates with cysteine and synthetic route to access these unsaturated electrophiles.

While most of the cysteine-reactive reagents described in this chapter feature good reactivity and cysteine-selectivity and often show very good product stabilities, the synthetic accessibility of these reagents is predominantly not straight-forward. Furthermore, the direct installation of these reagents on unprotected biomolecules is usually prohibited due to the lack of chemoselectivity of the synthetic routes or due to harsh reaction conditions. Tackling this issue, our group has recently reported unsaturated phosphonamidates as reagents for cysteine-selective protein labelling. These reagents can be synthesised from azides and unsaturated phosphonites by means of the chemoselective Staudinger-phosphonite reaction (SPhR), which is described in detail in chapter 1.4.

1.3.2 Selective modification of cysteine via radical reactions

All examples described in the previous chapter rely on the reactivity of the thiolate anion with electrophilic reagents. In a different concept, as cysteine thiyl radical, cysteine can also engage in reactions with electron-rich alkenes [149] and alkynes [150]. These radicals can be generated under photo-irradiation (typically at 365 nm), often promoted by radical-initiators (RI). Upon reaction with alkenes, a carbon radical is formed and the chain reaction can propagate via hydrogen abstraction from another sulfhydril group, leading to a new thiyl radical (Fig. 10A). Disulfide formation between two thiyl radicals eventually terminates the process. The thiol-ene reaction can be performed under aqueous conditions, features rapid kinetics (in chain reactions, the propagation kinetic constants range from 10^5-$10^6\,M^{-1}s^{-1}$, depending on the monomer structures [151, 152]) and is compatible with diverse functional groups. Next to applications in material science, these properties made the thiol-ene reaction also attractive for the functionalisation of proteins at cysteine residues.

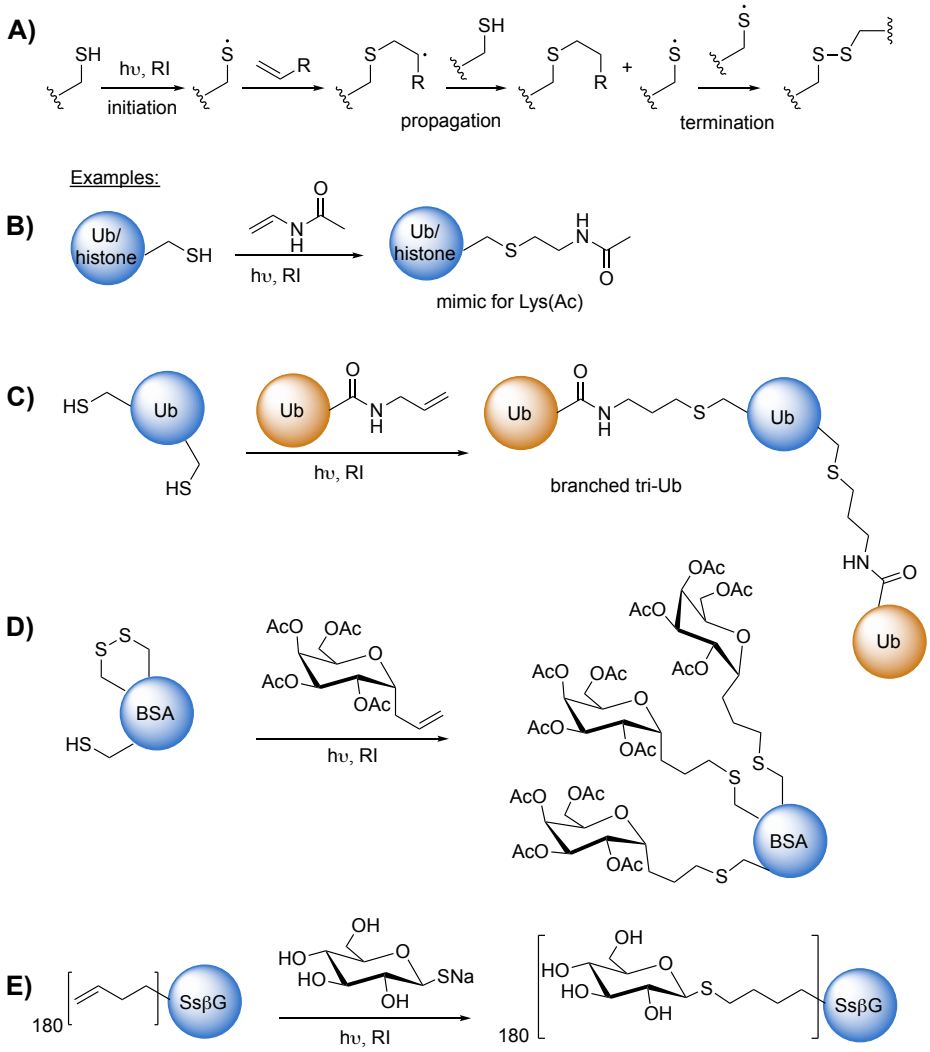

Fig. 10 Thiol-ene reaction: A) Reaction mechanism, B-E) application examples for the modification of proteins with the thiol-ene reaction. RI= radical initiator.

For example, Li *et al.* have employed the thiol-ene reaction on cysteine mutants of ubiquitin and histones H3 and H4 to generate mimics of the post-translational modifi-

cation Lys(Ac) (Fig. 10B). Thereby, they reacted the proteins with *N*-vinyl-acetamide under photo-irradiation in the presence of the radical initiator VA-044 obtaining excellent conversions above 90% [153]. In another example, the Strieter group used the thiol-ene reaction to generate diubiquitins and branched triubiquitins connected via unnatural isopeptide bonds Fig. 10C. To this end, they subjected cysteine mutants of ubiquitin to photo-irradiation in the presence of the radical initiator lithium acyl phosphinate (LAP) and a C-terminal allyl amide modified ubiquitin variant. When applied to proteins, the photo-irradiation-induced thiol-ene reaction can induce damage of the protein as like disulfide cleavage observed by Dondoni *et al.* [154]. In this study, BSA carrying a single free cysteine was subjected to the thiol-ene reaction with allyl α-C-galactoside, however the modification was not only found at the desired cysteine but also at two additional cysteines naturally engaged in a disulfife bridge (Fig. 10D). The authors hypothesise that photo-excited aromatic residues promoted electron transfer to the proximal disulfide bond, causing the cleavage of the latter. The thiol-ene reaction can also be performed the other way round, by introducing the ene-reagent into the protein and addressing it with an external thiol. Floyd *et al.* have for instance incorporated L-homoallylglycine into self-assembled, multimeric virus-like particle Qβ and modified it with glycosyl thiols (Fig. 10E) [155], giving rise to Qβ particles displaying 180 sugar modifications. In this case, structurally important intramolecular disulfide bonds were not affected, perhaps because no aromatic residues were in close proximity to promote damaging electron-tansfer. Next to the reactions with alkenes, thiyl radicals have also been employed with alkynes, mainly for applications in polymer synthesis [150, 156]. Thereby, two thiol groups add to a single alkyne, which has for instance been used for the synthesis of dendrimers [157]. In the context of protein modification, the thiol-yne reaction has only been applied in a handful of examples, for instance for the dual-modification of BSA with a fluorophore and a sugar moiety [158].

1.3.3 Transformation of cysteine into electrophilic handles

Compared to the wealth of nucleophilic functional groups in proteins, electrophilic moieties are rare. The most prominent example are disulfide bonds between two cysteine residues, which are important for the correct folding of proteins [159]. Cysteine disulfide bonds can be attacked by external nucleophilic thiols such as glutathione or by other cysteine residues to undergo disulfide shuffling. Nevertheless, the overall abundance of reactive electrophilic moieties in proteins is low. The installation of reactive electrophilic motifs thus provides a strategy for subsequent selective modification with nucleophiles, including the nucleophilic, natural amino acid residues. The latter concept is particularly attractive for the generation of site-selectively linked protein-protein conjugates. Such homogenous protein-protein conjugates are gaining increasing attention in pharmaceutical research (e.g. bispecific antibodies [160]) as well as in basic research, for example in the generation of site-selectively ubiquitinated proteins (e.g. Ref. [161, 162, 163]). Different electrophilic moieties have been incorporated into proteins as part of unnatural amino acids through genetical engineering methods [164]. For instance, the incorporation of an alkyl-bromide amino acid enabled protein stapling through nucleophilic lysine and histidine residues [165]. In a different example, Li *et al.* incorporated alkene-bearing amino acids into proteins for subsequent modification through the thiol-ene reaction [166]. Alternatively, natural amino acids can be transformed into electrophilic handles by means of chemical or enzymatic methods, thereby inducing reactivity for the subsequent modification with nucleophilic handles (Fig. 11). Several methods thereby make use of cysteine.

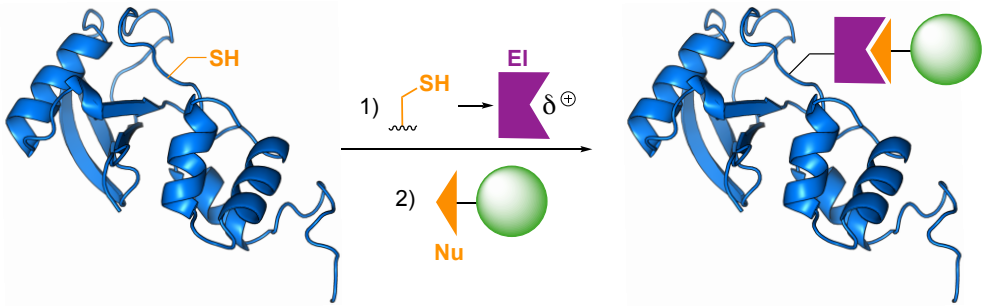

Fig. 11 General concept for the modification of cysteine with nucleophilic handles via intermediately installed electrophiles.

One possibility to install electrophilic handles on cysteine residue relies on the reaction with bis-electrophilic linkers (Fig. 12). Lee *et al.* for instance used a 3-bromo-2-bromomethyl-1-propene linker to construct several protein-small molecule conjugates [167]. They installed the homobifunctional linker on solvent-exposed cysteine residues, thereby inducing reactivity for the addition of small molecule thiol or amine nucleophiles. Following a similar approach, Holm *et al.* attached a homobifunctional *N,N*-ethylene bis(acrylamide) linker to a cysteine mutant of an affibody, enabling subsequent covalent capture of its antigen by affinity-induced nucleophilic addition to the weak acrylamide electrophile [168]. Moreover, Singh *et al.* employed chloroacetaldehyde as a bis-electrophilic linker for the conjugation of a cysteine mutant of α-globin and an amino-oxy ubiquitin derivative [169]. In order to avoid the formation of homo-dimers, it is necessary to use the linkers in excess, which necessitates a subsequent purification step before the addition of the nucleophilic modifier.

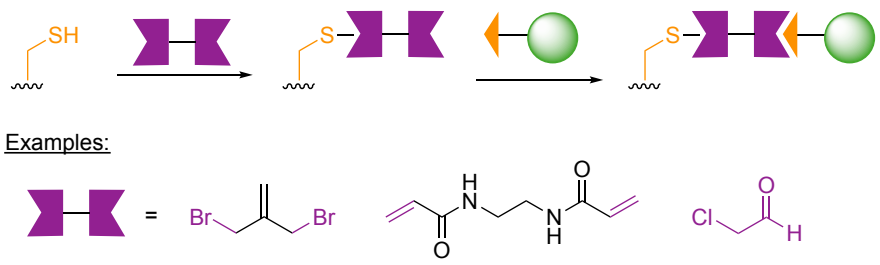

Fig. 12 Examples of bis-electrophilic linkers to install an electrophilic motif on cysteine.

Alternatively, rather than attaching a pre-existing electrophilic functional group to cysteine, a few approaches have been described to install an electrophilic motif on cysteine by means of chemoselective transformations. For instance, a formyl-glycine generating enzyme converts the cysteine within the peptide sequence CxPxR into electrophilic formyl-glycine (scheme 13). The aldehyde can then be addressed with a nucleophilic amino-oxy reagent to form a stable oxime. Hudak *et al.* have used this approach to install an azide and a dibenzoazacyclooctyne on human growth hormone and a full length human IgG antibody, which enabled subsequent site-selective chemical protein fusion via copper-free click reaction [170]. A nice feature of this method is that it enables the site-selective incorporation of the electrophilic aldehyde also in the presence of other cysteine residues. Nevertheless, the incorporation of the peptide recognition tag requires genetical engineering of the protein. Another disadvantage is the lability of the introduced aldehyde. As described by Hudak *et al.*, reducing agents had to be added to the buffer during protein purification in order to protect the protein

from oxidation. Furthermore, aldehydes are prone to react with amines from lysine residues to form imines, which can be another limitation of this method.

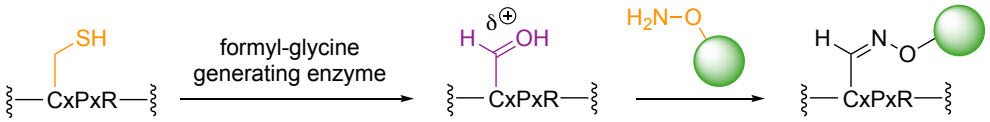

Scheme 13 The FGE-enzyme converts cysteine into an aldehyde, making it thereby amenable for subsequent modification with nucleophilic aminooxy reagents.

In addition to this tag-based chemoenzymatic conversion, there are chemical protocols that can deliver electrophiles from unpaired cysteines, which can then subsequently react selectively with canonical nucleophilic amino acids. A straight-forward protocol following this concept is the formation of electrophilic disulfides using the Ellman's reagent, which facilitates the formation of disulfide-linked protein-protein conjugates (scheme 14A). This strategy has been applied to various protein substrates, especially in the field of chemical ubiquitylation to construct ubiquitinated histones [161], ubiquitin-PCNA [162] and ubiquitin-α-Synuclein conjugates [163]. Notably, the applicability of this approach is limited due to the inherent lability of disulfides in reducing environments [171]. Also the thiolate leaving group can potentially re-open the disulfide conjugate by means of thiol-exchange. Nevertheless, this method is highly attractive as it allows the straight-forward conjugation of two proteins via natural amino acids in a selective manner. Moreover, site-selective conjugation can easily be achieved by placing the respective cysteines at the desired positions within the proteins by means of site-directed mutagenesis.

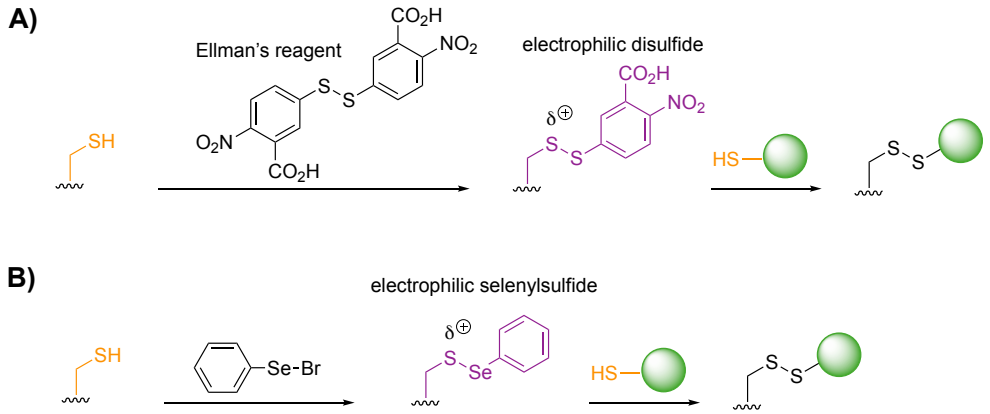

Scheme 14 Cysteine can be converted A) into electrophilic disulfides with Ellman's reagent or B) into electrophilic selenylsulfide with PhSeBr. These electrophiles undergo selective substitution with external thiols or cysteines from a second protein to give disulfides.

A similar strategy, introduced by Davis and co-workers makes use of electrophilic selenylsulfides, which can be efficiently converted to the respective disulfides with thiols [172] (scheme 14B). Using thiol derivatives of mono- and oligosaccharides, they have applied this approach for the site-selective generation of glycosylated proteins. The installation of the electrophilic selenylsulfide could be easily achieved by treating cysteine-containing proteins with phenylselenenyl bromide (PhSeBr) [173]. The resulting sulphur-selenium bond is highly polarised, which is the reason for its excellent reactivity towards nucle-

ophilic attack by other thiol nucleophiles [174]. As described in Ref. [172], quantitative conversions of selenylsulfide proteins with thiols could be achieved in under one hour with low excess of thiol modifiers. Nevertheless, a limitation of this method is that PhSeBr is a highly hazardous chemical, which makes it unattractive to work with.
In another approach, the Davis group and others converted cysteine residues chemoselectively into the electrophile dehydroalanine (Dha) [175, 176] (scheme 15). Dha is susceptible to thia- [177], selena- [178] and aza-Michael-additions [179], as well as to carbon-based free radical chemistry [180]. There are several methods that enable the conversion of cysteine into Dha [176]. In 2008, an oxidative amidation/Cope-type elimination protocol using *O*-mesitylenesulfonylhydroxylamine (MSH) was reported for Dha formation on the model protein subtilisin [181]. Given however that MSH is a reactive oxidizing and aminating reagent, side-reactions with nucleophilic amino acids (Met, Lys, His, Asp and Glu) were observed in some cases [175]. Thus, alternative methods were developed employing milder and more selective reagents to convert cysteine into Dha via bis-alkylation-elimination protocols [175]. The reagents 2,5-dibromohexanediamide (DBHDA) and 2,5-dibromopentanoate (MDBP) [179] proved to be particularly useful, given that they are water-soluble and easy to handle. Alternatively, selenocysteine (Sec) has been used as precursor to generate Dha on proteins. This naturally very low-abundant amino acid can be incorporated into proteins either cotranslationally [182], by native chemical ligation [183, 66] or in the form of PhSec by amber stop codon suppression [184]. Originally, generation of Dha from Sec has been achieved through oxidation of PhSec using hydrogen peroxide or sodium periodate [184, 185]. Here, intermediary formed selenoxides undergo a Cope-type elimination to give Dha. These protocols led to undesired oxidations of amino acids such as methionine and cysteine. A milder protocol to convert Sec into Dha makes use of DBHDA, which allows some selectivity over cysteine [183].

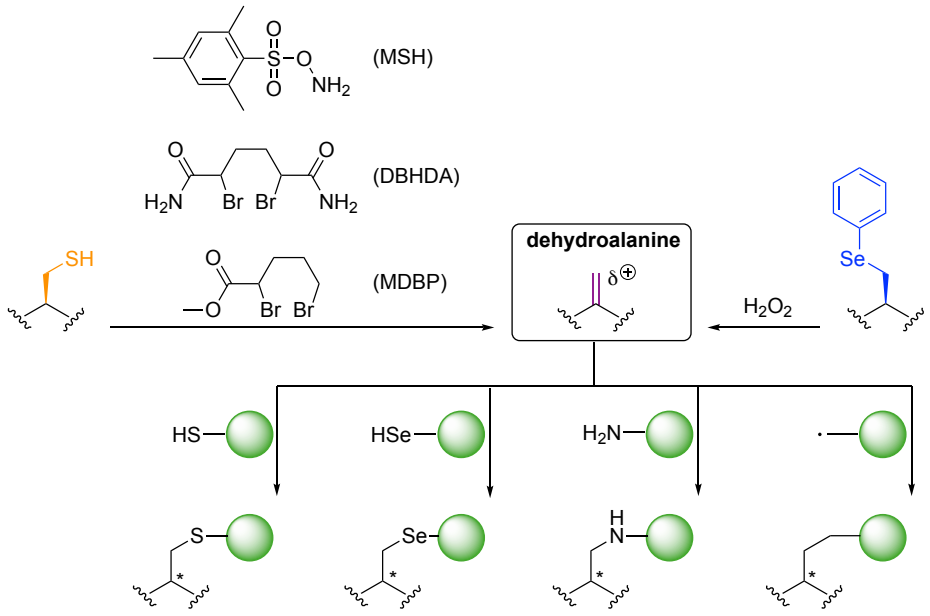

Scheme 15 Methods to generate dehydroalanine from cysteine or selenocysteine precursors and subsequent modification with nucleophiles or through radical addition.

Dha has been used for various protein modifications including the synthesis of protein-protein conjugates. Brik and co-workers for instance employed thiol addition of a Cys-peptide to Dha in combination with a subsequent native chemical ligation to construct protein-ubiquitin conjugates [186]. Furthermore, the same group used Dha on ubiquitin as activity-based probes to identify deubiquitinating enzymes (DUBs) [187, 188, 189]. To the best of our knowledge, no direct protein-protein conjugation using Dha derivatised proteins has however been reported for systems that are not based on affinity- induced reactivity. Furthermore, Dha has seen attention as precursor for the chemical synthesis of post-translational modifications [176]. Addition of sodium thiophosphate to Dha for instance gives rise to phospho-cysteine [181]. A general drawback of Dha modification is the generation of a mixture of diastereoisomers in the protein backbone [186], which can particularly be a problem when studying PTMs introduced with this method.

Despite the attractive possibilities for protein-protein conjugations that arise from the ability to introduce electrophilic moieties into proteins, there are still only few methods available that allow subsequent conjugations with canonical amino acids. Furthermore, the existing methods described above sometimes have disadvantages with regard to stability or selectivity.

1.4 Chemoselective bioconjugation with P(III) and P(V) reagents

1.4.1 Reactions of P(III) reagents with azides

A versatile family of chemoselective reactions for the modification of peptides and proteins employ the reactivity between azides and phosphorus(III) reagents. Historically, the development of these methods dates back to 1919, when Staudinger and Meyer described the reaction between organic azides and phosphines for the first time [190]. They noticed a spontaneous reaction between phenylazide and triphenylphosphine, resulting in an iminophosphorane. The latter could be hydrolysed to give triphenylphosphinoxide and aniline as products. The proposed mechanism of this Staudinger reaction is depicted in scheme 16. In the first step, the phosphine attacks the azide to form a phosphazide, which undergoes cyclisation. Upon release of gaseous nitrogen, an iminophosphorane is formed, which can also be described as the reactive aza-ylide form. Under aqueous conditions, the latter rapidly hydrolyses to the respective amine. Alternatively, the aza-ylide can be trapped with various electrophiles such as aldehydes to generate imines or with cyanates to give carbodiimides [191].

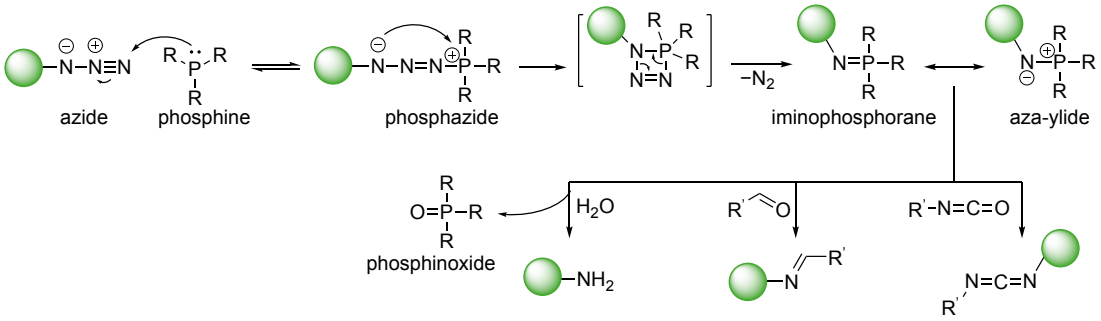

Scheme 16 Mechanism of Staudinger reduction and examples for reactions with electrophiles.

Given the absence of both the azide and the triphenylphosphine functional groups in natural systems, Bertozzi and co-workers recognised the potential to develop the Staudinger reaction further into a chemoselective ligation method. They found that the hydrolysis of the iminophosphorane intermediate could be circumvented in the presence of an intramolecular, electrophilic trap. By placing an ester into the phosphine reagent, intramolecular attack is favoured over hydrolysis, giving rise to an amide bond (scheme 17A). In this ground-breaking study, they applied the Staudinger ligation for the bioorthogonal cell-surface labelling of azido-containing sugars (incorporated by means of metabolic glyco-engineering). As a further refinement of the classical Staudinger ligation, the Bertozzi and the Raines group came up with a solution to eliminate the unnatural phosphine oxide residue, which is left back in the amide product [192, 193]. In the so-called traceless Staudinger ligation, the phosphine reagent is modified with an acylated leaving group as for instance phenol, thiophenol or the highly reactive methanethiol (scheme 17B). With these derivatives, a native amide bond is generated in the ligation product as a result of an acyl transfer to the nucleophilic iminophosphorane and liberation of the phosphine oxide after hydrolysis [194]. Generally, the traceless Staudinger reaction proceeds with excellent selectivity, nevertheless sometimes phosphine oxidation can be a limitation [195]. These positive features have prompted the use of the traceless Staudinger ligation in various applications [191], for instance for the ligation of peptides [196] or the generation of medium-sized lactams [197] and cyclised peptides [198].

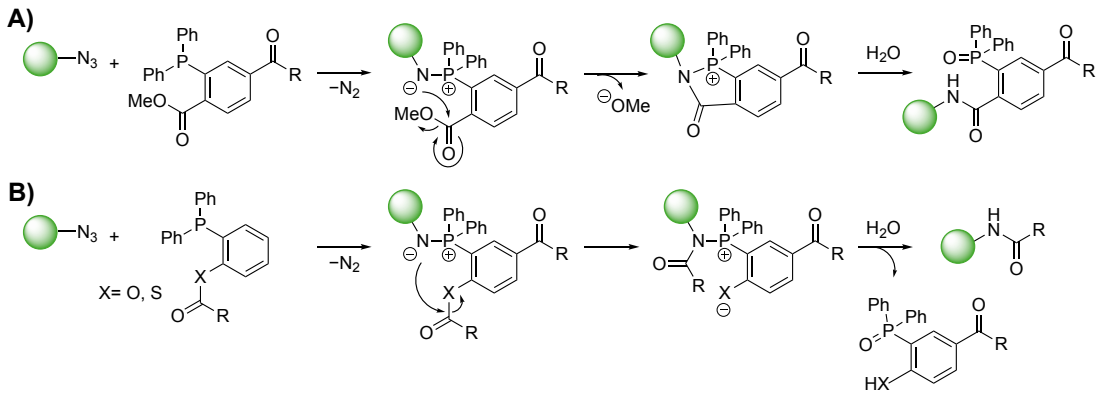

Scheme 17 A) Classical Staudinger ligation. B) Traceless Staudinger ligation.

Next to the phosphines described above, P-O bond containing phosphorus(III) species like phosphinites, phosphonites and phosphites [199, 200] can also undergo Staudinger-type reactions with azides, resulting in phosphinimidates, phosphonimidates and phosphorimidates, respectively (scheme 18).

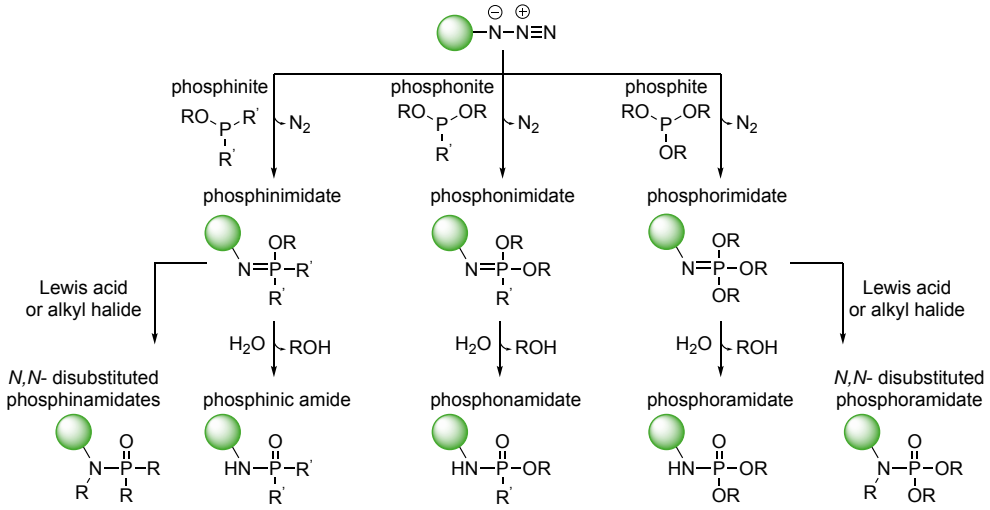

Scheme 18 Variations of the classical Staudinger reaction.

Owing to the more polarized P-O bonds, these derivatives are generally more labile than iminophosphoranes (containing all P-C bonds) [201]. As shown by our group and others, phosphinimidates and phosphorimidates can undergo rearrangements, catalysed by Lewis acids or alkyl halides, to yield *N,N*-disubstituted phosphinamidates and phosphoramidates [202, 203, 204, 205, 206]. Alternatively, the P=N species can be subjected to hydrolysis giving rise to phosphinic acids, phosphonamidates and phosphoramidates, respectively [200, 199, 207, 208, 209]. As opposed to the classical Staudinger reduction described above, here the P-N bond (as well as the P-C bonds) are preserved in the hydrolysis products. The reason for this is that alcoholates are generally better leaving groups compared to amines and thus get liberated preferentially. Nevertheless, reduction to the amine remains a side-reaction. The Staudinger-phosphite reaction has for instance been applied for the synthesis of DNA oligomers in organic solvents [210, 211]. In our group, the chemoselective Staudinger-phosphite reaction has been developed further as a tool for the site-selective modification of azide-containing biomolecules in

aqueous buffer conditions. In 2009, Serwa *et al.* succeeded to apply the Staudinger-phosphite reaction on azide-containing unprotected peptides and the model protein SecB [207]. In the latter case, an unnatural azido-phenylalanine amino acid was incorporated into the protein by means of the amber suppression technology. This was then treated with a water-soluble, light-cleavable phosphite in aqueous buffer at pH 8.0 to result in the respective phosphoramidate (scheme 19A). Subsequent photo-deprotection yielded a mimic of phospho-tyrosine, a post-translational modification found in proteins. Along these lines, Bertran-Vicente *et al.* were able to generate site-specifically phosphorylated lysine peptides from ϵ-azido lysine-containing peptides and either light- or base-cleavable phosphites (scheme 19B) [212]. Hence, the Staudinger-phosphite reaction enables the generation of homogenous phospho-peptides, thereby facilitating the investigation of these post-translational modifications. In a different direction, the Staudinger-phosphite reaction has been used to incorporate stabilising polyethylene-glycol (PEG) groups into peptides and proteins [213, 214], for instance into azido-containing analogues of erythropoietin (EPO) (scheme 19C) [215]. In another application, the Staudinger-phosphite reaction was employed to site-selectively install sugar moieties on peptides and polymers [216, 217].

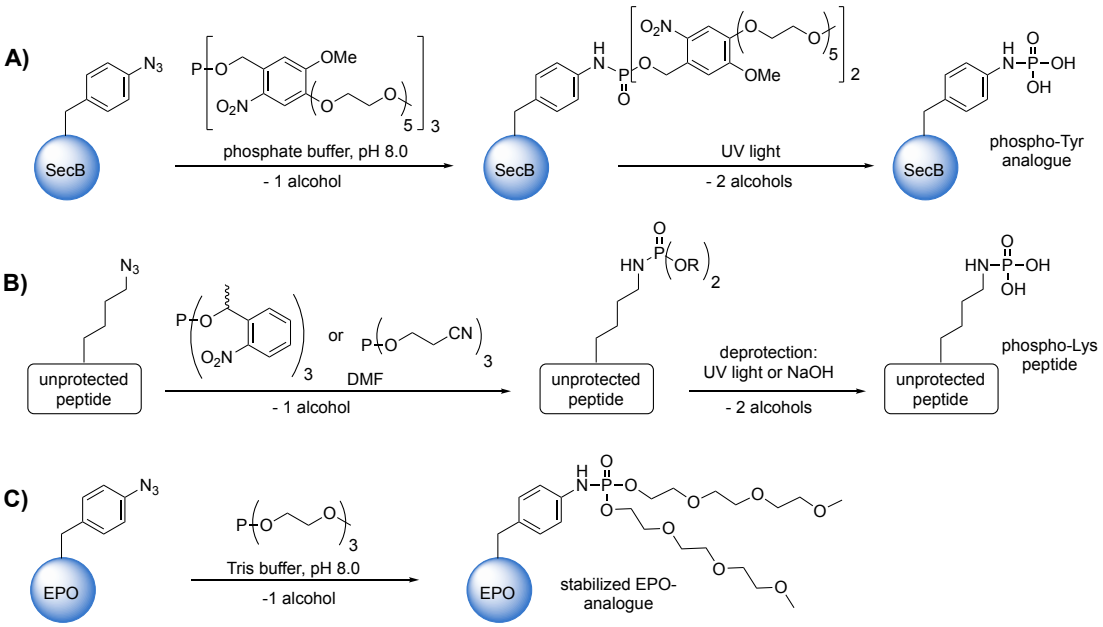

Scheme 19 Application examples for the Staudinger-phosphite reaction for peptide and protein modification: A) Site-selective installation of a phospho-tyrosine analogue on the protein SecB, B) Synthesis of phospho-lysine peptides, C) incorporation of water-soluble PEG chains into the protein erythropoietin (EPO).

In the above examples, symmetrical phosphites were used. Those were typically synthesised from phosphorus trichloride (PCl_3) through base-mediated nucleophilic substitutions with the desired alcohols or by treating the alcohols with hexamethylphophortriamide (scheme 20A). Alternatively, using dichloro-*N,N*-diisopropylaminophosphane [218] enables for the controlled, stepwise substitution with different alcohols, resulting in unsymmetrical phosphites (scheme 20B). These types of phosphites can be used to site-selectively introduce two different groups into biomolecules [219, 220].

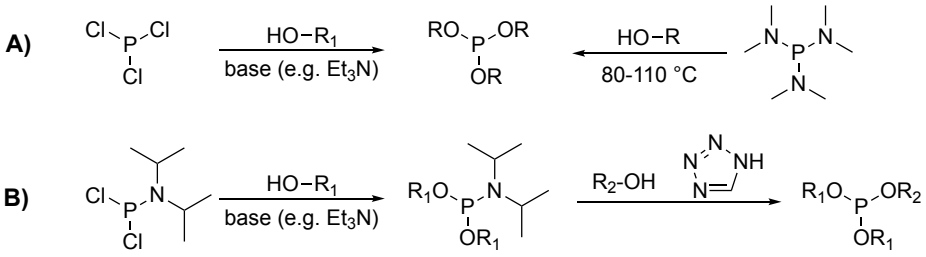

Scheme 20 Synthesis routes for A) symmetrical and B) unsymmetrical phosphites.

As depicted in scheme 18, azides can also be converted with phosphonites in the so-called Staudinger-phosphonite (SPhR) reaction, giving rise to phosphonamidates. However, compared to phosphites, phosphonites are more prone to auto-oxidation [221], which complicates their use in modifications of biomolecules. Nevertheless, as described by Vallee *et al.*, using an sp^2-hybridised aryl- rather than an alkyl-substituent at phosphorus led to increased stability of phosphonites when exposed to air [222]. To further avoid oxidation, they protected the phosphonites with borane, a process that can be reverted adding the base DABCO and gentle heating (scheme 21). Moreover, in order to increase water-solubility, they introduced oligoethylene units at the *O*-substituents. With these phosphonites, they could successfully modify azido-containing peptides and the protein calmodulin under buffer conditions in high conversions. Importantly, these reactions proved to run with excellent chemoselectivity.

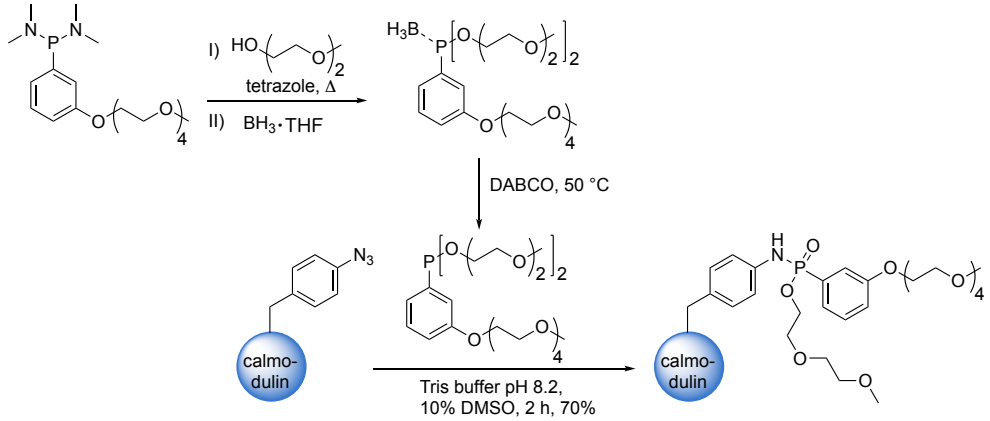

Scheme 21 First application of the Staudinger-phosphonite reaction for the site-selective modification of a protein.

Vallee *et al.* further expanded the scope of the Staudinger-phosphonite reaction to borane protected ethynylphosphonites [223]. With these substrates, a stepwise conjugation of two different azides could be achieved (scheme 22). In this study, borane-protected diethyl-ethynylphosphonites were used, which could be easily generated from diethylchlorophosphite and ethynylmagnesium bromide followed by the addition of BH_3, similar to a published protocol from Montchamp and co-workers [224]. This borane protected phosphonite was then first subjected to a copper-catalysed azide-alkyne cycloaddition (CuAAC), forming a triazole. In this step, the Staudinger reaction with the phosphorus is prevented due to the borane-adduct. Only subsequent deprotection by means of DABCO liberates the reactive triazole phosphonite, making it thereby amenable to react with a second azide. Similar as for the Staudinger-phosphite reaction described above, this system was made applicable to peptide and protein modification

in buffer conditions by the incorporation of stabilising oligo-ethylene glycol through the *O*-substituent [225]. Furthermore, as described by Siebertz *et al.*, the use of phosphites with *O-ortho*-nitrobenzyl-substituents enabled the UV-light-induced cleavage of the triazole-phosphonamidate conjugate [226].

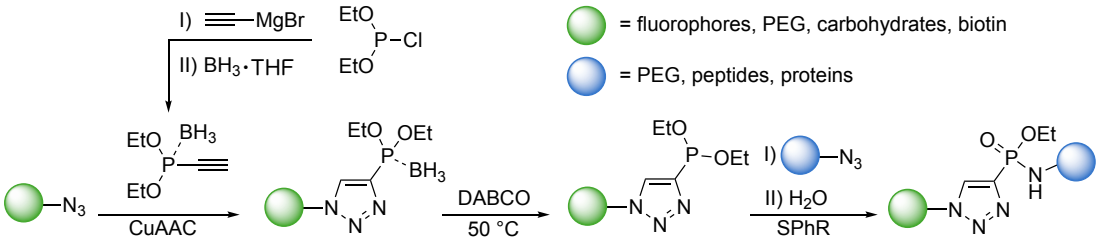

Scheme 22 Borane-protected ethynylphosphonites enable the modular coupling of two azides.

When reacting unprotected ethynylphosphonites directly with azides in the Staudinger-phosphonite reaction, ethynylphosphonamidates are being generated (scheme 23A) [208]. Our group discovered that this transformation induces reactivity for a subsequent thiol-addition to the alkyne group yielding stable thiol conjugates. The fact that thiol addition is only observed once the phosphonamidate has formed but not on the phosphonite stage could be explained by the electron-withdrawing nature of the P=O bond in the phosphonamidate. This likely renders the alkyne moiety more electron-poor and thus activates it toward nucleophilic attack by thiols. Importantly, both steps, the Staudinger-phosphonite reaction to make the phosphonamidate as well as the subsequent addition of thiols, proceed with excellent chemoselectivity. This feature is distinct from most other thiol/cysteine-selective methods, where the synthesis of the thiol-reactive reagent often requires several steps including protecting group manipulations (compare introduction, chapter 1.3.1).
As shown by Kasper *et al.*, *O*-ethyl-ethynylphosphonamidates could be efficiently synthesised in DMF from the respective azide-precursors and diethyl-ethynylphosphonite. As probed with reduced glutathione, the thiol-addition to an *O*-ethyl, *N*-aryl-EDANS-ethynylphosphonamidate proceeded with a bimolecular rate constant of 0.62 $M^{-1}s^{-1}$ at pH 8.5 [208]. Notably, the *Z*-isomer is thereby formed preferentially, which is in line with literature reports on the thiol-addition to other electron-deficient alkynes [227]. Next to small molecule derivatives, the Staudinger-phosphonite reaction was applied to install ethynylphosphonamidates on cyclic peptides, which could subsequently be conjugated to a cysteine-mutant of eGFP to enable intracellular delivery [208]. In the same study, the excellent cysteine-selectivity could further be demonstrated by labelling IgG antibodies. LC-MS/MS analysis of the trypsinated antibody revealed exclusive cysteine modification, while the other nucleophilic amino acids were not modified, even when using ethynylphosphonamidate in excess. Moreover, thiol-phosphonamidate conjugates exhibit high stability under physiological conditions; no thiol exchange or P-N bond hydrolysis was observed in the presence of excess free thiols or in cell lysate or human serum. These findings prompted the investigation of ethynylphosphonamidates as linkers for the generation of stable antibody-drug conjugates (see chapter 5 for background) [228]. Therefore, an ethynylphosphonite with an *O*-diethylenglycol substituent was synthesised starting from bis(diisopropylamino)-chlorophosphine with diethylene glycol (based on Ref. [224, 223, 226]) (scheme 23B). This phosphonite was subsequently subjected to the Staudinger-phosphonite reaction with an azide-containing NHS-ester to generate the respective ethynylphosphonamidate, which could further be coupled

to a toxin via a free amine. This derivative was then conjugated to a therapeutic antibody, giving rise to a stable and efficacious ADC.
Notably, the Staudinger-phosphonite reaction generates phosphonamidates as a racemic mixture, whereby the two enantiomers differ at the substituent configuration around the phosphorus atom. Consequently, cysteine addition leads to a mixture of diastereoisomers, which in some cases might be a limitation. However, Kasper *et al.* succeeded to separate the two enantiomers of an ethynylphosphonamidate-NHS building block by means of chiral HPLC [229]. Using these enantiomerically pure ethynylphosphonamidates, they were able to generate ADCs with high homogeneity.

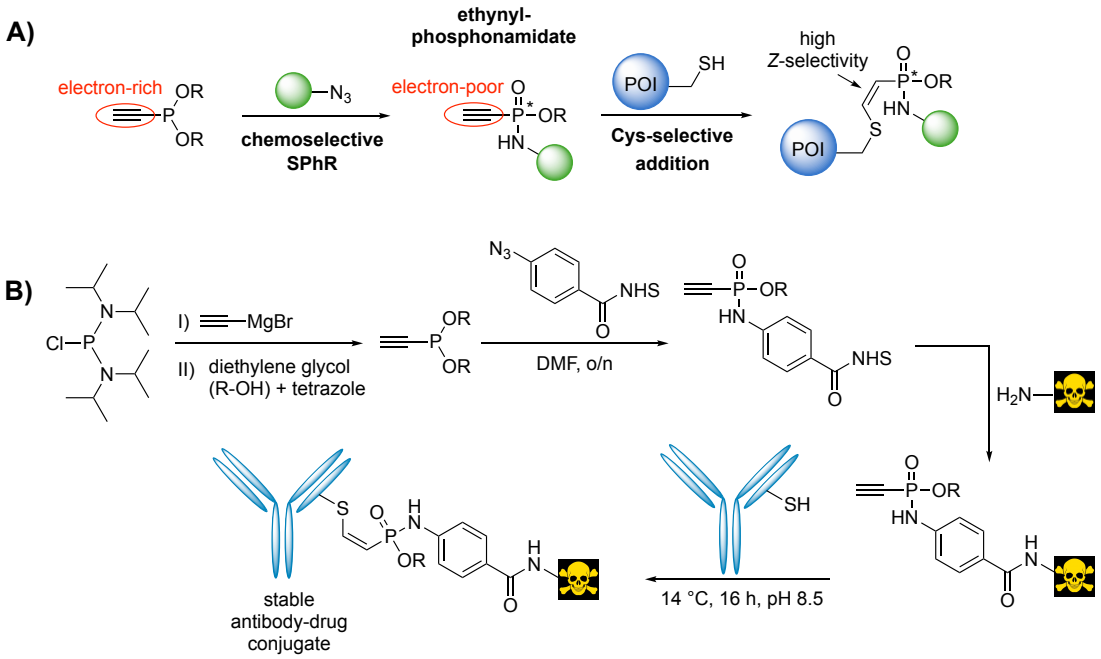

Scheme 23 A) Ethynylphosphonamidates can be accessed by the chemoselective Staudinger-phosphonite reaction (SPhR) from azides and ethynylphosphonites. Ethynylphosphonamidates react selectively with cysteines on proteins, giving the *Z*-isomer preferentially. The * marks a chiral center. B) Example for the synthesis of an ethynylphosphonamidate-toxin derivative, which was used to generate stable antibody-drug conjugates.

In a different study, Kasper and Glanz employed the Staudinger-phosphonite reaction to make vinylphosphonamidates using vinylphosphonites as the starting materials (scheme 24A) [209]. Analogously to ethynylphosphonamidates, vinylphosphonamidates could be used for cysteine-selective bioconjugations such as antibody labelling at cysteines. However, it was observed that vinylphosphonamidates are less reactive in thiol-additions compared to ethynylphosphonamidates owing to the less electrophilic sp^2-hybridised vinyl-carbon. Nevertheless, the reactivity of vinylphosphonamidates can be enhanced by varying the *N*- and *O*-substituents (scheme 24B). Generally speaking, the more electron-withdrawing these substituents are, the more reactive the vinyl bond gets towards nucleophilic attack by thiols. With two equivalents of glutathione at pH 8.5, an *N*-phenyl vinylphosphonamidate (10 mM) showed 80% conversion after 24 hours, while a comparable *N*-alkyl derivative was only converted 20% under the same conditions. The electron-withdrawing sp^2-aryl substituent thus increased the reactivity. The reactivity of the *N*-phenyl derivative could be further enhanced by replacing the *O*-ethyl

residue by a more electron-withdrawing *O*-trifluoroethyl substituent. This derivative reacted with glutathione in aqueous buffer at pH 8.5 with a bimolecular rate constant of 0.021 $M^{-1}s^{-1}$.

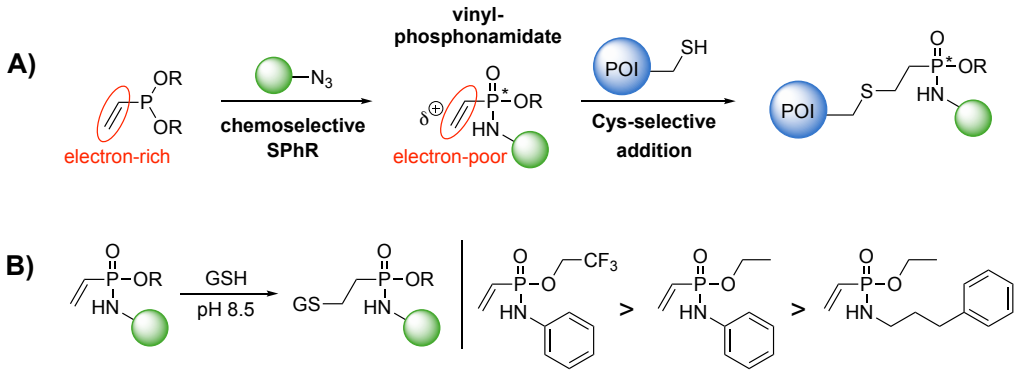

Scheme 24 A) Vinylphosphonamidates can be accessed by the chemoselective Staudinger-phosphonite reaction from azides and vinylphosphonites. Vinylphosphonamidates react selectively with cysteines on proteins. The * marks a chiral center. B) The reactivity of vinylphosphonamidates with thiols (e.g. glutathione, GSH) depends on the *N*- and *O*-substituents.

As depicted in scheme 25, the vinylphosphonites used in the above described studies were accessed via different routes (again based on Ref. [224, 223, 226]). In one route, phosphorus trichloride was first reacted with the desired alcohol and then treated with vinylmagnesium bromide to give the respective vinylphosphonite (route A). Alternatively, bis(diisopropylamino)-chlorophosphine was first alkylated with vinylmagnesium bromide and then subjected to tetrazole-mediated substitution with the desired alcohol (route B). Attempts to isolate unprotected vinylphosphonites failed in many cases due to product decomposition, hence they were protected with borane for isolation and storage. Before use in the Staudinger-phosphonite reaction, the borane protection was removed by treatment with DABCO. The diethyl-vinylphosphonite could be accessed from commercially available diethyl chlorophosphite and vinylmagnesium bromide (route C) and was used as crude mixture in the reaction with azides. Notably, a significant increase in thiol addition efficiency was observed when the SPhR was carried out in the presence of a thiol in a one-pot reaction. This variant of the SPhR enabled the facile stapling of a peptidic inhibitor as well as the macrocyclization of cell-penetrating peptides [209].

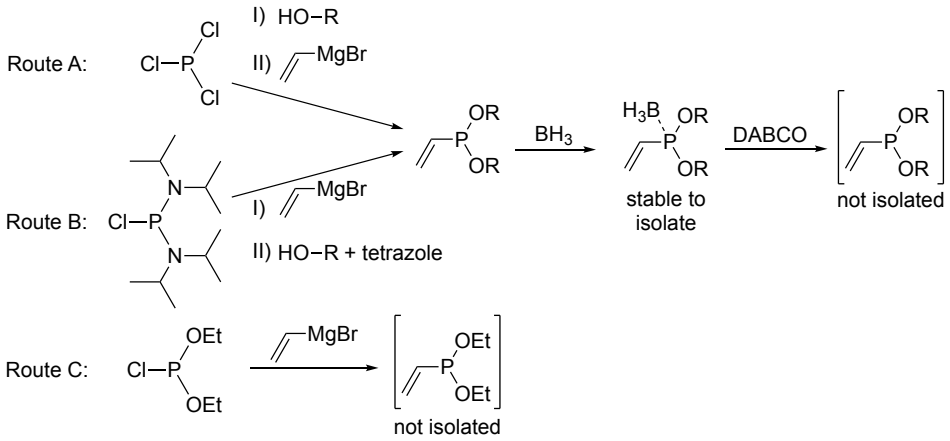

Scheme 25 Different synthetic routes to access vinylphosphonites.

1.4.2 Reactions of P(III) reagents with other electrophiles

Next to azides, the reactivity of phosphorus(III) reagents has also been explored with other electrophiles. In 1898, Michaelis described the reaction of phosphites with alkyl halides to generate phosphonates [230]. This reaction has further been elaborated by Arbuzov [231] (and several other investigators [232]), giving it the name Michaelis-Arbuzov reaction. The proposed mechanism of the classical Michaelis-Arbuzov reaction between phosphites and alkyl halides is depicted in scheme 26A. First, the lone pair electrons of the phosphite attack the electrophilic alkyl group of the alkyl halide, thereby substituting a halide anion. In the formed phosphonium salt intermediate, the alkyl group originating from the alkyl halide is attached at the phosphorus. Then, the displaced halide ion promotes the dissociation of an alkyl group of the phosphite from the reactive phosphonium intermediate, a process that is facilitated by the tendency of the phosphorus atom to withdraw electrons to expand its valency by forming a P=O bond. Overall, a trivalent phosphorus species (phosphite) is converted into pentavalent phosphorus species (phosphonate). In this process, a new alkyl halide is generated as a by-product. Typically, this transformation is carried out at elevated temperature.
Next to phosphites, the Michaelis-Arbuzov reaction can also be applied to phosphonites and phosphinites giving rise to phosphinates and phosphine oxides, respectively (scheme 26B).

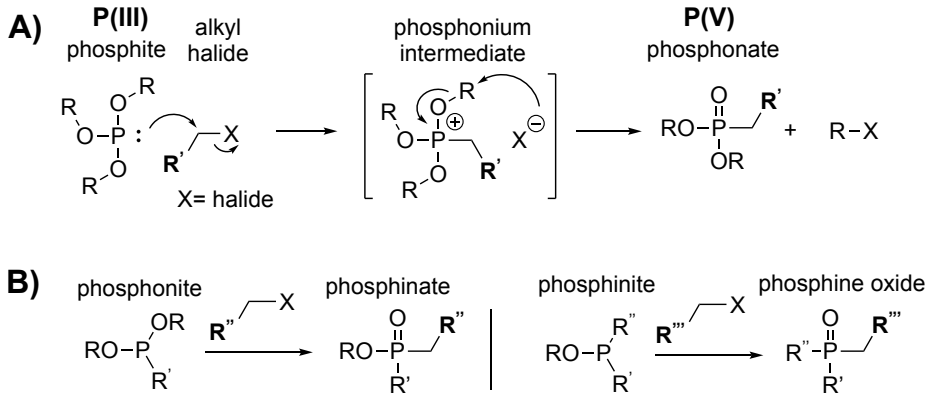

Scheme 26 A) Mechanism of the classical Michaelis-Arbuzov reaction between phosphites and alkyl halides for the generation of phosphonates. B) Variations with other P(III) reagents.

Moreover, it has been recognised early that besides alkyl halides, trialkyl phosphites are also reactive towards various other electrophiles [232], some of which are depicted in scheme 27. The reaction with β-halo-esters for instance gives rise to β-ester phosphonates, which serve as starting materials in the HWE reaction [233]. Similarly, phosphonates can be accessed using quaternary salts of Mannich bases [234] or alkyl *p*-toluenesulfonate esters [235]. While the latter substrate class requires elevated temperatures to convert effectively, more reactive starting materials such as sulfenyl chlorides have been shown to react readily at temperatures as low as –60 °C [236]. Notably, using sulfenyl chlorides as starting materials, thiophosphonates are formed, containing a phosphorus-sulphur bond.

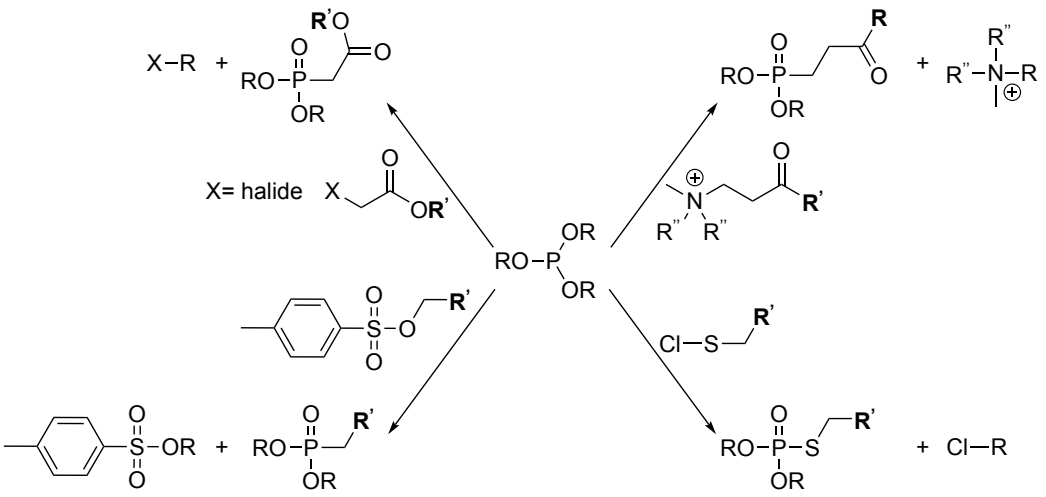

Scheme 27 Various electrophiles react with trialkyl phosphites in Arbuzov-type reactions.

Reactions of P(III) reagents with disulfides

Another well-known substrate class to readily react with phosphorus(III) reagents are disulfides. Treating them for instance with phosphines leads to the reduction of the disulfide bond to thiols. The water-soluble phosphine derivative tris(2-carboxyethyl)phosphine (TCEP) is widely used for the mild reduction of disulfide bonds in peptides and proteins in aqueous buffer (scheme 28).

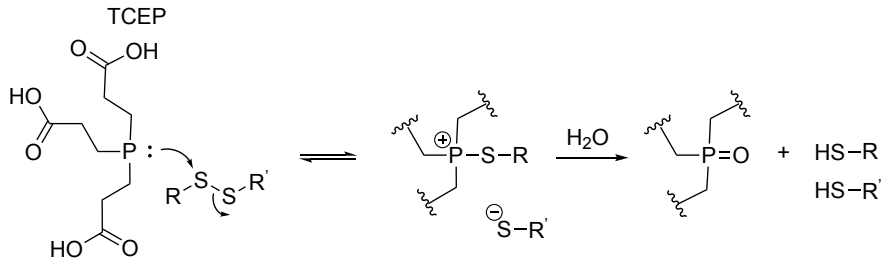

Scheme 28 Disulfide reduction by TCEP.

In 1955, Jacobson *et al.* reasoned that disulfides might as well be good substrates to react with phosphites, just like the other electrophiles described in scheme 27. Indeed, when they reacted diethyldisulfide and triethylphosphite together at 90 °C for 10 hours, they were able to obtain the desired ethylthiophosphonate in 77% yield (scheme 29A) [237]. Moreover, they found near quantitative amounts of diethyl sulfide as a by-product, indicating that the reaction followed an Arbuzov-like mechanism (compare scheme 26). A similar outcome was observed by Poshkus *et al.* when they treated triethylphosphite with a symmetrical, aromatic disulfide in boiling benzene (scheme 29B) [238]. However, here the product could be obtained in similar yield after significant shorter amount of time (ca. 2.5 h as reported in Ref. [239]). This circumstance can be explained by the fact that the disulfide bond in the aryl derivative is more polarised and hence more electrophilic than in the alkyl derivative owing to the electron-withdrawing effect of the sp^2-hybridised aryl substituent.

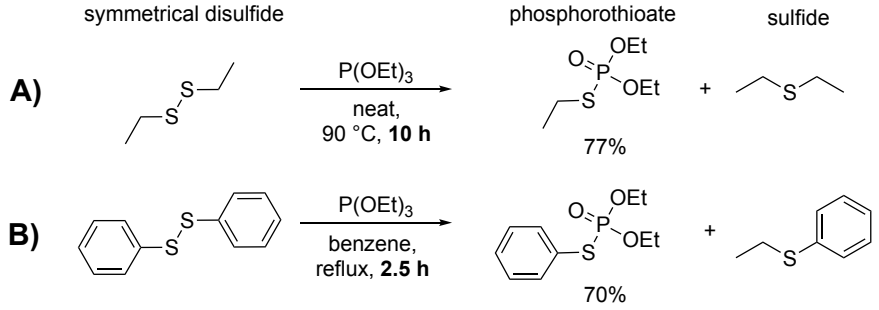

Scheme 29 Examples for the generation of phosphorothioates from the reaction of triethylphosphite with a symmetrical A) dialkyl- and B) diaryldisulfide as described in Ref. [237] and [238], respectively.

Along these lines, Harvey *et al.* thought that the reactivity of phosphites towards disulfides could be further enhanced by using unsymmetrical disulfides, reasoning that the sulphur-sulphur bond in the latter are yet more polarised and thus more electrophilic than in symmetrical disulfides [239]. Indeed, as demonstrated with a handful of unsymmetrical disulfides, they noticed striking enhancement of reactivity in the reaction with triethylphosphite (scheme 30B). In fact, those substrates reacted exothermically at room temperature and the desired phosphorothioates could be obtained in good yields next to the expected sulfides (by-products of the thiolate attacking the phosphonium intermediate, see scheme 30A).

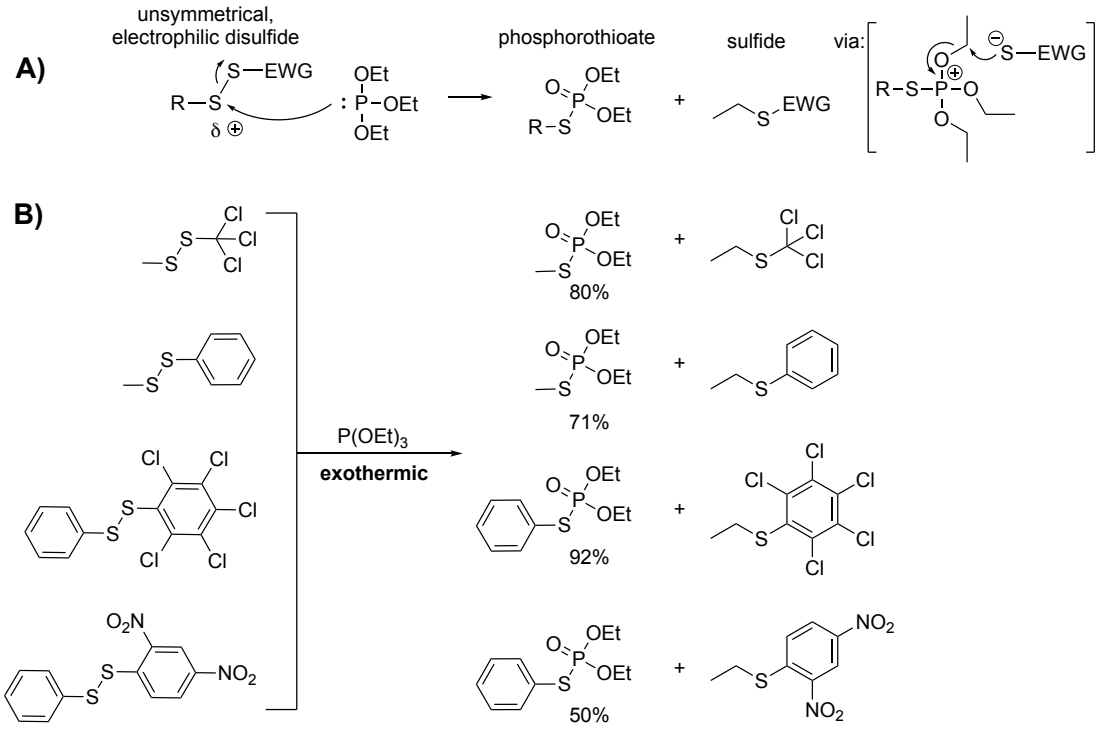

Scheme 30 A) Proposed mechanism of the reaction between triethylphosphite with unsymmetrical disulfides. B) First examples of this reaction reported by Harvey *et al.* [239].

Also other synthetic routes exist to generate phosphorothioates, for instance via nucleophilic substitution of $(RO)_2P(O)Cl$ halides with thiols (e.g. Ref. [240]). An alternative method, described by Zhu *et al.*, relies on the palladium-catalysed dehydrogenative coupling of H-phosphonates with thiols [241]. Moreover, phosphorothioates were synthesised in NHC-catalysed coupling reactions between H-phosphonates and disulfides [242]. Nevertheless, for the installation of phosphorothioates on biomolecules, the above described route relying on phosphites and activated disulfides seems most suitable, as it is independent of catalysts and proceeds efficiently under mild conditions. The applicability of the phosphite-disulfide reaction on biomolecules has for instance been demonstrated by Higson *et al.* for the synthesis of a diribonucleotide with a 3′-*S*-phosphorothiolate linkage, as depicted in scheme 31 [243]. They used a para-nitropyridine activated disulfide, which readily reacted with a ribonucleotide-substituted phosphite at ambient temperature.

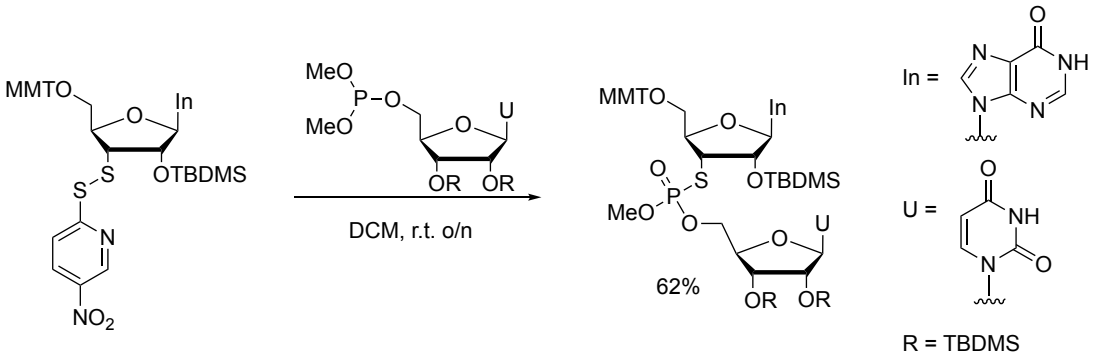

Scheme 31 Example for the reaction between a trialkylphosphite and an unsymmetrical disulfide to generate a phosphorothiolate-linked diribonucleotide as shown by Higson *et al.* [243].

In a different example, Bertran-Vicente *et al.* have made use of the chemoselective phosphite-disulfide reaction to generate site-specifically phosphorylated cysteine peptides (pCys) [244] (scheme 32). To this end, they activated cysteine peptides with the Ellman's reagent, which readily reacted with a photo-cleavable phosphite to the corresponding phosphorothiolate ester. Excellent conversion was observed when the reaction was run in DMF and the product could be isolated in 55% yield. Under aqueous conditions however, only 27% of the phosphorothiolate ester could be obtained and free cysteine peptide was observed as a side-product. A likely explanation of this observation is that water attacked the electrophilic phosphorus in the intermediary formed triester thiophosphonium cation, thereby substituting the cysteine residue (scheme 32). Nevertheless, with the intact phosphorothiolate ester in hand, pCys peptides could be obtained after UV-light mediated cleavage of the *O*-substituents. pCys is a post-translational modification of cysteine and is for instance known to function as an intermediate in the phosphoenolpyruvate-dependent phosphotransferase system [245] or in dephosphorylation of phosphotyrosine residues by protein tyrosine phosphatases [246, 247]. Chemoselective methods to access homogenous pCys peptides allows to study the properties and function of this PTM. Davis and co-workers managed to install pCys on a protein level [181]; however their protocol relying on the reaction of sodium thiophosphate with dehydroalanine (Dha) delivers an epimeric mixture of pCys proteins (compare chapter 1.3.3). In contrast, the method by Betran-Vicente *et al.* relying on the chemoselective phosphite-disuflide reaction proved to be epimerisation-free [244].

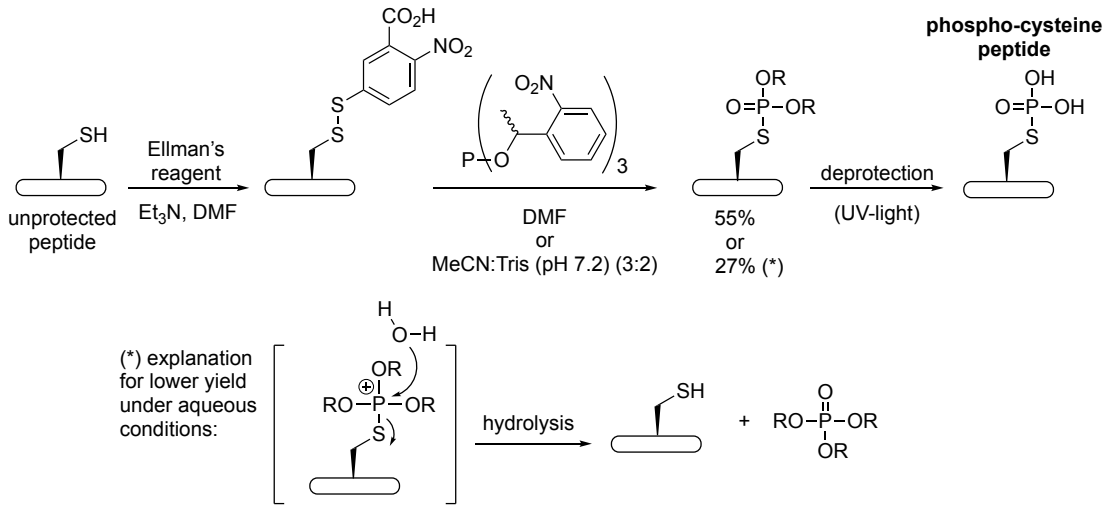

Scheme 32 Generation of site-specifically phosphorylated cysteine-peptides as reported by Bertran-Vicente *et al.* [244].

As illustrated with all the examples in this chapter, reactions between phosphorus(III) reagents and electrophilic substrates give rise to a broad variety of P(V) organophosphorus compounds with interesting properties. Phosphines can be used to reduce azides and disulfides or be employed in Staudinger-ligations. Moreover, phosphorus(III) reagents with one or several P-O bonds have been employed in conjugation reactions with various electrophiles. For instance, the Staudinger-phosphite and Staudinger-phosphonite reactions with azides give access to phosphoramidates and phosphonamidates, respectively (scheme 33). Interestingly, our group has found that unsaturated vinyl- and ethynylphosphonamidates are highly selective towards thiol-additions, which was employed to generate stable bioconjugates. On the other hand, the reaction between phosphites and disulfides (and in particular unsymmetrical disulfides) results in the formation of phosphorothiolates. Building up on all these results, it consequently seemed interesting to explore the reactivity between electrophilic disulfides and unsaturated vinyl- and ethynylphosphonites. The products expected from this transformation are unsaturated phosphonothiolates. Formally, these are analogues of unsaturated phosphonamidates, whereby sulphur instead of nitrogen is bonded to phosphorus. Very little has been reported so far about the synthesis of unsaturated phosphonothiolates from unsaturated phosphonites. Few examples exist on the reaction of phenyl-phosphonites with disufides [248, 249, 250] and in the late 1980s, Trishin *et al.* have synthesised vinylphosphonothiolate derivatives from sulfenyl chlorides and vinylphosphonites [251]. However, to the best of our knowledge, disulfides have not been explored as substrates in reactions with vinyl- or ethynylphosphonites. We hypothesised that unsaturated phosphonothiolates might as well react in thiol-additions to the corresponding thiol-conjugates. Again, to the best of our knowledge, this type of transformation has not been described before. Hence, a major goal within this thesis was to synthesise and evaluate unsaturated phosphonothiolates as reagents for cysteine-selective bioconjugations.

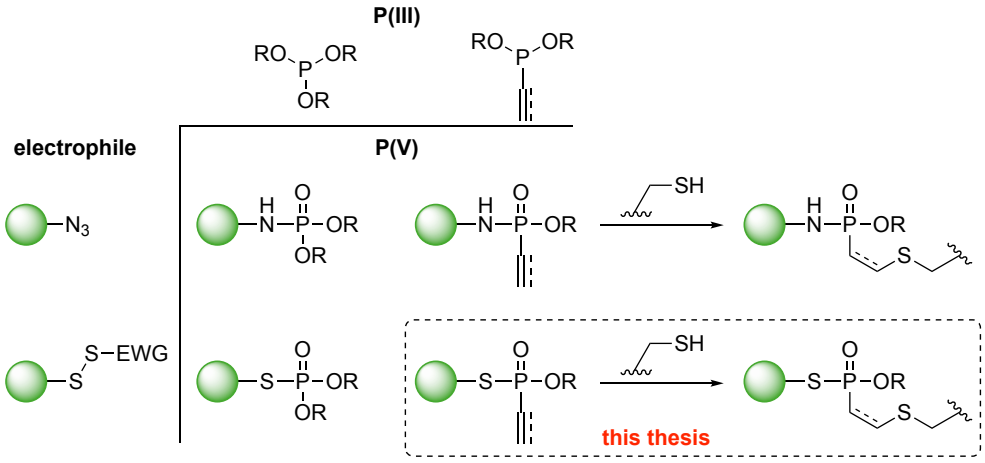

Scheme 33 Overview of products formed from the reaction of phosphites and phosphonites with azides and electrophilic disulfides. Unsaturated phosphonamidates react selectively with thiols, which prompted the question whether this reactivity could be extrapolated to unsaturated phosphonothiolates, which is the subject of this thesis. The dashed triple bond (before thiol addition) indicates that this can either be a double or a triple bond, resulting in either a single or a double bond in the thiol-conjugate.

2 Objectives

To date, a plethora of well-optimised strategies exist for the modification of proteins with various functional tags, including methods that rely on the incorporation of unnatural reactive handles as well as methods that specifically address canonical amino acids. The development of these methods gave access to a wide range of bioconjugates, including biopharmaceuticals and probes to study cellular processes in health and disease. While it seems that the bar for innovation in this advanced field is high, the challenge of applying organic chemistry on proteins with precise control still prevails. When relying on the modification of canonical amino acids and in particular cysteine, the repertoire of methods that feature both excellent selectivity as well as easy access to starting materials is still limited. As outlined in detail in the introduction (see chapter 1.3.1), the direct installation of electrophilic, cysteine-reactive handles into complex molecules such as polypeptides is prohibited for many of the currently available methods due to the lack of chemoselectivity in the synthesis of these handles. As a consequence, multi-step workarounds with protecting group manipulations are often needed to synthesise and install cysteine-reactive groups in these cases. On the other hand, methods that allow the installation of cysteine-reactive handles on complex substrates in a chemoselective manner are rare. In our group, this has been achieved in the chemoselective synthesis of cysteine-reactive phosphonamidates via the Staudinger-phosphonite reaction. This strategy is however limited to azide-containing substrates. When relying on canonical amino acids, the installation of cysteine-reactive electrophilic groups on proteins has only been demonstrated in a handful of examples as outlined in chapter 1.3.3. Importantly, these methods in principle allow for protein-protein conjugation solely based on canonical amino acids, which is highly attractive given that there is a great need for homogenous protein-protein conjugates in both pharmaceutical industry as well as in basic research.

In this thesis, our goal was to develop a chemoselective method that enables the installation of a cysteine-selective electrophilic group on cysteine residues, independent of unnatural amino acids. Specifically, we set out to investigate **unsaturated vinyl- and ethynylphosphonothiolates** as new classes of cysteine-reactive, electrophilic reagents (Fig. 13A). We hypothesised that these reagents could be incorporated chemoselectively into unprotected biomolecules by addressing activated cysteine residues with unsaturated phosphonites (see chapter 1.4.2). Assuming that unsaturated phosphonothiolates, similar to unsaturated phosphonamidates (see chapter 1.4.1), react selectively with cysteine, the proposed strategy in this thesis would allow selective thiol-thiol bioconjugations. Within the main objective of developing a cysteine-selective protein modification method based on unsaturated phosphonothiolates, the first step was to establish conditions that enable the efficient synthesis of these reagents from electrophilic disulfides and unsaturated phosphonites. The second step in the method development was to investigate the properties of unsaturated phosphonothiolates with respect to their reactivity and selectivity towards thiols as well as evaluating the stability of the resulting thiol-conjugates under physiologically relevant conditions. We thought that these aspects might be best studied with small molecule model systems before moving on to more complex substrates.

As mentioned above, the main aim for developing this method was the installation of electrophilic phosphonothiolates on unprotected peptides and proteins to enable site-selectively linked protein-protein conjugations (Fig. 13B). In two additional applications, we furthermore set out to employ unsaturated phosphonothiolates as linkers to generate antibody-drug conjugates, as well as protein-photocrosslinker conjugates to study dynamic protein-protein interactions.

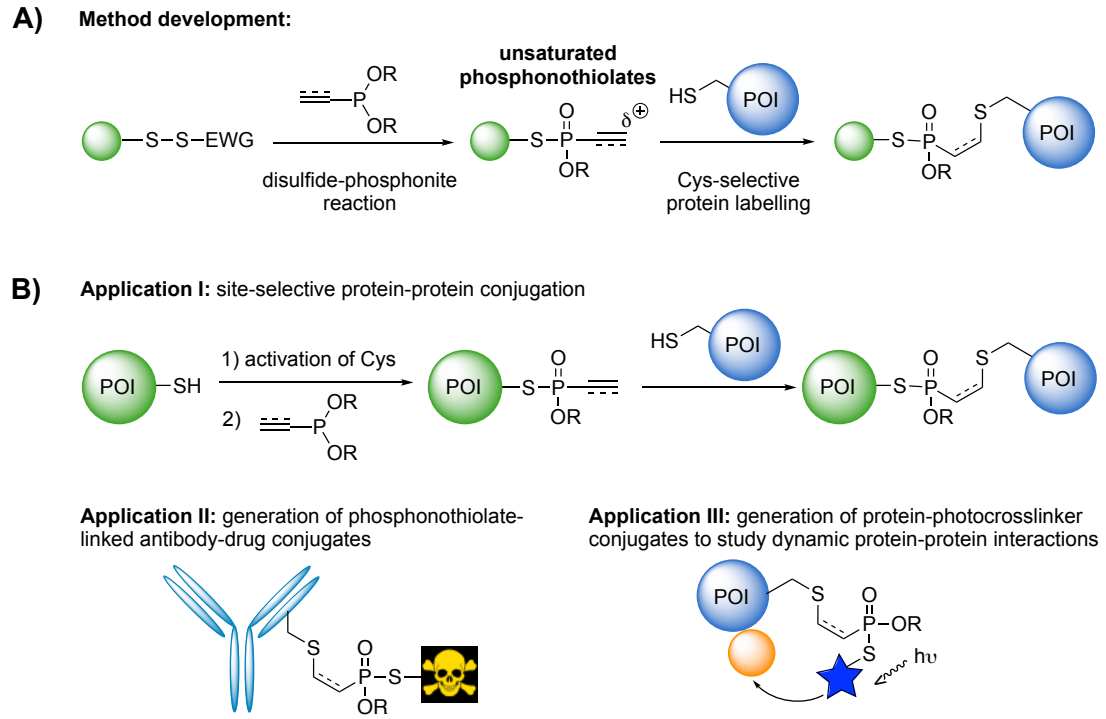

Fig. 13 Goals of this thesis. A) Synthesising phosphonothiolates and probing them for cysteine-selective protein labelling. B) Envisioned applications of unsaturated phosphonothiolates as linkers in bioconjugates. The dashed bond in the phosphonite and the phosphonothiolates indicates either a double or a triple bond and consequently a single or a double bond in the thiol-conjugate.

3 Method development: Chemically induced phosphonothiolate electrophiles for thiol-conjugations

Responsibility assignment
The research described in this chapter was conceptualised by Prof. Dr. Christian P. R. Hackenberger and the author and is based on previous work from the Hackenberger group and in particular from Dr. Jordi Betran-Vicente, Dr. Marc-André Kasper, Dr. Maria Glanz and Sergej Schwagerus [228, 208, 209, 244]. The author conducted the research described in this chapter with the following exceptions: The synthesis route to access unsaturated phosphonothiolates from phosphorus trichloride was developed together with Stephen Byrne. The finding that TFA inhibits the formation of the thiolate re-attack side-product was made together with Kevin Broi. Jahaziel Jahzerah assisted with the synthesis of small molecule phosphonothiolates. Molecular electrostatic potential maps were calculated by Songhwan Hwang from the group of Dr. Han Sun (FMP Berlin). LC-MS/MS measurements were performed by Dr. Michal Nadler-Holly and Heike Stephanowitz from the group of Dr. Fan Liu (FMP Berlin). MS/MS data was processed and analysed by Christian Stieger. The MMAE compound **49** used in this chapter was synthesised by Dr. Philipp Ochtrop and Dr. Marc-André Kasper. In addition, Dr. Marc-André Kasper synthesised the EDANS-phosphonamidate derivative **67** and performed the kinetic measurements with this substrate and also provided the Dabcyl-cysteine peptide used for the generation of FRET-pairs. Peter Schmieder and Nils Trieloff set up time-course ^{31}P-NMR experiments and assisted with the analysis. Ines Kretzschmar synthesised cysteine peptides. Dagmar Krause and Beate Kindt supported the author with some of the small molecule and peptide purifications by reverse-phase HPLC.
Parts of this chapter were published in and are adapted from A.L. Baumann*, S. Schwagerus*, K. Broi, K. Kemnitz-Hassanin, C. E. Stieger, N. Trieloff, P. Schmieder, C. P. R. Hackenberger. Chemically Induced Vinylphosphonothiolate Electrophiles for Thiol–Thiol Bioconjugations. *J. Am. Chem. Soc.* **2020**, *142*, 9544-9552 (* shared first authorship). In addition, parts of the technology described in this chapter are substance of a pending patent application by Alice Leonie Baumann, Marc-André Kasper, Stephen Byrne, Jonas Helma, Heinrich Leonhardt, Tina Stoschek, Marcus Gerlach, Jonas Helma, Dominik Schumacher, Christian P. R. Hackenberger. Chemoselective Thiol-Conjugation with Alkene or Alkyne-Phosphonothiolates and -Phosphonates (PCT/EP2019/055509).

3.1 Outline

Within this part of the thesis, the first goal was to investigate the reaction between electrophilic disulfides and unsaturated phosphonites to generate unsaturated phosphonothiolates (scheme 34 left). The second goal was to evaluate unsaturated phosphonothiolates as handles for the modification of proteins at cysteines (scheme 34 right).

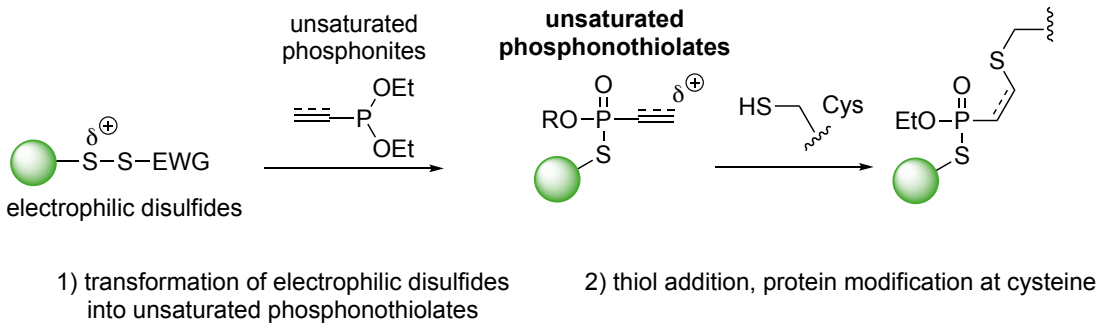

Scheme 34 Proposed synthetic route for the generation of electrophilic phosphonothiolates (left) and application of electrophilic phosphonothiolates as handles for protein modification at cysteine (right). The dashed bond in the phosphonite and the phosphonothiolate indicates either a double or a triple bond and consequently a single or a double bond in the thiol-conjugate.

3.2 Synthesis of small molecule phosphonothiolates from electrophilic disulfides

Small molecule electrophilic disulfides were synthesised as substrates to test the envisioned synthetic transformation with unsaturated phosphonites. Therefore, the thiol ethanethiol was reacted with the bis-disulfide reagents 5,5′-dithiobis-(2-nitrobenzoic acid) (Ellman's reagent) and 2,2′-dithiobis(5-nitropyridine) (DTNP) to give the respective electrophilic disulfides **1** and **2** in good yields (scheme 35). In principle, thiols can be activated to electrophilic disulfides with a number of reagents [252]. Ellman's reagent was chosen here based on our groups previous finding that Ellman's-activated cysteine residues reacted efficiently with phosphites in the synthesis of phospho-cysteine peptides (compare scheme 32) [244]. It was thus hypothesised that this type of electrophilic disulfide would be reactive also towards phosphonites. The DTNP reagent on the other hand has been used in the synthesis of a phosphorothiolate-linked diribonucleotide (compare scheme 31) [243]. Furthermore, DTNP has been described in the literature as a potent reagent to activate thiols for subsequent thiol-exchange as demonstrated for the generation of disulfide-linked antibody-drug conjugates [252].

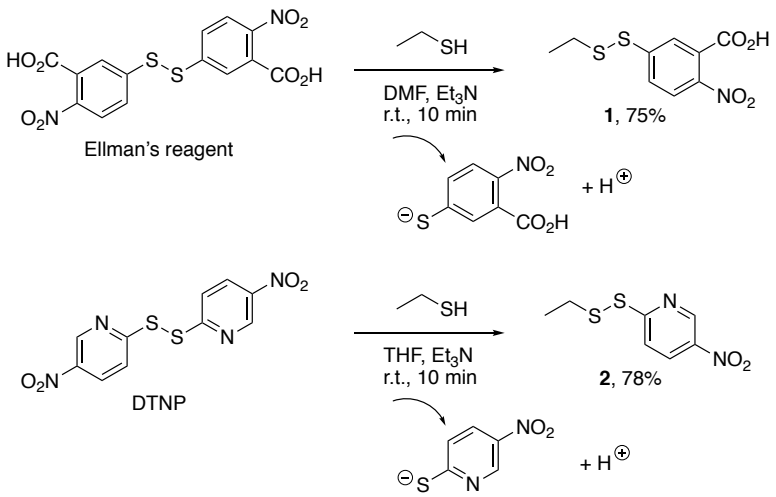

Scheme 35 Synthesis of small molecule electrophilic disulfides **1** and **2** from the reaction of ethanethiole with bis-disulfides.

As for the unsaturated phosphonite reaction partners, we commenced our investigations using the diethyl-ethynyl- and diethyl-vinylphosphonites **3** and **4**, respectively. These phosphonites can be readily synthesised from commercially available diethylchlorophosphine and ethynyl- or vinylmagnesiumbromide as previously reported by Montchamp and co-workers and our group (scheme 36) [224, 208, 209, 223, 226]. As observed before, unsaturated diethyl-phosphonites are prone to oxidize upon exposure to air and hence they must either be isolated in protected form or used freshly as crude mixtures. Here, the unsaturated diethyl-phosphonites **3** and **4** were employed as crude mixtures as it was more straight-forward to start with.

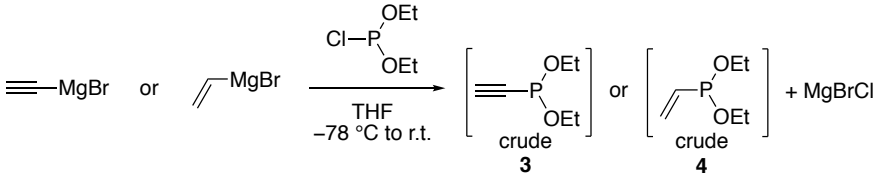

Scheme 36 Synthesis of diethyl-ethynyl- and diethyl-vinylphosphonites **3** and **4**.

Subsequently, the unsaturated crude diethyl-phosphonites **3** and **4** were employed in reactions with the above synthesised electrophilic disulfides to test whether this conversion would lead to the targeted unsaturated vinyl- and ethynylphosphonothiolates, respectively. In a first test reaction, electrophilic disulfide **1** was mixed with one equivalent of crude diethyl-ethynylphosphonite **3** in THF at room temperature (Fig. 14A). ^{31}P-NMR analysis of the reaction mixture indicated the formation of two phosphorus-containing species (at 37.2 ppm and at 36.6 ppm, Fig. 14B), which could be isolated and be assigned to the undesired addition products **5** and **6** (Fig. 14A). The desired ethynylphosphonothiolate product **7** was not observed. Notably, the product **6** was found to be esterified by an ethyl group at the carboxylic acid. This can be explained when the the carboxylate residue of the Ellman's group attacked an ethyl group in the phosphonium cation intermediate, pointing towards an Arbuzov-like mechanism (compare introduction, chapter 1.4.2).

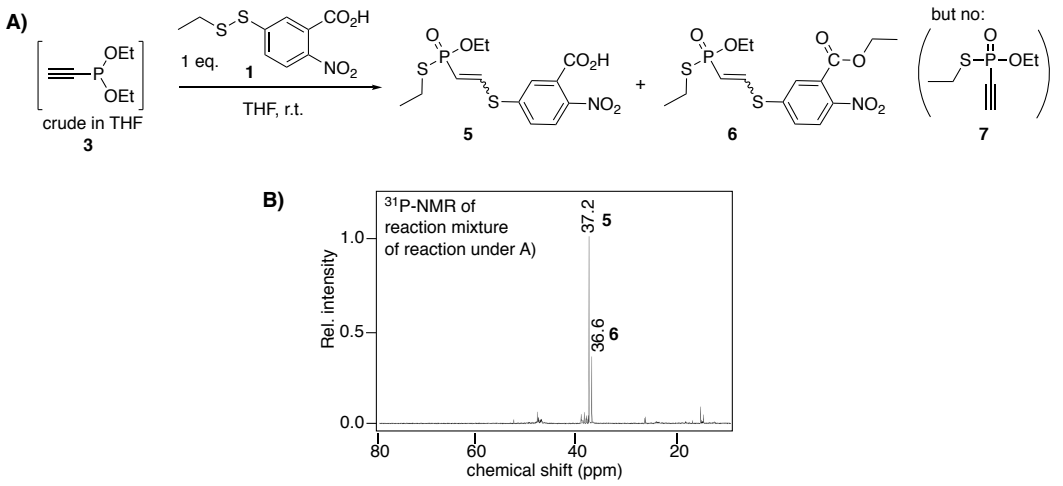

Fig. 14 A) Reaction between ethynylphosphonite **3** and electrophilic disulfide **1** did not give the desired product **7** but the re-attack products **5** and **6** instead. B) ^{31}P-NMR spectra of the reaction mixture in THF.

The formation of **5** and **6** indicated that the targeted ethynylphosphonothiolate **7** had been formed intermediately but reacted *in situ* with the thiolate group originating from the reaction of **3** with electrophilic disulfide **1** as depicted in scheme 37. This side reaction is hereafter referred to as *re-attack*.

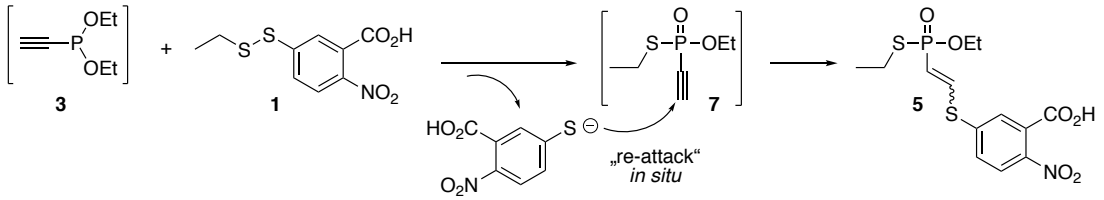

Scheme 37 Re-attack of the thiolate leaving group to ethynylphosphonothiolate **7** *in situ*.

It was furthermore noticed that the reaction between phosphonite **3** and disulfide **1** proceeded very quickly, as the phosphonite was fully converted to the products **5** and **6** when checked by ^{31}P-NMR after a few minutes (Fig. 14B). Any attempts to inhibit the undesired re-attack reaction by the addition of thiol-scavengers to the reaction mixture (such as maleimides or iodoacetamide) were not successful. From these first observations, it could be deduced that unsaturated phosphonites indeed react with electrophilic disulfides to form phosphonothiolates as hypothesised. Moreover, the re-attack phenomenon pointed towards high reactivity of unsaturated phosphonothiolates with thiolates. Since thiolate re-attack in the reaction with electrophilic disulfide **1** and ethynylphosphonite **3** could not be suppressed by adding thiol scavengers, the disulfide-phosphonite reaction was next investigated with vinylphosphonite **4** instead. Our group has recently reported that thiol additions to vinylphosphonamidates are significantly slower compared to ethynylphosphonamidate derivatives (see introduction, chapter 1.4.1) [209]. Hence, it was hypothesised that this reactivity trend might also translate to the respective phosphonothiolate derivatives and that less re-attack for the reaction between electrophilic disulfide **1** and vinylphosphonite **4** would be obtained consequently (Fig. 15A). Indeed, for this reaction, the desired vinylphosphonothiolate product **8** was found next to the re-attack product **9** in a ratio of approximately 1:1.4 based on ^{31}P-NMR signal intensities (Fig. 15B).

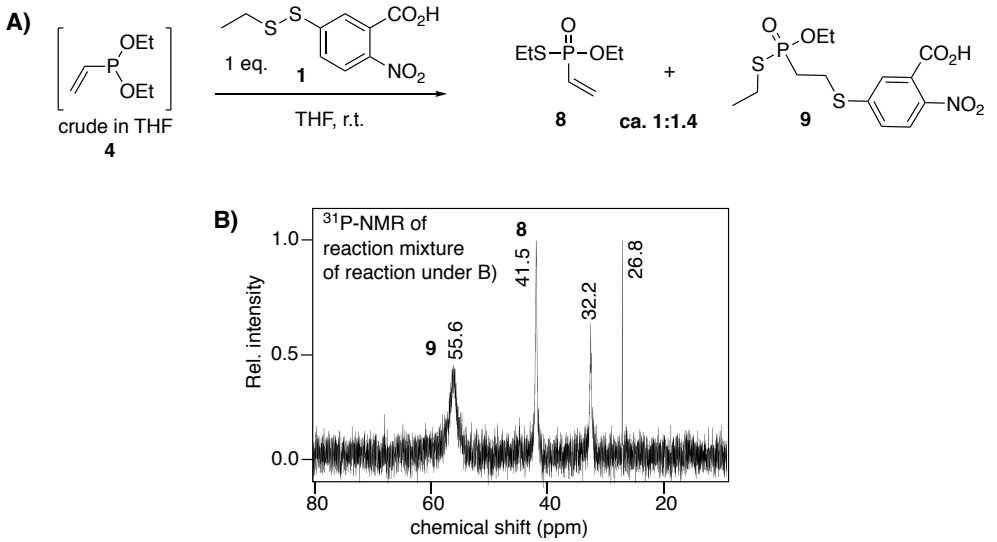

Fig. 15 A) Reacting vinylphosphonite **4** with electrophilic disulfide **1** gave a mixture of the desired product **8** and re-attack product **9**. B) ^{31}P-NMR spectrum of the reaction mixture in THF. The signal at 32.2 ppm corresponds to triphenylphosphinoxide, which was used as internal standard in this experiment. The signal at 26.8 ppm might be vinylphosphonic acid (compare Fig. 17) but this was not confirmed here.

Continuing with the vinylphosphonite **4**, even lesser re-attack occurred when the DTNP-activated electrophilic disulfide **2** was used (Fig. 16A). With this substrate, the ratio between vinylphosphonothiolate **8** to re-attack product **10** was approximately 3:1 based on ^{31}P-NMR analysis of the reaction mixture (Fig. 16B).

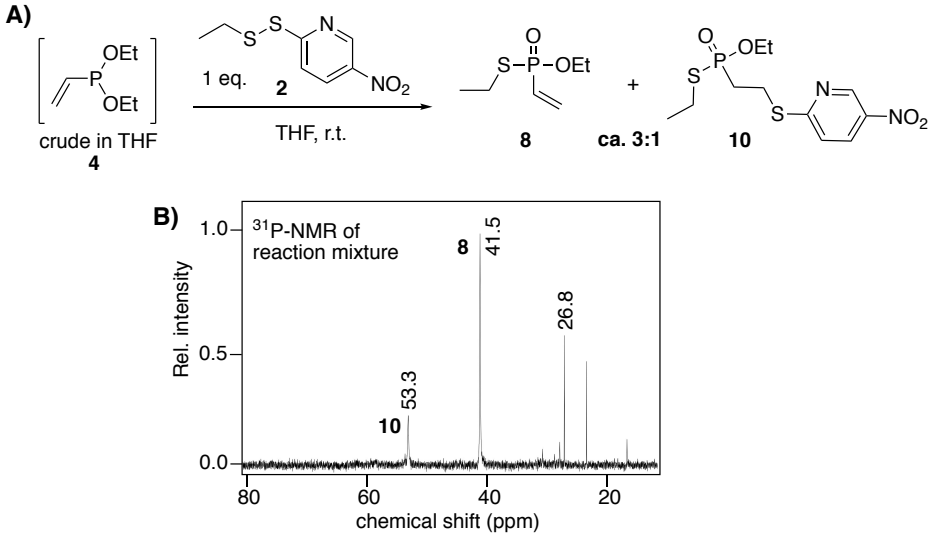

Fig. 16 Compared to substrate **1**, less re-attack side-product is formed *in situ* for the substrate **2** as judged from ^{31}P-NMR analysis of the crude reaction mixture. The signal at 26.8 ppm might be vinylphosphonic acid (compare Fig. 17) but this was not confirmed here.

The circumstance that less re-attack product formed in the reaction with DTNP-activated disulfide **2** compared to Ellman's activated disulfide **1** might be explained by the different nucleophilicities of the respective leaving groups 5-nitropyridine-2-thiolate versus 3-carboxy-4-nitrobenzenethiolate. The more electron-withdrawing the aryl

substituents are, the better stabilised is the thione form (S=C-R), which is less nucleophilic. Along these lines, it will be interesting to test even less nucleophilic leaving groups in future optimisations. One could for instance use *N*-methylated pyridine derivatives or alternatively, incorporate a second electron-withdrawing nitro-group into the disulfide activator.

Keeping in mind that THF would not be a suitable solvent when applying the disulfide-phosphonite reaction on peptide substrates, more polar solvents were considered for the further optimisation of the reaction conditions. The ideal solvent for the installation of phosphonothiolates on biomolecules would be water or an appropriate aqueous buffer. However, when reacting electrophilic disulfide **2** and vinylphosphonite **4** under aqueous conditions (DMSO/H_2O= 3:1[3]), no desired vinylphosphonothiolate **8** was observed (Fig. 17A). Instead, species at 27.3 and 18.2 ppm were detected in the ^{31}P-NMR of the reaction mixture (Fig. 17C). Although these phosphorus-containing species were not isolated here, it was hypothesised that they are vinylphosphonate **11** and vinylphosphinate **12**, respectively (Fig. 17A). As for the vinylphosphonate **11** this assumption is based on comparison to a commercial sample of this exact compound, which showed the same chemical shift under these conditions (see Appendix Fig. 143). Vinylphosphinate **12** on the other hand has been characterised by Montchamp and co-workers [253]. Although measured in a different solvent ($CDCl_3$), the ^{31}P-NMR shift they report (25.1 ppm) is close to the one observed here (27.3 ppm). Furthermore, when crude vinylphosphonite **4** alone was subjected to the same conditions (DMSO/H_2O= 3:1), the species at 27.3 ppm was observed almost exclusively (Fig. 18).

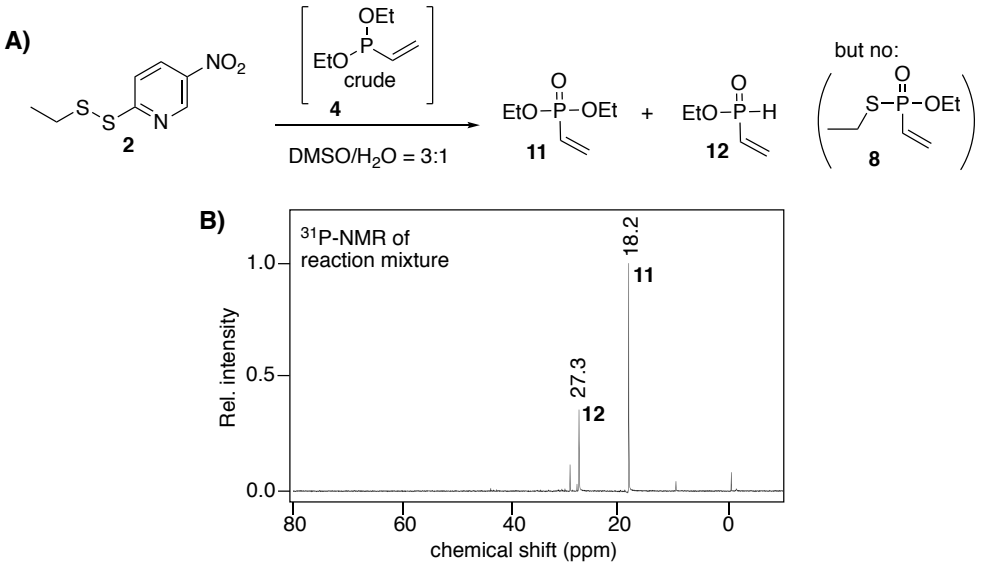

Fig. 17 A) Under aqueous conditions, the reaction between electrophilic disulfide **2** and diethyl-vinylphosphonite **4** did not yield vinylphosphonothiolate **8** but vinylphosphonate **11** and vinylphosphinate **12** instead. B) ^{31}P-NMR of the reaction mixture in DMSO/H_2O= 3:1.

[3] 75% of DMSO was necessary for solubilising both reagents.

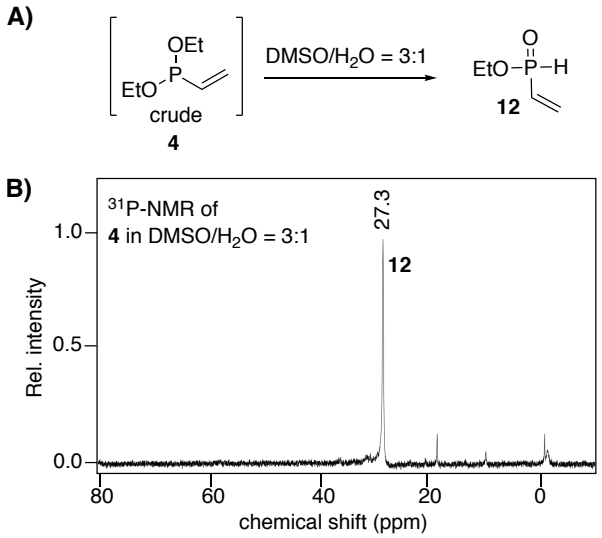

Fig. 18 When subjecting crude vinylphosphonite **4** to a mixture of DMSO/H_2O= 3:1, the main observed species is presumably vinylphosphinate **12**.

In order to shed light on the side-reactions occurring under aqueous conditions, the reaction between disulfide **4** and vinylphosphonite **2** was repeated in DMSO supplemented with one equivalent of ^{18}O-labelled water (scheme 38). Analysis of the reaction product by ^{31}P-NMR and MS clearly indicated the formation of phosphonate **11** along with its re-attack product (see Experimental Fig. 68 and Fig. 70). Thereby, a mixture of ^{16}O- and ^{18}O-labelled phosphonate (in similar intensities) was observed. Vinylphosphonothiolate and its re-attack product were also observed in about the same amount, however, containing exclusively the normal ^{16}O-isotope in their P=O bond. These findings can be rationalised by having a closer look at the Arbuzov-type mechanism (introduced in chapter 1.4.2) the phosphonite-disulfide likely follows (scheme 38A). First, vinylphosphonite **4** attacks the disulfide **2** at its more electrophilic sulphur, liberating thereby 5-nitropyridine-2-thiolate. The formed phosphonium intermediate can then undergo different transformations. In the desired case, the vinylphosphonothiolate is formed, mediated by a nucleophile attacking the methylene group of one of the *O*-ethyl groups (scheme 38A). Possible nucleophiles that drive the formation of the vinylphosphonothiolate **8** are the thiolate leaving group[4] or halide ions originating from the phosphonite synthesis (Fig. 38A). In a different scenario, the cationic phosphorus in the phosphonium intermediate gets attacked by nucleophiles such as water. When this happens, the thiolate residue is liberated preferentially over the alkoxide as it is less basic (Fig. 38B) [254]. This explains why diethyl-vinylphosphonate was formed in the presence of water (scheme 38, Fig. 17). As mentioned above, in the reaction between disulfide **2** and phosphonite **4**, both ^{16}O- and ^{18}O-labelled phosphonates were observed. A simple explanation can be that the reaction mixture was contaminated with H_2O^{16}.

[4]The ethyl sulfide of the leaving group could be isolated from the reaction mixture (see Experimental, chapter 8.2.3 for its characterisation).

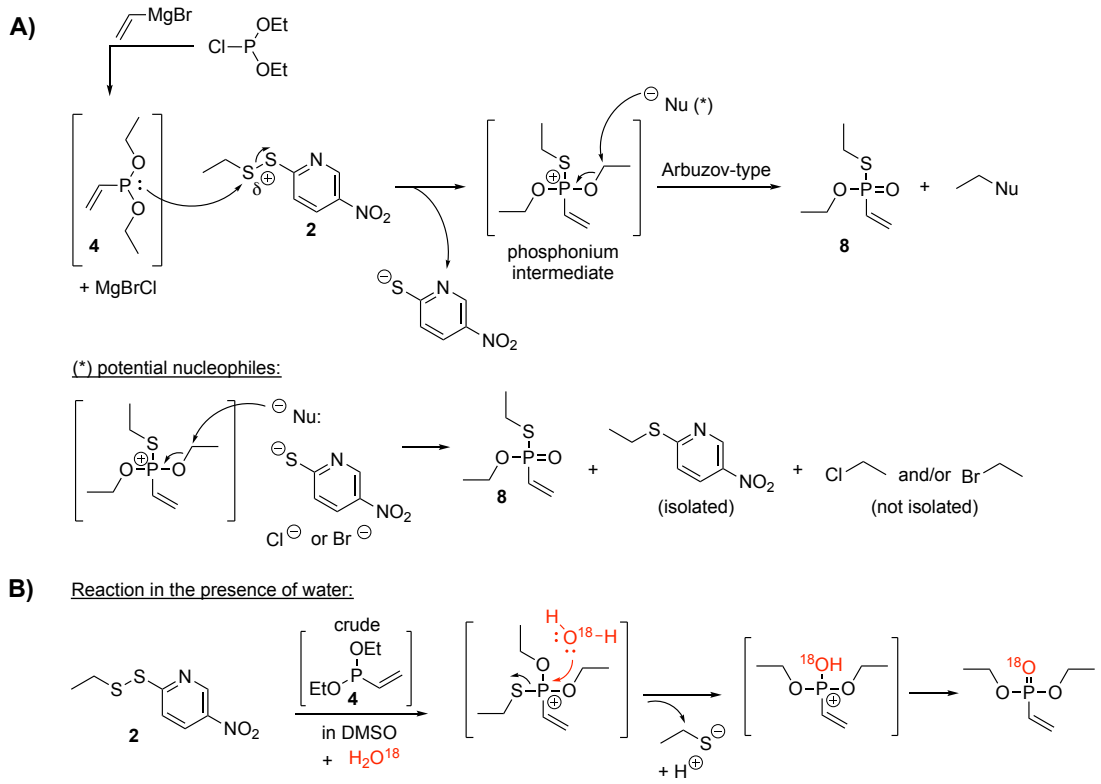

Scheme 38 A) Mechanistic proposal for the disulfide-phosphonite reaction. B) Hydrolysis of the phosphonium intermediate results in release of the thiol residue and the formation of a phosphonate.

The finding that the reaction between electrophilic disulfides and unsaturated phosphonite **4** is not compatible with aqueous conditions, narrowed down the possibilities for appropriate, polar solvents. Further optimisation studies were continued in dry dimethylsulfoxide (see below). Nevertheless, in the future one could try to optimise the reaction for aqueous conditions by using more electron-withdrawing *O*-substituents in the phosphonite. Perhaps, this way at least a partial competition between thiolate versus alkoxide leaving group would be achieved. However, by employing a phosphonite with electron-withdrawing *O*-substituents, also the initial attack to the disulfide would be expected to be slower, owing to the less nucleophilic phosphorus in this case. Another consequence of using an electron-withdrawing *O*-substituent (e.g. trifluoroethyl) could be decreased stability of the phosphonothiolate product. As a P-O(trifluoroethyl) bond would be more polarised than the P-O(ethyl) bond, hydrolysis through nucleophilic attack of water to the phosphorus in the phosphonothiolate could be enhanced in such a system (compare chapter 3.7). A different way to decrease undesired hydrolysis of the phosphonium intermediate could be to incorporate a nucleophile into the phosphonite side chain, thereby promoting intramolecular rearrangement of the phosphonium intermediate to the phosphonothiolate.

As mentioned above, further optimisations using the diethyl-vinylphosphonite **4** were carried out in dry DMSO (Fig. 19). In this case, the desired vinylphosphonothiolate **8** and the re-attack product **10** were observed in a ratio of approximately 1:1 based on ^{31}P-NMR signal intensities (Fig. 19B). For comparison, the same reaction in THF gave a better ratio of phosphonothiolate to re-attack product (ca. 3:1, see Fig. 16). A likely explanation of this difference is the better solubility of the thiolate leaving group in the

more polar solvent DMSO. In fact, for the reaction in THF, an orange precipitate was observed, indicating partial insolubility of the leaving group, which can explain why it re-attacked the vinylphosphonothiolate to a lesser extent. As can be seen in the ^{31}P-NMR spectrum in Fig. 19B, next to the phosphonothiolate and its re-attack product, also a shift likely corresponding to vinylphosphonate **11** was observed. The formation of this by-product can be explained by the mechanism discussed above as a consequence of contamination with water. Notably, when subjecting the vinylphosphonite **4** alone to DMSO, no significant oxidation was observed within about one hour (data not shown here).

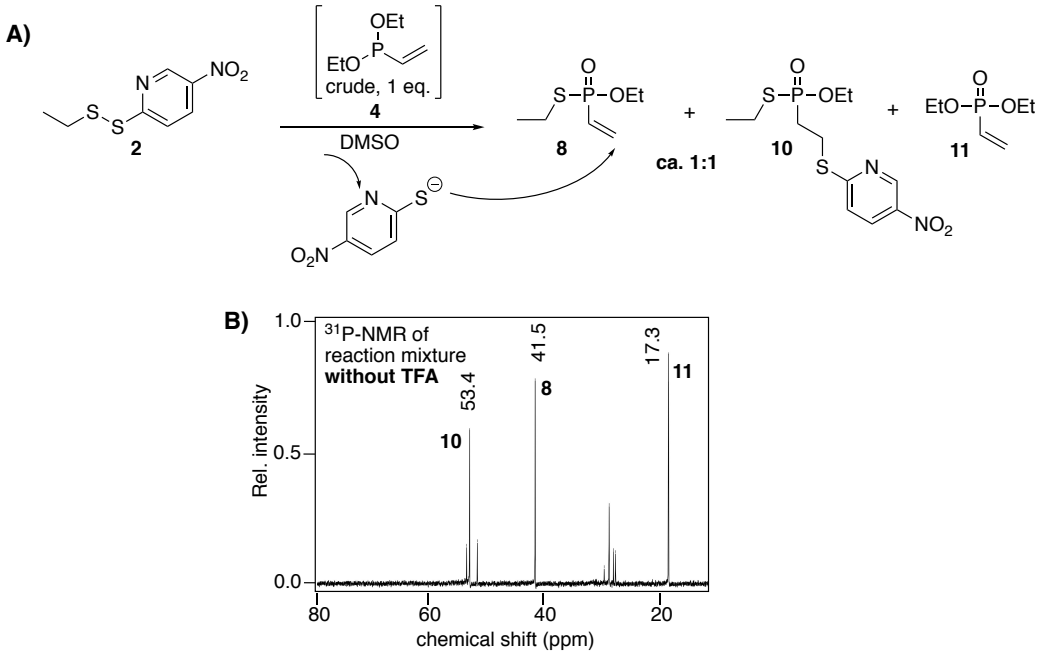

Fig. 19 A) The reaction between electrophilic disulfide **2** and phosphonite **4** in DMSO results in a mixture of the desired vinylphopshonothiolate **8** and re-attack by-product **10** in a ratio of ca. 1:1. B) ^{31}P-NMR spectrum of the reaction mixture in THF. The phosphorus-containing species, which are not labelled with numbers could not be identified.

Eventually, it was found that re-attack of the thiolate leaving group to the unsaturated phosphonothiolate **8** could be suppressed when the reaction mixture was supplemented with trifluoroacetic acid (TFA) (Fig. 20). Presumably, under acidic conditions, the thiolate leaving group gets protonated and is hence no longer a good nucleophile. Complete inhibition of re-attack could be achieved in the presence of ten equivalents of TFA. Under these conditions, the desired vinylphosphonothiolate **8** was observed as the main product by ^{31}P-NMR (Fig. 20B). Next to traces of vinylphosphonate **11**, another minor side-product, characterised by two douplet peaks at around 44 and 55 ppm was observed. It was hypothesised that these signals can be assigned to the structure **13** (Fig. 20A)[5].

[5]Although this product was not isolated here, the assumption that it is in fact compound **13** is reasonable given than an analogous side-product was observed on peptide level (see scheme 43), where it has been isolated and characterised (see Experimental scheme 58 and Appendix Fig. 167 & Fig. 168).

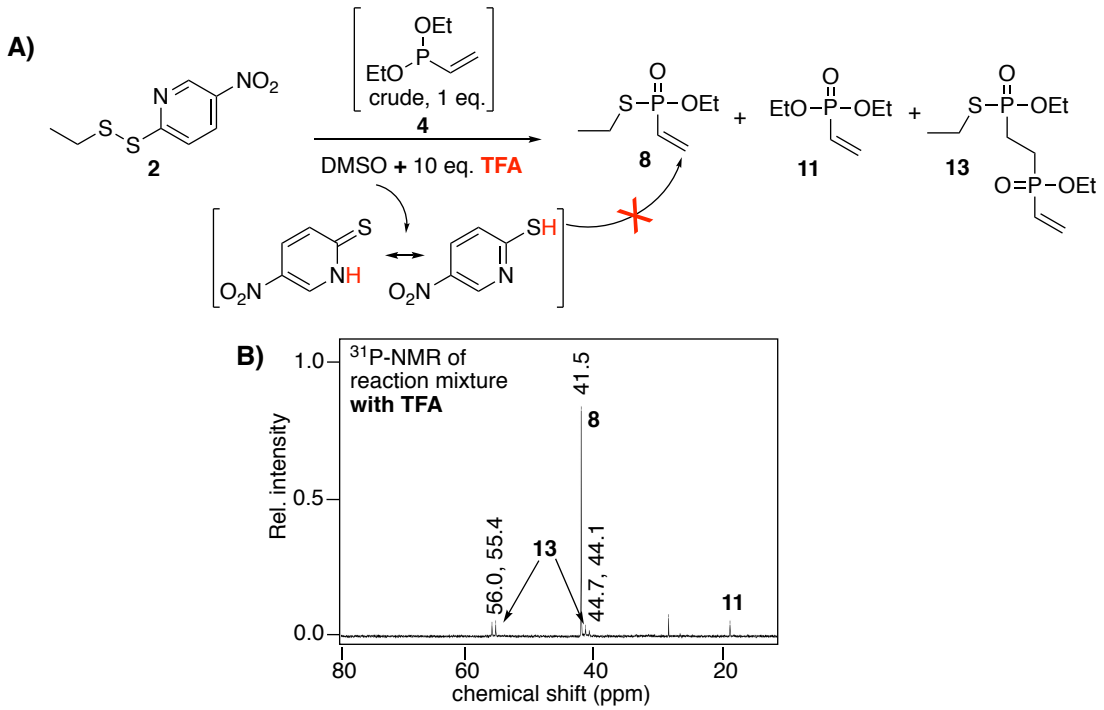

Fig. 20 A) In the presence of TFA, the re-attack reaction is fully suppressed. B) ^{31}P-NMR spectrum of the reaction mixture.

As depicted in scheme 39, the side-product **13** presumably forms when vinylphosphonite attacks the formed vinylphosphonothiolate **8** at its electrophilic vinyl-bond. The resulting phosphonium intermediate can then get attacked by a nucleophile (such as the thiolate leaving group as discussed above), giving rise to phosphonothiolate-phosphonate **13**.

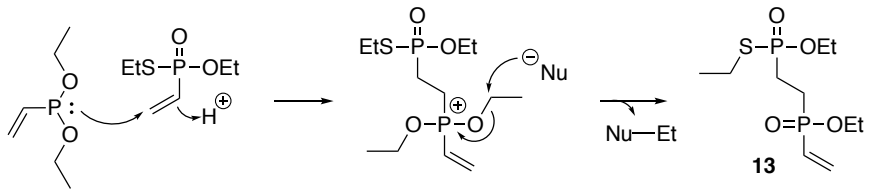

Scheme 39 Mechanistic proposal for the formation of side-product **13**.

It was further found that a slight excess (1.5-2 equivalents) of vinylphosphonite was needed to obtain full conversion of the electrophilic disulfide **2** in DMSO containing 10 eq. TFA. The reason for this is that diethyl-vinylphosphonite **4** oxidises to diethyl-vinylphosphonate **11** under these conditions. In fact, when subjecting crude vinylphosphonite **4** alone to DMSO/TFA, quick oxidation to vinylphosphonate was observed by ^{31}P-NMR analysis. Consequently, the order of mixing the reagents was important. Vinylphosphonite **4** had to be added to the disulfide dissolved in DMSO/TFA and not vice versa to minimise oxidation of the phosphonite.

Using the optimised conditions (two equivalents of phosphonite in DMSO supplemented with ten equivalents TFA), full conversion of **2** was obtained (judged by TLC) and the desired vinylphosphonothiolate **8** could be isolated in 80 % yield (scheme 40).

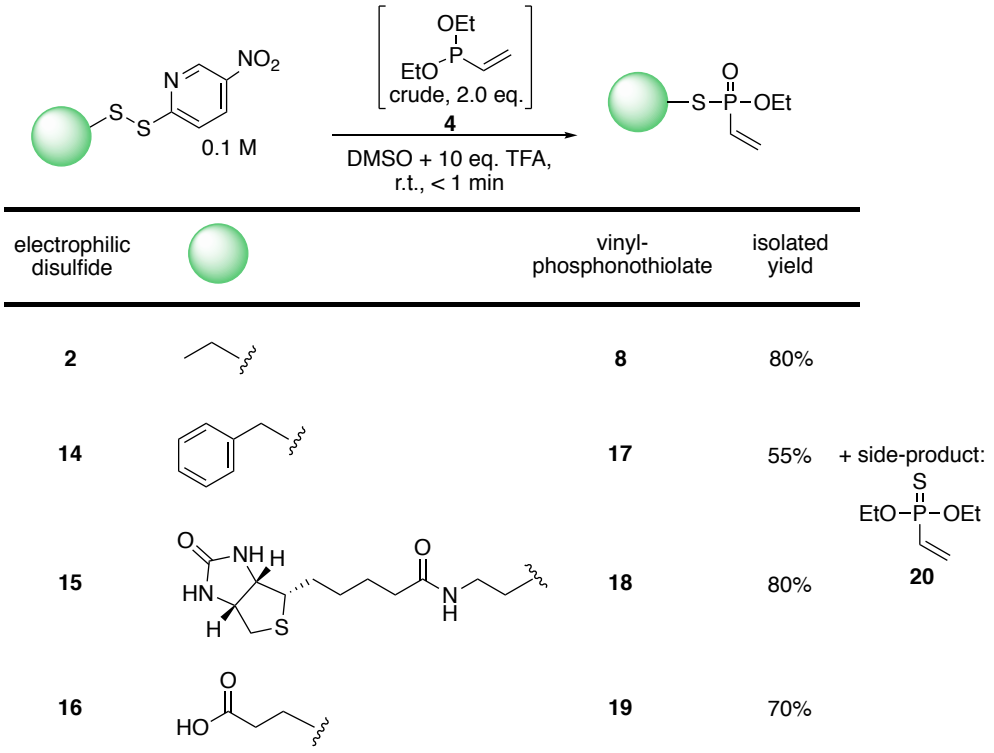

Scheme 40 Synthesis of small molecule vinylphosphonothiolates under optimized reaction conditions.

Next, the phosphonite-disulfide reaction was tested on a few other derivatives. Therefore, benzylmercaptan, a biotinthiol derivative and mercaptopropionic acid were first activated with DTNP to the corresponding electrophilic disulfides **14-16**. These were then subjected to the reaction with crude vinylphosphonite **4** under the optimised conditions with DMSO/TFA. For all substrates, the targeted vinylphosphonothiolates **17-19** could be isolated in good yields. While the yields for the derivatives **18** and **19** were comparable to the ethylderivative **8** (80% and 70%, respectively), the benzyl-derivative **17** was obtained only in 55% yield. For the latter substrate, the phosphonothioate side-product **20** was observed in the reaction mixture. Based on the mechanism discussed above, the formation of this side product can be explained looking at the corresponding phosphonium intermediate (scheme 41). In this case, the electrophilic, benzylic position of the thiol residue competes for nucleophilic attack with the methylene group of the *O*-ethyl substituent, giving rise to a mixture of **20** and **17**.

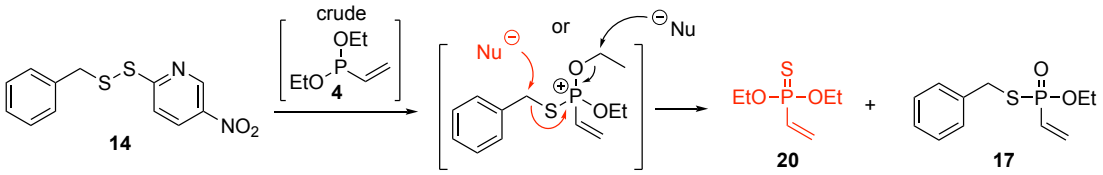

Scheme 41 Mechanistic explanation for the formation of phosphonothioate side-product **20**.

The optimised protocol for the disulfide-phosphonite reaction was also successfully applied for the synthesis of ethynylphosphonothiolate **7** from ethynylphosphonite **3** and electrophilic disulfide **2** (scheme 42). Here, no re-attack product was observed and the desired ethynylphosphonothiolate could be isolated in 58% yield. This result is in sharp

contrast to the reaction between ethynylphosphonite **3** and disulfide **1**, where exclusive formation of re-attack products was observed (compare Fig. 14). The finding that TFA inhibits re-attack *in situ* was thus very important to enable the isolation of the reactive ethynylphosphonothiolate.

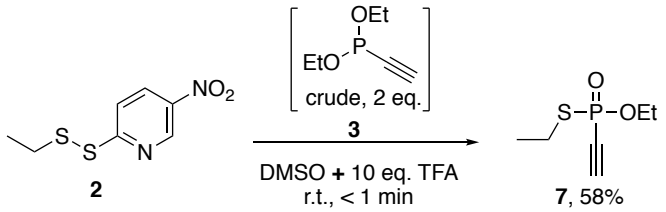

Scheme 42 Synthesis of ethynylphosphonothiolate **7** from electrophilic disulfide **2** and ethynylphosphonite **3** using the optimised protocol. Running the reaction under acidic conditions was key to suppress re-attack.

Taken together, the results described in this chapter demonstrate that unsaturated phosphonothiolates can be synthesised from electrophilic disulfides in an efficient manner by suppressing the formation of re-attack by-products under acidic conditions.

3.3 Synthesis of peptide phosphonothiolates

Based on the promising results with small molecule vinylphosphonothiolates, we next set out to install vinylphosphonothiolates on unprotected peptides to test whether the disulfide-phosphonite reaction was chemoselective in the presence of other functional groups (scheme 43). Therefore a set of DTNP- activated disulfide model peptides **23-27** with the general sequence KYRCXK were used, whereby X stands for one of the amino acids alanine (A), serine (S), histidine (H), aspartic acid (D) or methionine (M). Together with lysine (K), arginine (R) and tyrosine (Y), the potentially interfering functional groups of natural amino acids were thereby covered. As for the small molecule substrates, the peptides **23-27** reacted quickly with vinylphosphonite **4** in DMSO/TFA to yield the desired vinylphosphonothiolates **28-32** in 29-41% after reverse-phase HPLC purification. No reaction with any of the other amino acids was observed, which demonstrated the excellent chemoselectivity of this transformation on unprotected peptides. The purified peptides were analysed by ^{31}P-NMR, whereby a 1:1 mixture of two diastereoisomers was observed as a consequence of the racemic phosphonothiolate (Appendix, e.g. Fig. 161). The two main side products in this transformation were reduced cysteine peptides (10-14%) and phosphonite addition products (5-8%).

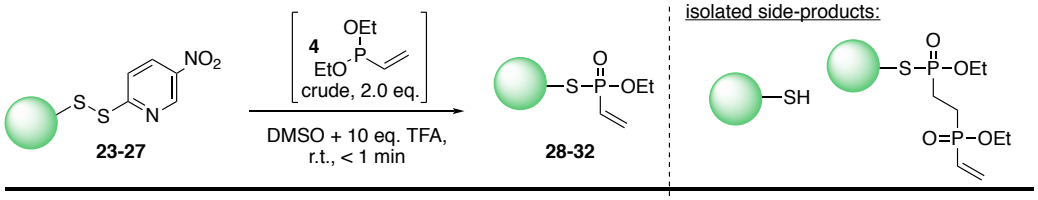

electrophilic disulfide		vinyl-phosphonothiolate peptides	product isolated yield	reduced Cys-peptides isolated yield	phosphonite-addition product isolated yield
23	H_2N–KYRC**A**K–NH_2	**28**	41%	10%	5%
24	H_2N–KYRC**S**K–NH_2	**29**	33%	14%	7%
25	H_2N–KYRC**H**K–NH_2	**30**	32%	13%	7%
26	H_2N–KYRC**D**K–NH_2	**31**	29%	13%	8%
27	H_2N–KYRC**M**K–NH_2	**32**	35%	14%	5%

Scheme 43 Installation of vinylphosphonothiolate on cysteine-activated peptides. The indicated yields are isolated yields after reverse-phase HPLC purification.

3.4 Synthesis of small molecule phosphonothiolates from phosphorus trichloride

Next to the chemoselective disulfide-route described above, an alternative route for the synthesis of vinyl- and ethynylphosphonothiolates was developed starting from phosphorus trichloride (PCl_3) as depicted in scheme 44. Thereby, PCl_3 was first converted in a three-step one-pot reaction to the vinyl- or ethynyl-intermediates **33** or **34** (protocol adapted from Ref. [255]). Subsequent tetrazole-mediated substitution of the diisopropyl-amine residue with thiols and oxidation with *t*-BuOOH delivered unsaturated phosphonothiolates (protocol adapted from Ref. [256]). This route was followed for the synthesis of benzylderivatives **35** and **17** as well as for the synthesis of Boc-protected amine derivatives **36** and **37**.
This route is longer compared to the above discussed disulfide route. Here, starting from PCl_3, five steps are needed to obtain phosphonothiolates, whereas the disulfide route contains only 2 steps (disulfide activation and treatment with phosphonite). Also the overall yields are lower. Here, the overall yield of vinylphosphonothiolate **17** (starting from PCl_3) is 13%, whereas it was 44% for the same compound via the disulfide route (starting from benzylmercaptan). Moreover, the PCl_3 route can not be used to install unsaturated phosphonothiolate chemoselectively on biomolecules. Nevertheless, synthesising unsaturated phosphonothiolates via this route provides an alternative solution to avoid re-attack (compare previous chapter).

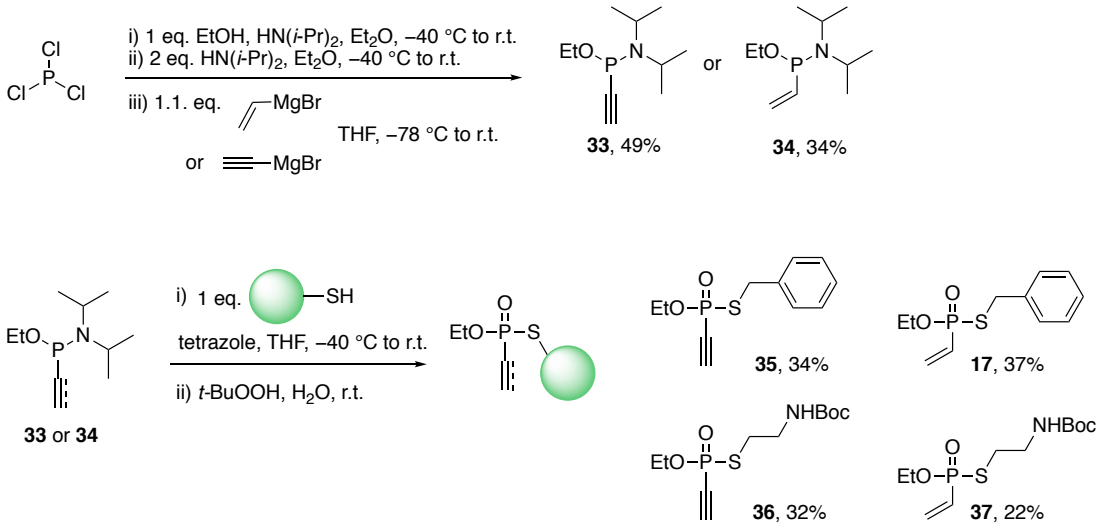

Scheme 44 Synthesis of unsaturated phosphonothiolates from PCl_3.

3.5 Functionalisation of general building blocks

Carboxylic acid and amine phosphonothiolate derivatives could be further derivatised by means of amide couplings (scheme 45). Carboxylic acid derivative **19** was for instance activated to electrophilic NHS-ester **38** and subsequently coupled to EDANS, yielding the fluorescent vinylphosphonothiolate derivative **39** (scheme 45A). The Boc-protected amine-derivatives **36** and **37** were deprotected with TFA and then coupled to EDANS-derivative **42**, biotin or succinic acid to give derivatives **43-48** (scheme 45B). The phosphonothiolate derivatives **50** and **51** carrying cytotoxins were synthesised from **47** and **48** (scheme 45C). These derivatives were later used for the generation of antibody-drug conjugates (see chapter 5). Photoreactive derivatives **54** and **55** (used in chapter 6.4) were obtained from amine precursor **41** (scheme 45D).

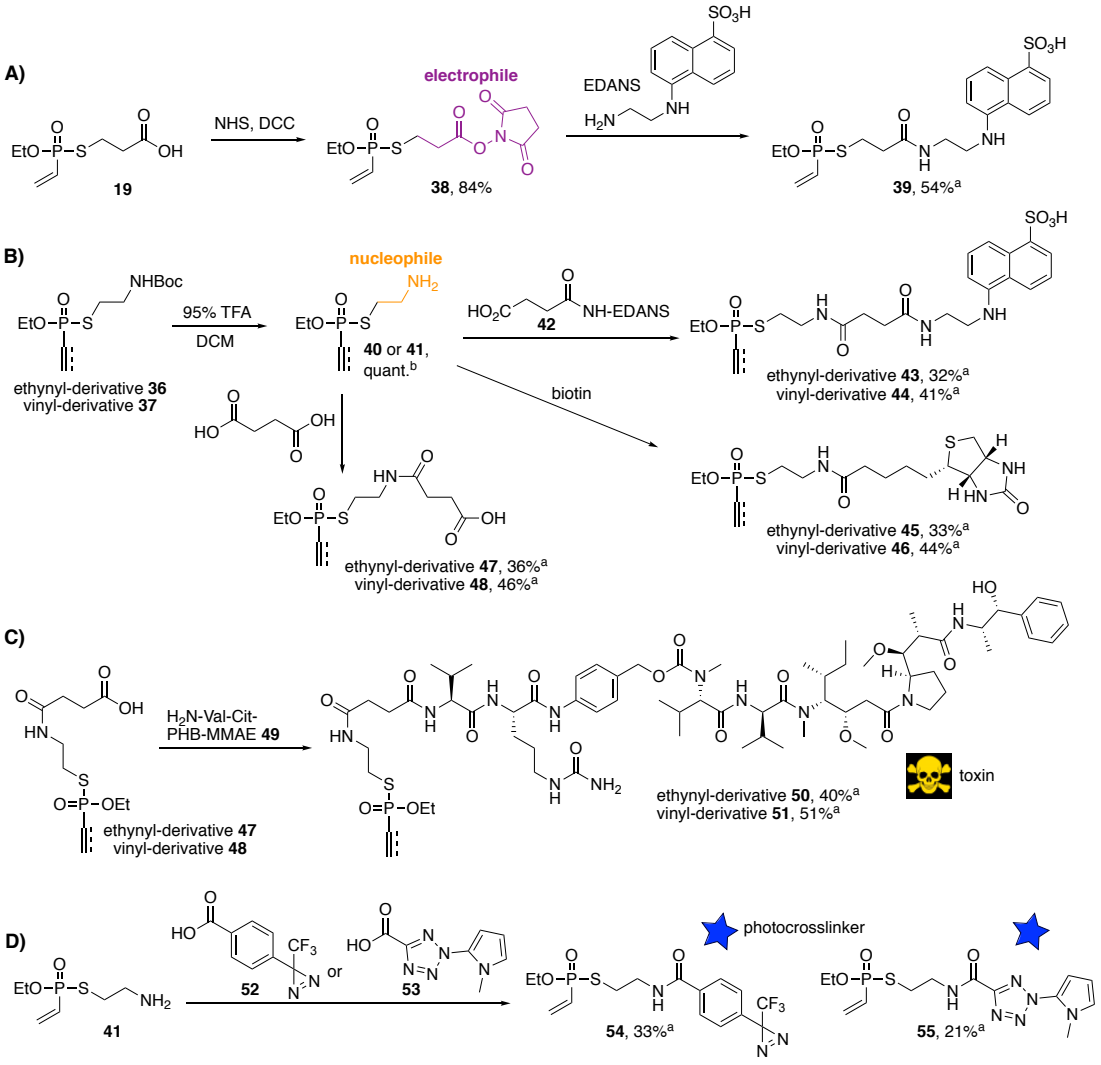

Scheme 45 Derivatisation of amine and carboxylic acid phosphonothiolates through amide couplings. HATU was used as coupling agent in amide couplings. [a]Isolated yields after reverse-phase HPLC-purification. [b]Used as crude product without further purification.

3.6 Thiol additions to unsaturated phosphonothiolates

Having successfully synthesised vinyl- and ethynylphosphonothiolates, the next aim was to investigate the reactivity of these compounds in thiol additions. In a first proof-of-concept experiment, the *S*-benzyl vinylphosphonothiolate derivative **17** was mixed with reduced glutathione in aqueous buffer at pH 8.5 and the reaction was followed by UV-LC-MS (Fig. 21). To our delight, clean conversion was observed and the thiol-conjugate product **56** could be obtained in 77% yield after reverse-phase HPLC purification.

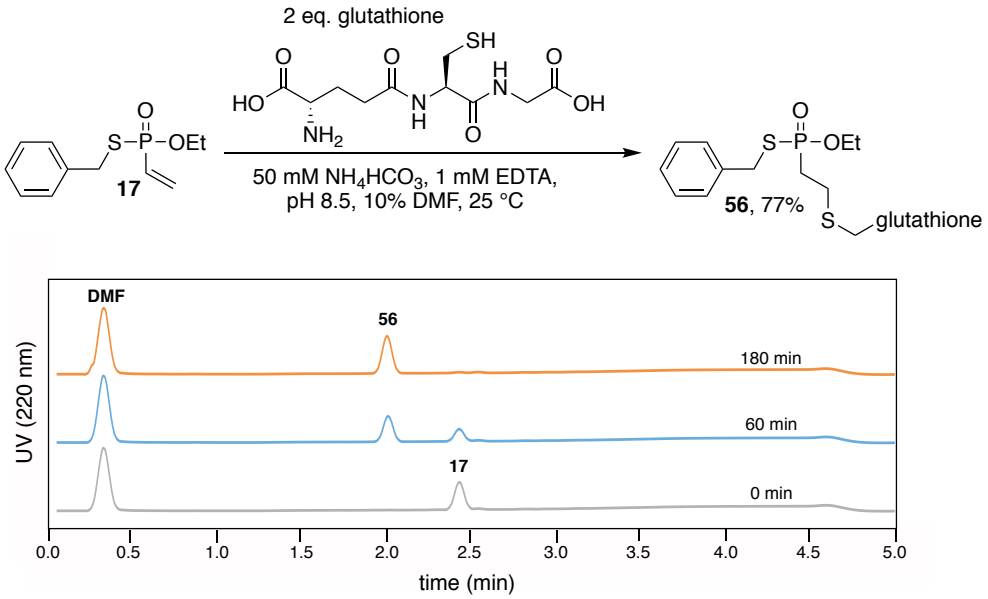

Fig. 21 Glutathione (GSH) addition to **17** (10 mM) gave thiol-conjugate **56**. The reaction was monitored by LC-UV (220 nm).

Similarily, glutathione addition to ethynylphosphonothiolate **7** gave the conjugate **57** (scheme 46). The thiol addition thereby gave the *Z*-double bond isomer preferentially (E/Z=1:10), which is in line with previous observations made by our group and others for the thiol addition to electron-deficient alkynes [208, 227].

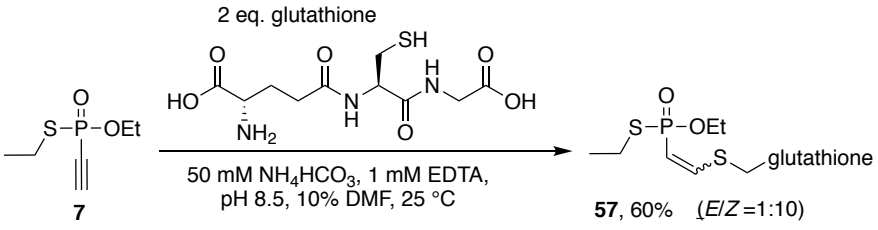

Scheme 46 Glutathione addition to ethynylphosphonothiolate derivative **7**.

Next, bimolecular rate constants for the thiol addition to vinyl- and ethynylphosphonothiolates were determined from equimolecular reactions between reduced glutathione and water-soluble, fluorescent EDANS-derivatives **39** and **43**, respectively (Fig. 22A). Thereby it was found that glutathione addition to vinylphosphonothiolate derivative **39** proceeds with a bimolecular rate constant of $0.0020\,M^{-1}s^{-1}$ in PBS at pH 7.4 (Fig. 22B). At pH 8.5, the thiol addition to **39** is roughly an order of magnitude faster with a bimolecular rate constant of $0.074\,M^{-1}s^{-1}$. This finding can be explained by the fact that with increasing pH, there is more glutathione present in the reactive, deprotonated thiolate form. The thiol addition to ethynyl-derivative **43** on the other hand proceeded approximately 600 times faster compared to the vinyl derivative **39** with a bimolecular rate constant of $1.32\,M^{-1}s^{-1}$ at pH 7.4. This result coincides with the observation that more re-attack product was created in the synthesis of ethynylphosphonothiolates as compared to vinylphosphonothiolates under neutral conditions. The higher reactivity of ethynyl- over vinylphosphonothiolates is further in line with previous work from our group on unsaturated phosphonamidates, where the same reactivity trend was observed for vinyl- versus ethynylphosphonamidates [208, 209]. The higher reactivity/-electrophilicity of ethynylphosphonothiolates could also be visualised by electrostatic potential maps (Fig. 22C). Therein, the ethynylphosphonothiolate **7** shows lower electron density at the terminal carbon (more on the blue end of the scale) compared to the vinyl derivative **8**, which is an indication for higher electrophilicity of the ethynyl-residue over the vinyl-residue.

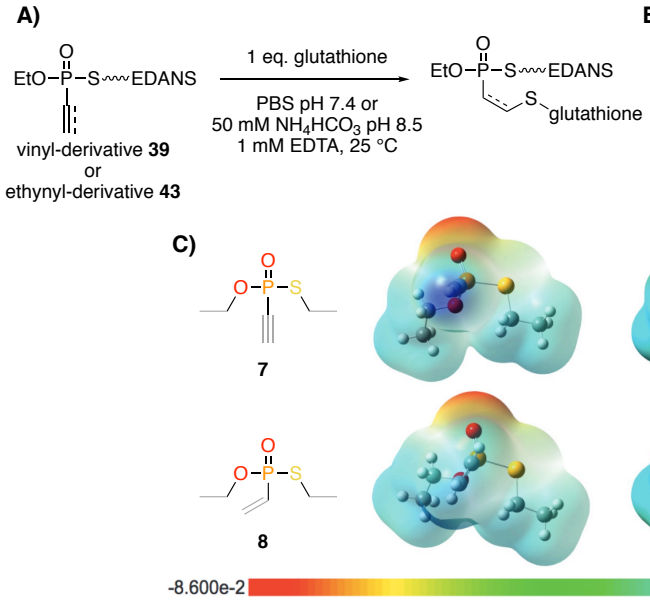

Fig. 22 A/B) Bimolecular rate constants for the thiol addition to unsaturated phosphonothiolates **39** and **43**. C) Electrostatic potential maps. The atoms in the structures **7** and **8** are colour-coded with respect to the transparent maps on the left. The black wedges point at the most positive values of the terminal carbons of the triple and the double bond, respectively.

Next, the cysteine-selectivity of the thiol addition to vinyl- and ethynylphosphonothiolates was investigated on protein level using the monoclonal IgG antibodies Cetuximab and Trastuzumab. IgG antibodies are large globular proteins with a molecular weight of about 150 kDa consisting of two identical light and heavy chains (LC, HC), which are covalently connected via interchain disulfide bridges. These interchain disulfides can be reduced under mild conditions with DTT or TCEP [228, 257, 258], thereby setting free eight sulfhydril groups for labelling with unsaturated phosphonothiolates. In non-DTT-treated controls, no modification was expected as IgG antibodies typically do not contain additional unpaired cysteines. First, to compare the cysteine-selectivity of vinyl- versus ethynylphosphonothiolates, an excess (50 eq.) of the respective biotin derivatives **45** and **46** were allowed to react with DTT-reduced antibody Cetuximab in buffer at pH 8.5 for 16 hours (Fig. 23A). Subsequent Western-blot analysis revealed labelling of the heavy and the light chains for both biotin-phosphonothiolate derivatives (Fig. 23B). A higher degree of modification was observed for the more reactive ethynyl-derivative **45** compared to the vinyl-derivative **46**. Importantly, in the negative controls (-DTT), no labelling was observed for vinylphosphonothiolate **46**, indicating excellent cysteine-selectivity of this derivative. In contrast, with ethynylphosphonothiolate **45**, some labelling was also observed in the negative control, pointing towards unselective modification. Lowering the pH improved the cysteine-selectivity for derivative **45** (Fig. 23C).

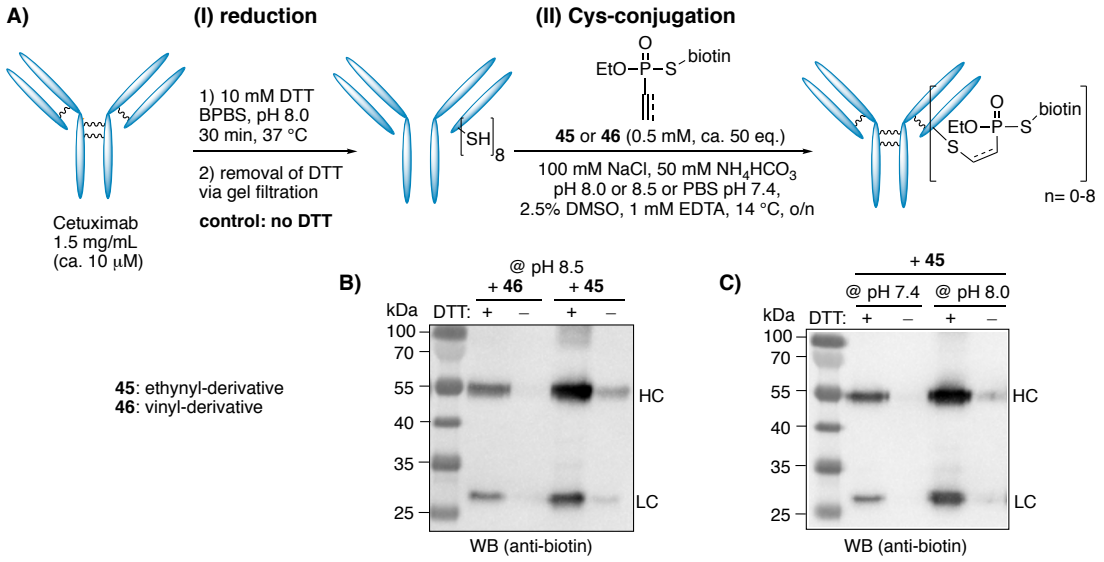

Fig. 23 A) Modification of the antibody Cetuximab with biotin derivatives **45** (ethynylphosphonothiolate) and **46** (vinylphosphonothiolate) via a mild reduction/alkylation protocol. B) Western-blot analysis (anti-biotin) of Cetuximab after modification with **45** and **46** at pH 8.5. C) Same analysis for derivative **45** after modification at pH 7.4 and pH 8.0.

In comparison to a maleimide-biotin derivative (**58**), antibody labelling with vinylphosphonothiolate **18** is less efficient (based on Western-blot analysis) but features superior cysteine-selectivity (Fig. 24). Cross-reactivity of maleimides with other nucleophilic amino acids (mainly lysine and histidine) is a known phenomenon, especially under slightly basic conditions [107, 208, 259].

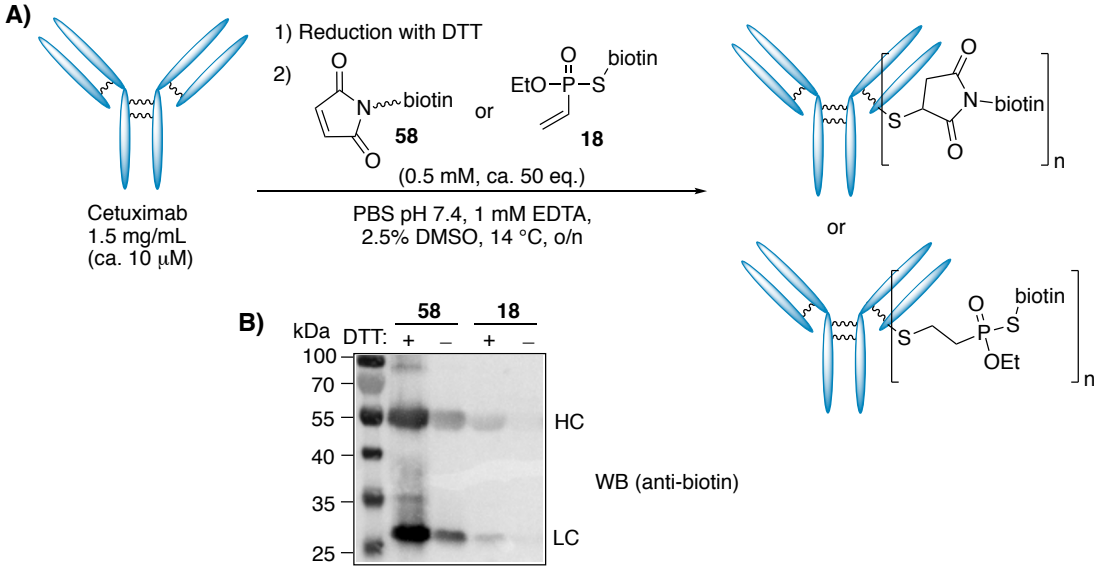

Fig. 24 Modification of Cetuximab with vinylphosphonothiolate **18** or maleimide-biotin **58**.

The cysteine-selectivity and labelling efficiency of vinyl- and ethynylphosphonothiolates was further investigated by means of intact protein MS. Therefore, the IgG antibody Trastuzumab was reacted with either *S*-ethyl ethynyl- or vinylphosphonothiolate derivatives **7** or **8**, respectively (scheme 47). Here, a larger excess of phosphonothiolates (100 eq.) were used at higher antibody concentration (5 mg/mL) to challenge the chemoselectivity. After the modification, the antibodies were deglycosylated and reduced before analysis by middle-up MS analysis (Fig. 25). The labelling degrees were estimated based on MS signal intensities.

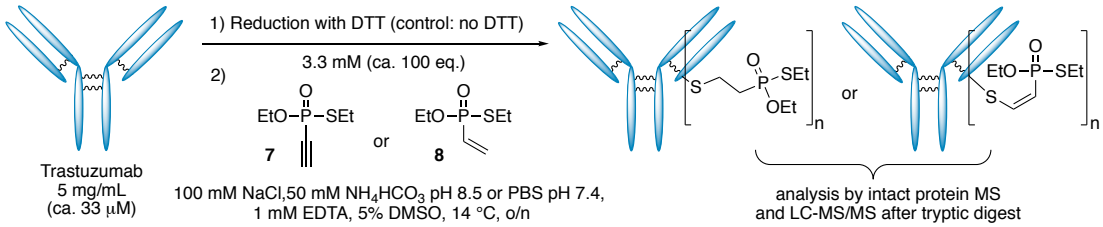

Scheme 47 Labelling of Trastuzumab with phosphonothiolates **7** and **8**.

The MS analysis revealed average modification ratios per antibody of 1.0 with vinylphosphonothiolate **8** and 2.5 with ethynylphosphonothiolates **7** at pH 7.4 (Fig. 25A/E). At pH 8.5, almost maximal labelling of ca. 7.6-7.7 modifications per antibody was observed for both derivatives (Fig. 25C/G). In the negative controls (-DTT) for vinylphosphonothiolate **8**, no labelling was observed at either pH 7.4 or at pH 8.5 (Fig. 25B/D). In the negative control for the modification with ethynylphosphonothiolate **7** at pH 8.5 however, some labelling (ca. 0.3 modifications per antibody) was observed (Fig. 25H), which is in line with the Western-blot analysis above (see Fig. 23). MS/MS analysis

of this sample after tryptic digest revealed that these modifications were at distinct histidine, tyrosine and threonine residues, as well as at certain cysteine residues (see Experimental chapter 8.2.9). An explanation for unexpected cysteine labelling in this negative control might be that the interchain disulfide bridges spontaneously opened to some extent and thereby free sulfhydril groups became accessible for the reaction with ethynylphosphonothiolates. A detailed MS/MS analysis of all the different reaction conditions further revealed –next to labelling of the targeted inter-chain cysteines – modification at certain histidine residues also for the vinylphosphonothiolate probe **8** at both pH 7.4 and pH 8.5 as well as labelling of the N-termini and a distinct threonine residue with this probe at pH 8.5. Given however that both intact protein MS as well as Western-blotting are sensitive analytical methods and that in the respective spectra (Fig. 25) and blots (Fig. 23), no or only traces of labelling could be observed in the negative controls, still demonstrates that cysteine-selectivity for both unsaturated phosphonothiolate derivatives is high. Moreover, large excess of both reagents was used in these experiments and the selectivity might thus further be improved by decreasing the number of equivalents. Nevertheless, depending on the local environment within a protein, cross-reactivity with other nucleophilic side chains cannot be excluded and should be analysed carefully from case to case.

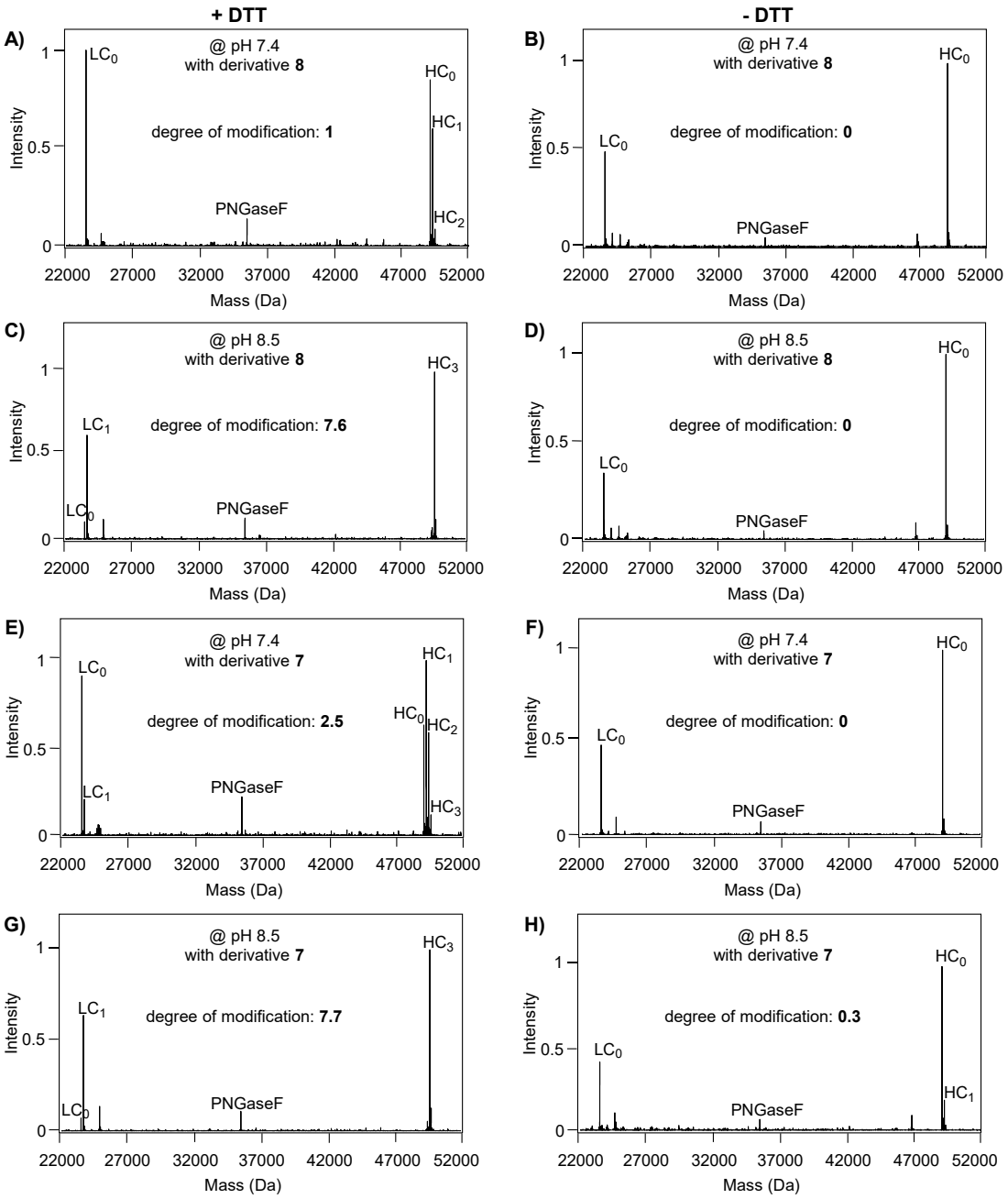

Fig. 25 Deconvoluted MS spectra (ESI-TOF) of Trastuzumab after labelling with vinylphosphonothiolate **8** (panels A-D) or ethynylphosphonothiolate **7** (panels E-H) at either pH 7.4 or pH 8.5. Left column: Trastuzumab was treated with DTT before the addition of the phosphonothiolates, right column: control reactions without prior DTT reduction. Trastuzumab samples were deglycosylated with the enzyme PNGaseF and reduced with DTT before MS analysis. LC: light chain, HC: heavy chain, subscripts: number of modifications. Modification degrees were estimated based on signal intensities.

3.7 Stability of phosphonothiolates

Next to the selectivity in the labelling of proteins, the stability of vinyl- and ethynylphosphonothiolates was investigated under conjugation conditions. Therefore, the water-soluble phosphonothiolates **39** and **43** were subjected to aqueous solutions at pH 7.4 (PBS) or pH 8.5 (50 mM NH_4HCO_3) and their degradation at 25 °C and at 37 °C was monitored over time via ^{31}P-NMR (Fig. 26). For both derivatives, hydrolysis of the phosphorus-sulphur bond was observed, giving rise to the respective phosphonic acids and free thiol-EDANS (Fig. 26A). The degradation was monitored over 90 hours, revealing that vinylphosphonothiolate **39** is significantly more stable than ethynylphosphonothiolate **43**: At pH 7.4 and 25 °C, more than 90% of vinylphosphonothiolate **39** remained intact after 90 hours, while under the same conditions 50% of ethynylphosphonothiolate **43** was hydrolysed (Fig. 26B). At pH 8.5, the hydrolysis proceeded faster, particularly for ethynyl derivative **43**. The same trends, but more pronounced, were observed at 37 °C (Fig. 26C). The circumstance that ethynylphosphonothiolates are less stable in buffer than vinylphosphonothiolates may be explained by the higher electrophilicity of the phosphorus atom as a consequence of the more electron-withdrawing effect of the ethynyl-residue compared to the vinyl-residue. Notably, for both substrates, hydrolysis at pH 7.4 and 8.5 occurs on a slower time scale than the reaction with thiols under these conditions and hence instability of these reagents is not a critical issue under conjugation conditions.

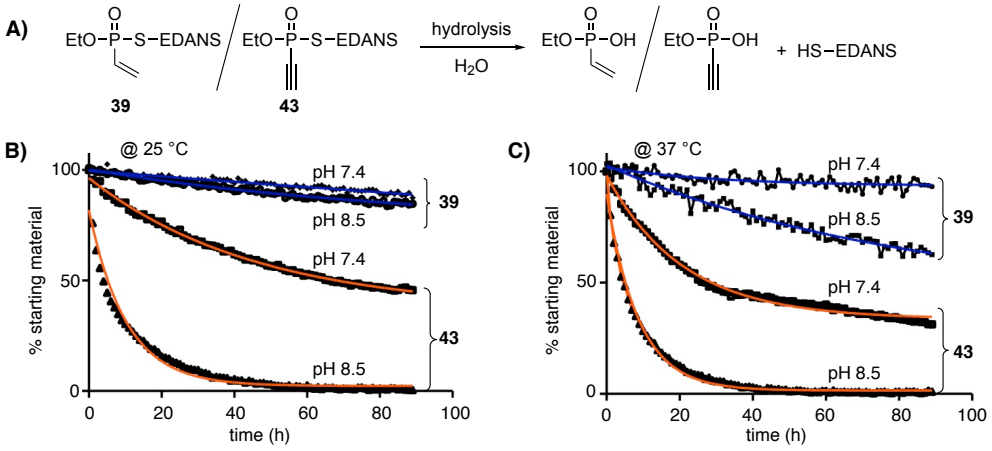

Fig. 26 Aqueous stability of unsaturated phosphonothiolates (**39**=vinyl-derivative, **43**=ethynyl-derivative) at 25 °C (B) and at 37 °C (C). Initial concentration (100% starting material)= 5 mM.

The stability of vinylphosphonothiolates was further investigated on peptide level using the purified peptides **28-32** described above. Therefore, the vinylphosphonothiolate peptides **28-32** were subjected to conjugation buffer at pH 7.4 or pH 8.5 and were monitored by UV-LC-MS over time (Fig. 27). Exemplary LC-UV traces are shown for peptide **28** (X=A) at pH 7.4 and pH 8.5 in Fig. 27 B and D, respectively. Thereby, several new species were observed and assigned according to their m/z to the structures depicted in Fig. 27A. Not surprising, P-S bond hydrolysis was observed, giving rise to reduced cysteine peptides (II). The cysteine peptides (II) further reacted with remaining vinylphosphonothiolate peptides (I) to the respective thiol-conjugates (III). In addition, a new species with the same m/z as the starting materials was observed for all tested peptides (see Experimental Fig. 83 and 84 for extracted ion chromatograms).

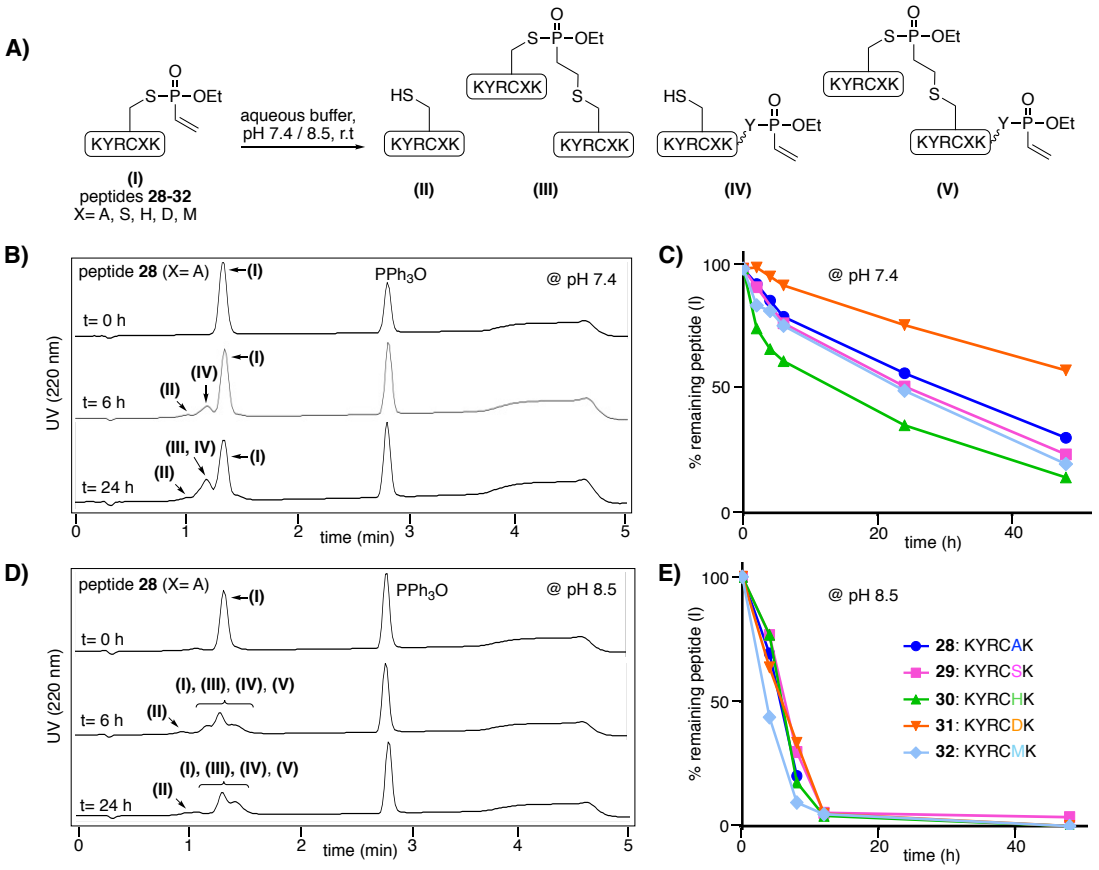

Fig. 27 A) Structures of observed products upon incubation of vinylphosphonothiolate peptides **28-32** in aqueous buffers. The Y in structure (IV) stands for any of the nucleophilic amino acids in the sequence. B) Exemplary LC-UV chromatograms for peptide **28** (X=A) in PBS pH 7.4 over time. C) Quantification of remaining vinylphosphonothiolate peptides **28-32** over time at pH 7.4. Shown are percentages of remaining intact peptides (I) based on extracted ion intensities (see Experimental for details). For legend see panel (E). D, E) Analogous analysis at pH 8.5 (50 mM NH_4HCO_3).

This observation indicated the migration of the vinyl-*O*-ethylphosphate group to other nucleophilic residues, giving rise to peptides with the general structure (IV). As this phenomenon was observed for all the tested peptides **28-32** to similar extents, it is likely that the P(V) moiety got transferred to the amine groups of either the N-terminus or lysine, which are present in all the peptides. The migration products (IV) further reacted with remaining vinylphosphonothiolate peptides (I) to give conjugates of the general structure (V). As a consequence of all these processes, approximately 50% of peptides **28-32** (I) were decomposed or consumed after 24 h at neutral pH (Fig. 27C). The quantification is based on extracted ion intensities (see Experimental for details). At pH 8.5, all the described processes were faster, leaving approximately 50% of peptides **28-32** (I) intact after about 8 hours (Fig. 27D).

While these results clearly show that vinylphosphonothiolate peptides undergo hydrolysis and other side-reaction in aqueous buffer, employing the freshly synthesised peptides **28-32** directly with reduced glutathione under the same conditions (PBS pH 7.4 or 50 mM NH_4HCO_3 pH 8.5) resulted in clean conversion into the thiol addition products (Fig. 28). Migration of the P(V) moiety to other residues was not observed for any of the peptides **28-32** (exemplified for peptide **28** in Fig. 28). It could thus be concluded that both the migration of the P(V) moiety to other nucleophilic residues, as

well as the hydrolysis of the P-S bond are slower than the thiol addition and that these processes do therefore not constitute a major problem under conjugation conditions with thiols.

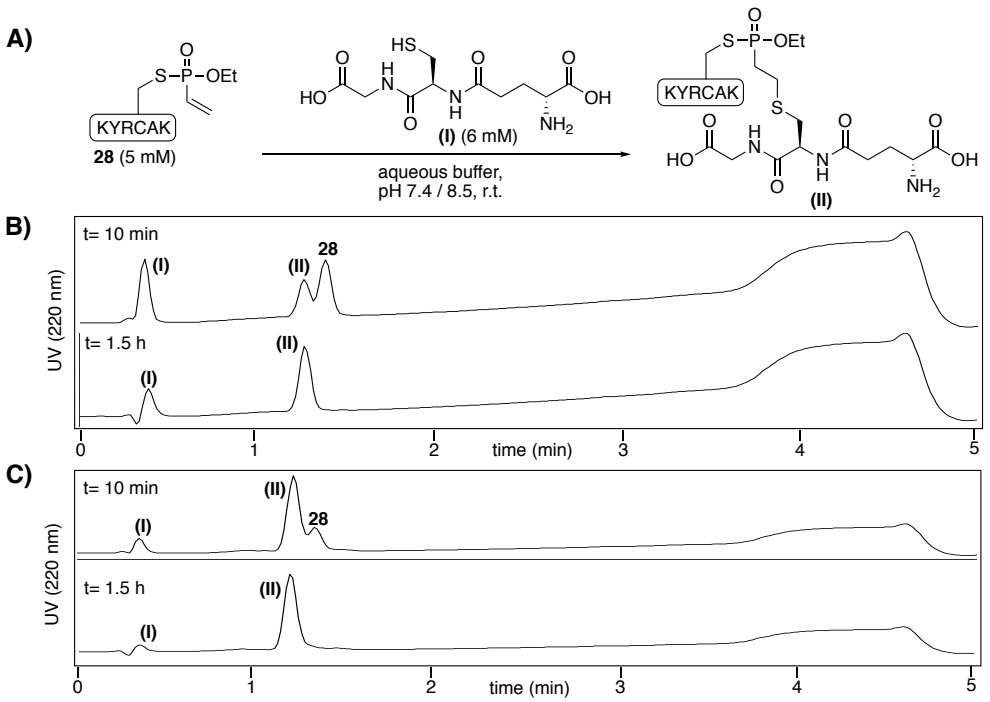

Fig. 28 Glutathione addition to vinylphosphonothiolate peptide **28** at pH 7.4 (B) or pH 8.5 (C). Shown are LC-UV chromatograms of the reaction mixtures.

Next, the stability of the thiol-phosphonothiolate conjugates was investigated under physiologically relevant conditions such as cell lysate (HeLa), human serum, PBS (pH 7.4) or in the presence of excess glutathione. Therefore, a previously established FRET quencher pair assay was employed [208] using the ethynyl- and vinylphosphonothiolate-linked conjugates **59** and **60**, respectively (Fig. 29A). Upon cleavage of the conjugates, fluorescent EDANS-thiol is liberated and generates a fluorescence signal (the more cleavage, the higher the fluorescence value). In a 1 M NaOH solution for instance, both conjugates hydrolyse to full extent within approximately 2 hours (Fig. 29 B/C, red curve). Compared to this maximum fluorescence, both conjugates showed good stability in neutral buffer, HeLa lysate or in the presence of excess free thiols. In human serum however, significant cleavage was observed for the ethynyl-linked conjugate **59** (orange curves, Fig. 29B).

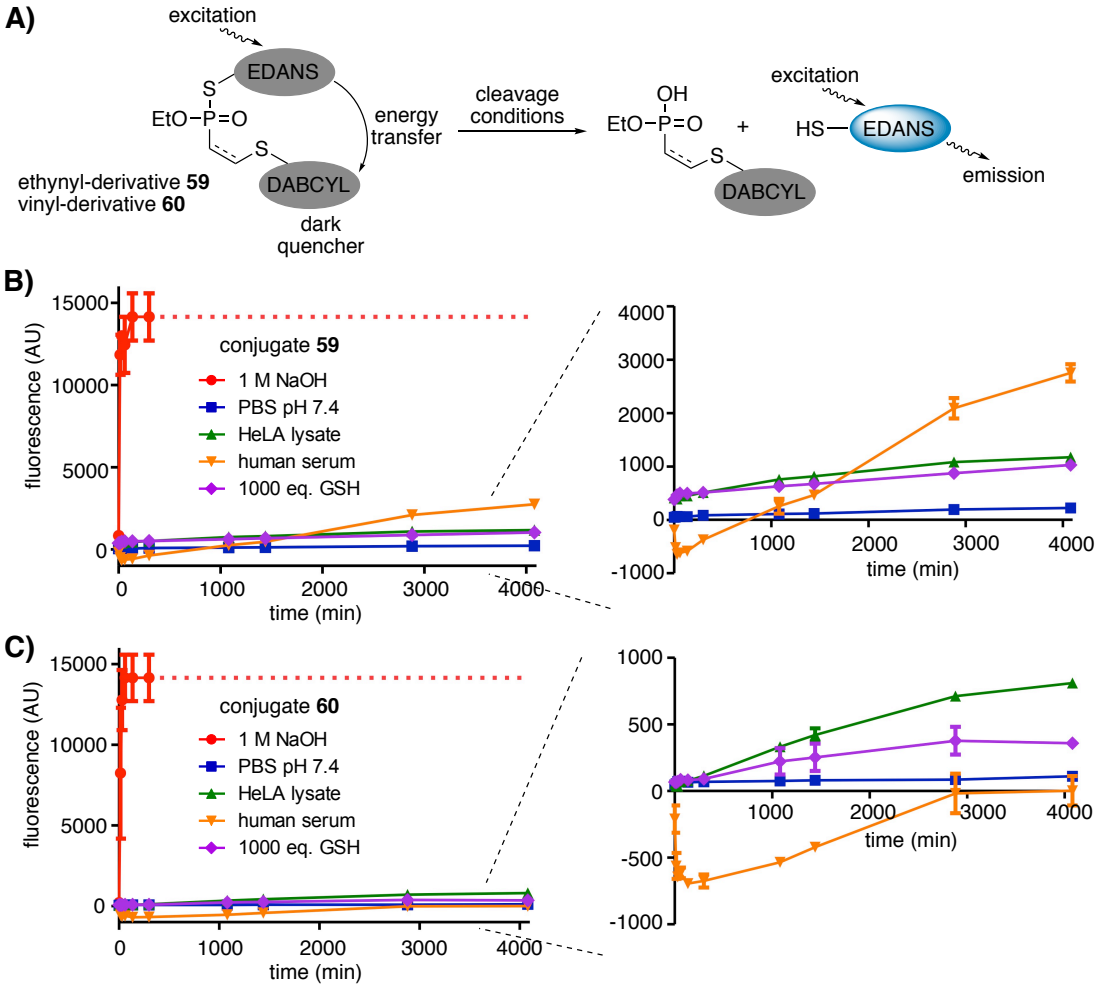

Fig. 29 A) Principle of the fluorescence-quenching assay (adapted from [208]). B) and C) Stabilities of ethynyl- and vinylphosphonothiolate-linked conjugates **59** and **60**, respectively. Shown are mean values and error bars of triplicates. Negative values for serum samples might be due to serum autofluorescence.

3.8 Comparison of unsaturated phosphonothiolates to unsaturated phosphonates and phosphonamidates

After having discovered that unsaturated vinyl- and ethynylphosphonothiolates are reactive towards thiol additions and that the resulting thiol-conjugates possess good stability, we were interested in comparing these aspects for thiol additions to other unsaturated phosphorus(V) electrophiles, in particular to phosphonates and phosphonamidates. These compound classes differ in the kind of heteroatom bound to the phosphorus. Phosphonothiolates contain a P-S bond; phosphonates and phosphonamidates a P-O and a P-N bond, respectively (Fig. 30). As outlined in the introduction (see chapter 1.4.1), our group has intensively investigated unsaturated vinyl- and ethynylphosphonamidates for cysteine-selective bioconjugations [228, 208, 209]. On the other hand, unsaturated phosphonates have not seen a lot of attention for cysteine-bioconjugation [146].

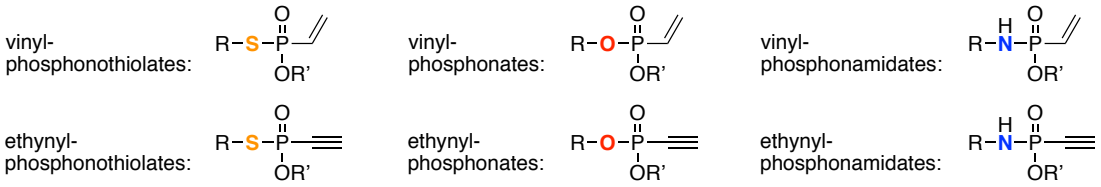

Fig. 30 General structures and nomenclature of unsaturated P(V)-electrophiles.

In order to access unsaturated phosphonates derivatives for comparative studies, the route described in chapter 3.4 using the precursors **33** and **34** was adapted to alcohols (scheme 48). Using this route, Boc-protected amine-derivatives **61** and **62** were generated. These were then further modified into the water-soluble, fluorescent EDANS-derivatives **65** and **66**, respectively by means of Boc-deprotection with TFA and subsequent coupling to EDANS derivative **42**.

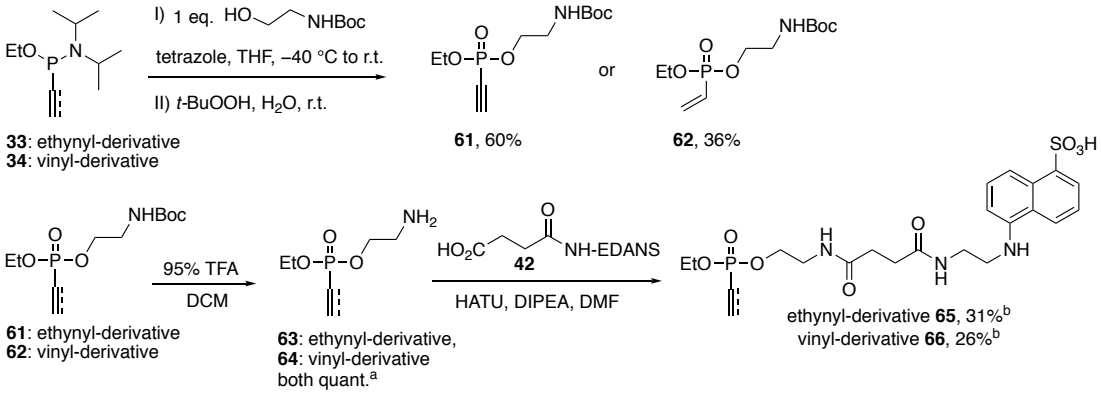

Scheme 48 Synthesis of vinyl- and ethynylphosphonate derivatives. [a]Used as crude product, [b]isolated via reverse-phase HPLC.

Using the generated fluorescent derivatives **65** and **66**, the bimolecular rate constants for thiol additions with glutathione at pH 7.4 were determined analogously to the phosphonothiolate study (compare Fig. 22). For the ethynylphosphonate derivative **65** the bimolecular rate constant was found to be 0.146 ± 0.009 $M^{-1}s^{-1}$ at pH 7.4 (Fig. 31C). Under the same conditions, the vinylphosphonate derivative **66** reacted too slowly with glutathione to deduce an accurate rate constant. In comparison to unsaturated phosphonothiolate derivatives, unsaturated phosphonates react thus roughly an order of magnitude slower in thiol additions under neutral conditions. As for unsaturated phosphonamidates, the ethynyl-derivative **67** was used for comparison (see structure in Fig. 31A). Notably, this derivative bears an aryl residue at the nitrogen. The bimolecular rate constant for the glutathione addition to this compound was determined to 0.0493 ± 0.0023 $M^{-1}s^{-1}$ at pH 7.4. Since aryl-substituted phosphonamidates are more reactive than alkyl-substituted derivatives [209], the rate constant for the respective alkyl-derivative would be estimated to be slightly lower. Overall, it can thus be concluded that unsaturated phosphonothiolates are clearly the most reactive derivates, followed by unsaturated phosphonates and phosphonamidates.

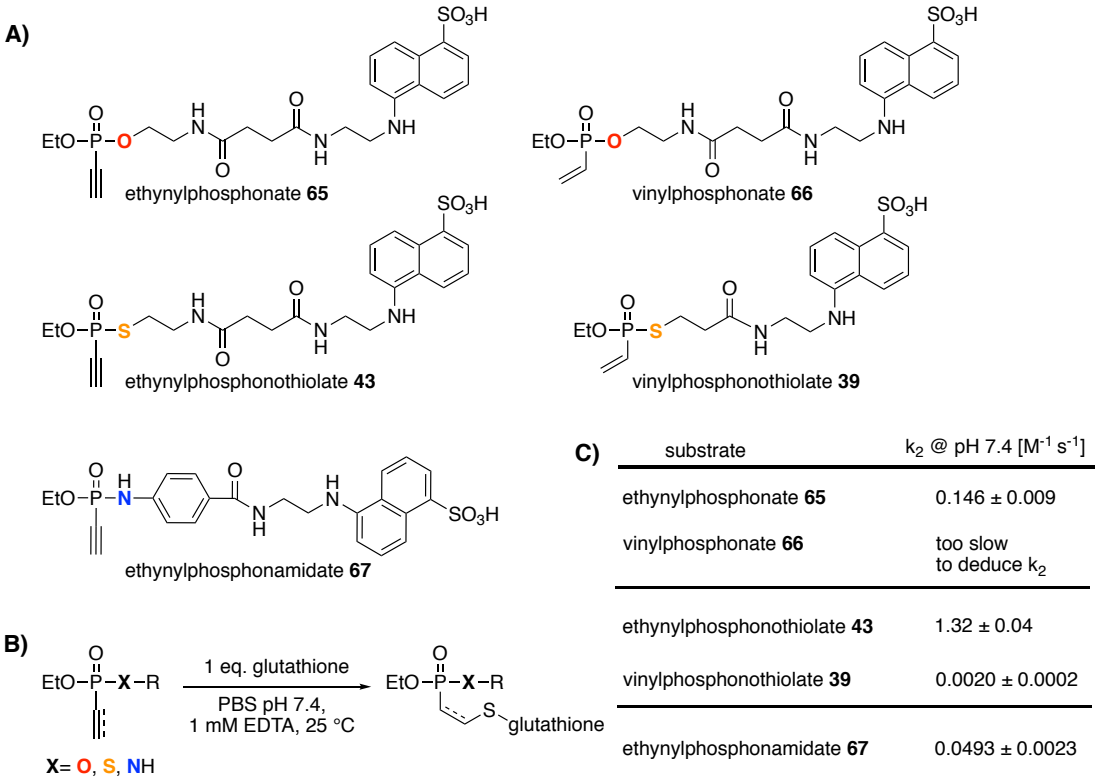

Fig. 31 Comparison of reactivities for the thiol addition to unsaturated P(V)-electrophiles. A) Structures of the investigated compounds, B) general reaction conditions for the addition of glutathione, C) experimentally obtained bimolecular rate constants.

While one would generally assume that electron-withdrawing substituents around the phosphorus atom would render the terminal carbon of the vinyl- and alkynyl groups more electropositive and thus more reactive for nucleophilic thiolate addition, the observed rate constants do not correlate with the electronegativities of the heteroatoms (N, O, S). If this was the case, unsaturated phosphonates would expected to be the most electrophilic/reactive in thiol additions, followed by phosphonamidates and phosphonothiolates. The unprecedented finding that unsaturated phosphonothiolates are

considerably more reactive than the other P(V)-derivatives must thus have additional reasons, likely to be found in the nature of the phosphorus-sulphur bond. In order to understand these reactivities better, a collaborator is currently working on DFT calculations to predict reaction energy profiles for the thiol addition to P(V)-electrophiles, from which information about the reaction rates might be derived. In addition to the general trend of phosphonothiolates being the most reactive derivatives, followed by phosphonates and phosphonamidates, the ethynyl-derivatives react much faster with thiols than the respective vinyl-derivatives within all three compound classes. These differences in reactivity are also reflected in the electrostatic potential maps as shown in Fig. 32. The ethynyl-residues show less electron density at the terminal carbon than the vinyl-residues, indicating higher electrophilicites.

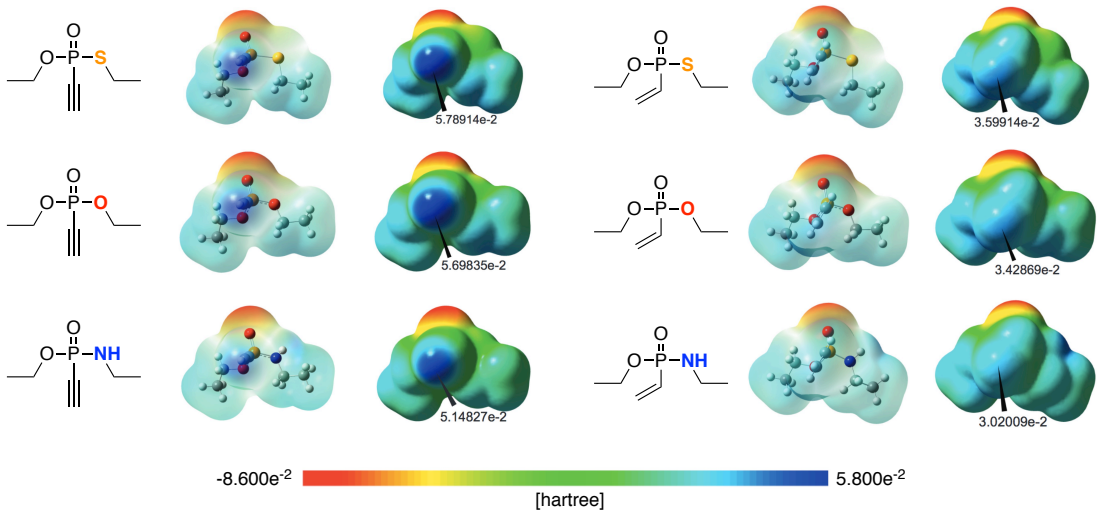

Fig. 32 Electrostatic potential maps of unsaturated P(V)-electrophiles. The black wedges point at the most positive values of the terminal carbons of the triple and double bonds, respectively.

Next to the reactivities of different P(V) electrophiles in thiol additions, also the stability of the respective thiol-conjugates was compared. From the study described in chapter 3.7, it could be concluded that thiol-phosphonothiolate conjugates are stable in aqueous, neutral buffer as well as in HeLa lysate and in the presence of excess free thiols. In serum however, some P-S bond hydrolysis was observed over time, particularly for the ethynylphosphonothiolate derivative (Fig. 29B). In contrast, ethynylphosphonamidates employ excellent stability also in serum as well as under the other conditions, as described in references [208] and [228]. The stability of thiol-phosphonate conjugates was investigated here using the same assay as described before and good stability was observed for both ethynyl- and vinyl-conjugates **68**/**69** under all tested conditions (Fig. 33).

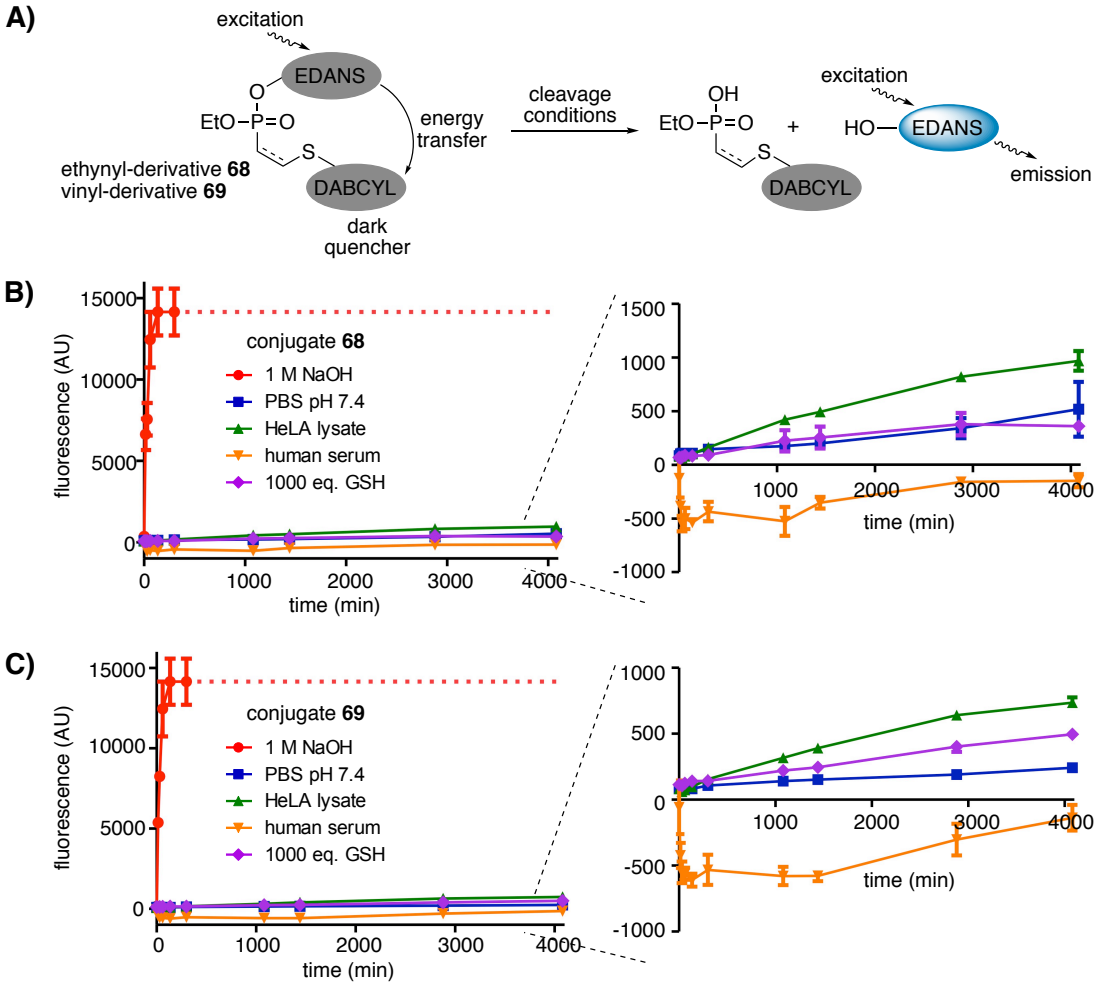

Fig. 33 A) Fluorescence-quenching assay using phosphonate-linked conjugates **68** and **69**. B/C) Stabilities of ethynyl- and vinylphosphonate-linked conjugates **68** and **69**, respectively. Shown are mean values and error bars of triplicates.

In conclusion, all three P(V) compound classes can be used to generate thiol-conjugates. Ethynylphosphonothiolates are the most reactive derivatives, followed by ethynylphosphonates and ethynylphosphonamidates. The respective vinyl-P(V) derivatives are significantly less reactive. The stability of the thiol-P(V) conjugates is generally very good under physiological relevant conditions. An exception are the most reactive ethynylphosphonothiolate derivatives, where significant hydrolysis was observed both for the unconjugated reagents (compare Fig. 26) as well as for the thiol-conjugates in serum (compare Fig. 29). One might thus draw the general conclusion that high reactivity of unsaturated P(V) electrophiles in thiol additions is compromised by decreased stability of these compounds.

4 Phosphonothiolate-linked protein-protein conjugates

Responsibility assignment
The research described in this chapter was conceptualised by Prof. Dr. Christian P. R. Hackenberger, Sergej Schwagerus and the author. Most of the herein presented experiments were conducted by Sergej Schwagerus, as specified at the beginning of each section. Briefly, Sergej Schwagerus established the synthesis of vinylphosphonothiolate-ubiquitin **72** and did most of the protein-protein conjugations with this substrate. He furthermore performed CD measurements of the synthetic diubiquitin **78**, as well as the stability assay against DUBs and the enzymatic ubiquitination of conjugate **80**. Moreover, Sergej Schwagerus worked together with Kristin Kemnitz-Hassanin on the expression and purification of the proteins used in this chapter. LC-MS/MS measurements were performed by Dr. Michal Nadler-Holly and the MS/MS data was analysed by Christian Stieger. Parts of this chapter were published in and are adapted from A. L. Baumann*, S. Schwagerus*, K. Broi, K. Kemnitz-Hassanin, C. E. Stieger, N. Trieloff, P. Schmieder, C. P. R. Hackenberger. Chemically Induced Vinylphosphonothiolate Electrophiles for Thiol–Thiol Bioconjugations. *J. Am. Chem. Soc.* **2020**, *142*, 9544-9552 (* shared first authorship).

4.1 Background and Outline

Building up on the results described in chapter 3, where we could show that vinylphosphonothiolates can be chemoselectively installed on unprotected peptides, we wanted to expand our method to install electrophilic vinylphosphonothiolates on proteins. As described in chapter 1.3.3, introducing an electrophilic moiety into proteins in principle enables the subsequent conjugation to other proteins via canonical nucleophilic amino acid residues. The generation of heterobifunctional proteins is not only gaining interest for next-generation biopharmaceuticals such as IgG Fc domain fusions [260] but is also needed in various applications in basic research for example to study protein ubiquitinations. While heterobifunctional proteins can be generated as genetic fusions, this approach is limited to connecting the proteins at their N- and C-termini. On the other hand, chemical approaches give access to more diverse topologies through conjugation of proteins via side-chain residues. This is not only important for cases where unmodified termini are required for optimal bioactivity but is also crucial to study the function of ubiquitinated proteins. As the largest post-translational modifications of proteins, ubiquitinations regulate various cellular processes from protein degradation and trafficking to DNA repair and transcription [261]. As outlined in chapter 6.4, the site at which a substrate protein is modified with ubiquitin, as well as the connectivity in-between poly-ubiquitins, determines the fate of the substrate protein [261]. For instance, ubiquitination at distinct lysine residues of α–Synuclein have been identified in filamentous α–Synuclein depositions, which are a hallmark of various neurodegenerative diseases [262]. In order to study the effect of distinct

ubiquitinations, there is thus a great need for methods that allow the generation of homogeneous, site-specifically ubiquitinated substrate proteins for functional investigations. Important contributions in this field have been made by the groups of B. Crosas [263], H. Dohlman and S. Campbell [264], A. Brik [265, 266, 267, 268], A. Marx [269], M. R. Pratt [270], E. Strieter [271, 272] and very recently by the Liu group [273]. Out of these methods, only a few allow the generation of uncleavable ubiquitinated proteins by replacing the natural isopeptide bonds with unnatural, stable linkages, that both resist cleavage by deubiquitinating enzymes as well as reduction by external thiols under physiological conditions. Such uncleavable ubiquitin-protein conjugates are powerful tools to dissect ubiquitin signalling [274]. One of the first contributions toward this goal has been made by the Marx group, who has generated protease-resistant ubiquitin chains via stable triazoles linkages from click reactions between genetically incorporated unnatural alkyne- and azide- containing amino acids [269]. Following a similar goal, the Brik group has generated uncleavable ubiquitinated proteins via oxime ligations [267]. In their very recent publication, the Liu group has reported yet a new kind of DUB-resistant ubiquitin probes based on isopeptide-*N*-ethylated dimeric or polymeric Ub chains, which they prepared using a chemoenzymatic protocol. On an impressive scale, they used their method to generate various homotypic and branched ubiquitin probes in excellent yields [273].
Complementing these approaches, we set out to generate non-cleavable and site-selectively linked ubiquitin-protein conjugates using our herein developed phosphonothiolate linkers (scheme 49). Thereby, we wanted to install the electrophilic vinylphosphonothiolate moiety on a ubiquitin mutant containing an activated cysteine and subsequently conjugate our probe to proteins of interest via cysteine conjugation. As opposed to the methods above, our method would allow the generation of (presumably) non-cleavable ubiquitin-protein conjugates via canonical amino acids in an enzyme-independent manner.

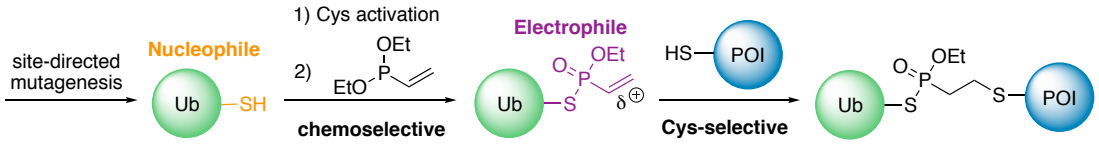

Scheme 49 Outline for the synthesis of phosphonothiolate-linked ubiquitin-protein conjugates.

4.2 Synthesis of vinylphosphonothiolate-ubiquitin

Note: The synthesis of vinylphosphonothiolate-ubiquitin ***72*** *was first established by Sergej Schwagerus. The author repeated this synthesis, based on the established protocol. The herein presented data for the aqeuous stability of* ***72*** *was also obtained from Sergej Schwagerus.*

In order to install the vinylphosphonothiolate-electrophile on ubiquitin, the UbG76C mutant **70**, carrying a single cysteine at the C-terminus was first activated to the respective electrophilic disulfide **71**. Here, Ellman's reagent was used instead of DTNP because it employs better water-solubility. Following the protocol established for the installation of vinylphosphonothiolates on unprotected peptides (compare chapter 3.3), activated ubiquitin **71** was then subjected to DMSO containing 1% TFA, before diethylvinylphosphonite **4** (50 eq.) was added as a crude mixture. The reaction mixture was analysed by intact protein MS, indicating the formation of the desired vinylphosphonothiolate-Ub **72** as well as reduced Ub-Cys as a side-product. This result proved that the developed protocol can also be applied to more complex substrates. While after 8 hours, there was still starting material **71** detected by intact protein MS, adding another portion of diethyl-vinylphosphonite (50 eq.) resulted in full conversion of the starting material **71** and the desired UbG76C-vinylphosphonothiolate **72** was obtained in 24% isolated yield after semi-preparative HPLC purification.

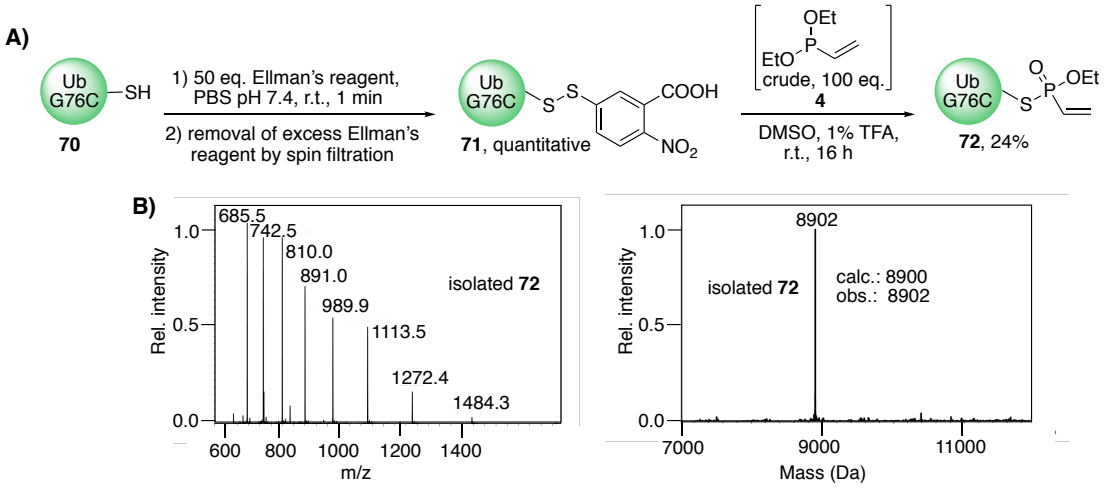

Fig. 34 Installation of the vinylphosphonothiolate moiety on protein level. A) Conversion of cysteine-ubiquitin mutant **70** into vinylphosphonothiolate-ubiquitin **72** via electrophilic disulfide **71**. B) Raw and deconvoluted MS spectra of purified **72**.

The fact that more equivalents of vinylphosphonite were needed here to obtain full conversion of the electrophilic disulfide as opposed to the analogous reaction on peptide level, might be due to the lower concentration of ubiquitin used here (ca. 1.5 mM of Ub **71** as opposed to 30 mM of peptides **28-32**, (compare chapter 3.3)) as well as due to the more complex structure of the substrate. Furthermore, diethyl-vinylphosphonite **4** can oxidize over time to the unreactive diethyl-vinylphosphonate **11**. Consequently, to compensate for this side-reaction, more equivalents of diethyl-vinylphosphonite **4** are needed, especially at low substrate concentrations. Given that the formation of vinylphosphonothiolates was very rapid on small molecule as well as on peptide level, the long reaction time reported here for the analogous reaction on ubiquitin seems

surprising. However, since the reaction on ubiquitin could only be followed by intact protein MS, close and accurate monitoring of the conversion was challenging for this substrate and further complicated by the small scale these reactions were performed at. Therefore, when optimising this protocol in the future, it might be worth to re-evaluate the necessary reaction time to complete disulfide conversion.
Next, the stability of the generated vinylphosphonothiolate-ubiquitin **72** was investigated under protein conjugation conditions (Fig. 35). Therefore, vinylphosphonothiolate-Ub **72** was subjected to aqueous buffers at pH 7.4 or pH 8.5 and followed over time by SDS-PAGE (Fig. 35B). Similar to the observed behaviour of peptide vinylphosphonothiolates **28-32**, P-S bond hydrolysis was observed over time at pH 8.5 at r.t., as well as to a smaller extent at pH 7.4 and more pronounced at 37 °C than at r.t. Because of the P-S bond hydrolysis, the free thiol ubiquitin **73** reacts with intact **72** to form C-terminal ubiquitin homodimers **74**.

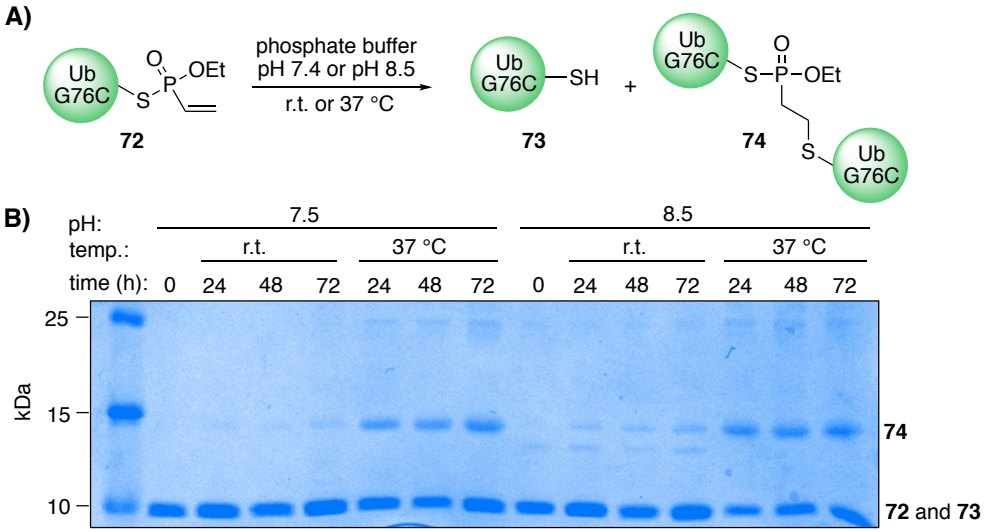

Fig. 35 Stability of vinylphosphonothiolate-ubiquitin **72** in aqueous buffer. A) Assay conditions and decomposition products, B) SDS-PAGE gel (Coomassie) indicates the formation of covalent homodimer **74**.

4.3 Ubiquitin-protein conjugations

Ubiquitin-eGFP conjugation

Note: The herein presented Ub-eGFP conjugation was conducted by Sergej Schwagerus.

With the ubiquitin-vinylphosphonothiolate probe **72** in hand, ubiquitin-protein conjugation was first probed in a model system using the eGFP cysteine mutant (C70M S147C) **75**, carrying a single accessible cysteine residue. The conjugation between **72** and **75** was monitored by intact protein MS (see Experimental, Fig. 93) and SDS-PAGE (Fig. 36). Thereby, the targeted conjugation product **76** could be detected, proving that thiol addition to ubiquitin probe **72** gives access to covalent protein-protein conjugates. At pH 8.5 and 37 °C, more than 80% of eGFP C70M S147C **75** had reacted after 24 hours with Ub-phosphonothiolate **72** to Ub-eGFP conjugate **76**. On the other hand, at pH 7.4 the reaction was significantly slower. In addition, the expected side-products **73** and **74** were observed; at pH 8.5 more than at pH 7.4. As a consequence, we decided to

perform further conjugation reaction at pH 8.0, which constitutes a compromise between reactivity and stability.

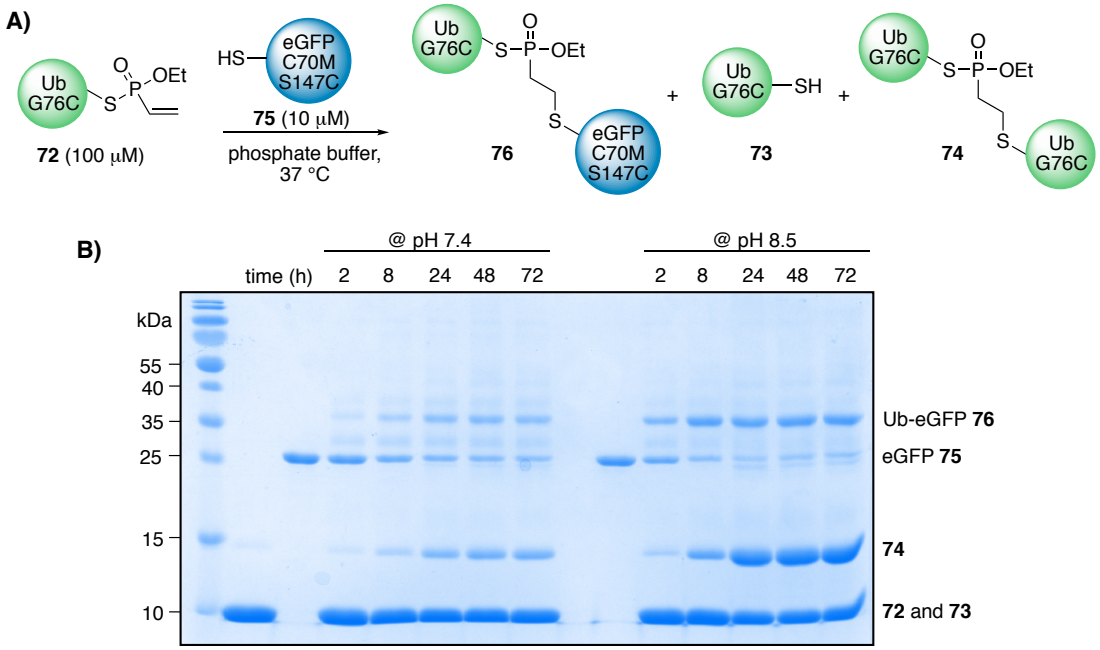

Fig. 36 Conjugation of vinylphosphonothiolate-Ub **72** to eGFP cysteine mutant **75**. A) Reaction conditions and side-products. B) Monitoring of the reaction by SDS-PAGE (Coomassie).

Ubiquitin-ubiquitin conjugation

Note: The conjugation between vinylphosphonothiolate ubiquitin ***72*** *and ubiquitin mutant* ***77*** *was first established by Sergej Schwagerus. The author repeated and optimised the protocol slightly. The data shown in Fig. 37 has been produced by the author. All the data shown in Fig. 38 were obtained by Sergej Schwagerus.*

Next, we set out to generate a phosphonothiolate-linked diubiquitin between vinylphosphonothiolate-Ub **72** and the ubiquitin-cysteine mutant UbK48C **77** (Fig. 37). While in the reaction with eGFP, the vinylphosphonothiolate-Ub **72** had been used in excess (ten times over eGFP), for this conjugation, UbK48C **77** was used in excess to economise **72**. We reacted vinylphosphonothiolate-Ub **72** with UbK48C **77** at pH 8.0 at 37 °C and the reaction was monitored by SDS-PAGE (Fig. 37B) and intact protein MS (see Experimental Fig. 94), which indicated maximal conversion after 24 hours and the formation of the covalent protein-protein conjugate **78**. The product **78** could be isolated in 27% yield after size-exclusion chromatography and showed the correct mass by intact protein MS (Fig. 37C). In order to confirm site-selective linkage to phosphonothiolate-ubiquitin, the conjugate **78** was subjected to LC-MS/MS analysis after tryptic digest. The respective crosslinked peptide was found (see Experimental, Fig. 98) and no P(V)-transfer conjugation products were observed on protein level.

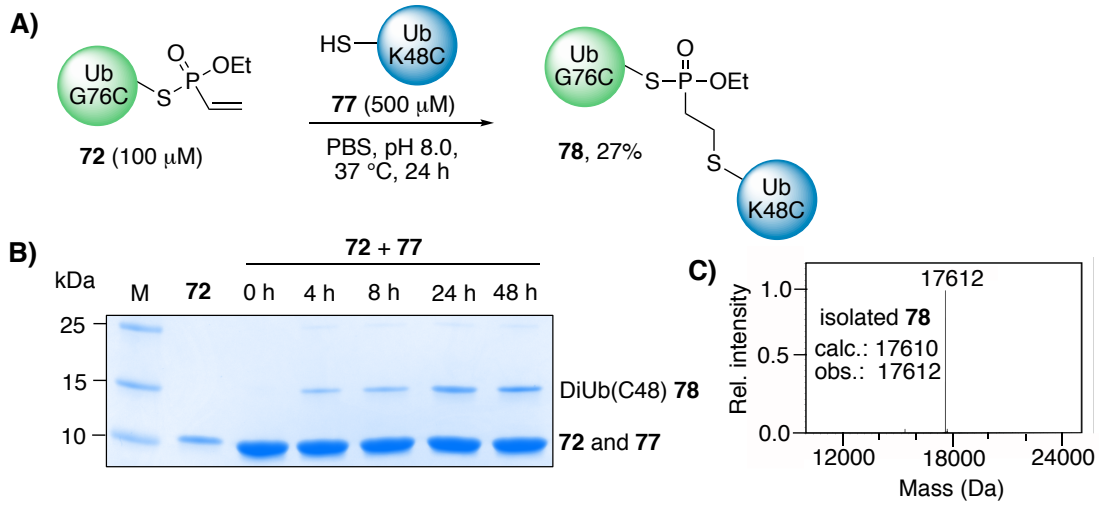

Fig. 37 Conjugation of vinylphosphonothiolate-Ub **72** to ubiquitin mutant UbK48C **77**. A) Reaction conditions, B) Monitoring the conversion by SDS-PAGE (Coomassie), C) Deconvoluted MS-spectrum of purified conjugate **78**.

We were then able to demonstrate that the isolated phosphonothiolate-linked DiUb(C48) **78** does not get hydrolysed by the deubiquitinating enzyme USP2CD, as opposed to wild-type DiUb(K48) (Fig. 38A).

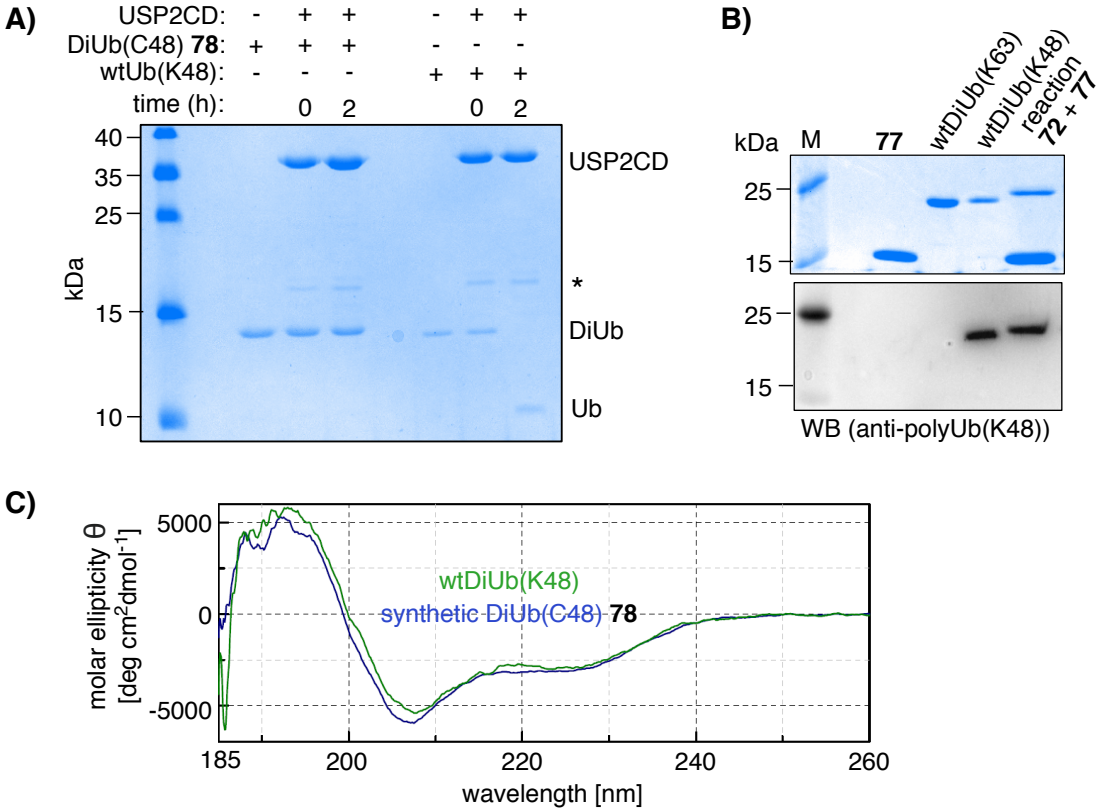

Fig. 38 A) Comparison of hydrolytic stability of the conjugate **78** and the wild-type DiUb(K48), SDS-PAGE gel (Coomassie), (*): impurity arising from the USP2CD sample. B) Confirmation that conjugate **78** is linked via cysteine C48. Top: SDS-PAGE (Coomassie), bottom: Western blot (anti-polyUb(K48C)). C) CD-spectra of synthetic phosphonothiolate-linked DiUb(C48) **78** compared to wild-type DiUb(K48).

Furthermore, the synthetic DiUb **78** shows similar ellipticity in CD-spectra compared to the wild-type diubiquitin (K48) (Fig. 38B). In addition, the site-selective linkage at position C48 was verified by Western-blot analysis (Fig. 38C) and by MS/MS analysis after tryptic digest (see Experimental Fig. 98A). Taken together, these results prove that synthetic phosphonothiolate linked DiUb **78** is hydrolytically stable and employs similar properties as the wild-type DiUb(K48), which is linked via an isopeptide bond.

Ubiquitin-α–Synuclein conjugation

*Note: The conjugation between vinylphosphonothiolate ubiquitin **72** and α–Synuclein **79** was first established by Sergej Schwagerus. The author repeated and optimised the protocol slightly. The experiment shown in Fig. 39 has been conducted by the author. The enzymatic ubiquitination of conjugate **80** (data shown in Fig. 40) has been conducted by Sergej Schwagerus.*

In a final example, vinylphosphonothiolate **72** was conjugated to the α–Synuclein cysteine mutant **79** (Fig. 39A). Also here, maximal conversion was observed after approximately 24 hours, as shown by SDS-PAGE analysis (Fig. 39B). Pure phosphonothiolate-linked Ub-α-Synuclein conjugate **80** could be obtained in 16% isolated yield after size-exclusion chromatography and showed the correct mass (Fig. 39C). Furthermore, the selective linkage at cysteine C6 of α–Synuclein was confirmed by MS/MS analysis (see Experimental Fig. 98B).

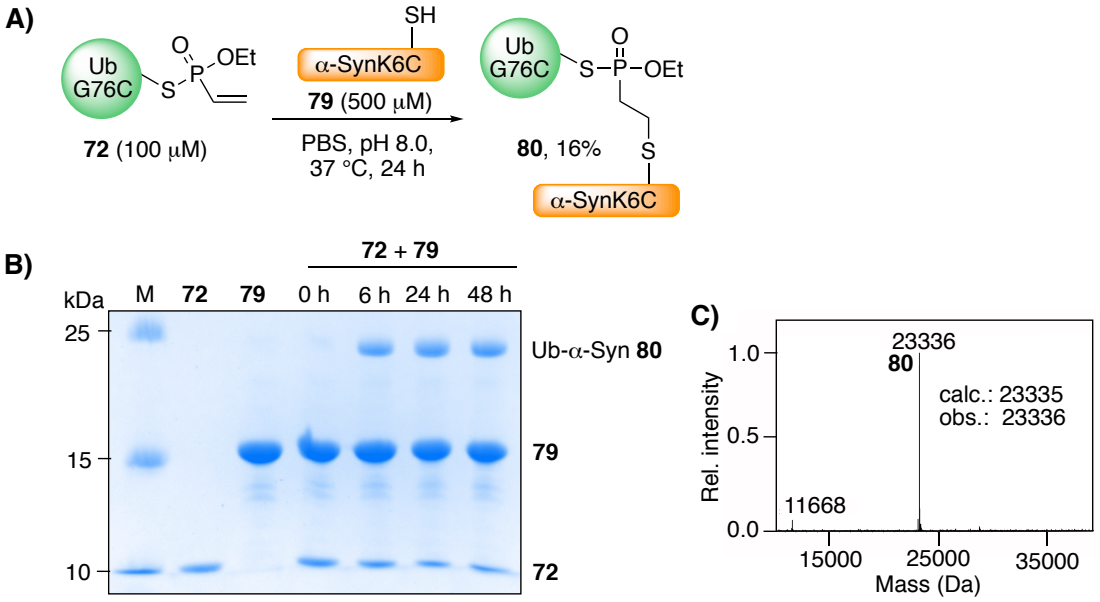

Fig. 39 Conjugation of vinylphosphonothiolate-ubiquitin **72** to α–Synuclein cysteine mutant **79**. A) Reaction conditions, B) SDS-PAGE gel (Coomassie) showing the formation of covalent conjugate **80**, C) intact protein MS (ESI) of purified Ub-α–Synuclein conjugate **80**.

Finally, in order to prove that the non-hydrolysable phosphonothiolate-linked ubiquitinated proteins can be recognised by ubiquitin-binding proteins, α-Synuclein-ubiquitin conjugate **80** was mixed with K48M ubiquitin mutant **81** and the enzymes Ubc1 (E2-25k) and E1 to enable enzymatic ubiquitination (Fig. 40A). The ubiquitin-conjugating enzyme Ubc1 catalyses the formation of K48-linked ubiquitin chains from mono ubiqui-

tin [275, 276]. In this assay, the dead-end K48M ubiquitin mutant **81** was used to avoid poly-ubiquitination. After 24 h incubation at 37 °C, the formation of di-ubiquitinated α-Synuclein **82** was detected by ESI-MS (Fig. 40B), demonstrating that the ubiquitinating enzymes indeed recognise the synthetic phosphonothiolate-linked ubiquitin as a substrate. By Western-blot using a specific anti-polyUb(K48) antibody (Fig. 40C), it could additionally be confirmed that conjugate **82** is linked via the K48 residue.

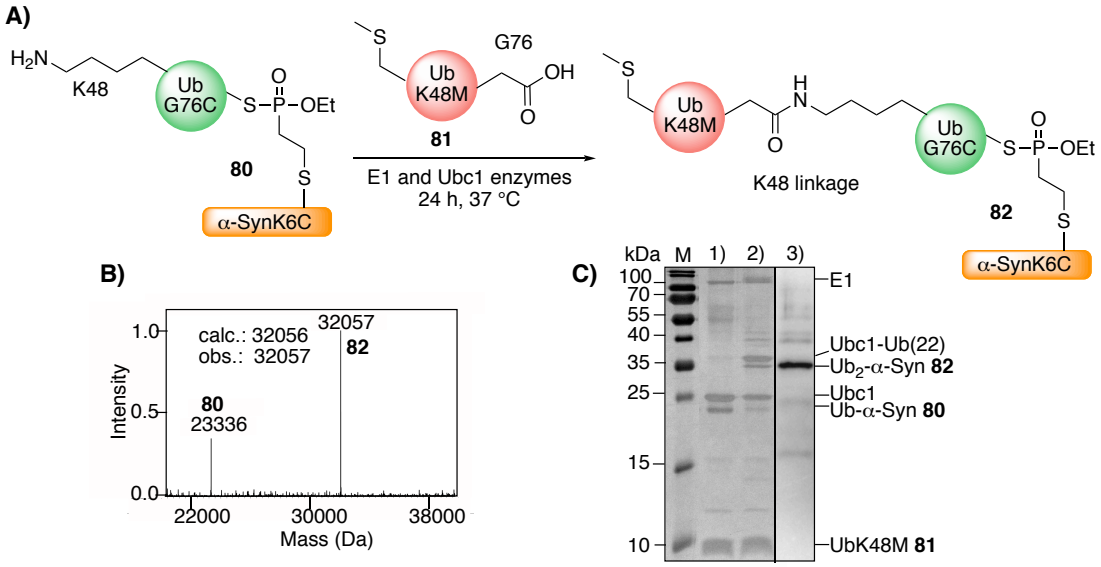

Fig. 40 Enzymatic ubiquitination of α-Synuclein-ubiquitin conjugate **80**. A) Reaction conditions, B) Intact protein MS spectrum of the reaction mixture, showing the formation of Ub_2-α-Syn conjugate **82**. C) lanes 1) and 2): SDS-gel (silver stain) of the reaction mixture at time 0 and 24 hours, respectively, lane 3) Western-blot (anti-polyUb(K48)).

Taken together, the results in this chapter demonstrate that vinylphosphonothiolate electrophiles could be installed site-selectively on a cysteine residue in a single cysteine-containing ubiquitin mutant. The resulting electrophilic ubiquitin-vinylphosphonothiolate **72** could be conjugated to Cys-containing mutants of α-Synuclein and ubiquitin, generating non-hydrolysable conjugates, which were accepted as substrates for subsequent enzymatic ubiquitination. The herein described method thus enables the conjugation of two biomolecules containing single free cysteines in a site-selective manner.

In addition to using electrophilic phosphonothiolates for cysteine-selective protein-protein conjugations, a further goal in this thesis was to apply phosphonothiolates as linkers in antibody-drug conjugates (ADCs) (see next chapter 5).

5 Phosphonothiolate-linked antibody-drug conjugates

Responsibility assignment

The research described in this chapter was conceptualised by Prof. Dr. Christian P. R. Hackenberger and Dr. Marc-André Kasper and is based on previous work from our group on phosphonamidate-linked ADCs [228]. The author conducted the research described in this chapter with the following exceptions: The evaluation of the herein generated ADCs in cytotoxic assays was performed by Stefanie Boldt and Dr. Marcus Gerlach from the company *Tubulis*. The stability study of ADCs in rat serum was performed together with Dr. Marc-André Kasper.
Parts of the technology described in this chapter are substance of a pending patent application by Alice Leonie Baumann, Marc-André Kasper, Stephen Byrne, Jonas Helma, Heinrich Leonhardt, Tina Stoschek, Marcus Gerlach, Jonas Helma, Dominik Schumacher, Christian P. R. Hackenberger. Chemoselective Thiol-Conjugation with Alkene or Alkyne-Phosphonothiolates and -Phosphonates. PCT/EP2019/055509.

5.1 Background and Outline

ADCs have emerged as one of the most promising concepts for targeted cancer therapeutics [8]. In this concept, highly potent cytotoxic molecules are selectively delivered to cancer cells by means of cancer-targeting antibodies (Fig. 41A). As opposed to non-targeted cancer therapies, the ADC-approach delivers a higher concentration of the cytotoxic agent at the cancer site, while (in an ideal case) not affecting healthy tissue. To guarantee a safe and efficient delivery it is crucial that the cytotoxic agents are linked via stable, covalent bonds to the antibody in order to prevent premature release during blood circulation associated with off-target toxicity. Several of the recently approved ADCs are conjugated via cysteine residues [8]. The ADC Adcetris® (**83**) for instance is a maleimide-linked conjugate between the antibody brentuximab (targeting the CD30 receptor) and the construct Val-Cit-PAB-MMAE with an average drug-to-antibody ratio (DAR) of 4 (Fig. 41B) [277].

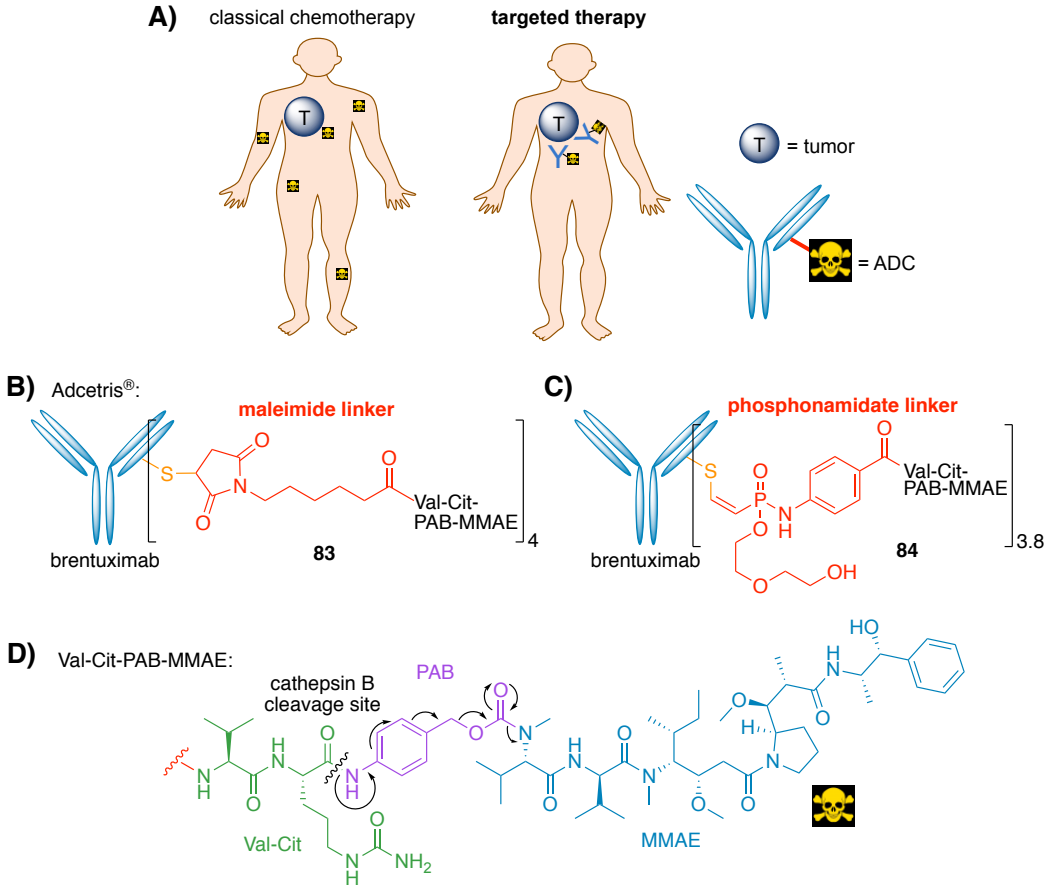

Fig. 41 A) Concept of targeted cancer-therapy using ADCs, B) Adcetris®, C) phosphonamidate-linked ADC, D) structure of Val-Cit-PAB-MMAE and cleavage mechanism.

The cleavable valin-citrulin-para-amino-benzyl (Val-Cit-PAB) linker enables the release of the toxin Monomethyl auristatin E (MMAE) after ADC internalisation into cells by means of cathepsin B cleavage and subsequent self-immolation of the para-amino-benzyl (PAB) linker (Fig. 41D). While Adcetris® shows good efficacy in treatments of refractory Hodgkin lymphoma [278] and systemic anaplastic large cell lymphoma [279], its stability during blood circulation is suboptimal. As demonstrated by Kasper

et al., thiol-exchange of the thiol-maleimide conjugate leads to significant transfer of toxins to serum proteins [228]. Tackling this issue, our group has recently introduced a stable analogue to Adcetris®, wherein the thiol-maleimide linkage is replaced with a thiol-phosphonamidate linkage (Fig. 41C) [228]. As opposed to Adcetris®, the phosphonamidate-linked ADC **84** proved to be stable in rat serum and showed excellent anti-tumour efficacy in mice models.
In this chapter, unsaturated ethynyl- and vinylphosphonothiolates are evaluated as alternative linkers for the generation of ADCs. Specifically, the antibody brentuximab was conjugated with ethynyl- and vinylphosphonothiolate Val-Cit-PAB-MMAE derivatives **47** and **48**, thereby making use of the earlier introduced reduction-alkylation protocol for the modification of IgG antibodies (scheme 50).

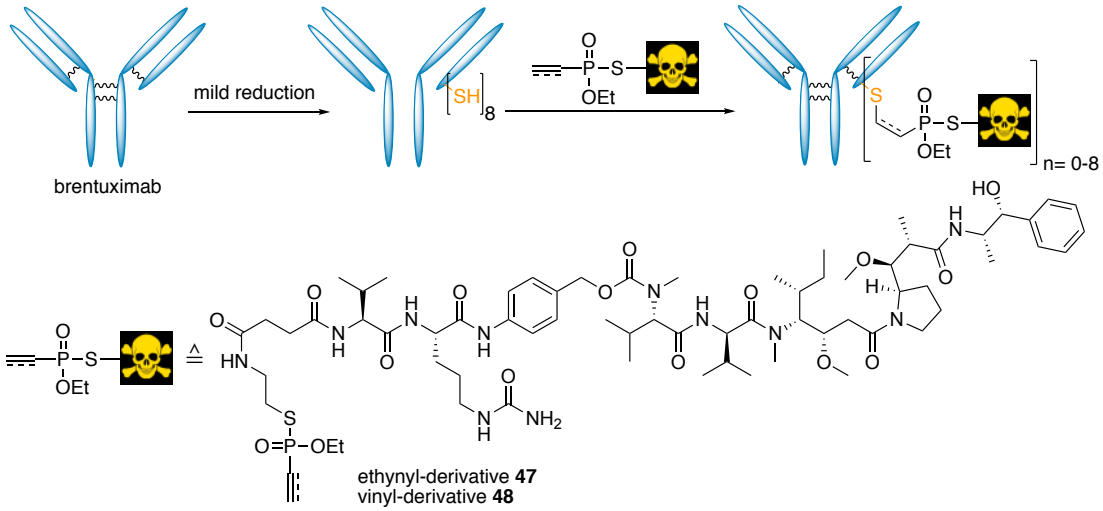

Scheme 50 General scheme for the generation of phosphonothiolate-linked ADCs via a reduction-alkylation protocol and structures of the employed phosphonothiolate-toxin derivatives.

5.2 Ethynylphosphonothiolates as linkers for ADC generation

First, ethynylphosphonothiolate-MMAE derivative **47** was employed in a screen to find conditions to generate an ADC with an average DAR of around 4 for direct comparison to Adcetris®. Therefore, brentuximab was reduced with DTT and reacted with different concentrations of ethynylphosphonothiolate-toxin **47** (scheme 51).

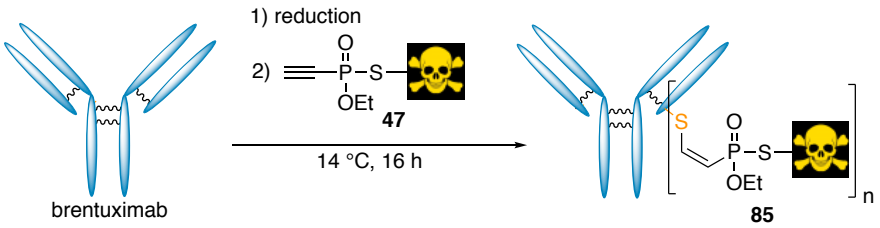

Scheme 51 General conditions for the generation of brentuximab-MMAE ADCs **85** with ethynylphosphonothiolate-toxin **47**. Reduction: 1000 eq. DTT, pH 8.0, 37 °C, 40 min. DTT was removed before the addition of **47** by gel filtration. The pH during modification and the number of eq. of **47** was varied according to table 2.

After modification, antibody samples were deglycosylated and reduced for analysis by middle-up LC-MS. The drug-to-antibody ratios were then estimated based on MS signal intensities. First, no modification was observed when employing an antibody concentration of 1 mg/mL and 25 eq. of **47** at pH 7.4 (table 2, entry 1). Increasing the antibody concentration to 5 mg/mL and using 4-50 eq. of **47** increased the modification efficiency and delivered average DARs between 1.14 and 6.63 (entries 2-6). Increasing the pH to 8.5 even allowed efficient labelling at lower antibody concentration (entry 7).

Table 2 Screening conditions for the modification of brentuximab with ethynylphosphonothiolate-MMAE derivative **47**.

Entry	Conc. antibody [mg/mL]	pH	eq. 47	DAR (n)
1	1	7.4	25	0
2	5	7.4	4	1.14
3	5	7.4	8.8	3.15
4	5	7.4	25	4.60
5	5	7.4	16	5.70
6	5	7.4	50	6.63
7	1	8.5	25	3.15

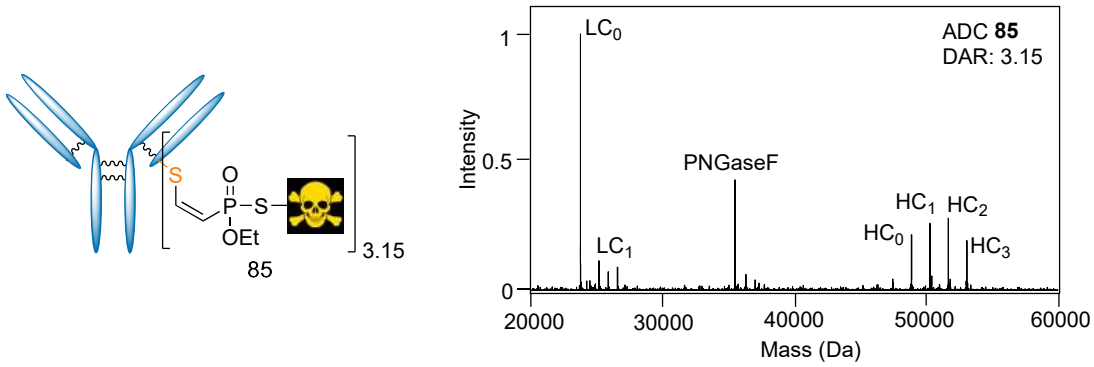

Fig. 42 Middle-up protein MS (deconvoluted spectrum) of purified ADC **85** after deglycosylation and reduction. PNGaseF: enzyme used for deglycosylation, LC= light chain, HC= heavy chain, subscripts indicate number of modifications. LC_0 exp: 23724, obs: 23725; LC_1 exp: 25122, obs: 25123; HC_0 exp: 48877, obs: 48877; HC_1 exp: 50275, obs: 50277; HC_2 exp: 51673, obs: 51677; HC_3 exp: 53071, obs: 53075 Da.

The purified ADC with a DAR of 3.15 (ADC **85**, see Fig. 42 for MS spectrum) was then evaluated in a cell-viability assay using a CD30-overexpressing cell line. Here, the phosphonothiolate-linked ADC **85** showed potent toxin- and CD-30-dependent cell killing (IC_{50} = 2.23 ± 0.17 pM), comparable to that of Adcetris® (IC_{50} = 2.24 ± 0.16 pM) (Fig. 43).

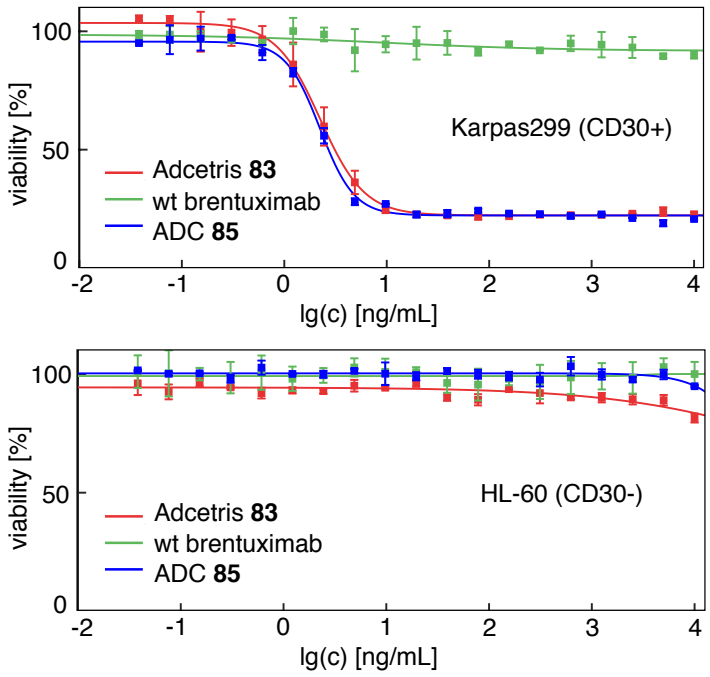

Fig. 43 Cell viability assays for ADC **85**, Adcetris® and wild-type brentuximab.

As for the stability of ADCs generated with ethynylphosphonothiolates however, it was found that the phosphorus-sulphur bond in the conjugates is prone to hydrolysis (scheme 52). For an ADC with a DAR of 5.70, approximately 25% of the toxins were lost after incubation for 16 hours in PBS at pH 7.4 and 25 °C (see Appendix Fig. 235 for MS spectra). At 37 °C, even 35% of the toxins were lost as a result of P-S bond hydrolysis, resulting in a DAR of 3.68. This finding was surprising since the small molecule ethynylphosphonothiolate conjugate **59** was found to be stable in neutral buffer (compare FRET-based stability assay in Fig. 29B). The local environment of the phosphonothiolate linkage however is different on ADCs than in the previously employed model and nucleophilic side chains of the antibody might catalyse and promote hydrolysis of the phosphonothiolate moiety.

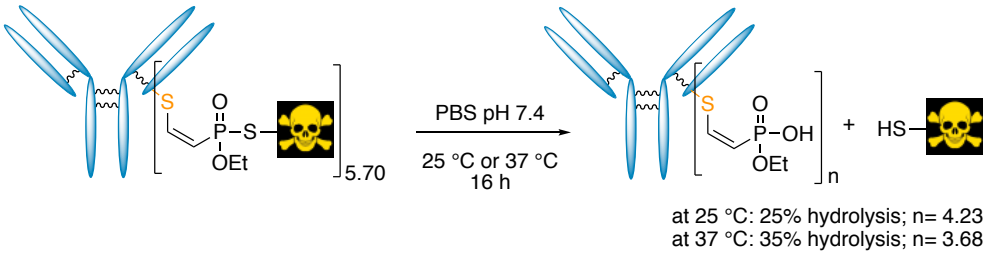

Scheme 52 Hydrolysis of ADC **85** in PBS pH 7.4 results in loss of the toxin.

5.3 Vinylphosphonothiolates as linkers for ADC generation

Assuming that ADCs generated with vinylphosphonothiolates would be more stable than the above described ADC **85**, we set out to generate the respective brentuximab-MMAE ADC employing vinylphosphonothiolate-toxin **48** (scheme 53).

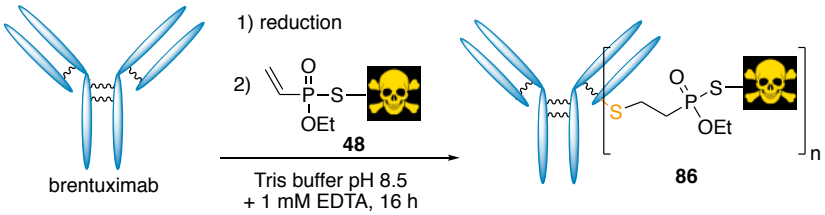

Scheme 53 General conditions for the generation of brentuximab-MMAE ADCs **86** with vinylphosphonothiolate-toxin **48**. The reduction protocol, the temperature and the number of eq. of **48** was varied according to table 3.

Using the modification conditions producing high DARs for the ethynyl-derivative **47** (5 mg/mL antibody, 50 eq. of toxin) only gave a DAR of 0.14 with 50 eq. of vinyl-derivative **48** at pH 8.5 (table 3, entry 1). The observation that antibody modification with **48** is less efficient compared to the ethynyl-derivative **47** was expected as our previous analysis showed that thiol additions to vinylphosphonothiolates are orders of magnitudes slower than to ethynylphosphonothiolates (compare Fig. 22). As a consequence of this slow modification rate, thiol addition to **48** competes with re-oxidation of the interchain cysteines. While additional DTT could in principle be added to restore accessible cysteines for modification with **48**, DTT itself would react with vinylphosphonothiolate in a thiol addition and thereby consume **48**. We therefore considered an alternative reduction protocol based on TCEP for further optimisation. As shown by Kasper *et al.* for the generation of phosphonamidate-linked ADCs, a one-pot reduction-alkylation protocol with TCEP enabled effective antibody modification while circumventing the removal of the reducing agent [228]. Although TCEP can also add to vinylphosphonothiolates, these by-products can be minimised by using only few eq. of TCEP. As shown by Bahou *et al.* [280] as well as our group [228], efficient reduction of the interchain disulfide bridges of IgG antibodies can be achieved with stoichiometric amounts of TCEP. Indeed, using 6 eq. of TCEP in one pot with only 10 eq. of vinylphosphonothiolate **48** gave a DAR of 0.12 (table 3, entry 2), which is comparable to the initially applied two-step DTT-reduction alkylation protocol with 50 eq. of **48** (entry 1). The average DAR could further be doubled to 0.24 by using 10 eq. TCEP and 10 eq. **48** (entry 3) and yet increased to 0.89 using 50 eq. **48** (entry 4). To reach yet higher average DARs though, the antibody concentration had to be increased to 12 mg/mL (entry 5 and 6). Under these concentrated conditions, **48** was not fully soluble when used with 50 eq. Increasing the temperature to 25 °C let to a slight improvement of the average DAR to 2.09 (entry 7). To reach the targeted DAR of 4, the temperature was further increased to 37 °C and additional portions of TCEP and **48** had to be added over the course of several days (entry 8). Not surprisingly, these harsh conditions led to the formation of antibody aggregates and the final DAR of the soluble fraction after purification by size-exclusion chromatography (SEC) was 3.10 (ADC **86**, see Fig. 44 for MS spectrum).

Table 3 Screening conditions for the generation of vinylphosphonothiolate-linked brentuximab-MMAE ADCs. [a]DAR=4.36 before purification; DAR=3.10 after purification by SEC. For reduction with DTT, 1000 eq. were used.

Entry	Conc. antibody [mg/mL]	Temp [°C]	DTT or eq. TCEP	eq. 48	DAR (n)
1	5	14	DTT	50	0.14
2	5	14	6	10	0.12
3	5	14	10	10	0.24
4	5	14	10	50	0.89
5	12	14	10	25	1.15
6	12	14	10	50	1.71
7	12	25	10	50	2.09
8	12	25/37	10+10+10+10	50+25	4.36 (3.10)[a]

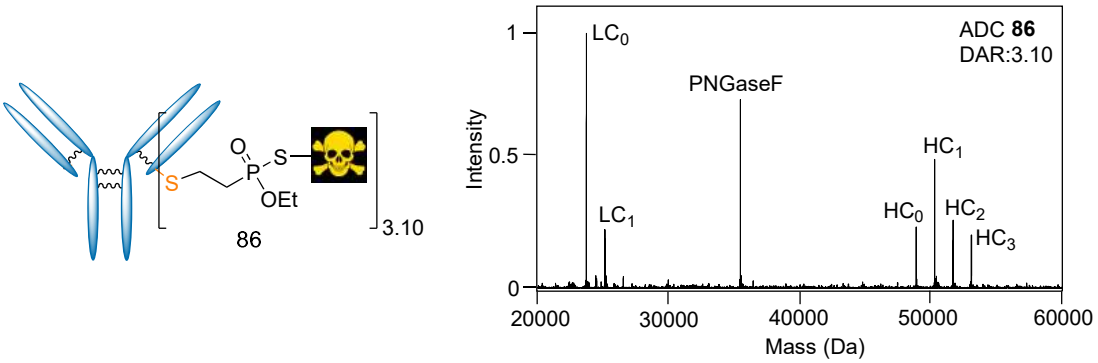

Fig. 44 Middle-up protein MS (deconvoluted spectrum) of purified ADC **86** after deglycosylation and reduction. PNGaseF: enzyme used for deglycosylation, LC= light chain, HC= heavy chain, subscripts indicate number of modifications, LC_0 exp: 23724, obs: 23724; LC_1 exp: 25124, obs: 25124; HC_0 exp: 48876, obs: 48876; HC_1 exp: 50276, obs: 50277; HC_2 exp: 51676, obs: 51677; HC_3 exp: 53076, obs: 53078 Da.

To our delight, the ADC **86** not only showed potent *in vitro* cell killing (ADC **86**: IC_{50} = 3.62 ± 0.26 pM, Adcetris®: IC_{50} = 4.15 ± 0.25 pM, Fig. 45) but also improved stability under neutral conditions compared to ADC **85**. In PBS at pH 7.4, no hydrolysis of ADC **86** was observed in neutral buffer.

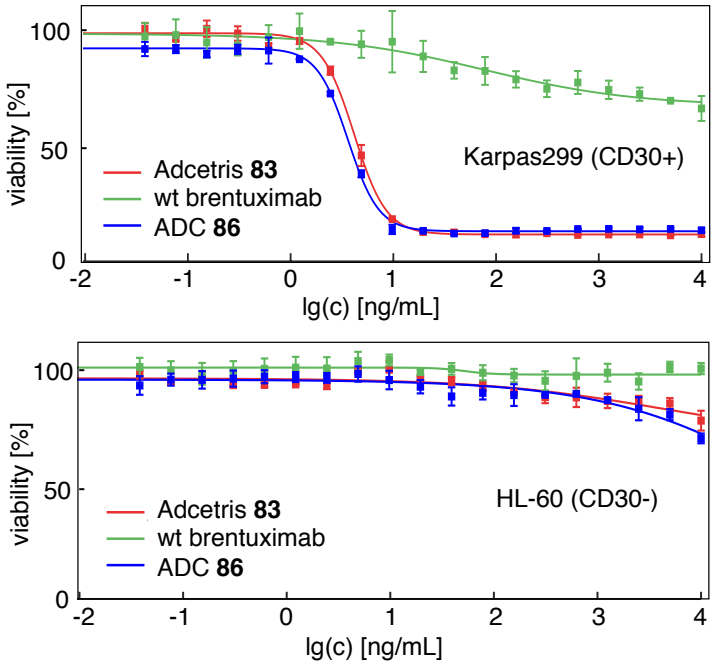

Fig. 45 Cell viability assays for ADC **86**, Adcetris® and wild-type brentuximab.

Moving on to more physiological relevant conditions, the stability of ADC **86** was next investigated in rat serum at 37 °C. Thereby, hydrolysis of the phosphorus-sulphur bond in the conjugate was observed, leading to approximately 30 % loss of the toxin after seven days incubation at 37 °C (see Experimental Fig. 100 for MS spectra). In comparison, under the same conditions, Adcetris® approximately lost 70% of toxin already after three days as shown by Kasper *et al.* in Ref. [228]. As for the phosphonamidate-linked ADC **83**, only 10% of toxin was lost after seven days.
Overall, these results indicate that unsaturated phosphonothiolate and in particular vinylphosphonothiolates do have potential as linkers in ADCs, however, both the stability of the conjugates as well as the modification efficiency remain to be optimised.
In comparison to ethynylphosphonamidates (see ADC **84** Fig. 41), unsaturated phosphonothiolates seem less suitable as linkers for the efficient generation of stable antibody-drug conjugates. The phosphonamidate-linked ADC **84** with a DAR of 3.8 could be obtained with as little 4 equivalents of *O*-diethylene glycol ethynylphosphonamidate as linker at pH 8.5 and an antibody concentration of 5 mg/mL [228]. Furthermore, this ADC proved to be highly stable under serum conditions [228].

6 Studying dynamic protein-protein interactions by photocrosslinking

Responsibility assignment
The research described in the first part of this chapter (subchapter 6.1) was conceptualised by Prof. Dr. Christian P. R. Hackenberger, Prof. Dr. Janine Kirstein, Manuel Iburg and the author. The author performed the herein described antibody-photocrosslinker conjugations, photocrosslinking experiments and SDS-PAGE/Western-blot analysis together with Manuel Iburg. In addition, Manuel Iburg expressed and purified the herein used proteins. The polyclonal antibodies were provided by the Kirstein group and were purified by Manuel Iburg.
The research described in the second part of this chapter (subchapter 6.4) was conceptualised by Prof. Dr. Christian P. R. Hackenberger and Prof. Dr. Yogesh Kulathu. Dr. Michal Nadler-Holly performed LC-MS/MS measurements and Christian Stieger analysed the MS/MS data.

6.1 Studying dynamic interactions of chaperone proteins: Background and Outline

An efficient protein homeostasis system is of fundamental importance for the survival of any cell and organism. Protein misfolding and aggregation are associated with many age onset diseases, including neurodegenerative diseases like Huntington's disease, Alzheimer's disease and Parkinson's disease [281]. In the view of that it is crucial that cells have the capacity to maintain protein homeostasis by either correctly refolding or eliminating aggregated proteins. As for the quality control of proteins in cells, molecular chaperones play a central role. Chaperones assist the *de novo* folding of proteins, prevent protein misfolding and aggregation and also facilitate the disaggregation and refolding of denatured proteins (Fig. 46) [282]. On the other hand, well-known processes for the elimination of damaged proteins are autophagy and the ubiquitin-proteasome system [283]. Rampelt *et al.* have recently identified a novel mechanism for aggregate-clearance in metazoans: a protein disaggregase that is formed by a triage chaperone complex HSP-110-HSP-70-HSP-40 [284] [6]. This chaperone complex has the ability to disaggregate and subsequently refold protein aggregates and thereby can restore the function of endogenous proteins that have been sequestered into aggregates.

[6] Molecular chaperones (also called heat-shock proteins (HSP)) are classified for *C. elegans* into the following families according to their molecular weight: small HSPs, HSP-40 (also called J- or DNJ-proteins), HSP-60, HSP-70 and HSP-90. HSP-110 is a member of the HSP-70 family.

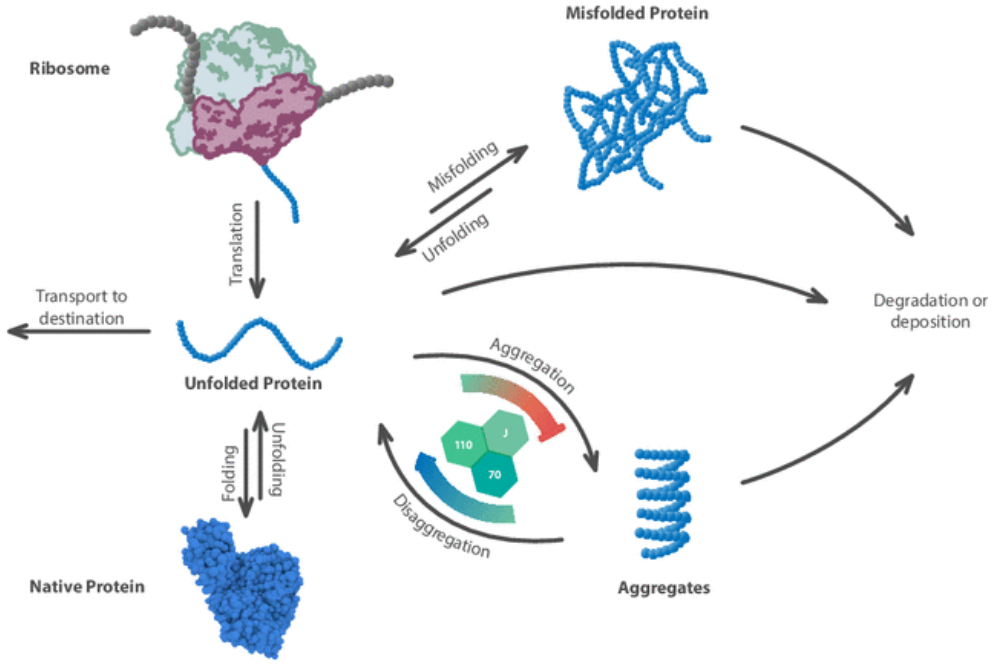

Fig. 46 A chaperone network maintains protein homeostasis. A protein complex composed of chaperones HSP-110, HSP-70 and HSP-40 (J-proteins) facilitates the disaggregation of aggregated proteins into their native form. *This figure has been kindly provided by Prof. Dr. Janine Kirstein.*

To date, only little is known about the composition of the three chaperone families within the disaggregase complex and the initial substrate recognition. Metazoans like *C. elegans* encode for only one HSP-110 protein but for ten different HSP-70 and about 30 HSP-40 chaperones. Any combination of these three chaperone families has in principal the potential to form a specific disaggregase complex. Nillegoda *et al.* have for instance identified specific complexes consisting of HSP-110, HSP-1[7] and DNJ-12 or DNJ-13 that have the ability to disaggregate preformed amorphous protein aggregates [285]. And a different complex composed of HSP-110, HSP-1 and DNJ-13 can inhibit the formation of HttExon1Q48 amyloid fibrils [286]. The identification of yet further specific chaperone complexes in an efficient manner has turned out to be an experimental challenge. Given the large number of possible chaperone combinations, individual testing with purified chaperone proteins was regarded as prohibitively laborious. On the other hand, conventional co-immunoprecipitations analyses will miss out on a large number of potential interaction partners as the interaction with protein substrates and chaperone interaction partners is too dynamic. To address this challenge in collaboration with the Kirstein group, we proposed that the interactions between chaperones in active disaggregase complexes as well as the interaction with specific aggregated substrate proteins could be identified by means of photocrosslinking. As demonstrated for other dynamic protein interactions, photocrosslinking is a powerful method to covalently link transiently interacting proteins, thereby enabling pull-downs under denaturing conditions and subsequent identification of the isolated proteins by means of LC-MS/MS analysis [287].

[7] a member of the HSP-70 family

Here, we wanted to conjugate photocrosslinkers (by means of P(V)-electrophiles) to polyclonal antibodies, which the Kirstein group had generated against a number of individual chaperone proteins from immunising rabbits [286]. These antibody-photocrosslinker conjugates would then be subjected to lysates of *C. elegans*, where they would bind specifically to their target chaperone proteins. Upon irradiation with UV light, any adjacent, interacting proteins would be covalently crosslinked, thus enabling the isolation of stable protein complexes and subsequent identification of chaperone-interacting proteins (Fig. 47). We expected that these antibody-crosslinker tools would eventually enable us to study specific chaperone-protein interactions in neurodegenerative disease models of *C. elegans*.

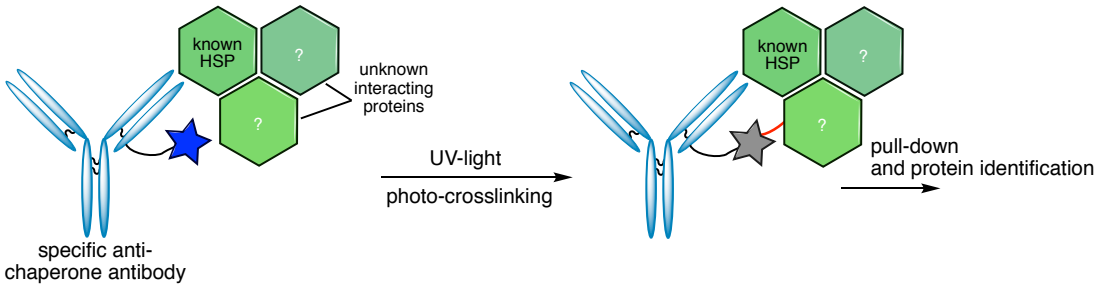

Fig. 47 Envisioned approach to capture interacting proteins of specific chaperones by means of light-induced covalent crosslinking.

Given that the position of the target chaperones with respect to their protein interaction partners is dynamic, the crosslinkers were designed to be long and flexible in order to reach possible interacting proteins within a large space. Therefore, PEG-spacers were incorporated between the antibody attachment site and the photoreactive moieties. In addition, biotin was introduced in the crosslinker for detection and pull-down purpose (see Fig. 48 for structure). Trifluoromethyl-aryldiazirine [288] and 2-phenyl-5-carboxytetrazole [289] were employed as photo-reactive groups (scheme 54). The choice fell for these two types of photocrosslinkers as they have proven to be efficient in many reported applications to crosslink dynamic protein interactions [287]. The activation of diazirines with UV-light (typically at 350-365 nm) generates reactive carbenes, which can insert into S-H, N-H, O-H, as well as C-H bonds [290] (scheme 54A). We considered the unspecific reactivity profile of diazirines to be an advantage for the proposed application of crosslinking chaperone interacting proteins, as these types of bonds are ubiquitous in proteins. Crosslinking would thus be independent of specific amino acid residues in the protein to be captured, thereby increasing the chance of successful crosslinking events. Nevertheless, carbenes are very short-lived reactive species and are prone to be quenched by water, hampering crosslinking yields [291]. In this regard, 2-aryl-5-carboxytetrazole photocrosslinkers proved to be attractive alternatives to diazirines. As recently demonstrated by Herner *et al.*, photocrosslinking with 2-aryl-5-carboxytetrazoles can be more efficient compared to diazirine [289].

Upon irradiation of 2-aryl-5-carboxytetrazoles (typically at 302 nm), a carboxy-nitrile imine is formed, which is more stable and thus more long-lived than carbenes, which can result in higher photocrosslinking yields [292] (scheme 54B). A distinct difference to carbenes is that nitrile imines react selectively with nucleophiles. On proteins, stable adducts are formed with carboxylate residues of aspartic and glutamic acids [289]. Attack of carboxylates to carboxy nitrile imines, followed by a 1,4-acyl shift, gives rise to stable photo-adducts. Although nitrile imines can also react with thiols [293], the resulting adduct is less stable as it can not undergo an acyl shift. Thus, other than diazirines, 2-aryl-5-carboxytetrazoles have a less broad reactivity profile, which might be a disadvantage.

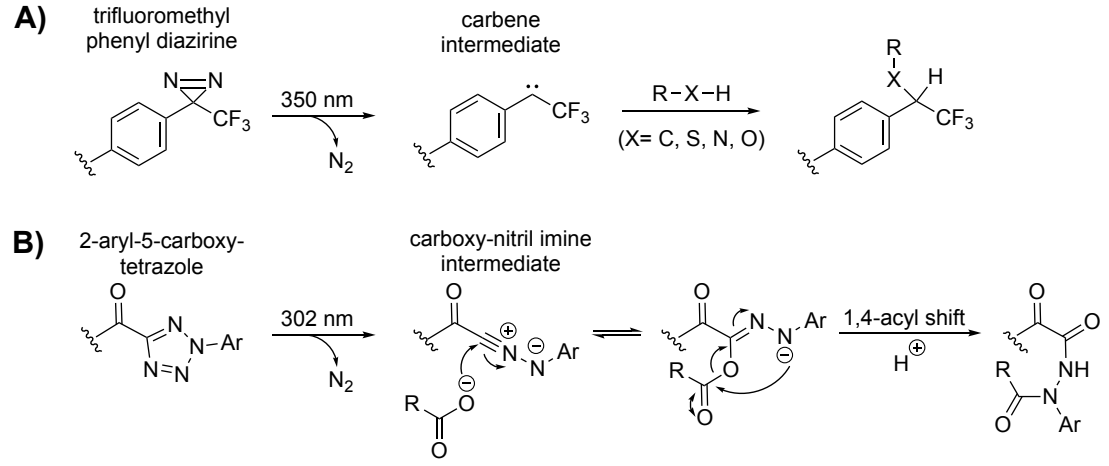

Scheme 54 Proposed photocrosslinking mechanisms for A) trifluoromethyl-aryldiazirine and B) 2-aryl-5-carboxytetrazole.

6.2 Modification of anti-chaperone antibodies with photocrosslinkers

We started our investigations by generating photocrosslinker conjugates of chaperone-specific polyclonal antibodies, and in particular with anti-HSP-1 and anti-DNJ-12 antibodies (Fig. 48 and Fig. 49, respectively). The crosslinker molecules were synthesised by means of solid-phase peptide synthesis (SPPS) (see Experimental chapter 8.5.1). To start with, four diethylene-glycol units were incorporated between the P(V)-electrophile and the photo-reactive head-groups. These constructs were then conjugated to the anti-chaperone antibodies using the previously described reduction-alkylation protocol with DTT. As can be seen in the Western-blots in Fig. 48B and Fig. 49B, both anti-HSP-1 and anti-DNJ-12 antibodies were successfully modified with the photocrosslinker molecules.

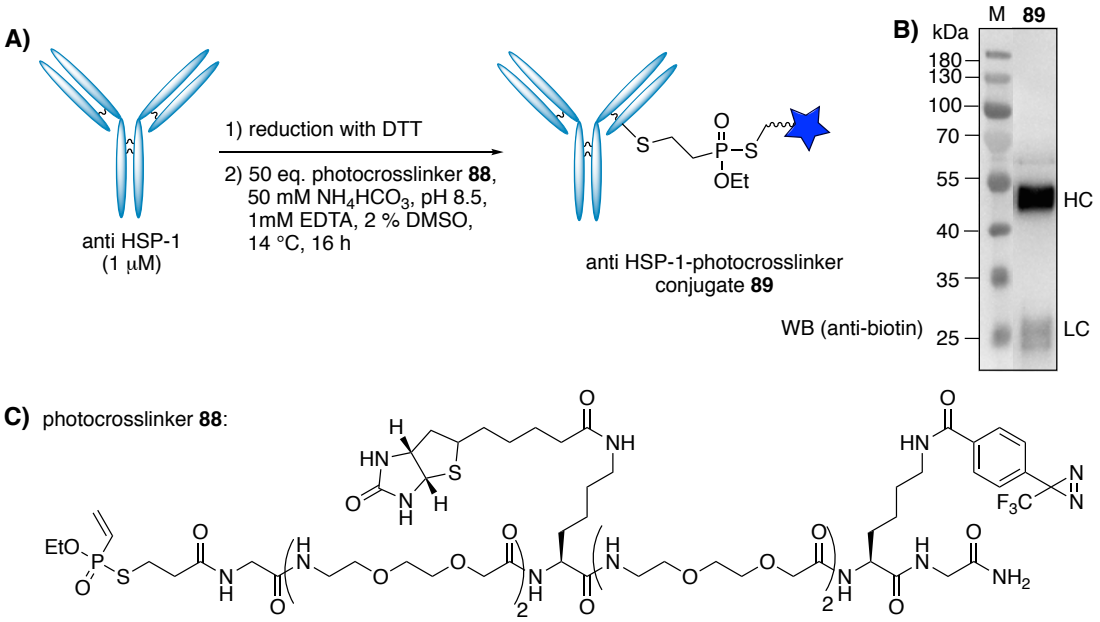

Fig. 48 Modification of polyclonal anti-HSP-1 antibody with photocrosslinker **88**. A) Modification conditions, B) Western blot (anti-biotin) of the modified antibody. HC: heavy chain, LC: light chain, M: marker C) Structure of the photocrosslinker **88**.

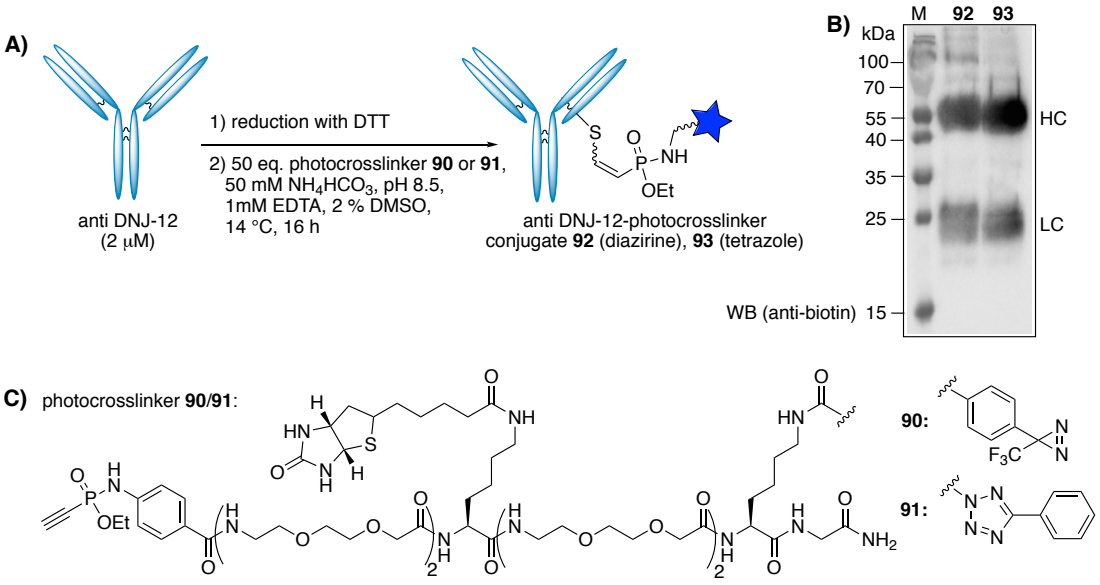

Fig. 49 Modification of polyclonal anti-DNJ-12 antibody with diazirine- and tetrazole-photocrosslinkers **90** and **91**, respectively. A) Modification conditions, B) Western blot (anti-biotin) of the modified antibodies (**90**=diazirine derivative, **91**=tetrazole derivative). HC: heavy chain, LC: light chain, M: marker C) Structure of the photocrosslinkers **90** and **91**.

6.3 Photocrosslinking

With the generated antibody-photocrosslinker conjugates **89**, **92** and **93** we first wanted to see whether those conjugates would have the ability to crosslink their primary target proteins HSP-1 or DNJ-12, respectively. Therefore, the anti-DNJ-12-photocrosslinker conjugates **92**/**93** (diazirine and tetrazole derivatives, respectively) were mixed separately with purified DNJ-12 protein and the mixtures were irradiated with UV-light (Fig. 50A).

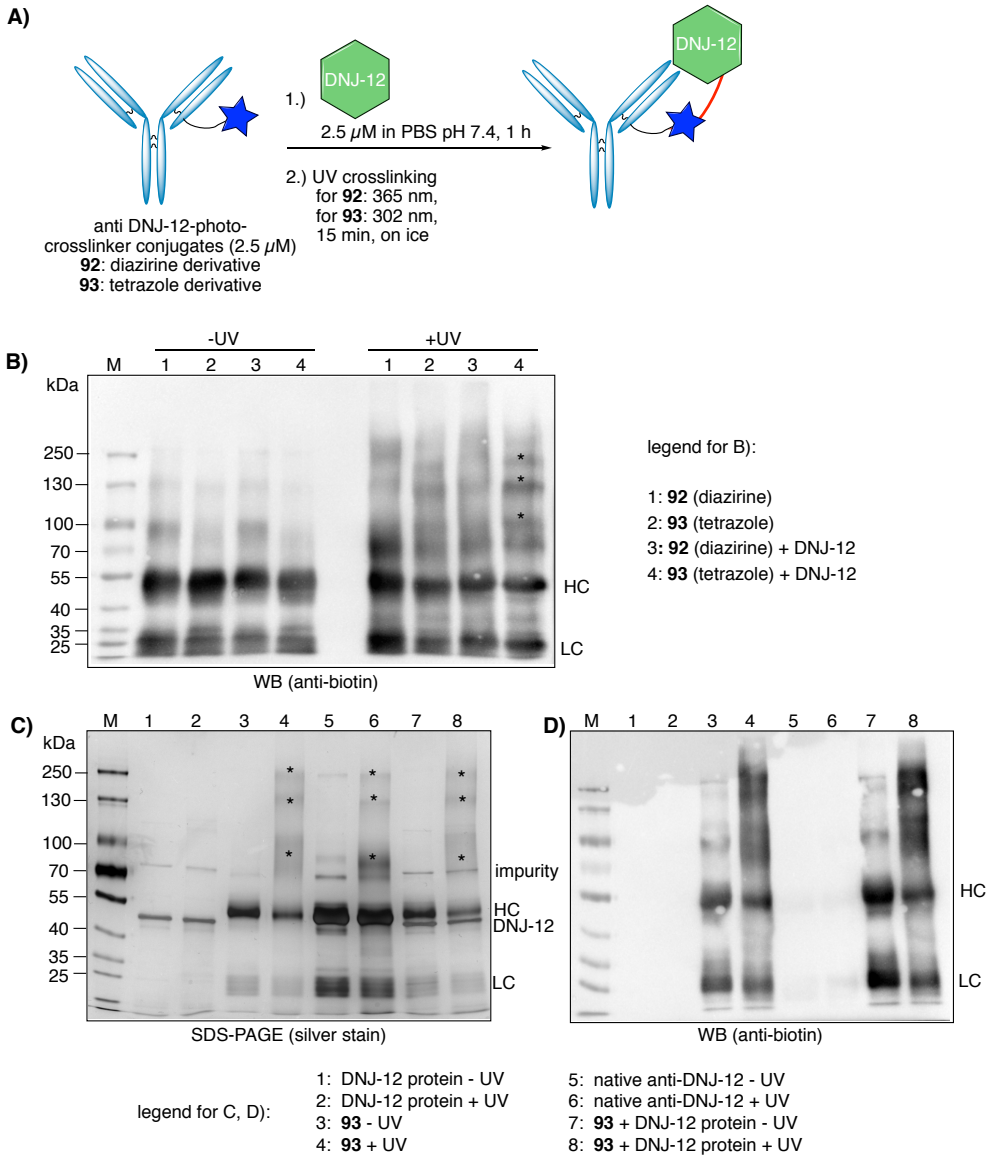

Fig. 50 Attempt to crosslink DNJ-12 protein. A) Reaction conditions, B) Comparison between photocrosslinker **92** and **93** C-D) Additional control reactions for conjugate **93**.

If crosslinking to DNJ-12 occurs, the respective covalent conjugates between either the heavy or the light chain of the antibody and DNJ-12 were expected to be seen by a band shift in SDS-PAGE/Western-blot analysis. While some higher molecular species were detected for both conjugates compared to non-irradiated controls (Fig. 50B), they did not seem to originate from crosslinking to DNJ-12 but rather be a consequence of UV-

induced aggregation of the antibodies, themselves. The same species (indicated with *) were also observed in the absence of DNJ-12 (Fig. 50C, lane 4), as well as in the control of the native DNJ-12 antibody carrying no photocrosslinker (Fig. 50C, lane 6). Similar observations were also made in the analogous photocrosslinking experiment with the anti-HSP-1-photocrosslinker conjugate **89** (Fig. 51). These experiments were repeated under various conditions, screening different antibody and chaperone concentrations, temperatures, UV-irradiation times and intensities. Moreover, shorter as well as longer crosslinkers were tested, by varying the number of diethyleneglycol units between two and six. In none of these trials though was specific crosslinking observed.

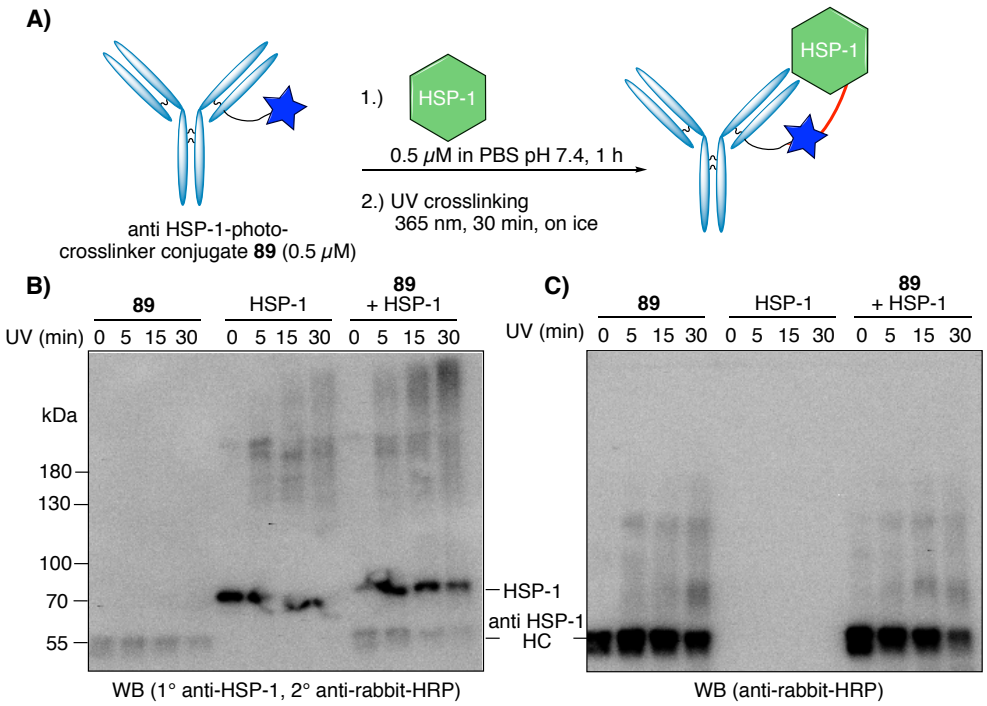

Fig. 51 Attempt to crosslink HSP-1 protein. A) Reaction conditions, B) Western-blot against HSP-1, C) Western-blot against anti-HSP-1.

Although crosslinking to the primary targets was not successful, it still remained possible that crosslinking to secondary, interacting proteins would work. To test this, the experiment with anti-HSP-1-photocrosslinker conjugate **89** was repeated in the presence of the chaperone DNJ-13, which is a known interaction partner of HSP-1 (Fig. 52). Denatured luciferase was added to simulate physiological conditions. After irradiation with UV light, the protein mixture was subjected to a pull-down (strepatavidin) to enrich for crosslinked species. Crosslinks between DNJ-13 and either the light or the heavy chain of **89** would be expected between 55-90 kDa (DNJ-13 plus light or heavy chain of the antibody). However, no distinct bands of similar molecular weight could be detected by SDS-PAGE/Western-blot analysis (Fig. 52B).

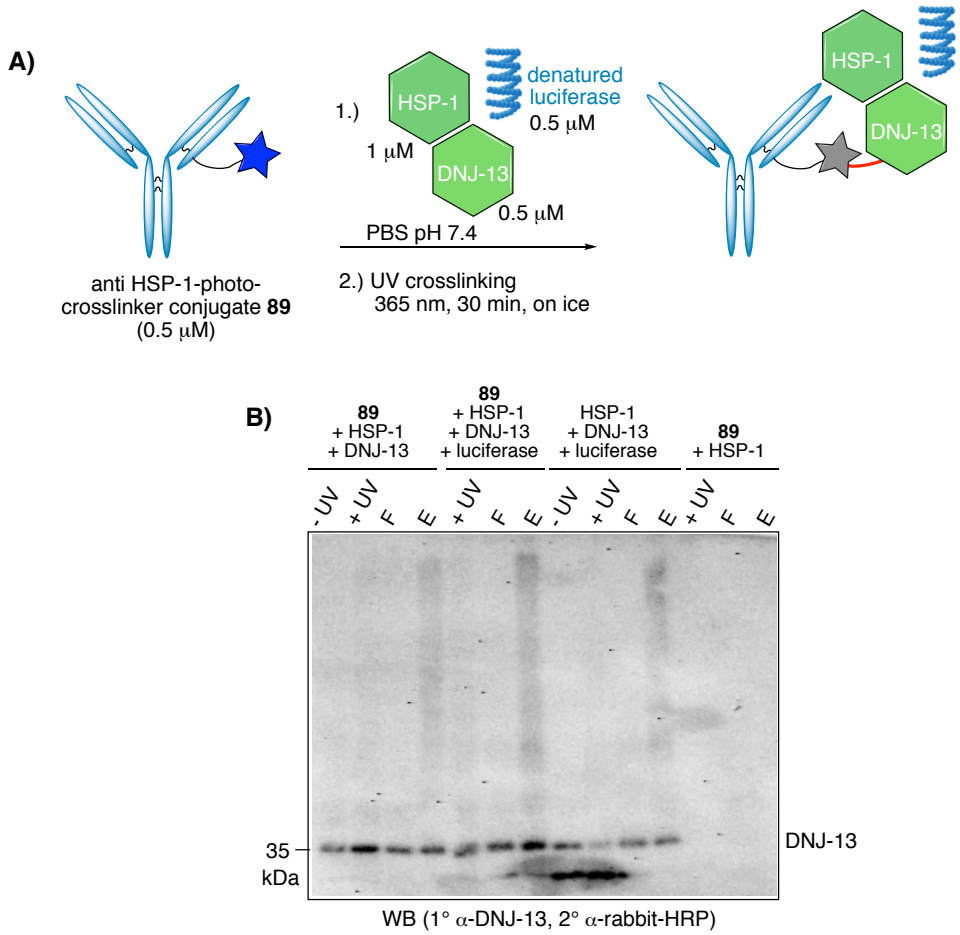

Fig. 52 A) Attempt to crosslink DNJ-13 with antibody-crosslinker conjugate **89** mediated by HSP-1 and denatured luciferase. B) Western blot against DNJ-13, detected by anti-rabbit-HRP (chemiluminescence). F: flow-through after pull-down, E: elution from streptavidin-coated beads.

The fact that no crosslinking of chaperone proteins was observed in any of these preliminary test experiments pointed towards a general problem of this strategy. Next to the observed UV-induced aggregation of antibodies, the other main problem seemed to be lacking pre-organisation of the photocrosslinker with respect to the proteins to be captured. The initial idea was to compensate for the unknown binding architectures between the chaperone proteins and their substrates by using long and flexible crosslinkers of different length by varying the number of PEG groups inside the linker. However, these molecules will not adopt a linear conformation in water but rather fold up in an unpredictable way. This makes it virtually impossible to predict which space the photoreactive moiety covers in solution and if it could in principle reach the desired protein, especially given that the position of the proteins to be captured is a further unknown parameter, also because polyclonal antibodies were used here. Lacking pre-organisation and hence proximity of the photocrosslinker and the target proteins decreases the probability of specific crosslinking events. More likely outcomes are inactivation of the short-lived reactive intermediates by other surrounding molecules such as water or by the antibody itself (self-crosslinking) (Fig. 53).

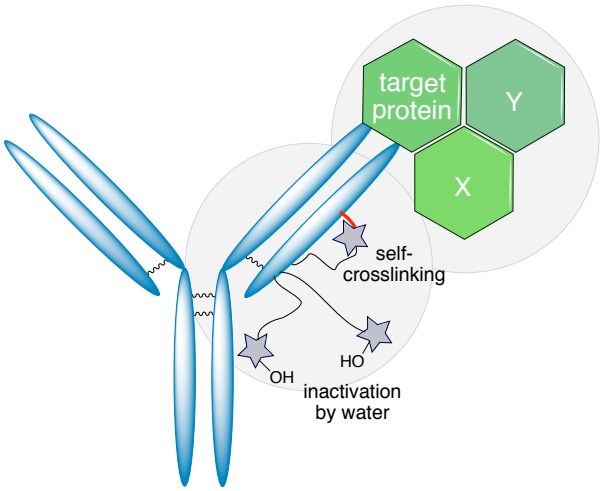

Fig. 53 The main problem identified with the antibody-photocrosslinker approach is lacking pre-organisation between the photocrosslinkers and the proteins to be captured. As a consequence, inactivation of photocrosslinkers by water or self-crosslinking are more likely events.

Another complication was the characterisation of the antibody-photocrosslinker conjugates. At the time of these experiments, intact-protein analysis was not available for us and the antibody-photocrosslinker conjugates were only characterised by means of anti-biotin Western blots. Thereby, the presence of the photocrosslinker could only be indirectly detected via the biotin included in the linker. The integrity of the photocrosslinker moieties as well as the number of photocrosslinkers attached to the antibody remained unknown. Even if MS analysis was available, the interpretation of the spectra might have been complicated by the fact that polyclonal antibodies were used here.
An alternative, more promising approach for the system we tried to study here, could be to apply a global crosslinking method by using for instance lysine-reactive DSSO crosslinkers [294].

Still, we were convinced that photocrosslinking is in principle a powerful tool to study dynamic protein-protein interactions, in particular for better defined systems that allow more rational and controlled placing of the photocrosslinker with respect to the targets to be captured. Motivated by these thoughts, we therefore turned our attention to study different kinds of dynamic protein-protein interactions and in particular specific interactions between deubiquitinating enzymes and their substrates (see next chapter, 6.4).

6.4 Studying substrate specificity of DUBs: Background and Outline

The post-translational modification of proteins with ubiquitin controls almost every process in cells, in particular through regulation of protein levels by providing proteasomal and lysosomal targeting signals and by controlling signalling networks [295, 296, 297]. Ubiquitins are commonly attached to substrate proteins at lysine residues catalysed by a complex enzyme machinery involving ubiquitin ligases E1, E2 and E3. These enzymes install ubiquitin either as a single moiety or in the form of polymeric chains, in which ubiquitin molecules are connected through specific isopeptide bonds via internal lysine residues (Lys6, Lys11, Lys27, Lys29, Lys33, Lys48 and Lys63) and their carboxyl terminus [298].
On the other hand, to dynamically regulate this process, there are around 100 deubiquitinating enzymes (DUBs) that revert ubiquitination by means of hydrolysis of the isopeptide bonds within ubiquitins as well as between ubiquitins and their substrate proteins (Fig. 54) [299, 297]. The combination of these two dynamic processes gives rise to distinct "ubiquitin codes", which are tightly coupled to the regulation of protein levels [261]. Malfunction of this complex system have been implicated with various diseases ranging from cancer to neurological disorders [261, 300, 301].

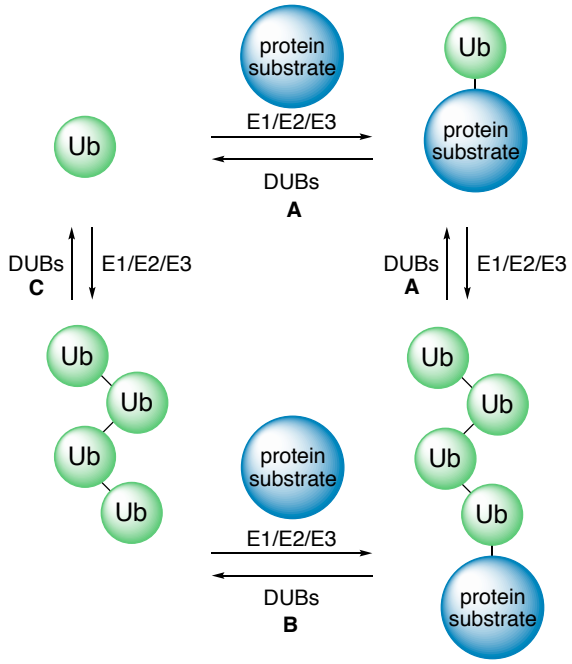

Fig. 54 Functions of DUBs in the ubiquitin pathway. A: Editing or rescue of ubiquitin conjugates, B: recycling of ubiquitin or ubiquitin oligomers from ubiquitin-protein conjugates, C: disassembly of unanchored ubiquitin oligomers. *The graph was adapted from Ref. [299].*

One of the predominant research question towards understanding the ubiquitin code is to decipher substrate specificity of DUBs. DUB-specificity can be mediated by unique protein-protein interaction domains [302] or through recognition of specific topologies of ubiquitin chains [303, 304]. To date, around 100 different DUBs, the majority of which are cysteine proteases, have been identified and are grouped into seven distinct families [297]. Although a few substrates have been identified for some DUBs in these families, the specificity of most DUBs is still poorly defined. Given that most DUBs are cysteine proteases, they are well suited for activity-based studies [274, 305]. To that end, non-hydrolysable, synthetic ubiquitin probes are typically equipped with electrophilic handles that allow covalent trapping of the active site cysteine of DUBs. This approach facilitates pull-down and subsequent identification of the covalently-linked conjugates. In this chapter, we thought to investigate the substrate specificity from the other side by employing DUBs themselves as reactive probes. Specifically, we set out to equip DUBs with photoreactive crosslinkers through conjugation with vinylphosphonothiolates (Fig. 55). In a next step, these DUB-photocrosslinker conjugates would then be subjected to substrate proteins and irradiation with UV-light would trigger covalent crosslinking between the DUBs and their interacting substrates (Fig. 55B).

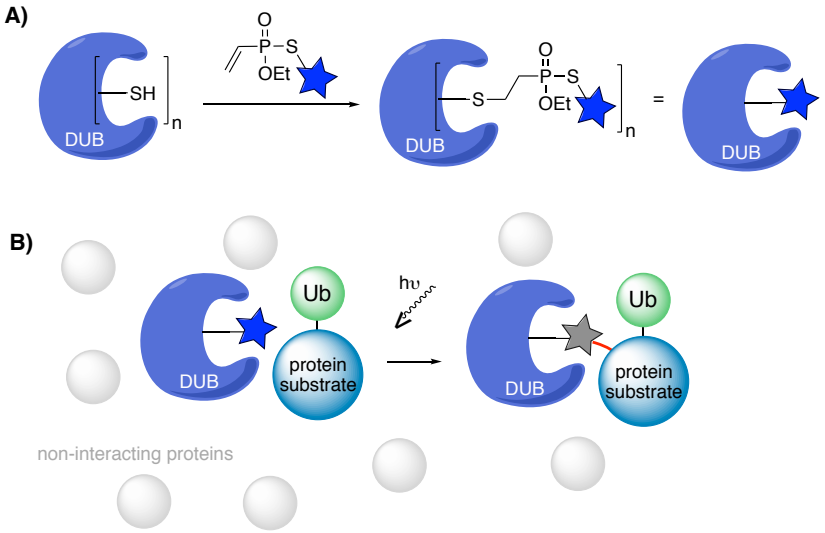

Fig. 55 Envisioned approach to study substrate specificities of DUBs in this thesis. A) Modification of DUBs with photoreactive crosslinkers by means of cysteine-selective conjugation with vinylphosphonothiolates, B) photocrosslinking specifically interacting ubiquitinated substrate proteins within complex environments.

In first proof-of-concept experiments, the cysteine protease DUBs USP2CD and UCHL3 were employed. Next to the active site cysteine, both of these DUBs contain several additional cysteines. It remained to evaluate experimentally, which of those cysteines were addressable for the conjugation with the photocrosslinkers and importantly, how the positioning of the photocrosslinker would influence the outcome of the photocrosslinking experiment.

6.5 Modification of DUBs with photocrosslinkers

To begin, the two DUBs USP2CD and UCHL3 were each conjugated to two different photocrosslinkers via vinylphosphonothiolates. Crosslinker **54** carries a diazirine photoreactive group and crosslinker **55** a *N*-methylpyrroletetrazole (mPyT) as depicted in Fig. 56. The latter type of photocrosslinker, developed by Tian *et al.*, is an improved version of the phenyltetrazole derivative used in chapter 6.1. After conjugation, the DUBs were digested and subjected to MS/MS in order to analyse which cysteine residues carried the photocrosslinkers. Crystal structures of both DUBs in complex with ubiquitin are depicted in Fig. 56 and Fig. 57, respectively and the cysteines that were found to be modified with the photocrosslinkers (based on the MS/MS analysis) are marked therein. In the USP2CD-photocrosslinker conjugate **94**, the vinylphosphonothiolate photocrosslinker **54** modified cysteines C476 and C477 (Fig. 56B). Interestingly, for the same DUB, modification with photocrosslinker **55** was found additionally on the cysteines C458 and C276, the latter of which is the active site cysteine (highlighted in magenta).

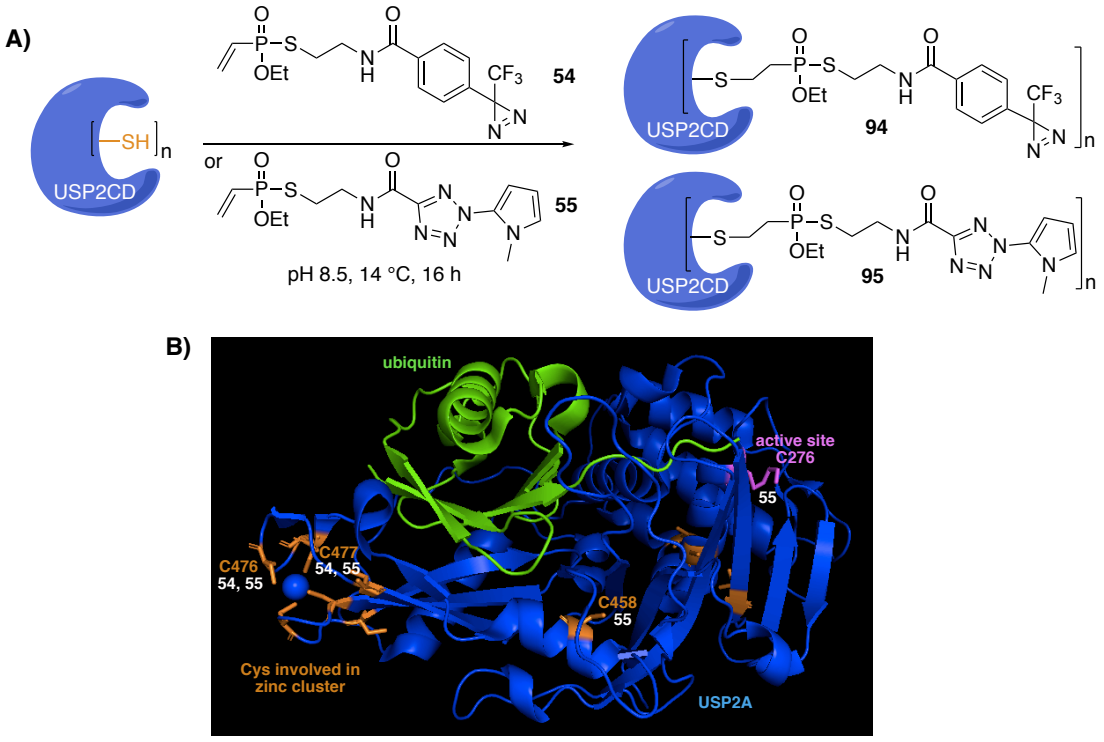

Fig. 56 A) Conjugation of the DUB USP2CD (25 μM) with photocrosslinkers **54** and **55** (625 μM). B) Crystal structure of USP2A (USP2CD) (blue) in complex with ubiquitin (green), PDB entry: 3NHE. Cysteine residues are highlighted in orange and magenta (active site cysteine). The cysteines modified with the photocrosslinkers are labelled with the respective numbers **54** and **55**.

As for UCHL3, modifications with photocrosslinkers **54** and **55** were found both at the active site cysteine C95 (highlighted in magenta, Fig. 57B) and in addition at the cysteine C209.

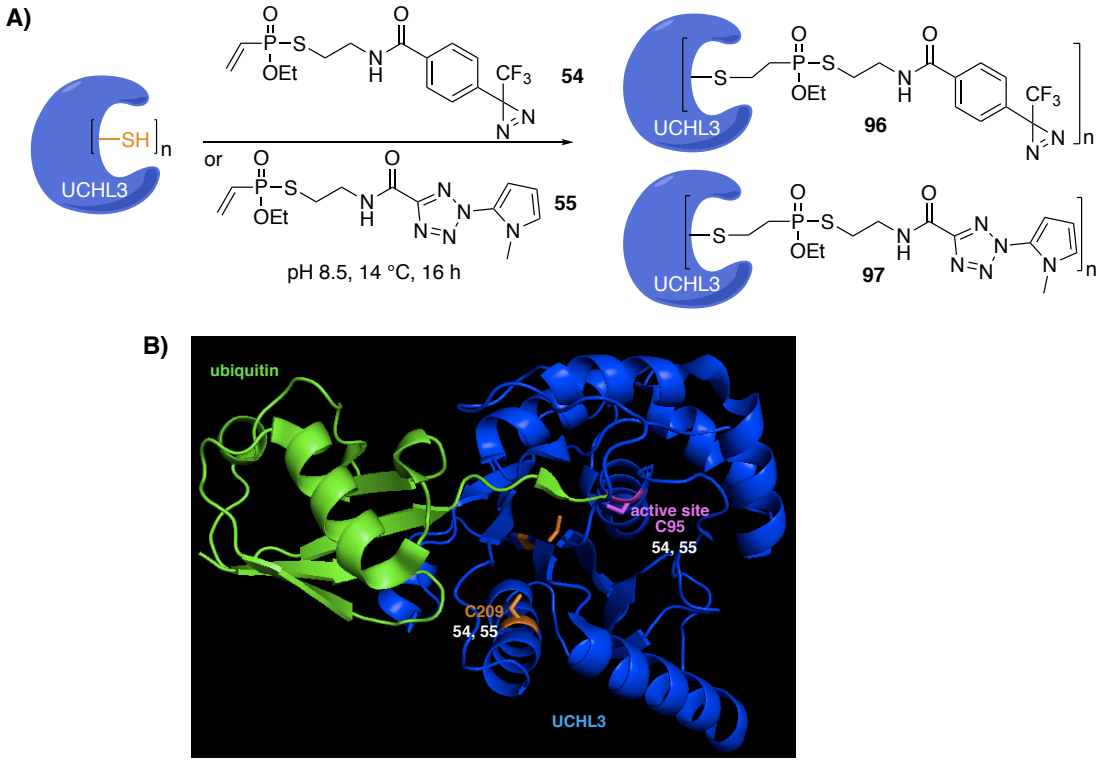

Fig. 57 A) Conjugation of the DUB UCHL3 (25 μM) with photocrosslinkers **54** and **55** (625 μM). B) Crystal structure of UCHL3 (blue) in complex with a ubiquitin-VME probe (green), PDB entry: 1XD3. Cysteine residues are highlighted in orange and magenta (active site cysteine). The cysteines modified with the photocrosslinkers are labelled with the respective numbers **54** and **55**.

6.6 Photocrosslinking

Next, it was evaluated whether the modified DUB-photocrosslinker conjugates **94-97** retained their ability to interact with ubiquitin. First, USP2CD-photocrosslinker conjugates **94** (diazirine head group) and **95** (mPyT head group) were mixed with wild-type ubiquitin and irradiated with UV-light (Fig. 58A). In control reactions, GFP was added to check for specificity. As can be seen in the gel in Fig. 58B, covalent crosslinks between USP2CD and wild-type ubiquitin formed for both conjugates and the crosslinking to ubiquitin was specific in the presence of GFP. This experiment proved that it was possible to covalently and specifically crosslink ubiquitin with the DUB-photocrosslinker conjugate. It was further observed that the crosslinking with the tetrazole crosslinker (conjugate **95**) was approximately twice as efficient compared to the diazirine crosslinker (conjugate **95**).

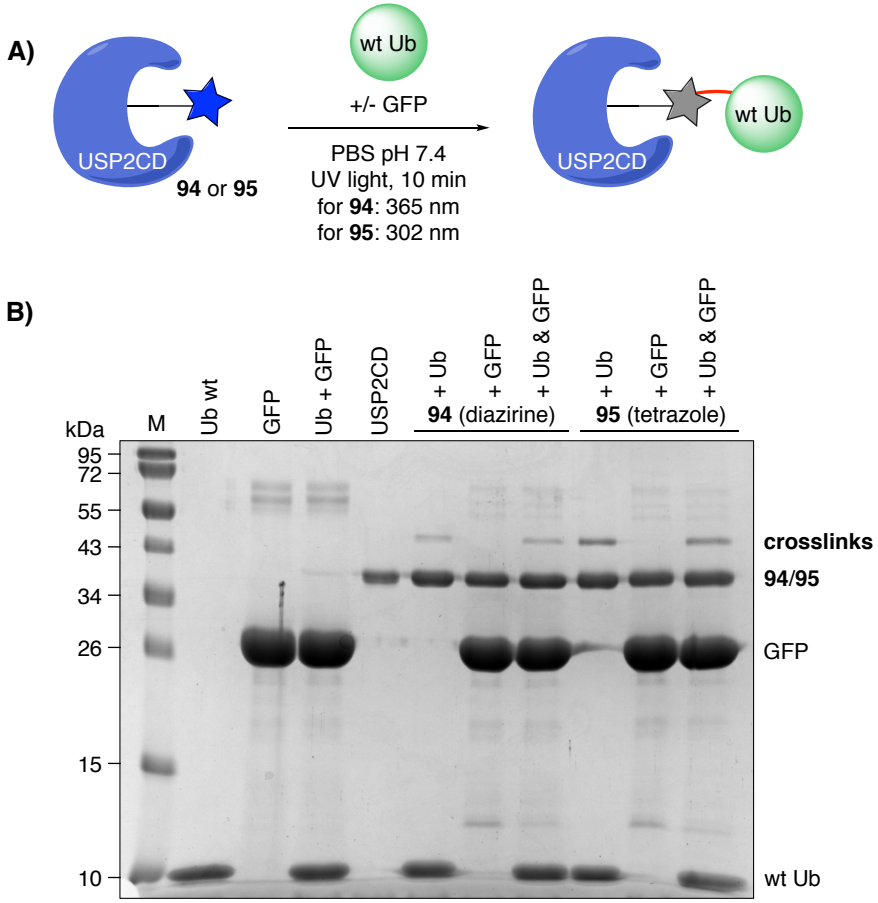

Fig. 58 A) Photocrosslinking between USP2CD-photocrosslinker conjugates **94** & **95** (each 6 μM) with wild-type ubiquitin (wt Ub, 25 μM) alone or in the presence of GFP (25 μM). B) SDS-PAGE (Coomassie). All samples were irradiated with UV-light.

The analogous experiment with UCHL3-photocrosslinker conjugates **96** & **97** (Fig. 59A) also resulted in covalent DUB-ubiquitin crosslinks and again, the photocrosslinking was more efficient with the tetrazole derivative (conjugate **97**, Fig. 59B).

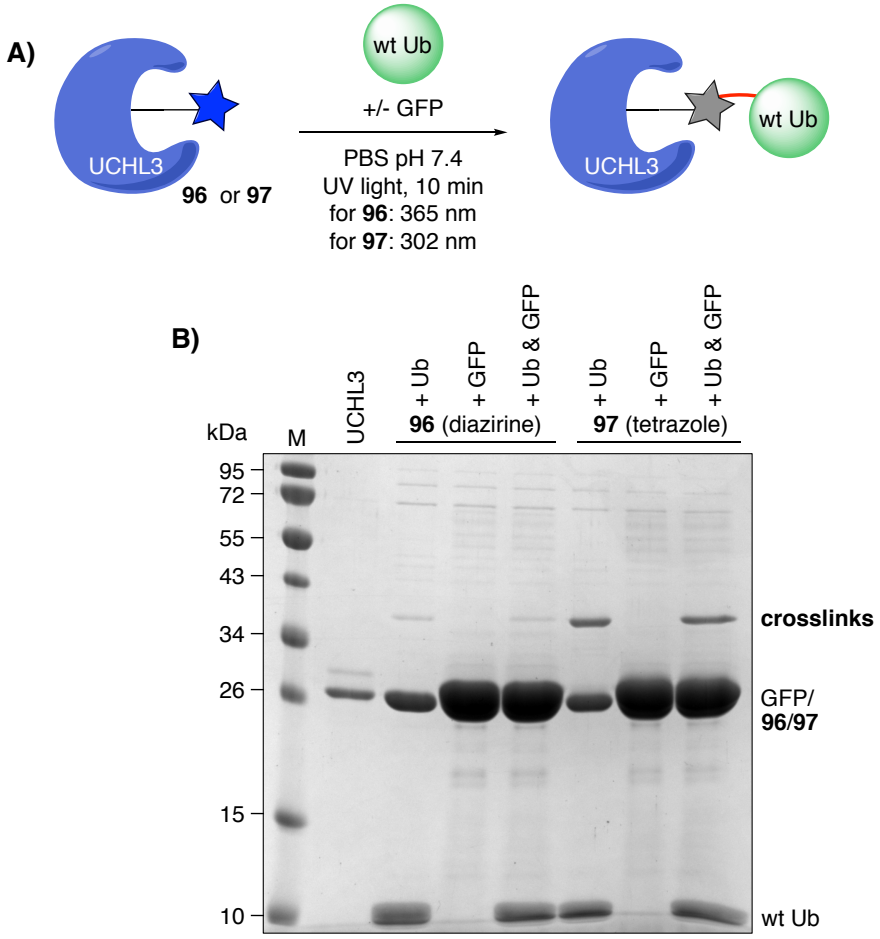

Fig. 59 A) Photocrosslinking between UCHL3-photocrosslinker conjugates **96** & **97** (each 6 μM) with wild-type ubiquitin (25 μM) alone or in the presence of GFP (25 μM). B) SDS-PAGE (Coomassie). All samples were irradiated with UV-light.

Based on these promising results, photocrosslinking was next attempted with diubiquitin (DiUb) substrates and in particular with K48- and K63-linked DiUb (Fig. 60A). As for USP-DUBs it has been shown that they can recognise both types of linkages [306]. UCHL3 on the other hand interacts preferentially with K27-linked ubiquitins and to a much lesser extent with other DiUbs as demonstrated by Zhang *et al.* [307]. As shown in Fig. 60B, covalent crosslinks between DUBs and DiUbs were obtained also in this experiment. Interestingly, differences in-between the different DUBs also with regard to the photo-reactive moieties were observed. Covalent crosslinking to DiUb(K48) was for instance observed for USP2CD-tetrazole conjugate **95** (see 1* in Fig. 60B) but not for the respective USP2CD-diazirine conjugate **94**. This might be either due to differences in the efficiencies of the photo-reactive groups or reflect the different positions of the photocrosslinkers in conjugate **94** and **95**. As shown in Fig. 56, the MS/MS analysis of these two conjugates revealed that modification with photocrosslinker **54** (diazirine) was found only at cysteines C476 and C477, while modification with photocrosslinker **55** was additionally found at the cysteines C458 and C276, the latter being the active

site cysteine. It may thus be that crosslinking to DiUbK48 happened with conjugate **95** through the crosslinkers attached at one of these additional sites. In future experiments it will be important to determine the crosslinked sites by means of MS/MS. This analysis will also aid to rationally decide where to place the crosslinker best for efficient and specific crosslinking.

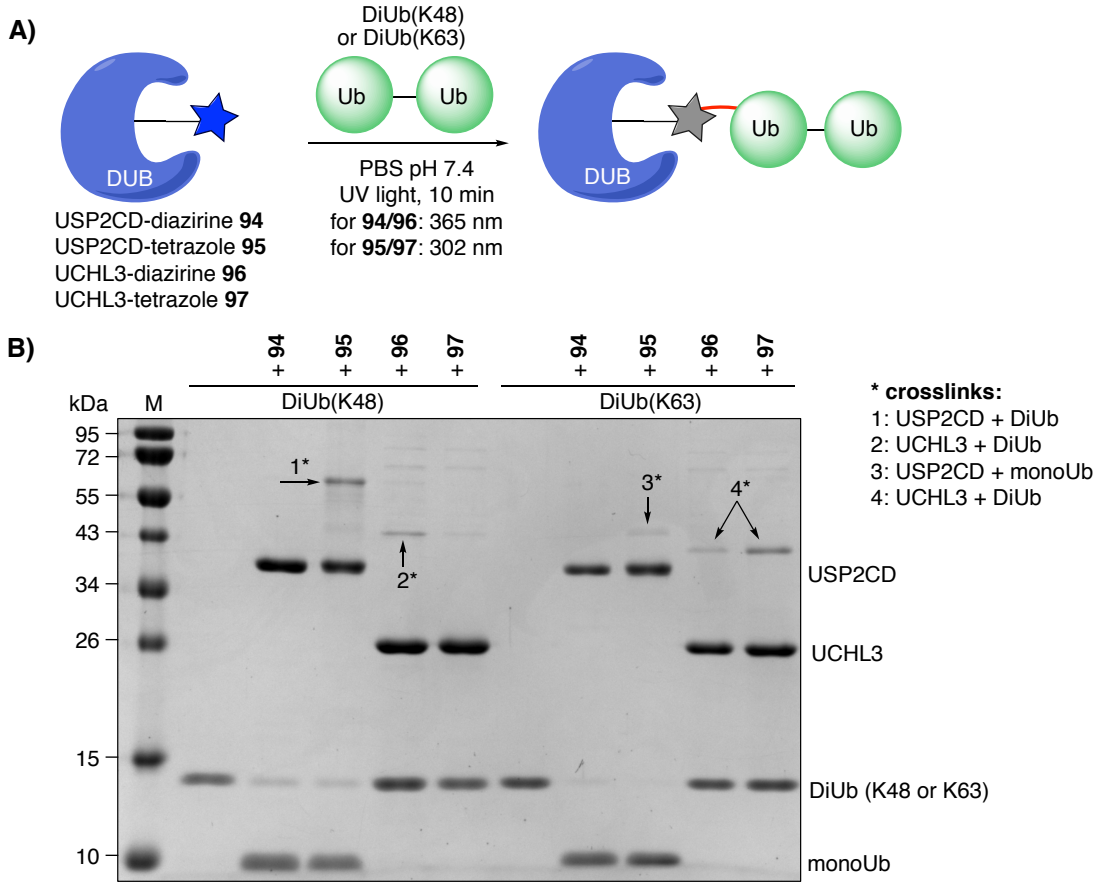

Fig. 60 A) Photocrosslinking between DUB-photocrosslinker conjugates (3 μM) and diubiquitins (DiUb, 6 μM). B) SDS-PAGE (Coomassie). All samples were irradiated with UV-light.

For the UCHL3-photocrosslinker conjugates **96** and **97** the opposite outcome was observed in the crosslinking experiment with DiUb(K48). Here, the diazirine-modified UCHL3 **96** showed more efficient crosslinking (2*) than the tetrazole-UCHL3 **97**. This finding is particularly interesting because for UCHL3, both photocrosslinkers were found at the same two cysteine residues (C209 and C95 (active site), see Fig. 57B). A possible reason for the observed difference between the crosslinkers can be that the carbene species, resulting from irradiation of the diazirine, react unselectively with various functional groups, while the carboxynitrilimine species of the activated tetrazole derivative reacts more selectively with carboxylates and maybe other nucleophilic side chain residues [289, 308]. Consequently, the absence of nucleophilic residues in proximity to the tetrazole photocrosslinker might be the reason why crosslinking was not efficient with this substrate. Again, the SDS-PAGE analysis does not reveal at which site crosslinking between UCHL3 and the diubiquitin happened and further MS/MS analysis will be necessary to gain more insight. Another observation was that in the samples containing USP2CD, diubiquitins hydrolysed to a large extent to

monoubiquitins (monoUb, see bottom of the gel in Fig. 60). This remaining protease activity of USP2CD conjugates can be explained by incomplete modification of the active site cysteine.
As for the experiment with K63-linked DiUb, the outcomes were yet different. Here, only little crosslinking was observed with USP2CD (3*) but the band shift of this species indicates crosslink to *mono*-ubiquitin (monoUb). There are two scenarios that can lead to this outcome. Either USP2CD-tetrazole conjugate **95** first crosslinked DiUb(K63) followed by hydrolysis or USP2CD crosslinking happened with monoUb present in the mixture originating from previous DiUb(K63) hydrolysis. Thus, for future experiments in lysates it will be important to test whether crosslinked substrates are still amenable to cleavage by DUBs. This would mean, that the pulled-down species do not necessarily correlate with the initially recognised substrates.
Using DiUb(K63) together with UCHL3 resulted in crosslinking for the UCHL3-tetrazole conjugate **97** and also for UCHL3-diazirine conjugate **96** (see 4* for both). In general, UCHL3 did not significantly hydrolyse the DiUbs over the course of the experiment, which was expected based on the low activity of UCHL3 towards K48- and K63-linked diubiquitins [307]. This finding also indicates, that substrates with a certain affinity to DUBs might be crosslinked although the activity of the DUB towards the hydroylsis of this substrate is low.

In the next steps of this project, we will carefully evaluate the positioning of the photocrosslinkers within the tested DUBs to investigate its impact on the selectivity and the efficiency for substrate crosslinking. Site-selective placing of the crosslinker might then be achieved via site-directed mutagenesis of cysteine residues. Alternatively, unnatural amino acids could be incorporated into DUBs and be addressed selectively using bioorthogonal labelling strategies. Apart from the chosen model DUBs used in these first proof-of-concept experiments, the approach will be extended to recently identified DUBs with yet unexplored substrate specificity. Finally, for photocrosslinking experiments in cell lysates, an appropriate handle for pull-down purpose has to be incorporated into the DUB. As mentioned above, a critical aspect in the evaluation of pulled-down substrate proteins will be to confirm if these hits are true-positives and indeed reflect substrate specificity. Overall, the preliminary data described in this chapter point towards promising possibilities of using DUB-photocrosslinker conjugates as tools to study DUB-substrate interactions and we are hopeful that this approach will enable the identification of specific substrate proteins in complex environments.

7 Summary & Outlook

In this work, vinyl- and ethynylphosphonothiolates were synthesised and explored as a new class of electrophilic reagents for cysteine-selective bioconjugations.

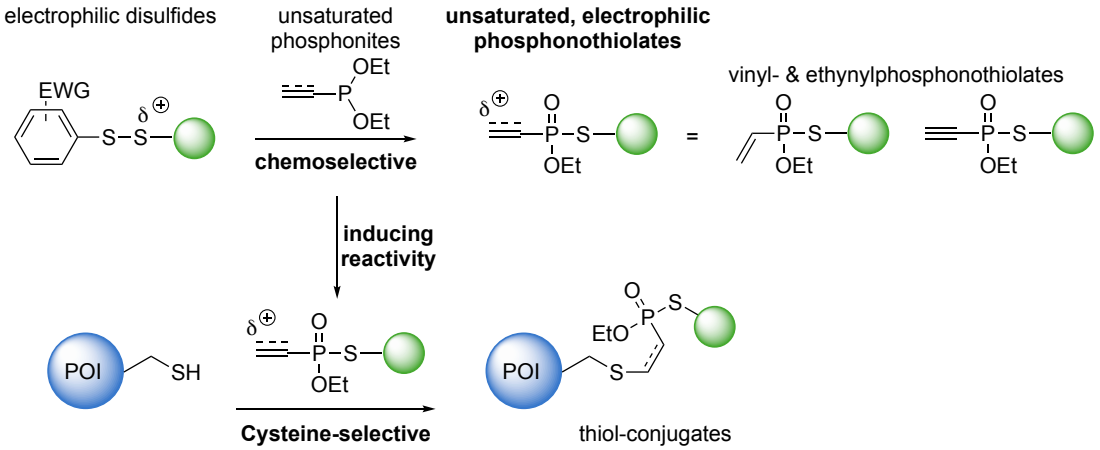

Fig. 61 The method developed in this thesis enables the chemoselective synthesis of unsaturated phosphonothiolates, thereby inducing reactivity for subsequent cysteine-selective thiol additions.

Vinyl- and ethynylphosphonothiolates have not been investigated for bioconjugation purpose and also their synthesis has not seen a lot of attention so far. In this work, we thus aimed at developing first an efficient synthetic protocol to access unsaturated phosphonothiolates in order to then evaluate their properties as handles in protein modifications. Based on previous work from our group and others, where it has been shown that phosphorus(III) species react efficiently with disulfides [237, 239, 243, 309, 244], we hypothesised that vinyl- and ethynylphosphonothiolates could be synthesised from electrophilic disulfides and unsaturated phosphonites. This thesis documents that we succeeded in accessing vinyl- and ethynylphosphonothiolates from electrophilic disulfides and vinyl- and ethynylphosphonites (scheme 55A). We optimised this disulfide-phosphonite reaction using unsymmetrical 5-nitropyridine disulfide derivatives and discovered that this reaction proceeds very quickly in organic solvents, following presumably an Arbuzov-type mechanism. In the presence of water, the targeted phosphonothiolates could not be obtained, which might be due to substitution of the thiol residue in the phosphonium intermediate by water. We further found that the disulfide-phosphonite reaction must be performed under acidic conditions in order to inhibit the formation of a side-product originating from the addition of the thiolate leaving group to the unsaturated phosphonothiolates. Under the optimised conditions, various small molecule derivatives could be obtained in good yields.

In addition, an alternative synthetic route was developed to access unsaturated phosphonothiolates in five steps from phosphorus trichloride (scheme 55B). Both routes allowed us to synthesise general building blocks, which could further be derivatised by means of amide couplings.
Importantly, it was found that the disulfide-phosphonite reaction proceeds with excellent chemoselectivity, as demonstrated for the installation of vinylphosphonothiolate electrophiles at activated cysteine residues on unprotected peptides and the protein ubiquitin. This method thus enables the site-selective installation of an electrophilic moiety into unprotected polypeptides, a strategy that gives rise for subsequent modification with nucleophiles.

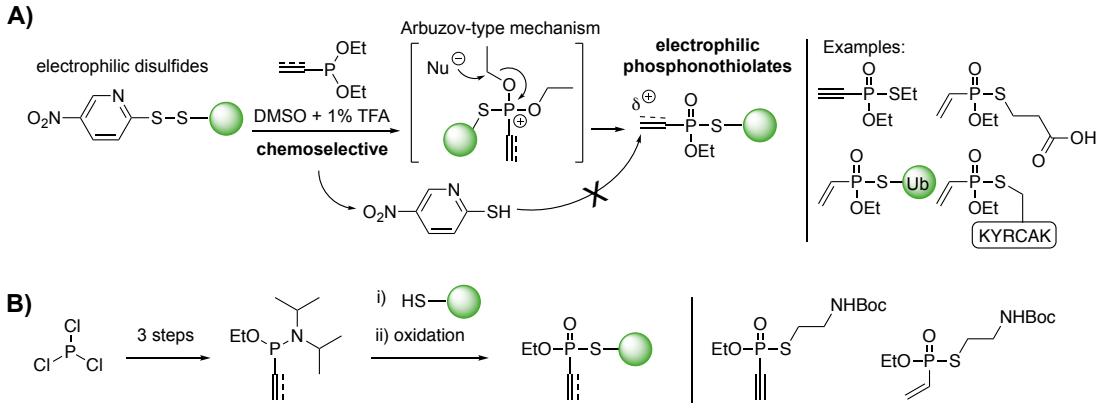

Scheme 55 A) Chemoselective synthetic route to access unsaturated phosphonothiolates from electrophilic disulfides. B) Alternative synthetic route starting from PCl_3.

Using the generated vinyl- and ethynylphosphonothiolates, we then explored their reactivity towards thiol additions. It was found, that the ethynyl-derivatives are significantly more reactive in thiol additions with bimolecular rate constants in the low $M^{-1}s^{-1}$ range, as opposed to $mM^{-1}s^{-1}$ rates for the thiol addition to the respective vinyl-derivatives at neutral pH (scheme 56).
The enhanced reactivity of ethynylphosphonothiolates is however compromised by the stability of these reagents in aqueous buffer. We found that the phosphorus-sulphur bond in ethynylphosphonothiolates is prone to hydrolysis, especially under basic conditions. P-S bond hydrolysis was also observed for vinylphosphonothiolate reagents but on a much slower time scale compared to the ethynyl-derivatives. This trend was also found for the respective thiol-conjugates, although the thiol-conjugates are generally more stable than the unconjugated phosphonothiolates.
Notably, thiol addition to both vinyl- and ethynylphosphonothiolates is irreversible, also in the presence of excess free thiols, as opposed to thiol conjugates formed from maleimides for example.
As for the chemoselectivity of the thiol additions to vinyl- and ethynylphosphonothiolates, we found that both compound classes employ high, although not exclusive, cysteine-selectivity in the modification of IgG antibodies.

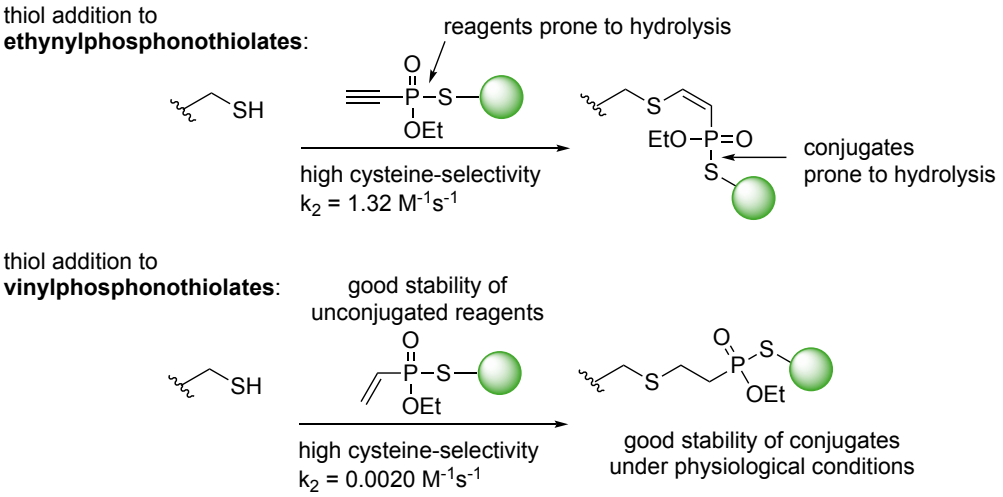

Scheme 56 Thiol additions to ethynyl- and vinylphosphonothiolates.

Based on the promising results documented in this thesis, further optimisations will likely help to improve the synthesis of unsaturated phosphonothiolates and their use in thiol-conjugation reactions. One limitation of the developed system in its current stage is the low reactivity of vinylphosphonothiolates, necessitating relatively high concentrations of the reaction partners to obtain sufficient labelling. Ethynylphosphonothiolates on the other hand react almost three orders of magnitude faster with thiols but the P-S bond in these reagents and the corresponding thiol conjugates is prone to hydrolysis. As previously shown by our group [208, 209], the more electron-withdrawing the substituents around the phosphorus are, the more reactive unsaturated P(V)-reagents become towards thiol addition. Following this logic, vinylphosphonothiolates could be rendered more reactive by introducing more electron-withdrawing residues at the *O*-substituent. However, such derivatives would expected to be less stable, as a consequence of the more electropositive phosphorus being more prone towards nucleophilic attack by water. The compromise of decreased stability for increased reactivity must thus be kept in mind when developing new electrophilic phosphonothiolate derivatives. Another limitation of the current system concerns the synthesis of unsaturated phosphonothiolates. As demonstrated in this thesis, the disulfide-phosphonite reaction requires dry conditions as the reactive intermediates otherwise can get quenched by water. This is particularly a problem for peptide and protein substrates, as it limits the applicability of this method to polypeptides that are soluble in organic solvents and can subsequently be refolded. Also here, one could try to derivatise the vinylphosphonite such, that the Arbuzov-mechanism is favoured over hydrolysis. This might be achieved by means of introducing more electron-withdrawing substituents at the *O*-residue or maybe also by incorporating a nucleophile into the phosphonite side chain to promote intramolecular rearrangement. A further parameter that can be changed is the type of activated disulfide employed. Using less nucleophilic leaving groups might obviate the need for acidic conditions to inhibit re-attack of the respective thiolate leaving group to the desired unsaturated phosphonothiolates. Although there is room for optimising the developed method in the future, the potential of unsaturated phosphonothiolates as linkers to generate functional bioconjugates could be demonstrated in this thesis in three different applications (Fig. 62).

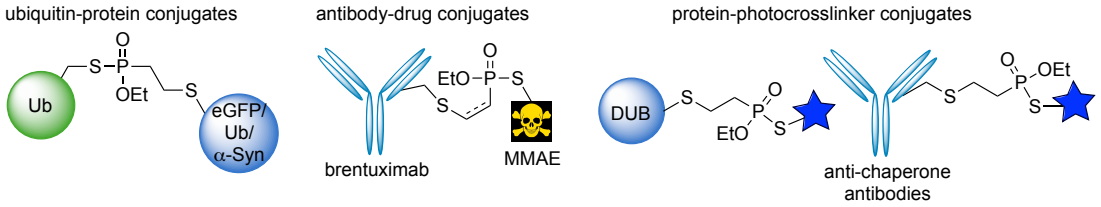

Fig. 62 Overview of generated phosphonothiolate-linked bioconjugates.

First, we succeeded in generating site-selectively ubiquitinated protein conjugates using a vinylphosphonothiolate-ubiquitin probe. In particular, we generated a non-hydrolysable diubiqutin as well as a ubiquitin-α-Synuclein conjugate. The chemoselective installation of electrophilic vinylphosphonothiolates on ubiquitin thus enabled the generation of protein-protein conjugates relying solely on canonical amino acids.
In a second application, we evaluated unsaturated phosphonothiolates as linkers in antibody-drug conjugates (ADCs). Specifically, brentuximab-MMAE conjugates were generated. While ethynylphosphonothiolates allowed for the efficient generation of brentuximab-MMAE ADCs with high average drug to antibody ratios (DARs), these ADC hydrolysed under physiological conditions. On the other hand, the generation of ADCs with decent DARs was more challenging using the less reactive vinylphosphonothiolate derivatives but the resulting ADCs proved to be more stable. Compared to the clinically approved ADC Adcetris®, the ADC generated with vinylphosphonothiolate was more stable in rat serum and showed similar *in vitro* efficacy.
In a final application, vinylphosphonothiolates were employed as linkers to modify proteins with photoreactive crosslinkers to study dynamic protein-protein interactions. On the one hand, we equipped chaperone-specific antibodies with photocrosslinkers and tried to crosslink chaperone interacting proteins. This approach was not successful, most likely because the photocrosslinkers were too flexible and thus did not reach the target proteins, thereby prohibiting successful crosslinking. On the other hand, we modified deubiquitinating enzymes with photocrosslinkers. With these tools, we were able to efficiently crosslink model ubiquitin substrates, which indicates potential of DUB-photocrosslinker conjugates for the identification of specific substrate proteins.

Taken together, the herein developed method enables the chemoselective transformation of activated disulfides into electrophilic vinyl- and ethynylphosphonothiolates, thereby inducing reactivity for subsequent cysteine-selective thiol additions. We believe that this formal conjugation of two complex thiol-containing molecules will be used for the generation of homogenous peptide and protein conjugates without the need for non-canonical amino acids.

8 Experimental

Contents

8.1 General information

8.1.1 Chemicals and solvents

If not mentioned specifically, chemicals and solvents were purchased from Merck (Merck group, Germany), TCI (Tokyo chemical industry CO., LTD., Japan) and Acros Organics (Thermo Fisher scientific, USA) and used without further purification. Dry solvents were purchased from Acros Organics (Thermo Fisher scientific, USA).

8.1.2 Flash- and thin layer chromatography

Flash column chromatography was performed using NORMASIL 60® silica gel (40-63 μm, VWR international, USA) or high purity grade (60 μm, Davisil Grade 633, Sigma-Aldrich Co., USA). Aluminium TLC plates (silica gel 60 coated with fluorescent indicator UV254) were purchased from Macherey-Nagel (Macherey-Nagel GmbH & Co. Kg, Germany). Spots were visualised by fluorescence depletion with a 254 nm lamp or manganese staining (10 g K_2CO_3, 1.5 g $KMnO_4$, 0.1 g NaOH in 200 mL H_2O), followed by heating.

8.1.3 Preparative HPLC

Preparative HPLC was performed on a Gilson PLC 2020 system (Gilson Inc, WI, Middleton, USA) using a VP 250/32 Macherey-Nagel Nucleodur C18 HTec Spum column (Macherey-Nagel GmbH & Co. Kg, Germany).

8.1.4 Semipreparative HPLC

Semipreparative HPLC was performed on a Shimadzu prominence HPLC system (Shimadzu Corp., Japan) with a CBM20A communication bus module, a FRC-10A fraction collector, 2 pumps LC-20AP, and a SPD-20A UV/VIS detector, using a VP250/21 Macherey-Nagel Nucleodur C18 HTec Spum column (Macherey-Nagel GmbH & Co. Kg, Germany). For protein purification a Vydac® protein C4 column (10 μm, 300 , 10 mm ID x 250 mm L, Cat#214TP1010) was used. Eluents: A = H_2O + 0.1% TFA, B = MeCN + 0.1% TFA.

8.1.5 Analytical HPLC

Analytical HPLC for thiol addition kinetic measurements was conducted on a Shimadzu prominence HPLC system (Shimadzu Corp., Japan) with a CBM-20A communication bus module, a SIL-20A auto sampler, 2 pumps LC-20AT, and a SPD-M20A UV/VIS detector, a CTO-20A column oven and a RF-10AXL fluorescence detector, using an Agilent Eclipse C18 5 μm, 250 x 4.6 mm RR-HPLC column (Agilent Technologies, USA) with a flow rate of 1.0 mL/min. The following gradients were used: (A = H_2O + 0.1% TFA, B = MeCN + 0.1% TFA), 2% B 0-5 min, 2-45% B 5-35 min, 45-95% B 35-36 min, 95% B 36-40 min, 95 to 2% B 40-41 min, 2% B 41-45 min. Fluorescence spectra with Ex/Em 336/490 nm were recorded.

8.1.6 UPLC-UV/MS

UPLC-UV/MS traces were recorded on a Waters H-class instrument equipped with a quaternary solvent manager, a Waters autosampler, a Waters TUV detector and a Waters Acquity QDa detector with an Acquity UPLC BEH C18 1.7 μm, 2.1 x 50 mm RP column with a flow rate of 0.6 mL/min (Waters Corp., USA). The following gradients were used: A = H_2O + 0.1% TFA in; B = MeCN + 0.1% TFA. Long gradient: 5% B 0-1.5 min, 5- 95% B 1.5-13.0 min, 95% B 13.0-13.9 min, 5% B 13.9-15 min. Short gradient: 3% B 0-0.5 min, 3-60% B 0.5-3.0 min, 95% B 3.0-3.9 min, 3% B 3.9-5 min.

8.1.7 Size-exclusion chromatography

Protein purification by size-exclusion chromatography was conducted with an ÄKTA FPLC system (GE Healthcare, United States) equipped with a P-920 pump system, a UPC-900 detector and a FRAC-950 fraction collector. For antibody purification a 5 mL *HiTrap*® desalting column was used with a flow-rate of 1.5 mL/min. For ubiquitin and α-Synuclein proteins or protein conjugates, a Superdex 75 10/300 GL column (GE Healthcare, USA) was used with a flow-rate of 0.8 mL/min.

8.1.8 High resolution MS

High-resolution ESI-MS spectra were recorded on two different instruments: 1) Agilent 6220 TOF Accurate Mass coupled to an Agilent 1200 LC (Agilent Technologies, USA). On this system, samples were measured at 35 °C between 100-2000 m/z. The used column was an Accucore RP-MS (30 x 2.1 mm; 2.6 μm particle size) eluted with a flow of 0.8 mL/min and the following gradient (A = H_2O + 0.1% TFA, B = MeCN + 0.1% TFA), gradient: 5% B 0-0.2 min, 5-99% B 0.2-1.1 min, 99% B 1.1-2.5 min. 2) Agilent Technologies 6230 Accurate Mass TOF LC/MS linked to Agilent Technologies HPLC 1260 Series; Column: Thermo Accuore RP-MS; Particle Size: 2.6 μM; Dimension: 30 x 2.1 mm. The following gradient was used: A = H_2O + 0.1% formic acid, B = MeCN + 0.1% formic acid, 5% B 0.0-0.2 min, 5-99% B 0.2-1.1 min, 99% B 1.1-3.6 min, 5% B 3.6-4.9 min. Flow rate: 0.8 mL/min; UV-detection: 220 nm, 254 nm, 300 nm.

8.1.9 Intact protein MS

Intact proteins were analysed using a Waters H-class instrument equipped with a quaternary solvent manager, a Waters sample manager-FTN, a Waters PDA detector and a Waters column manager with an Acquity UPLC protein BEH C4 column (300 , 1.7 μm, 2.1 mm x 50 mm). Proteins were eluted at a column temperature of 80 °C with a flow

rate of 0.3 ml/min. For proteins the following gradient was used: A = H_2O + 0.01% formic acid, B = MeCN + 0.01% formic acid. 5-95% B 0-6 min at 40 °C. Mass analysis was conducted with a Waters XEVO G2-XS QTof analyzer. Proteins were ionized in positive ion mode applying a cone voltage of 40 kV. Raw data was deconvoluted with MaxEnt 1.

8.1.10 NMR

NMR spectra were recorded with a Bruker AV-III 300 MHz spectrometer and a Bruker AV III 600 MHz spectrometer, both equipped with a broadband probe (BBFO). For stability measurements at 25 °C or 37 °C, a Bruker AV-III 600 MHz spectrometer equipped with a QCI cryoprobe with one-axis self-shielding gradients and a cooled ^{31}P-coil and preamplifier was used. Chemical shifts δ are reported in ppm relative to residual solvent peaks ($CDCl_3$: 7.26 [ppm]; DMSO−d_6: 2.50 [ppm]; CD_3CN 1.94 [ppm]; 4.79 D_2O [ppm] for ^{1}H-spectra and $CDCl_3$: 77.16 [ppm]; DMSO−d_6: 39.52 [ppm]; CD_3CN 1.32 [ppm]; for ^{13}C-spectra.

8.1.11 UV-irradiation for photocrosslinking experiments

Protein samples in photocrosslinking experiments were irradiated using an Analytik Jena bench-top 8-Watt UV-lamp (UVLMS-38) equipped with a switch to choose between 254/302/365 nm. The samples were typically placed with a distance of 2-3 cm to the UV-lamp and directly irradiated from the top.

8.1.12 Tryptic digest of proteins and LC-MS/MS analysis

Note: LC-MS/MS measurements were done by Dr. Michal Nadler-Holly and Heike Stephanowitz from the group of Dr. Fan Liu (FMP Berlin). Christian Stieger analysed MS/MS data and wrote the corresponding Experimental.
For MS/MS analysis, proteins were run on a SDS-gel, stained with Coomassie brilliant blue and further processed by in-gel protein digest using trypsin. For this, the desired protein band was cut into pieces and transferred in a 1 mL test tube. 200 µL of washing buffer (50 mM triethylammonium bicarbonate (TEAB from Sigma) pH 8.5/ acetonitrile 1:1) was added and the mixture was shaken for 10 min at 30 °C. The washing buffer was removed and 200 µL of 50 mM TEAB pH 8.5 was added and the sample was again shaken for 10 min at 30 °C. The buffer was removed and the gel pieces were shrunk by the addition of 200 µL acetonitrile. The last step was repeated one additional time and then the solvent was removed. Next, 100 µL of a DTT solution (5 mM in 50 mM TEAB) was added and the mixture was shaken for 45 min at 56 °C. The supernatant was removed and immediately afterwards, 100 µL of chloroacetamide (CAA) solution (40 mM in 50 mM TEAB) was added and shaken for 30 min in the dark at r.t. The buffer was removed and the residue was washed with 200 µL washing buffer. After buffer removal, the gel pieces were shrunk by the addition of 200 µL acetonitrile (two times). Subsequently, 0.1 µg trypsin in 40 µL of digest buffer (50 mM TEAB pH 8.5) was added and the mixture was shaken over night at 37 °C. The sample was then shortly centrifuged and 30 µL of 0.5% trifluoroacetic acid in acetonitrile was added to stop the digest. The supernatant was transferred from the test tube into a glass MS vial. The remaining gel pieces were shrunk by the addition of 20 µL acetonitrile and this supernatant was combined with the solution in the MS vial. The solvent was then removed under vacuum and the residue was redissolved in 6 µL H_2O/acetonitrile 95/5 containing 0.1% TFA and subjected to LC-MS/MS analysis:

Peptide mixtures after tryptic digest were analysed by a reversed-phase capillary liquid chromatography system (Dionex Ultimate 3000 NCS-3500RS Nano, Thermo Scientific) connected to an Orbitrap Fusion mass spectrometer (Thermo Fisher Scientific, Germany). For sample loading, a PepMap C-18 trap-column (Thermo Fischer Scientific) of 0.075 mm ID x 50 mm length, 3 μm particle size, 100 Å pore size was used. The loading mobile phase A contained 1% acetonitrile and 0.1% TFA in water, and mobile phase B 0.1% TFA acid in acetonitrile. LC separation was performed with a 200 cm μPACTM column (PharmaFluidics, Ghent, Belgium) at an eluent flow rate of 750 nL/min using a gradient of 4-50% B in 59 min. The separation mobile phase A contained 0.1% formic acid in water, and mobile phase B 0.1% formic acid in acetonitrile. FT survey scans were acquired in a range of 350 to 1500 m/z with a resolution of 120000 (FWHM) and an AGC target value of 4e5. Precursor ions with charge states 2-5 were isolated with a mass selecting quadrupole (isolation window m/z 1.2) with 10 s dynamic exclusion. Precursor ions were fragmented using stepped higher-energy collisional dissociation (HCD). Stepped HCD MS/MS spectra were acquired with 27-30-33% normalised collision energy (NCE). The maximum injection time was set to 54 ms to collect 2e4 precursor ions. Fragment ion spectra were acquired in the Orbitrap with a resolution of 15000 (FWHM).

8.1.13 SDS-PAGE and Western-blot analysis

SDS-PAGE
SDS-gels were prepared using standard protocols. All probes were boiled in SDS sample buffer containing β-mercaptoethanol prior to loading. Gels were run in a Mini-PROTEAN system from Bio-Rad at 250 V for 30 min. Bands were detected with standard Coomassie stain.
Silver staining
For silver staining, gels were fixed and rinsed in fixing solution (40% methanol (v/v), 10% acetic acid (v/v), 50% H_2O (v/v)) over 18 h. Gels were then rinsed in 20% EtOH in water over 10 min, followed by incubation in 10 % sodium thiosulfate for 1 min. After washing the gel two times in H_2O for 1 min each, the gel was incubated in 0.2 % silver nitrate for 20 min. The gel was briefly washed in H_2O for 1 min, followed by developing solution (3% K_2CO_3 (w/v); 25 μL formaldehyde (37%), 12.5 μL sodium thiosulfate (10%) in 100 mL H_2O). After sufficient visualisation had been acquired, developing solution was replaced with stopping solution (4% Tris (w/v), 2% acetic acid (v/v)) for at least 30 min of incubation. The gel was then washed twice in H_2O for at least 30 min each.
Western blotting
Western blotting was carried out after SDS-PAGE in a wet chamber (Bio-Rad). In brief, the gel and a PVDF membrane were equilibrated in transfer buffer (25 mM Tris, 190 mM glycine, 10% EtOH (v/v)) for 5 min before the transfer sandwich was assembled. Western blots were performed at constant current of 250 mA for 60 min. After blotting, membranes were stained with Ponceau (0.1% Ponceau S (w/v), 5% acetic acid (v/v) in H_2O) and then blocked for 1 h with ROTI®Block (Roth) (ROTI®Block: 0.01% Tween in PBS (v/v) = 1:9) or in 5% milk powder (w/v). After blocking, the membrane was washed two times with 0.01% Tween in PBS (v/v) for 2 min. Primary antibody incubation (with anti-HSP-1 or anti-DNJ-13, 1:5000 dilution from serum) was carried out overnight at 4 °C in 1x Roti Block in H_2O). Secondary antibody (Thermo Fisher Scientific, goat-anti-rabbit IgG (H+L), peroxidase conjugated, 1:15000) was incubated for 90 min in 1x Roti Block in H_2O. Alternatively, for anti-biotin Western-blotting, the

membrane was incubated with 0.03% Streptavidin-POD conjugate (Roche Diagnostics GmbH) (v/v) in PBS containing 0.01% Tween (v/v) and 1% ROTI®Block (v/v) for 1 hour at r.t. Detection was carried out using the ECL-reagent (Thermo Fisher Scientific), following the manufacturer's instructions and utilising a ChemiDoc XRS Imaging System (Universal Hood III, BioRad Laboratories GmbH).

8.2 Experimental part for method development chapter

8.2.1 Synthesis of electrophilic disulfides

5-(ethyldisulfaneyl)-2-nitrobenzoic acid (1)

A round-bottom flask equipped with a magnetic stir bar was charged with Ellman's reagent (255 mg, 0.64 mmol, 2.0 eq.) and DMF (3 mL). To this stirred, clear solution was added triethylamine (466 μL, 3.2 mmol, 10 eq.) and ethanethiol (24 μL, 0.32 mmol, 1.0 eq.), and the resulting clear red solution was stirred at 10 min at r.t. The solvents were evaporated under reduced pressure and the residue was dissolved in 0.5 mL DCM and purified by flash column chromatography on silica (EtOAc/hexane (containing 0.1% formic acid) = 2:1 to 1:1). Pure product-containing fraction were pooled and solvents were evaporated under reduced pressure to yield the title compound as a yellow solid (62 mg, 0.24 mmol, 75%). ^{1}H-NMR: (600 MHz, $CDCl_3$): δ = 7.95 (d, J = 2.1 Hz, 1H), 7.91 (d, J = 8.6 Hz, 1H), 7.78 (dd, J = 8.6, 2.1 Hz, 1H), 2.81 (q, J = 7.3 Hz, 2H), 1.34 (t, J = 7.3 Hz, 3H). ^{13}C-NMR: (151 MHz, $CDCl_3$): δ = 170.60, 146.43, 145.90, 128.63, 127.40, 126.48, 124.82, 33.12, 14.36. HR-MS (ESI+) for $C_9H_{10}NO_4S_2^+$ [M+H$^+$] calcd.: 260.0046, found: 260.0051.

General procedure 1 for the activation of small molecule thiols with DTNP

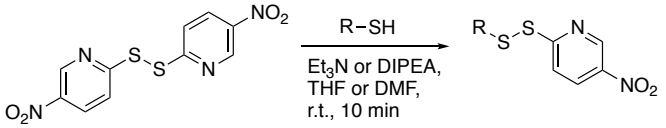

A round-bottom flask equipped with a magnetic stir bar was charged with thiol (1.0 eq.) dissolved in THF or DMF at a concentration of 0.1 M. Triethylamine or DIPEA (3.0 eq.) and disulfide 2,2′-dithiobis(5-nitropyridine) (DTNP) (1.2 eq.) were subsequently added, resulting in a colour-change from colourless to yellow-red and the reaction mixture was stirred at r.t. When full conversion was achieved (approximately after 10 min), the volatiles were evaporated under reduced pressure and the crude product was purified by flash column chromatography on silica gel or by reverse-phase HPLC.

2-(Ethyldisulfaneyl)-5-nitropyridine (2)

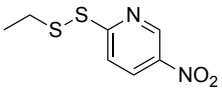

Compound **2** was prepared according to general procedure 1 from ethanethiol (103 μL, 1.34 mmol) in THF with Et_3N. The crude product was purified by flash column chromatography on silica gel (*n*-hexane/EtOAc = 10:1) to yield the title compound as a yellow oil (228 mg, 1.05 mmol, 78%). ^{1}H-NMR: (300 MHz, $CDCl_3$): δ = 9.24 (d, J = 2.6 Hz, 1H), 8.39 (dd, J = 8.9 Hz, 2.6 Hz, 1H), 7.92 (d, J = 8.9 Hz, 1H), 2.85 (q, J = 7.3 Hz, 2H), 1.34 (t, J = 7.3 Hz, 3H). ^{13}C-NMR: (75 MHz, $CDCl_3$): δ = 169.40, 145.13, 141.97, 131.65, 119.16, 32.99, 14.34. HR-MS (ESI+) for $C_7H_9N_2O_2S_2^+$ [M+H$^+$], calcd.: 217.0100, found: 217.0106.

2-(Benzyldisulfaneyl)-5-nitropyridine (14)

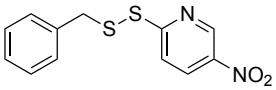

Compound **14** was prepared according to general procedure 1 from benzyl mercaptan (48 μL, 0.41 mmol) in THF with Et_3N. The crude product was purified by flash column chromatography on silica gel (*n*-hexane/EtOAc = 10:1) to yield the title compound as a colourless solid (91 mg, 0.33 mmol, 80%). ^{1}H-NMR: (300 MHz, $CDCl_3$): δ = 9.18 (d, J = 2.6 Hz, 1H), 8.15 (dd, J = 8.9 Hz, 2.6, 1H), 7.49 (d, J = 8.9 Hz, 1H), 7.30-7.24 (m, 2H), 7.24-7.17 (m, 3H), 4.04 (s, 2H). ^{13}C-NMR: (75 MHz, $CDCl_3$): δ = 168.90, 144.86, 141.81, 136.10, 131.17, 129.50 (2C), 128.83 (2C), 128.04, 119.03, 43.86. HR-MS (ESI+) for $C_{12}H_{11}N_2O_2S_2^+$ [M+H$^+$], calcd.: 279.0256, found: 279.0271.

2-(Biotinyldisulfaneyl)-5-nitropyridine (15)

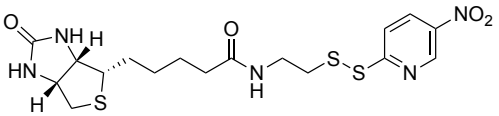

Following a literature procedure [310], D-biotin was first converted into the corresponding biotin-succinimidyl-ester and then reacted with 2-aminoethane-1-thiol to give the respective biotin-thiol derivative. This biotin-thiol derivative (44 mg, 0.179 mmol) was then activated with DTNP according to general procedure 1 in DMF with DIPEA. The crude product was purified by flash column chromatography on silica gel (DCM/MeOH = 20:1 to 10:1) to yield the title compound as a yellow solid (53 mg, 0.134 mmol, 75%). ^{1}H-NMR: (300 MHz, DMSO$-$d$_6$): δ = 9.25 (d, J = 2.2 Hz, 1H), 8.57 (dd, J = 8.9, 2.7 Hz, 1H), 8.11-7.97 (m, 2H), 6.39 (d, J = 18.1 Hz, 2H), 4.30 (dd, J = 7.7, 5.0 Hz, 1H), 4.12 (ddd, J = 7.4, 4.4, 1.8 Hz, 1H), 3.32 (m, 2H), 3.15 - 3.02 (m, 1H), 2.95 (t, J = 6.6 Hz, 2H), 2.81 (dd, J = 12.4, 5.0 Hz, 1H), 2.59 (m, 1H), 2.06 (t, J = 7.3 Hz, 2H), 1.65-1.19 (m, 6H). ^{13}C-NMR: (75 MHz, DMSO$-$d$_6$): δ = 172.42, 167.35, 162.81, 145.03, 142.34, 132.76, 119.59, 61.11, 59.27, 55.50, 40.43, 37.74, 37.62, 35.21, 28.27, 28.10, 25.25. HR-MS (ESI+) for $C_{17}H_{24}N_5O_4S_3^+$ [M+H$^+$], calcd.: 458.0985, found: 458.1010.

3-((5-Nitropyridin-2-yl)disulfaneyl)propanoic acid (16)

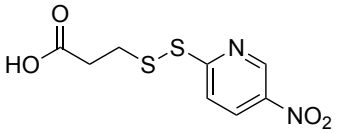

Compound **16** was prepared according to general procedure 1 from mercaptopropionic acid (250 μL, 2.85 mmol) in THF with Et_3N. The crude product was purified by flash column chromatography on silica gel (*n*-hexane/EtOAc = 1:1 + 0.1% formic acid) to yield the title compound as a yellow oil (80 mg, 1.54 mmol, 54%). ^{1}H-NMR: (300 MHz, $CDCl_3$): δ = 9.94 (s, broad), 9.27 (d, J = 2.6 Hz, 1H), 8.41 (dd, J = 8.9, 2.6 Hz, 1H), 7.87 (d, J = 8.8 Hz, 1H), 3.10 (t, J = 6.9 Hz, 2H), 2.82 (t, J = 6.8 Hz, 2H). ^{13}C-NMR: (75 MHz, $CDCl_3$): δ = 177.23, 168.03, 145.32, 142.33, 131.89, 119.66, 33.67, 33.31. HR-MS (ESI+) for $C_8H_9N_2O_4S_2^+$ [M+H$^+$], calcd.: 260.9998, found: 261.0005.

Synthesis of DTNP activated cysteine peptides 23-27

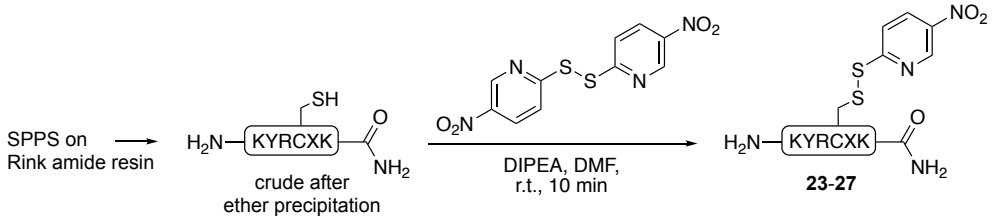

Peptides with the general sequence KYRCXK (X= A, S, H, D, M) were obtained from Fmoc-based solid-phase-peptide synthesis on a Rink-amide resin[8]. The crude peptides (0.1 mmol, 1.0 eq.) and 2,2'-dithiobis(5-nitropyridine) (47 mg, 0.15 mmol, 1.5 eq.) were dissolved in 1.0 mL DMF containing DIPEA (87 μL, 0.5 mmol, 5.0 eq.) and the mixtures were shaken at r.t. for 10 min. Solvents were then removed under reduced pressure and the residues were redissolved in 5 mL H_2O/MeCN 9:1 + 0.1% TFA, filtered and subsequently purified by semipreparative HPLC (gradient: A = H_2O + 0.1% TFA, B = MeCN + 0.1% TFA, 3-60% B in A over 50 min, flow-rate: 30 mL/min). Products **23-27** were obtained as yellow powder after lyophilization and analysed by UPLC-UV (long gradient) and HR-MS.

Table 4 Isolated yields of electrophilic disulfide peptides after HPLC purification.

sequence	compound No.	amount (mg)	amount (mmol)	yield (%)
KYRCAK	**23**	33.5	0.0364	36
KYRCSK	**24**	21.7	0.0232	23
KYRCHK	**25**	13.5	0.0137	14
KYRCDK	**26**	31.0	0.0321	32
KYRCMK	**27**	17.9	0.0182	18

[8]The author thanks Ines Kretzschmar for peptide synthesis.

HR-MS (ESI) analysis of peptides **23-27**:
peptide **23**: for $C_{38}H_{61}N_{14}O_9S_2^+$ [M+H$^+$] calcd.: 921.4182, found: 921.4268.
peptide **24**: for $C_{38}H_{61}N_{14}O_{10}S_2^+$ [M+H$^+$] calcd.: 937.4131, found: 937.4155.
peptide **25**: for $C_{41}H_{63}N_{16}O_9S_2^+$ [M+H$^+$] calcd.: 987.4400, found: 987.3994.
peptide **26**: for $C_{39}H_{61}N_{14}O_{11}S_2^+$ [M+H$^+$] calcd.: 965.4080, found: 965.4174.
peptide **27**: for $C_{40}H_{65}N_{14}O_9S_3^+$ [M+H$^+$] calcd.: 981.4216, found: 981.4238.

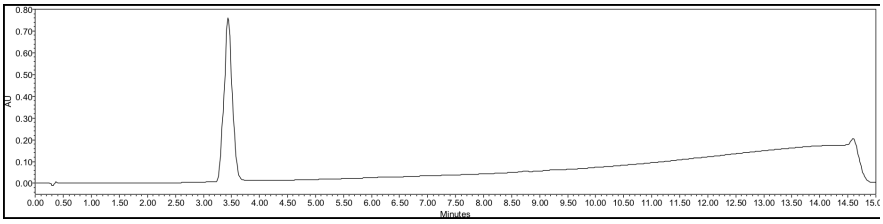

Fig. 63 UPLC-UV analysis (220 nm) of purified peptide **23**.

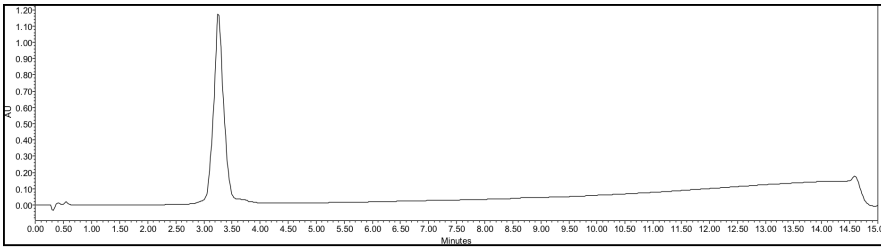

Fig. 64 UPLC-UV analysis (220 nm) of purified peptide **24**.

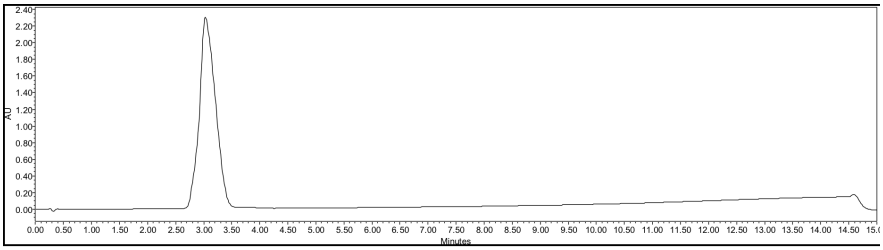

Fig. 65 UPLC-UV analysis (220 nm) of purified peptide **25**.

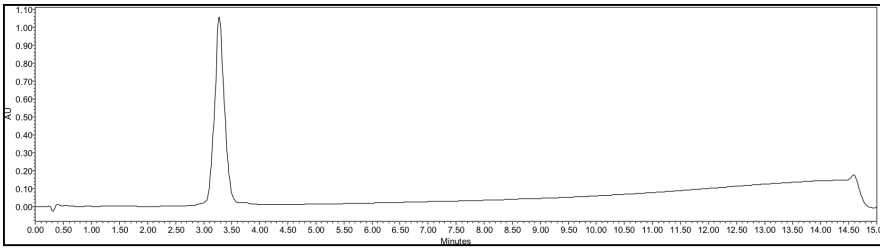

Fig. 66 UPLC-UV analysis (220 nm) of purified peptide **26**.

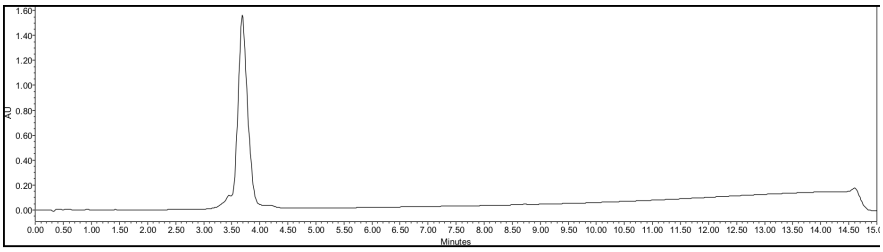

Fig. 67 UPLC-UV analysis (220 nm) of purified peptide **27**.

8.2.2 Synthesis of phosphonites

Diethyl-ethynylphosphonite (3)

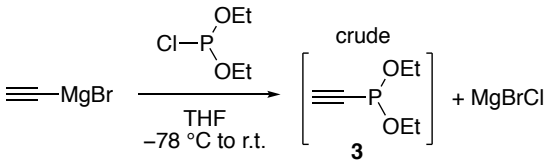

The procedure described here for the synthesis of diethyl-ethynylphosphonite is based on Ref. [208]: A Schlenk-flask was charged with diethyl chlorophosphite (Sigma, 278 μL, 2.00 mmol, 1.0 eq.) under an argon atmosphere, cooled to –78 °C (in an aceton dry-ice bath) and ethynylmagnesium bromide solution (Sigma, 0.5 M in THF, 4.40 mL, 2.20 mmol, 1.1 eq.) was added drop-wise and stirred for 10 min at –78 °C. The solution was allowed to warm to r.t. and used without further dilution for subsequent reactions. ^{31}P-NMR: (122 MHz, crude in THF): δ = 128.02.

Diethyl-vinylphosphonite (4)

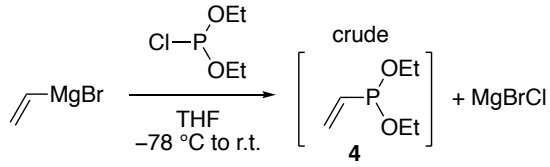

The procedure described here for the synthesis of diethyl-vinylphosphonite is based on Ref. [209]: A Schlenk-flask was charged with diethyl chlorophosphite (Sigma, 278 μL, 2.00 mmol, 1.0 eq.) under an argon atmosphere, cooled to –78 °C and vinylmagnesium bromide solution (Sigma, 1.0 M in THF, 2.20 mL, 2.20 mmol, 1.1 eq.) was added drop-wise and stirred for 10 min at –78 °C. The solution was allowed to warm to r.t. and used without further dilution for subsequent reactions. ^{31}P-NMR: (122 MHz, crude in THF): δ = 158.60.

8.2.3 Synthesis of phosphonothiolates from electrophilic disulfides

Test reaction between electrophilic disulfide (1) and ethynylphosphonite (3) in THF

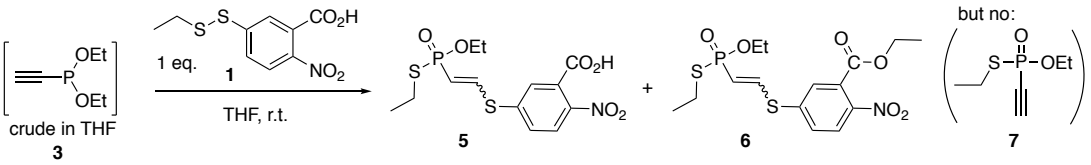

Ellman's-activated disulfide **1** (63 mg, 0.243 mmol, 1.0 eq.) was dissolved in dry THF (0.6 mL). To this stirred solution was added drop-wise freshly synthesized diethyl-ethynylphosphonite **3** (crude in THF, ca. 0.45 M, 0.54 mL, 0.243 mmol, 1.0 eq.) at r.t. and the mixture was stirred at r.t. for 1.5 hours and analysed by ^{31}P-NMR (see Fig. 14B). The crude products were then purified by silica gel chromatography (*n*-hexane/EtOAc = 1:1 + 0.1% formic acid to MeOH/DCM = 5:95 + 0.1% formic acid) to give products **5** (13 mg, 0.0344 mmol, 14%, ca. 75% pure according to ^{1}H-NMR) and **6** (3 mg, 0.0074 mmol, 3%, ca. 95% pure according to ^{1}H-NMR). The low yields can be explained by incomplete conversion of electrophilic disulfide **1** (33 mg, 0.127 mmol of **1** were recovered.) The product were characterized by ^{1}H-NMR, ^{31}P-NMR and low-resolution MS:

Re-attack product **5**:
^{1}H-NMR: (300 MHz, $CDCl_3$): δ = 8.08-7.87 (m, 2H), 7.83 (d, J = 8.5 Hz, 1H), 7.56 (dd, J = 8.5, 2.0 Hz, 1H), 6.09 (dd, J = 21.0, 16.6 Hz, 1H), 4.31-4.18 (m, 2H), 2.89 (dt, J = 13.4, 7.4 Hz, 2H), 1.39 (t, J = 7.2 Hz, 6H). ^{31}P-NMR: (122 MHz, $CDCl_3$): δ = 42.65. LR-MS (ESI+) for $C_{13}H_{17}NO_6PS_2^+$ [M+H$^+$], calcd.: 378.02, found: 378.16.

Re-attack product **6**:
^{1}H-NMR: (300 MHz, $CDCl_3$): δ = 7.96 (d, J = 8.5 Hz, 1H), 7.72 (d, J = 2.0 Hz, 1H), 7.64 (dd, J = 8.5, 2.1 Hz, 1H), 7.53 (dd, J = 20.6, 16.5 Hz, 1H), 6.03 (dd, J = 19.5, 16.4 Hz, 1H), 4.42 (q, J = 7.2 Hz, 2H), 4.27-4.12 (m, 2H), 2.84 (dq, J = 14.5, 7.3 Hz, 2H), 1.37 (three overlapping triplets, 9H). ^{31}P-NMR: (122 MHz, $CDCl_3$): δ = 39.29. LR-MS (ESI+) for $C_{15}H_{21}NO_6PS_2^+$ [M+H$^+$], calcd.: 406.05, found: 406.17.

Test reaction between electrophilic disulfide (1) and vinylphosphonite (4) in THF

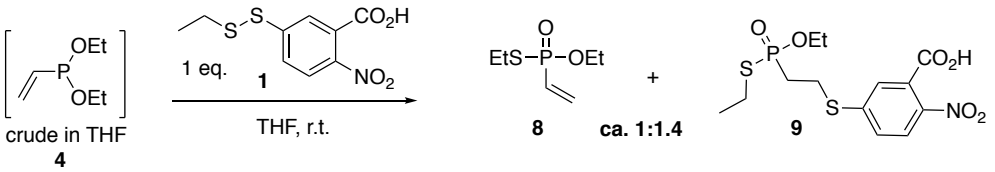

Ellman's-activated disulfide **1** (105 mg, 0.405 mmol, 1.0 eq.) was dissolved in dry THF (3.5 mL). To this stirred solution was added drop-wise freshly synthesized diethyl-vinylphosphonite **4** (crude in THF, ca. 0.80 M, 506 μL, 0.405 mmol, 1.0 eq.)

containing internal standard triphenylphosphineoxide (PPh_3O) at r.t. and the mixture was stirred at r.t. for 30 min and analysed by ^{31}P-NMR (see Fig. 15B. The crude products were then purified by silica gel chromatography (*n*-hexane/EtOAc = 1:1 + 0.1% formic acid to MeOH/DCM = 5:95 + 0.1% formic acid) to give products **8** and **9**.

Vinylphosphonothiolate **8**:
^{1}H-NMR: (300 MHz, $CDCl_3$): δ = 6.40-5.98 (m, 3H), 4.30-4.06 (m, 2H), 2.89-2.72 (m, 2H), 1.41-1.30 (m, 6H). ^{13}C-NMR: (75 MHz, $CDCl_3$): δ = 133.92 (d, J = 1.5 Hz), 130.86 (d, J= 145.4 Hz), 61.83 (d, J = 6.7 Hz), 24.98 (d, J = 3.0 Hz), 16.57 (d, J = 5.3 Hz), 16.45 (d, J=6.9 Hz). ^{31}P-NMR (122 MHz, $CDCl_3$): δ = 42.12. HR-MS (ESI+) for $C_6H_{14}O_2PS^+$ [M+H$^+$] calcd.: 181.0447, found: 181.0460.

Re-attack product **9**:
^{1}H-NMR: (600 MHz, $CDCl_3$): δ = 8.68 (s, 1H), 7.86 (d, J = 8.6 Hz, 1H), 7.60 (d, J = 2.1 Hz, 1H), 7.46-7.41 (m, 1H), 4.32-4.14 (m, 2H), 3.42-3.32 (m, 2H), 2.97-2.88 (m, 2H), 2.45-2.36 (m, 2H), 1.39 (t, J = 7.6 Hz, 3H), 1.38 (t, J = 7.2 Hz, 3H). ^{13}C-NMR: (151 MHz, $CDCl_3$): δ = 167.64, 144.98, 144.43, 129.38, 129.17, 127.22, 124.73, 62.82 (d, J = 7.5 Hz), 33.05 (d, J = 102.4 Hz), 25.62 (d, J = 3.5 Hz), 25.05, 16.88 (d, J = 5.0 Hz), 16.27 (d, J = 7.1 Hz). ^{31}P-NMR: (243 MHz, $CDCl_3$): δ = 52.77. HR-MS (ESI+) for $C_{13}H_{19}NO_6PS_2^+$ [M+H$^+$] calcd.: 380.0386, found: 380.0380.

Test reaction between electrophilic disulfide (2) and vinylphosphonite (4) in THF

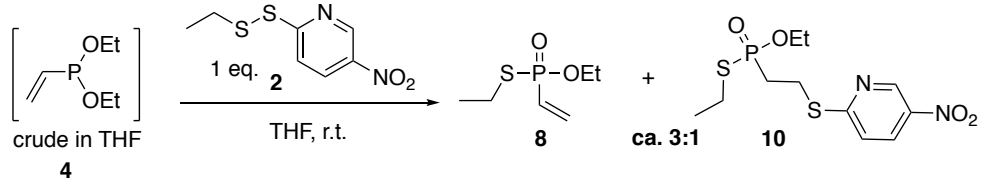

Scheme 57 Test reaction between electrophilic disulfide **2** and vinylphosphonite **4** in THF

DTNP-activated disulfide **2** (98 mg, 0.453 mmol, 1.0 eq.) was dissolved in dry THF (4 mL) under an argon atmosphere. To this stirred solution was added drop-wise freshly synthesized diethyl-vinylphosphonite **4** (crude in THF, ca. 0.80 M, 566 μL, 0.453 mmol, 1.0 eq.) at r.t.. The mixture was stirred at r.t. for 30 min and analysed by ^{31}P-NMR (see Fig. 16B). The crude mixture was purified by silica gel chromatography (*n*-hexane/EtOAc= 4:1 to 2:1 to 1:1), giving vinylphosphonothiolate **8** (43 mg, 0.140 mmol, 53%) and re-attack product **10** (20 mg, 0.060 mmol, 13%). The characterization of vinylphosphonothiolate **8** is described above.
Re-attack product **10**: ^{1}H-NMR: (300 MHz, $CDCl_3$): δ = 9.25 (dd, J = 2.7, 0.7 Hz, 1H), 8.24 (dd, J = 8.9, 2.7 Hz, 1H), 7.30 (dd, J = 8.9, 0.7 Hz, 1H), 4.35-4.05 (m, 2H), 3.58-3.47 (m, 2H), 3.00-2.86 (m, 2H), 2.56-2.39 (m, 2H), 1.42 (t, J = 7.5 Hz, 3H), 1.37 (t, J = 7.2 Hz, 3H). ^{13}C-NMR: (75 MHz, $CDCl_3$): δ = 166.79, 145.25, 141.42, 130.66, 121.78, 61.76 (d, J = 7.6 Hz), 34.37, 33.02, 25.30 (d, J = 3.3 Hz), 23.94, 17.06 (d, J = 4.5 Hz), 16.42 (d, J = 6.7 Hz). ^{31}P-NMR (122 MHz, $CDCl_3$): δ = 53.30. HR-MS (ESI+) for $C_{11}H_{18}N_2O_4PS_2^+$ [M+H$^+$] calcd.: 337.0440, found: 337.0446.

Reaction between electrophilic disulfide (2) and vinylphosphonite (4) in DMSO + H_2O^{18}

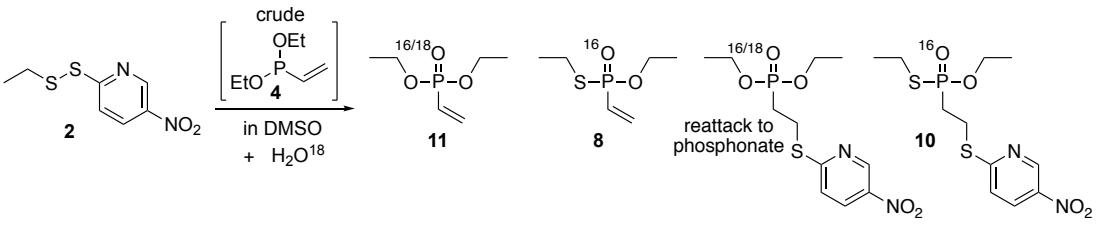

DTNP-activated electrophilic disulfide **2** (26 mg, 0.12 mmol, 1.0 eq.) was dissolved in dry DMSO (1 mL) containing H_2O^{18} (Sigma, 2.4 μL, 0.12 mmol, 1.0 eq.). To this stirred mixture was added vinylphosphonite **4** (crude in THF, ca. 0.78 M, 154 μL, 1.0 eq.) drop-wise at r.t. and the mixture was analysed by means of ^{31}P-NMR (Fig. 68).

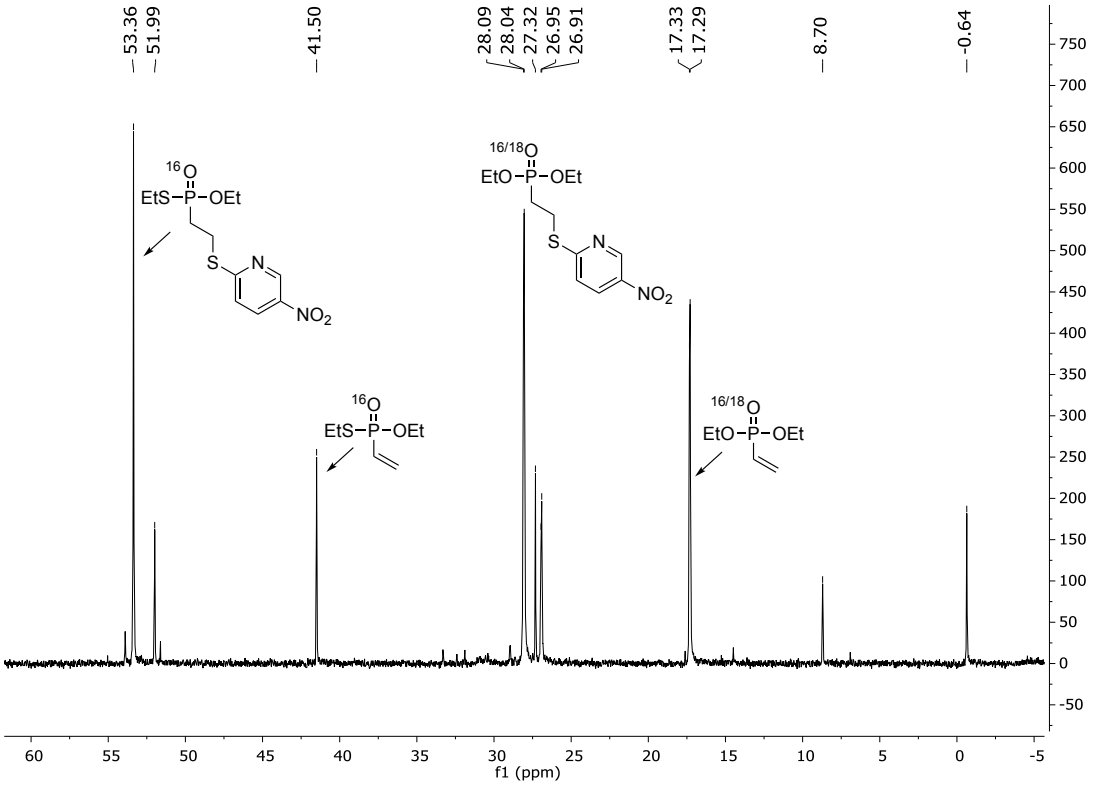

Fig. 68 ^{31}P-NMR of the reaction mixture of the reaction between electrophilic dislufide **2** and vinylphosphonite **4** in DMSO + H_2O^{18}. The identified products are indicated; for the re-attack-phosphonate species, the corresponding signal is in the range of 27-28 ppm but could not be unambiguously assigned in this crude ^{31}P-NMR spectrum.

The crude mixture was subjected to purification via semipreparative HPLC (5-70% MeCN + 0.1% TFA in H_2O + 0.1% TFA over 50 min, flow: 10 mL/min) and the two re-attack products were thereby isolated, see characterization below.
The vinylphosphonothiolate **8** and the vinylphosphonate **11** were not isolated here. The vinylphosphonothiolate **8** has been characterized above and has a characteristic

^{31}P-NMR chemical shift of ca. 42 ppm, which fits to the signal observed in Fig. 68. The assignment of vinylphosphonate **8** in the crude ^{31}P-NMR shown in Fig. 68 is based on comparison to the commercially available diethylvinylphosphonate (Sigma), which was characterized in DMSO−d_6 below and has a ^{31}P-NMR shift of ca. 17 ppm in DMSO.

Re-attack product **10**:

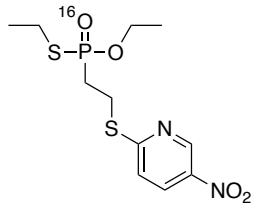

The NMR and HR-MS analysis is in line with the above described characterization for this compound. UPLC-MS analysis of the HPLC-purified **10** is shown below (Fig. 69). The observed mass corresponds to the ^{16}O-isotope.

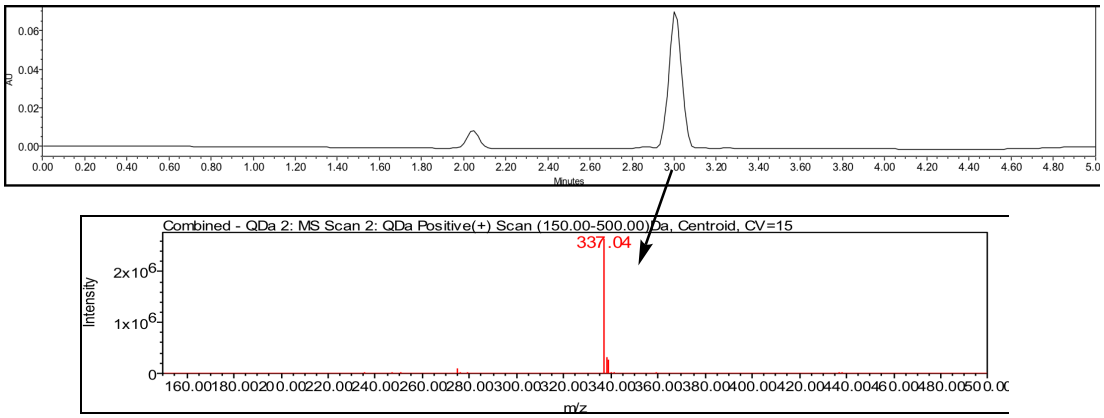

Fig. 69 UPLC-MS analysis of isolated product **10**. LR-MS for $C_{11}H_{18}N_2O_4PS_2^+$ [M+H$^+$] calcd.: 337.04, found: 337.04.

Re-attack product to phosphonate:

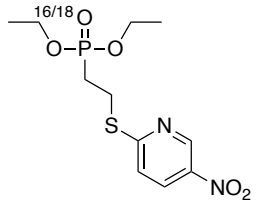

^{1}H-NMR: (300 MHz, $CDCl_3$): δ = 9.27 (dd, J = 2.7, 0.7 Hz, 1H), 8.26 (dd, J = 8.9, 2.7 Hz, 1H), 7.34-7.29 (m, 1H), 4.27-4.10 (m, 4H), 3.55-3.40 (m, 2H), 2.37-2.19 (m, 2H), 1.45-1.34 (m, 6H). ^{31}P-NMR (122 MHz, $CDCl_3$): δ = 27.82, 27.78. HR-MS (ESI+) for $C_{11}H_{18}N_2O_5PS^+$ [M+H$^+$] calcd.: 321.0669, found: 321.0667. HR-MS (ESI+) for $C_{11}H_{18}N_2O_4O^{18}PS^+$ [M+H$^+$] calcd.: 323.0711, found: 323.0711.

UPLC-MS analysis is shown below in Fig. 70.

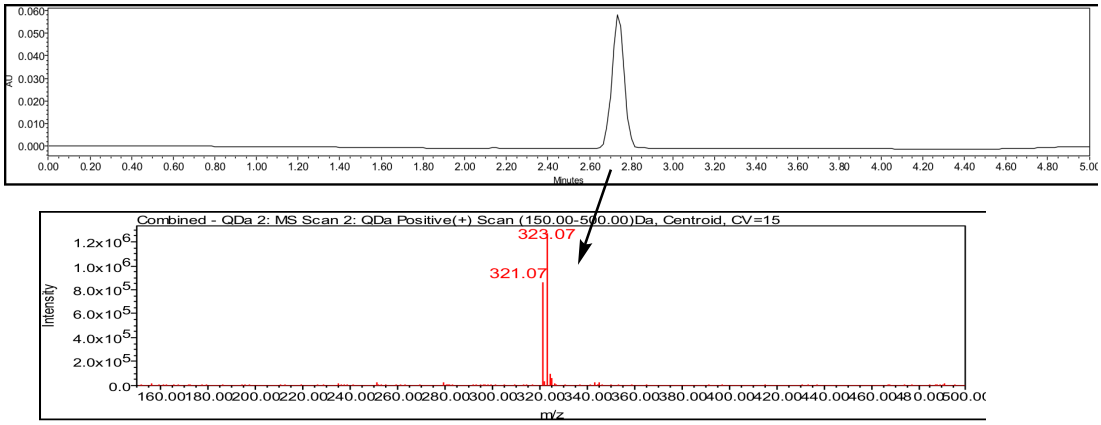

Fig. 70 UPLC-MS analysis of isolated re-attack to phosphonate. LR-MS for $C_{11}H_{18}N_2O_5PS^+$ [M+H$^+$] calcd.: 321.07, found: 321.07 and for $C_{11}H_{18}N_2O_4O^{18}PS^+$ [M+H$^+$] calcd.: 323.07, found: 323.07.

Commercial vinylphosphonate **11** (Sigma):

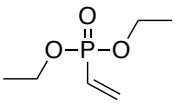

^{1}H-NMR: (300 MHz, DMSO−d$_6$): δ = 6.30-6.00 (m, 3H), 3.97 (dq, J = 8.3, 7.1 Hz, 4H), 1.23 (t, J = 7.1 Hz, 6H). ^{13}C-NMR (75 MHz, DMSO−d$_6$): δ = 135.50 (d, J = 1.8 Hz), 126.47 (d, J = 179.7 Hz), 61.35 (d, J = 5.7 Hz), 16.22 (d, J = 6.0 Hz). ^{31}P-NMR (122 MHz, DMSO−d$_6$): δ = 16.97.

Test reaction between electrophilic disulfide (2) and vinylphosphonite (4) in DMSO without TFA

DTNP-activated electrophilic disulfide **2** (80 mg, 0.370 mmol, 1.0 eq.) was dissolved in dry DMSO (3.7 mL) to reach a disulfide concentration of 0.1 M. To this stirred mixture was added drop-wise a solution of diethyl-vinylphosphonite (crude, ca. 0.78 M in THF, 474 μL, 1.0 eq.) at r.t. The reaction mixture was stirred at r.t., analysed by ^{31}P-NMR (see Fig. 19B) and then purified by silica-gel chromatography (n-hexane/EtOAc = 4:1 to 2:1 to 1:1) to give vinylphosphonothiolate **8** (26 mg, 0.144 mmol, 39%), re-attack product **10** and the alkylated leaving group (30 mg, 0.163 mmol, 44%).

Vinylphosphonothiolate **8** and re-attack product **10** have been characterized above. Characterization of alkylated leaving group:

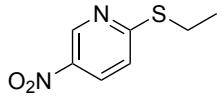

^{1}H-NMR: (300 MHz, $CDCl_3$): δ = 9.22 (dd, J = 2.7, 0.7 Hz, 1H), 8.20 (dd, J = 8.9, 2.7 Hz, 1H), 7.31-7.21 (m, 1H), 3.25 (q, J = 7.3 Hz, 2H), 1.39 (t, J = 7.4 Hz, 3H). ^{13}C-NMR (75 MHz, $CDCl_3$): δ = 168.25, 145.15, 141.04, 130.34, 121.51, 25.06, 14.40. HR-MS (ESI+) for $C_7H_9N_2O_2S^+$ [M+H$^+$] calcd.: 185.0379, found: 185.0382.

General procedure 2 for the synthesis of small molecule phosphonothiolates using the optimized protocol

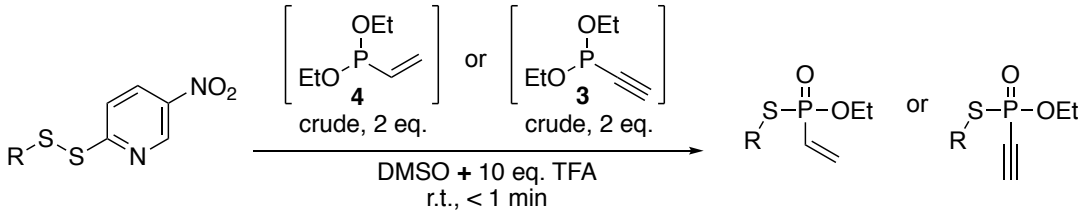

DTNP-activated electrophilic disulfides (1.0 eq.) were dissolved in dry DMSO containing trifluoroacetic acid (10 eq.) to reach a disulfide concentration of 0.1 M. To this stirred mixture was added drop-wise a solution of diethyl-vinyl- or ethynylphosphonite (crude in THF, 2.0 eq.) at r.t. Typically, the reactions were complete within one minute. The crude products were purified by flash column chromatography.

S,O-Diethyl vinylphosphonothiolate (8)

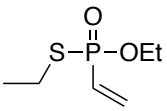

Compound **8** was prepared according to general procedure 2 from mixed electrophilic disulfide **2** (100 mg, 0.462 mmol). The crude product was purified by flash column chromatography (n-hexane/EtOAc = 4:1 to 2:1 gradient) to yield the title compound as a colourless oil (67 mg, 0.370 mmol, 80%). This product has been characterized above.

S-Benzyl *O*-ethyl vinylphosphonothiolate (17)

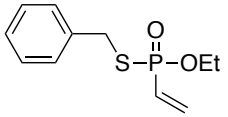

Compound **17** was prepared according to general procedure 2 from mixed electrophilic disulfide **14** (100 mg, 0.359 mmol). The crude product was purified by flash column chromatography (*n*-hexane/EtOAc = 4:1 to 1:1 gradient) to yield the title compound as a colourless oil (48 mg, 0.198 mmol, 55%). ^{1}H-NMR: (300 MHz, $CDCl_3$): δ = 7.39-7.21 (m, 5H), 6.34-5.91 (m, 3H), 4.27-3.95 (m, 4H), 1.32 (t, J = 7.0 Hz, 3H). ^{13}C-NMR: (75 MHz, $CDCl_3$): δ = 163.06, 137.15 (d, J = 5 Hz), 134.68 (d, J = 1.6 Hz), 129.70 (d, J = 146.5 Hz), 129.00, 128.71, 127.70, 62.36 (d, J = 6.9 Hz), 34.51 (d, J = 2.8 Hz), 16.22 (d, J = 6.9 Hz). ^{31}P-NMR (122 MHz, $CDCl_3$): δ = 42.69. HR-MS (ESI+) for $C_{11}H_{15}O_2PS^+$ [M+H$^+$] calcd.: 242.0525, found: 242.0551.
The phosphonothioate by-product (S=P-R) (compare for example scheme 41) was not isolated/characterized but its indicative ^{31}P-NMR-shift at 85 ppm in DMSO (observed in the crude reaction mixture), is in line with literature [311]. Furthermore, when vinylphosphonite was treated with molecular sulphur in DMSO, a single species with the same shift of 85 ppm was observed by ^{31}P-NMR.

S-(4-biotinamidoethyl) *O*-ethyl vinylphosphonothiolate (18)

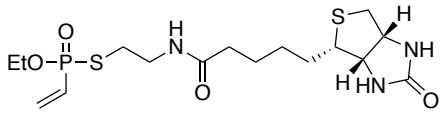

Compound **18** was prepared according to general procedure 2 from mixed electrophilic disulfide **15** (15 mg, 0.0328 mmol). The crude product was purified by flash column chromatography (DCM/MeOH = 50:1 to 9:1 gradient) to yield the title compound as a colourless solid (11 mg, 0.0262 mmol, 80%).
^{1}H-NMR: (600 MHz, DMSO−d_6): δ = 8.02 (t, J = 5.7 Hz, 1H), 6.47-6.12 (m, 5H), 4.33-4.27 (m, 1H), 4.12 (ddd, J = 8.4, 4.8, 1.8 Hz, 1H), 4.11-4.04 (m, 2H), 3.26 (q, J = 6.7 Hz, 2H), 3.09 (ddd, J = 8.5, 6.1, 4.4 Hz, 1H), 2.85-2.73 (m, 3H), 2.58 (d, J = 12.4 Hz, 1H), 2.06 (t, J = 7.4 Hz, 2H), 1.61 (ddt, J = 12.2, 9.7, 6.1 Hz, 1H), 1.55-1.42 (m, 3H), 1.36-1.29 (m, 2H), 1.28 (t, J = 7.0 Hz, 3H). ^{13}C-NMR: (151 MHz, DMSO−d_6): δ = 172.20, 162.67, 134.39, 130.55 (d, J = 144 Hz), 61.43 (d, J = 7.3 Hz), 61.02, 59.18, 55.39, 40.06, 35.10, 29.05, 28.15, 28.01, 25.17, 16.12 (d, J = 7 Hz). ^{31}P-NMR (243 MHz, DMSO−d_6): δ = 41.34. HR-MS (ESI+) for $C_{16}H_{29}N_3O_4PS_2^+$ [M+H$^+$] calcd.: 422.1332, found: 422.1340.

S-Propanoic acid *O*-ethyl vinylphsophonothiolate (19)

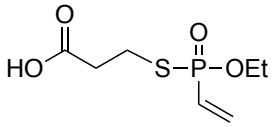

Compound **19** was prepared according to general procedure 2 from mixed electrophilic disulfide **16** (146 mg, 0.561 mmol). The crude product was purified by flash column chromatography (gradient: *n*-hexane/EtOAc=4:1 to EtOAc + 0.1% formic acid) to yield the title compound as a colourless oil (88 mg, 0.393 mmol, 70%). ^{1}H-NMR: (600 MHz, $CDCl_3$): δ = 9.25 (s, 1H), 6.38-6.07 (m, 3H), 4.26-4.13 (m, 2H), 3.09-2.96 (m, 2H), 2.74 (t, J = 7.2 Hz, 2H), 1.35 (t, J = 7.1 Hz, 3H). ^{13}C-NMR: (151 MHz, $CDCl_3$): δ = 174.98, 134.92, 130.18 (d, J = 145.9 Hz), 62.52 (d, J = 6.9 Hz), 35.73 (d, J = 3.5 Hz), 25.02 (d, J = 2.8 Hz), 16.38 (d, J = 6.9 Hz). ^{31}P-NMR (243 MHz, Chloroform-d): δ = 43.17. HR-MS (ESI+) for $C_7H_{14}O_4PS^+$ [M+H$^+$] calcd.: 225.0345, found: 225.0358.

O,S-Diethyl ethynylphosphonothiolate (7)

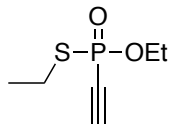

Compound **7** was prepared according to general procedure 2 from mixed electrophilic disulfide **2** (100 mg, 0.462 mmol). The crude product was purified by flash column chromatography (*n*-hexane/EtOAc = 2:1 to 100% EtOAc gradient) to yield the title compound as a colourless oil (48 mg, 0.270 mmol, 58%). ^{1}H-NMR: (300 MHz, $CDCl_3$): δ = 4.24 (dq, J = 9.6, 7.1 Hz, 2H), 3.17 (d, J = 12.5 Hz, 1H), 3.07-2.87 (m, 2H), 1.41 (td, J = 7.2, 5.9 Hz, 6H). ^{13}C-NMR: (75 MHz, $CDCl_3$): δ = 89.23 (d, J = 42.8 Hz), 77.33 (d, J = 236.9 Hz), 63.93 (d, J = 6.8 Hz), 25.72 (d, J = 3.7 Hz), 16.21 (d, J = 7.4 Hz), 16.12 (d, J = 6.4 Hz). ^{31}P-NMR (122 MHz, $CDCl_3$): δ = 17.40. HR-MS (ESI+) for $C_6H_{12}O_2PS^+$ [M+H$^+$] calcd.: 179.0290, found: 179.0301.

Synthesis of vinylphosphonothiolate peptides (28-32)

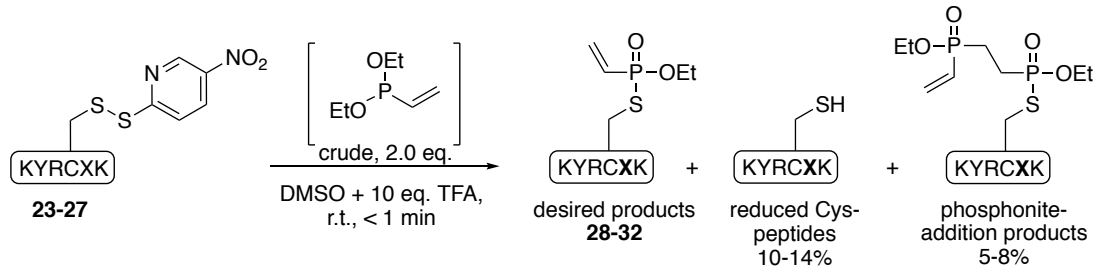

Scheme 58 Synthesis of vinylphosphonothiolate peptides and observed side-products.

DTNP-activated cysteine peptides **23-27** (0.010 mmol, 1.0 eq.) were dissolved in dry DMSO containing trifluoroacetic acid (10 eq.) to reach a peptide concentration

of 30 mM. To these stirred mixtures was added drop-wise a solution of diethylvinylphosphonite (crude in THF, 2.0 eq.). After the reaction was complete (typically less than 2 minutes), the reaction mixtures were diluted with 4.5 mL H_2O and purified by semipreparative HPLC (gradient: 5-50% MeCN + 0.1% TFA, 95-40% H_2O + 0.1% TFA over 40 min, flow: 5 mL/min), yielding products **28-32** as white powders after lyophilization. The purified peptides were analysed by UPLC-UV, HR-MS and ^{31}P-NMR (see Appendix). The ^{31}P-NMR spectra show two species in a ratio of 1:1, which correspond to the two diastereoisomers of the product, as the phosphonite-disulfide reaction results in a racemic mixture of the phosphonothiolate. In case of peptide **32**, the two diastereoisomers could be separated by HPLC and were analysed separately. Next to the desired phosphonothiolate peptide products, two side products were identified. The main side product in this reaction is reduced cysteine peptide (ca. 10-14% isolated yields). In addition, ca. 5-8% of the addition products of vinylphosphonite to vinylphosphonothiolate peptides were isolated (see Appendix for ^{31}P-NMR spectrum).

Table 5 Isolated yields of vinylphosphonothiolate peptides and side-products after HPLC purification.

sequence	**compound No.**	**amount (mg)**	**amount (μmol)**	**yield (%)**	Cys-peptide (%)	phosphonite-addition (%)
KYRCAK	**28**	3.6	4.07	41	10	5
KYRCSK	**29**	3.0	3.33	33	14	7
KYRCHK	**30**	3.0	3.15	32	13	7
KYRCDK	**31**	2.7	2.91	29	13	8
KYRCMK	**32**	1.7+1.6	3.49	35	14	5

HR-MS (ESI) analysis of peptides **28-32**:
peptide **28**: for $C_{37}H_{66}N_{12}O_9PS^+$ [M+H$^+$] calcd.: 885.4529, found: 885.4482.
peptide **29**: for $C_{37}H_{66}N_{12}O_{10}PS^+$ [M+H$^+$] calcd.: 901.4478, found: 901.3964.
peptide **30**: for $C_{40}H_{68}N_{14}O_9PS^+$ [M+H$^+$] calcd.: 951.4747, found: 951.5656.
peptide **31**: for $C_{38}H_{66}N_{12}O_{11}PS^+$ [M+H$^+$] calcd.: 929.4427, found: 929.4526.
peptide **32**: for $C_{39}H_{70}N_{12}O_9PS_2{}^+$ [M+H$^+$] calcd.: 945.4562, found: 945.4465.

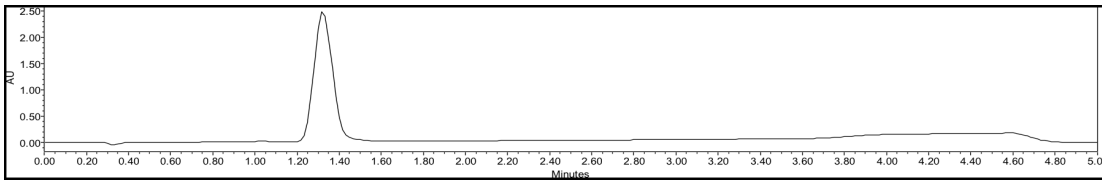

Fig. 71 UPLC-UV analysis (220 nm) of purified peptide **28**.

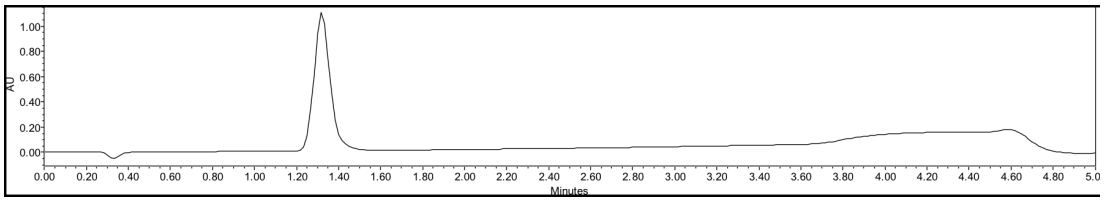

Fig. 72 UPLC-UV analysis (220 nm) of purified peptide **29**.

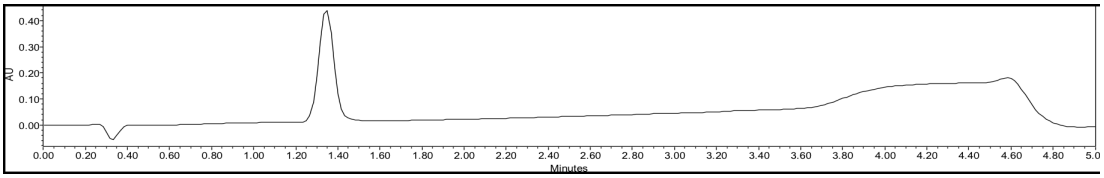

Fig. 73 UPLC-UV analysis (220 nm) of purified peptide **30**.

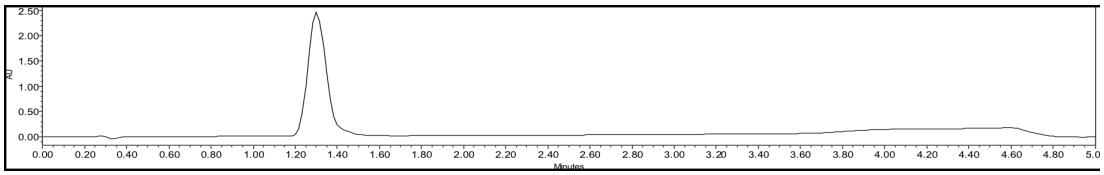

Fig. 74 UPLC-UV analysis (220 nm) of purified peptide **31**.

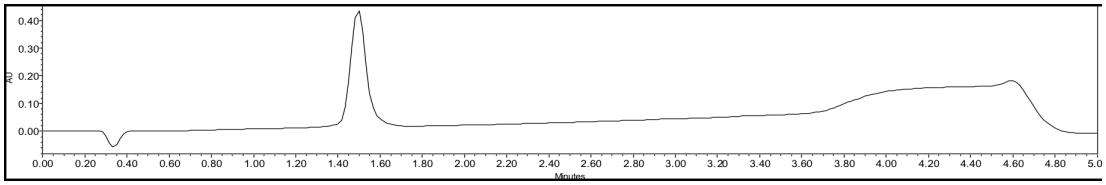

Fig. 75 UPLC-UV analysis (220 nm) of purified peptide **32**.

8.2.4 Synthesis of phosphonothiolates via PCl_3 route

Synthesis of precursors 33 and 34

1-ethoxy-1-ethynyl-*N,N*-diisopropylphosphanamine (33)

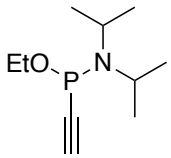

A flame-dried round bottom Schlenk flask was charged with phosphorus trichloride (12.5 mmol, 1090 μL, 1.0 eq.) and dry ether (50 mL) under an argon atmosphere and cooled to –30 °C in an aceton dry ice bath. Ethanol (12.5 mmol, 728 μL, 1.0 eq.) and triethylamine (12.5 mmol, 1.733 mL, 1.0 eq.) were added and the solution was stirred at –30 °C for 10 min before warming to r.t. and stirred for another hour. The resulting white suspension was quickly filtered over celite. The filtrate was collected in a flame-dried round bottom Schlenk flask and cooled again to –30 °C under an argon atmosphere. Diisopropylamine (25 mmol, 3.528 mL, 2.0 eq.) was added and the reaction mixture was stirred at –30 °C for 10 min before warming up to r.t. and stirred for another hour. The resulting suspension was filtered over celite again. The clear filtrate was cooled to –78 °C under an argon atmosphere and a solution of ethylmagnesium bromide (Sigma, 0.5 M in THF, 13.75 mmol, 27.5 mL, 1.1 eq.) was added, stirred for 10 min at –78 °C and then at r.t. for another hour. The reaction mixture was then concentrated to roughly 20 mL under reduced pressure, diluted with saturated aqueous $NaHCO_3$ (60 mL) and extracted with EtOAc (3x 120 mL). The combined organic layers were dried over $NaSO_4$, filtered and the solvents were removed under reduced pressure. The resulting oily residue was purified by silica gel (Sigma, Davisil Grade 633, pore size 60 Å, 200-425 mesh particle size) chromatography (*n*-hexane + 1% Et_3N) to yield the titled compound as a yellow oil (1.236 g, 6.14 mmol, 49%). ^{1}H-NMR: (300 MHz, CD_3CN): δ = 3.77-3.63 (m, 4H), 3.33 (d, J = 1.8 Hz, 1H), 1.21-1.13 (m, 15H). ^{13}C-NMR: (75 MHz, ceCD3CN): δ = 92.75 (d, J = 7.4 Hz), 86.85 (d, J = 18.5 Hz), 62.86 (d, J = 16.20 Hz), 48.36, 24.37, 17.40 (d, J = 7.5 Hz). ^{31}P-NMR (122 MHz, CD_3CN) δ = 92.22. HR-MS (ESI+) for $NaC_{10}H_{20}NOP^+$ [M+Na^+] calcd.: 224.1180, found: 224.1270.

1-ethoxy-*N,N*-diisopropyl-1-vinylphosphanamine (34)

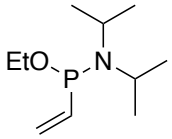

A flame-dried round bottom Schlenk flask was charged with phosphorus trichloride (12.5 mmol, 1090 μL, 1.0 eq.) and dry ether (50 mL) under an argon atmosphere and cooled to –30 °C in a dry ice bath. Ethanol (12.5 mmol, 728 μL, 1.0 eq.) and triethylamine (12.5 mmol, 1.733 mL, 1.0 eq.) were added and the solution was stirred at –30 °C for 10 min before warming to r.t. and stirred for another hour. The resulting white suspension was quickly filtered over celite. The filtrate was collected in a flame-dried round bottom Schlenk flask and cooled again to –30 °C under an argon atmosphere. Diisopropylamine (25 mmol, 3.528 mL, 2.0 eq.) was added and the reaction mixture was stirred at –30 °C for 10 min before warming up to r.t. and stirred for another hour. The resulting suspension was filtered over celite again. The clear filtrate was cooled to –78 °C under an argon atmosphere and a solution of vinylmagnesium bromide (Sigma, 1.0 M in THF, 13.75 mmol, 13.75 mL, 1.1 eq.) was added, stirred for 10 min at –78 °C and then at r.t. for another hour. The reaction mixture was then concentrated to roughly 20 mL under reduced pressure, diluted with saturated aqueous $NaHCO_3$ (60 mL) and extracted with EtOAc (3x 120 mL). The combined organic layers were dried over $NaSO_4$, filtered and the solvents were removed under reduced pressure. The resulting oily residue was purified by silica gel (Sigma, Davisil Grade 633, pore size 60 Å, 200-425 mesh particle size) chromatography (*n*-hexane + 1% Et_3N) to yield the titled compound as a colourless oil (852 mg, 4.19 mmol, 34%). ^{1}H-NMR: (300 MHz, CD_3CN): δ = 6.36-6.14 (m, 1H), 5.77-5.53 (m, 2H), 3.81-3.61 (m, 2H), 3.53-3.38 (m, 2H), 1.23-1.04 (m, 15H). ^{13}C-NMR: (75 MHz, CD_3CN): δ = 142.23 (d, J = 7.0 Hz), 125.34 (d, J = 19.7 Hz), 63.01 (d, J = 21.0 Hz), 46.63 (d, J = 9.5 Hz), 24.83 (dd, J = 22.3, 6.9 Hz), 17.59 (d, J = 7.6 Hz). ^{31}P-NMR (122 MHz, CD_3CN) δ = 113.79. HR-MS (ESI+) for $C_{10}H_{23}NOP^+$ [M+H$^+$] calcd.: 204.1517; found: 204.1596.

General procedure 3: Synthesis of ethynyl- and vinylphosphonothiolates from intermediates 33 and 34

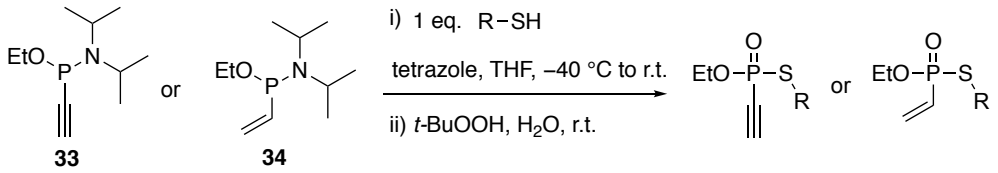

Scheme 59 Synthesis of ethynyl- and vinylphosphonothiolates from **33** and **34**, respectively.

A round bottom flask was charged with **33** or **34** (1.0 eq.), dissolved in dry acetonitrile (to reach a concentration of 0.1 M) and cooled to –40 °C. Separately, a solution of the desired thiol (1.0 eq.) and tetrazole (Sigma, 0.45 M in MeCN, 2.0 eq.) was prepared and added drop-wise to the first stirred solution at –40 °C. The reaction mixture was stirred for 10 min at –40 °C before allowed to warm to r.t. and stirred for another 30 min. Then, a tert-butyl hydroperoxide solution (70 wt. % in H_2O, 1.0 eq.) was added at r.t. and stirred for 10 min. The reaction mixture was then diluted with H_2O (e.g. 3 mL for 0.1 mmol scale) and extracted with DCM (3x 10 mL). The combined organic layers were dried over Na_2SO_4, filtered and the solvents were removed under reduced pressure. The crude product was purified by silica gel chromatography.

***S*-benzyl *O*-ethyl ethynylphosphonothiolate (35)**

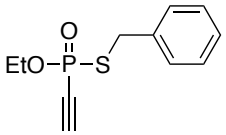

Compound **35** was prepared according to general procedure 3 starting from **33** (25 mg, 0.123 mmol) and mercaptobenzyl (14.4 μL, 0.123 mmol). Purification by silica gel chromatography (100% EtOAc) gave the desired compound as a colourless oil (10 mg, 0.042 mmol, 34%). ^{1}H-NMR: (300 MHz, $CDCl_3$): δ = 7.40-7.27 (m, 5H), 4.27-3.99 (m, 4H), 3.10 (d, J = 12.5 Hz, 1H), 1.33 (td, J = 7.1, 0.6 Hz, 3H). ^{13}C-NMR: (75 MHz, $CDCl_3$): δ = 136.58 (d, J = 6.3 Hz), 129.21, 128.86, 127.95, 88.99 (d, J = 42.7 Hz), 77.41 (d, J = 238.2 Hz), 63.62 (d, J = 6.5 Hz), 35.16 (d, J = 3.4 Hz), 16.17 (d, J = 7.5 Hz). ^{31}P-NMR (122 MHz, $CDCl_3$): δ = 15.36. HR-MS (ESI+) for $C_{11}H_{14}O_2PS^+$ [M+H$^+$] calcd.: 241.0447; found: 241.0447.

S-Boc-ethylamine *O*-ethyl ethynylphosphonothiolate (36)

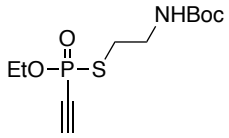

Compound **36** was prepared according to general procedure 3 starting from **33** (93 mg, 0.465 mmol) and tert-butyl (2-mercaptoethyl)carbamate (82 mg, 0.465 mmol). Purification by silica gel chromatography (100% EtOAc) gave the desired compound as a colourless oil (44 mg, 0.15 mmol, 32%). ^{1}H-NMR: (600 MHz, DMSO−d_6): δ = 5.02 (d, J = 12.7 Hz, 1H), 4.33 (dq, J = 10.1, 7.0 Hz, 2H), 3.11 (dt, J = 15.5, 6.9 Hz, 2H), 2.69 (p, J = 1.8 Hz, 2H), 1.57 (s, 9H), 1.49 (t, J = 7.0 Hz, 3H). ^{13}C-NMR: (151 MHz, DMSO−d_6): δ = 155.42, 93.47 (d, J = 40.6 Hz), 77.93, 77.11 (d, J = 234 Hz), 63.18 (d, J = 6.7 Hz), 40.19, 30.01, 28.15, 15.86 (d, J = 7.1 Hz). ^{31}P-NMR (243 MHz, DMSO−d_6): δ = 11.75. HR-MS (ESI+) for $C_{11}H_{20}NO_4PSNa^+$ [M+Na^+] calcd.: 316.0743; found: 316.0746.

S-benzyl *O*-ethyl vinylphosphonothiolate (17)

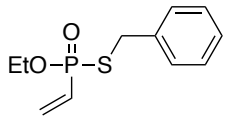

Compound **17** was prepared according to general procedure 3 starting from **34** (25 mg, 0.123 mmol) and mercaptobenzyl (14.4 μL, 0.123 mmol). Purification by silica gel chromatography (100% EtOAc) gave the desired compound as a colourless oil (11 mg, 0.0454 mmol, 37%). This compound has already been characterized above.

S-Boc-ethylamine *O*-ethyl vinylphosphonothiolate (37)

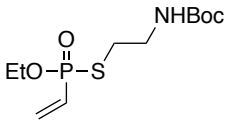

Compound **37** was prepared according to general procedure 3 starting from **34** (93 mg, 0.465 mmol) and tert-butyl (2-mercaptoethyl)carbamate (82 mg, 0.465 mmol). Purification by silica gel chromatography (100% EtOAc) gave the desired compound as a colourless oil (30 mg, 0.10 mmol, 22%). ^{1}H-NMR: (300 MHz, $CDCl_3$): δ = 6.41-5.98 (m, 3H), 4.30-4.09 (m, 2H), 3.39 (t, J = 6.5 Hz, 2H), 3.06-2.80 (m, 2H), 1.44 (s, 9H), 1.36 (t, J = 7.1 Hz, 3H). ^{13}C-NMR: (75 MHz, $CDCl_3$): δ = 155.95, 134.62, 130.27 (d, J = 145 Hz), 79.66, 62.55 (d, J = 6 Hz), 41.41, 30.19, 28.44, 16.32 (d, J = 6.7 Hz). ^{31}P-NMR (122 MHz, Chloroform-d): δ = 42.26.

8.2.5 Derivatisation of general phosphonothiolate building blocks

_S_-Propanoic NHS ester _O_-ethyl vinylphosphonothiolate (38)

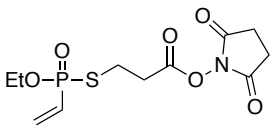

Carboxylic acid **19** (10 mg, 0.0446 mmol, 1.0 eq) and _N_-hydroxysuccinimide (5.1 mg, 0.0446 mg, 1.0 eq.) were dissolved in 400 μL of a 1,4-dioxane/EtOAc = 1:1 mixture and cooled to 0 °C. Dicyclohexylcarbodiimide (9.2 mg, 0.0446 mmol, 1.0 eq.) was added to the stirred solution and the mixture was allowed to warm to r.t. After 1 h, the suspension was filtered and the clear residue was dried under reduced pressure to yield compound **38** (12 mg, 0.0374 mmol, 84%). ^{1}H-NMR: (600 MHz, $CDCl_3$): δ = 6.39-6.09 (m, 3H), 4.29-4.13 (m, 2H), 3.19-2.99 (m, 4H), 1.37 (t, J = 7.1 Hz, 3H). ^{13}C-NMR: (151 MHz, $CDCl_3$): δ =168.92, 166.85, 134.76, 130.50 (d, J = 146.2 Hz), 62.41 (d, J = 6.8 Hz), 33.03 (d, J = 3.0 Hz), 25.71, 24.57 (d, J = 2.9 Hz), 16.40 (d, J = 6.9 Hz). ^{31}P-NMR (243 MHz, $CDCl_3$): 41.44. HR-MS (ESI+) for $C_{11}H_{17}NO_6PS^+$ [M+H$^+$] calcd: 322.0509, found: 322.0540.

_S_-EDANS _O_-ethyl vinylphosphonothiolate (39)

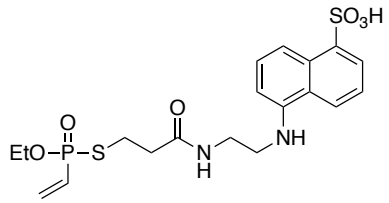

NHS ester **38** (30 mg, 0.0934 mmol, 1.0 eq.) and EDANS (Biomol, 30 mg, 0.103 mmol, 1.1 eq.) were dissolved in 470 μL DMF in an Eppendorf tube. DIPEA (33 μL, 0.189 mmol, 2.0 eq.) was added and the suspension was stirred at r.t. for 15 min. The volatiles were evaporated under reduced pressure and the crude product was purified by preparative HPLC (5-60% MeCN in 40 min, flow: 16 mL/min) to yield compound **39** (24 mg, 0.0508 mmol, 54%) as a white powder after lyophilisation. ^{1}H-NMR: (600 MHz, DMSO$-d_6$): δ = 8.32 (d, J = 8.6 Hz, 1H), 8.22 (t, J = 5.8 Hz, 1H), 8.07 (d, J = 8.5 Hz, 1H), 7.96 (d, J = 7.0 Hz, 1H), 7.40 (dd, J = 8.5, 7.1 Hz, 1H), 7.34 (t, J = 8.1 Hz, 1H), 6.81 (d, J = 7.3 Hz, 1H), 6.38 (ddd, J = 28.0, 18.4, 12.4 Hz, 1H), 6.25-6.11 (m, 2H), 4.14 ,Äì 3.98 (m, 2H), 3.41 (t, J = 6.2 Hz, 2H), 3.32 (t, J = 6.5 Hz, 2H), 2.93 (ddt, J = 18.0, 12.9, 6.6 Hz, 2H), 1.26 (t, J = 7.0 Hz, 3H). ^{13}C-NMR: (151 MHz, DMSO$-d_6$): δ = 170.42, 144.21, 134.28, 130.60 (d, J = 142 Hz), 130.09, 125.92, 124.59, 124.07, 123.23, 122.62, 61.37 (d, J = 6.7 Hz), 44.79, 37.23, 36.23 (d, J = 4.0 Hz), 25.42 (d, J = 2.8 Hz), 16.10 (d, J = 6.5 Hz). ^{31}P-NMR (243 MHz, DMSO$-d_6$): δ = 41.29. HR-MS (ESI+) for $C_{19}H_{26}N_2O_6PS_2^+$ [M+H$^+$] calcd.: 473.0964, found: 473.0984.

S-ethylamine *O*-ethyl ethynylphosphonothiolate (40)

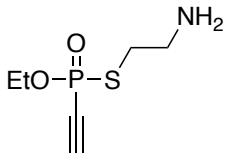

Boc-protected ethynylphosphonothiolate derivative **36** was dissolved in TFA/H_2O=95:5 at a concentration of 0.1 M. The solution was stirred for 10 min at r.t. and then diluted with water (1:10). The product **40** (an oil) was obtained quantitatively after lyophilization and was directly used for subsequent reactions.

S-ethylamine *O*-ethyl vinylphosphonothiolate (41)

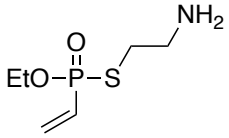

Boc-protected vinylphosphonothiolate derivative **37** was dissolved in TFA/H_2O=95:5 at a concentration of 0.1 M. The solution was stirred for 10 min at r.t. and then diluted with water (1:10). The product **41** (an oil) was obtained quantitatively after lyophilization and was directly used for subsequent reactions.

4-oxo-4-((2-((5-sulfonaphthalen-1-yl)amino)ethyl)amino)butanoic acid (42)

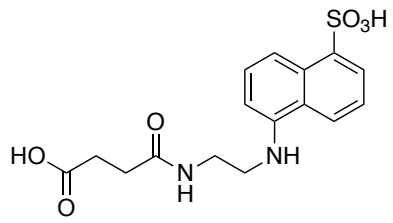

HATU (690 mg, 1.814 mmol, 1.0 eq.) and succinic acid (214 mg, 1.814 mmol, 1.0 eq.) were dissolved in 6 mL DMF containing DIPEA (1.263 mL, 7.254 mmol, 4.0 eq.). This solution was added to EDANS (483 mg, 1.814 mmol, 1.0 eq.) dissolved in 3 mL DMF and the mixture was stirred at r.t. for 30 min. The solvents were then removed under reduced pressure and the crude product was purified by preparative HPLC, giving product **42** (508 mg, 1.387 mmol, 76%) as a slightly greenish powder after lyophilization.

S-EDANS derivative O-ethyl ethynylphosphonothiolate (43)

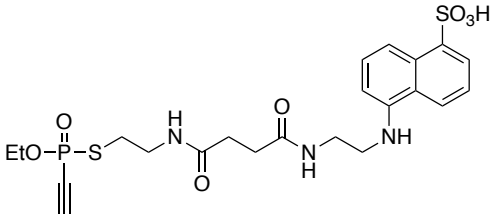

A solution containing HATU (24.2 mg, 0.0635 mmol, 1.1 eq.), EDANS-derivative **42** (23.3 mg, 0.0635 mmol, 1.1 eq.) and DIPEA (30 μL, 0.173 mmol, 3.0 eq.) in 0.2 mL DMF was added to amine derivative **40** (11.2 mg, 0.0578 mmol, 1.0 eq.) dissolved in 0.1 mL DMF and the mixture was stirred at r.t. for 30 min. The solvents were then evaporated under reduced pressure and the crude product was purified via semipreparative HPLC (gradient: 10-50% MeCN+0.1% TFA in H_2O+0.1% TFA over 50 min, flow: 5 mL/min) giving product **43** (10 mg, 0.0185 mmol, 32%) as a white powder after lyophilization. ^{1}H-NMR: (600 MHz, DMSO−d_6): δ = 8.40 (m, broad, 1H), 8.17-8.05 (m, 3H), 8.01-7.95 (m, 1H), 7.45-7.40 (m, 1H), 7.39-7.34 (m, 1H), 6.93 (m, broad, 1H), 4.83 (d, J = 12.8 Hz, 1H) 4.13 (dq, J = 10.1, 7.0 Hz, 2H), 3.41 (q, J = 6.1 Hz, 2H), 3.33 (p, J = 6.6, 5.9 Hz, 4H), 3.11-3.04 (m, 1H), 2.92 (dtd, J = 16.2, 6.9, 2.7 Hz, 2H), 2.38-2.32 (m, 4H), 1.29 (t, J = 7.1 Hz, 3H), 1.16 (t, J = 7.3 Hz, 1H). ^{13}C-NMR: (151 MHz, DMSO−d_6): δ = 172.22, 171.59, 144.19, 130.09, 125.90, 124.71, 124.35, 124.21, 123.80, 123.60, 123.40, 122.66, 93.55 (d, J = 41.8 Hz), 77.12 (d, J = 232.1 Hz), 63.29 (d, J = 6.6 Hz), 45.78, 38.94 (d, J = 5.4 Hz), 30.69, 30.61, 29.70, 15.90 (d, J = 7.2 Hz), 8.61. ^{31}P-NMR (243 MHz, DMSO−d_6): δ = 11.77. HR-MS (ESI+) for $C_{22}H_{29}N_3O_7PS_2^+$ [M+H$^+$] calcd.: 542.1179, found: 542.1156.

S-EDANS derivative O-ethyl vinylphosphonothiolate (44)

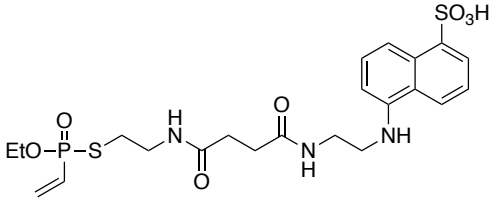

A solution containing HATU (20.6 mg, 0.0541 mmol, 1.1 eq.), EDANS-derivative **42** (19.8 mg, 0.0541 mmol, 1.1 eq.) and DIPEA (26 μL, 0.147 mmol, 3.0 eq.) in 0.2 mL DMF was added to amine derivative **41** (9.6 mg, 0.0490 mmol, 1.0 eq.) dissolved in 0.1 mL DMF and the mixture was stirred at r.t. for 30 min. The solvents were then evaporated under reduced pressure and the crude product was purified via semipreparative HPLC (gradient: 10-50% MeCN+0.1% TFA in H_2O+0.1% TFA over 50 min, flow: 5 mL/min) giving product **44** (11 mg, 0.0202 mmol, 41%) as a white powder after lyophilization. ^{1}H-NMR: (600 MHz, DMSO−d_6): δ = 8.39 (d, J = 8.7 Hz, 1H), 8.11 (dt, J = 10.8, 5.7 Hz, 2H), 8.07 (d, J = 8.7 Hz, 1H), 7.98 (d, J = 7.1 Hz, 1H), 7.43 (t, J = 7.8 Hz, 1H), 7.37 (t, J = 8.1 Hz, 1H), 6.46-6.33 (m, 1H), 6.25-6.11 (m, 2H), 4.15-4.01 (m, 2H), 3.40 (q, J = 6.2 Hz, 2H), 3.33 (t, J = 6.4 Hz, 2H), 3.25 (q, J = 6.7 Hz, 2H), 3.08 (qd, J = 7.3, 4.8 Hz, 1H), 2.77 (dqt, J = 19.9, 13.1, 6.9 Hz, 2H), 2.38-2.30 (m, 4H), 1.26 (t, J = 7.0 Hz, 3H), 1.16 (t, J = 7.3 Hz, 2H). ^{13}C-NMR:

(151 MHz, DMSO−d_6): δ = 172.22, 171.52, 144.17, 134.41, 130.54 (d, J = 142.1 Hz), 130.07, 125.92, 124.71, 124.27, 123.56, 122.68, 61.45 (d, J = 7.7 Hz), 45.78, 37.07, 30.71, 30.62, 28.98, 16.11 (d, J = 6.5 Hz), 8.61. ^{31}P-NMR (243 MHz, DMSO−d_6): δ = 38.38. HR-MS (ESI+) for $C_{22}H_{31}N_3O_7PS_2^+$ [M+H$^+$] calcd.: 544.1341, found: 544.1316.

_S_-4-(ethylamido)-4-biotin _O_-ethyl ethynylphosphonothiolate (45)

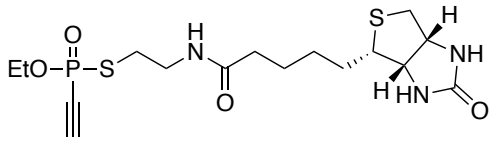

A solution containing HATU (61 mg, 0.160 mmol, 1.1 eq.), biotin (39 mg, 0.160 mmol, 1.1 eq.) and DIPEA (76 μL, 0.435 mmol, 3.0 eq.) in 0.4 mL DMF was added to amine derivative **40** (28 mg, 0.145 mmol, 1.0 eq.) dissolved in 0.2 mL DMF and the mixture was stirred at r.t. for 30 min. The solvents were then evaporated under reduced pressure and the crude product was purified via semipreparative HPLC (gradient: 10-50% MeCN+0.1% TFA in H_2O+0.1% TFA over 50 min, flow: 10 mL/min) giving product **45** (20 mg, 0.0477 mmol, 33%) as a white powder after lyophilization. ^{1}H-NMR: (600 MHz, DMSO−d_6): δ = 8.06 (t, J = 5.7 Hz, 1H), 4.83 (d, J = 12.6 Hz, 1H), 4.30 (ddd, J = 7.7, 5.2, 1.0 Hz, 1H), 4.19-4.10 (m, 3H), 3.33 (td, J = 6.8, 5.6 Hz, 2H), 3.10 (ddd, J = 8.5, 6.3, 4.4 Hz, 1H), 2.94 (dtd, J = 15.7, 6.8, 3.0 Hz, 2H), 2.85-2.80 (m, 1H), 2.58 (d, J = 12.3 Hz, 1H), 2.50 (p, J = 1.9 Hz, 1H), 2.07 (t, J = 7.4 Hz, 2H), 1.61 (m, 1H), 1.56-1.41 (m, 3H), 1.36-1.26 (m, 5H (a multiplet (2H) and a triplet (3H) are overlaying)). ^{13}C-NMR: (151 MHz, DMSO−d_6): δ = 177.26, 162.67, 93.51 (d, J = 40.8 Hz), 77.12 (d, J = 234.1 Hz), 63.26 (d, J = 6.4 Hz), 61.01, 59.18, 55.37, 38.80 (d, J = 5.4 Hz), 35.09, 29.80, 28.13, 28.00, 25.16, 15.89 (d, J = 7.0 Hz). ^{31}P-NMR (243 MHz, DMSO−d_6): δ = 11.77. HR-MS (ESI+) for $C_{16}H_{27}N_3O_4PS_2^+$ [M+H$^+$] calcd.: 420.1175, found: 420.1154.

_S_-4-(ethylamido)-4-biotin _O_-ethyl vinylphosphonothiolate (46)

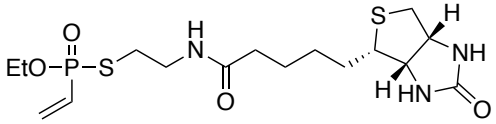

A solution containing HATU (31.7 mg, 0.0834 mmol, 1.1 eq.), biotin (20.4 mg, 0.0834 mmol, 1.1 eq.) and DIPEA (40 μL, 0.227 mmol, 3.0 eq.) in 0.4 mL DMF was added to amine derivative **41** (14.8 mg, 0.0758 mmol, 1.0 eq.) dissolved in 0.1 mL DMF and the mixture was stirred at r.t. for 30 min. The solvents were then evaporated under reduced pressure and the crude product was purified via semipreparative HPLC (gradient: 10-50% MeCN+0.1% TFA in H_2O+0.1% TFA over 50 min, flow: 10 mL/min) giving product **46** (14 mg, 0.0332 mmol, 44%) as a white powder after lyophilization. This compound has been characterized above (compare compound **18**).

_S_-4-(ethylamido)-4-oxobutanoic acid _O_-ethyl ethynylphosphonothiolate (47)

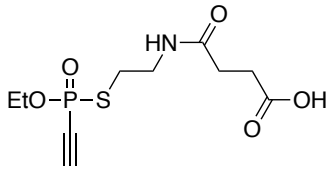

A solution containing HATU (122 mg, 0.321 mmol, 1.0 eq.), succinic acid (38 mg, 0.321 mmol, 1.0 eq.) and DIPEA (167 μL, 0.962 mmol, 3.0 eq.) in 1.0 mL DMF was added to amine derivative **40** (62 mg, 0.321 mmol, 1.0 eq.) dissolved in 1.0 mL DMF and the mixture was stirred at r.t. for 30 min. The solvents were then evaporated under reduced pressure and the crude product was purified via semipreparative HPLC (gradient: 20-60% MeCN+0.1% TFA in H_2O+0.1% TFA over 60 min, flow: 10 mL/min) giving product **47** (34 mg, 0.116 mmol, 36%) as a white powder after lyophilization. ^{1}H-NMR: (600 MHz, DMSO−d_6): δ = 12.05 (s, broad, 1H), 8.12 (t, J = 5.8 Hz, 1H), 4.84 (d, J = 12.7 Hz, 1H), 4.19-4.10 (m, 2H), 3.36-3.30 (m, 2H, overlay with H_2O), 2.97-2.88 (m, 2H), 2.42 (t, J = 6.9 Hz, 2H), 2.31 (t, J = 6.9 Hz, 2H), 1.30 (t, J = 7.0 Hz, 3H). ^{13}C-NMR: (151 MHz, DMSO−d_6): δ = 173.71, 171.18, 93.50 (d, J = 40.1 Hz), 77.12 (d, J = 233.6 Hz), 63.27 (d, J = 6.9 Hz), 38.93 (d, J = 5.4 Hz), 29.91, 29.67 (d, J = 3.7 Hz), 29.00, 15.88 (d, J = 6.7 Hz). ^{31}P-NMR (243 MHz, DMSO−d_6): δ = 11.75. HR-MS (ESI+) for $C_{10}H_{17}NO_5PS^+$ [M+H^+] calcd.: 294.0560, found: 294.0558.

_S_-4-(ethylamido)-4-oxobutanoic acid _O_-ethyl vinylphosphonothiolate (48)

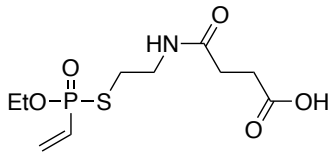

A solution containing HATU (117 mg, 0.308 mmol, 1.0 eq.), succinic acid (36 mg, 0.308 mmol, 1.0 eq.) and DIPEA (160 μL, 0.923 mmol, 3.0 eq.) in 1.0 mL DMF was added to amine derivative **41** (60 mg, 0.308 mmol, 1.0 eq.) dissolved in 1.0 mL DMF and the mixture was stirred at r.t. for 30 min. The solvents were then evaporated under reduced pressure and the crude product was purified via semipreparative HPLC (gradient: 20-60% MeCN+0.1% TFA in H_2O+0.1% TFA over 60 min, flow: 10 mL/min) giving product **48** (42 mg, 0.142 mmol, 46%) as a white powder after lyophilization. ^{1}H-NMR: (300 MHz, $CDCl_3$): δ = 7.79 (s, broad, 1H), 7.46 (t, J = 5.4 Hz, 1H), 6.43-6.02 (m, 3H), 4.27-4.09 (m, 2H), 3.61-3.42 (m, 2H), 3.09-2.78 (m, 2H), 2.73-2.61 (m, 2H), 2.60-2.48 (m, 2H), 1.35 (t, J = 7.1 Hz, 3H). ^{13}C-NMR: (75 MHz, $CDCl_3$): δ = 175.52, 173.12, 135.41 (d, J = 1.6 Hz), 129.78 (d, J = 145.9 Hz), 62.90 (d, J = 7.0 Hz), 40.79 (d, J = 2.8 Hz), 30.79, 29.92, 28.97 (d, J = 2.8 Hz), 16.39 (d, J = 6.9 Hz). ^{31}P-NMR (122 MHz, $CDCl_3$): δ = 44.28. HR-MS (ESI+) for $C_{18}H_{19}NO_5PS^+$ [M+H^+] calcd.: 296.0716, found: 296.0724.

S-Val-Cit-PHB-MMAE *O*-ethyl ethynylphosphonothiolate (50)

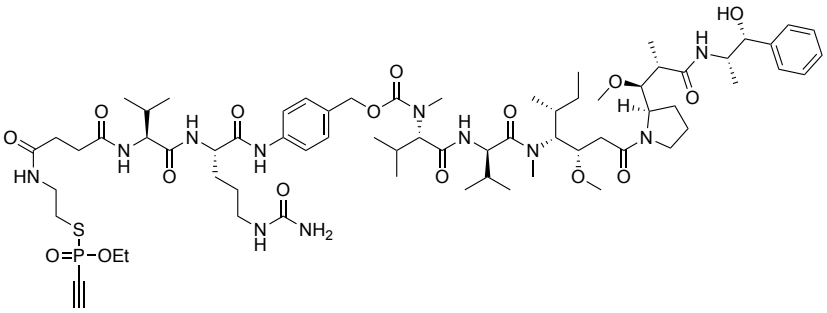

A solution containing HATU (2.44 mg, 6.41 μmol, 1.2 eq.), carboxylic acid ethynylphosphonothiolate derivative **47** (1.88 mg, 6.41 μmol, 1.2 eq.) and DIPEA (4.7 μL, 26.7 μmol, 5 eq.) in 100 μL DMF was mixed with a solution of Val-Cit-PHB-MMAE **49**[9] (6 mg, 5.34 μmol, 1.0 eq.) in 100 μL DMF. The mixture was shaken at r.t. for 1 hour before diluted with water (4 mL). The crude product was purified by semipreparative HPLC (gradient: 30-99% MeCN + 0.1% TFA in H_2O + 0.1% TFA over 50 min, flow: 5 mL/min) to give product **50** (3 mg, 2.14 μmol, 40%) as a white powder after lyophilization.
HR-MS (ESI+) for $C_{68}H_{110}N_{11}O_{16}PS^{2+}$ [M+2H$^+$] calcd.: 699.8790; found: 699.8792.

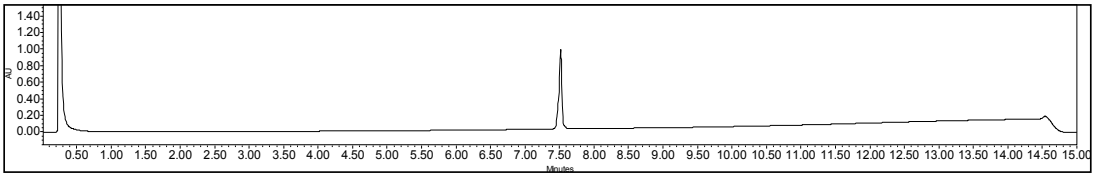

Fig. 76 UPLC-UV analysis (220 nm) of purified compound **50**.

S-Val-Cit-PHB-MMAE *O*-ethyl vinylphosphonothiolate (51)

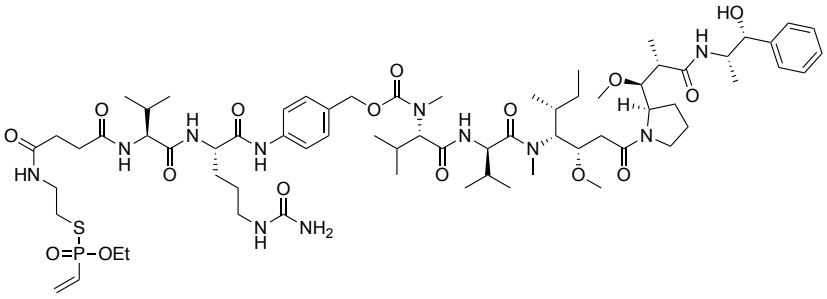

A solution containing HATU (3.0 mg, 7.90 μmol, 1.2 eq.), carboxylic acid vinylphosphonothiolate derivative **48** (2.33 mg, 7.90 μmol, 1.2 eq.) and DIPEA (5.8 μL, 32.9 μmol, 5 eq.) in 150 μL DMF was mixed with a solution of Val-Cit-PHB-MMAE **49** (7.4 mg, 6.59 μmol, 1.0 eq.) in 150 μL DMF. The mixture was shaken at r.t. for 15 min before diluted with water (5 mL). The crude product was purified by semipreparative HPLC

[9] *Compound **49** was synthesized and has been kindly provided by Dr. Philipp Ochtrop and Dr. Marc-André Kasper.*

(gradient: 30-99% MeCN + 0.1% TFA in H_2O + 0.1% TFA over 50 min, flow: 5 mL/min) to give product **51** (4.74 mg, 3.38 μmol, 51%) as a white powder after lyophilization. HR-MS (ESI+)for $C_{68}H_{112}N_{11}O_{16}PS^{2+}$ [M+2H$^+$]: calcd.: 700.8868; found: 700.8866.

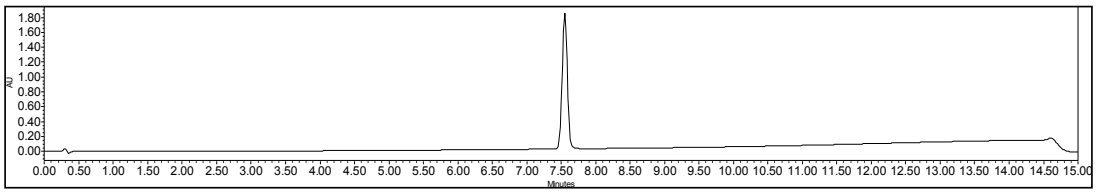

Fig. 77 UPLC-UV analysis (220 nm) of purified compound **51**.

Tetrazole synthesis

Compound **53** was synthesized according to Ref. [308] with some adaptions.

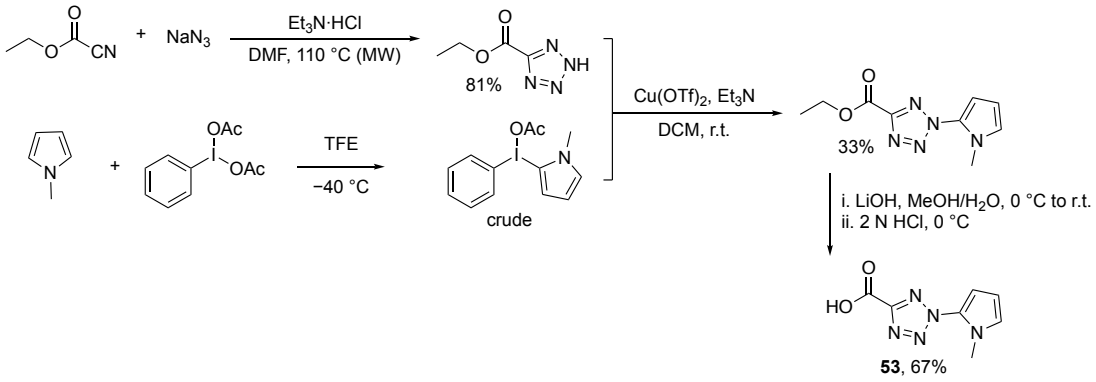

Ethyl 2H-tetrazole-5-carboxylate

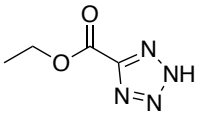

To a solution of ethyl cyanoformate (1.50 g, 15 mmol, 1.0 eq.) in DMF (10 mL) in a microwave tube was added NaN_3 (1.97 g, 30 mmol, 2.0 eq.) and Et_3N•HCl (4.20 g, 30 mmol, 2.0 eq.). The mixture was stirred at 110 °C under microwave irradiation for 2 h (Biotage, Initiator$^+$). Then 2 N HCl (10 mL) was added at 0 °C and the mixture was extracted with EtOAc (3 times with 20 mL). The combined organic layer was washed with brine, dried over anhydrous Na_2SO_4, filtered and concentrated. The residue was redissolved in water and lyophilized. After lyophilization, the title compound was obtained as a yellowish solid (1.73 g, 12.17 mmol, 81%).

Ethyl 2-(1-methyl-1H-pyrrol-2-yl)-2H-tetrazole-5-carboxylate

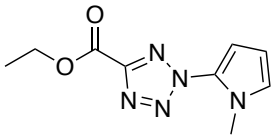

To a solution of 1-methyl-1H-pyrrole (1 g, 12.5 mmol, 2.5 eq.) in trifluoroethanol (10 mL) under an argon atmosphere was added $PhI(OAc)_2$ (4.00 g, 12.5 mmol, 2.5 eq.) at –40 °C. The mixture was stirred at –40 °C for 2 h, then concentrated under reduced pressure. The residue was dissolved in dry DCM (20 mL), then ethyl 2H-tetrazole-5-carboxylate (710 mg, 5 mmol, 1.0 eq.), $Cu(OTf)_2$ (722 mg, 2 mmol, 0.4 eq.) and Et_3N (3.43 mL, 25 mmol, 5.0 eq.) were added at r.t.. The mixture was stirred at r.t. under an argon for 16 h, then washed with saturated NH_4Cl, brine, dried over anhydrous Na_2SO_4, filtered and concentrated. The residue was purified by silica gel flash chromatography (*n*-hexane/EtOAc = 3:1) to afford the title compound as a brown oil (368 mg, 1.66 mmol, 33%). ^{1}H-NMR: (300 MHz, $CDCl_3$): δ = 6.62 (dd, J = 3.0, 2.0 Hz, 1H), 6.47 (dd, J = 4.0, 2.0 Hz, 1H), 6.05 (dd, J = 4.0, 2.9 Hz, 1H), 4.39 (q, J = 7.1 Hz, 2H), 3.60 (s, 3H), 1.32 (t, J = 7.1 Hz, 3H). ^{13}C-NMR: (75 MHz, $CDCl_3$): δ = 157.28, 156.94, 124.43, 123.72, 107.42, 105.94, 62.42, 34.65, 13.85.

2-(1-methyl-1H-pyrrol-2-yl)-2H-tetrazole-5-carboxylic acid (53)

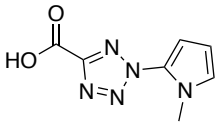

To a solution of ethyl 2-(1-methyl-1H-pyrrol-2-yl)-2H-tetrazole-5-carboxylate (463 mg, 2.181 mmol) in MeOH/H_2O (1:1, 8 mL) was added a 1 N LiOH solution in H_2O (1.6 mL) at 0 °C. The mixture was stirred at r.t. for 30 min. Then, the solution was acidified with 1 N HCl at 0 °C to pH = 2-3, and the mixture was extracted with DCM (3 times 10 mL). The combined organic layer was washed with brine, dried over anhydrous Na_2SO_4, filtered and concentrated to afford the title compound as a brown solid (284 mg, 1.47 mmol, 67%). ^{1}H-NMR: (300 MHz, $CDCl_3$): δ = 6.75 (dd, J = 2.9, 2.0 Hz, 1H), 6.71 (dd, J = 4.0, 1.9 Hz, 1H), 6.26 (dd, J = 4.0, 2.9 Hz, 1H), 3.79 (s, 3H). HR-MS (ESI+) for $C_7H_8N_5O_2^+$ $[M+H]^+$ calcd.: 194.0673, found: 194.0674.

***S*-diazirine derivative, *O*-ethyl vinylphosphonothiolate (54)**

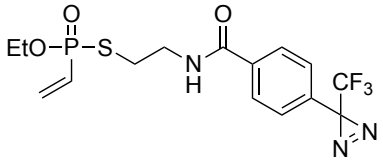

A solution containing HATU (41 mg, 0.108 mmol, 1.5 eq.), 4-[3-(trifluoromethyl)-3H-diazirin-3-yl]benzoic acid (TCI, 25 mg, 0.108 mmol, 1.5 eq.) and DIPEA (37 μL,

0.215 mmol, 3.0 eq.) in 0.3 mL DMF was added to a solution of amine vinylphosphonothiolate derivative **41** (14 mg, 0.717 mmol, 1.0 eq.) in 0.1 mL DMF. The mixture was stirred at r.t. for 1 hour before diluted with water (4 mL). The crude product was purified by semipreparative HPLC (gradient: 5-99% MeCN + 0.1% TFA in H_2O+0.1% TFA over 40 min, flow: 5 mL/min). After lyophilization, the titled product was obtained as a white powder (9.7 mg, 0.0238 mmol, 33%).
^{1}H-NMR: (300 MHz, $CDCl_3$): δ = 8.24 (s, 1H), 8.16-7.96 (m, 3H), 7.32-7.19 (m, overlap with $CDCl_3$ signal), 6.43-6.01 (m, 3H), 4.23-4.06 (m, 2H), 3.90-3.63 (m, 2H), 3.24-2.96 (m, 2H), 1.31 (t, J = 7.1 Hz, 3H). ^{13}C-NMR: (75 MHz, $CDCl_3$): δ = 168.93, 166.57, 135.30, 135.08, 132.35, 130.52, 128.89 (d, J = 146.6 Hz), 127.88, 126.57, 122.02 (q, J = 275 Hz), 62.95 (d, J = 7.2 Hz), 42.01, 28.75 (d, J = 2.7 Hz), 28.55 (d, J = 46.6 Hz), 16.36 (d, J = 6.9 Hz). ^{31}P-NMR: (122 MHz, $CDCl_3$): δ = 45.04. HR-MS (ESI+) for $C_{15}H_{18}F_3N_3O_3PS^+$ $[M+H]^+$ calcd.: 408.0753, found: 408.0761.

_S_-methyl-pyrrol-tetrazole derivative, _O_-ethyl vinylphosphonothiolate (55)

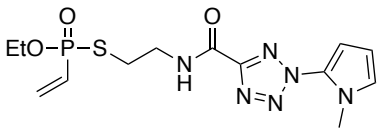

A solution containing HATU (58 mg, 0.154 mmol, 3.0 eq.), methyl-pyrrole-tetrazole carboxylic acid derivative **53** (30 mg, 0.154 mmol, 3.0 eq.) and DIPEA (27 μL, 0.154 mmol, 3.0 eq.) in 0.2 mL DMF was added to a solution of amine vinylphosphonothiolate derivative **41** (10 mg, 0.0512 mmol, 1.0 eq.) in 0.1 mL DMF. The mixture was stirred at r.t. for 1 hour before diluted with water (4 mL). The crude product was purified by semipreparative HPLC (gradient: 5-99% MeCN + 0.1% TFA in H_2O+0.1% TFA over 40 min, flow: 5 mL/min). After lyophilization, the title product was obtained as a white powder (4 mg, 0.0108 mmol, 21%). ^{1}H-NMR: (600 MHz, DMSO−d_6): δ = 9.33 (s, 1H), 7.05 (dd, J = 2.9, 2.0 Hz, 1H), 6.63 (dd, J = 3.9, 2.0 Hz, 1H), 6.50-6.12 (m, 4H, the vinyl protons and one proton from the pyrrol ring overlap), 4.15-4.07 (m, 2H), 3.65 (s, 3H), 3.60-3.53 (m, 2H), 2.97 (ddt, J = 14.0, 8.8, 6.9 Hz, 2H), 1.28 (t, J = 7.0 Hz, 3H). ^{13}C-NMR: (151 MHz, DMSO−d_6): δ = 159.24, 156.14, 134.52, 130.44 (d, J = 142.0 Hz), 124.31, 124.09, 107.17, 106.05, 61.49 (d, J = 6.7 Hz), 40.05, 34.09, 28.45, 16.09 (d, J = 6.5 Hz). ^{31}P-NMR: (243 MHz, DMSO−d_6): δ = 38.20. HR-MS (ESI+) for $C_{13}H_{20}N_6O_3PS^+$ $[M+H]^+$ calcd.: 371.1050, found: 371.1047.

FRET pair (59)

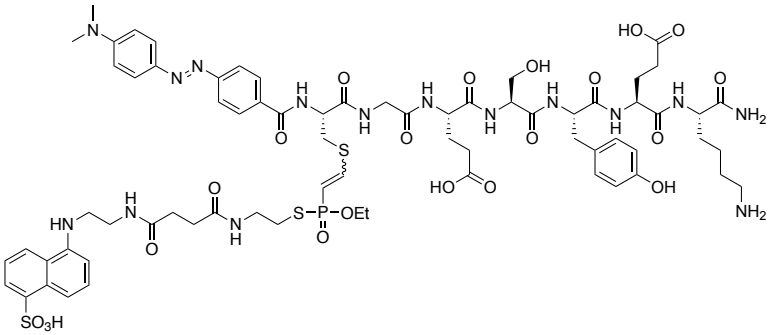

To a solution of Dabcyl peptide[10] (2.5 mg, 2.35 μmol, 1.0 eq.) in aqueous 50 mM NH_4HCO_3 buffer containing 1 mM EDTA at pH 8.5 was added EDANS ethynylphosphonothiolate derivative **43** (1.5 mg, 2.82 μmol, 1.2 eq.) dissolved in DMF (280 μL). The reaction mixture was shaken at r.t. for 1 hour and then diluted with water (4.7 mL) for purification via semipreparative HPLC (gradient: 10-50% MeCN+0.1% TFA in H_2O+0.1% TFA over 45 min, flow: 16 mL/min). After lyophilization, product **59** was obtained as a red powder (3 mg, 1.87 μmol, 80%).
HR-MS (ESI+) for $C_{70}H_{94}N_{15}O_{21}PS_3^+$ $[M+H]^+$ calcd.: 803.7819, found: 803.7806.

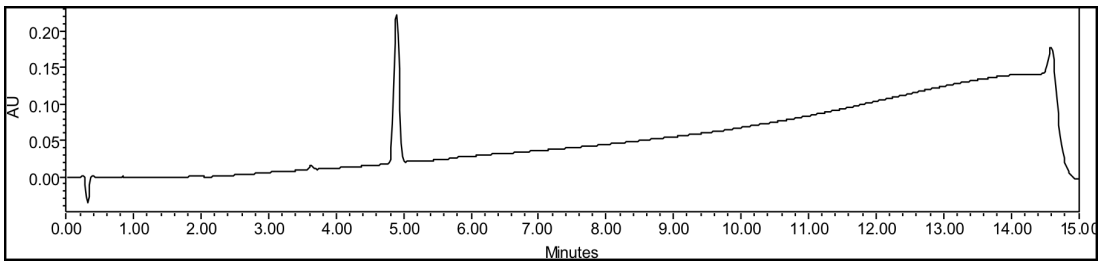

Fig. 78 UPLC-UV analysis (220 nm) of compound **59**.

[10] *The Dabcyl-cysteine peptide was kindly provided by Dr. Marc-André Kasper, who synthesized it according to Ref. [208].*

FRET pair (60)

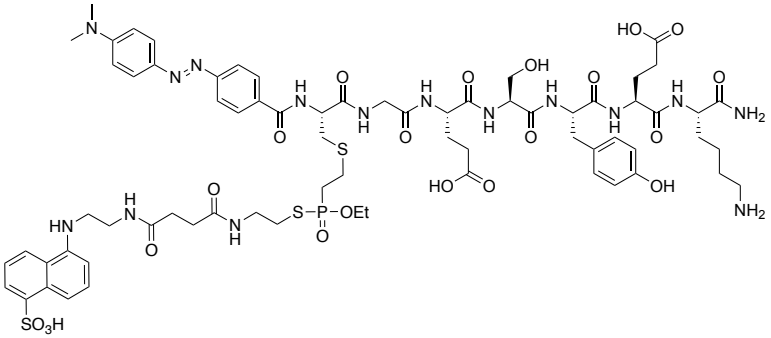

To a solution of Dabcyl peptide (2.5 mg, 2.35 μmol, 1.0 eq.) in aqueous 50 mM NH_4HCO_3 buffer containing 1 mM EDTA at pH 8.5 was added EDANS vinylphosphonothiolate derivative **44** (1.5 mg, 2.82 μmol, 1.2 eq.) dissolved in DMF (280 μL). The reaction mixture was shaken at r.t. for 3 hours and then diluted with water (4.7 mL) for purification via semipreparative HPLC (gradient: 10-50% MeCN+0.1% TFA in H_2O+0.1% TFA over 45 min, flow: 16 mL/min). After lyophilization, product **60** was obtained as a red powder (3 mg, 1.87 μmol, 80%).
HR-MS (ESI+) for $C_{70}H_{96}N_{15}O_{21}PS_3^+$ $[M+H]^+$ calcd.: 804.7897, found: 804.7889.

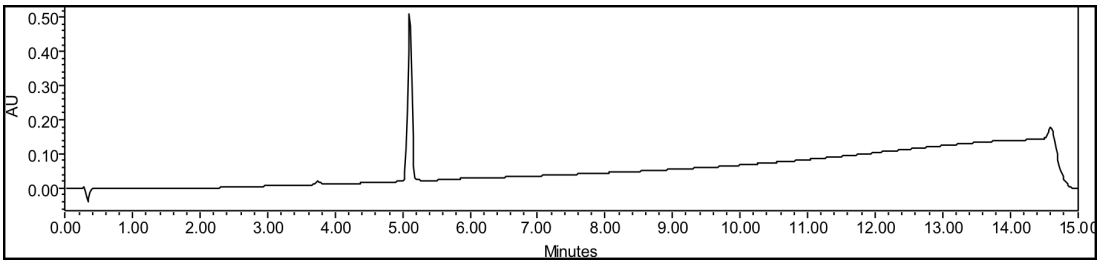

Fig. 79 UPLC-UV analysis (220 nm) of compound **60**.

8.2.6 Glutathione addition to phosphonothiolates

Glutathione addition to vinylphosphonothiolate (17)

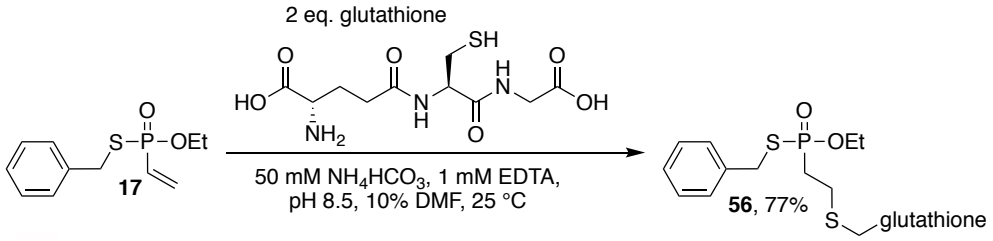

Reduced glutathione (20.3 mg, 0.066 mmol, 2.0 eq.) was dissolved in 1.32 mL aqueous 50 mM NH_4HCO_3 buffer at pH 8.5 containing 1 mM EDTA and added to a solution of vinylphosphonothiolate **17** (8 mg, 0.033 mmol, 1.0 eq.) dissolved in 0.33 mL DMF and the mixture was stirred at r.t. for 180 min. The solvents were then removed under reduced pressure and the residue was redissolved in 5 mL H_2O and purified via semipreparative HPLC (gradient: 20-60% MeCN + 0.1% TFA in H_2O + 0.1% TFA over 40 min, flow: 16 mL/min). After lyophilization product **56** was obtained as a white powder (14 mg, 0.026 mmol, 77%). ^{1}H-NMR: (300 MHz, D_2O): δ = 7.46-7.28 (m, 5H), 4.50 (dd, J = 8.4, 5.3 Hz, 1H), 4.19-3.93 (m, 7H), 2.90 (dd, J = 14.1, 5.3 Hz, 1H), 2.76 (ddd, J = 14.1, 8.4, 1.9 Hz, 1H), 2.69-2.47 (m, 4H), 2.25-2.01 (m, 4H), 1.26 (t, J = 7.1 Hz, 3H). ^{13}C-NMR: (75 MHz, D_2O): δ = 174.29, 172.82, 172.51, 172.08, 137.34, 128.95, 128.84, 127.95, 63.15 (d, J = 7.7 Hz), 52.79, 52.60, 41.06, 33.90, 32.66, 31.37, 30.93, 25.58, 23.95, 15.38 (d, J = 6.5 Hz). ^{31}P-NMR: (122 MHz, D_2O): δ = 60.52. HR-MS (ESI+) for $C_{21}H_{33}N_3O_8PS^+$ [M+H$^+$] calcd.: 550.1441, found: 550.1451.

Glutathione addition to ethynylphosphonothiolate (7)

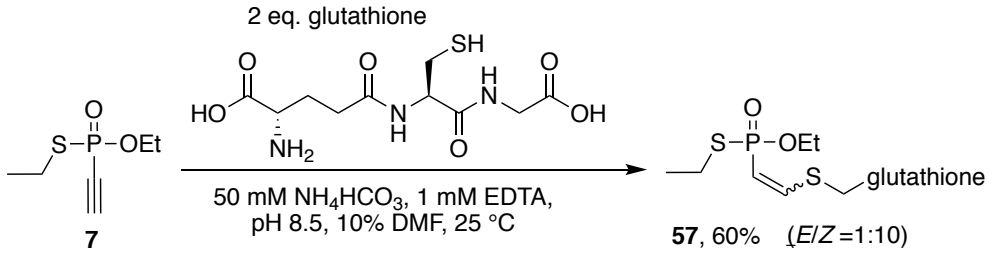

Reduced glutathione (141 mg, 0.460 mmol, 2.0 eq.) was dissolved in 10.35 mL aqueous 50 mM NH_4HCO_3 buffer at pH 8.5 containing 1 mM EDTA and added to a solution of ethynylphosphonothiolate **7** (41 mg, 0.230 mmol, 1.0 eq.) in 1.15 mL DMF and the mixture was stirred at r.t. for 90 min. The solvents were then removed under reduced pressure and the residue was redissolved in 5 mL H_2O and purified via semipreparative HPLC (gradient: 5-90% MeCN + 0.1% TFA in H_2O + 0.1% TFA over 40 min, flow: 10 mL/min). The *E*- and *Z*-double bond isomers could be separated and were lyophilized individually to give: *E*-isomer of **57** (6 mg, 0.0124, 5%) and *Z*-isomer of **57** (61 mg, 0.1256, 55%).

E-double bond isomer of **57**:
^{1}H-NMR: (600 MHz, D_2O): δ = 7.57 (dd, J = 22.6, 16.6 Hz, 1H), 6.08 (ddd, J = 21.3, 16.6, 1.4 Hz, 1H), 4.78-4.75 (m, 1H, overlaps with D_2O signal), 4.23 (dq, J = 9.3, 7.1 Hz, 2H), 4.06 (s, 2H), 4.00 (t, J = 6.5 Hz, 1H), 3.46 (dd, J = 14.4, 5.5 Hz, 1H), 3.29 (ddd, J = 14.4, 7.9, 1.6 Hz, 1H), 2.91-2.80 (m, 2H), 2.66-2.54 (m, 2H), 2.24 (q, J = 8.1, 7.7 Hz, 2H), 1.39 (t, J = 7.1 Hz, 3H), 1.35 (t, J = 7.4 Hz, 3H). ^{13}C-NMR (151 MHz, D_2O): δ = 177.19, 175.66, 175.15, 174.57, 165.58, 152.82 (d, J = 9.7 Hz), 115.13 (d, J = 151 Hz), 66.28 (d, J = 5.9 Hz), 55.66, 55.22, 43.96, 35.52, 33.79, 28.38, 27.45, 18.24 (d, J = 6.3 Hz). ^{31}P-NMR: (243 MHz, D_2O): δ = 45.25 (d, J = 9.1 Hz). HR-MS (ESI+) for $C_{16}H_{31}N_3O_8PS_2^+$ [M+H^+] calcd.: 488.1285, found: 488.0925.

Z-double bond isomer of **57**:
^{1}H-NMR: (600 MHz, D_2O): δ = 7.53 (ddd, J = 49.8, 12.3, 2.4 Hz, 1H), 5.97 (dt, J = 21.5, 12.0 Hz, 1H), 4.70 (ddd, J = 20.1, 8.6, 5.2 Hz, 1H), 4.23 (dq, J = 9.3, 7.1 Hz, 2H), 4.08 (td, J = 6.6, 1.5 Hz, 1H), 4.04 (s, 2H), 3.43 (ddd, J = 14.4, 5.2, 3.8 Hz, 1H), 3.23 (dt, J = 14.4, 8.5 Hz, 1H), 2.92-2.82 (m, 2H), 2.66-2.58 (m, 2H), 2.30-2.21 (m, 2H), 1.38 (t, J = 7.1 Hz, 3H), 1.35 (td, J = 7.4, 4.3 Hz, 3H). ^{13}C-NMR (151 MHz, D_2O): δ = 176.89, 175.55, 174.60 (d, J = 11.6 Hz), 174.4, 165.64 (q, J = 35 Hz), 154.88 (d, J = 17.9 Hz), 119.06 (q, J = 292 Hz, acetonitrile contamination?), 116.15 (dd, J = 148.6, 30.3 Hz), 66.04 (dd, J = 10.1, 6.9 Hz), 56.36 (d, J = 6.7 Hz), 55.12, 43.91, 39.08 (d, J = 11.0 Hz), 33.79, 28.28 (d, J = 6.0 Hz), 27.40, 18.30. ^{31}P-NMR: (243 MHz, D_2O): δ = 44.90 (d, J = 9.8 Hz). HR-MS (ESI+) for $C_{16}H_{31}N_3O_8PS_2^+$ [M+H^+] calcd.: 488.1285, found: 488.1016.

Glutathione addition to vinylphosphonothiolate peptides (28-32)

HPLC-purified peptides **28-32** were dissolved in 200 μL conjugation buffer (PBS pH 7.4 or 50 mM NH_4HCO_3 pH 8.5). To start the reaction, 50 μL of a 30 mM solution of reduced glutathione in conjugation buffer was added to reach a final glutathione concentration of 6 mM and peptide concentrations of 5 mM. The solutions were shaken at 700 rpm at 25 °C. Samples were drawn in a volume of 8 μL, diluted into 30 μL of H_2O and subjected to UPLC-MS analyses (short gradient), injecting 5 μL each (compare Fig. 28).

8.2.7 Phosphonate synthesis

_O_-Boc-ethylamine _O_-ethyl ethynylphosphonate (61)

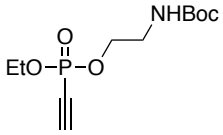

A round bottom flask was charged with **33** (201 mg, 1.0 mmol, 1.0 eq.), dissolved in dry acetonitrile (10 mL) and cooled to –40 °C. Separately, a solution of Boc-protected ethanolamine (161 mg, 1.0 mmol, 1.0 eq.) and tetrazole (Sigma, 0.45 M in MeCN, 4.4 mL, 2.0 mmol, 2.0 eq.) was prepared and added drop-wise to the first stirred solution at –40 °C. The reaction mixture was stirred for 10 min at –40 °C before allowed to warm to r.t. and stirred for another 30 min. Then, a tert-butyl hydroperoxide solution (70 wt. % in H_2O, 286 μL, 1.0 mmol, 1.0 eq.) was added at r.t. and stirred for 10 min. The reaction mixture was then diluted with 30 mL H_2O and extracted with DCM (3 times 60 mL). The combined organic layers were dried over Na_2SO_4, filtered and the solvents were removed under reduced pressure. After purification by silica gel chromatography (100% EtOAc) the titled product was obtained as a colourless oil (168 mg, 0.60 mmol, 60%). ^{1}H-NMR: (300 MHz, $CDCl_3$): δ = 4.18-3.96 (m, 4H), 3.31 (q, J = 5.5 Hz, 2H), 3.06 (d, J = 13.4 Hz, 1H), 1.33 (s, 9H), 1.27 (td, J = 7.1, 0.8 Hz, 3H). ^{13}C-NMR: (75 MHz, $CDCl_3$): δ = 155.78, 88.61 (d, J = 51.1 Hz), 79.61, 73.69 (d, J = 291.1 Hz), 66.58 (d, J = 6.4 Hz), 63.85 (d, J = 6.0 Hz), 40.70 (d, J = 7.1 Hz), 28.34, 16.02 (d, J = 7.0 Hz). ^{31}P-NMR: (122 MHz, $CDCl_3$): δ = -8.03. HR-MS (ESI+) for $C_{11}H_{21}NO_5P^+$ [M+H^+] calcd.: 278.1157, found: 278.1149.

_O_-Boc-ethylamine _O_-ethyl vinylphosphonate (62)

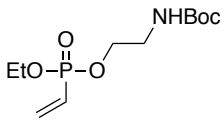

A round bottom flask was charged with **34** (203 mg, 1.0 mmol, 1.0 eq.), dissolved in dry acetonitrile (10 mL) and cooled to –40 °C. Separately, a solution of Boc-protected ethanolamine (177 mg, 1.0 mmol, 1.0 eq.) and tetrazole (Sigma, 0.45 M in MeCN, 4.4 mL, 2.0 mmol, 2.0 eq.) was prepared and added drop-wise to the first stirred solution at –40 °C. The reaction mixture was stirred for 10 min at –40 °C before allowed to warm to r.t. and stirred for another 30 min. Then, a tert-butyl hydroperoxide solution (70 wt. % in H_2O, 286 μL, 1.0 mmol, 1.0 eq.) was added at r.t. and stirred for 10 min. The reaction mixture was then diluted with 30 mL H_2O and extracted with DCM (3 times 60 mL). The combined organic layers were dried over Na_2SO_4, filtered and the solvents were removed under reduced pressure. After purification by silica gel chromatography (100% EtOAc) the titled product was obtained as a colourless oil (100 mg, 0.36 mmol, 36%). ^{1}H-NMR: (300 MHz, $CDCl_3$): δ = 6.395.87 (m, 3H), 5.14 (s, 1H), 4.153.96 (m, 4H), 3.36 (q, J = 5.4 Hz, 2H), 1.40 (s, 9H), 1.30 (t, J = 7.0 Hz, 3H). ^{13}C-NMR: (75 MHz, $CDCl_3$): δ = 158.89, 136.28 (d, J = 2.0 Hz), 125.38 (d, J = 183.9 Hz), 79.54, 65.14 (d, J = 6.0 Hz), 62.26 (d, J = 5.5 Hz), 41.13 (d, J = 6.0 Hz), 28.43, 16.40 (d, J = 6.2 Hz). ^{31}P-NMR: (122 MHz, $CDCl_3$): δ = 17.97. HR-MS (ESI+) for $NaC_{11}H_{22}NO_5P^+$ [M+Na^+] calcd.: 302.1133, found: 302.1120.

S-ethylamine O-ethyl ethynylphosphonate (63)

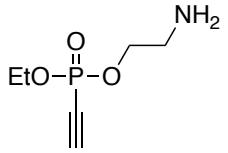

Boc-protected ethynylphosphonate derivative **61** was dissolved in TFA/H_2O=95:5 at a concentration of 0.1 M. The solution was stirred for 10 min at r.t. and then diluted with water (1:10). The product **63** (an oil) was obtained quantitatively after lyophilization and was directly used for subsequent reactions.

S-ethylamine O-ethyl vinylphosphonate (64)

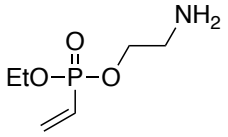

Boc-protected vinylphosphonate derivative **62** was dissolved in TFA/H_2O=95:5 at a concentration of 0.1 M. The solution was stirred for 10 min at r.t. and then diluted with water (1:10). The product **64** (an oil) was obtained quantitatively after lyophilization and was directly used for subsequent reactions.

O-EDANS derivative O-ethyl ethynylphosphonate (65)

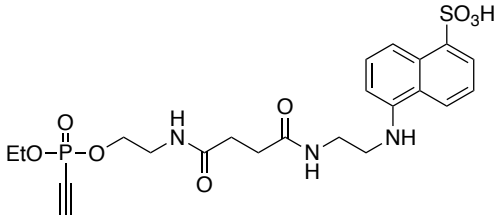

A solution containing HATU (33.2 mg, 0.087 mmol, 1.1 eq.), EDANS-derivative **42** (32 mg, 0.087 mmol, 1.1 eq.) and DIPEA (47 μL, 0.237 mmol, 3.0 eq.) in 0.2 mL DMF was added to amine derivative **63** (14 mg, 0.079 mmol, 1.0 eq.) dissolved in 0.1 mL DMF and the mixture was stirred at r.t. for 30 min. The solvents were then evaporated under reduced pressure and the crude product was purified via semipreparative HPLC (gradient: 10-50% MeCN+0.1% TFA in H_2O+0.1% TFA over 50 min, flow: 5 mL/min) giving product **65** (13 mg, 0.0248 mmol, 31%) as a white powder after lyophilization. ^{1}H-NMR: (600 MHz, DMSO−d_6): δ = 8.27 (d, J = 8.6 Hz, 1H), 8.13-8.04 (m, 3H), 7.95 (m, 1H), 7.40-7.29 (m, 2H), 6.76 (d, J = 7.4 Hz, 1H), 4.55 (d, J = 13.5 Hz, 1H), 4.08 (dq, J = 9.0, 7.1 Hz, 2H), 3.99-3.95 (m, 2H), 3.39 (q, J = 6.1 Hz, 2H), 3.30 (q, J = 6.3, 5.9 Hz, 4H), 2.35 (s, 4H), 1.27 (t, J = 7.1 Hz, 3H). ^{13}C-NMR: (151 MHz, DMSO−d_6): δ = 15.82 (d, J = 6.7 Hz), 16.72, 18.07, 30.65 (d, J = 14.8 Hz), 37.23, 41.84, 53.61, 64.18 (dd, J = 285.2, 5.7 Hz), 72.86 Hz, 74.75 Hz, 92.55 (d, J = 48.8 Hz), 122.61, 123.23, 124.05, 125.58, 125.94, 130.11, 144.25, 171.74, 172.16. ^{31}P-NMR: (243 MHz, DMSO−d_6): δ = –8.38. HR-MS (ESI+) for $C_{22}H_{29}N_3O_8PS^+$ [M+H^+] calcd.: 526.1413, found: 526.1387.

O-EDANS derivative *O*-ethyl vinylphosphonate (66)

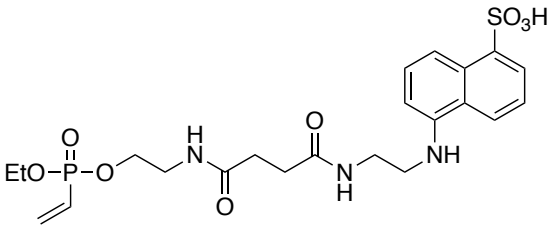

A solution containing HATU (30 mg, 0.079 mmol, 1.1 eq.), EDANS-derivative **42** (29 mg, 0.079 mmol, 1.1 eq.) and DIPEA (38 μL, 0.215 mmol, 3.0 eq.) in 0.2 mL DMF was added to amine derivative **64** (13 mg, 0.072 mmol, 1.0 eq.) dissolved in 0.1 mL DMF and the mixture was stirred at r.t. for 30 min. The solvents were then evaporated under reduced pressure and the crude product was purified via semipreparative HPLC (gradient: 10-50% MeCN+0.1% TFA in H_2O+0.1% TFA over 50 min, flow: 5 mL/min) giving product **66** (10 mg, 0.0190 mmol, 26%) as a white powder after lyophilization.
^{1}H-NMR: (300 MHz, DMSO$-d_6$): δ = 8.26 (d, J = 8.6 Hz, 1H), 8.18-8.01 (m, 3H), 7.95 (d, J = 7.4 Hz, 1H), 7.44-7.23 (m, 2H), 6.75 (d, J = 7.6 Hz, 1H), 6.30-6.04 (m, 3H), 4.03-3.93 (m, 2H), 3.87 (dt, J = 7.5, 5.7 Hz, 2H), 3.38 (t, J = 5.7 Hz, 2H), 3.32-3.23 (m, 4H), 2.34 (s, 4H), 1.22 (t, J = 7.0 Hz, 3H). ^{13}C-NMR: (151 MHz, D_2O): δ = 178.59, 177.53, 142.00, 141.10, 134.34, 131.81, 129.73, 129.49, 129.29, 128.61, 126.64, 125.50 (d, J = 182 Hz), 67.49 (d, J = 5.4 Hz), 66.49 (d, J = 5.8 Hz), 52.09, 42.14 (d, J = 6.7 Hz), 39.01, 33.35, 18.20 (d, J = 6.2 Hz). ^{31}P-NMR: (122 MHz, DMSO$-d_6$): δ = 17.33.
HR-MS (ESI+) for $C_{22}H_{31}N_3O_8PS^+$ [M+H$^+$] calcd.: 528.1570, found: 528.1543.

FRET pair (68)

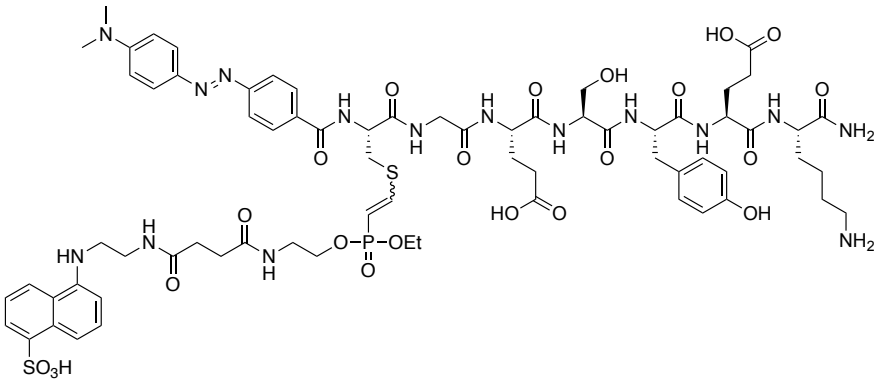

To a solution of Dabcyl peptide (2.5 mg, 2.35 μmol, 1.0 eq.) in aqueous 50 mM NH_4HCO_3 buffer containing 1 mM EDTA at pH 8.5 was added EDANS ethynylphosphonate derivative **65** (1.5 mg, 2.82 μmol, 1.2 eq.) dissolved in DMF (280 μL). The reaction mixture was shaken at r.t. for 1 hour and then diluted with water (4.7 mL) for purification via semipreparative HPLC (gradient: 10-50% MeCN+0.1% TFA in H_2O+0.1% TFA over 45 min, flow: 16 mL/min). After lyophilization, product **68** was obtained as a red powder (3 mg, 2.01 μmol, 86%).
HR-MS (ESI+) for $C_{70}H_{94}N_{15}O_{22}PS_2^+$ [M+H^{2+}] calcd.: 795.7933, found: 795.7931.

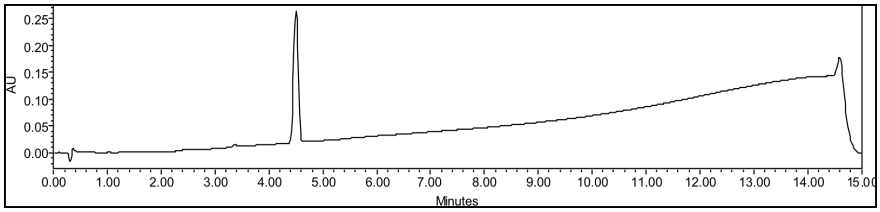

Fig. 80 UPLC-UV analysis (220 nm) of compound **68**.

FRET pair (69)

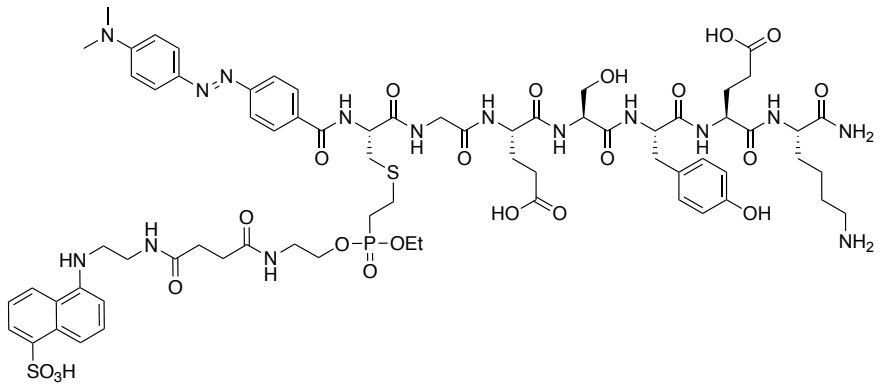

To a solution of Dabcyl peptide (2.5 mg, 2.35 μmol, 1.0 eq.) in aqueous 50 mM NH_4HCO_3 buffer containing 1 mM EDTA at pH 8.5 was added EDANS vinylphosphonate derivative **66** (1.5 mg, 2.82 μmol, 1.2 eq.) dissolved in DMF (280 μL). The reaction mixture was shaken at r.t. for 3 hours and then diluted with water (4.7 mL) for purification via semipreparative HPLC (gradient: 10-50% MeCN+0.1% TFA in H_2O+0.1% TFA over 45 min, flow: 16 mL/min). After lyophilization, product **69** was obtained as a red powder (3 mg, 2.01 μmol, 86%).
HR-MS (ESI+) for $C_{70}H_{96}N_{15}O_{22}PS_2^+$ [M+H^{2+}] calcd.: 796.8012, found: 796.8002.

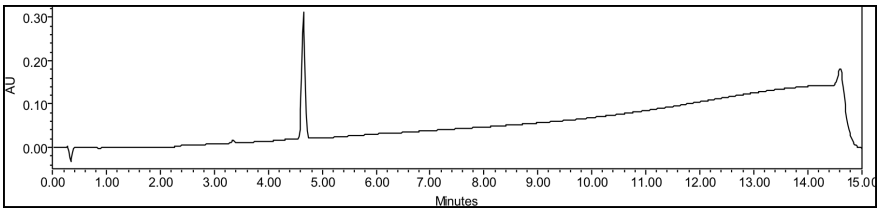

Fig. 81 UPLC-UV analysis (220 nm) of compound **69**.

8.2.8 Determination of second order rate constants for thiol additions to unsaturated P(V) electrophiles

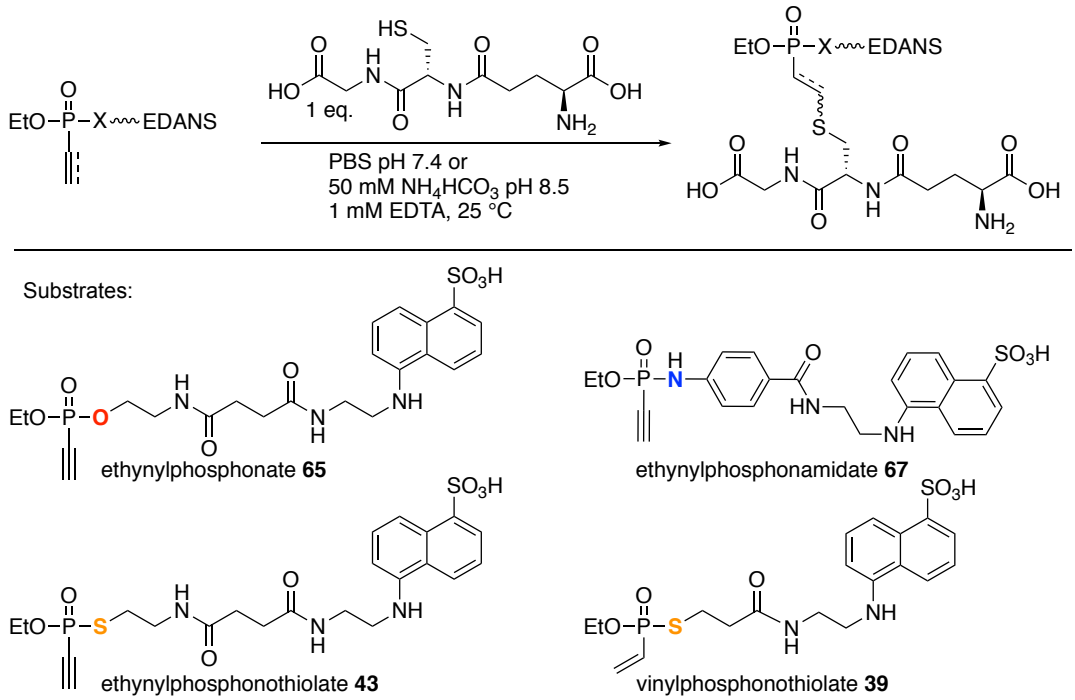

Scheme 60 Glutathione addition to unsaturated P(V) electrophiles.

Glutathione additions to EDANS-P(V)-electrophiles were conducted at different concentrations, depending on the reactivity of the compounds: For ethynylphosphonate **65**, ethynylphosponamidate **67** and ethynylphosphonothiolate **43** at pH 7.4 and for vinylphosphonothiolate **49** at pH 8.5 reactions were run at 100 μM while for vinylphosphonothiolate **49** at pH 7.4 the conjugation with glutathione was run at 1 mM. Therefore, 2.5 μL of either a 20 mM or a 200 mM solution of EDANS-P(V) electrophile in DMF (for reactions at 100 μM or 1 mM, respectively) and 5 μL of a 10 mM or a 100 mM solution of unconjugated EDANS (as an internal standard) in 1:1 DMF/conjugation buffer (PBS + 1 mM EDTA pH 7.4 or 50 mM NH_4HCO_3 + 1 mM EDTA adjusted to pH 8.5 with aqueous ammonia buffer) were added to 488 μL conjugation buffer. Then, 5 μL of a 10 mM/100 mM solution of reduced glutathione in conjugation buffer was added to start the reaction. Samples were drawn in a volume of 2 μL (for reactions at 1 mM) or 20 μL (for reactions at 100 μM) and immediately diluted into 98 or 80 μL of 50 mM NaOAc buffer at pH 3.5 to stop the reaction. The first sample (t = 0) was drawn before the addition of glutathione. Samples were subjected to HPLC analysis injecting 20 μL (see general information in chapter 8.1 for details). In Fig. 82A, exemplary chromatogram traces are shown for the glutatione addition to vinylphosphonothiolate **39**. Signal intensities were quantified by integration of the area under the peak for both the P(V) electrophiles and the internal standard EDANS. The concentration of remaining P(V) starting material (SM) at time point x ($[SM]_x$) was calculated as follows: $[SM]_x = ((SM_x/EDANS_x)/(SM_0/EDANS_0)) * [SM]_0$ whereas SM and EDANS are the measured intensities of the respective peaks at a given time point and $[SM]_0$ is the initial concentration of P(V) electrophiles (either 0.1 mM or 100 μM). The inverse

concentrations of remaining P(V) electrophile ($1/[SM]_0$) were plotted against time and second order rate constants were deduced from the slopes of the fitted curves through the mean values of three independent measurements.

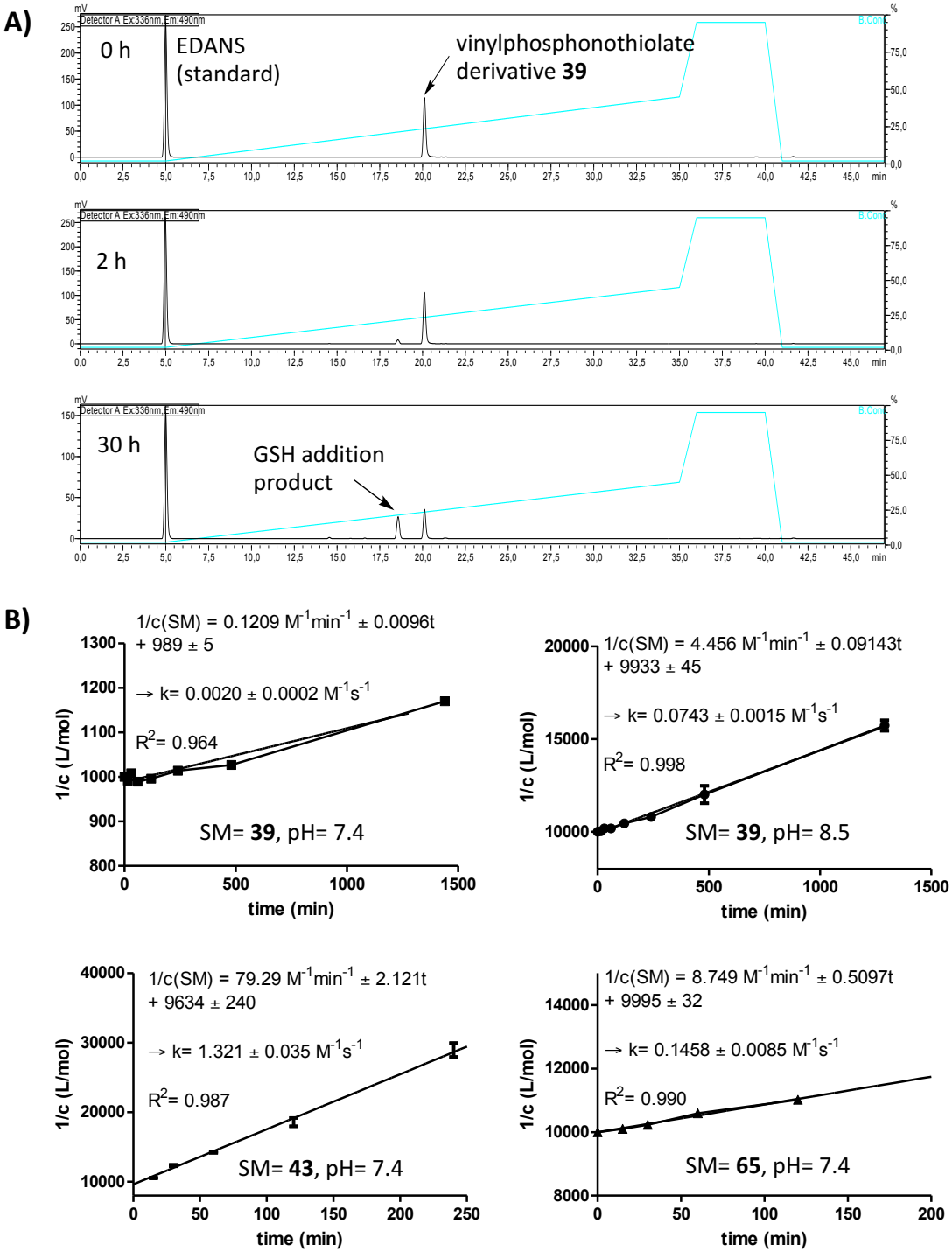

Fig. 82 A) Exemplary HPLC traces (fluorescence at 490 nm) of the reaction mixture of vinylphosphosphonothiolate **39** and glutathione. B) 1/concentration of P(V) electrophiles over time for reactions with glutathione and linear plot. The slopes of the linear plots are the second order rate constants k.

8.2.9 Antibody labelling with unsaturated phosphonothiolates

Cetuximab labelling with phosphonothiolate-biotin derivatives 18, 45 and 46 or maleimide-biotin derivative 58

Cetuximab[11] (Erbitux®, Merck KGaA, 1.5 mg/mL, ca. 10 μM in PBS buffer containing 50 mM borate pH 8.0, 10 μL per condition) was reduced with 1000 eq. DTT (1 μL of a 100 mM solution in borate PBS pH 8.0) at 37 °C for 30 min. DTT removal and buffer exchange to conjugation buffer (50 mM NH_4HCO_3, 100 mM NaCl containing 1 mM EDTA pH 8.5 or PBS pH 7.4 containing 1 mM EDTA) was conducted using spin desalting columns (75 μL ZebaTM, 7 K MWCO, Thermo Fisher Scientific, USA) following the manufacturers instructions. Then, ethynyl- or vinylphosphonothiolate derivatives **45**, **46** or **18** or maleimide-biotin derivative **58** (Sigma Aldrich) (0.25 μL of a 20 mM solution in DMSO, resulting in a final reagent concentration of ca. 0.5 mM (50 eq.) and 2.5% DMSO in the reaction mixture) was added quickly and the mixture was shaken at 850 rpm and 14 °C for 16 h. For control reactions, compounds **45**, **46**, **18** or **58** were directly added to unreduced Cetuximab in conjugation buffer. After conjugation, removal of excess reagent and buffer exchange to PBS pH 7.4 was conducted using spin desalting columns (75 μL ZebaTM, 7 K MWCO, Thermo Fisher Scientific, USA). For SDS-PAGE/Western-blot analysis, 3 μL of the antibody solution after gel filtration were mixed with 27 μL of mercaptoethanol-containing Laemmli buffer and heated at 95 °C for 10 min. Thereof, 10 μL were loaded on a 12% acrylamide SDS-gel and then then subjected to Western-blotting using the commercially available Streptavidin-POD conjugate (Roche Diagnostics GmbH) for hybridisation to the biotin-modified antibodies and indirect detection of biotin via chemiluminescence (see general information in chapter 8.1 for details).

Trastuzumab labelling with unsaturated phosphonothiolate derivatives 7 and 8

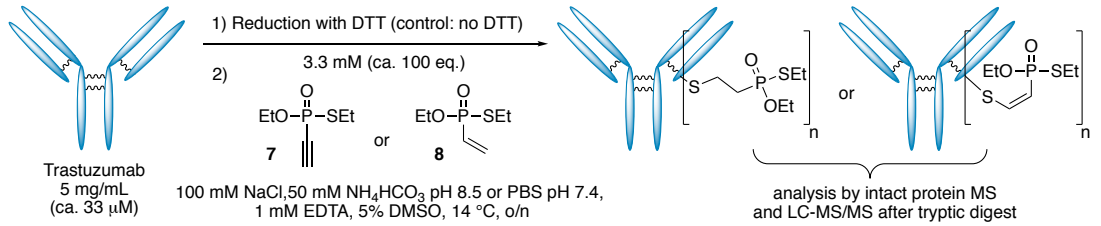

Scheme 61 Trastuzumab labeling with phosphonothiolates **7** and **8**.

Trastuzumab[12] (Herceptin, Roche, 5 mg/mL, ca. 33 μM in PBS buffer containing 50 mM borate pH 8.0, 20 μL per condition) was reduced with 1000 eq. DTT (2 μL of a 330 mM solution in borate PBS pH 8.0) at 37 °C for 30 min. DTT removal and buffer exchange to conjugation buffer (50 mM NH_4HCO_3, 100 mM NaCl containing 1 mM EDTA pH 8.5 or PBS pH 7.4 containing 1 mM EDTA) was conducted using spin desalting columns (75 μL ZebaTM, 7 K MWCO, Thermo Fisher Scientific, USA) following the manufacturers instructions. Then, ethynyl- or vinylphosphonothiolate derivatives **7** or **8**, respectively (1 μL of a 66 mM solution in DMSO, resulting in a final concentration of 3.3 mM phosphonothiolate derivative (100 eq.) and 5% DMSO in the reaction mixture) was added

[11] *We thank Dr. Kai Licha and Prof. Dr. Karsten Spiekermann for the provision of Cetuximab.*
[12] *We thank Prof. Dr. Karsten Spiekermann for the provision of Trastuzumab.*

quickly and the mixture was shaken at 850 rpm and 14 °C for 16 h. For control reactions, compounds **7** and **8** were directly added to unreduced Trastuzumab in conjugation buffer. After conjugation, removal of excess reagent and buffer exchange to PBS pH 7.4 was conducted using spin desalting columns (75 µL ZebaTM, 7 K MWCO, Thermo Fisher Scientific, USA).
For MS analysis, 10 µL of the antibody solution after gel filtration (diluted to 2 mg/mL with PBS pH 7.4) was mixed with 0.5 µL PNGase-F solution (Promega, Germany, recombinant, cloned from *Elizabethkingia miricola* 10 u/µL) and incubated at 37 °C for 2 h. Then, disulfide bridges were reduced by the addition of 1 µL DTT solution (100 mM in PBS, pH 7.4) and incubation at 37 °C for another 30 min. Samples were diluted with 30 µL distilled H_2O and subjected to MS analysis with the Waters H-class system (see general information in chapter 8.1 for details).
For MS/MS analysis, 3 µL of the antibody samples after gel filtration were mixed with 10 µL β-mercaptoethanol-containing Laemmli buffer, heated at 95 °C for 10 min and run on a 12 % SDS-gel. Bands were stained with Coomassie brilliant blue, cut out, alkylated with chloroacetamide and subjected to tryptic digest and LC-MS/MS analysis (see general information in chapter 8.1 for details).
For peptide identification, the RAW-files were loaded into Proteome Discoverer (v.2.4, Thermo Scientific) and a database search was performed with MSAmanda 2.0 [312]. Files were searched against a database containing the sequences of Trastuzumab heavy and light chain using the following search parameters: peptide mass tolerance of ±6 ppm, fragment mass tolerance of ±20 ppm, a maximum of three missed cleavages, minimum peptide length of 6 and a minimum MSAmanda score of 150. Modification with ethynylphosphonothiolate **7** (178.022 Da) or vinylphosphonothiolate **8** (180.037 Da) were considered as dynamic modifications to occur on all nucleophilic amino acids. Moreover, cysteine carbamidomethylation (57.021 Da) and methionine oxidation (15.995 Da) were considered as dynamic modifications. Spectra that identified a peptide carrying either **7** or **8** as modification were manually validated.
For each condition (labelling with either **7** or **8** at either pH 7.4 or pH 8.5 and respective -DTT controls), the MS/MS results are shown below. Sequence coverages are highlighted in green. A= cysteine modified with either **7** or **8**, C= cysteine carbamidomethylation, O= methionine oxidation. For peptides, which were found to be modified with either A or C (individually), the two letters stand on top of each other. For peptides containing several cysteines, a red bar indicates modifications that could not be unambiguously assigned to one or the other site. Exemplary MS/MS spectra of modified peptides are shown in the Appendix (see chapter 9.3).

Trastuzumab light chain, labeled with ethynylphosphonothiolate **7** at pH 7.4:

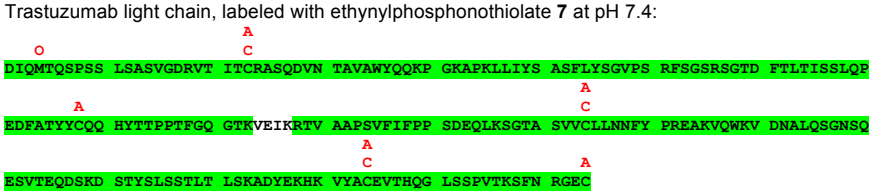

Trastuzumab heavy chain, labeled with ethynylphosphonothiolate **7** at pH 7.4:

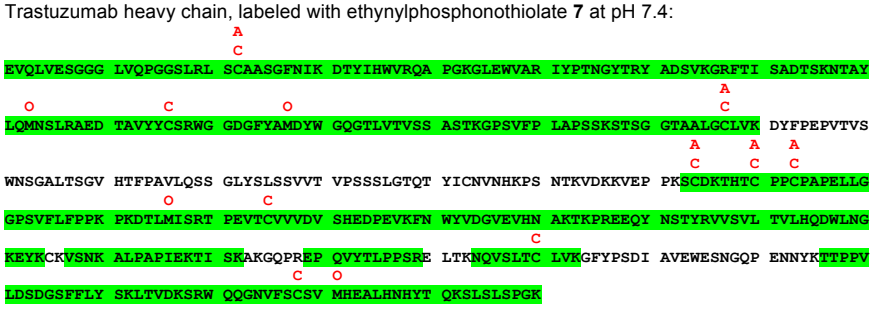

Trastuzumab light chain, labeled with ethynylphosphonothiolate **7** at pH 7.4 (-DTT control):

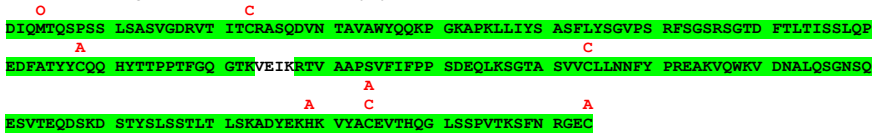

Trastuzumab heavy chain, labeled with ethynylphosphonothiolate **7** at pH 7.4 (-DTT control):

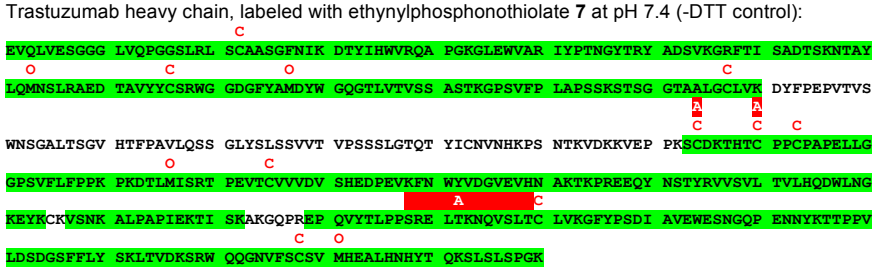

Trastuzumab light chain, labeled with ethynylphosphonothiolate **7** at pH 8.5:

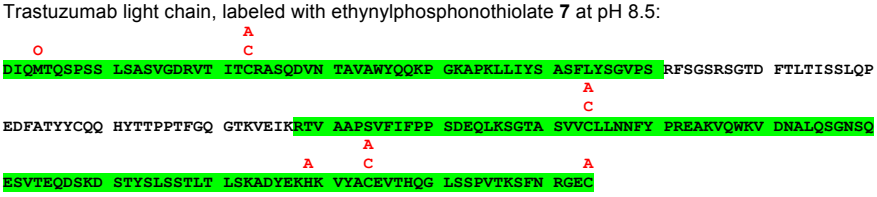

Trastuzumab heavy chain, labeled with ethynylphosphonothiolate **7** at pH 8.5:

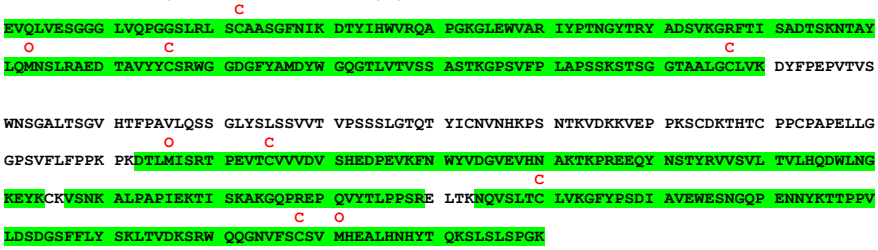

Trastuzumab light chain, labeled with ethynylphosphonothiolate **7** at pH 8.5 (-DTT control):

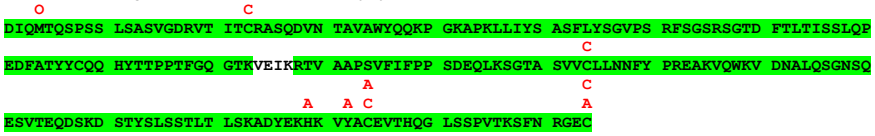

Trastuzumab heavy chain, labeled with ethynylphosphonothiolate **7** at pH 8.5 (-DTT control):

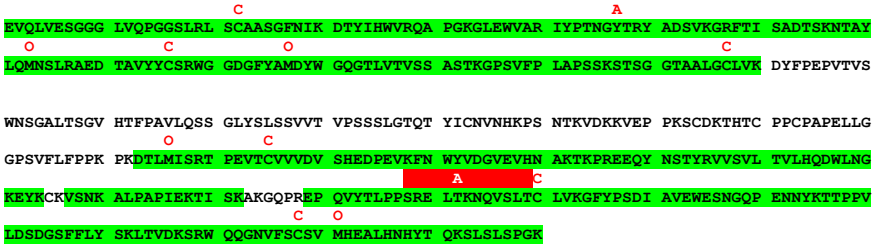

Trastuzumab light chain, labeled with vinylphosphonothiolate **8** at pH 7.4:

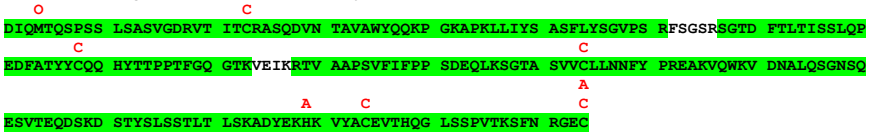

Trastuzumab heavy chain, labeled with vinylphosphonothiolate **8** at pH 7.4:

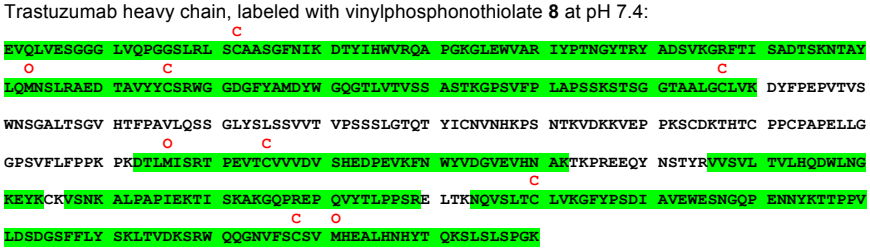

Trastuzumab light chain, labeled with vinylphosphonothiolate **8** at pH 7.4 (-DTT control):

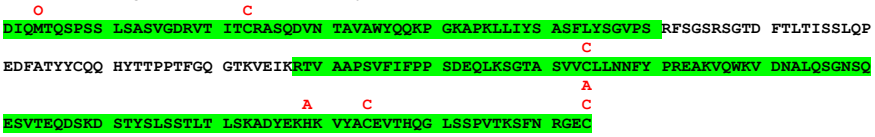

Trastuzumab heavy chain, labeled with vinylphosphonothiolate **8** at pH 7.4 (-DTT control):

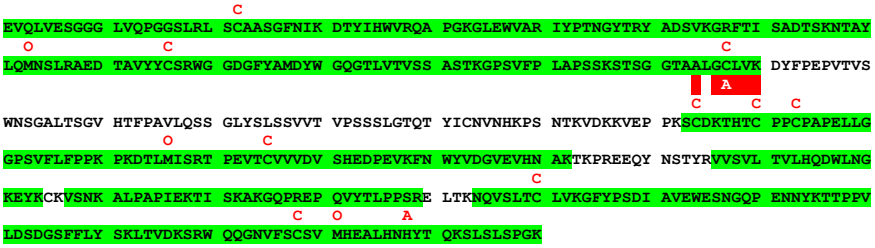

Trastuzumab light chain, labeled with vinylphosphonothiolate **8** at pH 8.5:

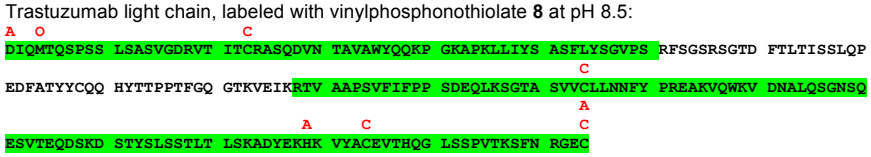

Trastuzumab heavy chain, labeled with vinylphosphonothiolate **8** at pH 8.5:

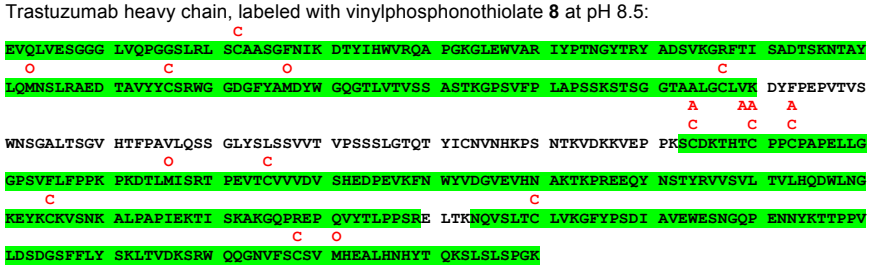

Trastuzumab light chain, labeled with vinylphosphonothiolate **8** at pH 8.5 (-DTT control):

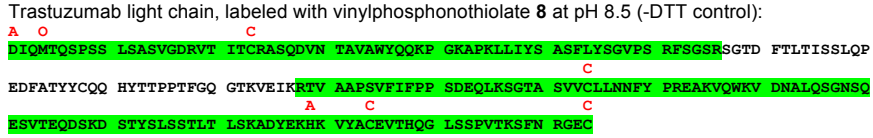

Trastuzumab heavy chain, labeled with vinylphosphonothiolate **8** at pH 8.5 (-DTT control):

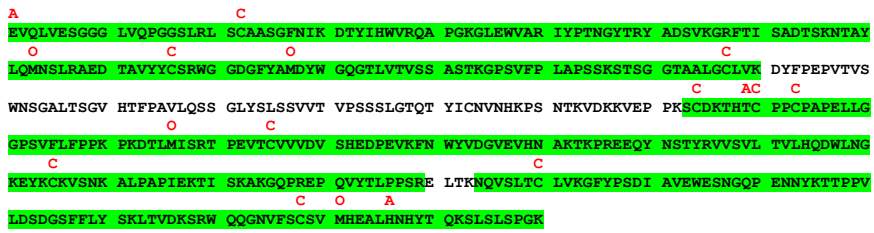

8.2.10 Stability studies of unsaturated phosphonothiolates

Aqueous stability of unsaturated phosphonothiolate derivatives 39 and 43

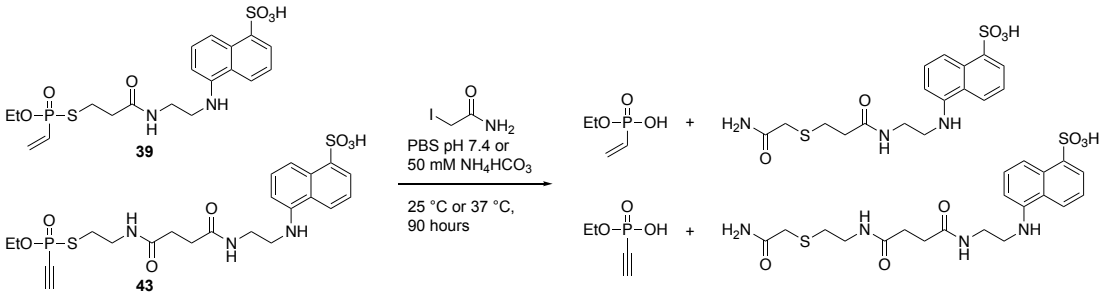

Scheme 62 Hydrolysis of unsaturated phosphonothiolate derivatives **39** and **43** in buffer.

Right before the measurement, vinyl- and ethynylphosphonothiolate derivatives **39** or **43** (3.0 μmol, 1.0 eq.), iodoacetamide (60 μmol, 20 eq.) and internal standard PMe_4Br (3.0 μmol, 1.0 eq., only for experiments at pH 8.5; for experiments at pH 7.4 the phosphate signal originating from the PBS buffer serves as internal standard) were weighed in as solids in an Eppendorf tube and dissolved in the test buffer solution (PBS pH 7.4 or 50 mM NH_4HCO_3 pH 8.5 containing 10% D_2O (540 μL buffer and 60 μL D_2O)). The role of iodoacetamide is to alkylate the thiolate, which gets released upon P-S bond hydrolysis, thereby circumventing re-attack, which would influence the experiment. The mixtures were transferred to NMR tubes and one-dimensional ^{31}P-NMR spectra with continuous broadband decoupling (using 32 scans, resulting in 3 min experiment time per spectrum) were recorded for each sample in intervals of 1 h over the course of 90 h on a Bruker AV-III 600 spectrometer. The samples were kept at either 25 °C or 37 °C during the whole experiment. For analysis, the spectra were Fourier-transformed, baseline corrected and the intensity of the ^{31}P-NMR signal of either **39** or **43** was obtained by integration.

Aqueous stability of vinylphosphonothiolate peptides 28-32

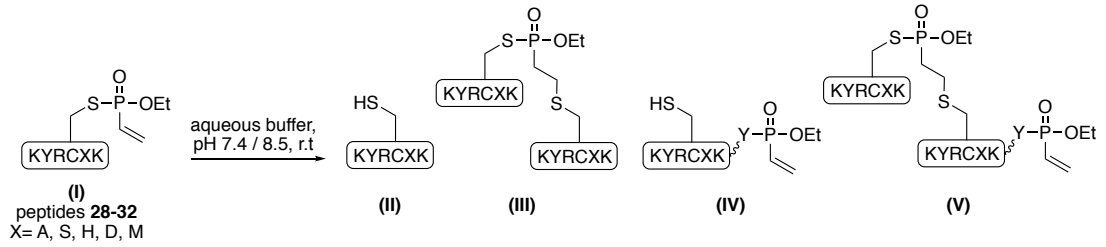

Scheme 63 Stability of vinylphosphonothiolate peptides in aqueous buffer: Hydrolysis of the P-S bond in the vinylphosphonothiolate peptides (I) can lead to free Cys-peptides (II) or P(V)-transfer to nucleophilic residues Y (structure IV). Peptides (II) and (IV) can react with residual (I) to form the conjugation products (III) and (V).

HPLC-purified peptides **28-32** were dissolved in either 250 μL PBS pH 7.4 or 50 mM NH_4HCO_3 containing 1 mM triphenylphosphine oxide (PPh_3O) as internal standard to reach final peptide concentrations of 5 mM. The solutions were shaken at 700 rpm at

25 °C. At t= 0, 2, 4, 8 and 24 hours, samples were drawn in a volume of 8 μL, diluted into 30 μL of H_2O and subjected to UPLC-UV/MS analyses (short gradient), injecting 5 μL each. For quantification (compare Fig. 27) the ratios between the extracted ion intensities of the doubly charged peptides (m/z: **28**: 443.2; **29**: 451.2; **30**: 476.3; **31**: 469.7; **32**: 473.2) and the internal standard PPh_3O (m/z: 279.1) at the given time points were determined and normalized to the respective ratios at t= 0 h. Exemplary LC-UV and TIC traces are shown for peptide **28** (X=A) in Fig. 83 for pH 7.4 and in Fig. 84 for pH 8.5. The observations for the peptides **29-32** were similar (UPLC-UV chromatograms and MS traces not shown here).

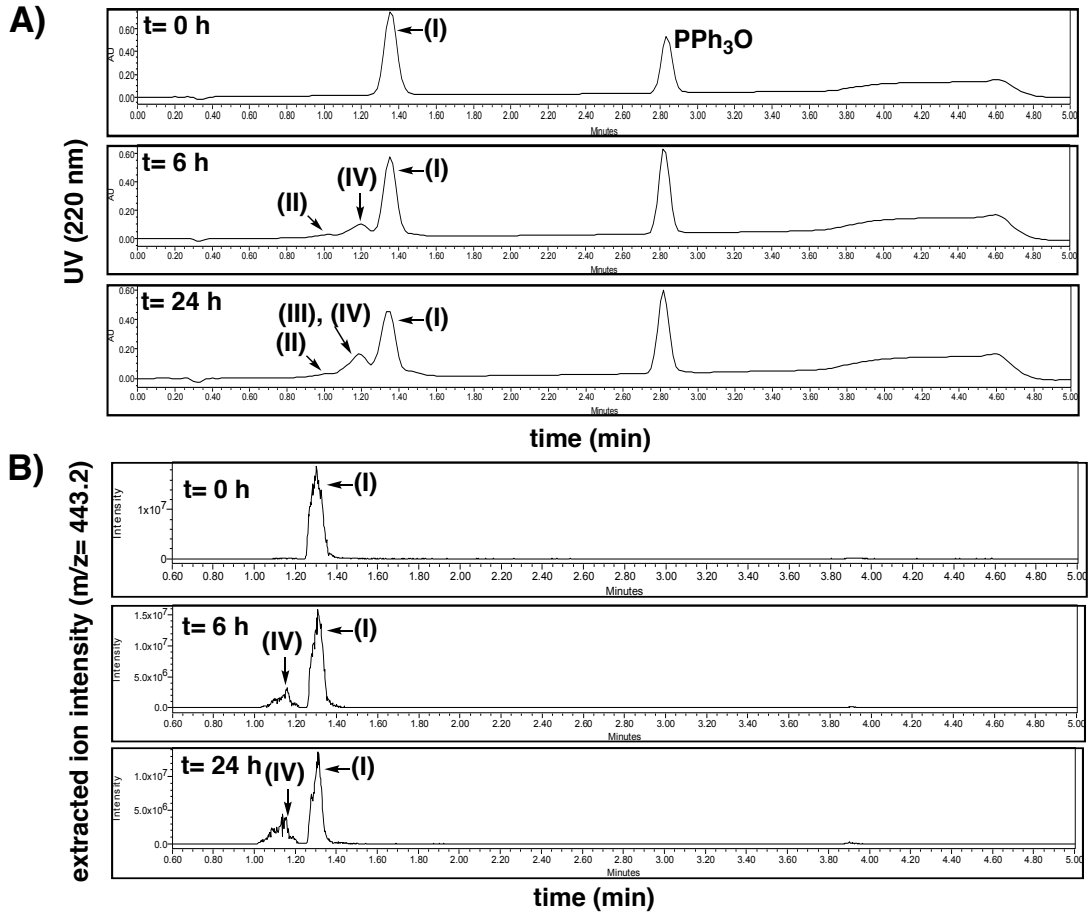

Fig. 83 A) UPLC-UV traces of peptide **28**, incubated in PBS buffer at pH 7.4. Over time, new peptide species arise, which were assigned by MS to the structures depicted in scheme 63. Note that the P(V)-transfer product (IV) has the same m/z as the vinylphosphonothiolate peptide (I) but runs at a different retention time. B) Corresponding traces of extracted ion intensities for the doubly charged peptide **28**. Triphenylphosphine oxide served as internal standard for quantification.

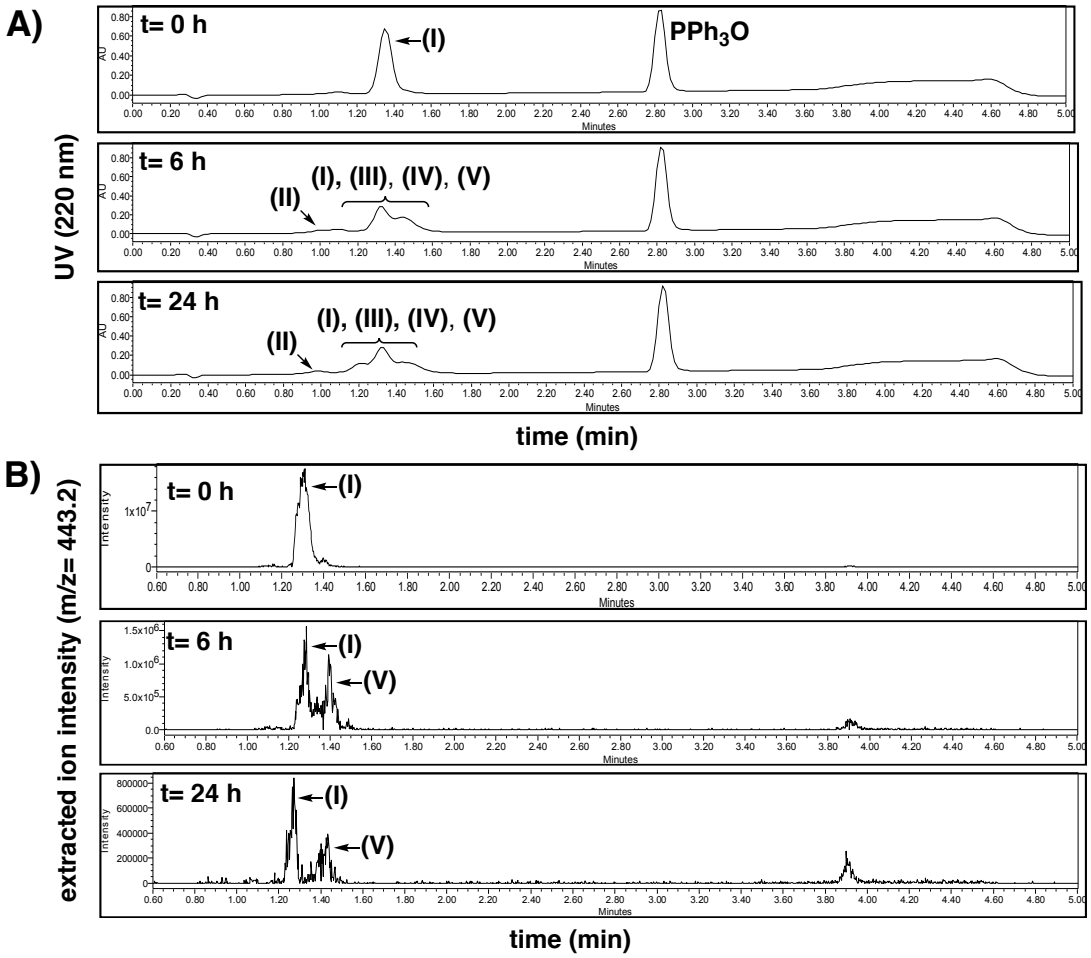

Fig. 84 A) UPLC-UV traces of peptide **28**, incubated in 50 mM NH_4HCO_3 buffer at pH 8.5. Over time, new peptide species arise, which were assigned by MS to the structures depicted in scheme 63. Some of these peptides co-elute. B) Corresponding traces of extracted ion intensities for the doubly charged peptide **28**. Note that product (V) $[M+4H^+]^{4+}$ has the same m/z as starting material (I) $[M+2H^+]^{2+}$ but runs at a different retention time. Triphenylphosphine oxide served as internal standard for quantification.

8.2.11 Stability of phosphonothiolate- and phosphonate-thiol conjugates

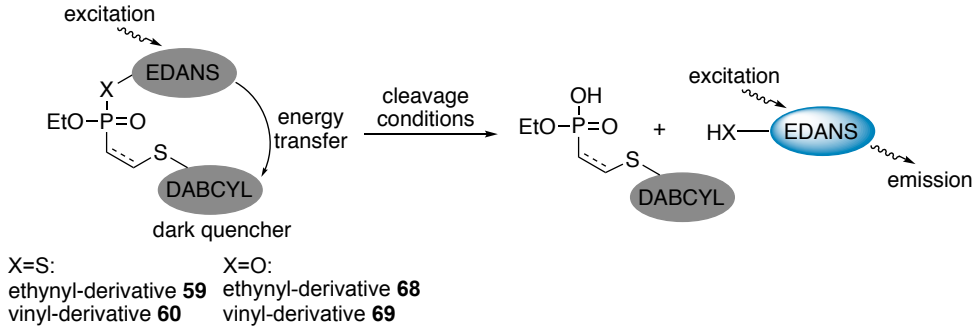

Scheme 64 Assay to investigate the stability of thiol-P(V) conjugates. The structures of the FRET pairs are depicted in the synthetic procedures.

Stability studies of Dabcyl-EDANS conjugates **59**, **60**, **68**, and **69** were conducted in 96-well plates (Corning 3615, black with clear, flat bottom). 5 μL of a 200 μM solution of each Dabcyl-EDANS conjugate in H_2O and 95 μL of the respective test solutions were mixed directly in the plate (exception: samples in 1 M NaOH were kept in Eppendorf tubes and only transferred to the plate after neutralization to protect equipment from corrosion). Fluorescence was measured on a Tecan Safire plate reader (Excitation: 360 nm, emission: 508 nm, bandwidth: 5 nm at 20 °C) from the same plate at different time points and corrected by the background measurement (test solution alone). Between measurements, the plate was kept at 25 °C. Mean values and standard deviation of three independent experiments were calculated (n = 3). HeLa cell lysate was generated from approximately $3.9*10^7$ cells, lysed in 2 mL PBS by sonification (final protein concentration: 1.0 mg/mL). Cells were grown on three 75 cm^2 cell culture plates, washed twice with PBS and harvested with a cell scraper. Human serum was purchased from Sigma Aldrich. Glutathione was dissolved at a concentration of 10 mM in PBS and the pH was adjusted to 7.4. 1 M NaOH studies were conducted at 200 μM in Eppendorf tubes, neutralized to pH 7.4 and diluted to 10 μM before fluorescence measurements.

8.2.12 Electrostatic potential maps

Note: Electrostatic potential maps were generated by Songwhan Hwang from the group of Dr. Han Sun (FMP Berlin). Songwhan Hwang also wrote this Experimental description.

All molecules were built using GaussView6 [313]. Geometry optimizations of the molecules were performed using the density functional theory (DFT) method with the aug-cc-pVTZ basis set at the B3LYP level in combination with the IEFPCM solvation model for water [314]. The molecular electrostatic potential was evaluated at each point on the isodensity surface with a value of 0.0004 electrons/$bohr^3$. Gaussian 16 [315] was used for all calculations.

8.3 Experimental part for protein-protein conjugation chapter

Note: The experimental data shown in this chapter (8.3) was obtained to a large extent by Sergej Schwagerus, as outlined in chapter 4. The data presented herein is published in Ref. [316] (shared first authorship together with Sergej Schwagerus). The text of the experimental descriptions shown in this chapter was written by Sergej Schwagerus and the author and is taken from the published paper (Ref. [316]). Kristin Kemnitz-Hassanin expressed and purified proteins together with Sergej Schwagerus. LC-MS/MS measurements were performed Dr. Michal Nadler-Holly, who also wrote the accompanying experimental description text. MS/MS data was analysed by Christian Stieger, who also wrote the accompanying text.

8.3.1 Protein expression

Expression and purification of UbG76C (70), UbK48C (77) and UbK48M (81)

The ubiquitin DNA sequence was synthesized by GeneArt AG and cloned into pET28a using NheI and XhoI restriction endonuclease sites. The NdeI restriction site was deleted.
Ubiquitin sequence:
5'GCTAGCCAGATTTTTGTTAAAACCCTGACCGGTAAAACCATTACCCTGGAAG
TTGAACCGAGCGATACCATTGAAAATGTGAAAGCCAAAATCCAGGACAAAGAA
GGTATTCCGCCTGATCAGCAGCGTCTGATTTTTGCAGGTAAACAGCTGGAAGA
TGGTCGTACCCTGAGCGATTATAACATTCAGAAAGAAAGCACCCTGCATCTGG
TTCTGCGTCTGCGTGGTGGT 3'

The mutations were introduced with classical PCR by the use of complementary primer pairs:

UbG76C **70**:
fwd: 5' GTGCTCGAGTTAGCAACCACGCAGACG 3'
rev: 5' CGTCTGCGTGGTTGCTAACTCGAGCAC 3'

UbK48C **77**:
fwd: 5' GCGTCTGATTTTTGCAGGTTGCCAGCTGGAAGATGGTCG 3'
rev: 5' CGACCATCTTCCAGCTGGCAACCTGCAAAAATCAGACGC 3'

UbK48M **81**:
fwd: 5' GATTTTTGCAGGTATGCAGCTGGAAGATG 3'
rev: 5' CATCTTCCAGCTGCATACCTGCAAAAATC 3'

The proteins were expressed in *E. coli* B834(DE3) using LB medium containing 30 μg/mL Kanamycin (Roth). Cells were grown at 37 °C, 180 rpm until an OD_{600} of 0.6-0.8 was reached, induced with 1 mM IPTG and incubated at 18 °C for 19 h. Lysis was performed in Dulbecco's PBS pH 7.4 using a high-pressure homogenizer (Microfluidics LM10 Microfluidizer) and debris centrifuged at 50.000 g for 15 min at 4 °C. The protein was purified with a BioRad NGC system (BioRad, USA) using a 5 mL HisTrap FF column (GE Healthcare, USA). Product-containing fractions were collected and dialyzed (MWCO: 3.5 kDa, Spectra/Pro®3 dialysis membrane) into the Thrombin

cleavage buffer (20 mM Tris-HCl pH 8.5, 150 mM NaCl, 2.5 mM $CaCl_2$). Then Thrombin was added (5 u/mL) and samples were incubated at 37 °C for 18 h. A second Ni-NTA purification was performed with a BioRad NGC system (BioRad, USA) using a 5 mL HisTrap FF (GE Healthcare, USA) column and the flow-through was collected and dialyzed (MWCO: 3.5 kDa, Spectra/Pro®3 dialysis membrane) into Dulbecco's PBS pH 7.4. The protein concentration was determined by NanoDrop® at 280 nm (ϵ = 1490 M^{-1} cm^{-1}). The pure protein was isolated in a yield of 20 mg/L for UbG76C, 9 mg/L for UbK48C and 13.6 mg/L for UbK48M. Protein aliquots were stored at –80 °C.

UbG76C **70**:
Protein sequence: His-tag highlighted in green; protease cleavage site highlighted in blue; UbG76C in black; G76C highlighted in red: MGSSHHHHHHSSGLVPRGSASQIFVKT LTGKTITLEVEPSDTIENVKAKIQDKEGIPPDQQRLIFAGKQLEDGRTLSDYNIQKE STLHLVLRLRGC

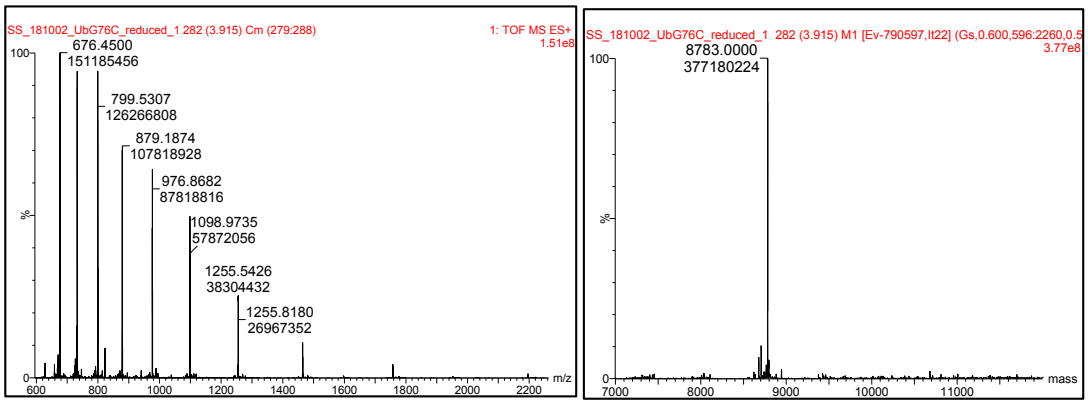

Fig. 85 Raw and deconvoluted HR-MS (ESI) spectra of UbG76C **70** after DTT reduction. Calcd.: 8782.0 Da, found: 8783.0 Da.

UbK48C **77**:
Protein sequence: His-tag highlighted in green; protease cleavage site highlighted in blue; UbK48C in black; K48C highlighted in red:
MGSSHHHHHHSSGLVPRGSASQIFVKTLTGKTITLEVEPSDTIENVKAKIQDKEGIP
PDQQRLIFAGCQLEDGRTLSDYNIQKESTLHLVLRLRGG

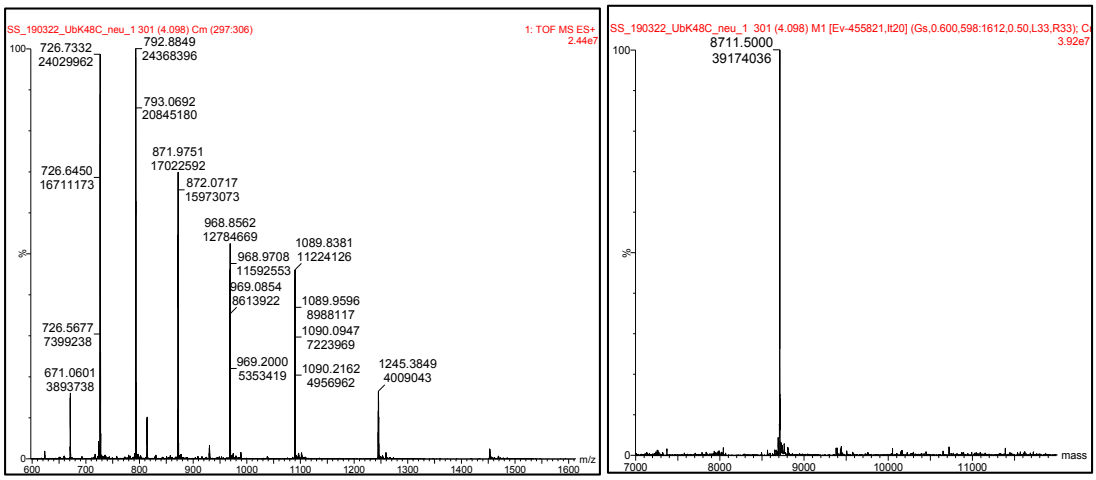

Fig. 86 Raw and deconvoluted HR-MS spectra (ESI) of UbK48C **77** after DTT reduction. Calcd.: 8710.9 Da, found: 8711.5 Da.

UbK48M **81**:
Protein sequence: His-tag highlighted in green; protease cleavage site highlighted in blue; UbK48M in black; K48M highlighted in red:
MGSSHHHHHHSSGLVPRGSASQIFVKTLTGKTITLEVEPSDTIENVKAKIQDKEGIP
PDQQRLIFAGMQLEDGRTLSDYNIQKESTLHLVLRLRGG

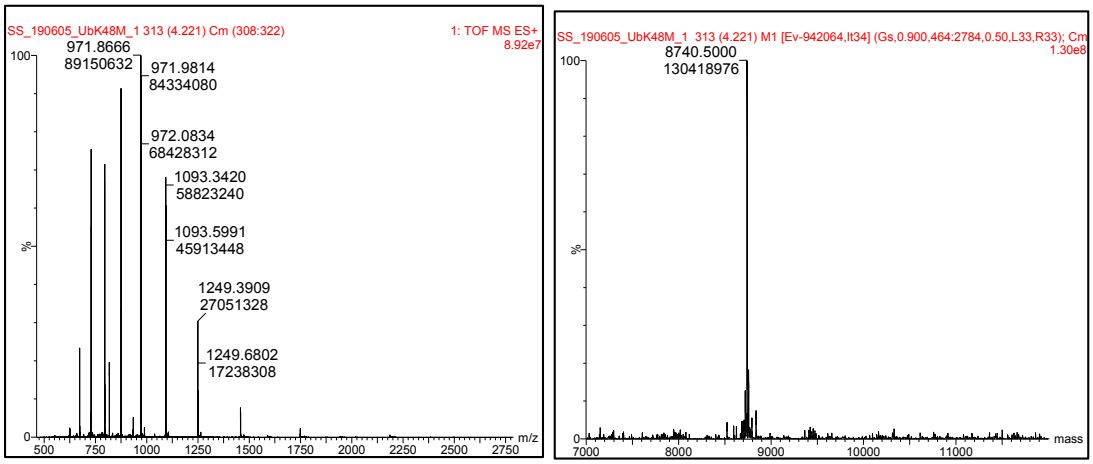

Fig. 87 Raw and deconvoluted HR-MS spectra (ESI) of UbK48M **81** after DTT reduction. Calcd.: 8738.9 Da, found: 8740.5 Da.

Expression and purification of α-SynucleinK6C 79

The protein was expressed and purified similar to Ref. [317]. The following α-SynucleinK6C sequence in vector pSVpT7 was used:

5'ATGGATGTATTCATGAAAGGACTTTCAAAGGCCAAGGAGGGAGTTGTGGCT
GCTGCTGAGAAAACCAAACAGGGTGTGGCAGAAGCAGCAGGAAAGACAAAA
GAGGGTGTTCTCTATGTAGGCTCCAAAACCAAGGAGGGAGTGGTGCATGGTG
TGGCAACAGTGGCTGAGAAGACCAAAGAGCAAGTGACAAATGTTGGAGGAGC
AGTGGTGACGGGTGTGACAGCAGTAGCCCAGAAGACAGTGGAGGGAGCAGGG
AGCATTGCAGCAGCCACTGGCTTTGTCAAAAAGGACCAGTTGGGCAAGAATG
AAGAAGGAGCCCCACAGGAAGGAATTCTGGAAGATATGCCTGTGGATCCTGAC
AATGAGGCTTATGAAATGCCTTCTGAGGAAGGGTATCAAGACTATGAACCTGA
AGCC 3'

The mutation was introduced with classical PCR by the use of complementary primer pairs:
fwd: 5' CATATGGATGTATTCATGTGCGGACTTTCAAAGG 3'
rev: 5' CCTTTGAAAGTCCGCACATGAATACATCCATATG 3'

The protein was expressed in *E. coli* Bl21(DE3) using LB medium containing 100 μg/mL ampicillin (LBAMP). Cells were grown at 37 °C, 180 rpm until an OD_{600} of 0.6-0.8 was reached. Expression was induced with 0.5 mM IPTG and incubated at 18 °C for 19 h. Lysis was performed in 10 mM Tris-HCl pH 8.0, 1 mM EDTA, 1 mM PMSF using a high-pressure homogenizer (Microfluidics LM10 Microfluidizer) and debris was boiled at 95 °C for 20 min, cooled down and centrifuged at 50.000 g for 15 min at 4 °C. Streptomycin sulfate (Roth) was added to the supernatant to a final concentration of 10 mg/mL and stirred for 15 min at 4 °C. After centrifugation at 50000 g for 15 min at 4 °C, ammonium sulfate (Roth) was added to the supernatant to reach a final concentration of 0.36 g/mL and stirred for 30 min at 4 °C. The suspension was centrifuged at 50000 g for 15 min at 4 °C and the pellet resuspended in 25 mM Tris-HCl pH 7.7. Then the protein was purified with a BioRad NGC system (BioRad, USA) using an anion-exchange-column Resource Q (GE Healthcare, USA) column with a NaCl gradient (0-600 mM). The α-SynucleinK6C was eluted at 300 mM NaCl. Subsequently, a size-exclusion chromatography (Superdex 75 10/300 GL column (GE Healthcare, USA) in Dulbecco's PBS pH 7.4 was performed to gel the clean α-SynucleinK6C **79** with a yield of 12 mg/L as determined by NanoDrop® at 280 nm ($\epsilon = 5960\,M^{-1}\,cm^{-1}$).

Protein sequence, K6C highlighted in red:
MDVFMCGLSKAKEGVVAAAEKTKQGVAEAAGKTKEGVLYVGSKTKEGVVHGV
ATVAEKTKEQVTNVGGAVVTGVTAVAQKTVEGAGSIAAATGFVKKDQLGKNEE
GAPQEGILEDMPVDPDNEA YEMPSEEGYQDYEPEA

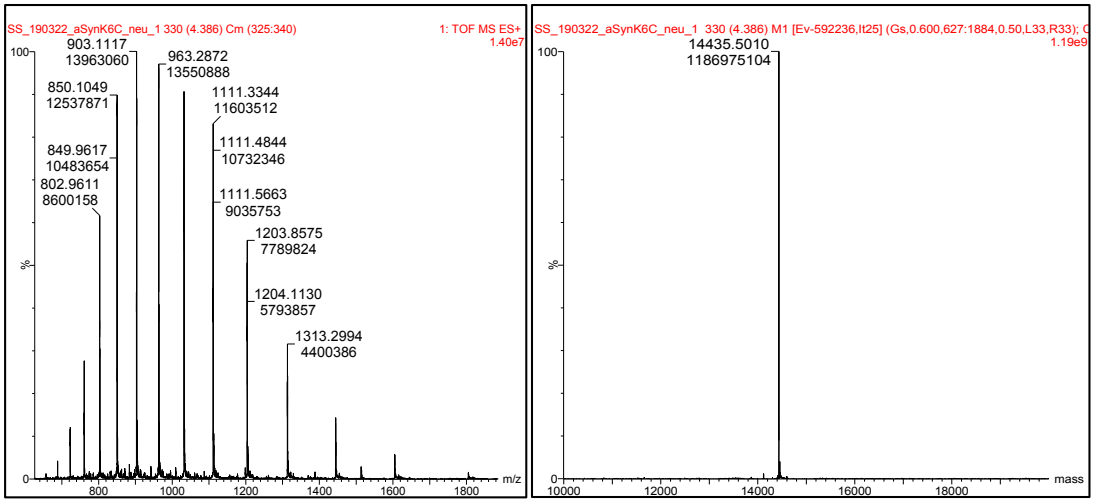

Fig. 88 Raw and deconvoluted HR-MS (ESI) spectra of α-SynucleinK6C **79** after DTT reduction. Calcd.: 14435.1 Da, found: 14435.5 Da

Expression and purification of eGFPC70MS147C 75

The protein was expressed and purified according to Ref. [208].

Protein sequence: His-tag highlighted in green; protease cleavage site highlighted in blue; eGFP highlighted in back; C70M and S147C highlighted in red:
MGSSHHHHHHSSGLVPRGSHMGSIQMVSKGEELFTGVVPILVELDGDVNGHKFSV
SGEGEGDATYGKLTLKFICTTGKLPVPWPTLVTTLTYGVQMFSRYPDHMKQHDF
FKSAMPEGYVQERTIFFKDDGNYKTRAEVKFEGDTLVNRIELKGIDFKEDGNILG
HKLEYNYNCHNVYIMADKQKNGIKVNFKIRHNIEDGSVQLADHYQQNTPIGDGP
VLLPDNHYLSTQSALSKDPNEKRDHMVLLEFVTAAGITLGMDELYK

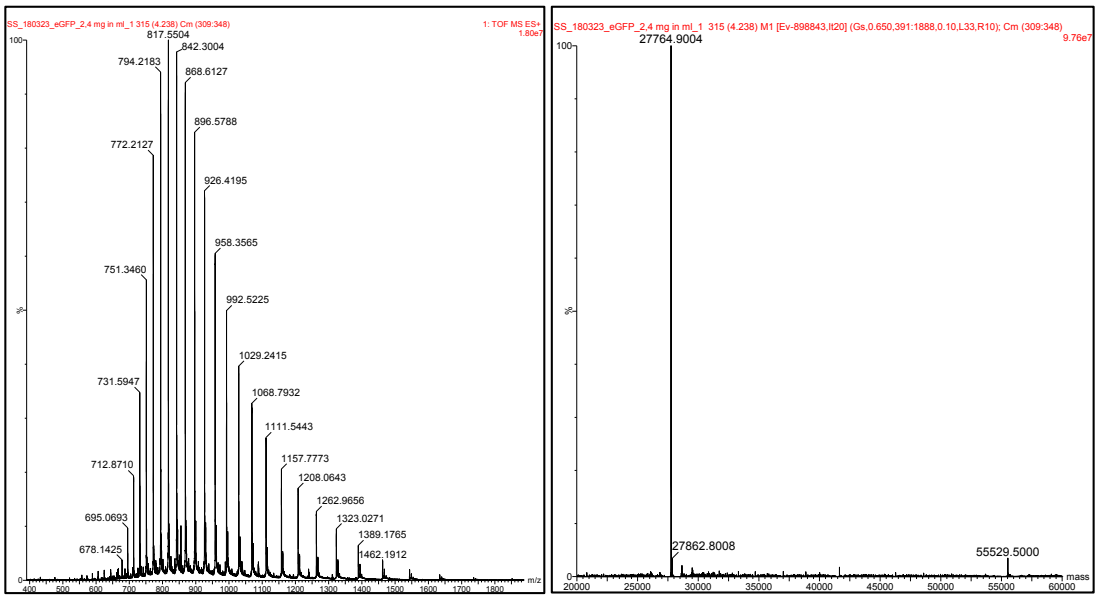

Fig. 89 Raw and deconvoluted HR-MS (ESI) spectra of eGFPC70MS147C **75**. Calcd.: 27766 Da, found: 27765 Da.

8.3.2 Synthesis and aqueous stability of vinylphosphonothiolate-Ub 72

Synthesis of Ellman's activated UbG76C 71

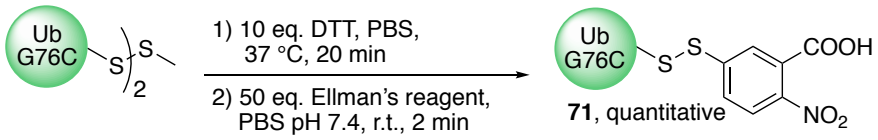

To a solution of UbG76C (mostly disulfide) (25.85 mg, 2.95 μmol) in 10 mL PBS pH 7.4 was added dithiothreitol (DTT) (4.5 mg, 29.5 μmol, 10 eq.) and the mixture was shaken for 20 min at 37 °C to reduce disulfides, which had formed during storage. Residual DTT was then thoroughly washed away by means of spin-filtration (MCWO: 3 kDa, Sartorius, Germany) using in total 50 mL of PBS pH 7.4 and the solution was finally concentrated to 2 mL. Subsequently Ellman's reagent (58.46 mg, 147.5 μmol, 50 eq.) was added and

the mixture was shaken for 2 min at r.t. The reaction mixture was washed with 50 mM NH_4HCO_3 pH 7.9 by means of spin-filtration (MCWO: 3 kDa, Sartorius, Germany) until the excess of Ellman's reagent was completely removed (requires approximately 50 mL of buffer) and then lyophilized, affording product **71** quantitatively (26.5 mg, 29.5 μmol).

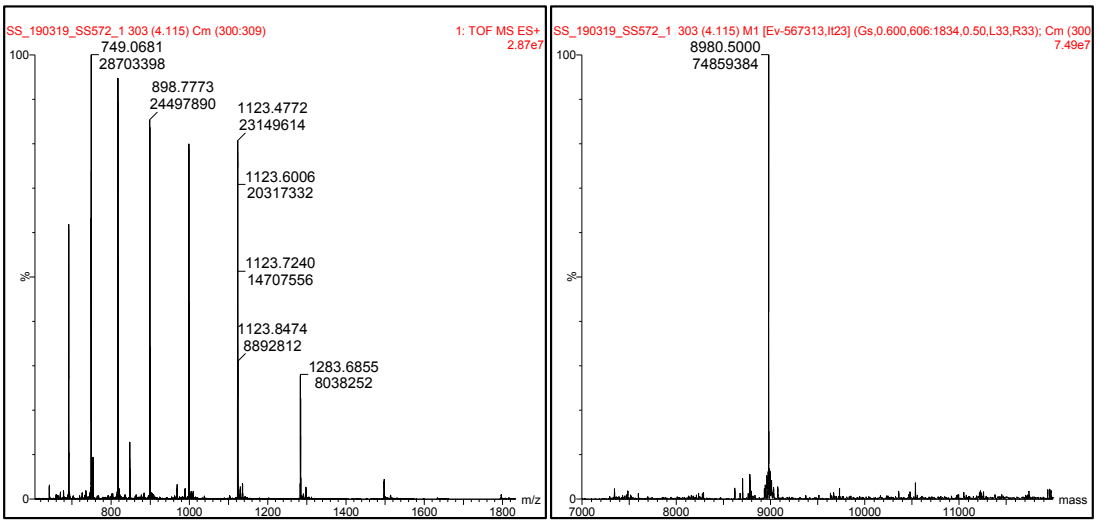

Fig. 90 Raw and deconvoluted HR-MS (ESI) spectra of Ellman's activated UbG76C **71**. Calcd.: 8979.2 Da, found: 8980.5 Da

Synthesis of vinylphosphonothiolate-Ub 72

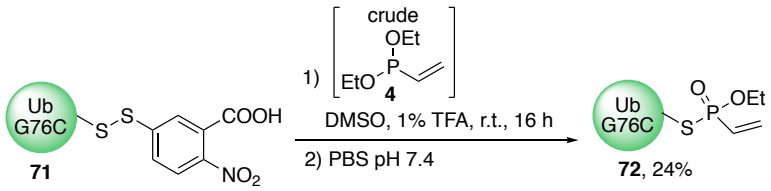

Lyophilized Ellman's activated UbG76C **71** (5.11 mg, 0.569 μmol) was dissolved in 380 μL dry DMSO containing 1% TFA in an Eppendorf tube. Freshly synthesized diethylvinylphosphonite **4** (crude, 36 μL, ca. 0.8 M in THF, 28.45 μmol, 50 eq.) was added and the mixture was immediately thoroughly vortexed to get the phosphonite in solution. The reaction mixture was shaken under an argon atmosphere overnight at r.t. ESI-MS analysis showed incomplete conversion, hence another portion of 50 eq. diethylvinylphosphonite (36 μL, 0.8 M in THF, 28.45 μmol) was added and the reaction mixture was shaken for 3 h. The crude mixture was diluted with 40 mL PBS pH 7.4 and concentrated to 5 mL by spin-filtration (MCWO: 3 kDa, Sartorius, Germany) to remove the DMSO. Subsequently, the crude was purified by semipreparative HPLC (Vydac protein C4 column, gradient: 30-70% MeCN + 0.1% TFA in H_2O + 0.1% TFA in 35 min) and the vinylphosphonothiolate UbG76C **72** was isolated as a pure fraction (2.43 mg, 0.273 μmol, 24%). The product was lyophilized and reconstituted before use by dissolving in DMSO and subsequent dilution in PBS pH 7.4.

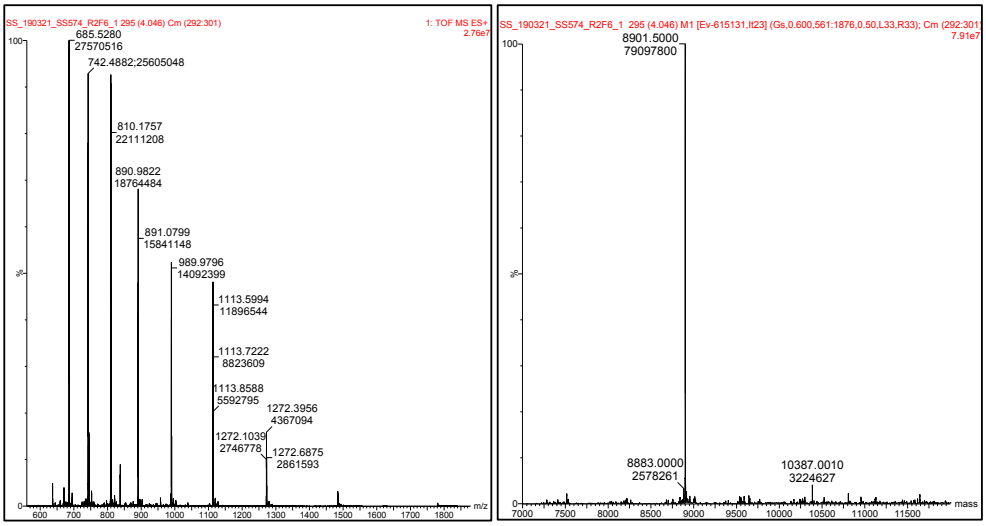

Fig. 91 Raw and deconvoluted HR-MS (ESI) spectra of purified vinylphosphonothiolate UbG76C **72**. Calcd.: 8900.1 Da, found: 8901.5 Da.

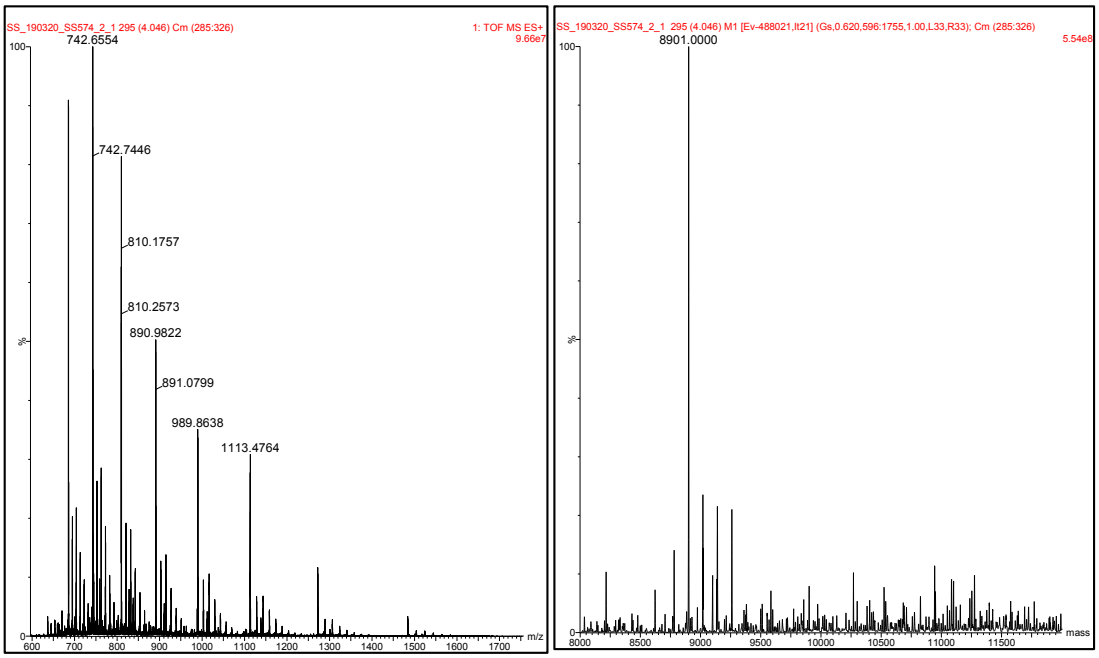

Fig. 92 Raw and deconvoluted HR-MS spectra of crude vinylphosphonothiolate UbG76C **72**.

Stability of vinylphosphonothiolate ubiquitin 72 in aqueous buffer

Vinylphosphonothiolate UbG76C **72** (1 μg/μL) in PBS pH 7.4 or in 50 mM Na_3PO_4 pH 8.5 was incubated at r.t. or at 37 °C. Samples were taken at 0, 24, 48 and 72 h and analysed by SDS-PAGE.

8.3.3 Protein conjugations to vinylphosphonothiolate-Ub 72

Conjugation of vinylphosphonothiolate-Ub 72 and eGFP mutant 75

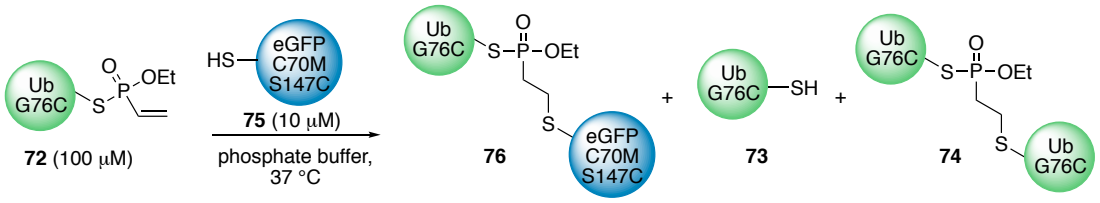

To a solution of eGFPC70MS147C **75** (2 μg/μL, 72 pmol, 2 μL) in PBS pH 7.4 or in 50 mM Na_3PO_4 pH 8.5 was added vinylphosphonothiolate UbG76C **72** (6.4 μL, 1 μg/μL, 719 pmol, 10 eq.) in PBS pH 7.4 or in 50 mM Na_3PO_4 pH 8.5. The reactions were shaken at 37 °C and samples were taken at 2, 8, 24, 48 and 72 h and analysed by SDS-PAGE gel (see Fig. 36) and by HR-MS (ESI).

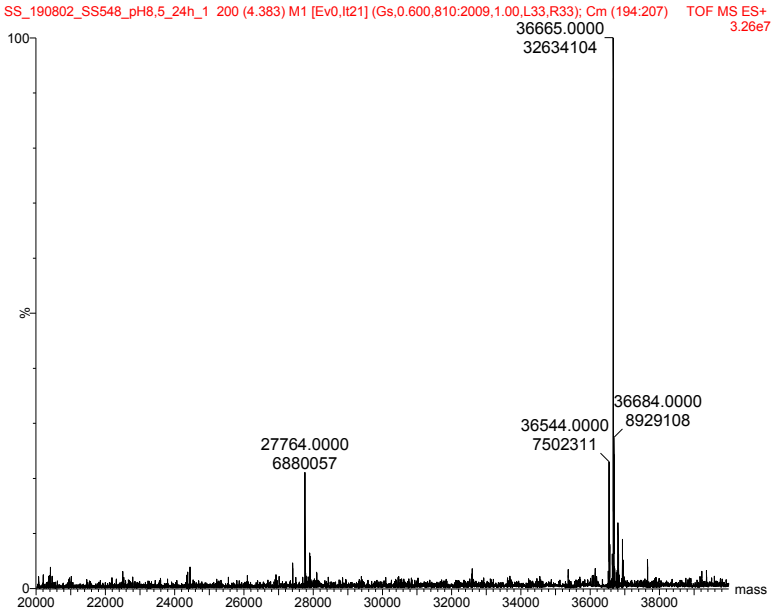

Fig. 93 Deconvoluted ESI-MS spectrum of the reaction mixture between eGFP mutant **75** and vinylphosphonothiolate ubiquitin **72** after 24 h, indicating the formation of Ub-GFP conjugate **76**: Calcd.: 36666 Da, found: 36665 Da.

Conjugation of vinylphosphonothiolate-Ub 72 and UbK48C 77

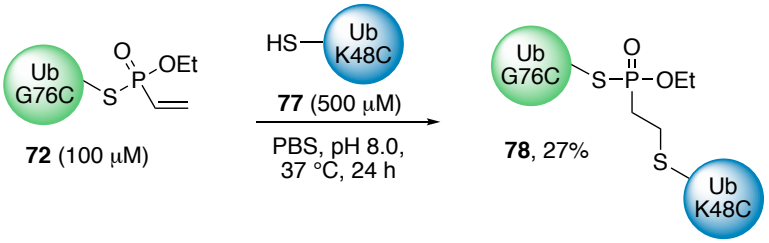

To a solution of UbK48C **77** (4.138 mg, 0.475 μmol, 5.0 eq.) in 2 mL PBS containing 5 mM EDTA at pH 7.4 was added dithiothreitol (DTT) (366 μg, 2.375 μmol, 25 eq.) and the mixture was shaken for 30 min at 37 °C. Residual DTT was washed away by means of spin-filtration (MCWO: 3 kDa, Sartorius, Germany) using 50 mL of the same buffer and the mixture was finally concentrated to 900 μL. To this was added a solution of vinylphosphonothiolate ubiquitin **72** (0.845 mg, 0.095 μmol, 1.0 eq.) in 100 μL 100 mM NH_4HCO_3 pH 8.5. The pH of the mixture was adjusted to pH 8.0 and the mixture was shaken at 37 °C. After 24 h the reaction mixture was treated with DTT (100 eq.) at 37 °C for 40 min to reduce disulfides of **77** because the latter would co-elute with the product **78**. The crude product was purified by size-exclusion chromatography (Superdex 75 10/300 GL column (GE Healthcare, USA)) in PBS pH 7.4. The conjugate DiUb(K48) **78** was isolated as a pure fraction (460 μg, 0.026 μmol, 27%). The protein concentration was determined by a BCA assay using dilutions of BSA in PBS as standards.

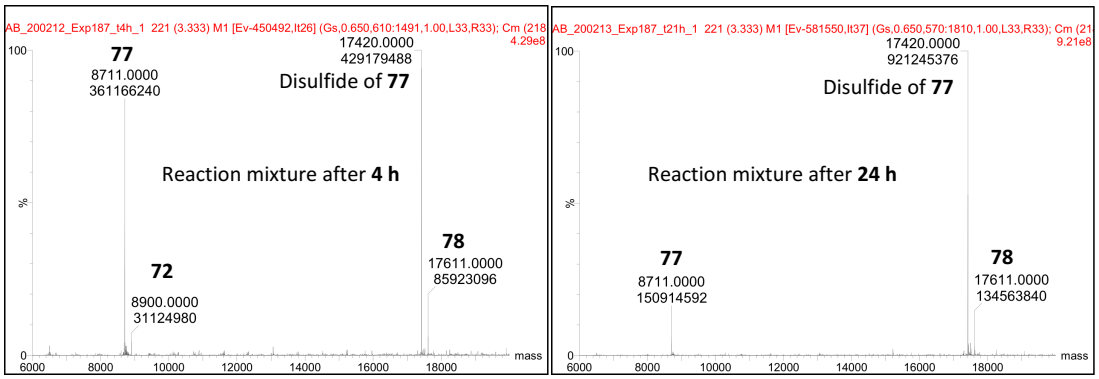

Fig. 94 Deconvoluted HR-MS spectra (ESI) of the reaction mixture of the conjugation between vinylphosphonothiolate ubiquitin **72** and UbK48C **77**.

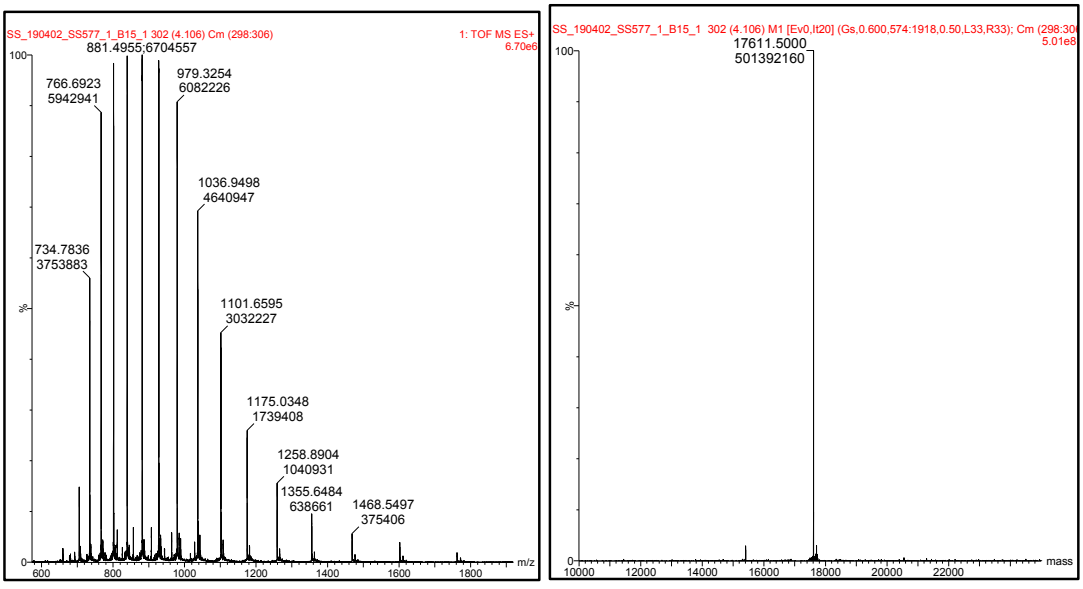

Fig. 95 Raw and deconvoluted HR-MS (ESI) spectra of purified DiUb(K48) conjugate **78**. Calcd.: 17610 Da, found: 17611 Da.

Hydrolytic stability of synthetic DiUb 78 against the DUB enzyme USP2CD

To the deubiquitinating enzyme USP2CD (1.6 μg, 40 pmol) (BostonBiochem) in 50 mM HEPES pH 8.0 containing 150 mM NaCl, 0.1 mM EDTA and 1 mM DTT was added either the DiUb(K48) **78** (1 μg, 56.8 pmol) in PBS pH 7.4 or wtDiUb(K48) (1 μg, 58.4 pmol) (Enzo Life Sciences) in PBS pH 7.4 and the mixtures were incubated for 2 h at 37 °C.

CD analysis of synthetic DiUb 78

The synthesized DiUb(K48) **78** conjugate was compared to commercially available wild-type DiUb(K48) (Enzo Life Sciences). DiUb(K48) samples were rebuffered to 50 mM Na_2HPO_4 pH 7.4 using spin filtration (MCWO: 10 kDa, Sartorius, Germany). The protein concentrations were determined by BCA assay (synthetic DiUb(K48) **78**: 9.34 μg/mL, wtDiUb(K48): 5.27 μg/mL). CD-Spectra were recorded at r.t. on a JASCO J-720 spectrometer using a 0.1 cm path length quartz cells at 260-185 nm rage with a scanning speed of 100 nm/min and 30 accumulations and a data pitch of 0.1 nm.

Conjugation of vinylphosphonothiolate-Ub 72 and α-SynucleinK6C 79

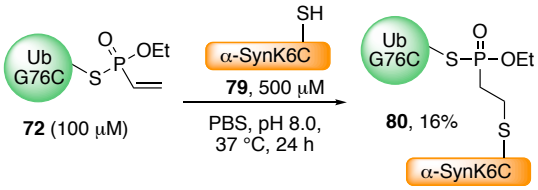

To a solution of α-SynucleinK6C (αSyn) **79** (6.86 mg, 0.475 μmol, 5.0 eq.) in 2 mL PBS containing 5 mM EDTA at pH 7.4 was added dithiothreitol (DTT) (366 μg, 2.375 μmol, 25 eq.) and shaken for 30 min at 37 °C. Residual DTT was washed away by means of spin-filtration (MCWO: 3 kDa, Sartorius, Germany) using approximately 50 mL of the same buffer and the mixture was concentrated to 900 μL. To this was added vinylphosphonothiolate ubiquitin **72** (0.845 mg, 0.095 μmol, 1.0 eq.) dissolved in 100 μL 100 mM NH_4HCO_3 pH 8.5 and the pH of the mixture was adjusted to pH 8.0. The mixture was shaken at 37 °C for 24 h. Thereafter the crude product was purified by size-exclusion chromatography (Superdex 75 10/300 GL column (GE Healthcare, USA)) in PBS pH 7.4. Other than for the conjugate DiUb(K48) **78** described above, this reaction mixture was not treated with DTT before size-exclusion chromatography because αSyn **79** and the product **80** have similar retention times and it is therefore beneficial to keep the αSyn **79** in the disulfide form for the purification in order to minimize mixed fractions. The conjugate Ub-αSyn conjugate **80** was isolated as a pure fraction (354 μg, 15.2 nmol, 16%). The protein amount was determined by a BCA assay using dilutions of BSA in PBS as standards.

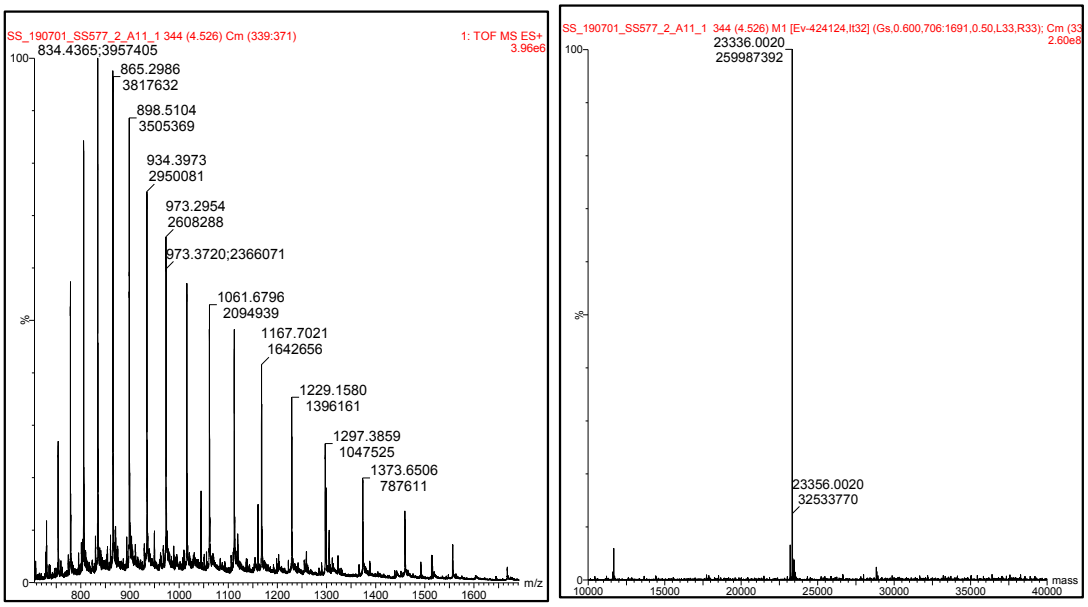

Fig. 96 Raw and deconvoluted HR-MS (ESI) spectra of purified Ub-αSyn conjugate **80**. Calcd.: 23335 Da, found: 23336 Da.

8.3.4 Enzymatic ubiquitination of α-Synuclein-ubiquitin conjugate 80

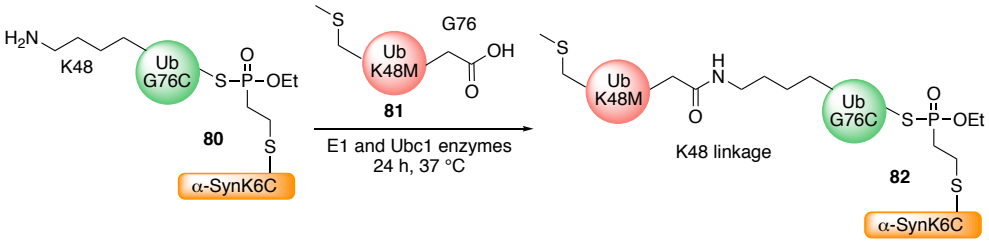

To a solution of UbK48M **81** (4 μL, 229 pmol, 5.3 eq.) in 50 mM Tris pH 7.4 containing 150 mM NaCl and 6 mM $MgCl_2$ was added E1 enzyme (Enzo Life Sciences, 2 μL, 1.8 pmol) and E2 enzyme (Ubc1) (Enzo Life Sciences, 1.2 μL, 20 pmol) and ATP (Thermo Fisher Scientific) (80 nmol, 0.8 μL). The mixture was left at r.t. for 10 min. Subsequently, α-Synuclein-ubiquitin conjugate **80** (2 μL, 43 pmol) in PBS pH 7.4 was added and the reaction was kept at 37 °C for over night. On the next day additional ATP (1 μL, 100 nmol) was added. The reaction was analysed by ESI-MS, SDS-PAGE (silver stain) and Western blot (see Fig. 40B/C).

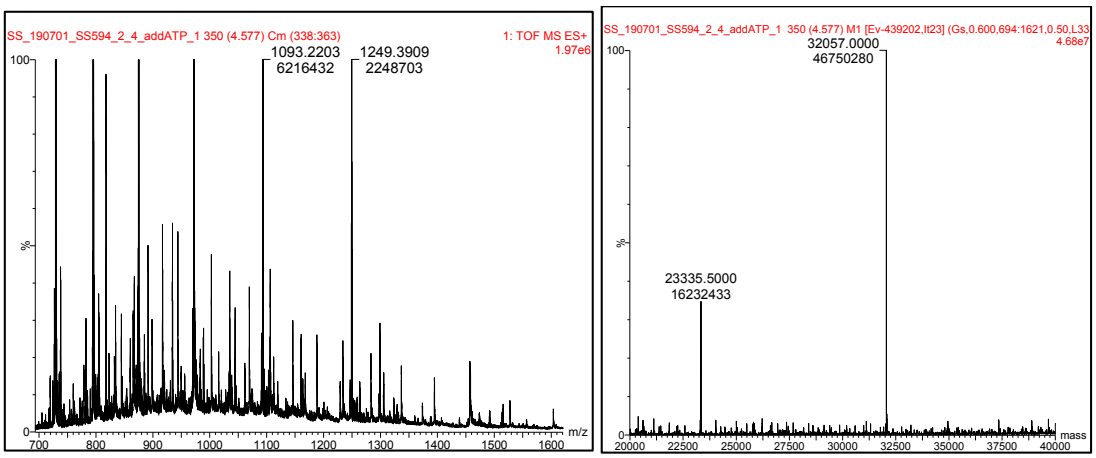

Fig. 97 Raw and deconvoluted HR-MS (ESI) spectra of the reaction mixture of UbK48M **81** and Ub-αSyn **80**. Calculated mass for diubiquitinated product **82**: 32056 Da, found: 32057 Da.

8.3.5 MS/MS analysis of phosphonothiolate-linked protein-protein conjugates

Purified protein conjugates **78** and **80** were run on a SDS-gel, stained with Coomassie and further processed by in-gel protein digest using trypsin. Digested peptides were analysed by LC-MS/MS as described in the general procedure in chapter 8.1.

For peptide identification, the RAW-files were loaded into Proteome Discoverer (v.2.4, Thermo Scientific) and a database search was performed with MSAmanda 2.0 [312]. Files were searched against a database containing the sequence of the two ubiquitin mutants and α-Synuclein, using the following search parameters: peptide mass tolerance of $\pm$5 ppm, fragment mass tolerance of $\pm$20 ppm, a maximum of two missed cleavages, minimum peptide length of 5 and a minimum MSAmanda score of 150. The P(V)-electrophile (118.0189 Da) and the P(V)-electrophile plus the attached ubiquitin C-terminus (296.0596 Da or 565.2448 Da) were considered as dynamic modifications to occur on all nucleophilic amino acids. Spectra that identified a peptide carrying one of these modifications were manually validated.
In addition, the files were searched with pLink 2.3 [318], a software designed to identify cross-linked peptides. Therefore, RAW-files were converted to MGF using Proteome Discoverer (v.2.4, Thermo Scientific). The following search parameters were used: peptide mass tolerance of $\pm$5 ppm, fragment mass tolerance of $\pm$20 ppm, a maximum of 4 missed cleavages, minimum peptide length of 2 and the P(V)-electrophile was set as a non-cleavable crosslinker with all nucleophilic amino acids as possible crosslink sites. Crosslink-containing spectra were manually validated and visualized using xiSPEC [319].

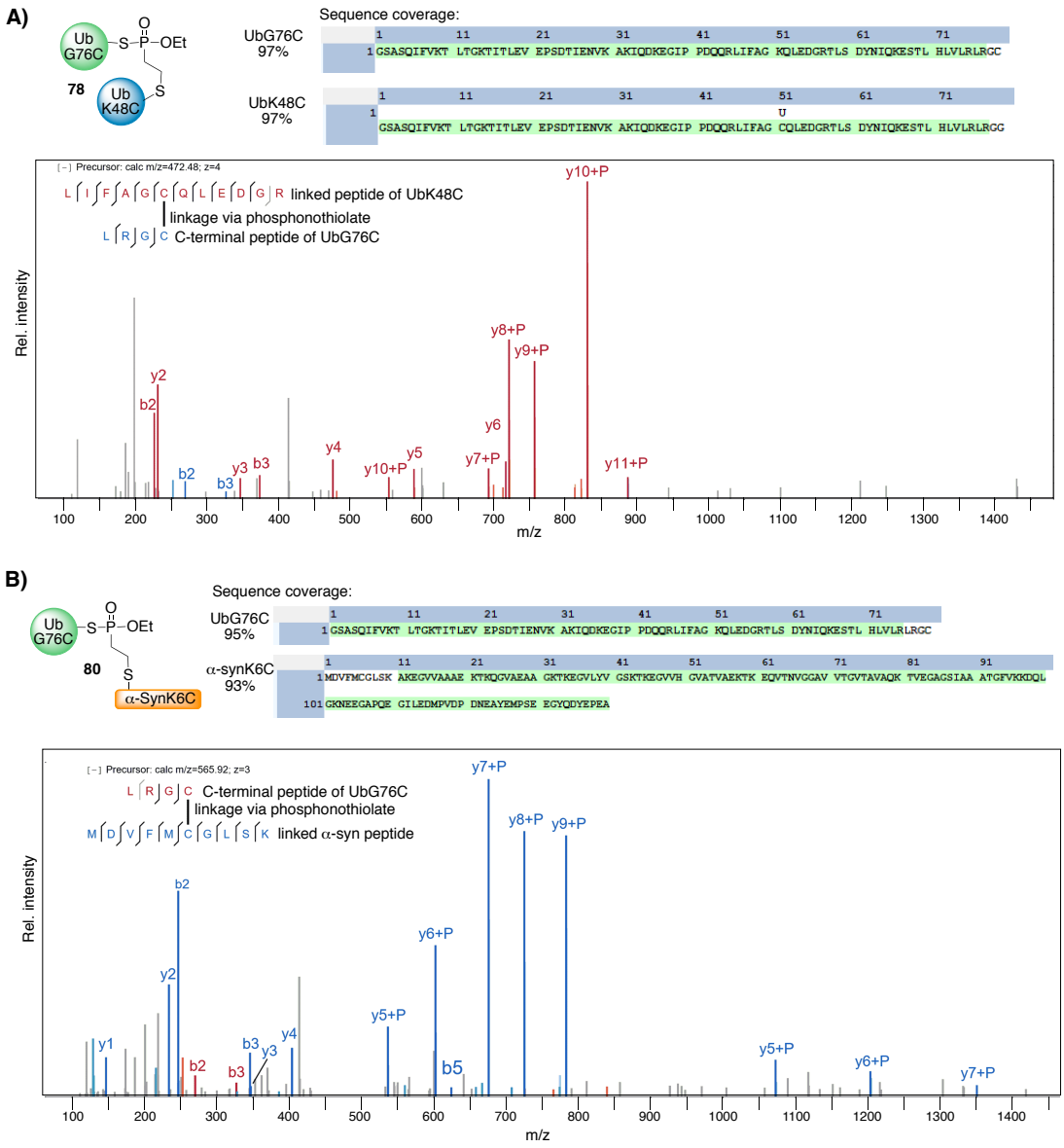

Fig. 98 MS/MS analysis of phosphonothiolate-linked protein-protein conjugates after tryptic digest for A) diubiquitin conjugate **78** and B) Ub-α-Synuclein conjugate **80**. Shown are the sequence coverages in green for the individual proteins and the MS/MS spectra of the phosphonothiolate-linked peptides, indicating site-specific conjugation to UbC76.

8.4 Experimental part for ADC chapter

The protocols used in this chapter are based on an adapted from Ref. [228]. Brentuximab was kindly provided by Stefanie Boldt and Marcus Gerlach from Tubulis GmbH.

8.4.1 Brentuximab modification with 47 and 48 (DAR screens)

Procedure for the modification of brentuximab (1 mg/mL) with different equivalents of 47

5 µl of a 70 mM solution of DTT in 50 mM sodium borate in PBS (pH 8.0) was added to 50 µl of a brentuximab solution (1.0 mg/mL) in 50 mM sodium borate in PBS (pH 8.0) and the mixture was incubated at 37 °C for 40 min. Excess DTT removal and exchange to the conjugation buffer (50 mM Tris, 1 mM EDTA, 100 mM NaCl, pH 8.5 or PBS, 1 mM EDTA, pH 7.4 at 14 °C) was conducted afterwards using 2 mL ZebaTM spin desalting columns with 7 K MWCO (Thermo Fisher Scientific, USA). The reduced antibody solutions were mixed quickly afterwards with the desired amount of compound **47** dissolved in DMSO to give a final amount of 5% DMSO. The mixture was shaken at 850 rpm and 14 °C for 16 hours.

Procedure for the modification of brentuximab (5 mg/mL) with different equivalents of 47 or with 48 using the full reduction protocol

5 µl of a 350 mM solution of DTT in 50 mM sodium borate in PBS (pH 8.0) was added to 50 µl of a brentuximab solution (5.0 mg/mL) in 50 mM sodium borate in PBS (pH 8.0) and the mixture was incubated at 37 °C for 40 min. Excess DTT removal and exchange to the conjugation buffer (50 mM Tris, 1 mM EDTA, 100 mM NaCl, pH 8.5 or PBS, 1 mM EDTA, pH 7.4 at 14 °C or at 25 °C) was conducted afterwards using 0.5 mL ZebaTM spin desalting columns with 7K MWCO (Thermo Fisher Scientific, USA). The reduced antibody solutions were mixed quickly afterwards with desired amount of compound **47** or **48** dissolved in DMSO to give a final amount of 5% DMSO (or 10% DMSO when using 100 eq. of **47**). The mixture was shaken at 850 rpm and 14 or 25 °C for 16 hours.

Procedure for the modification of brentuximab (5 mg/mL) with different equivalents of 48 using the partial reduction protocol with TCEP

10 µL of a brentuximab solution (5.0 mg/mL) in conjugation buffer (50 mM Tris, 1 mM EDTA, 100 mM NaCl, pH 8.5 at 14 °C) were mixed with 1 µL of a TCEP solution in conjugation buffer containing the appropriate amount of TCEP. Directly afterwards, the desired amount of compound **48** dissolved in DMSO were added to give a final amount of 5% DMSO. The mixture was shaken at 850 rpm and 14 °C for 16 hours.

Procedure for the modification of brentuximab (12 mg/mL) with different equivalents of 48 using the partial reduction protocol with TCEP

10 µL of a brentuximab solution of (12 mg/mL) in conjugation buffer (50 mM Tris, 1 mM EDTA, 100 mM NaCl, pH 8.5 at 14 °C) were mixed with 1 µL of a TCEP solution in conjugation buffer containing the appropriate amount of TCEP. Directly afterwards, the desired amount of compound **48** dissolved in DMSO were added to give a final amount of 10% DMSO. The mixture was shaken at 850 rpm and 14 °C, 25 °C or 37 °C for 16 hours.

8.4.2 Generation and purification of ADC 85 with a DAR of 3.15

28 µL of a 360 mM solution of DTT in 50 mM sodium borate in PBS (pH 8.0) were added to 300 µL of a brentuximab solution (5.0 mg/mL) in 50 mM sodium borate in PBS (pH 8.0) and the mixture was incubated at 37 °C for 40 min. Excess DTT removal and exchange to the conjugation buffer (50 mM Tris, 1 mM EDTA, 100 mM NaCl, pH 8.5) was conducted afterwards using 2 mL ZebaTM spin desalting columns with 7K MWCO (Thermo Fisher Scientific, USA). The reduced antibody solution was mixed quickly afterwards with 2.45 µL of a 36 mM solution of **47** dissolved in DMSO plus 14 µL DMSO to give a final amount of 5% DMSO and 8.8 eq. **47**. The solution was shaken at 850 rpm and 14 °C for 16 hours. The reaction mixture was purified in one portion by size-exclusion chromatography with a 25 mL SuperoseTM 6 Increase 10/300GL (GE healthcare, United States) and a flow of 0.7 mL/min eluting with sterile PBS (Merck, Germany). The antibody containing fractions were pooled and concentrated by spin-filtration to 225 µL (MWCO: 10 kDa, 6 mL, Sartorius, Germany) and the concentration was determined to 2 mg/mL (see chapter 8.4.4), which corresponds to 450 µg ADC and an overall yield of 30% based on the initial amount of brentuximab.

8.4.3 Generation and purification of ADC 86 with a DAR of 3.1

20 µL of a 8.8 mM solution of TCEP in conjugation buffer (50 mM Tris, 1 mM EDTA, 100 mM NaCl, pH 8.5) were added to 200 µL of a brentuximab solution (12.0 mg/mL) in conjugation buffer. Quickly afterwards, 12 µL of a 72 mM solution of **48** in DMSO was added to give a final amount of 5% DMSO, 10 eq. TCEP and 50 eq. **48**. The solution was shaken at 850 rpm and 25 °C for 16 hours. The next day, another portion of 10 eq. TCEP was added and quickly afterwards another portion of 25 eq. **48**. Two hours later, another portion of 10. eq. TCEP was added and the mixture was shaken at 850 rpm and 25 °C for 14 hours. The next day, based on the finding the DAR was still below 4 but free **48** was still detectable, another portion of 10 eq. of TCEP was added and the mixture was shaken at 850 rpm and 37 °C for 16 hours, resulting in a DAR of 4.36 as judged by intact protein MS from the reaction mixture. The reaction mixture was then purified in one portion by size-exclusion chromatography with a 25 mL SuperoseTM 6 Increase 10/300GL (GE healthcare, United States) and a flow of 0.7 mL/min eluting with sterile PBS (Merck, Germany). Thereby, a significant amount of aggregated antibody was separated from non-aggregated ADC. The latter fractions were pooled and concentrated by spin-filtration to 530 µL (MWCO: 10 kDa, 6 mL, Sartorius, Germany) and the concentration was determined to 2 mg/mL (see chapter 8.4.4), which corresponds to 1070 µg ADC and an overall yield of 44% based on the initial amount of brentuximab.

8.4.4 Analysis of ADCs

Determination of concentrations of purified ADCs

The final concentration of ADCs after purification by size-exclusion chromatography was determined in a 96-well plate with a PierceTM Rapid Gold BCA Protein Assay Kit (Thermo Fisher Scientific, USA) and a Bradford reagent B6916 (Merck, Germany) with pre-diluted protein assay standards of bovine gamma globulin (Thermo Fisher Scientific, USA). Results of both assays were arithmetically averaged.

Procedure for DAR determination of brentuximab conjugates by intact protein MS

For intact protein MS analysis of modified brentuximab, 10 μL of a solution of brentuximab (ca. 2 mg/mL) in PBS pH 7.4 were mixed with 0.5 μL PNGase-F solution (Promega, Germany, recombinant, cloned from *Elizabethkingia miricola* 10 u/μL) and incubated at 37 °C for 2 h. Then, 1 μL of DTT solution (10 mM in PBS, pH 7.4) was added and the mixture was incubated at 37 °C for another 30 min. Finally, samples were diluted with 30 μL distilled water and subjected to MS analysis with the Waters H-class system (for details see general information in chapter 8.1).

Resazurin assay

This protocol is based on Ref. [228]. HL60 and Karpas cell lines were cultured in RPMI-1640 supplemented with 10% FCS and 0.5% Penicillin-Streptomycin. SKBR3 and MDAMB468 cell lines were cultured in DMEM/F12 supplemented with 10% FCS and 0.5% Penicillin-Streptomycin. Cells were seeded at a density of $5*10^3$ cells/well (SKBR3, HL60 and Karpas) or $1*10^3$ cells/well (MDAMB468) in 96-well cell culture microplate. 1:4 serial dilutions of ADCs or antibodies were performed in cell culture medium starting at 3 μg/mL final concentration and transferred in duplicates to respective wells on the microplate. Plates were incubated for 96 h at 37 °C 5% CO_2. Subsequently, resazurin was added to a final concentration of 50 μM followed by incubation for 3–4 h at 37 °C, 5% CO_2. Metabolic conversion of resazurin to resorufin was quantified by the fluorescent signal of resorufin (λ_{Ex} = 560 nm and λ_{Em} = 590 nm) on a Tecan Infinite M1000 micro plate reader. Mean and standard deviation was calculated from duplicates, normalized to untreated control and plotted against antibody concentration. Data analysis was performed with MatLab R2016 software.

8.4.5 Stability studies of ADC 86 in rat serum

This protocol is based on Ref. [228]. In an Eppendorf-tube, 200 μL rat serum (Sigma Aldrich, United States) was mixed with 50 μL ADC **86** (2.0 mg/mL) to give a final solution of 0.4 mg/ml ADC in 80% rat serum. Samples were sterile filtered with UFC30GV0S centrifugal filter units (Merck, Germany) and incubated at 37 °C for 7 days. Samples for day 0 were directly processed further. Therefore, the supernatant of 50 μL anti human igG (Fc-Specific) agarose slurry (Sigma Aldrich, United States) was removed by centrifugation and the remaining resin washed three times with 200 μL PBS. The resin was incubated with 240 μL of the serum-ADC mix for 30 min at room temperature. Afterwards, the supernatant was removed and the resin washed 5 times with 200 μL PBS. Following by incubation for 5 minutes with 200 μL IgG elution buffer (ThermoFisher, United States) at room temperature. The supernatant was then transferred into a Spin filter (MWCO: 10 kDa, 0.5 ml, Sartorius, Germany), rebuffered to PBS pH 7.4 and concentrated to 100 μL. For analysis by intact protein MS, the samples were processed further as described in chapter 8.4.4. All measurements were performed in triplicates (n=3). Exemplary MS spectra at day 0 and day 7 are shown in Fig. 99 and Fig. 100/101, respectively.

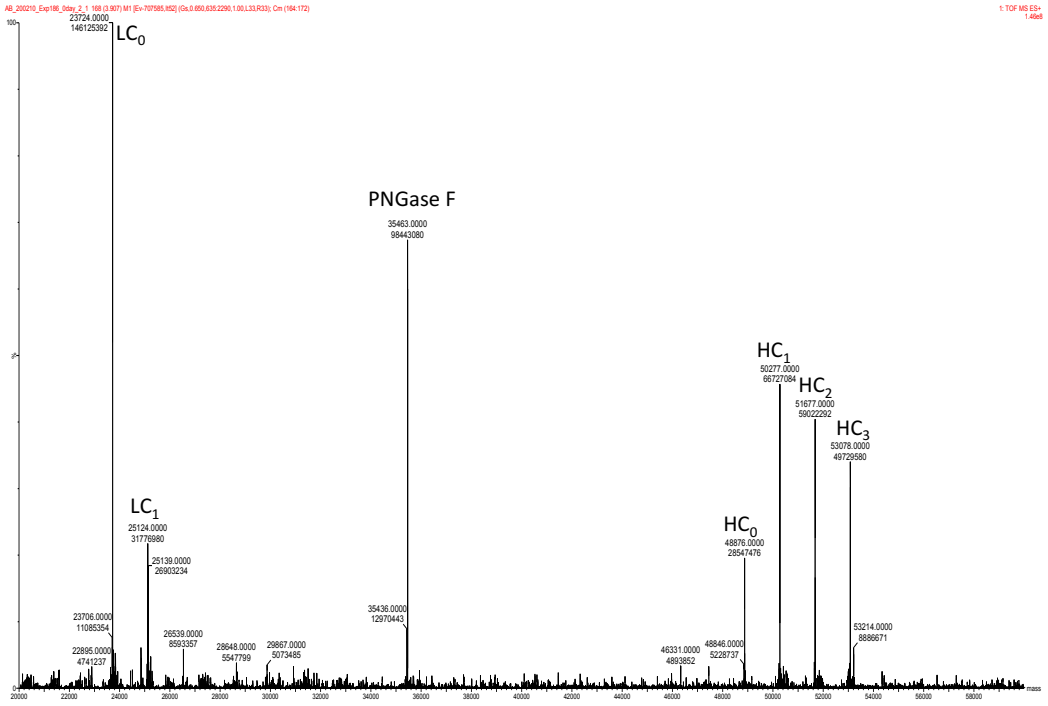

Fig. 99 Deconvoluted intact protein ESI-MS spectra of brentuximab ADC **86** after pull-down from rat serum at day 0.

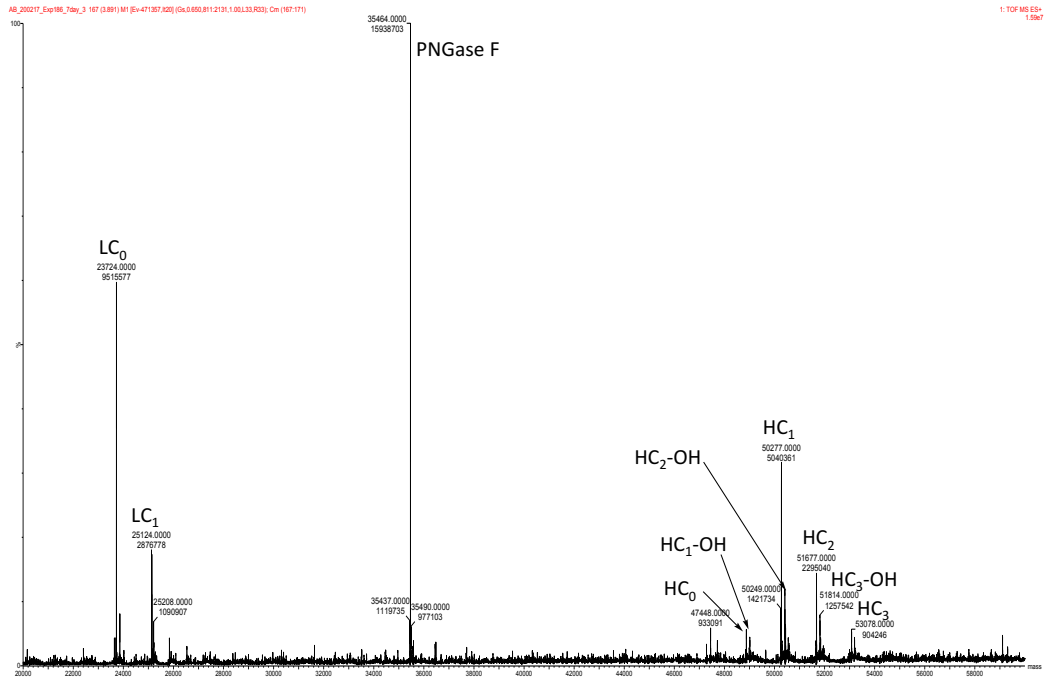

Fig. 100 Deconvoluted intact protein ESI-MS spectra of brentuximab ADC **86** after pull-down from rat serum at day 7, indicating P-S bond hydrolysis of the conjugate. Example: HC_2-OH is a heavy chain that carried initially 2 modifications, from which one was lost due to hydrolysis.

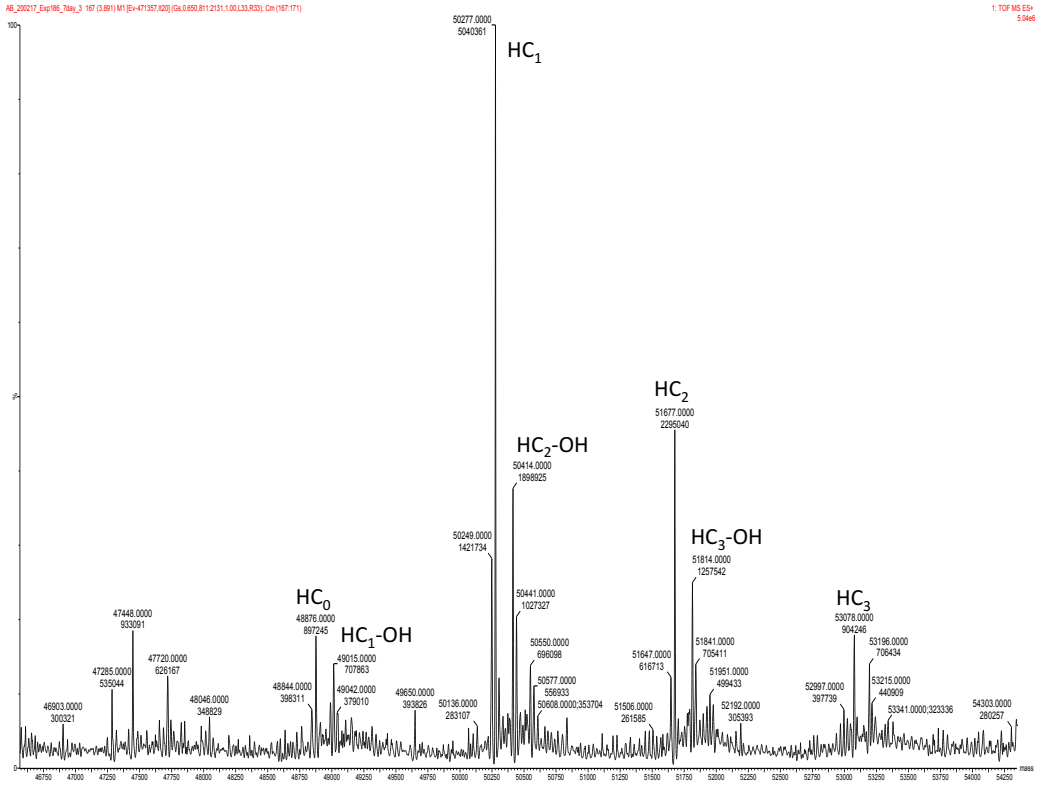

Fig. 101 Deconvoluted intact protein ESI-MS spectra of brentuximab ADC **86** after pull-down from rat serum at day 7 (zoomed in spectrum of Fig. 100).

8.5 Experimental part for chaperone photocrosslinking chapter

8.5.1 Synthesis of photocrosslinkers

Tetrazole building block synthesis

2-Phenyl-2H-tetrazole-5-carboxylic acid was synthesized based on protocols described in Ref. [320] and [289].

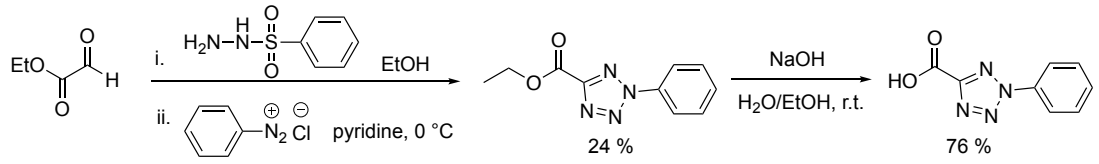

Ethyl 2-phenyl-2H-tetrazole-5-carboxylate

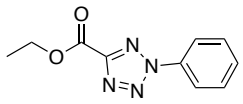

A solution of 50% ethyl 2-oxoacetate in toluene (3.042 g, 14.9 mmol, 1.4 eq.) and benzenesulfonyl hydrazide (1.72 g, 11.5 mmol, 1.07 eq.) in 60 mL EtOH was stirred at r.t. for 1 h. The solvent was removed under reduced pressure, and the residue was re-dissolved in 60 mL pyridine. Separately, to a stirred suspension of aniline (0.974 mL, 10.7 mmol, 1.0 eq.) and 4 mL concentrated HCl in 8 mL H_2O and 10 mL EtOH was added drop-wise a solution of $NaNO_2$ (0.775 g, 11.2 mmol, 1.05 eq.) in 3 mL H_2O at 0 °C. After 10 min, this solution was added drop-wise to the previously prepared pyridine solution over 50 min at –10 °C (ice/dry-ice bath). The mixture was warmed up to r.t. over 2 h with stirring before 100 mL H_2O was added. The solution was extracted with DCM (3 times 70 mL), and the organic layers were collected, combined, washed successively with 100 mL 2 N HCl (3 times) and 70 mL brine (one time). After drying over $NaSO_4$, the solvent was removed under reduced pressure. The dark brown oily residue was purified by silica gel flash chromatography (*n*-hexanes:EtOAc = 4:1) to give the crude product as a brown solid (1.153 g). The crude product was recrystallized from EtOH to give the title compound as a yellow solid (564 mg, 2.57 mmol, 24%). ^{1}H-NMR: (300 MHz, $CDCl_3$): δ = 8.23-8.13 (m, 2H), 7.63-7.49 (m, 3H), 4.56 (q, J = 7.1 Hz, 2H), 1.47 (t, J = 7.2 Hz, 3H). ^{13}C-NMR: (75 MHz, $CDCl_3$): δ = 157.87, 136.44, 130.73, 129.92, 120.39, 62.91, 14.30.

2-Phenyl-2H-tetrazole-5-carboxylic acid

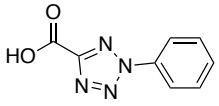

To a suspension of ethyl 2-phenyl-2H-tetrazole-5-carboxylate (500 mg, 2.281 mmol) in 26.5 mL H_2O was added 2.65 mL of a 2 M NaOH solution in EtOH (the mixture had to be heated and sonicated to get everything in solution). The solution was stirred at r.t.

for 2 hours, then acidified to pH = 2 by the addition of 2 N HCl and extracted with DCM (3 times with 30 mL). The combined organic layers were dried over Na_2SO_4 and filtered. The solvents were removed under reduced pressure to give the titled compound as a slightly pink solid (330 mg, 1.74 mmol, 76%). ^{1}H-NMR: (300 MHz, DMSO−d_6): δ = 8.18-8.02 (m, 2H), 7.77-7.56 (m, 3H). ^{13}C-NMR: (75 MHz, DMSO−d_6): δ = 158.66, 158.26, 135.99, 130.83, 130.26, 120.36. HR-MS (ESI+) for $C_8H_7N_4O_2^+$ $[M+H]^+$ calcd.: 191.0564, found: 191.0569.

Photocrosslinker 88

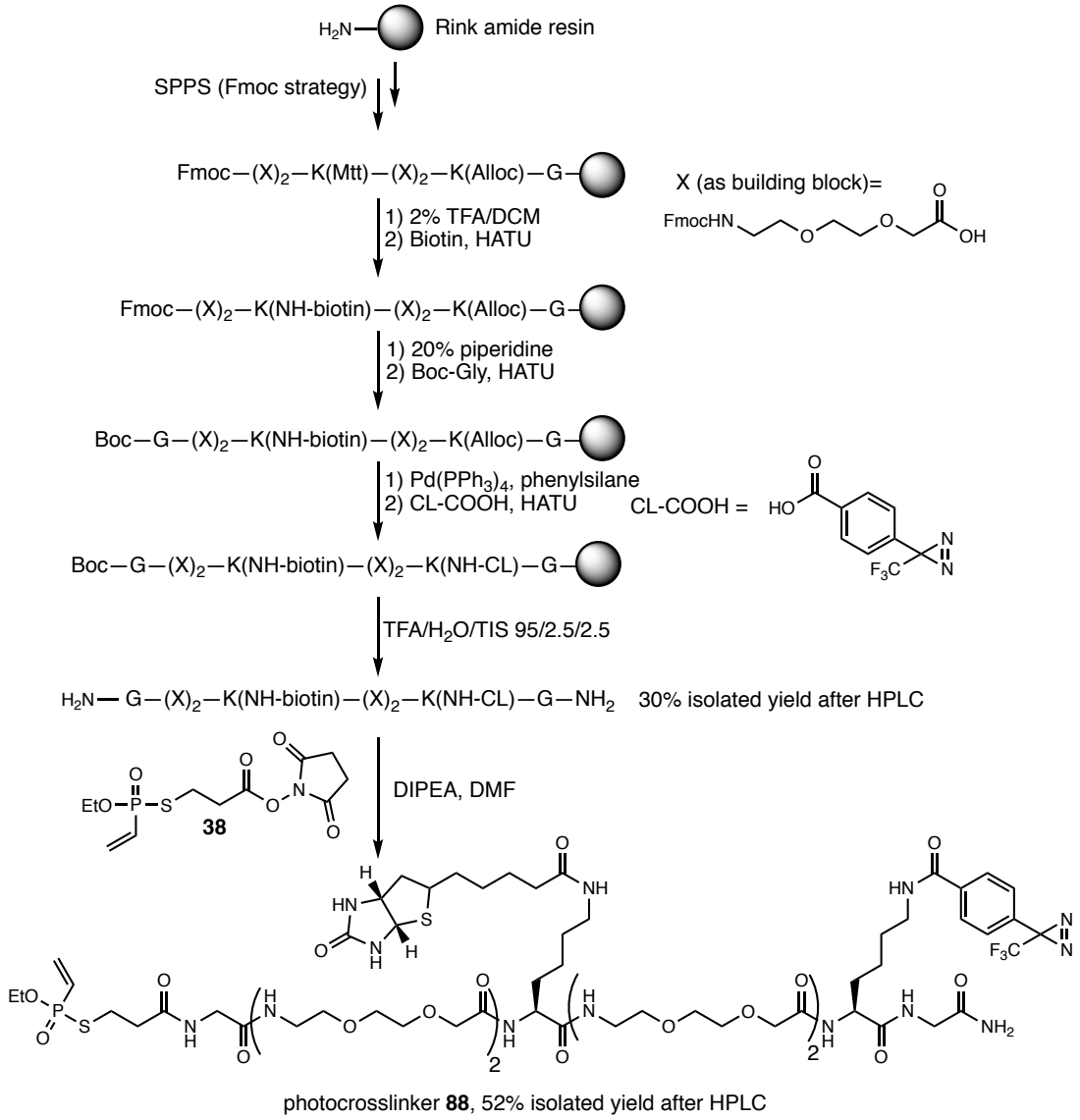

Scheme 65 Synthesis of photocrosslinker **88**. CL= photocrosslinker.

Photocrosslinker **88** was synthesized manually according to scheme 65 in a 50 μmol scale on a Rink amide resin with a loading of 0.47 mmol/g. Generally, the resin was washed with DMF, DCM and DMF again after amino acid couplings and Fmoc-deprotections. The amino acids G, K(Alloc) and K(Mtt) were coupled with single couplings (5 eq. amino acid for 1 h) with Oxyma and HCTU (5 eq. each) and DIPEA (10 eq.) in

DMF. The amino acid X (TCI, Fmoc-NH-PEG_2-CH_2COOH) was coupled in a single coupling (3 eq. for 1 h) with HATU (3 eq.) and DIPEA (6 eq.). Fmoc-deprotections were performed with piperidine/DMF (20:80; v:v, 3 times for 3 min). The Fmoc-protecting group on the last amino acid X was kept on during lysine modification with biotin. For K(Mtt) deprotection, the resin was first equilibrated in DCM and then treated with TFA/TIS/DCM (2:5:93; v:v:v, 3 times for 5 min). Biotin was then coupled in DMF in a single coupling (5 eq. biotin) with HATU (5 eq.) and DIPEA (10 eq.). Now the Fmoc-protecting group on the last amino acid (X) was removed by treatment with piperidine/DMF (20:80; v:v, 3 times for 3 min) and subsequently, Boc-protected glycine was coupled to the N-terminus (5 eq. Boc-glycine for 1 h) with Oxyma/HCTU (5 eq. each) and DIPEA (10 eq.). For K(Alloc) deprotection, the resin was first equilibrated in DCM and then treated with a solution of phenylsilane (0.025 eq.) and $Pd(PPh_3)_4$ (0.05 eq.) in DCM (2 times for 1 h with fresh solutions). The diazirine carboxylic acid was coupled to the deprotected lysine in a single coupling (3 eq. for 2 h) with HATU (3 eq.) and DIPEA (6 eq.). The final cleavage from resin was achieved by incubation with a mixture of TFA/TIS/H_2O (95:2.5:2.5; v:v:v) for 1.5 hours followed by precipitation in cold diethylether. The crude peptide was purified by semipreparative reverse-phase HPLC (gradient: 5-40% MeCN+0.1% TFA in H_2O+0.1% TFA over 40 min, flow: 16 mL/min) and the intermediate peptide was gained as a white powder (21 mg, 15 μmol, 30%) after lyophilization.
This purified intermediate peptide (10 mg, 7.2 μmol, 1.0 eq.) was dissolved in DMF (250 μL) and mixed with NHS derivative **38** (3.4 mg, 10.8 μmol, 1.5 eq.) and DIPEA (3.8 μL, 21.6 μmol, 3.0 eq.) and the mixture was shaken at r.t. for 15 min. The mixture was then diluted with water (4.5 mL) and the crude product was purified by semipreparative reverse-phase HPLC (gradient: 5-40% MeCN+0.1% TFA in H_2O+0.1% TFA over 40 min, flow-rate: 16 mL/min) to give photocrosslinker **88** (6.1 mg, 3.76 μmol, 52%) as a white powder after lyophilization.
HR-MS (ESI+) for $C_{66}H_{107}F_3N_{15}O_{22}PS_2^{2+}$ [M+2H$^+$]: calcd.: 806.8418; found: 806.8427.

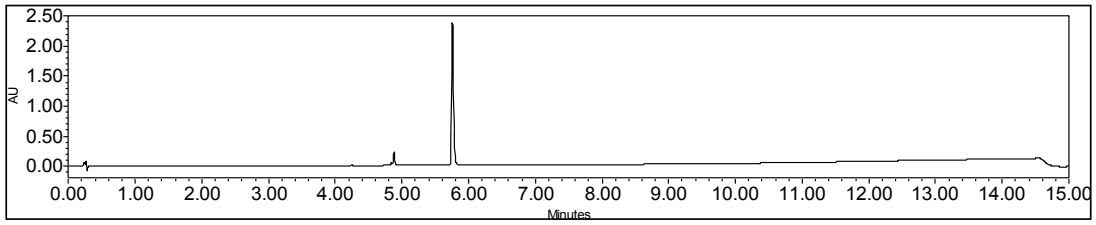

Fig. 102 UPLC-UV analysis (220 nm) of compound **88**.

Photocrosslinker 90 and 91

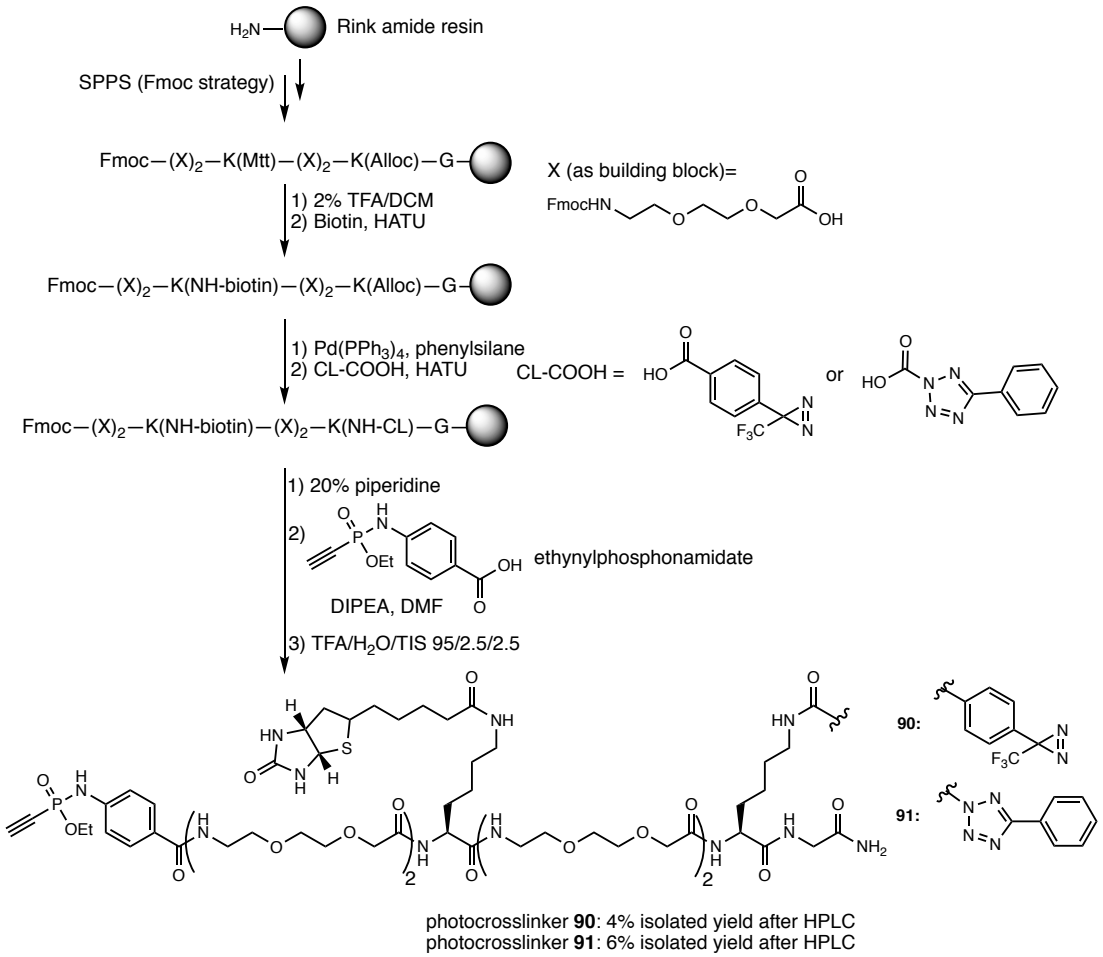

Scheme 66 Synthesis of photocrosslinkers **90** and **91**. CL= photocrosslinker.

Photocrosslinkers **90** and **91** were synthesized manually according to scheme 66 in a 130 μmol scale on a Rink amide resin with a loading of 0.40 mmol/g. Generally, the resin was washed with DMF, DCM and DMF again after amino acid couplings and Fmoc-deprotections. The amino acids G, K(Alloc) and K(Mtt) were coupled with single couplings (5 eq. amino acid for 1 h) with Oxyma and HCTU (5 eq. each) and DIPEA (10 eq.) in DMF. The amino acid X (TCI, Fmoc-NH-PEG_2-CH_2COOH) was coupled in a single coupling (3 eq. for 1 h) with HATU (3 eq.) and DIPEA (6 eq.). Fmoc-deprotections were performed with piperidine/DMF (20:80; v:v, 3 times for 3 min). The Fmoc-protecting group on the last amino acid X was kept on during lysine modification with biotin. For K(Mtt) deprotection, the resin was first equilibrated in DCM and then treated with TFA/TIS/DCM (2:5:93; v:v:v, 3 times for 5 min). Biotin was then coupled in DMF in a single coupling (5 eq. biotin) with HATU (5 eq.) and DIPEA (10 eq.). For K(Alloc) deprotection, the resin was first equilibrated in DCM and then treated with a solution of phenylsilane (0.025 eq.) and $Pd(PPh_3)_4$ (0.05 eq.) in DCM (2 times for 1 h with fresh solutions). The diazirine carboxylic acid (TCI) or tetrazole carboxylic acid (ethyl 2-phenyl-2H-tetrazole-5-carboxylate, see procedure above) was coupled to the deprotected lysine in a single coupling (3 eq. each for 2 h) with HATU (3 eq.) and DIPEA (6 eq.). Then, the N-terminal

Fmoc-protecting group was removed by treatment with piperidine/DMF (20:80; v:v, 3 times for 3 min) and subsequently, the ethynylphosphonamidate building block[13] (see scheme 66 for structure) was coupled on resin (1.5 eq. for 1 h) with HATU (1.5 eq.) and DIPEA (3.0 eq.). The final cleavage from resin was achieved by incubation with a mixture of TFA/TIS/H_2O (95:2.5:2.5; v:v:v) for 1 hour followed by precipitation in cold diethylether. The crude peptides were purified by semipreparative reverse-phase HPLC (gradient: 10-50% MeCN+0.1% TFA in H_2O+0.1% TFA over 30 min, flow: 16 mL/min) and the photocrosslinkers **90** (3.7 mg, 2.3 μmol, 4%) and **91** (6.0 mg, 3.9 μmol, 6%) were gained as white powders after lyophilization.

Photorosslinker **90**: LR-MS (ESI+) for $C_{68}H_{103}F_3N_{15}O_{21}PS^{2+}$ [M+2H$^+$] calcd.: 792.84; found: 793.04.

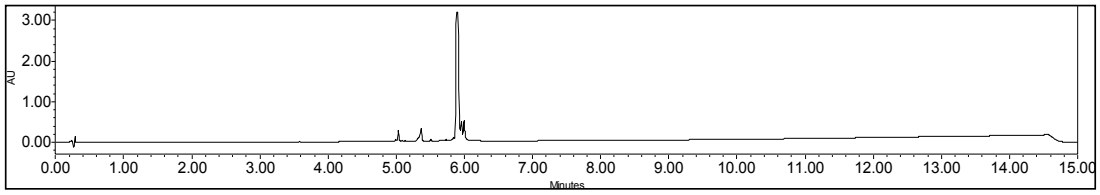

Fig. 103 UPLC-UV analysis (220 nm) of compound **90**.

Photorosslinker **91**: LR-MS (ESI+) for $C_{67}H_{104}N_{17}O_{21}PS^{2+}$ [M+2H$^+$] calcd.: 772.85; found: 773.08.

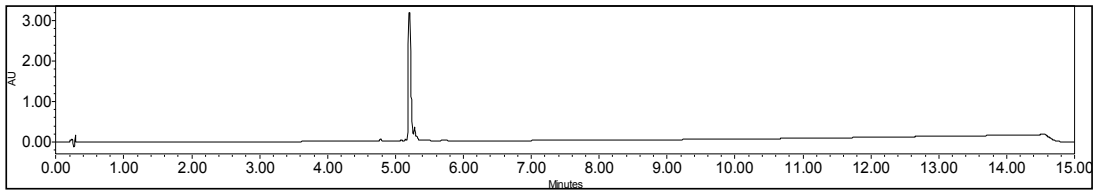

Fig. 104 UPLC-UV analysis (220 nm) of compound **91**.

[13] *The ethynylphosphonamidate building block was kindly provided by Dr. Marc-André Kasper, who synthesized it as described in Ref. [208].*

8.5.2 Conjugation of anti-chaperone antibodies with photocrosslinkers

Proteins and antibodies

The proteins HSP-1, DNJ-12 and DNJ-13 were expressed and purified by the Kirstein group. Polyclonal anti-HSP-1 and anti-DNJ-12 antibodies, provided by the Kirstein group, were generated by immunizing rabbits with purified chaperone proteins (Charles River, Germany) [286]. The immunized sera were tested against purified chaperone proteins and against wild-type *C. elegans* lysates. Anti-HSP-1 and anti-HSP-12 antibodies were purified by Manuel Iburg using immobilized target proteins on Sulflolink resin (Thermo Fisher Scientific, Waltham, USA). Briefly, 2 mL of the serum containing the antibodies (anti-HSP-1 or anti-DNJ-12) were added onto the column with the immobilized target proteins (HSP-1 or DNJ-12, respectively) and incubated over night at 4 °C. The next day, the resin was washed with washing buffer (20 mM Tris-HCl, 500 mM NaCl, 0.2% Triton X-100, pH=8.0), before eluting bound antibodies with elution buffer (150 mM glycine-HCl, 100 mM NaCl, pH= 2.5). Fractions were immediately neutralized by adding 50 μL of Tris-HCl pH=9.0 and samples were taken for analysis by SDS-PAGE. Before conjugations to photocrosslinkers, the purified antibodies were rebuffered to the desired conjugation buffer via spin filtration. Concentrations were determined with a BCA assay using BSA at defined concentrations as a standard.

Conjugation of anti-HSP-1 antibody with photocrosslinker 88

To the polyclonal anti-HSP-1 antibody (1 μM in 50 mM borate PBS pH 8.0, 50 μL) was added DTT (10 mM in BPBS buffer, 5 μL, final concentration in mixture: 1 mM) and the mixture was shaken at 37 °C and 800 rpm for 30 min. Removal of DTT and rebuffering to conjugation buffer (50 mM NH_4HCO_3, 100 mM NaCl, 1 mM EDTA) was achieved by means of gel filtration (Zeba spin column). Quickly afterwards, photocrosslinker **88** (2 mM in DMSO, 1.25 μL, final concentration in mixture: approx. 50 μM) was added and the mixture was shaken at 800 rpm for 16 hours at 14 °C. Removal of excess photocrosslinker and rebuffering to PBS pH 7.4 was achieved via spin-filtration and the antibody solution was concentrated to 1 μM. From this solution, 15 μL were mixed with 5 μL Laemmli buffer containing β-mercaptoethanol (4 times concentrated), heated at 95 °C for 15 min and run on a SDS-gel (12% SDS). For subsequent Western-blot analysis, the commercially available Streptavidin-POD conjugate (Roche Diagnostics GmbH) was used for hybridisation and indirect detection via chemiluminescence.

In order to test whether HSP-1-crosslinker conjugate **89** retained the ability to bind its target protein HSP-1, recombinant HSP-1 protein was blotted on a cellulose membrane and incubated with the anti-HSP-1-photocrosslinker conjugate **88** or unmodified anti-HSP-1 antibody as a control. Antibodies bound to target protein HSP-1 were subsequently detected with an anti-rabbit antibody-HRP as well as with streptavidin-HRP (Fig. 105).

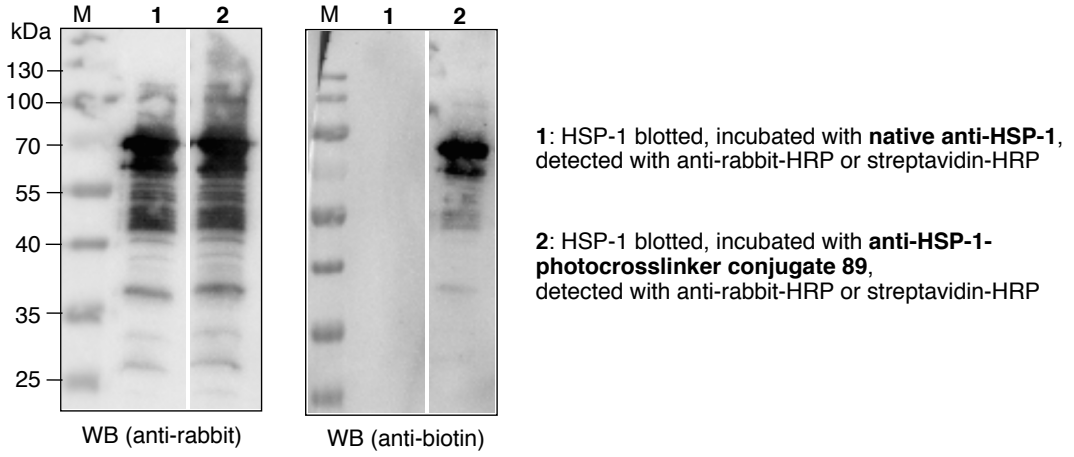

Fig. 105 Western-blots showing that anti-HSP-1-photocrosslinker conjugate **89** recognizes its target protein HSP-1. The intense band at ca. 70 kDa corresponds to anti-HSP-1 antibody bound to blotted HSP-1 protein.

Conjugation of anti-DNJ-12 antibody with photocrosslinker 90 and 91

To the polyclonal anti-DNJ-12 antibody (2 μM in 50 mM borate PBS pH 8.0, 300 μL) was added DTT (250 mM in BPBS buffer, 2.4 μL, final concentration in mixture: 2 mM) and the mixture was shaken at 37 °C and 800 rpm for 30 min. Removal of DTT and rebuffering to conjugation buffer (50 mM NH_4HCO_3, 100 mM NaCl, 1 mM EDTA) was achieved by means of gel filtration (Zeba spin column). Quickly afterwards, photocrosslinker **90** or **91** (5 mM in DMSO, 6 μL, final concentration in mixture: approx. 100 μM) was added and the mixture was shaken at 800 rpm for 16 hours at 14 °C. Removal of excess photocrosslinker and rebuffering to PBS pH 7.4 was achieved via spin-filtration and the antibody solution was concentrated to 5 μM. From this solution, 10 μL were mixed with 10 μL Laemmli buffer containing β-mercaptoethanol (2 times concentrated), heated at 95 °C for 15 min and run on a SDS-gel (12% SDS). For subsequent Western-blot analysis, the commercially available Streptavidin-POD conjugate (Roche Diagnostics GmbH) was used for hybridisation and indirect detection via chemiluminescence.

8.5.3 Photocrosslinking

Anti-DNJ-12-conjugates 92 and 93 and DNJ-12

Anti-DNJ-12-antibody-photocrosslinker conjugates **92** and **93** (5 μM in PBS pH 7.4, 40 μL) were each mixed with recombinant DNJ-12 protein (5 μM in PBS pH 7.4, 40 μL). For control reactions without DNJ-12, the conjugates **92** and **93** (40 μL) were diluted with 40 μL PBS pH 7.4 buffer instead. From these solutions, 40 μL were directly mixed with 14 μL β-mercaptoethanol containing Laemmli buffer (4 times concentrated) and heated at 95 °C for 15 min (non-irradiated control samples). The remaining volumes were shaken at 800 rpm at r.t. for 1 hour in the dark and then irradiated with UV-light (at 365 nm for conjugate **92** (diazirine) and at 302 nm for conjugate **93** (tetrazole)) for 15 min on ice. Afterwards, 14 μL of β-mercaptoethanol containing Laemmli buffer (4 times concentrated) was added and the samples were heated at 95 °C for 15 min and

subjected to SDS-PAGE (4-12.5% gradient gels), followed by Western-blot analysis using the commercially available Streptavidin-POD conjugate (Roche Diagnostics GmbH) for hybridisation and indirect detection via chemiluminescence. For additional control reactions (see Fig. 50C/D), the same procedure was followed using native anti-DNJ-12 antibody alternatively and two SDS-gels were run. One was used for Western-blot against biotin as described above and the other one was used for silver-stain (see general information for details).

Anti-HSP-1-conjugate 89 and HSP-1

Anti-HSP-1-antibody-photocrosslinker conjugate **89** (1 μM in PBS pH 7.4, 20 μL) was mixed with recombinant HSP-1 protein (1 μM in PBS pH 7.4, 20 μL). For control reactions without **89** or HSP-1 protein, the respective volume was replaced with buffer. From these mixtures, 5 μL were directly mixed with 5 μL β-mercaptoethanol containing Laemmli buffer (2 times concentrated) and heated at 95 °C for 15 min (non-irradiated control samples). The remaining volumes were shaken at 800 rpm at r.t. for 1 hour in the dark and then irradiated with UV-light at 365 nm for 30 min on ice. Samples of 5 μL were drawn after 5, 15 and 30 min, diluted with β-mercaptoethanol containing Laemmli buffer (2 times concentrated), heated at 95 °C for 15 min and subjected to SDS-PAGE (4-12.5% gradient gels, two identical SDS-gels were run) and subsequent Western-blot analysis. For one blot, the commercially available Streptavidin-POD conjugate (Roche Diagnostics GmbH) was used for hybridisation and indirect detection via chemiluminescence. For the other blot, first native rabbit anti HSP-1 antibody was used for hybridisation followed by detection with anti-rabbit-HRP (chemiluminescence).

Anti-HSP-1-conjugate 89 and HSP-1 + DNJ-13

Recombinant HSP-1 protein (final concentration: 1 μM), recombinant DNJ-13 protein (final concentration: 0.5 μM) and heat-denaturated recombinant luciferase (final concentration: 0.5 μM) were preincubated at r.t. for 1 hour, before anti-HSP-1-antibody-photocrosslinker conjugate **89** was added (final concentration: 0.5 μM) to give a final volume of 20 μL in PBS pH 7.4. This mixture was shaken at r.t. in the dark for 1 hour. 5 μL of this mixture were directly mixed with 5 μL β-mercaptoethanol containing Laemmli buffer (2 times concentrated) and heated at 95 °C for 15 min (non-irradiated control sample). The remaining volume was irradiated with UV-light at 365 nm for 30 min on ice. After 30 min, 5 μL of this mixture was diluted with β-mercaptoethanol containing Laemmli buffer (2 times concentrated) and heated at 95 °C for 15 min. The remaining volume was mixed with magnetic beads loaded with protein A/G (PierceTM Protein A/G magnetic beads Thermo Fisher Scientific, washed three times with TBST, one time with PBS). After incubation for 90 min, the beads were washed with TBST three times and samples were eluted by boiling in 2x SDS sample buffer. Separation of magnetic beads from liquid phase was carried out using a magnetic reaction vessel rack (GE Healthcare). Flow-through (wash fractions) and elution samples were mixed with Laemmli buffer, heated at 95 °C for 15 min and subjected to SDS-PAGE (4-12.5% gradient gel). For subsequent Western-blot analysis, native anti-DNJ-13 antibody was used for hybridisation and an anti-rabbit-HRP conjugate for indirect detection via chemiluminescence (see general information in chapter 8.1 for details).

8.6 Experimental part for DUB photocrosslinking chapter

8.6.1 Conjugation of DUBs to photocrosslinkers

In 0.5 mL Eppendorf tubes, USP2CD (R&D Systems, catalogue number E-504, 50 μM, 5 μL) or UCHL3 (R&D Systems, catalogue number E-325, 80 μM, 3.125 μL) plus 1.875 μL conjugation buffer (50 mM NH_4HCO_3 pH 8.5) were mixed with either compound **54** or **55** (1.25 mM in conjugation buffer containing 2.5% DMSO, 5 μL) resulting in DUB concentrations of 25 μM and crosslinker concentrations of 625 μM (= 25 eq.). The mixtures were shaken at 14 °C and 800 rpm for 16 hours. Removal of excess free crosslinker and rebuffering to PBS was then performed by gel filtration (Zeba Spin, with PBS). For MS/MS analysis, 2 μL of the mixtures after gel filtration were diluted with 10 μL Laemmli buffer containing β-mercaptoethanol, boiled at 95 °C for 5 min and subjected to SDS-PAGE (15% SDS). For tryptic digest and LC-MS/MS procedure, see general information in chapter 8.1.

8.6.2 MS/MS analysis of DUB-photocrosslinker conjugates

For peptide identification, the RAW-files were loaded into Proteome Discoverer (v.2.4, Thermo Scientific) and a database search was performed with MSAmanda 2.0 [312]. Files were searched against a database containing the sequences of the two DUBs using the following search parameters: peptide mass tolerance of ±8 ppm, fragment mass tolerance of ±20 ppm, a maximum of two missed cleavages, minimum peptide length of 5 and a minimum MSAmanda score of 150. Diazirine derivative **54** (407.068 Da) and tetrazole derivative **55** (370.098 Da) (both indicated with **A**) were considered as dynamic modifications to occur on cysteine. Moreover, cysteine carbamidomethylation (57.021 Da) (indicated with **C**) and methionine oxidation (15.995 Da) (indicated with **O**) were considered as dynamic modifications. Spectra that identified a peptide carrying **54** or **55** as modification were validated manually.

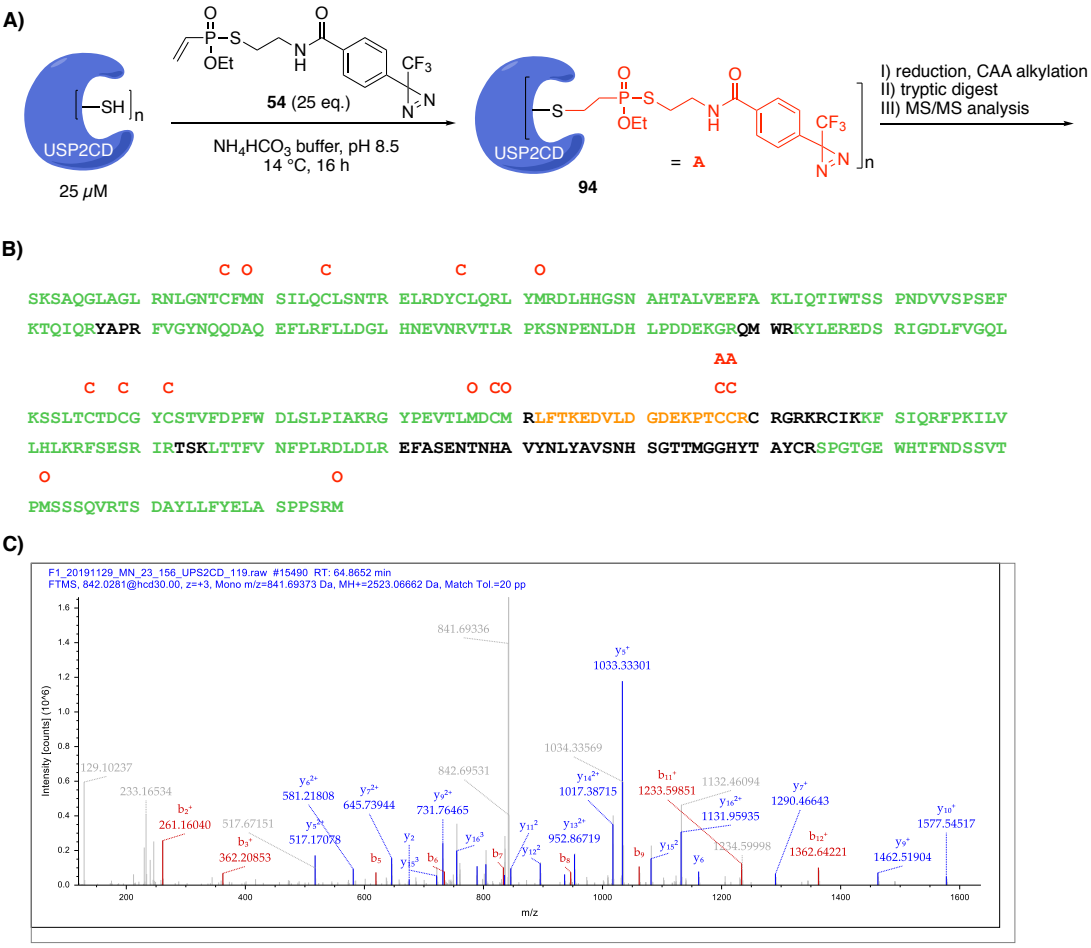

Fig. 106 A) Conjugation of USP2CD with photocrosslinker **54**. B) Amino acid sequence of USP2CD. MS sequence coverage is highlighted in green (84%). MS/MS recorded peptide is highlighted in orange. A= cysteine modified with crosslinker **54**, C= cysteine carbamidomethylation, O= methionine oxidation. C) Peptide spectrum match of the modified peptide LFTKEDVLDGDEKPTC(A/C)C(A/C)R (HCD spectrum). Both modifications A and C were found at these cysteines.

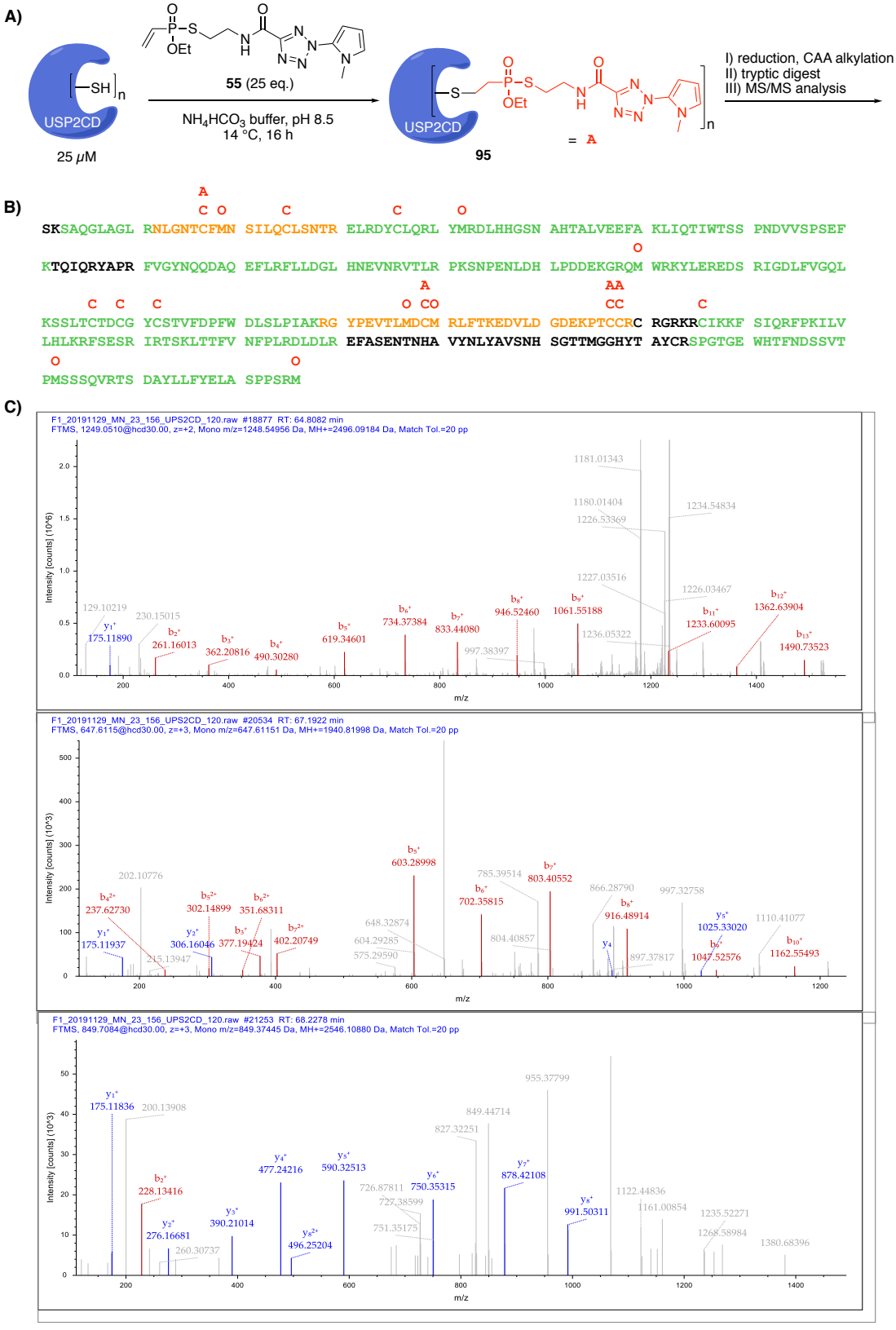

Fig. 107 A) Conjugation of USP2CD with photocrosslinker **55**. B) Amino acid sequence of USP2CD. MS sequence coverage is highlighted in green (85%). MS/MS recorded peptides are highlighted in orange. A= cysteine modified with crosslinker **55**, C= cysteine carbamidomethylation, O= methionine oxidation. C) Peptide spectra matches of the modified peptides, from top to bottom: LFTKEDVLDGDEKPTC(A/C)C(A/C)R; RGYPEVTLM(O)DC(A/C)M(O)R; NLGNTC(A/C)FM(O)NSILQC(C)LSNTR.

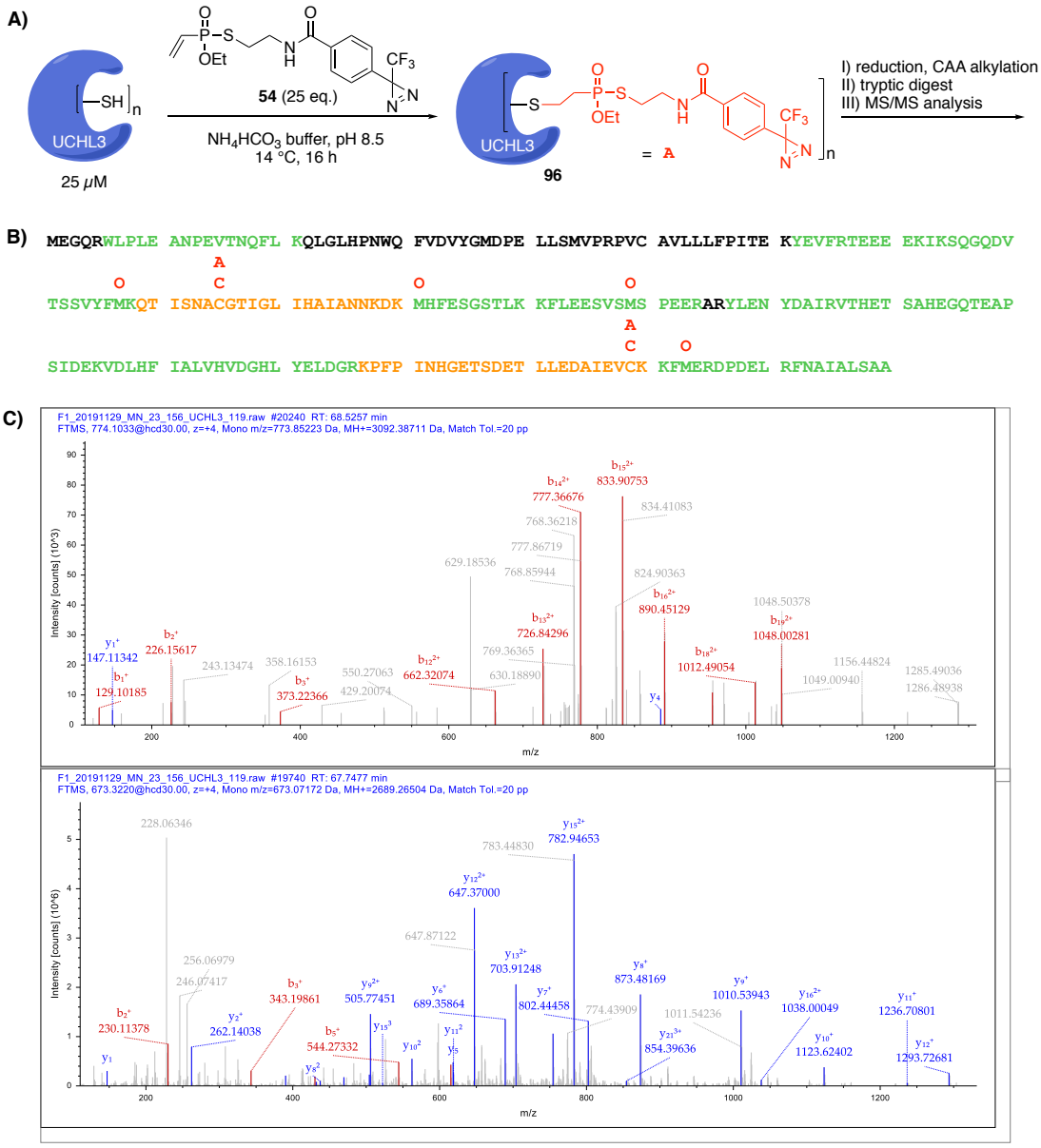

Fig. 108 A) Conjugation of UCHL3 with photocrosslinker **54**. B) Amino acid sequence of UCHL3. MS sequence coverage is highlighted in green (80%). MS/MS recorded peptides are highlighted in orange. A= cysteine modified with crosslinker **54**, C= cysteine carbamidomethylation, O= methionine oxidation. C) Peptide spectra matches of the modified peptides, from top to bottom: KPFPINHGETSDETLLEDAIEVC(C/A)K; QTISNAC(C/A)GTIGLIHAIANNKDK

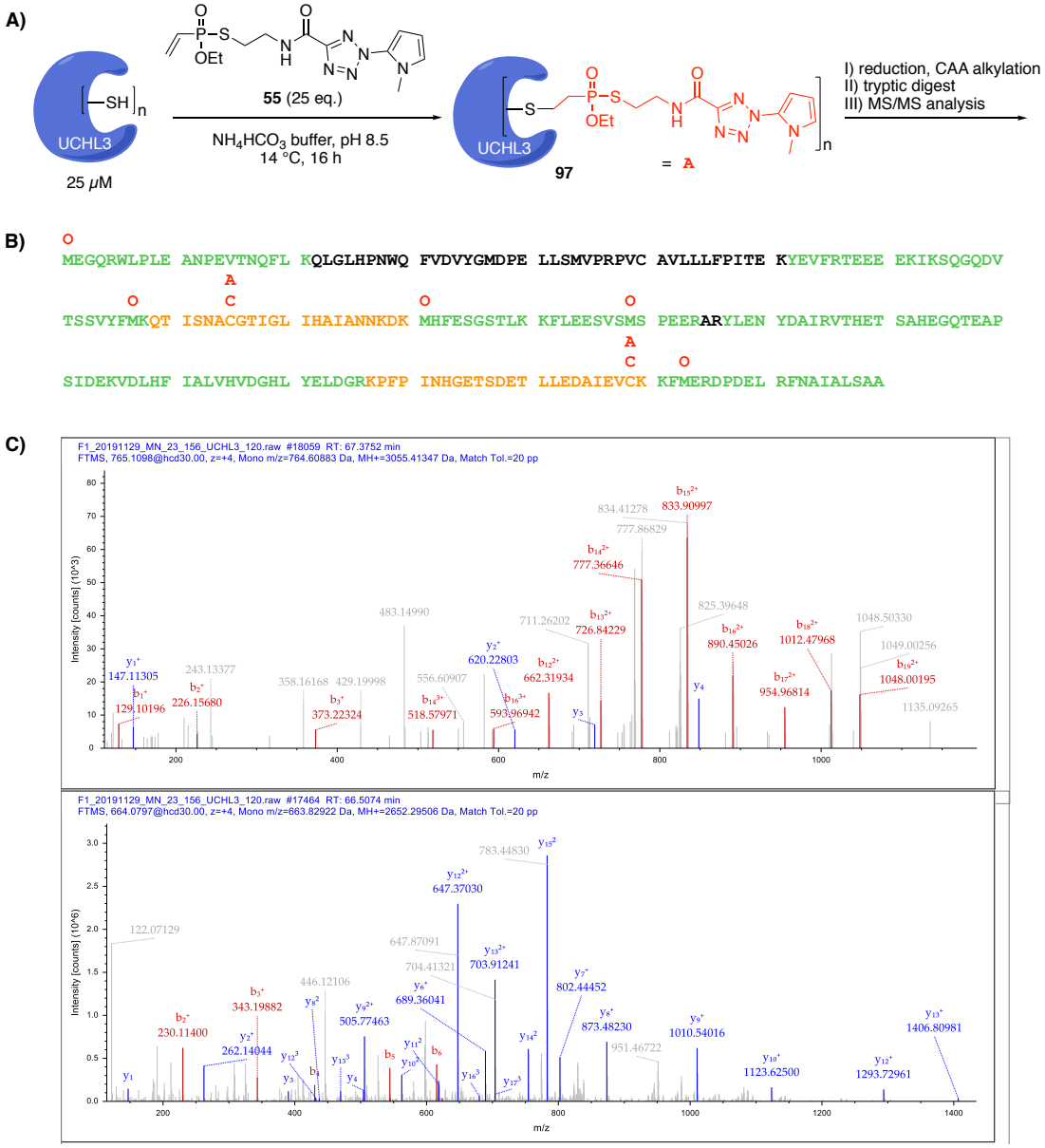

Fig. 109 A) Conjugation of UCHL3 with photocrosslinker **55**. B) Amino acid sequence of UCHL3. MS sequence coverage is highlighted in green (82%). MS/MS recorded peptides are highlighted in orange. A= cysteine modified with crosslinker **55**, C= cysteine carbamidomethylation, O= methionine oxidation. C) Peptide spectra matches of the modified peptides, from top to bottom: KPFPINHGETSDETLLEDAIEVC(C/A)K; QTISNAC(C/A)GTIGLIHAIANNKDK

8.6.3 Photocrosslinking

DUB-conjugates 94-97 and mono-ubiquitin

In lids of Eppendorf tubes, DUB-photocrosslinker conjugates **94-97** (25 μM in PBS pH 7.4, 2 μL) were mixed with wild-type ubiquitin (Ub wt) (100 μM in PBS pH 7.4, 2 μL) and GFP (50 μM in PBS pH 7.4, 4 μL) resulting in the following final concentrations: DUB-photocrosslinker conjugates: 6.25 μM; Ub wt: 25 μM; GFP: 25 μM. For control samples without ubiquitin or GFP, the respective volume was replaced with PBS pH 7.4. Without additional incubation time, the mixtures were directly irradiated with UV-light for 10 min at r.t at either 365 nm (diazirine conjugates **94** and **96**) or 302 nm (tetrazole conjugates **95** and **97**) in a distance of approximately 2 cm to the UV-lamp (see general procedure in chapter 8.1 for details). The samples were then diluted with 4 μL Laemmli buffer containing β-mercaptoethanol, boiled for 5 min at 95 °C and subjected to SDS-PAGE (15% SDS gels).

DUB-conjugates 94-97 and diubiquitins

In lids of Eppendorf tubes, DUB-photocrosslinker conjugates **94-97** (25 μM in PBS pH 7.4, 1 μL) were mixed with diubiquitins (DiUb(K63): Enzo, 1 mg/mL, ca. 55 μM, 1 μL or DiUb(K48): Enzo, 4.2 mg/mL, ca. 240 μM, 0.25 μL) and 6 μL PBS pH 7.4 resulting in the following final concentrations: DUB-photocrosslinker conjugates: ca. 3 μM; DiUbs: ca. 6-7 μM. Without additional incubation time, the mixtures were directly irradiated with UV-light for 10 min at r.t at either 365 nm (diazirine conjugates **94** and **96**) or 302 nm (tetrazole conjugates **95** and **97**) in a distance of approximately 2 cm to the UV-lamp (see general procedure in chapter 8.1 for details). The samples were then diluted with 4 μL Laemmli buffer containing β-mercaptoethanol, boiled for 5 min at 95 °C and subjected to SDS-PAGE (15% SDS gels).

9 Appendix

9.1 NMR spectra

Ethyl 2-(1-methyl-1H-pyrrol-2-yl)-2H-tetrazole-5-carboxylate

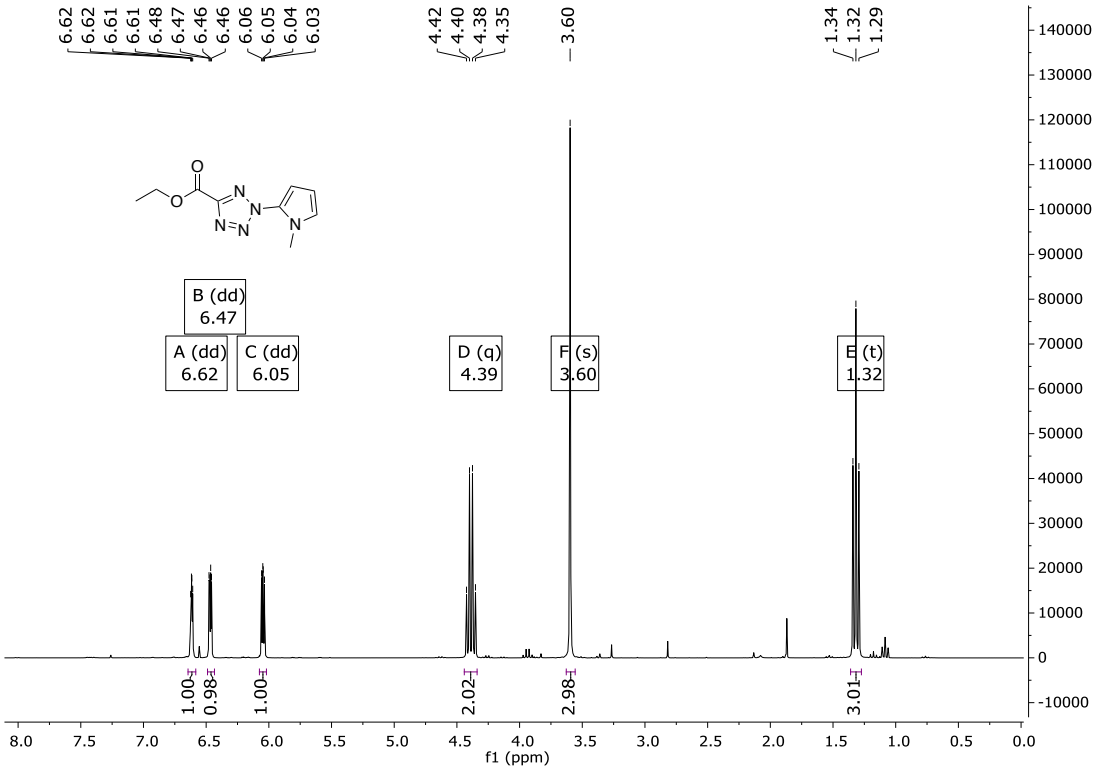

Fig. 110 ^{1}H-NMR spectrum of ethyl 2-(1-methyl-1H-pyrrol-2-yl)-2H-tetrazole-5-carboxylate in $CDCl_3$ (300 MHz).

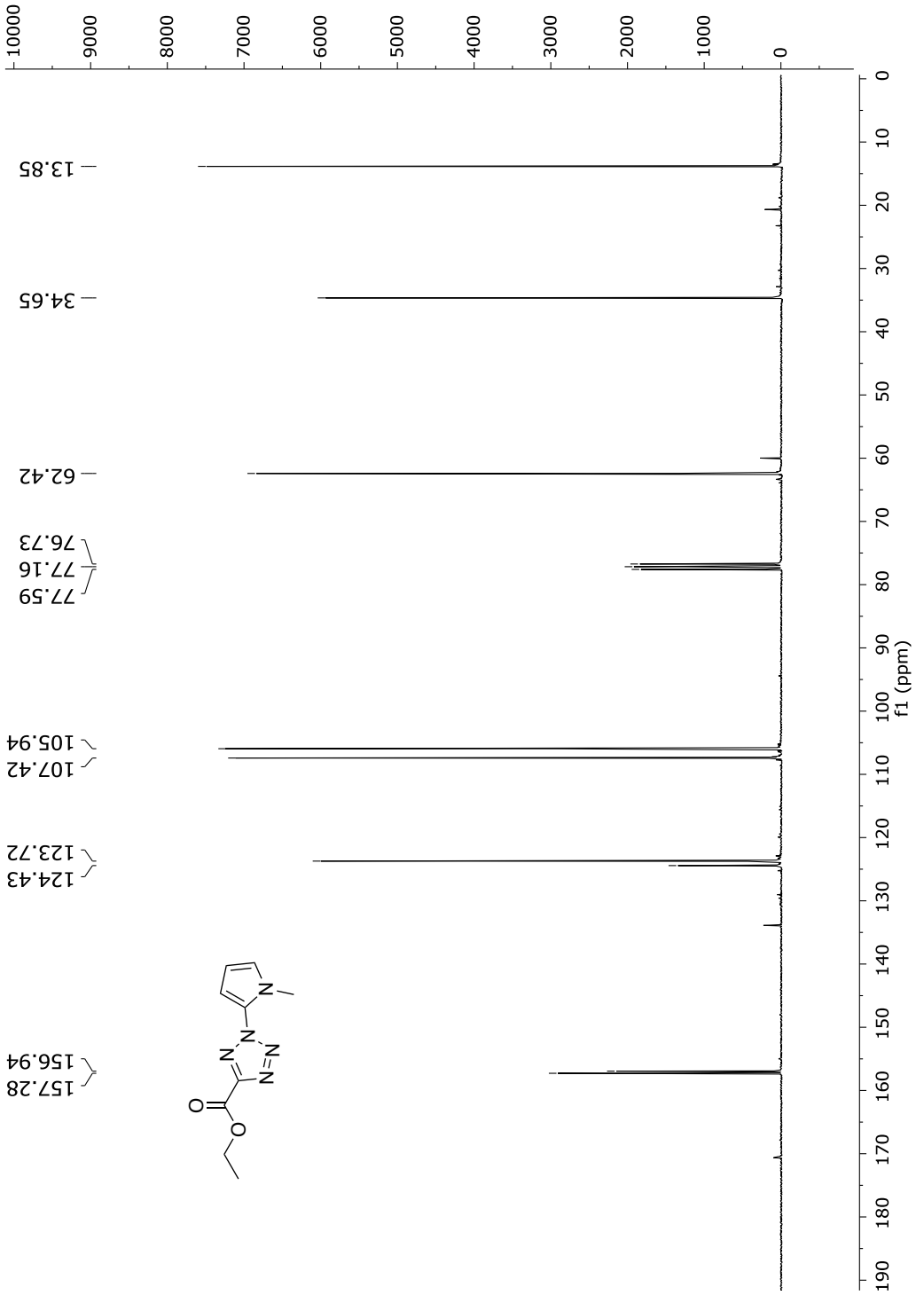

Fig. 111 ^{13}C-NMR spectrum of ethyl 2-(1-methyl-1H-pyrrol-2-yl)-2H-tetrazole-5-carboxylate in $CDCl_3$ (75 MHz).

Ethyl 2-phenyl-2H-tetrazole-5-carboxylate

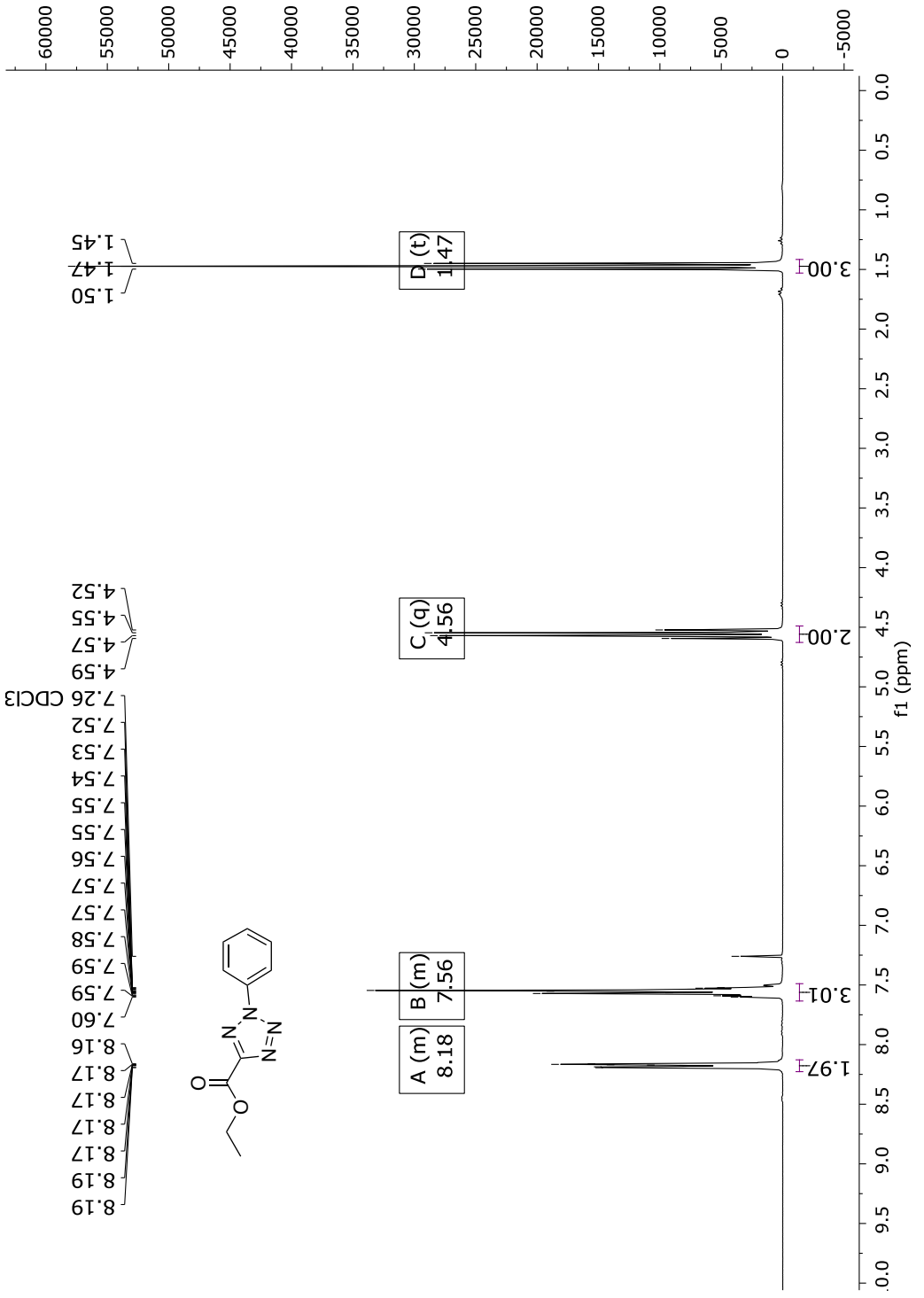

Fig. 112 ^{1}H-NMR spectrum of ethyl 2-phenyl-2H-tetrazole-5-carboxylate in $CDCl_3$ (300 MHz).

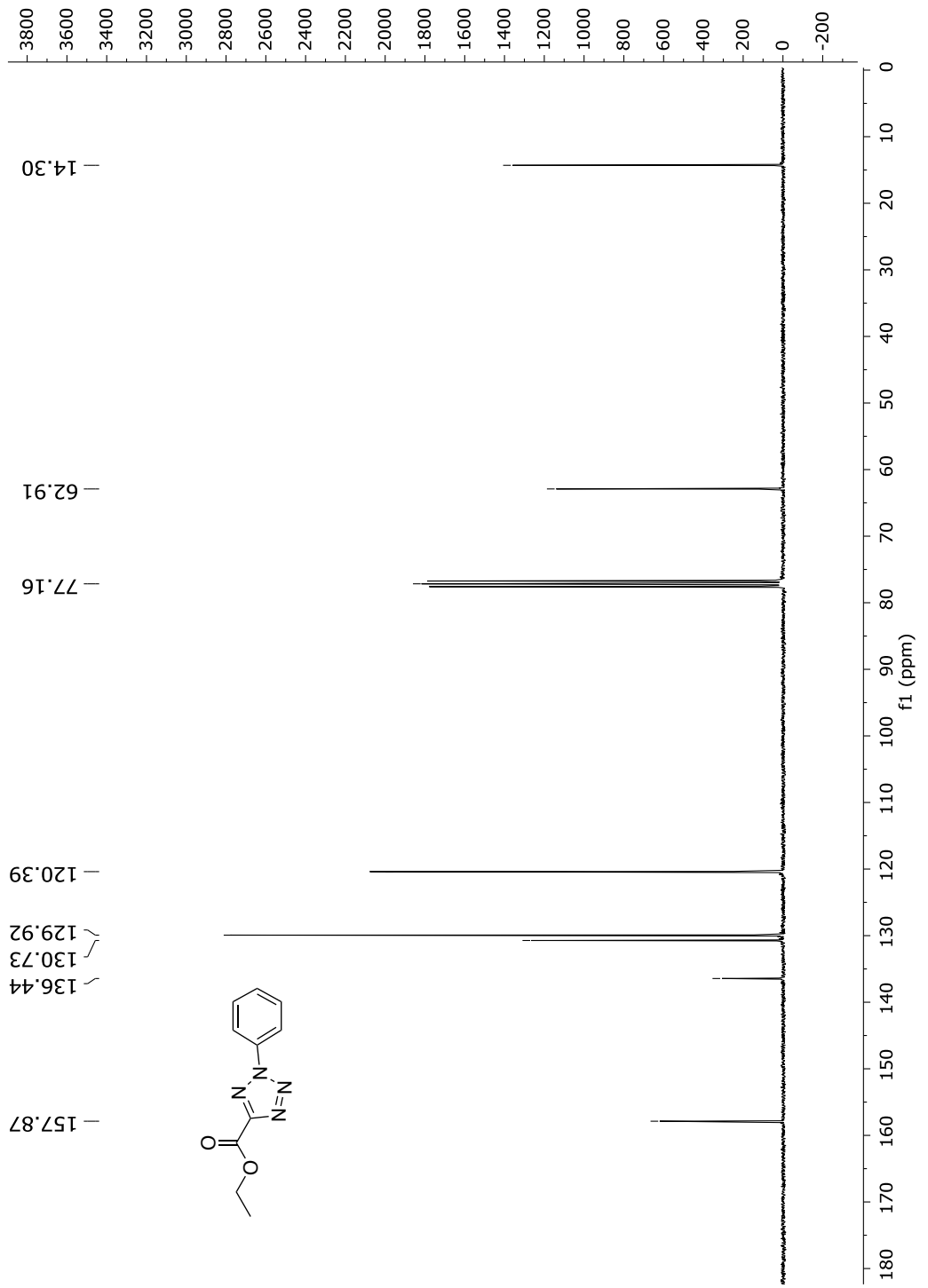

Fig. 113 ^{13}C-NMR spectrum of ethyl 2-phenyl-2H-tetrazole-5-carboxylate in $CDCl_3$ (75 MHz).

2-Phenyl-2H-tetrazole-5-carboxylic acid

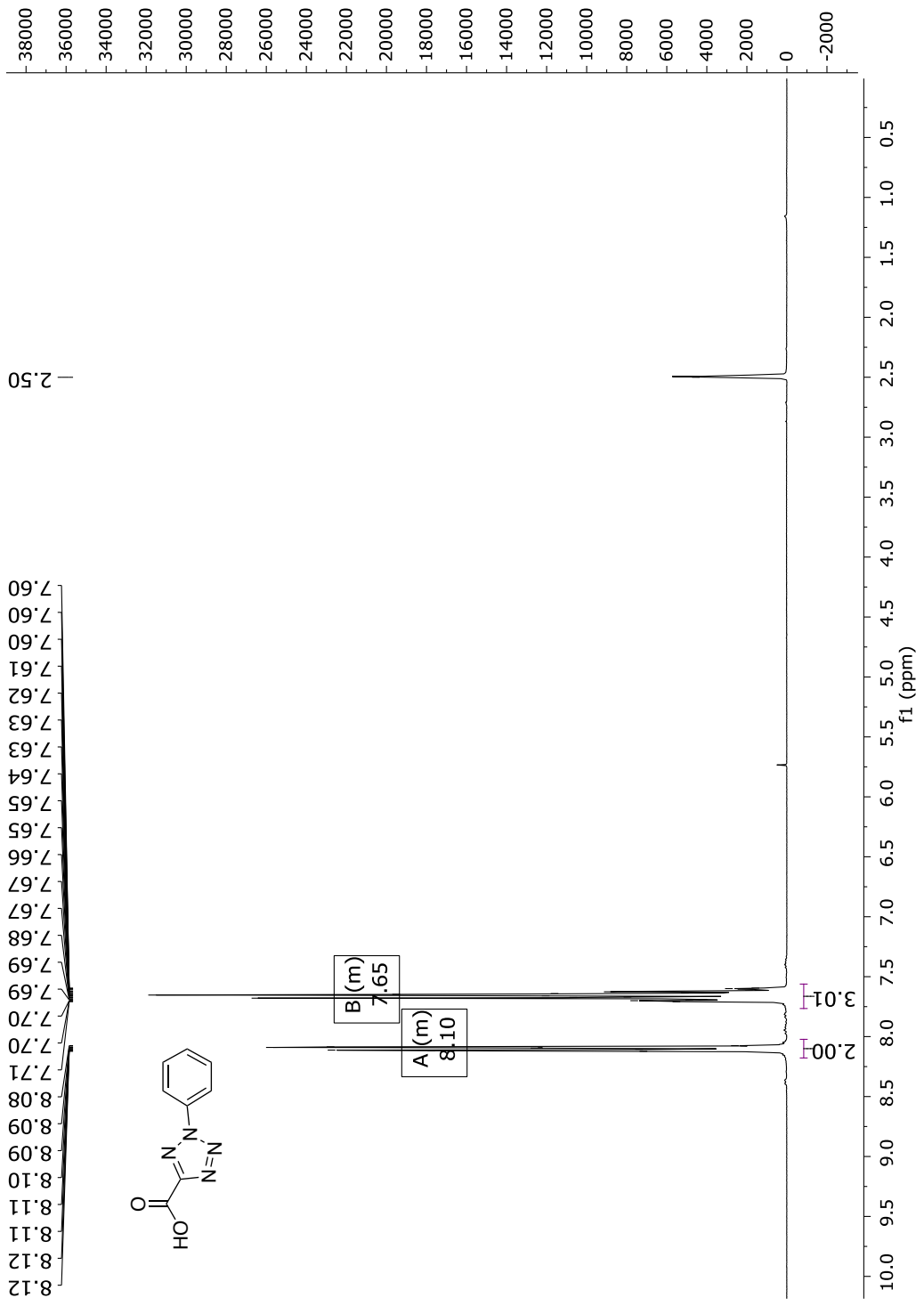

Fig. 114 ^{1}H-NMR spectrum of 2-Phenyl-2H-tetrazole-5-carboxylic acid in DMSO−d_6 (300 MHz).

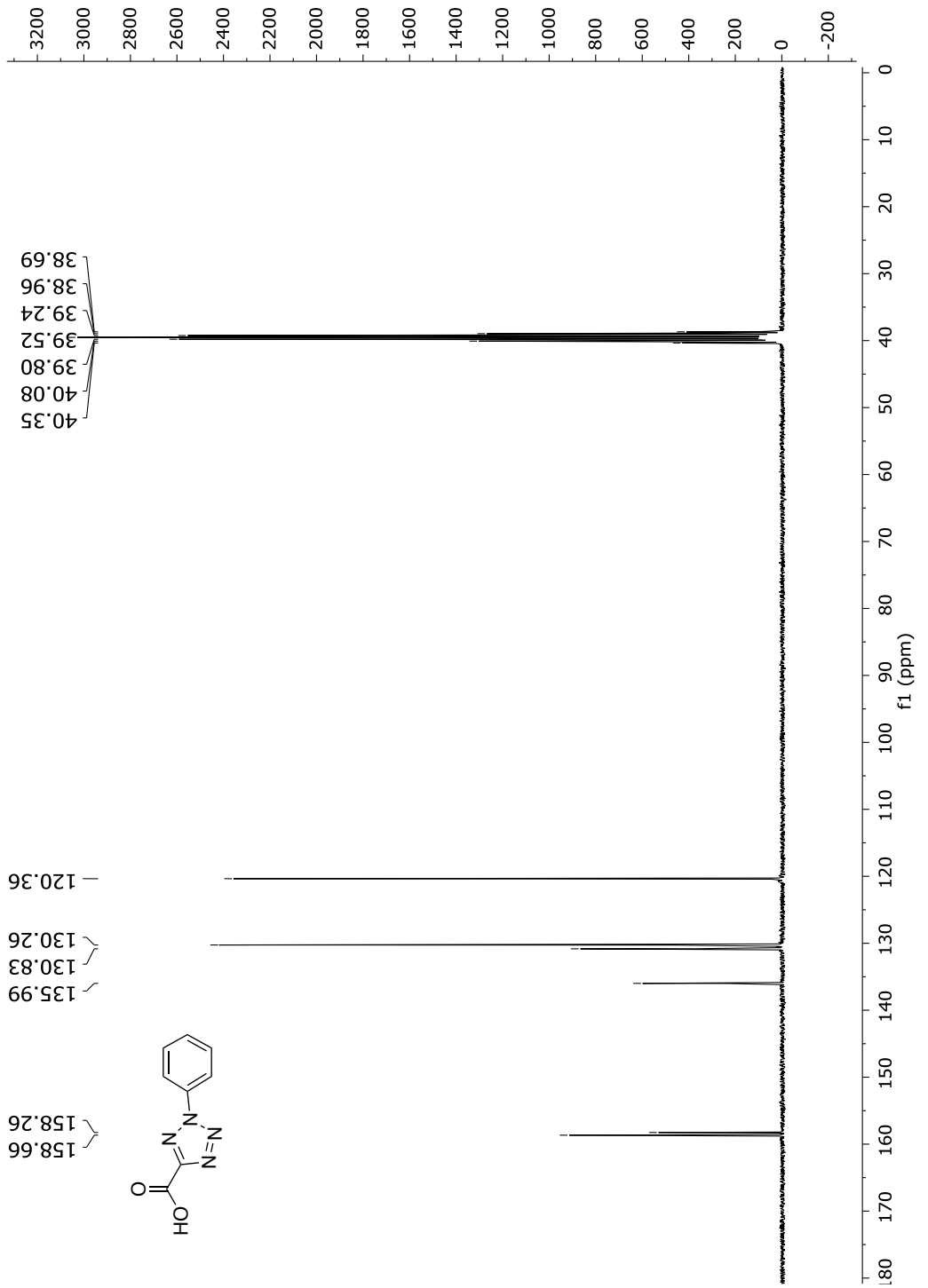

Fig. 115 ^{13}C-NMR spectrum of 2-Phenyl-2H-tetrazole-5-carboxylic acid in DMSO−d_6 (75 MHz).

5-(ethyldisulfaneyl)-2-nitrobenzoic acid (1)

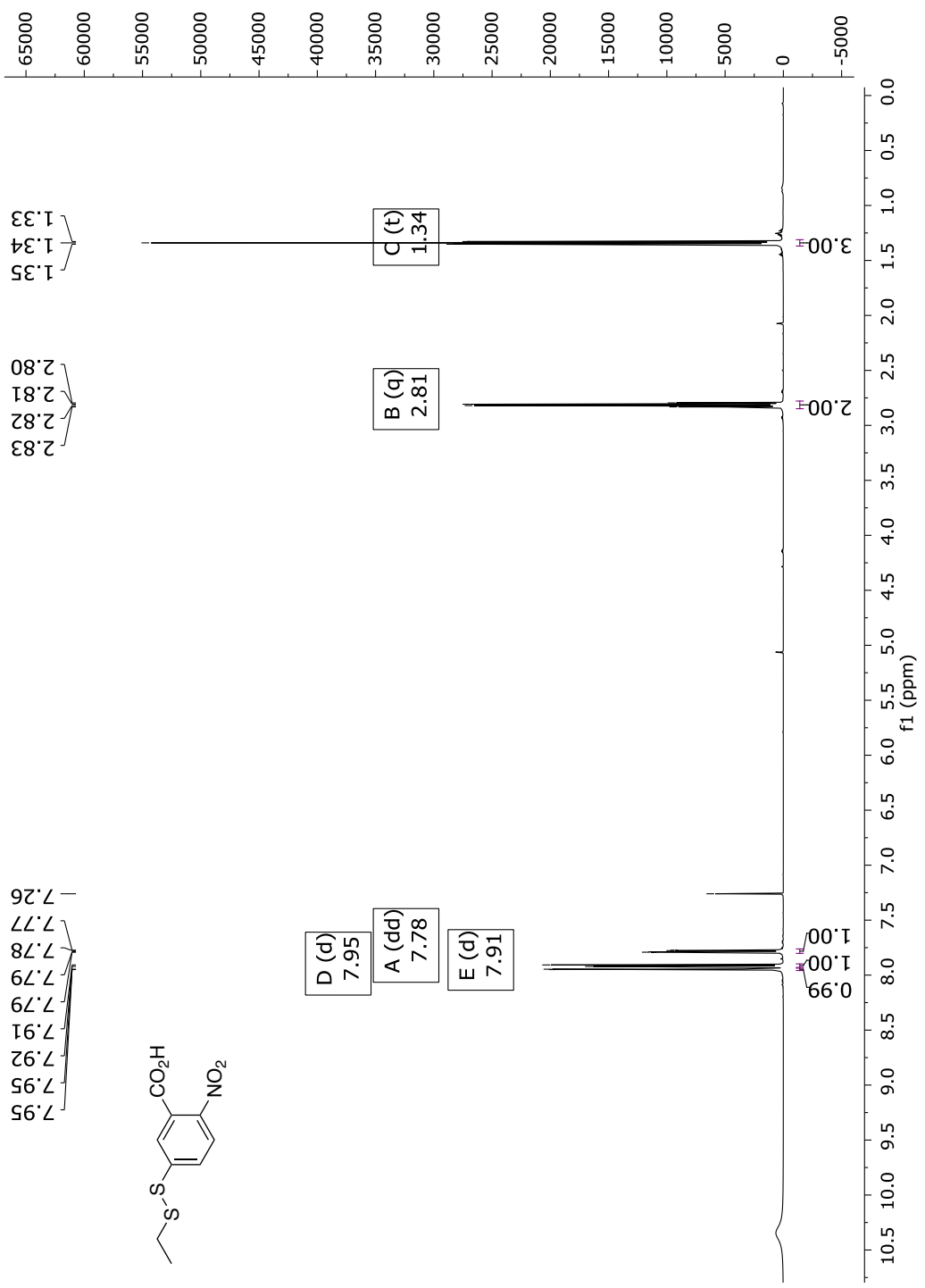

Fig. 116 ^{1}H-NMR spectrum of compound **1** in $CDCl_3$ (600 MHz).

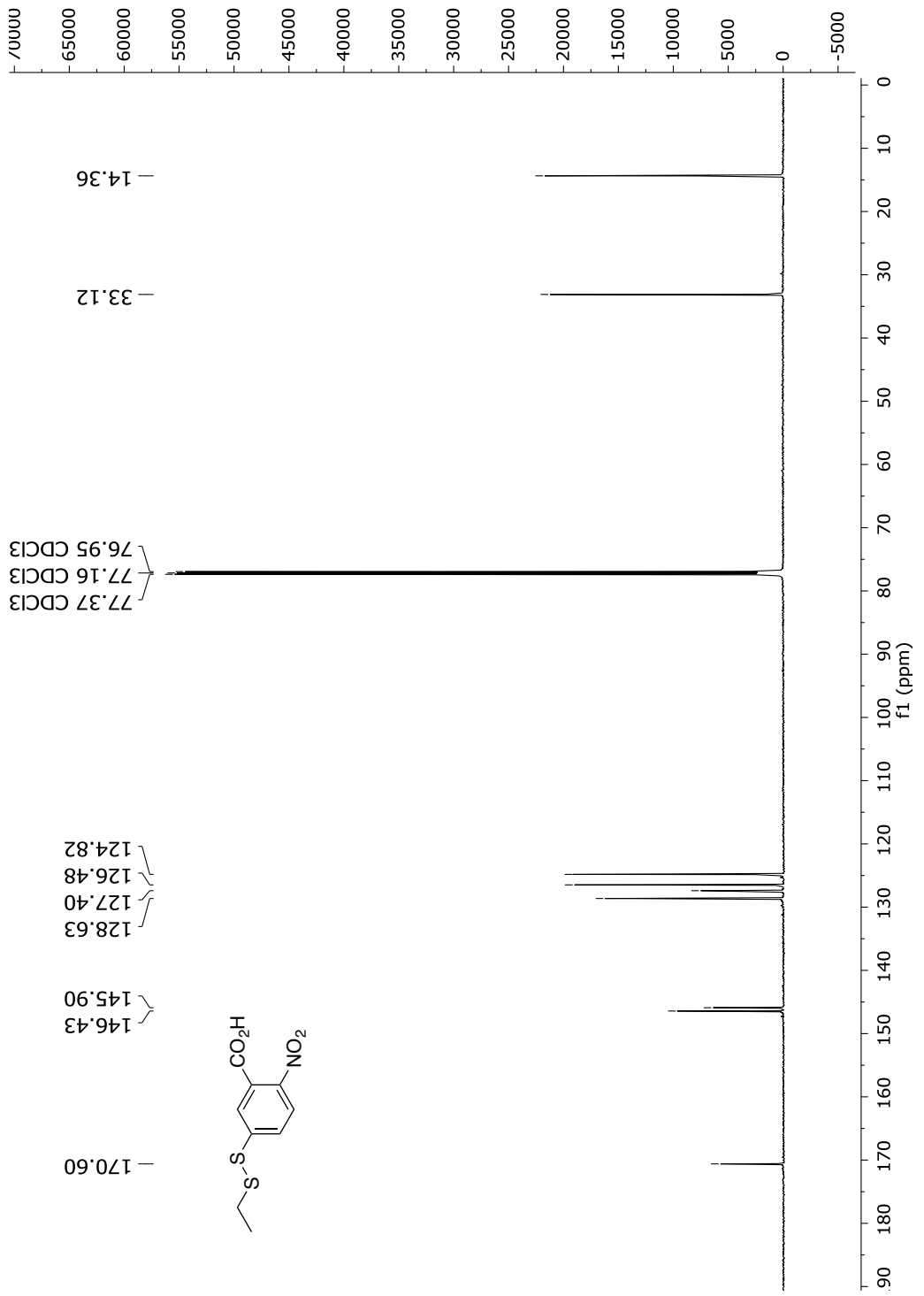

Fig. 117 ^{13}C-NMR spectrum of compound **1** in $CDCl_3$ (151 MHz).

2-(Ethyldisulfaneyl)-5-nitropyridine (2)

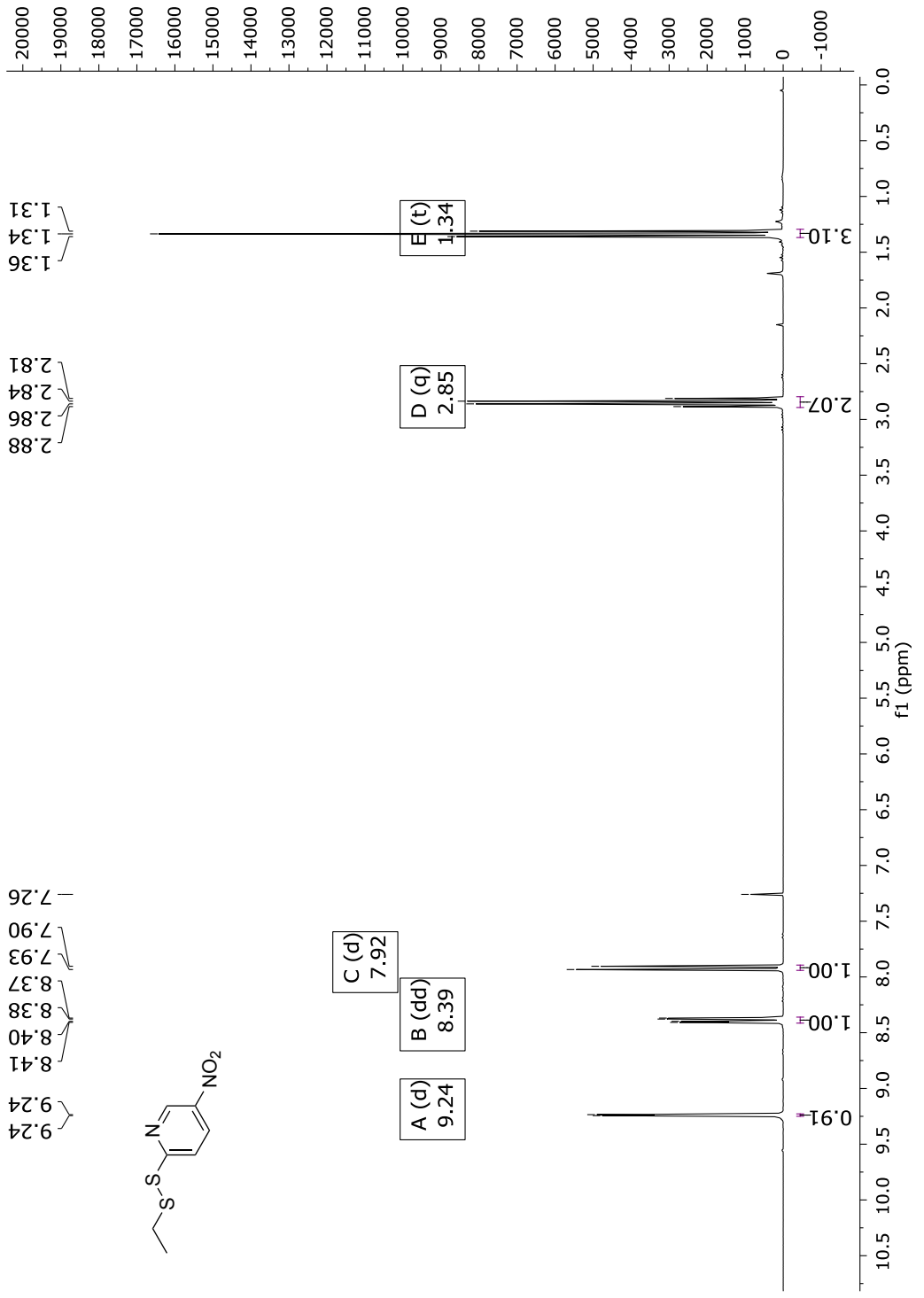

Fig. 118 ^{1}H-NMR spectrum of compound **2** in $CDCl_3$ (300 MHz).

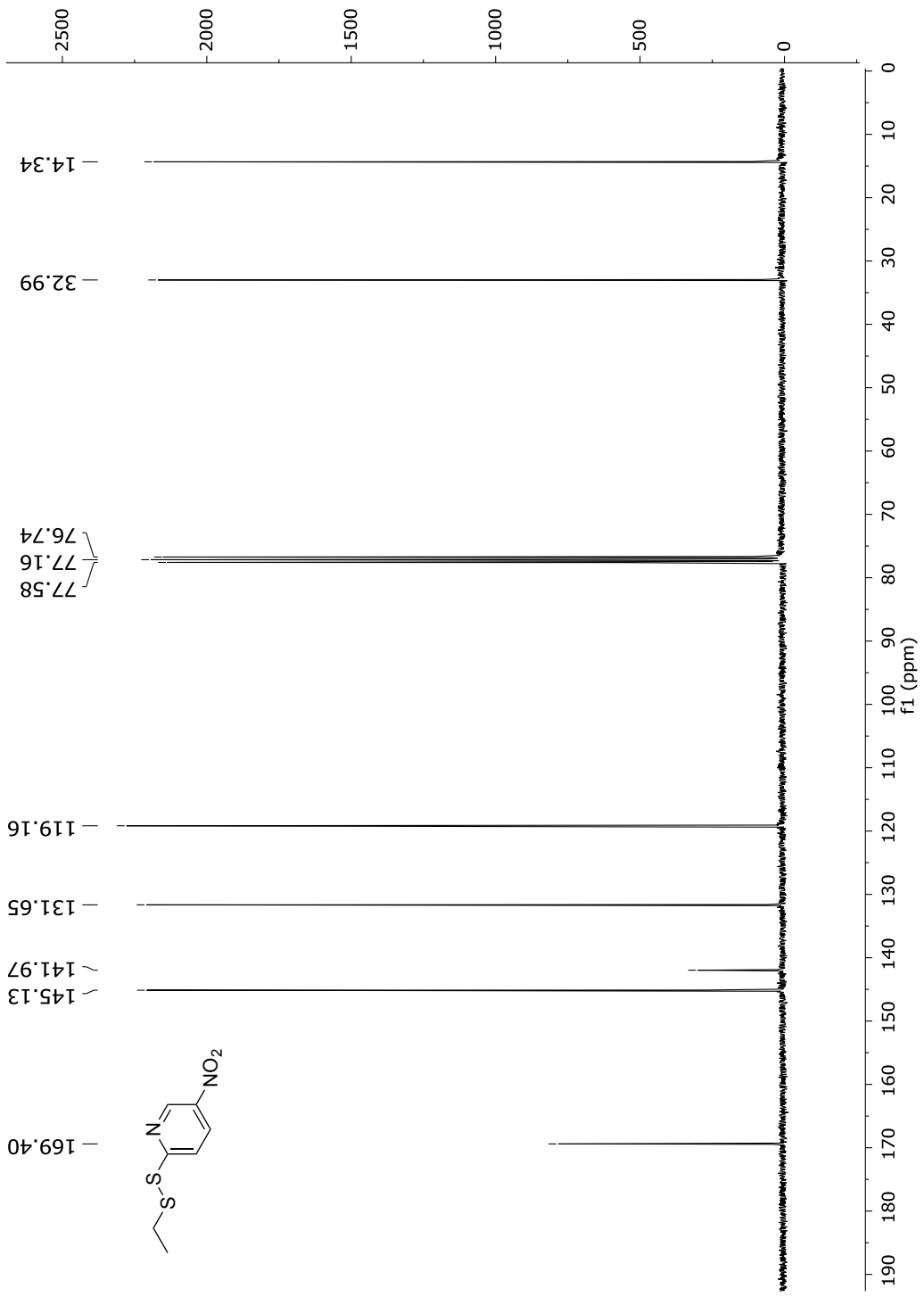

Fig. 119 ^{13}C-NMR spectrum of compound **2** in $CDCl_3$ (75 MHz).

Diethyl-ethynylphosphonite (3)

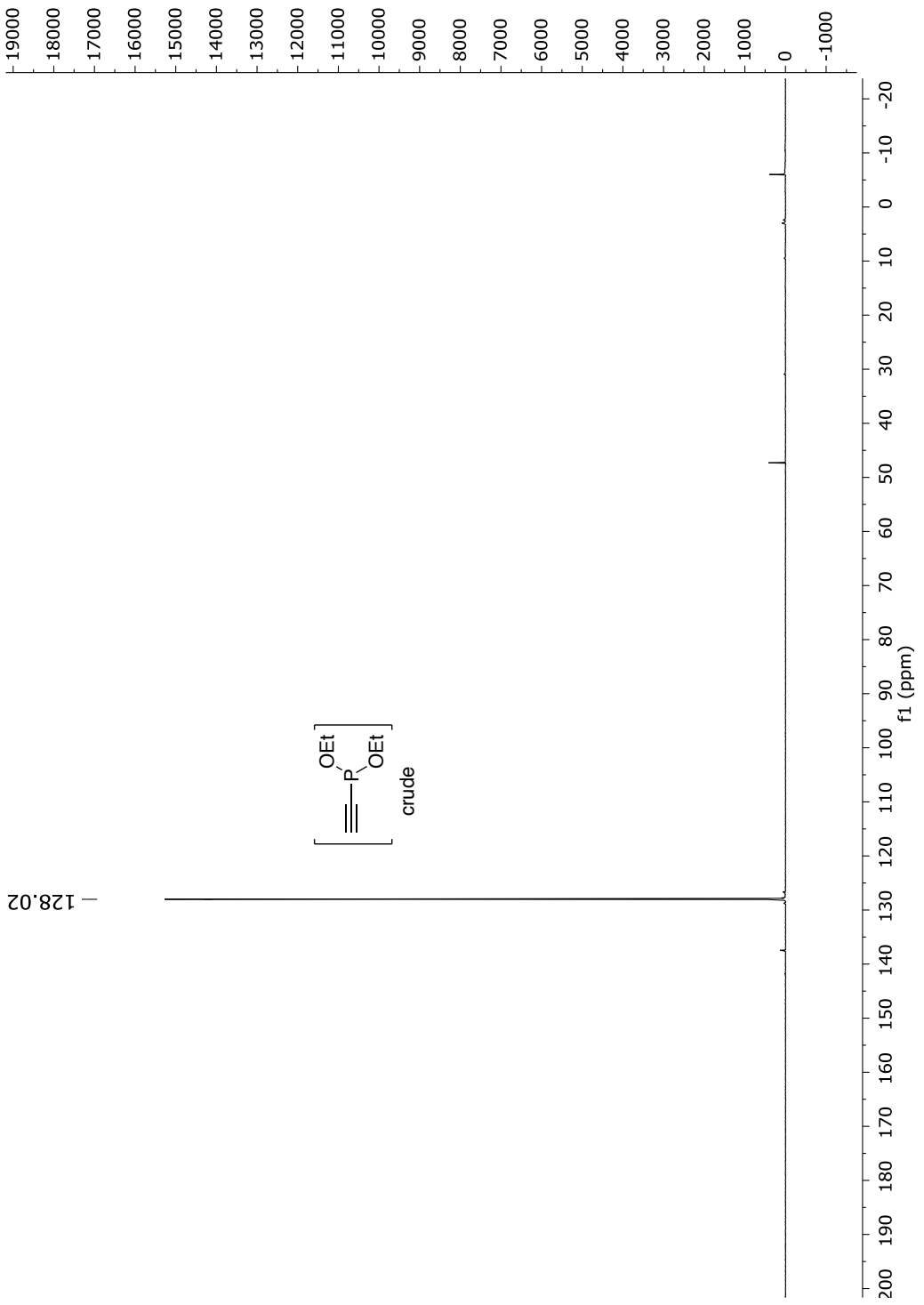

Fig. 120 ^{31}P-NMR spectrum of crude diethyl-ethynylphosphonite **3** in THF (122 MHz).

Diethyl-vinylphosphonite (4)

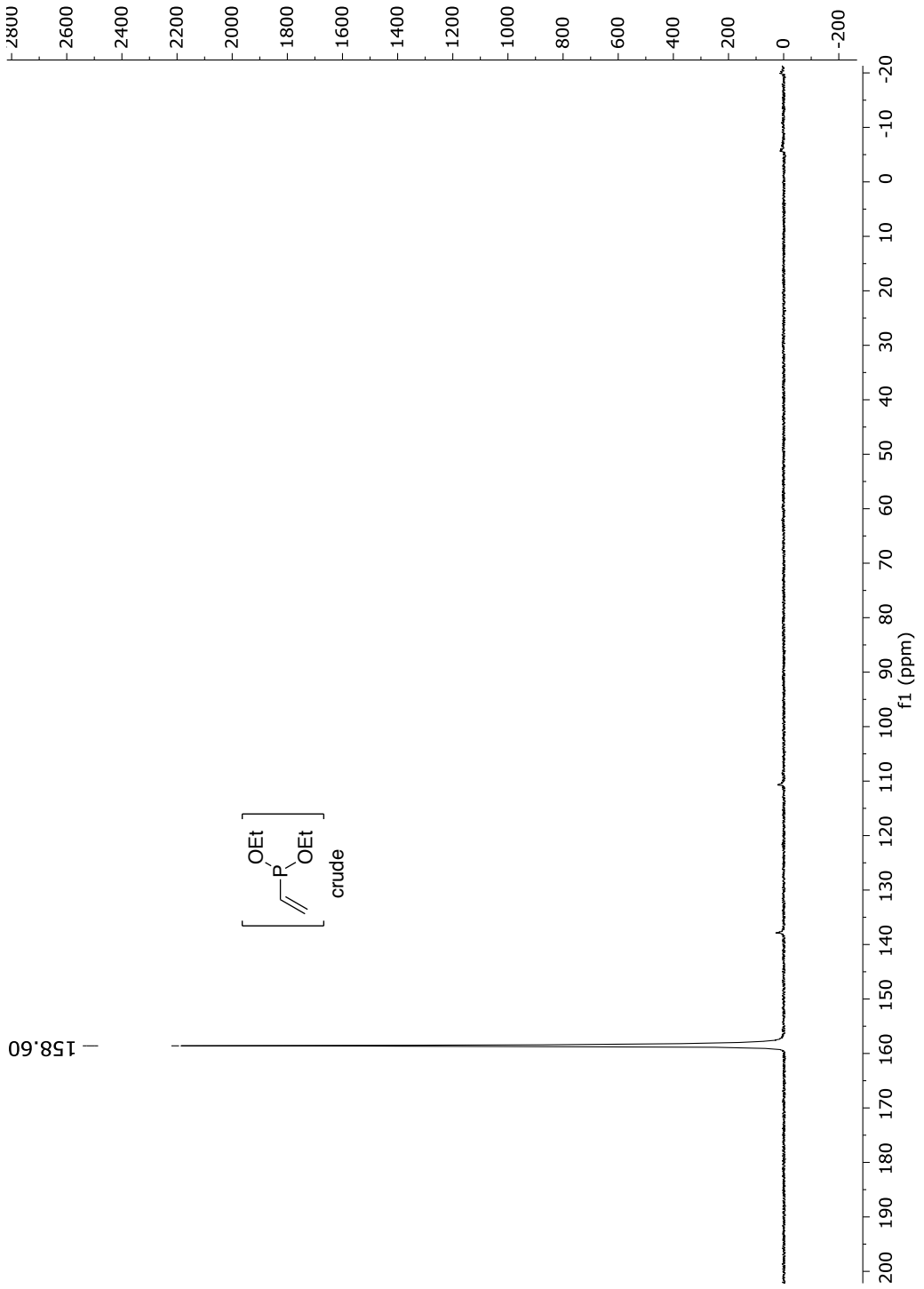

Fig. 121 ^{31}P-NMR spectrum of crude diethyl-vinylphosphonite **4** in THF (122 MHz).

Compound (5)

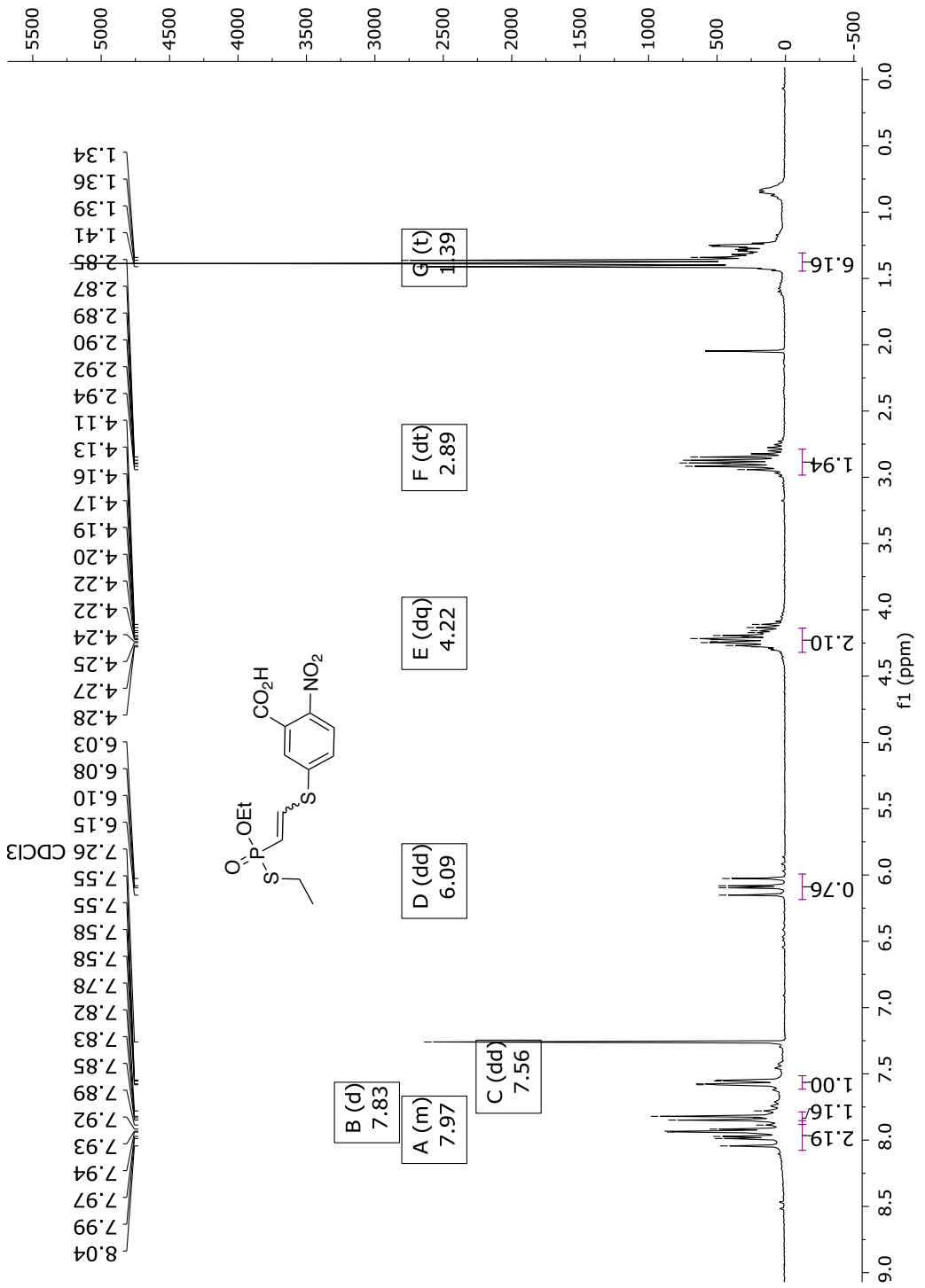

Fig. 122 ^{1}H-NMR spectrum of compound **5** in $CDCl_3$ (300 MHz).

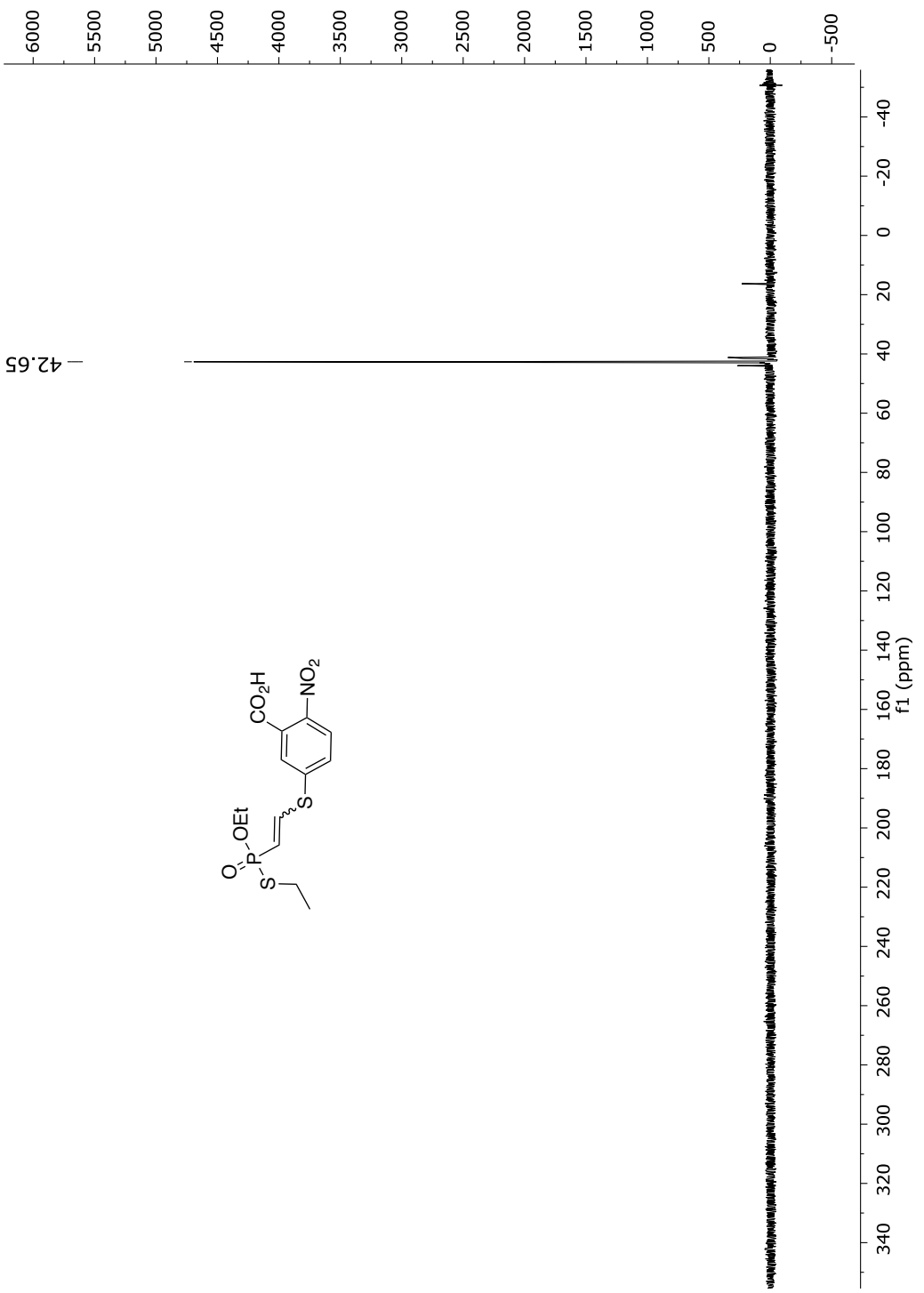

Fig. 123 ^{31}P-NMR spectrum of compound **5** in $CDCl_3$ (122 MHz).

Compound (6)

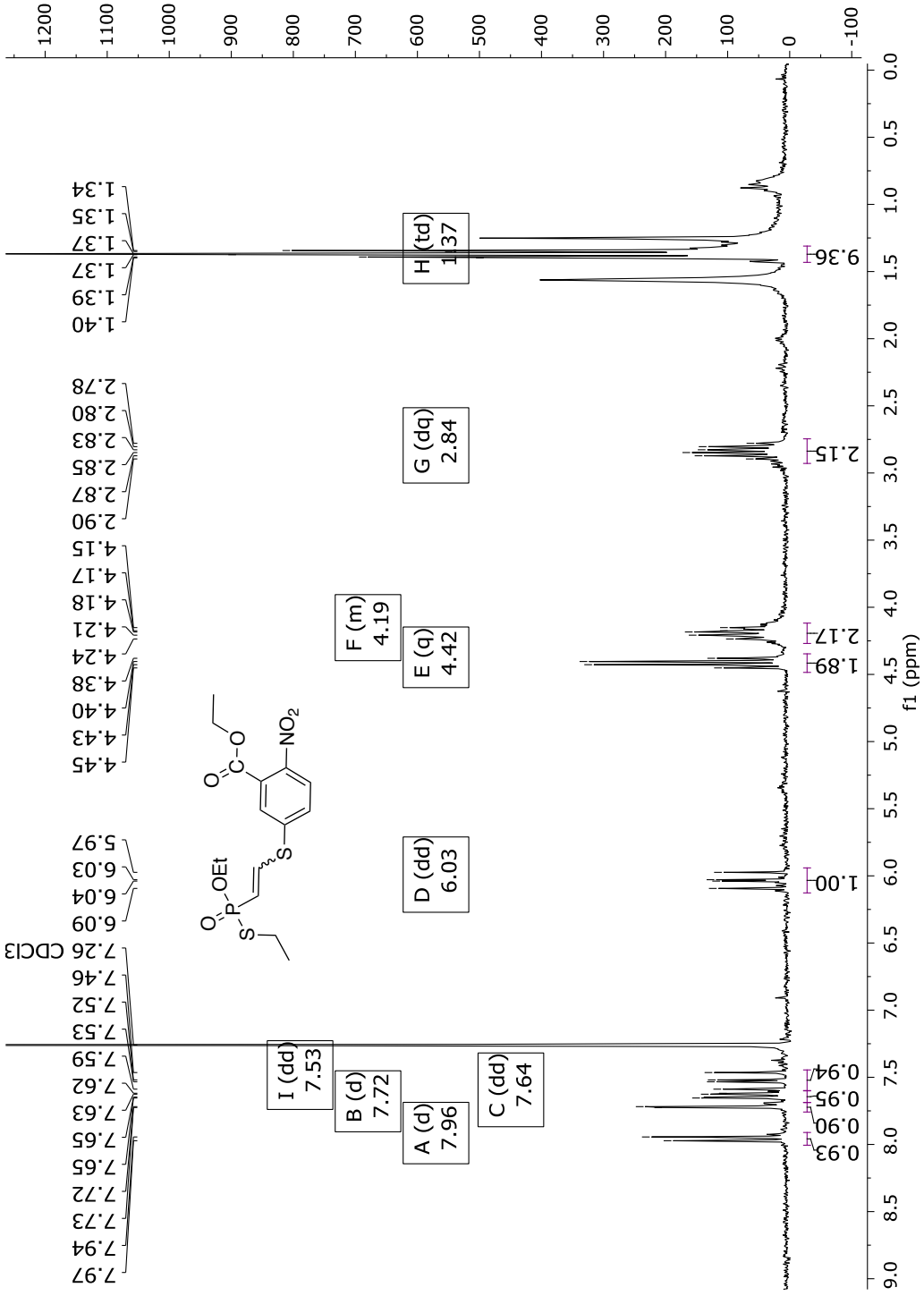

Fig. 124 ^{1}H-NMR spectrum of compound **6** in $CDCl_3$ (300 MHz).

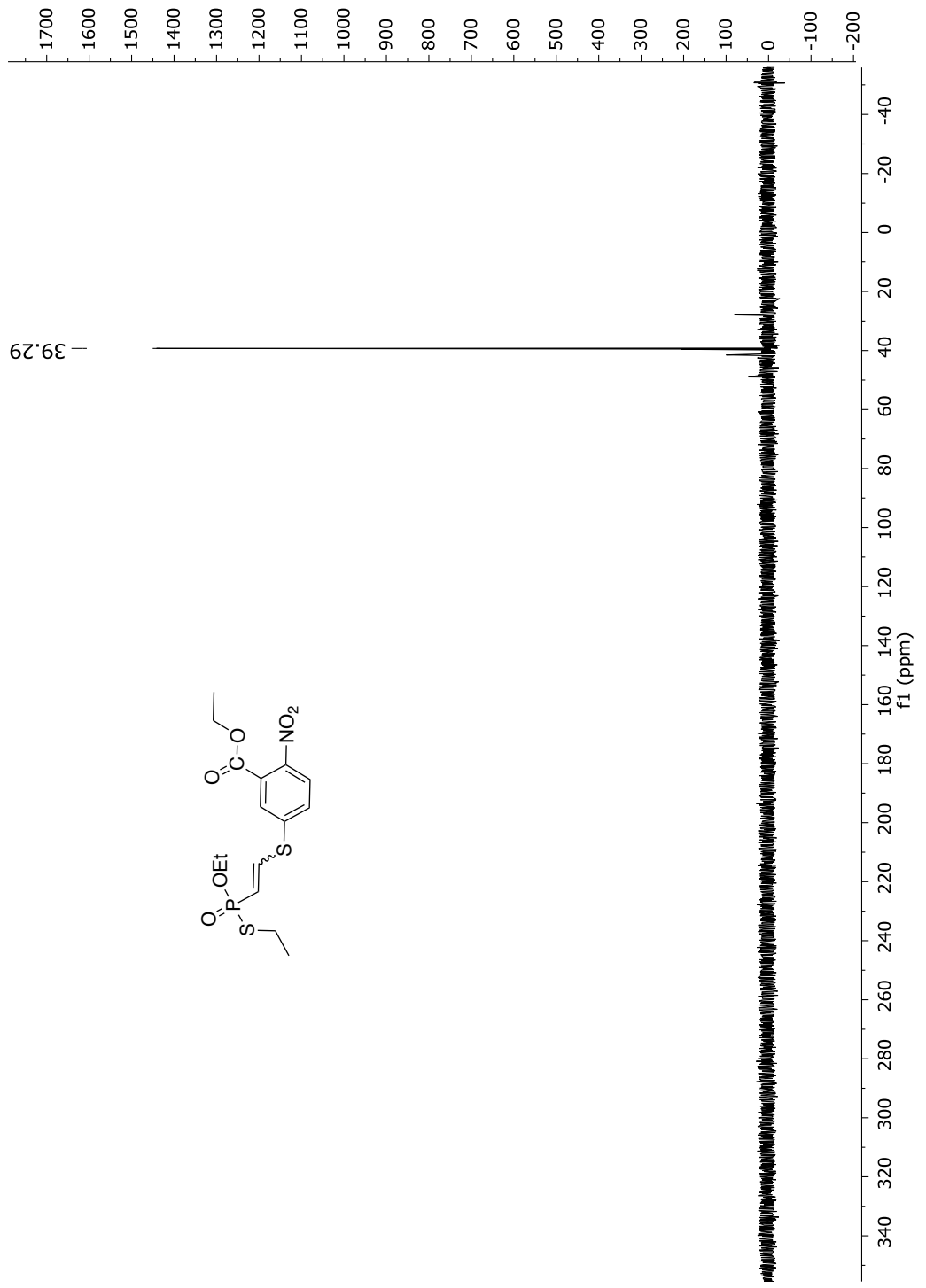

Fig. 125 ^{31}P-NMR spectrum of compound **6** in $CDCl_3$ (122 MHz).

O,S-Diethyl ethynylphosphonothiolate (**7**)

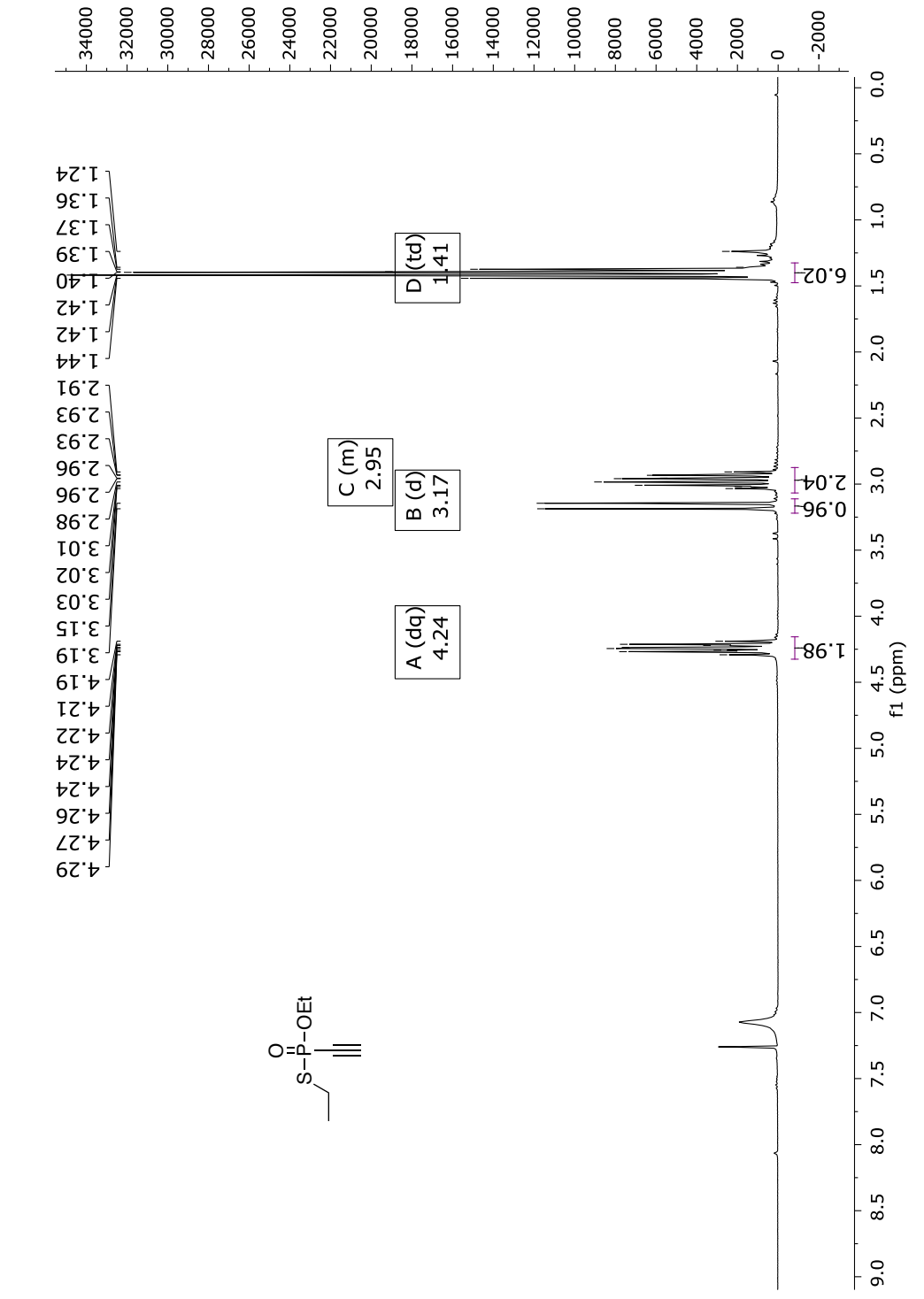

Fig. 126 ^{1}H-NMR spectrum of compound **7** in $CDCl_3$ (300 MHz).

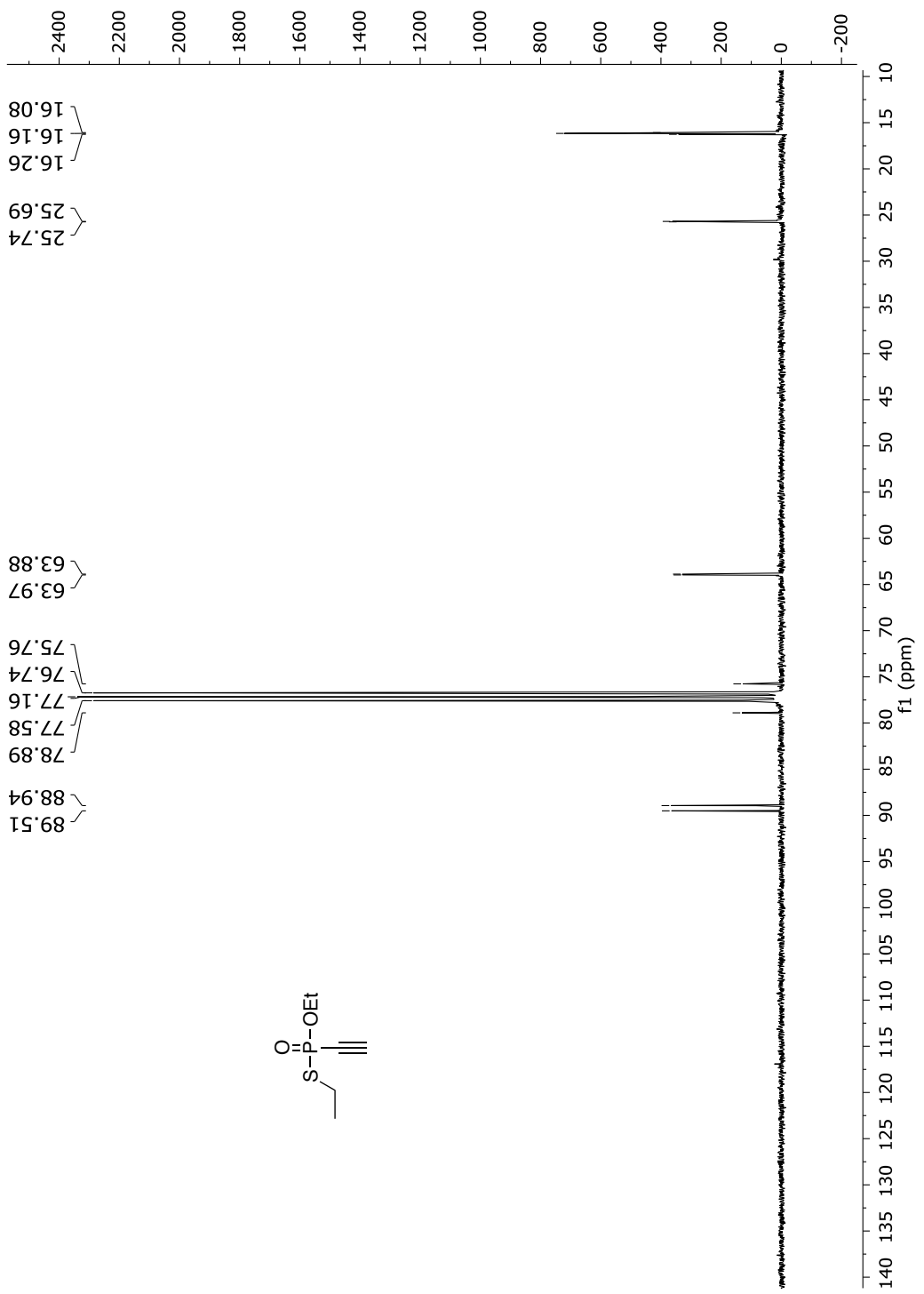

Fig. 127 ^{13}C-NMR spectrum of compound **7** in $CDCl_3$ (75 MHz).

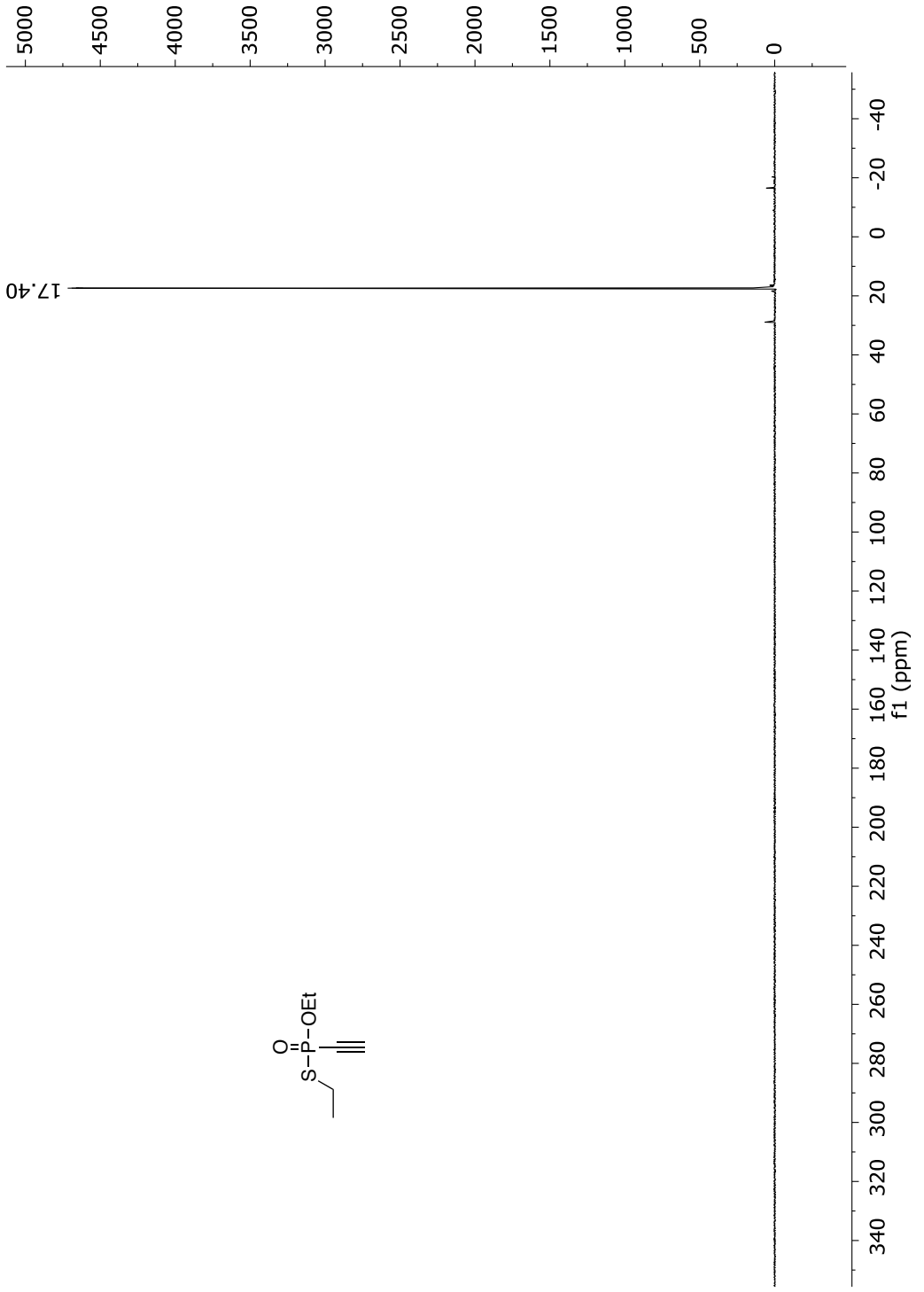

Fig. 128 ^{31}P-NMR spectrum of compound **7** in $CDCl_3$ (122 MHz).

O,S-Diethyl vinylphosphonothiolate (8)

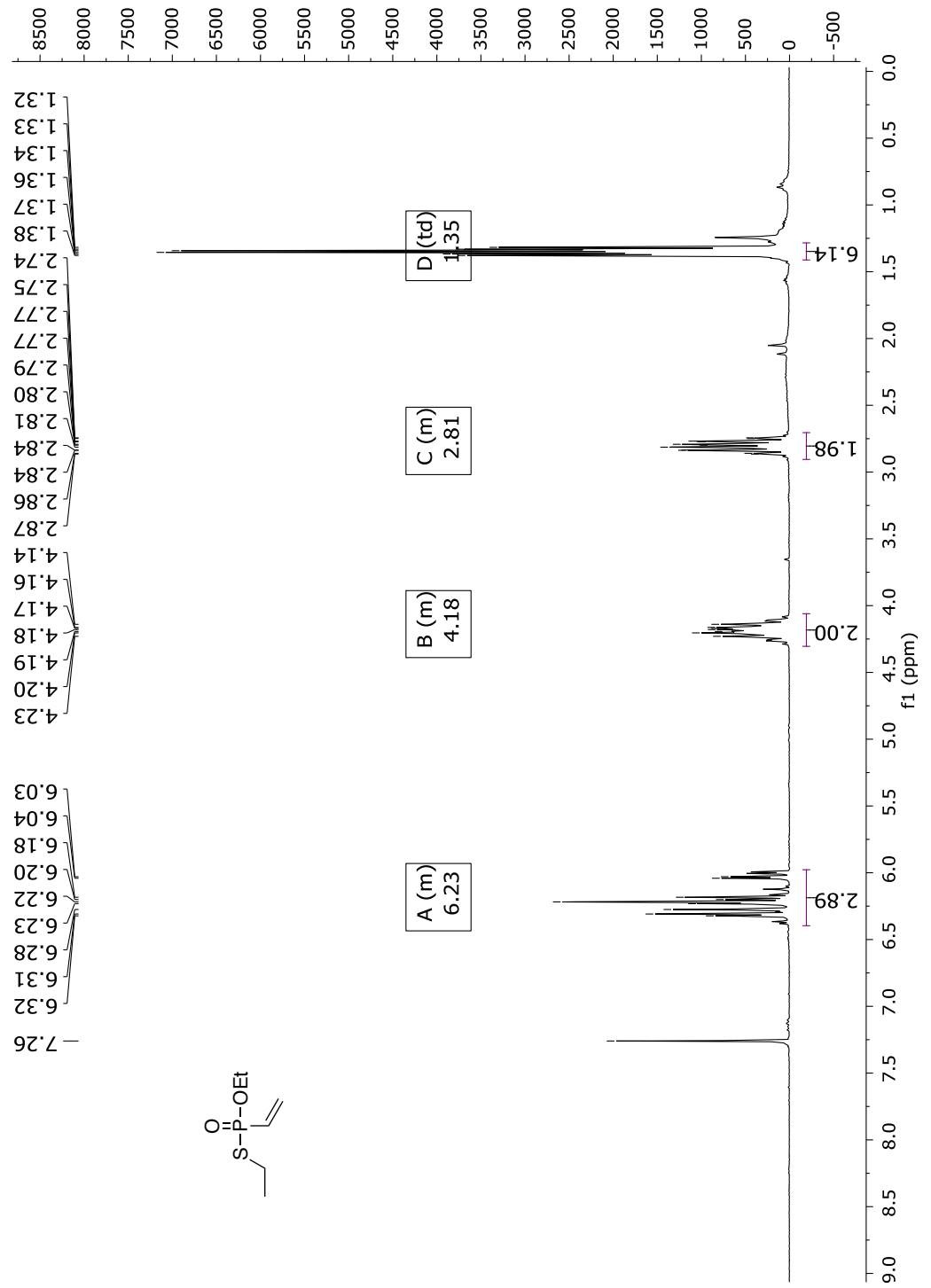

Fig. 129 ^{1}H-NMR spectrum of compound **8** in $CDCl_3$ (300 MHz).

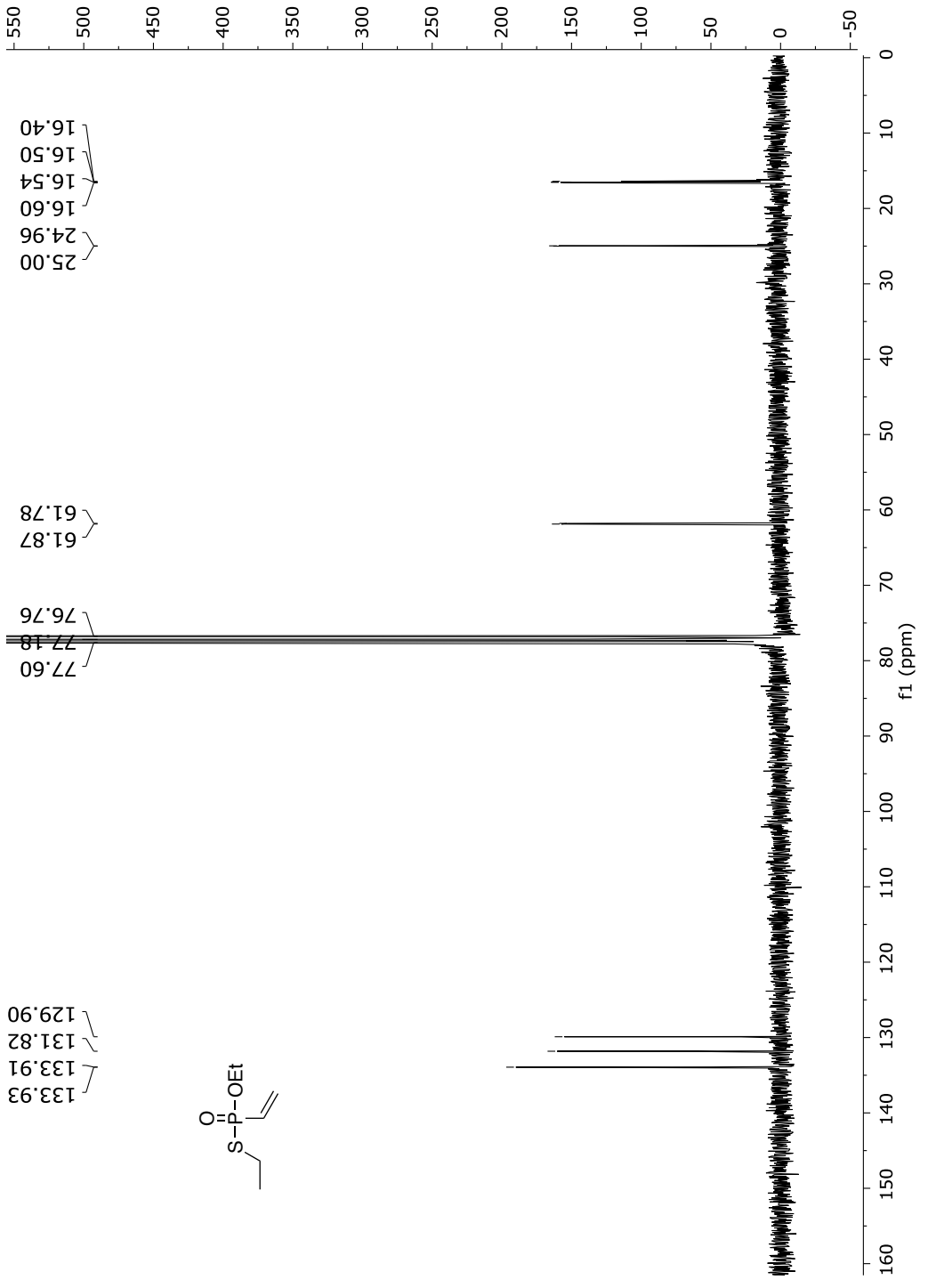

Fig. 130 ^{13}C-NMR spectrum of compound **8** in $CDCl_3$ (75 MHz).

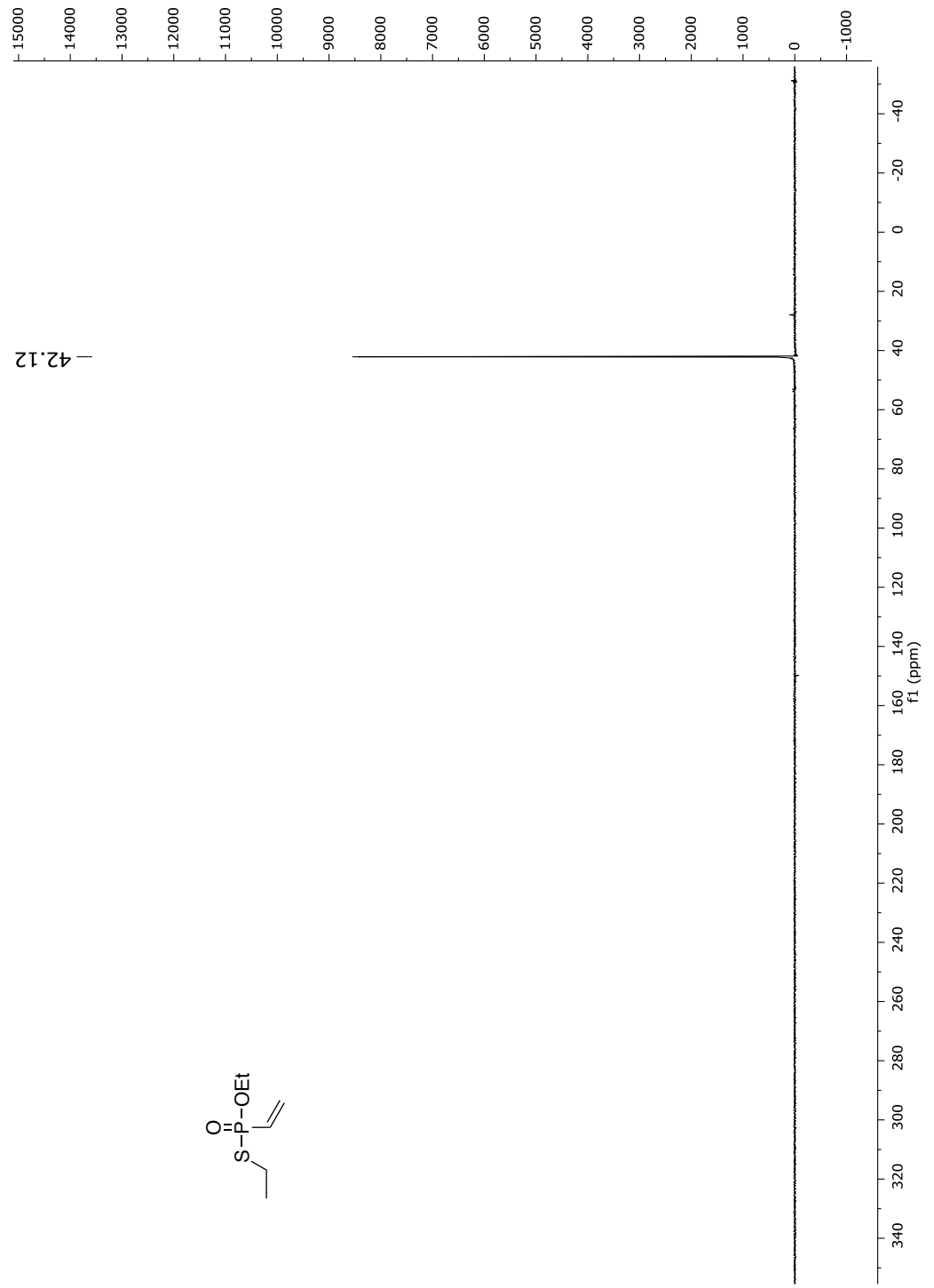

Fig. 131 ^{31}P-NMR spectrum of compound **8** in $CDCl_3$ (122 MHz).

Compound (9)

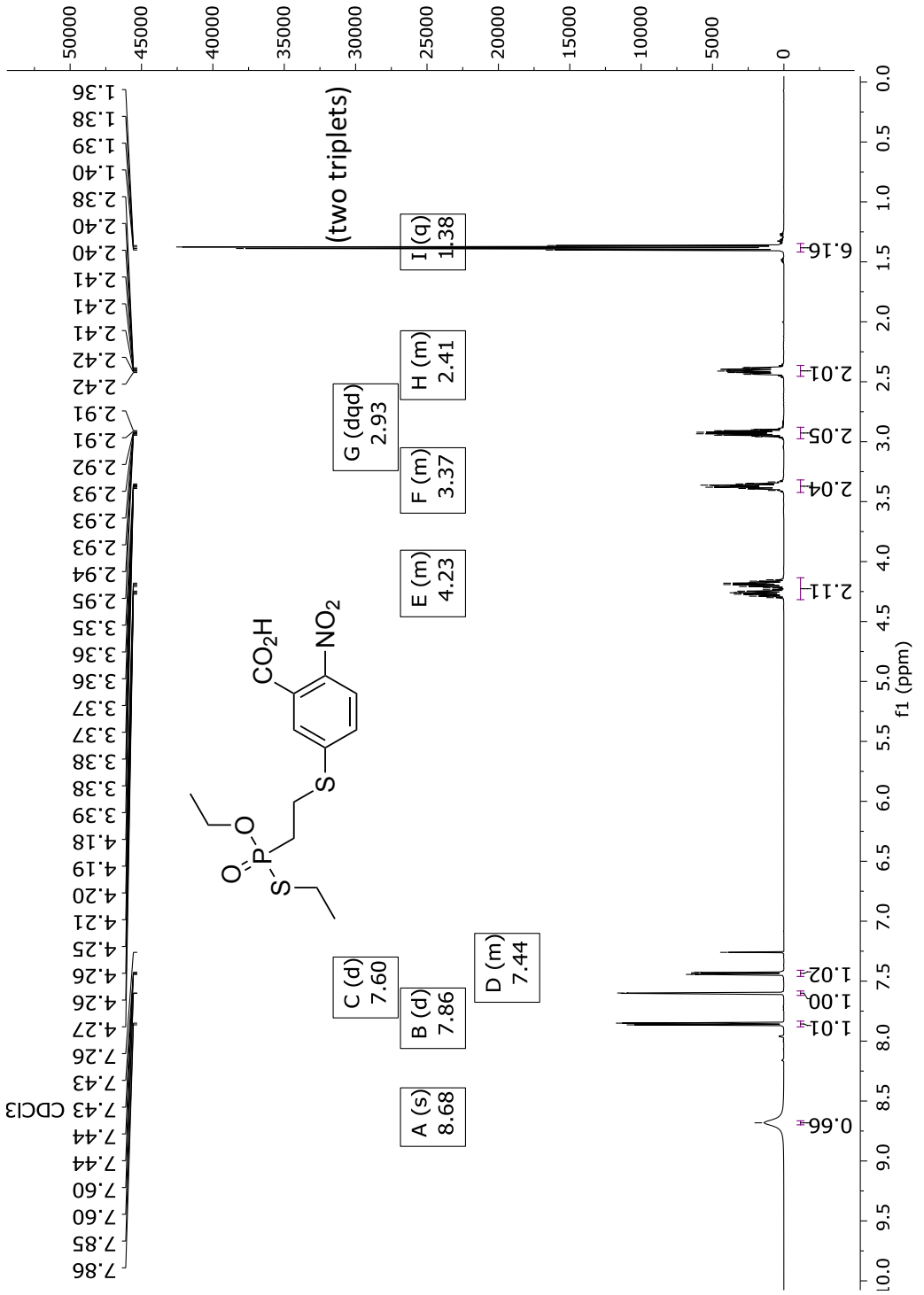

Fig. 132 ^{1}H-NMR spectrum of compound **9** in $CDCl_3$ (600 MHz).

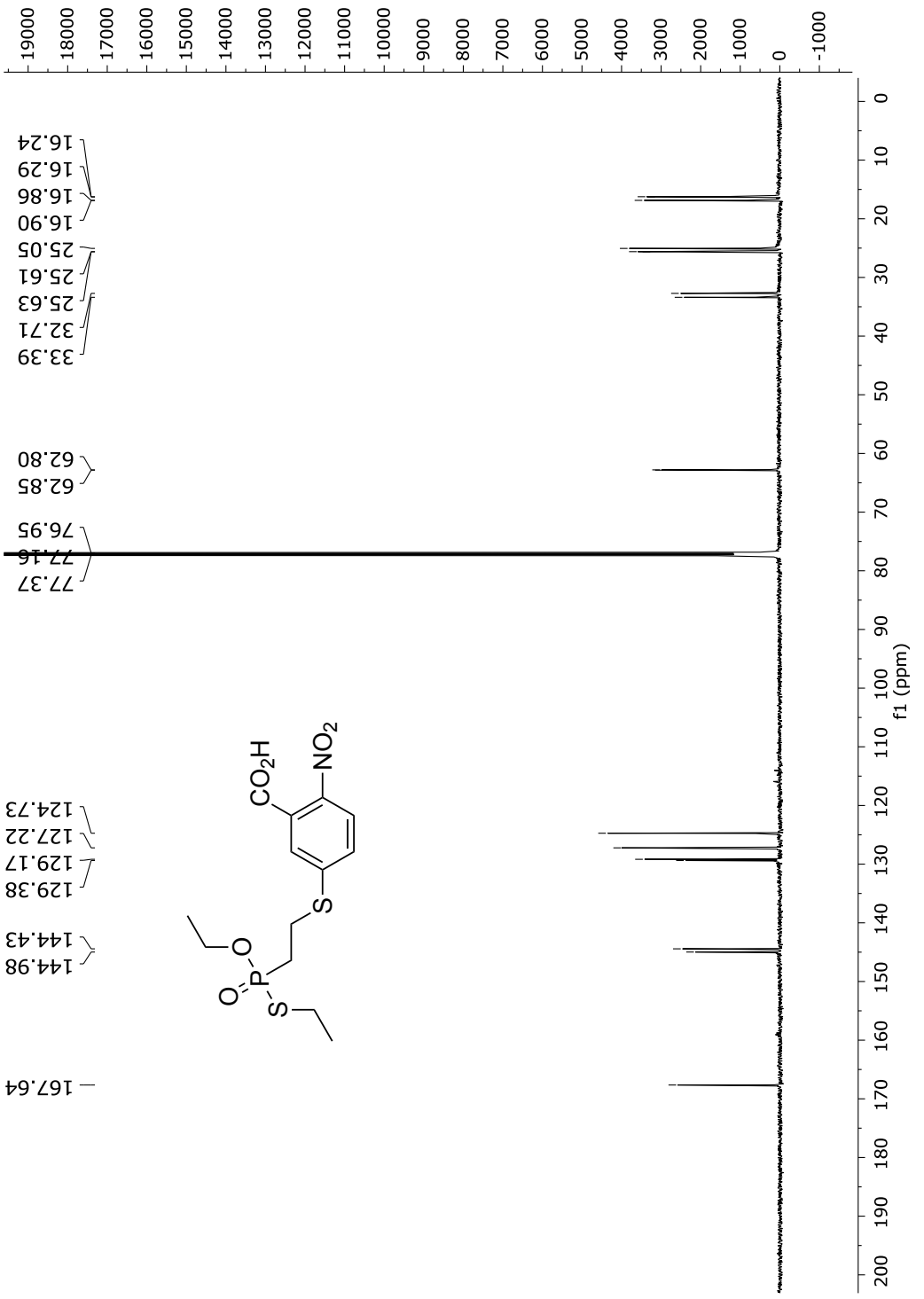

Fig. 133 ^{13}C-NMR spectrum of compound **9** in $CDCl_3$ (151 MHz).

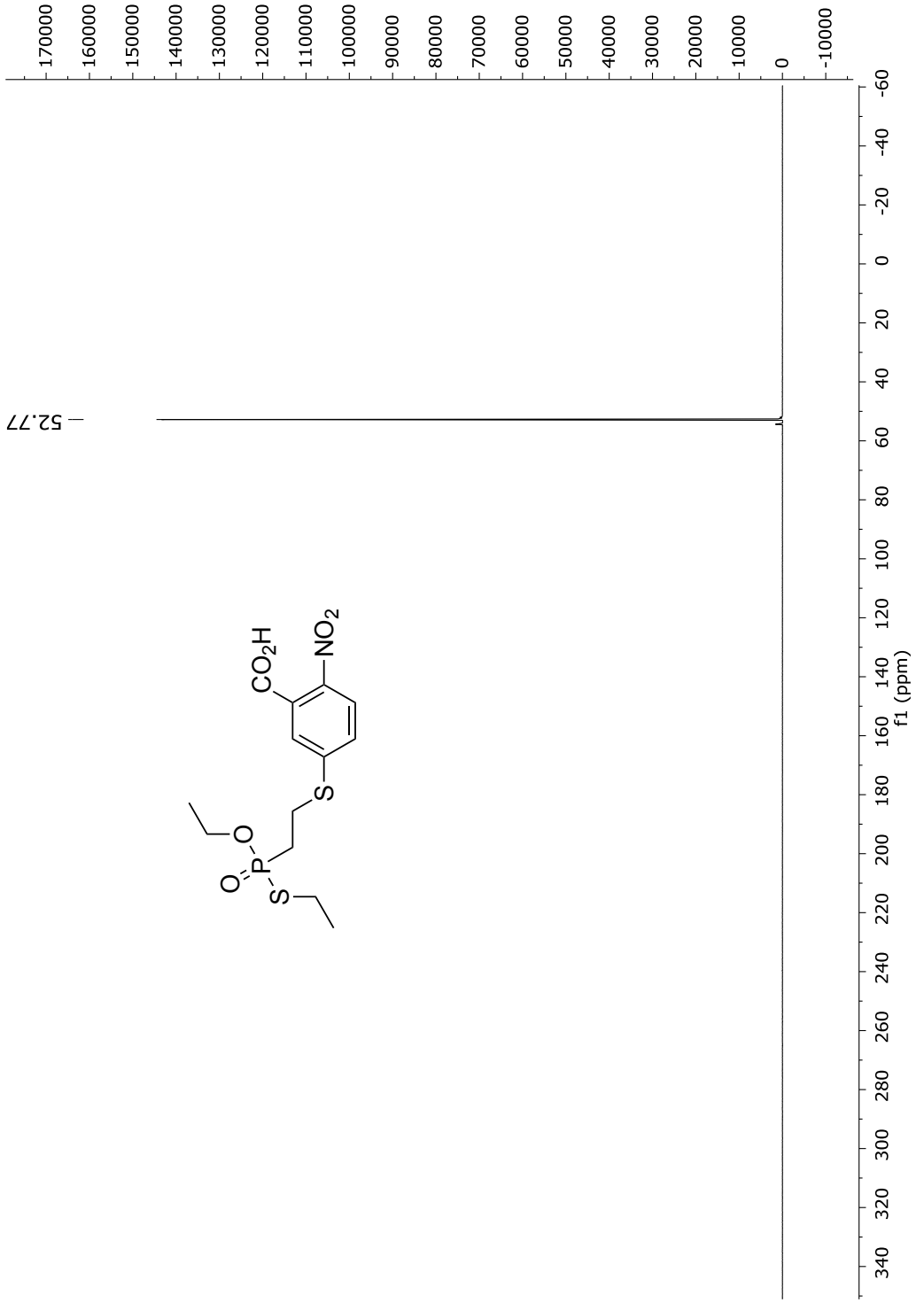

Fig. 134 ^{31}P-NMR spectrum of compound **9** in $CDCl_3$ (243 MHz).

Compound (10)

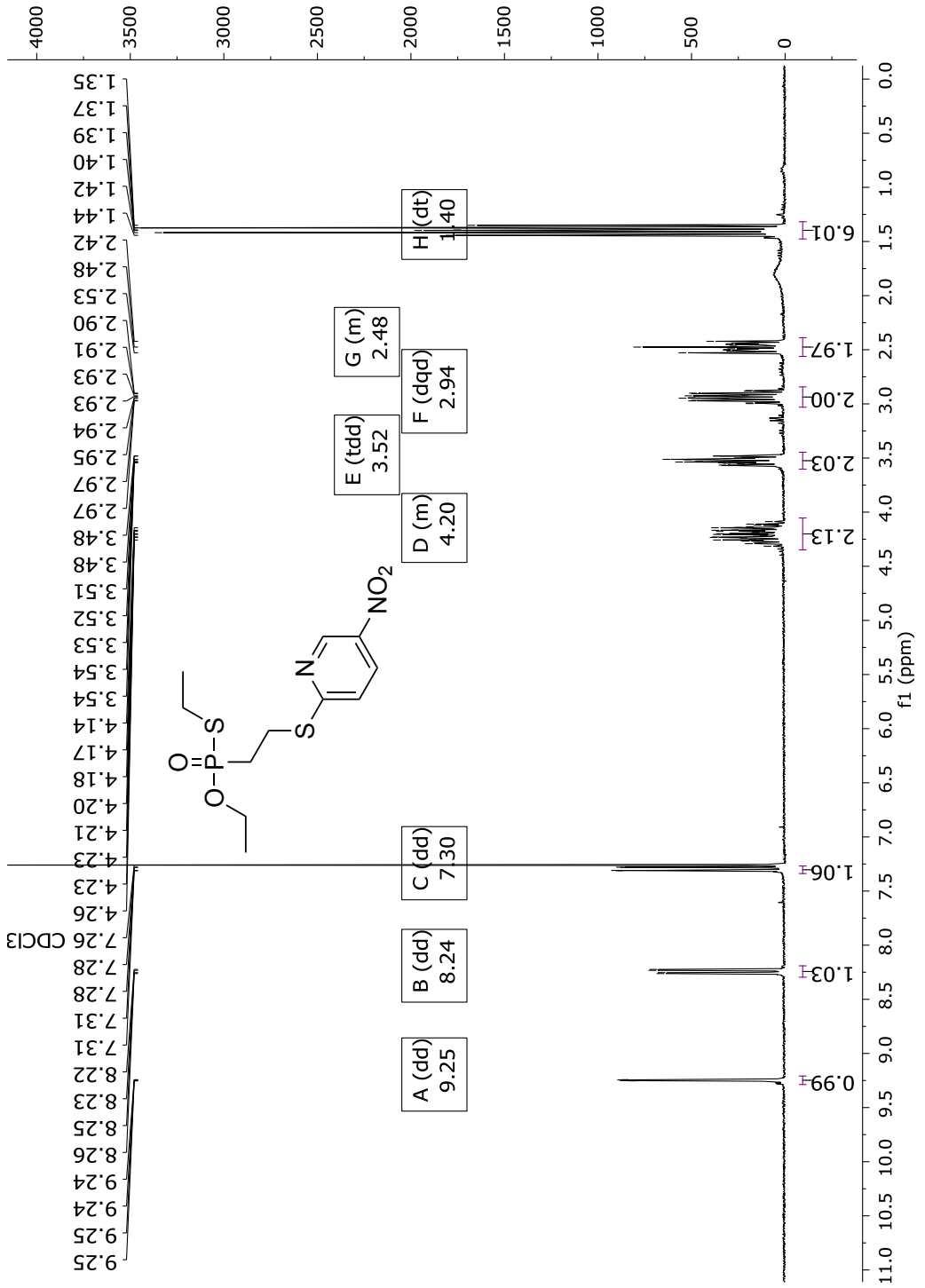

Fig. 135 ^{1}H-NMR spectrum of compound **10** in $CDCl_3$ (300 MHz).

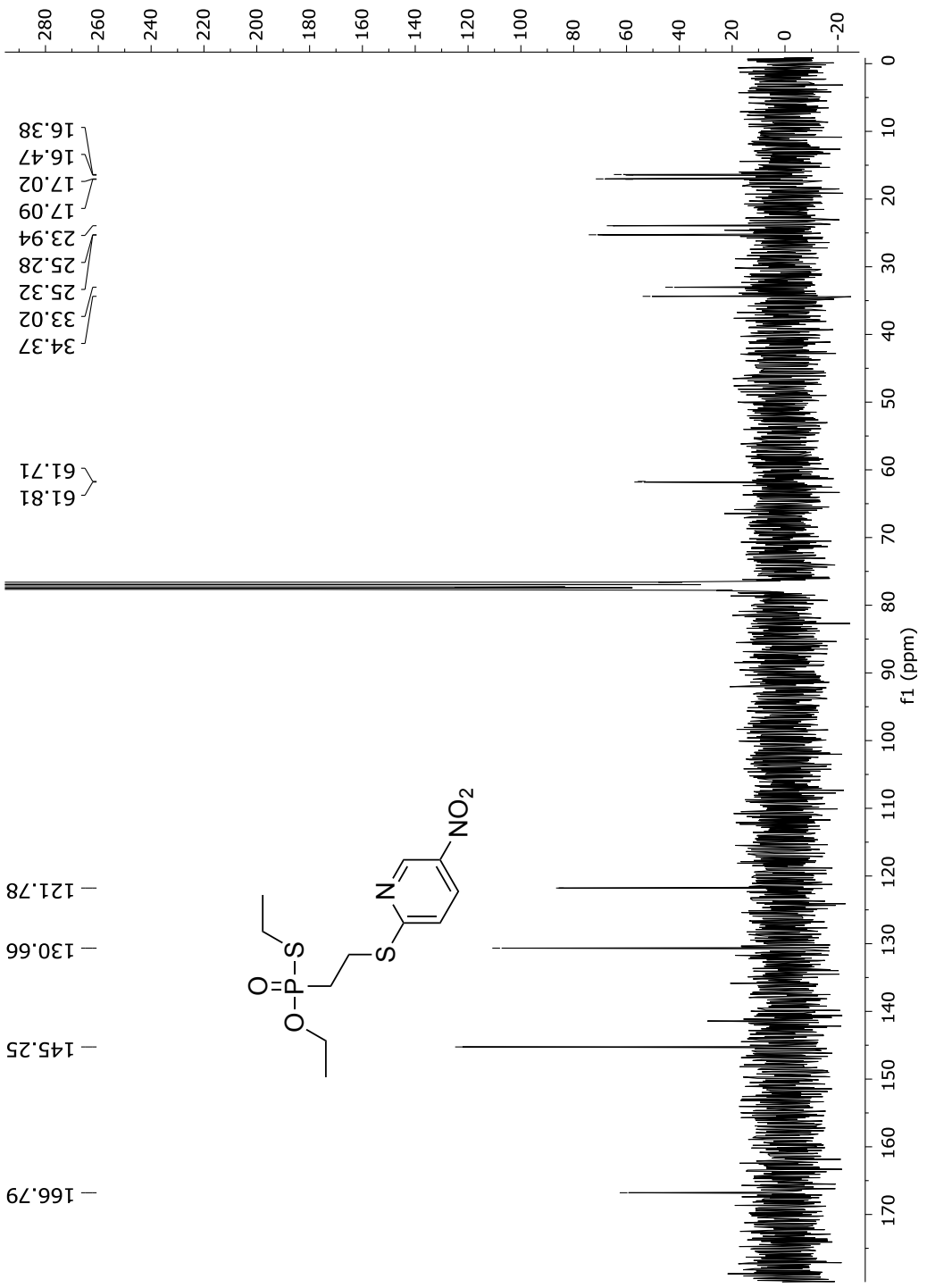

Fig. 136 ^{13}C-NMR spectrum of compound **10** in $CDCl_3$ (75 MHz).

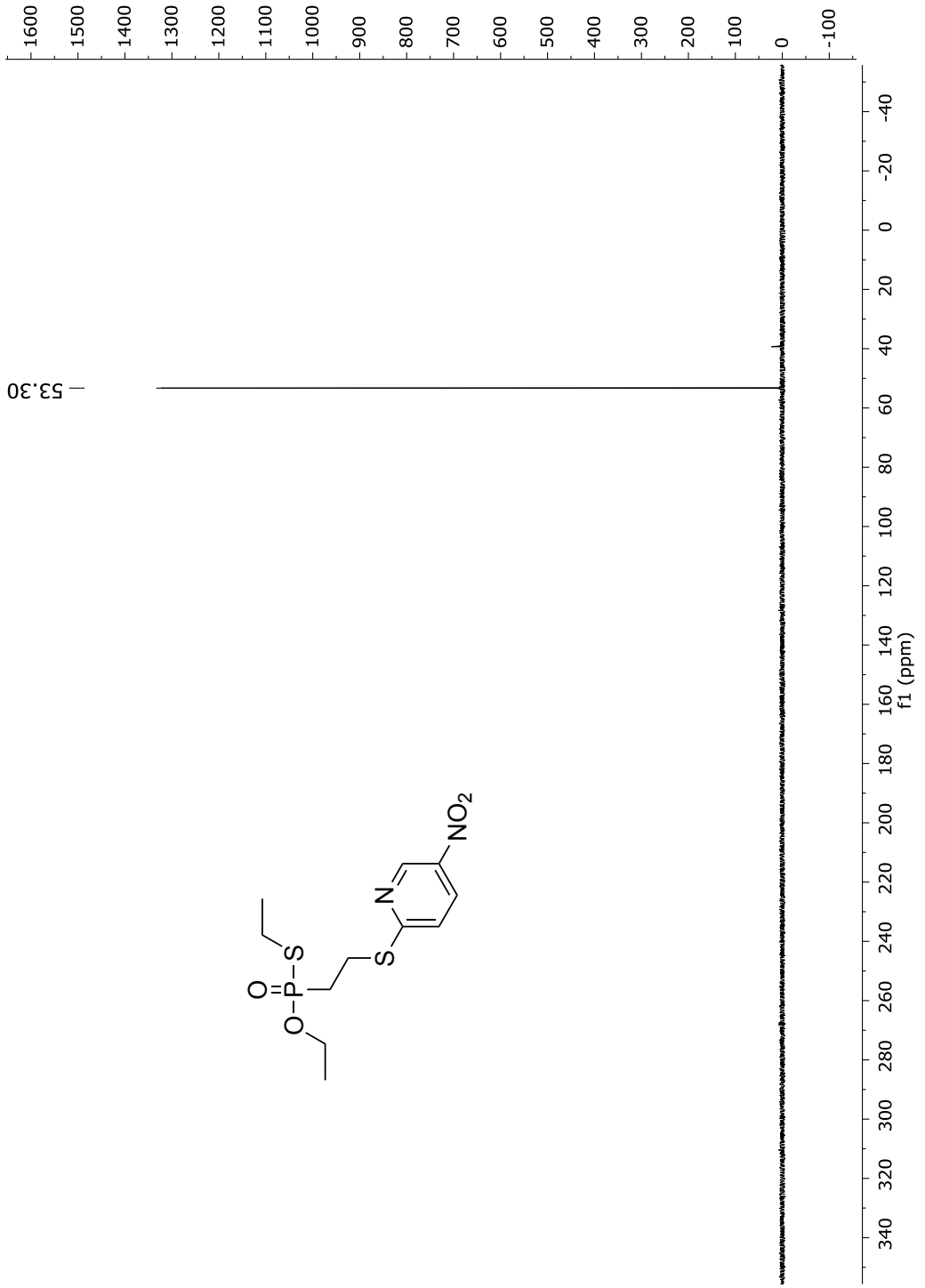

Fig. 137 ^{31}P-NMR spectrum of compound **10** in $CDCl_3$ (122 MHz).

Re-attack product to phosphonate 10

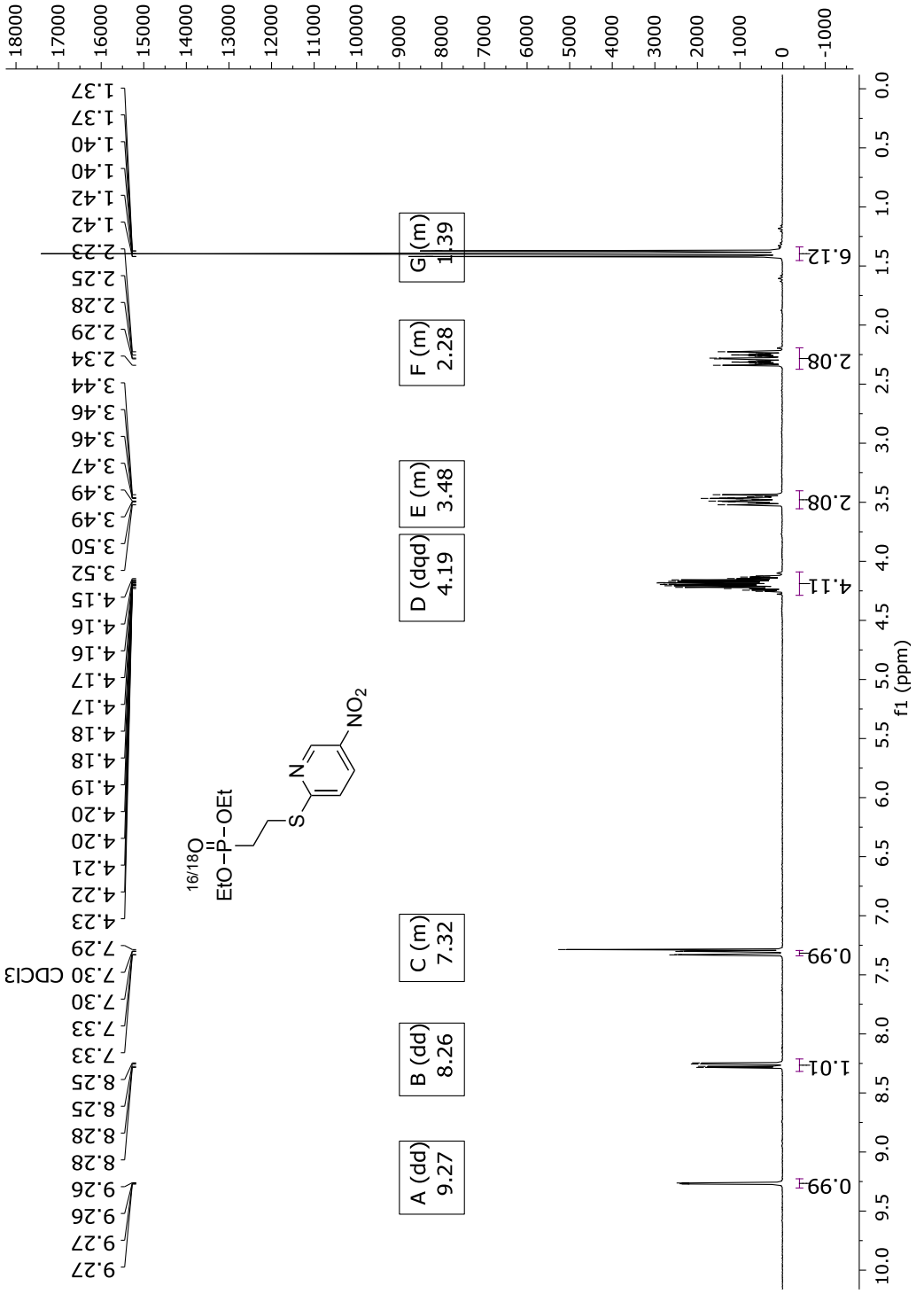

Fig. 138 ^{1}H-NMR spectrum of re-attack product to phosphonate **10** in $CDCl_3$ (300 MHz).

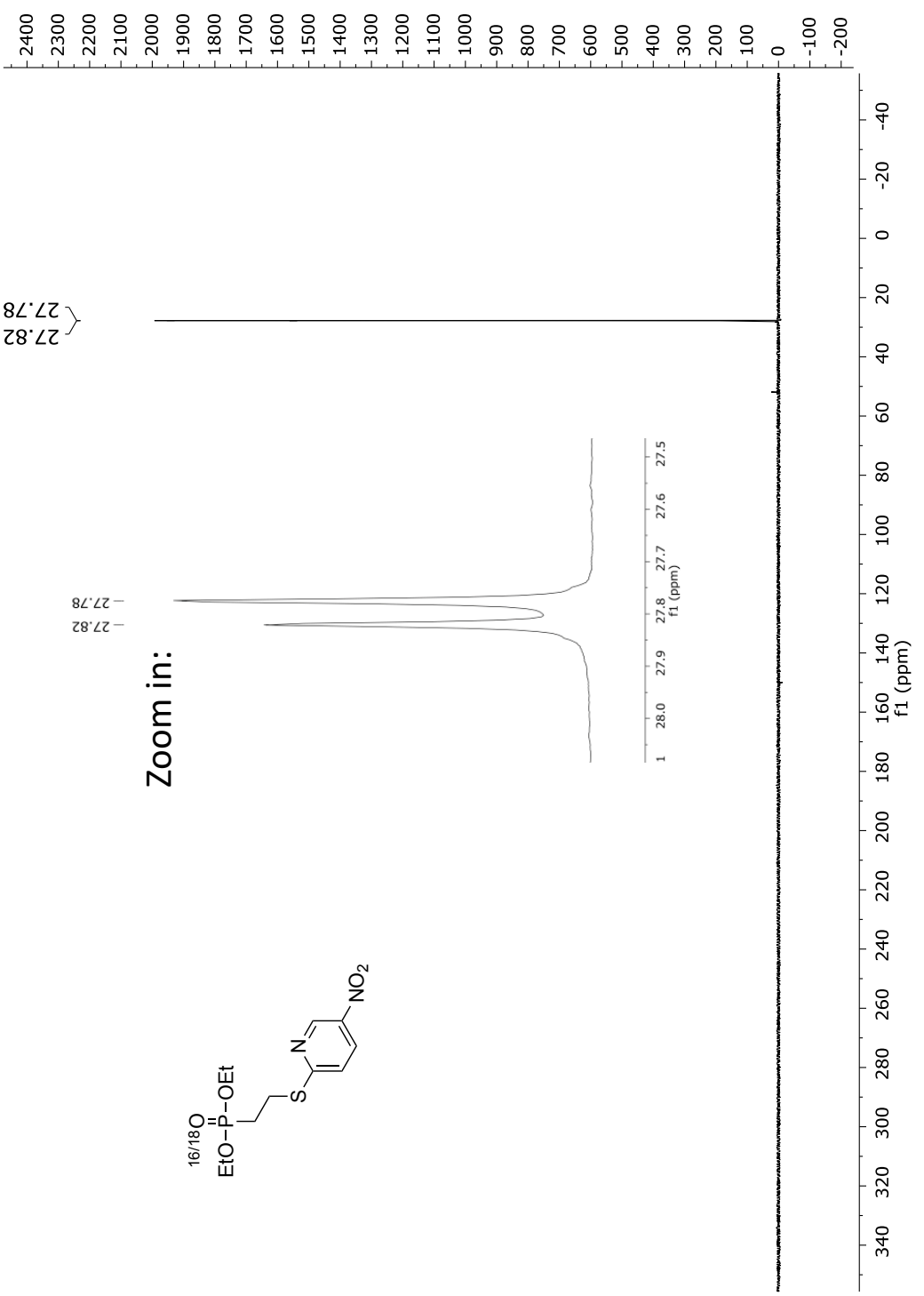

Fig. 139 ^{31}P-NMR spectrum of re-attack product to phosphonate **10** in $CDCl_3$ (122 MHz).

Diethyl-vinylphosphonate (11)

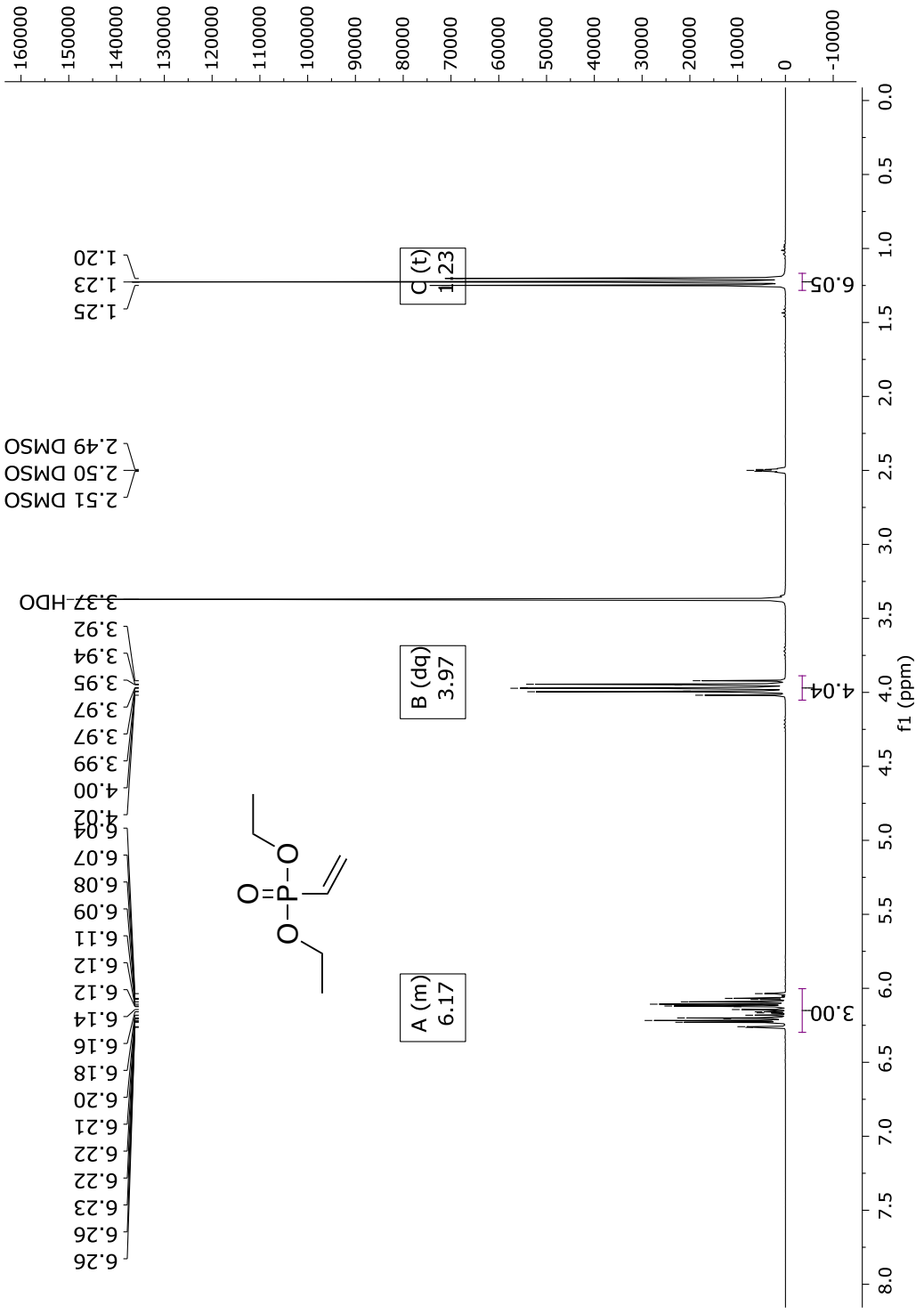

Fig. 140 ^{1}H-NMR spectrum of compound **11** (commercial from Sigma) in DMSO−d_6 (300 MHz).

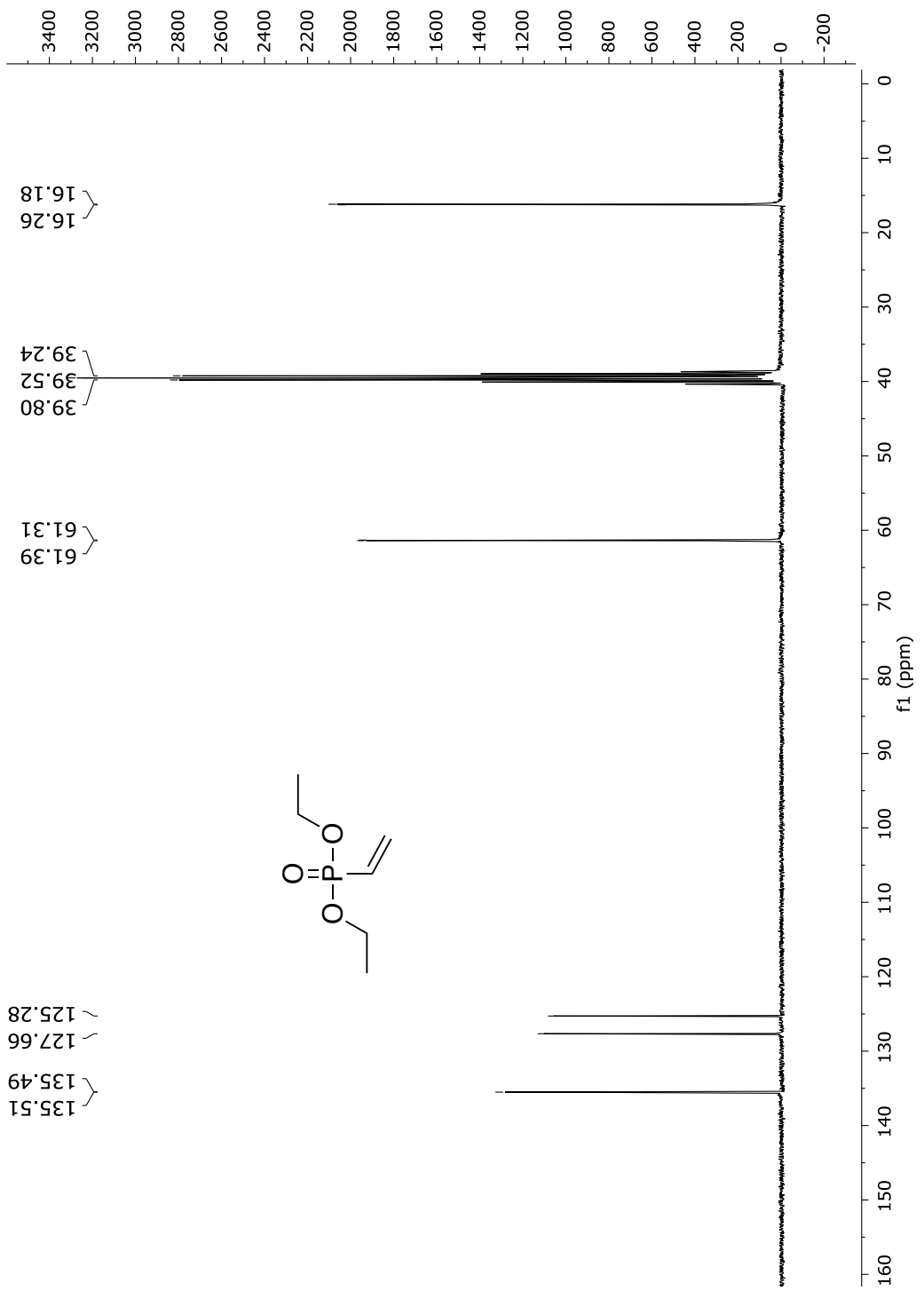

Fig. 141 ^{13}C-NMR spectrum of spectrum of compound **11** (commercial from Sigma) in DMSO−d_6 (75 MHz).

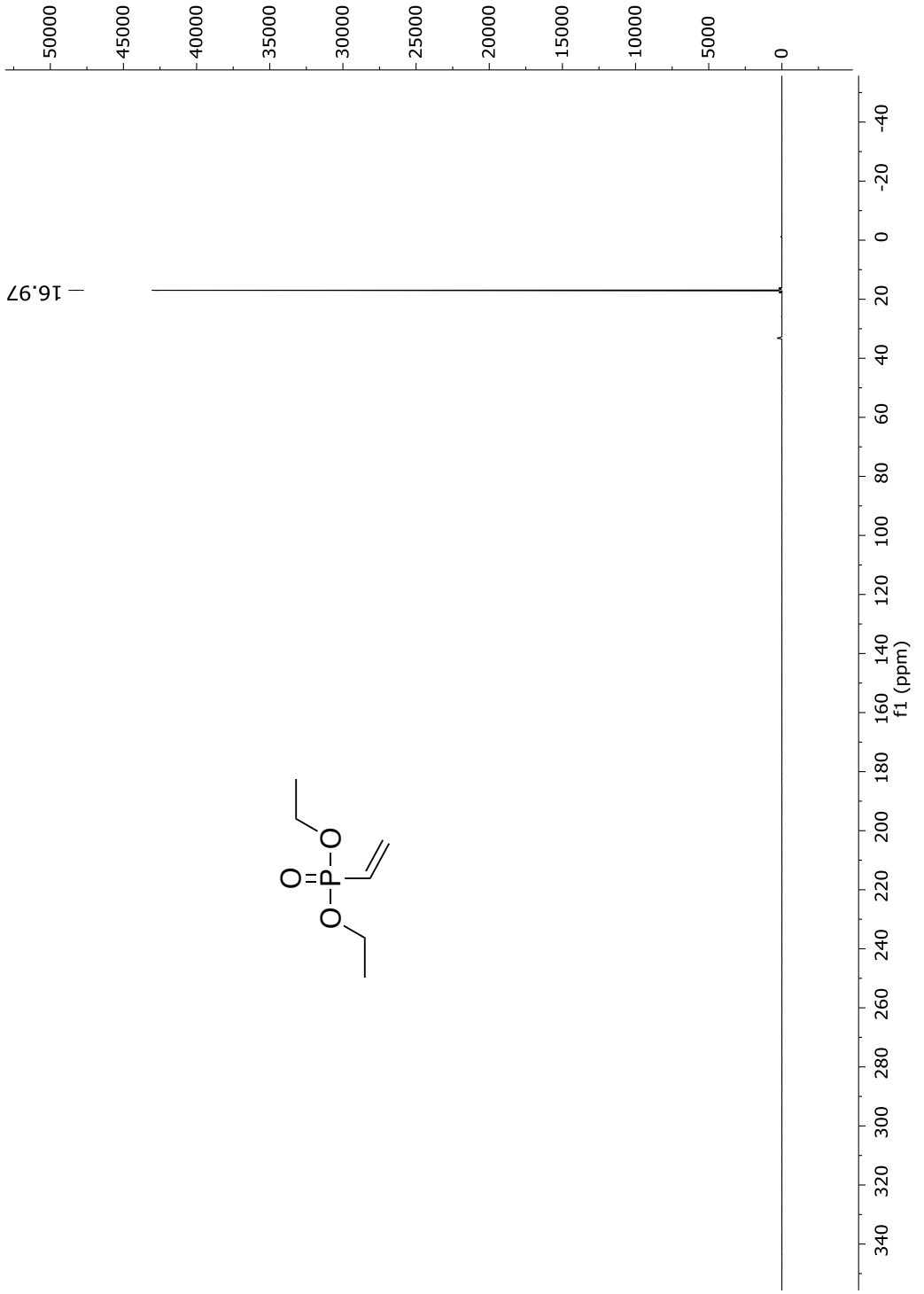

Fig. 142 ^{31}P-NMR spectrum spectrum of compound **11** (commercial from Sigma) in DMSO−d_6 (122 MHz).

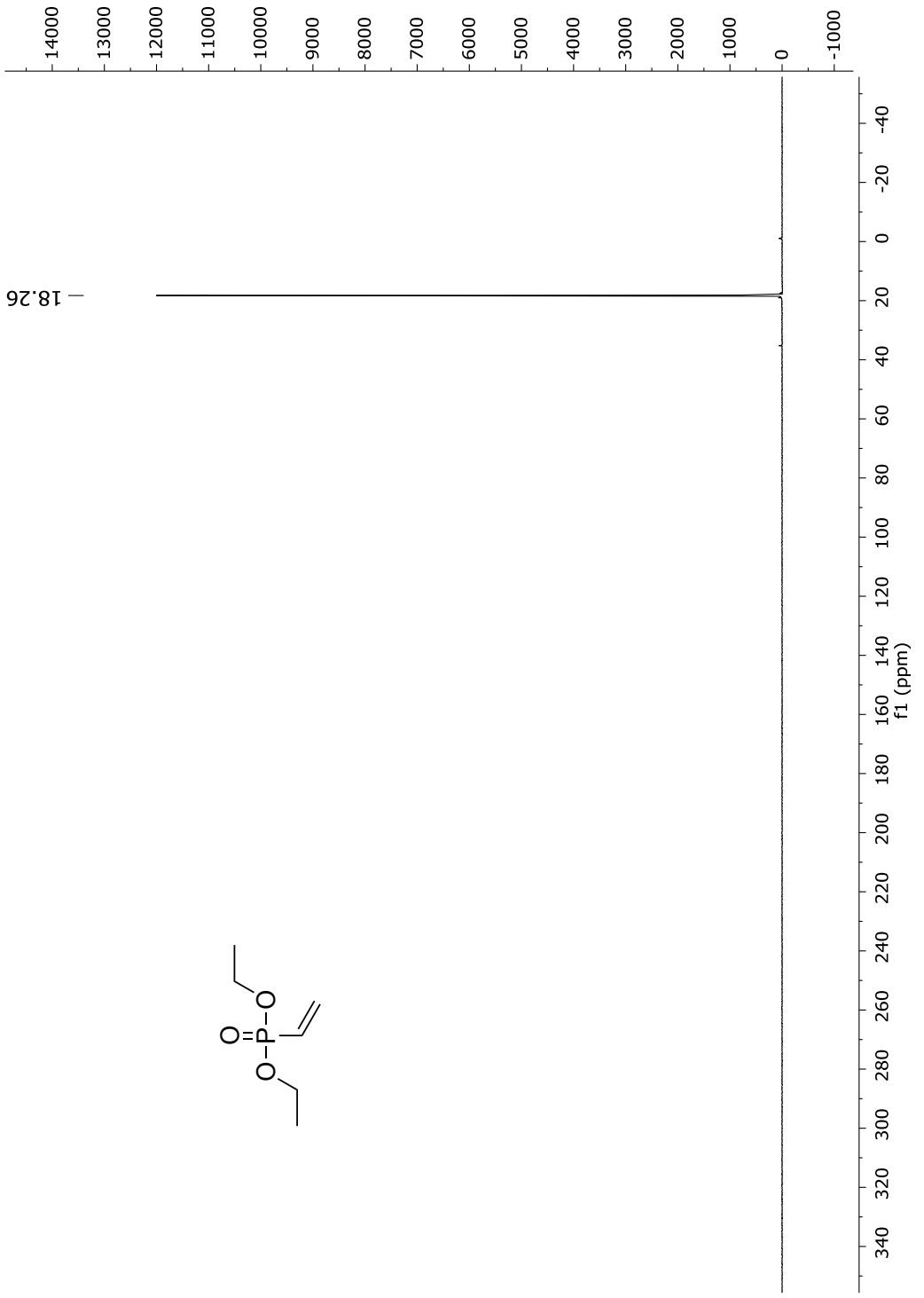

Fig. 143 ^{31}P-NMR spectrum spectrum of compound **11** (commercial from Sigma) in DMSO−d_6/H_2O=3:1 (122 MHz).

Alkylated leaving group

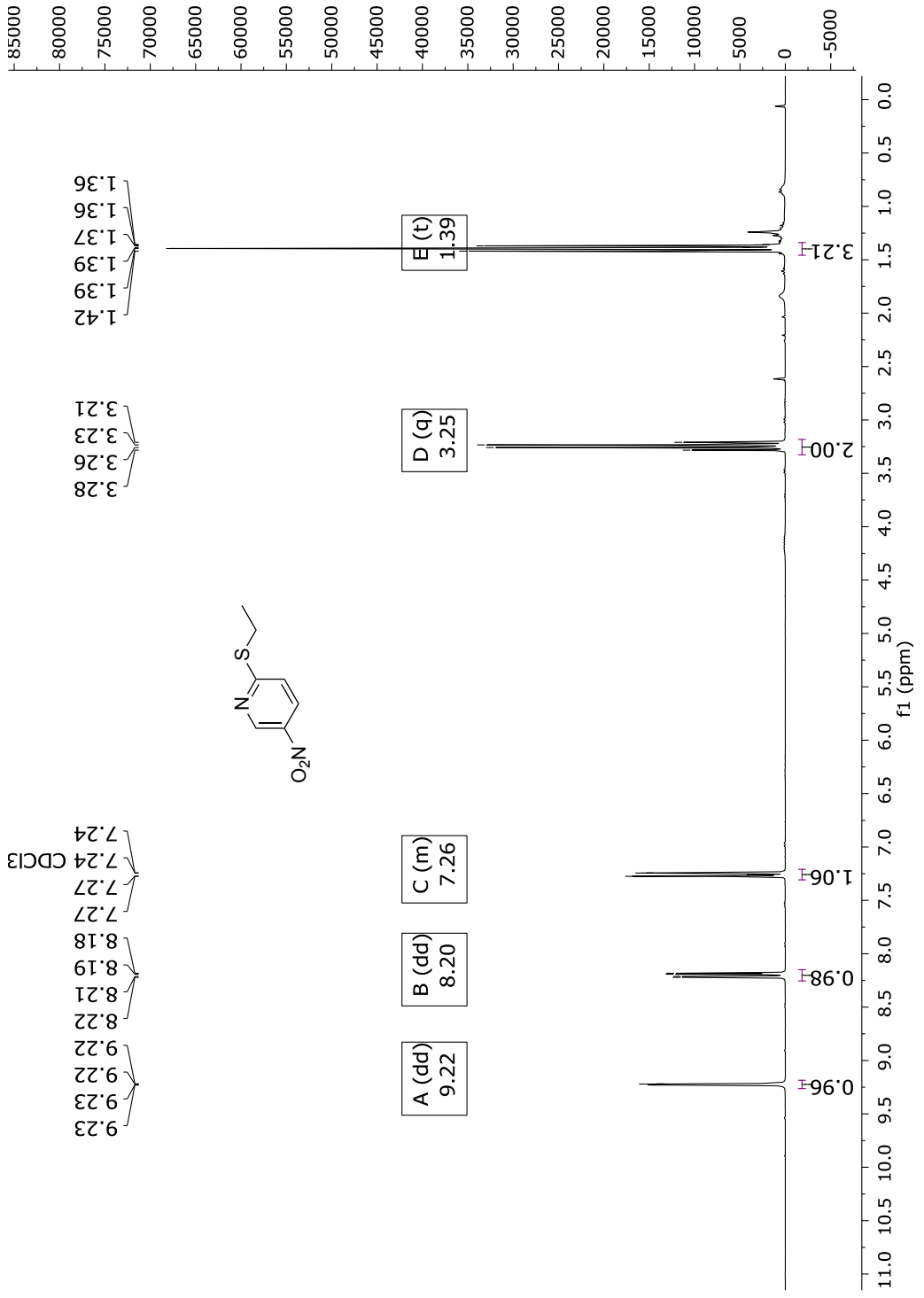

Fig. 144 ^{1}H-NMR spectrum of alkylated leaving group in $CDCl_3$ (300 MHz).

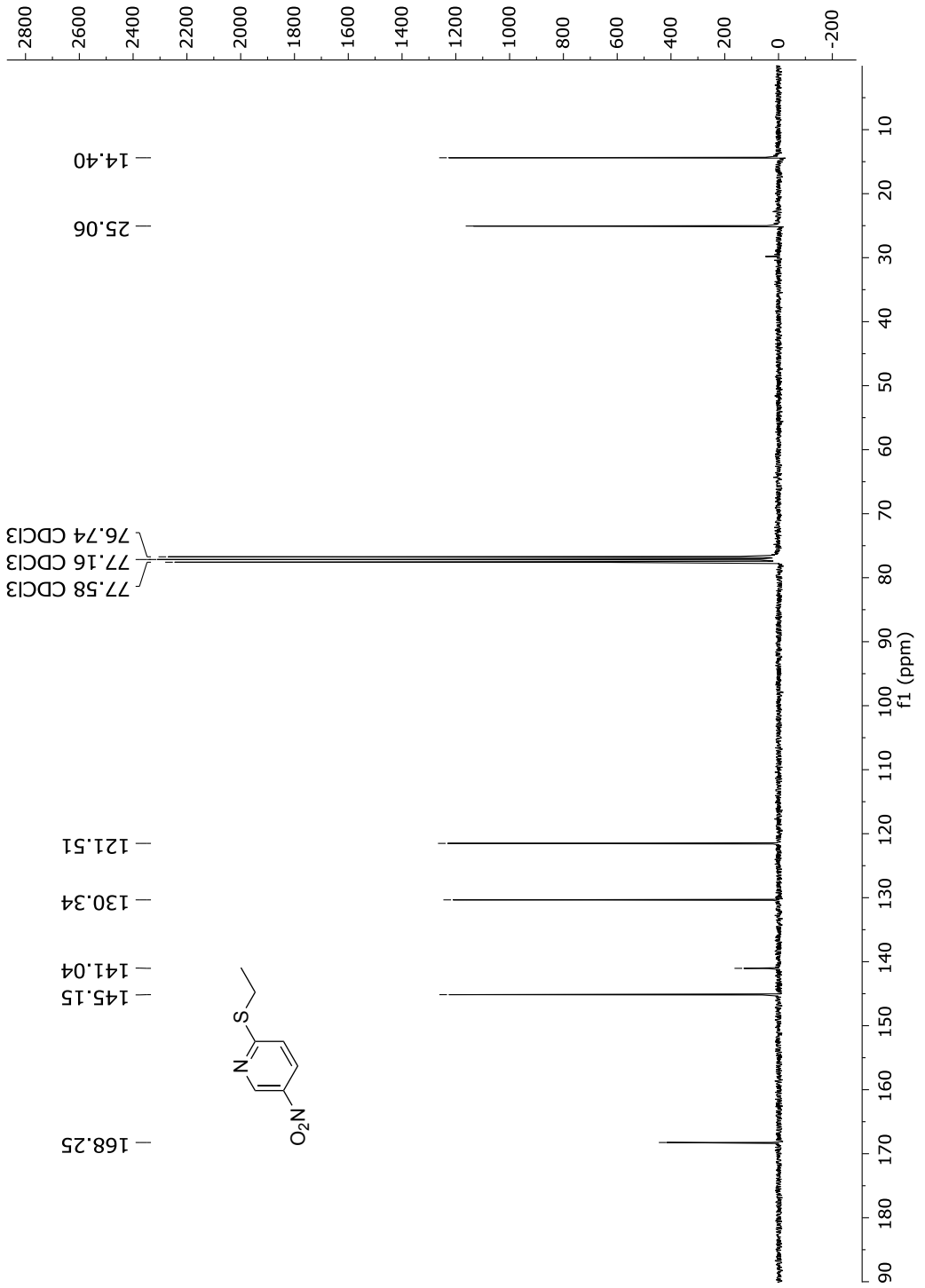

Fig. 145 ^{13}C-NMR spectrum of alkylated leaving group in $CDCl_3$ (75 MHz).

2-(Benzyldisulfaneyl)-5-nitropyridine (14)

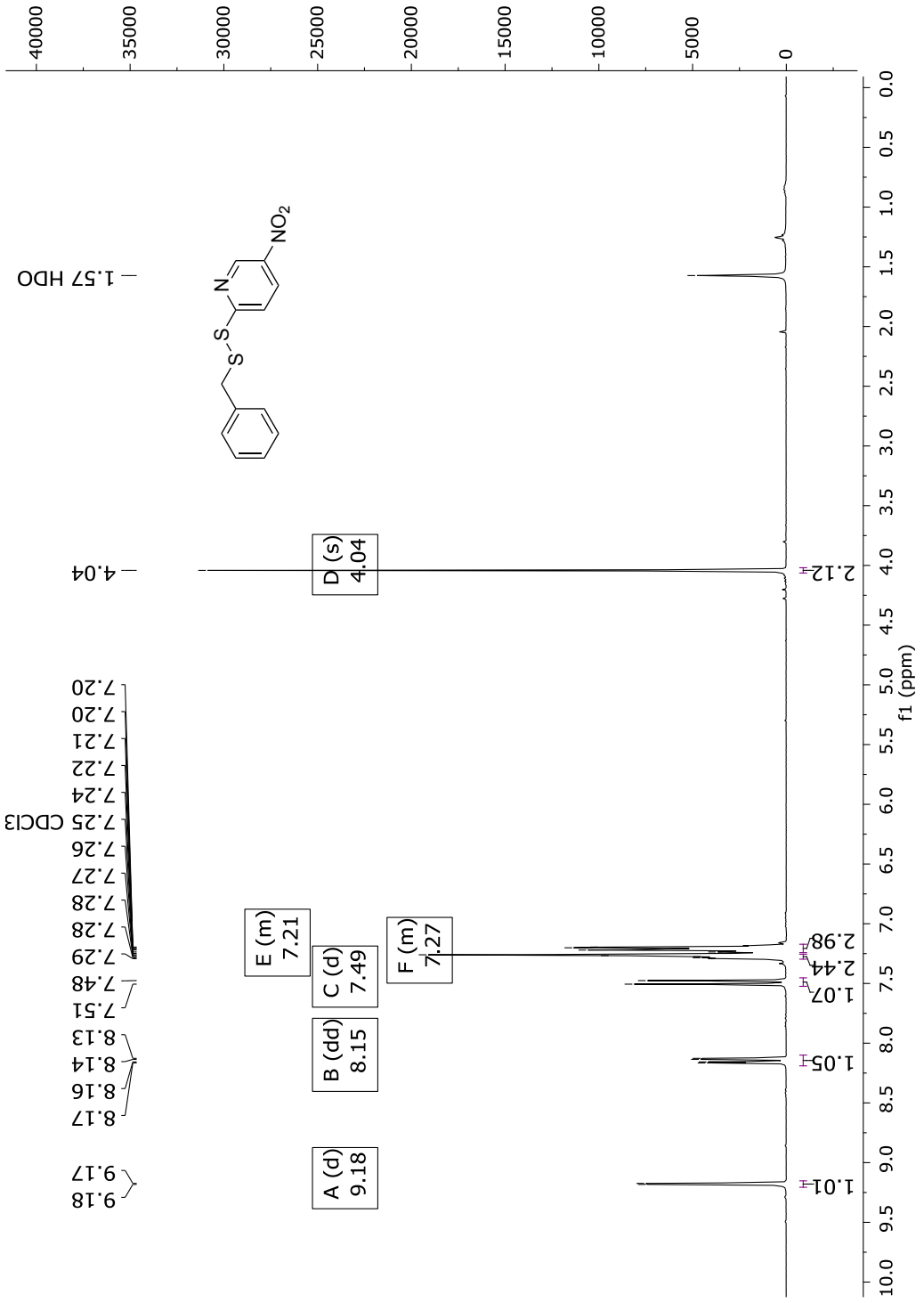

Fig. 146 ^{1}H-NMR spectrum of compound **14** in $CDCl_3$ (300 MHz).

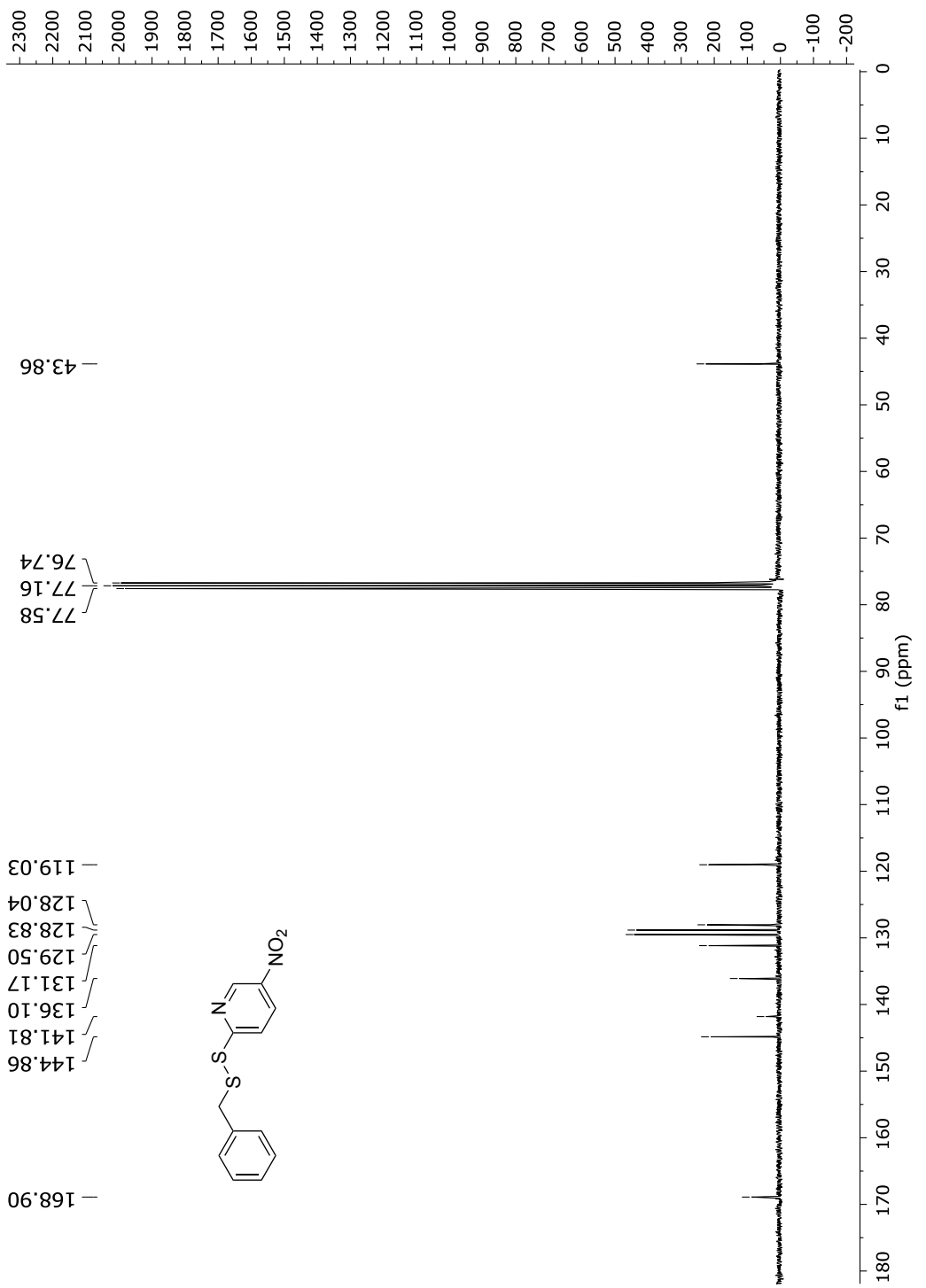

Fig. 147 ^{13}C-NMR spectrum of compound **14** in $CDCl_3$ (75 MHz).

2-(Biotinyldisulfaneyl)-5-nitropyridine (15)

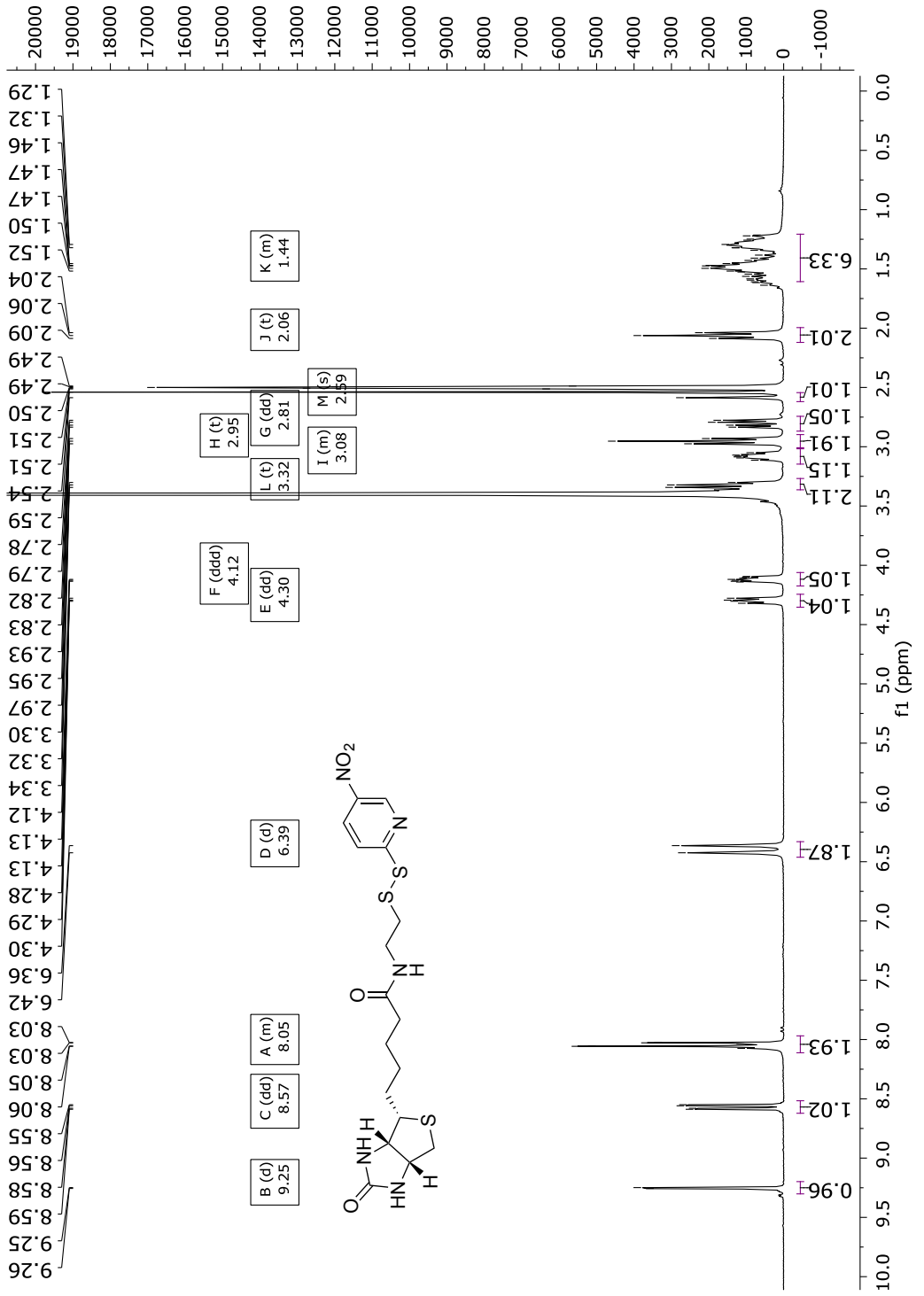

Fig. 148 ^{1}H-NMR spectrum of compound **15** in DMSO−d_6 (300 MHz).

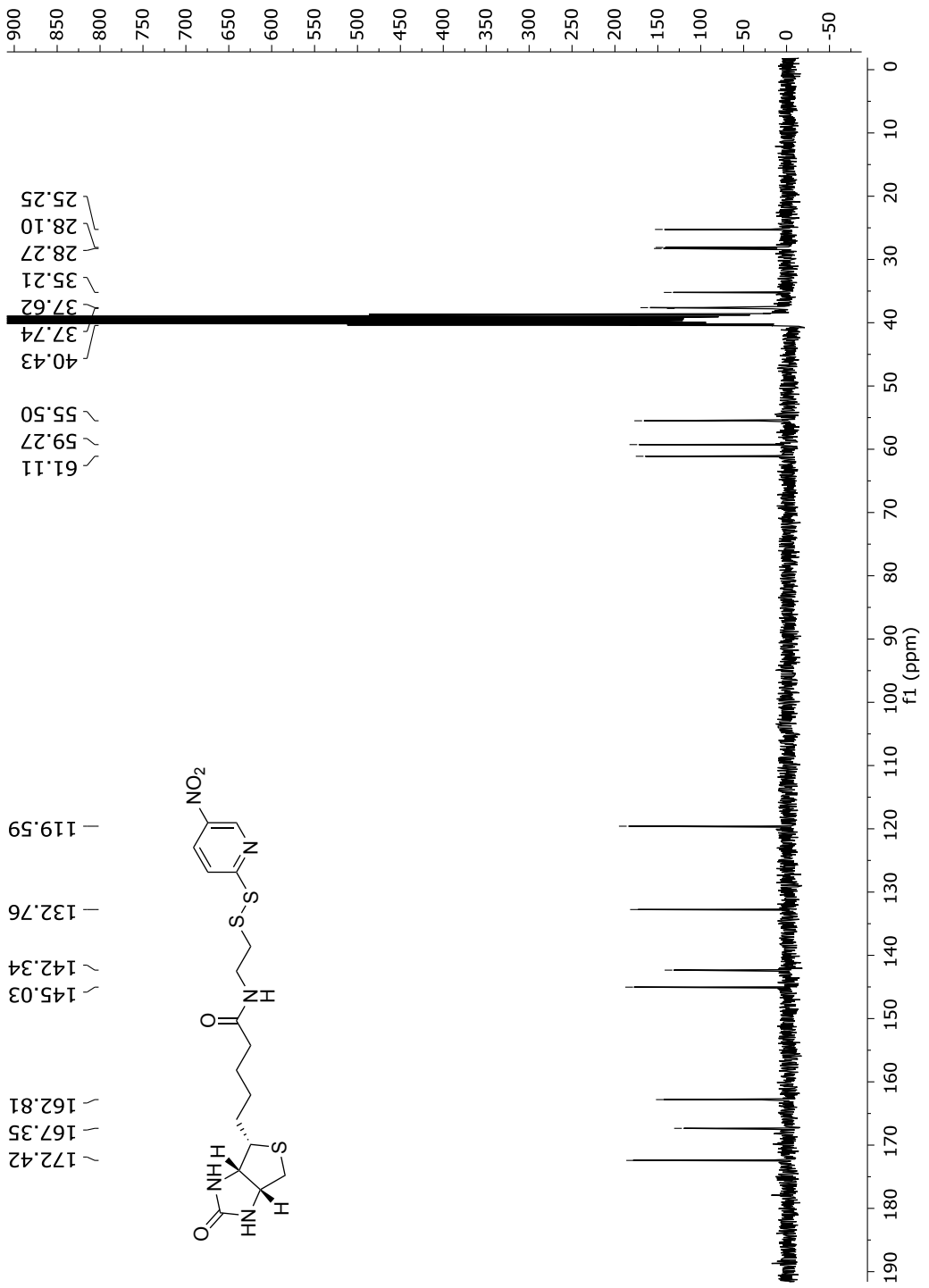

Fig. 149 ^{13}C-NMR spectrum of compound **15** in DMSO−d_6 (75 MHz).

3-((5-Nitropyridin-2-yl)disulfaneyl)propanoic acid (16)

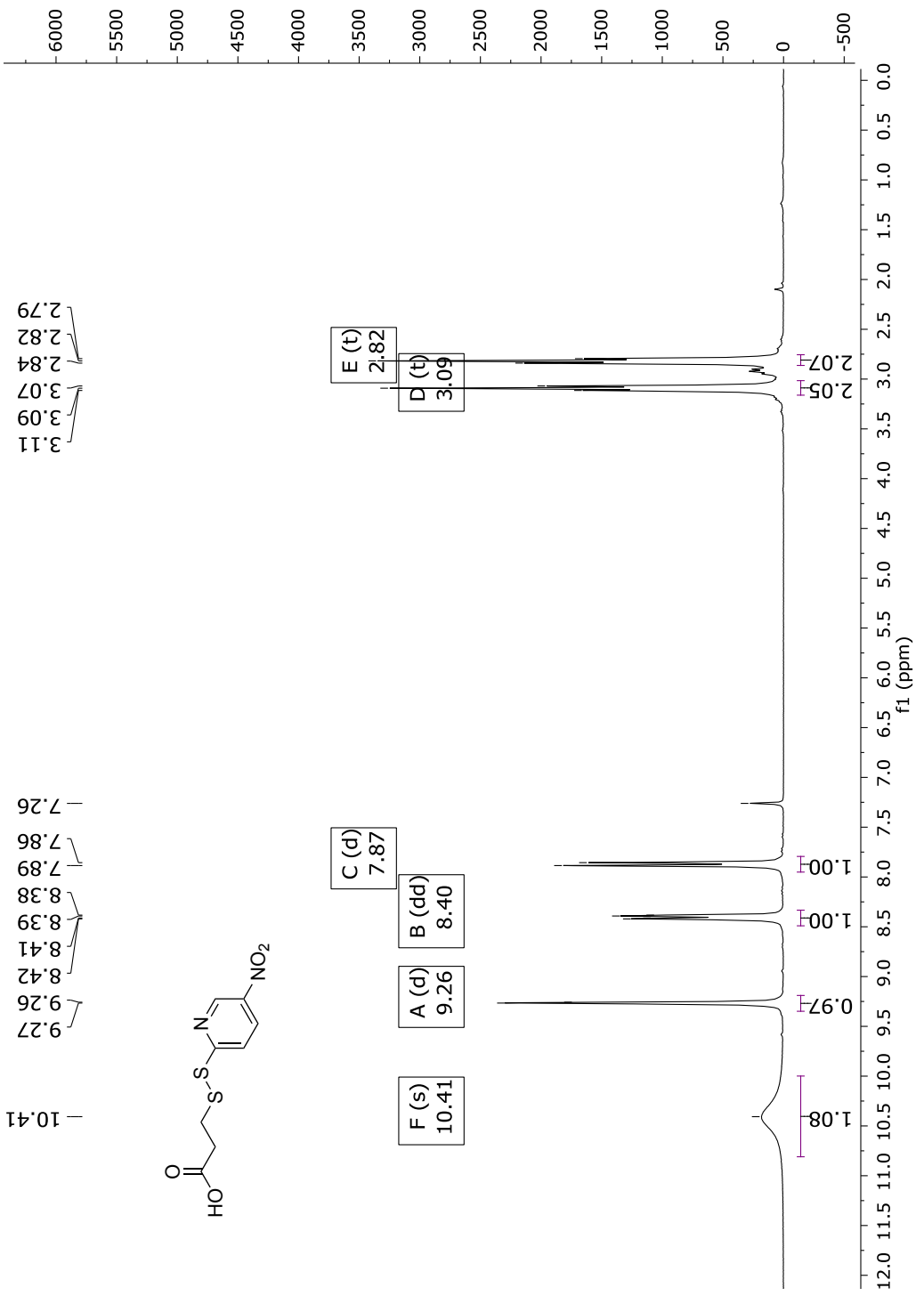

Fig. 150 ^{1}H-NMR spectrum of compound **16** in $CDCl_3$ (300 MHz).

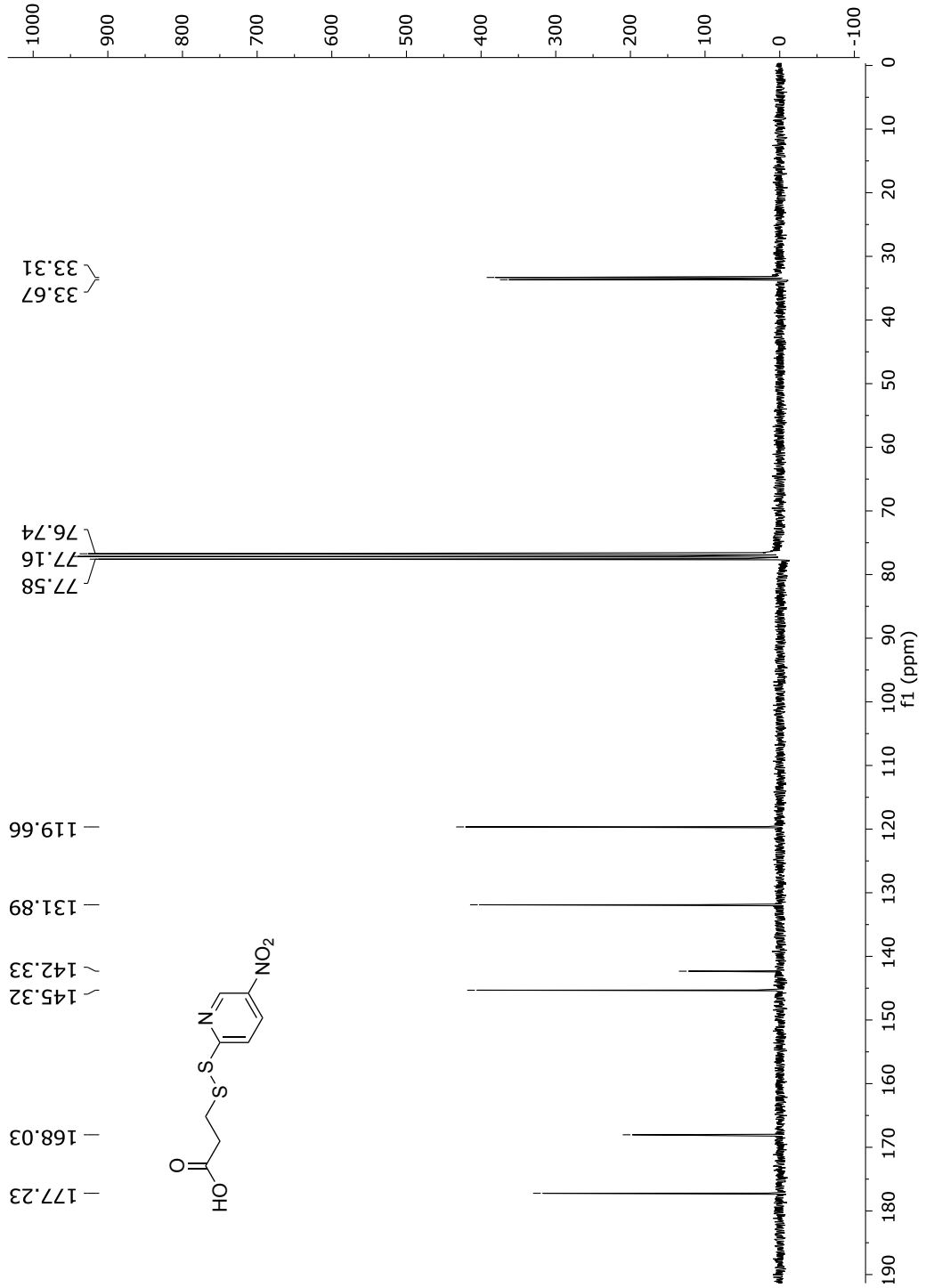

Fig. 151 ^{13}C-NMR spectrum of compound **16** in $CDCl_3$ (75 MHz).

_S_-Benzyl _O_-ethyl vinylphosphonothiolate (17)

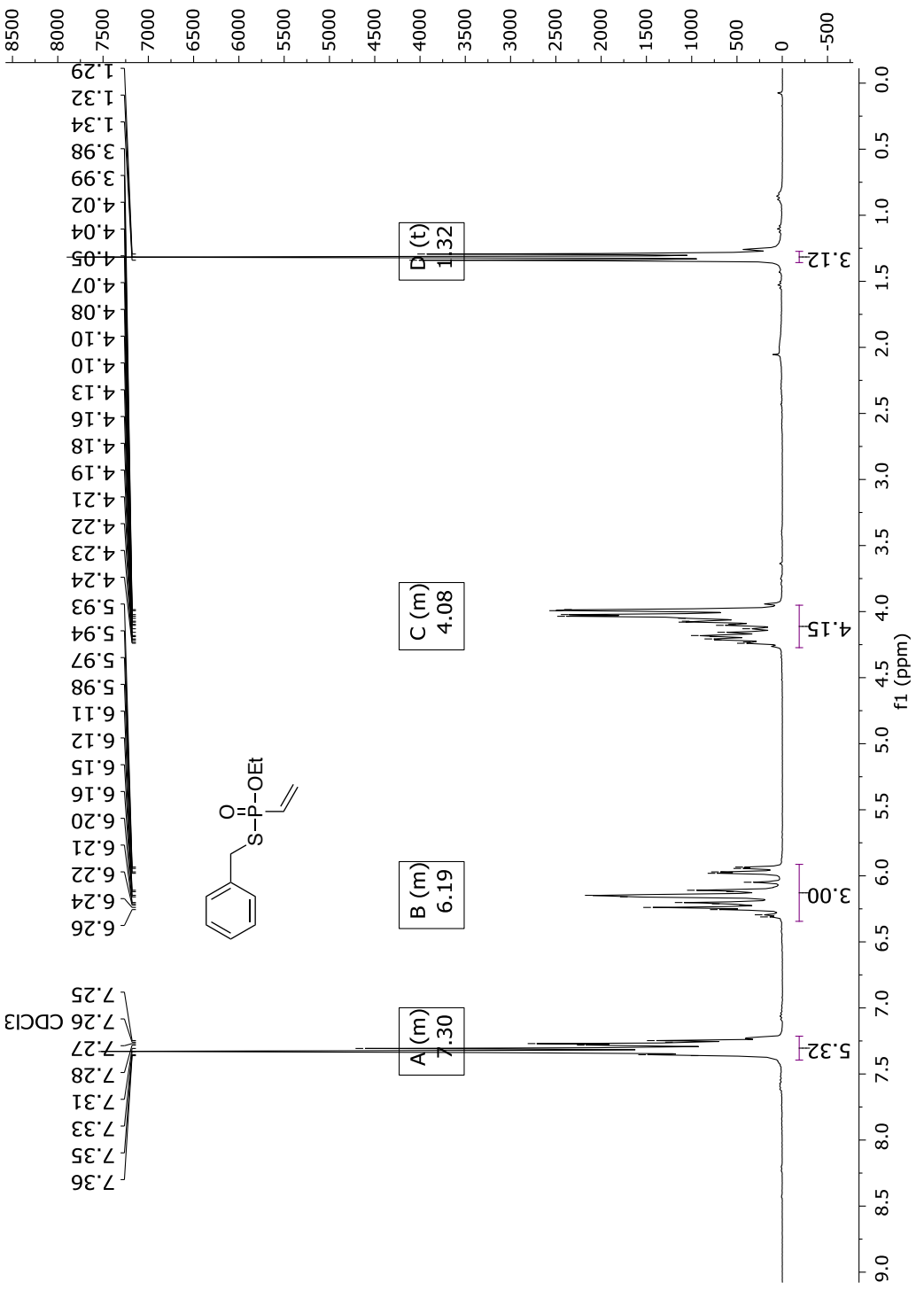

Fig. 152 ^{1}H-NMR spectrum of compound **17** in $CDCl_3$ (300 MHz).

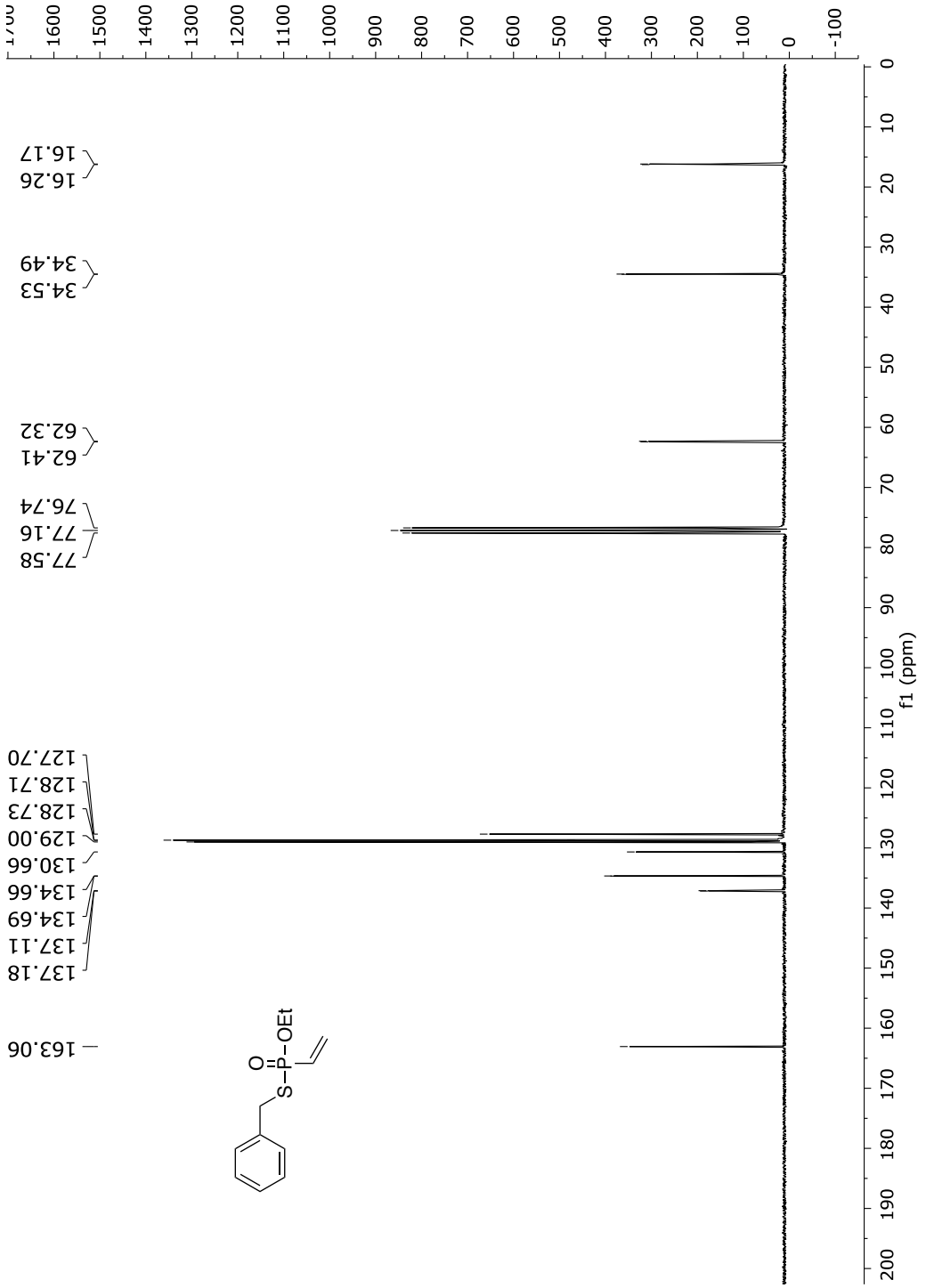

Fig. 153 ^{13}C-NMR spectrum of compound **17** in $CDCl_3$ (75 MHz).

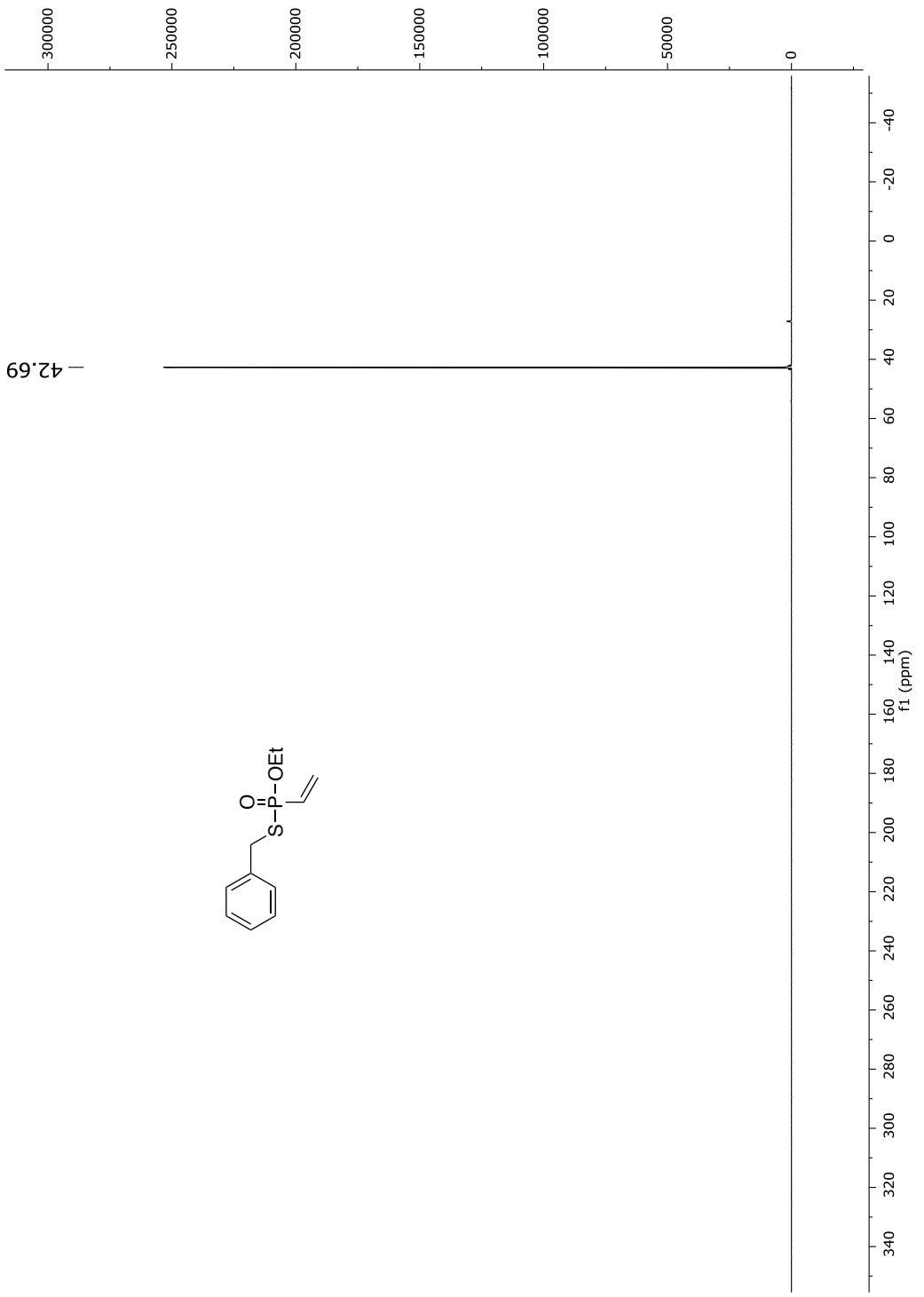

Fig. 154 ^{31}P-NMR spectrum of compound **17** in $CDCl_3$ (122 MHz).

S-Biotin O-ethyl vinylphosphonothiolate (18)

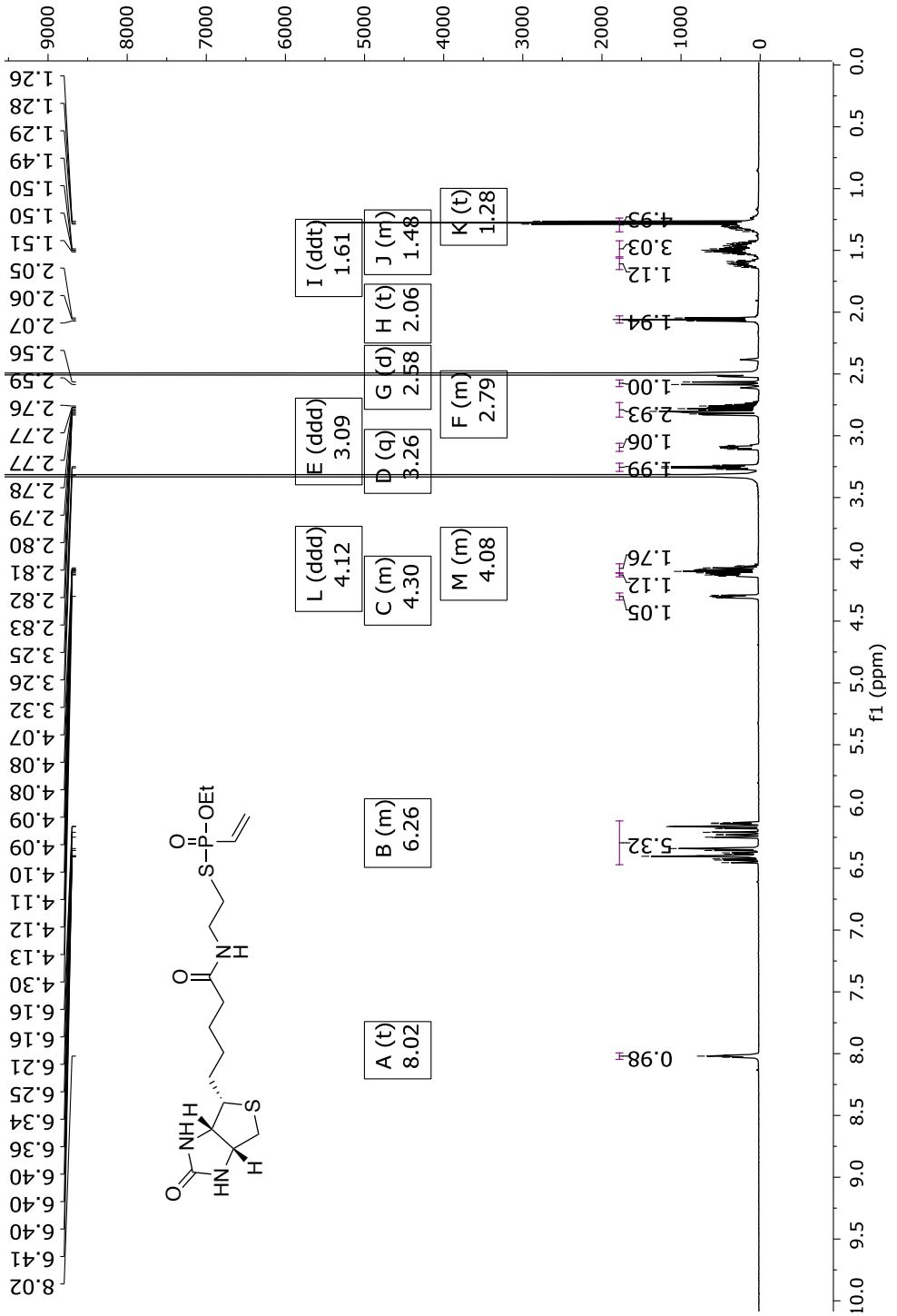

Fig. 155 ^{1}H-NMR spectrum of compound **18** in DMSO−d_6 (600 MHz).

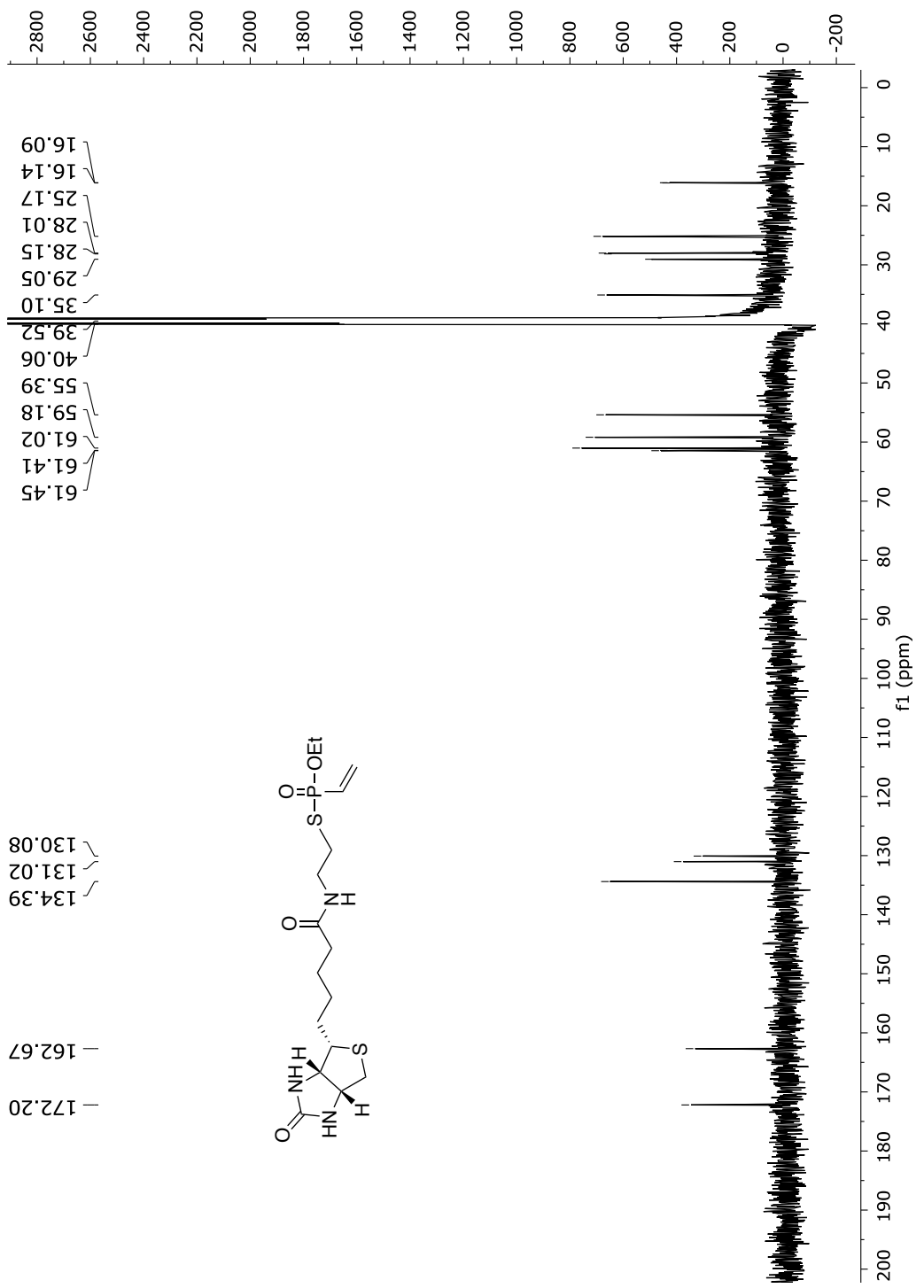

Fig. 156 ^{13}C-NMR spectrum of compound **18** in DMSO−d_6 (151 MHz).

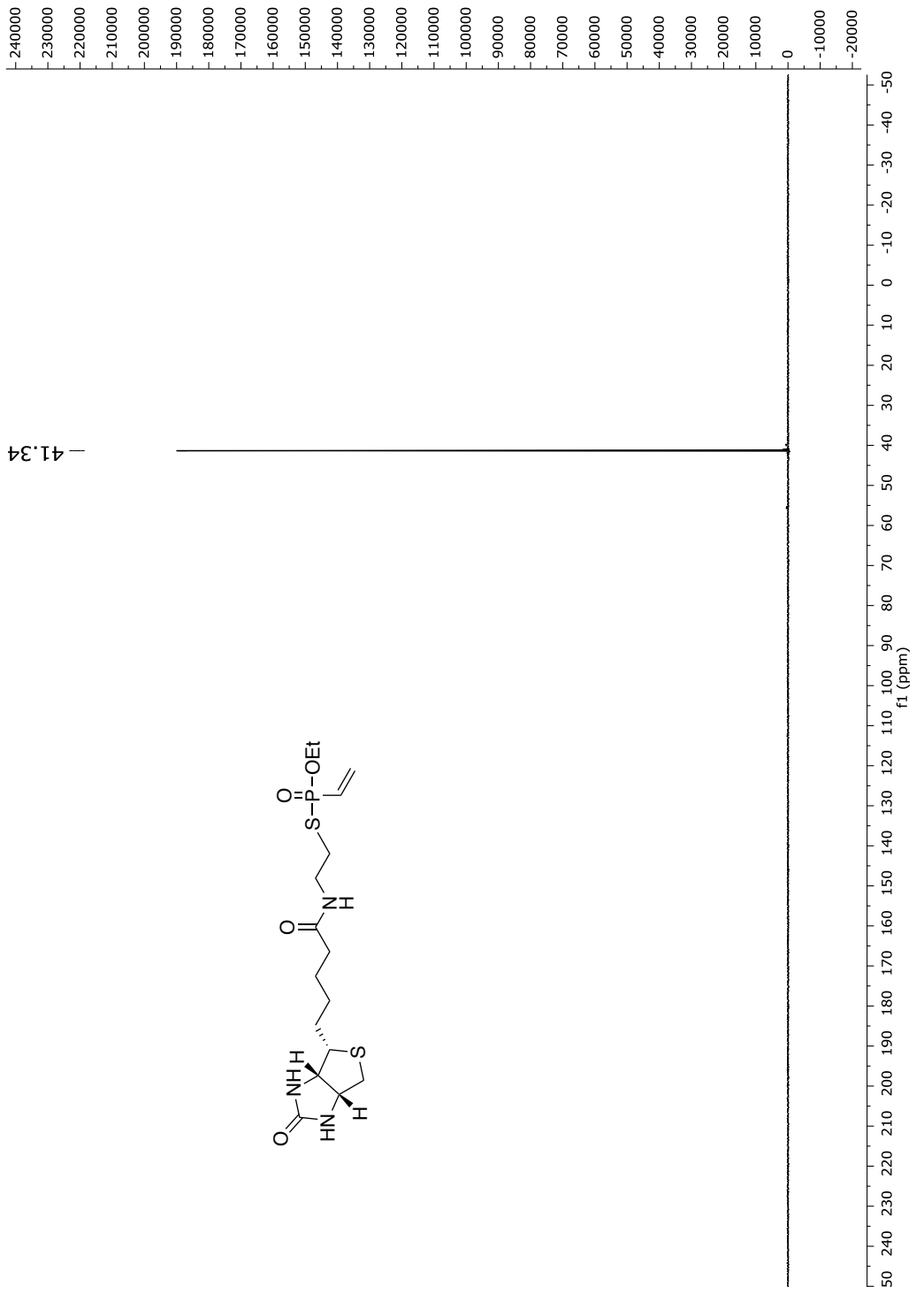

Fig. 157 ^{31}P-NMR spectrum of compound **18** in DMSO−d_6 (243 MHz).

_S_-Propanoic acid _O_-ethyl vinylphsophonothiolate (19)

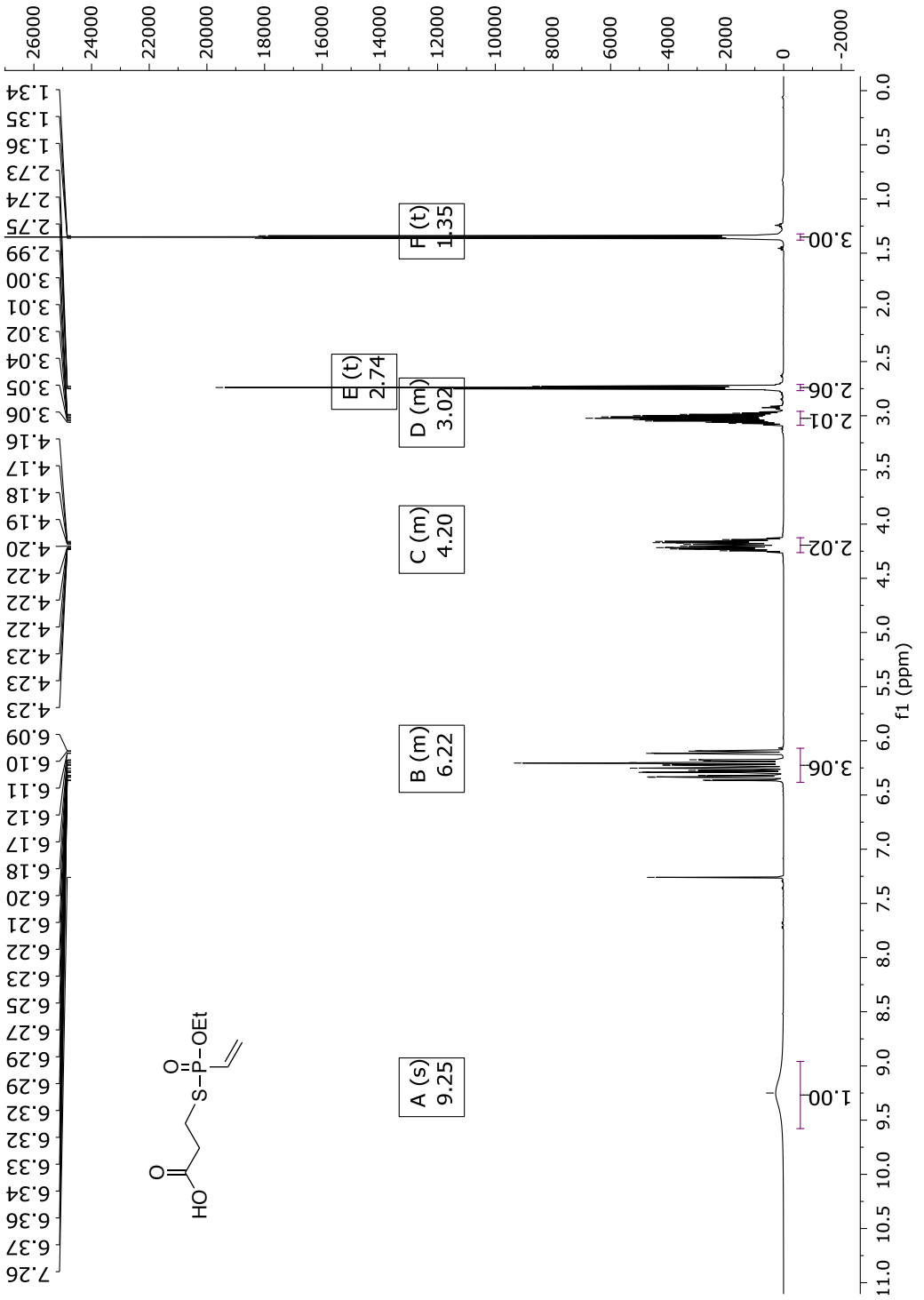

Fig. 158 ^{1}H-NMR spectrum of compound **19** in $CDCl_3$ (600 MHz).

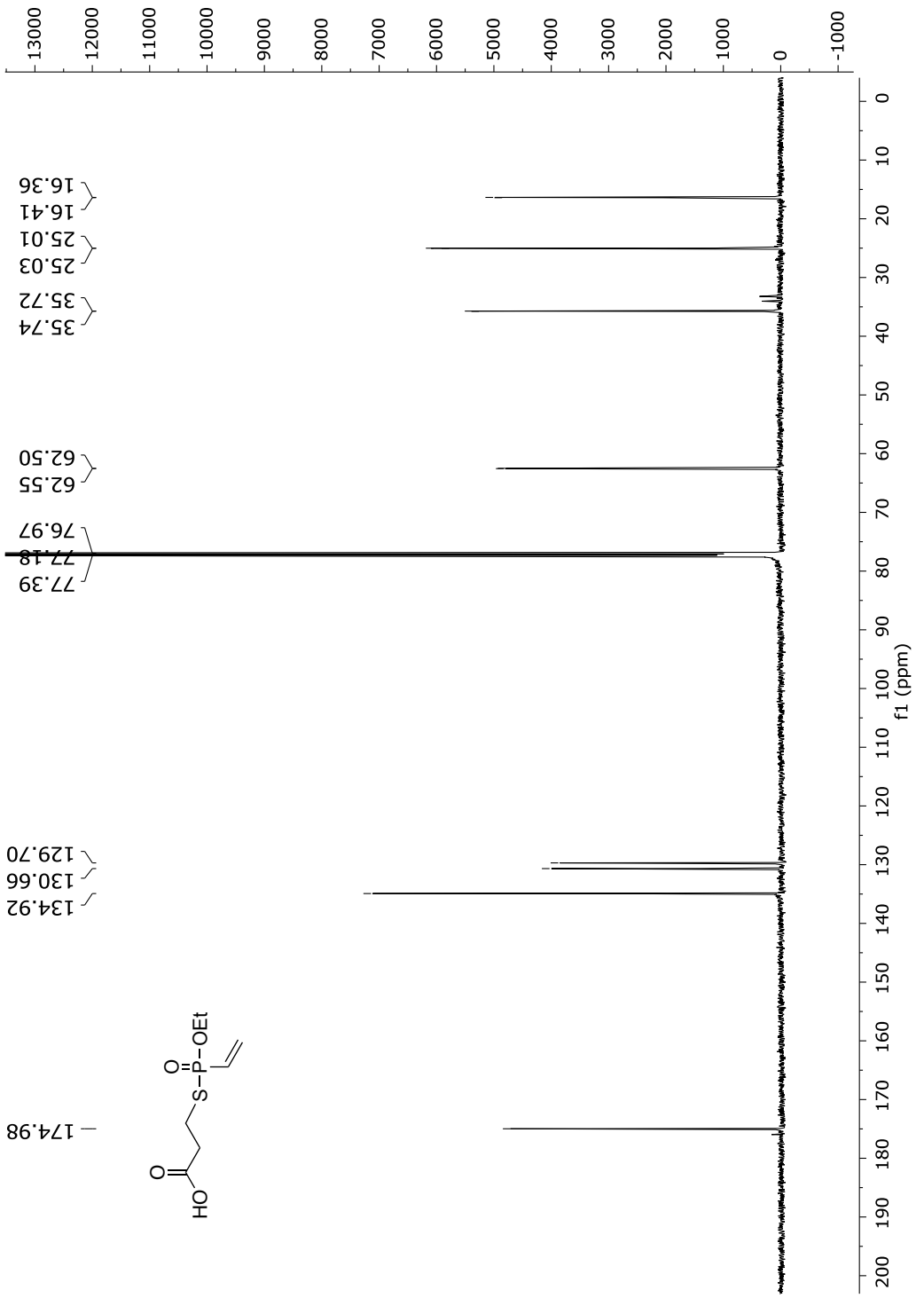

Fig. 159 ^{13}C-NMR spectrum of compound **19** in $CDCl_3$ (151 MHz).

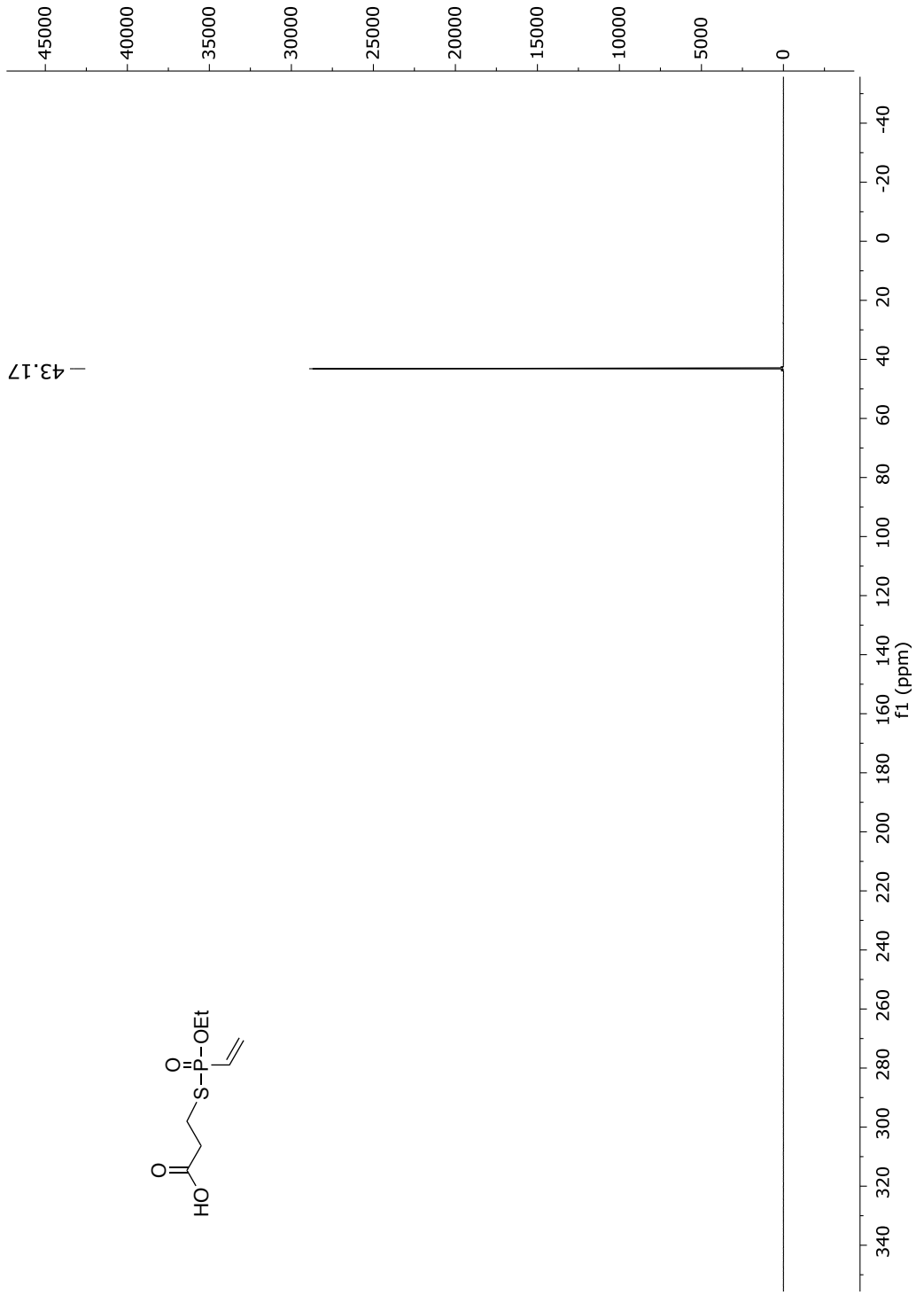

Fig. 160 ^{31}P-NMR spectrum of compound **19** in $CDCl_3$ (243 MHz).

vinylphosphonothiolate peptides (28-32)

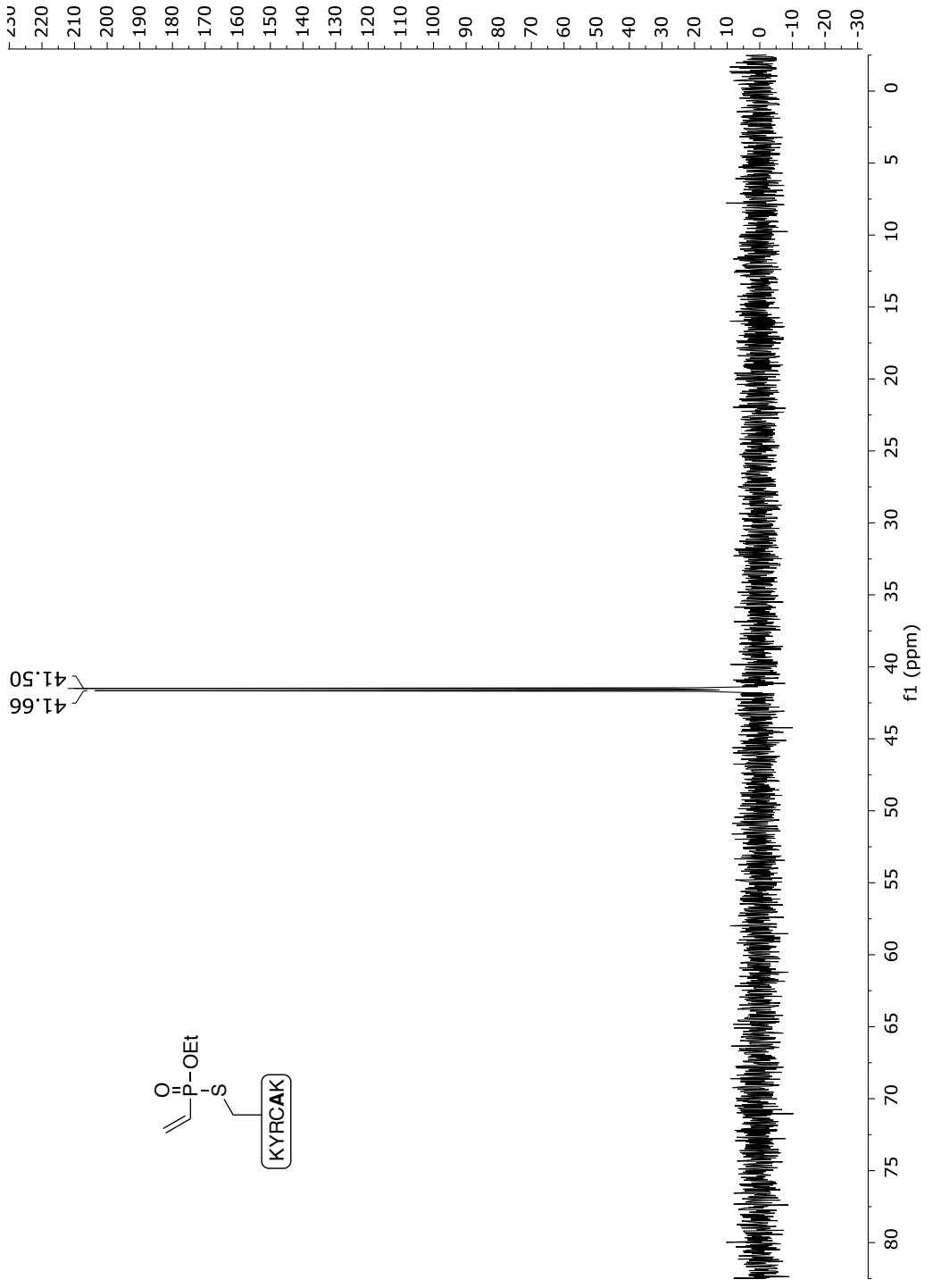

Fig. 161 ^{31}P-NMR spectrum of peptide **28** in DMSO−d_6 (two diastereoisomers) (122 MHz).

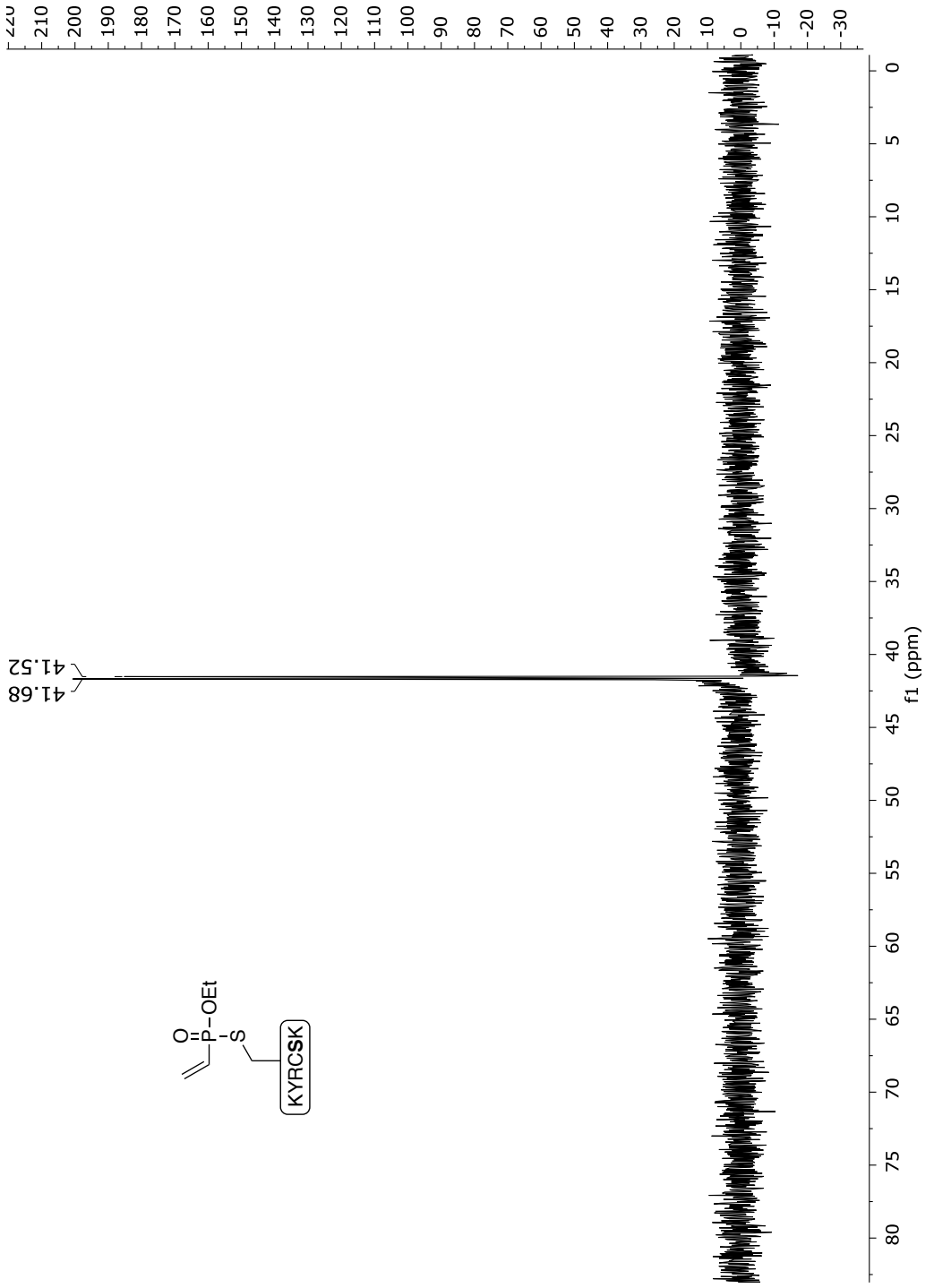

Fig. 162 ^{31}P-NMR spectrum of peptide **29** in DMSO−d_6 (two diastereoisomers) (122 MHz).

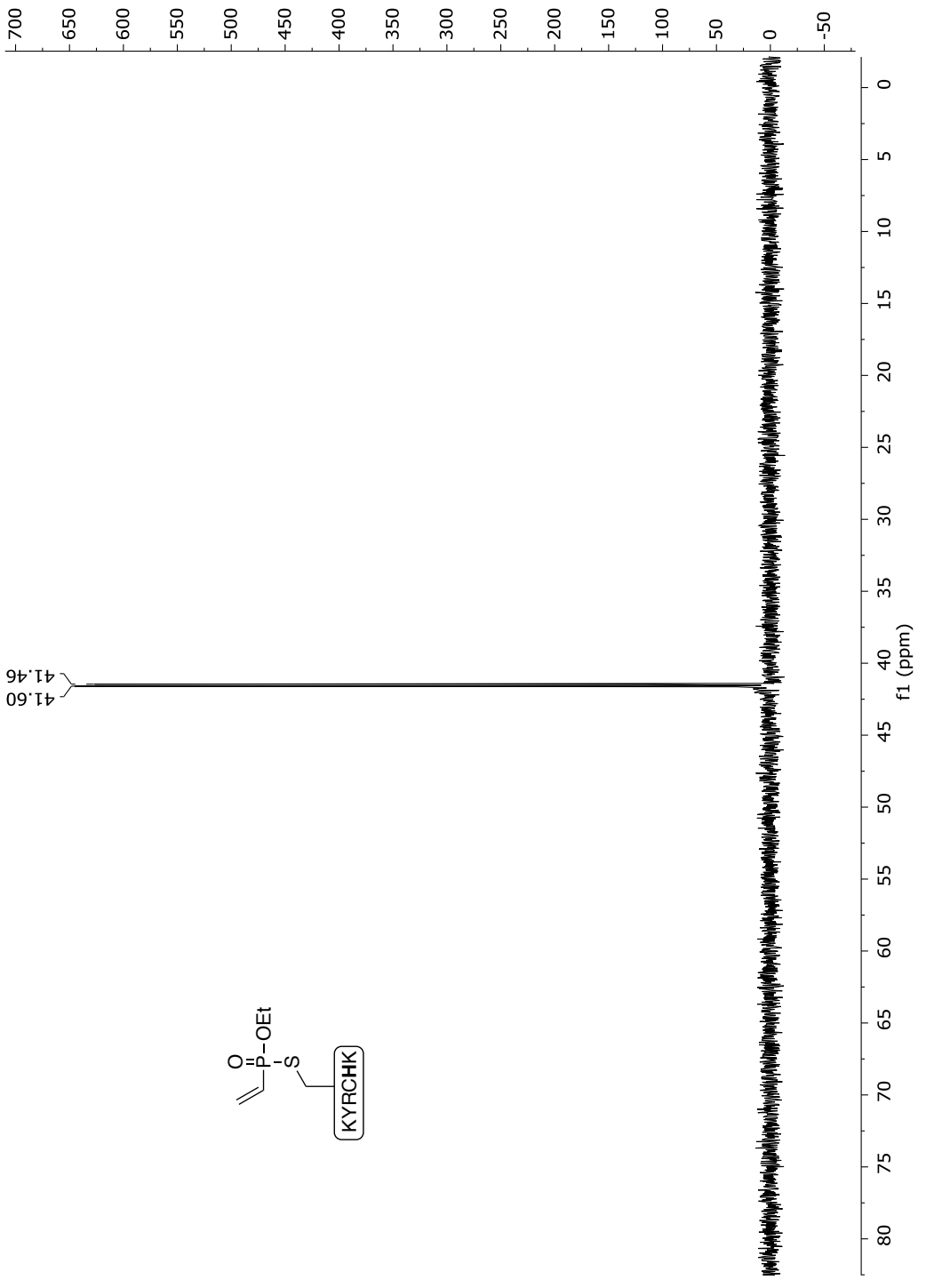

Fig. 163 ^{31}P-NMR spectrum of peptide **30** in DMSO−d_6 (two diastereoisomers) (122 MHz).

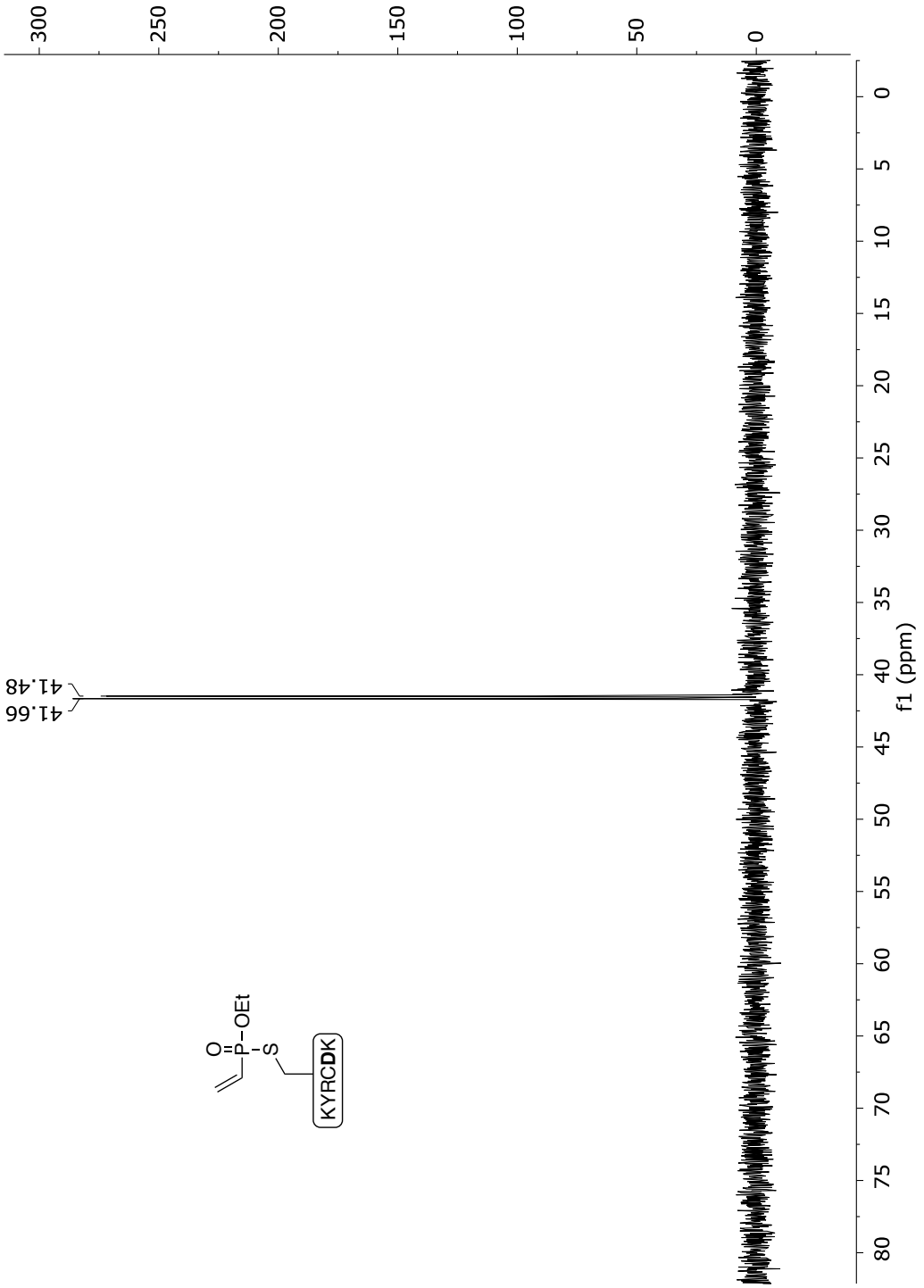

Fig. 164 ^{31}P-NMR spectrum of peptide **31** in DMSO−d_6(two diastereoisomers) (122 MHz).

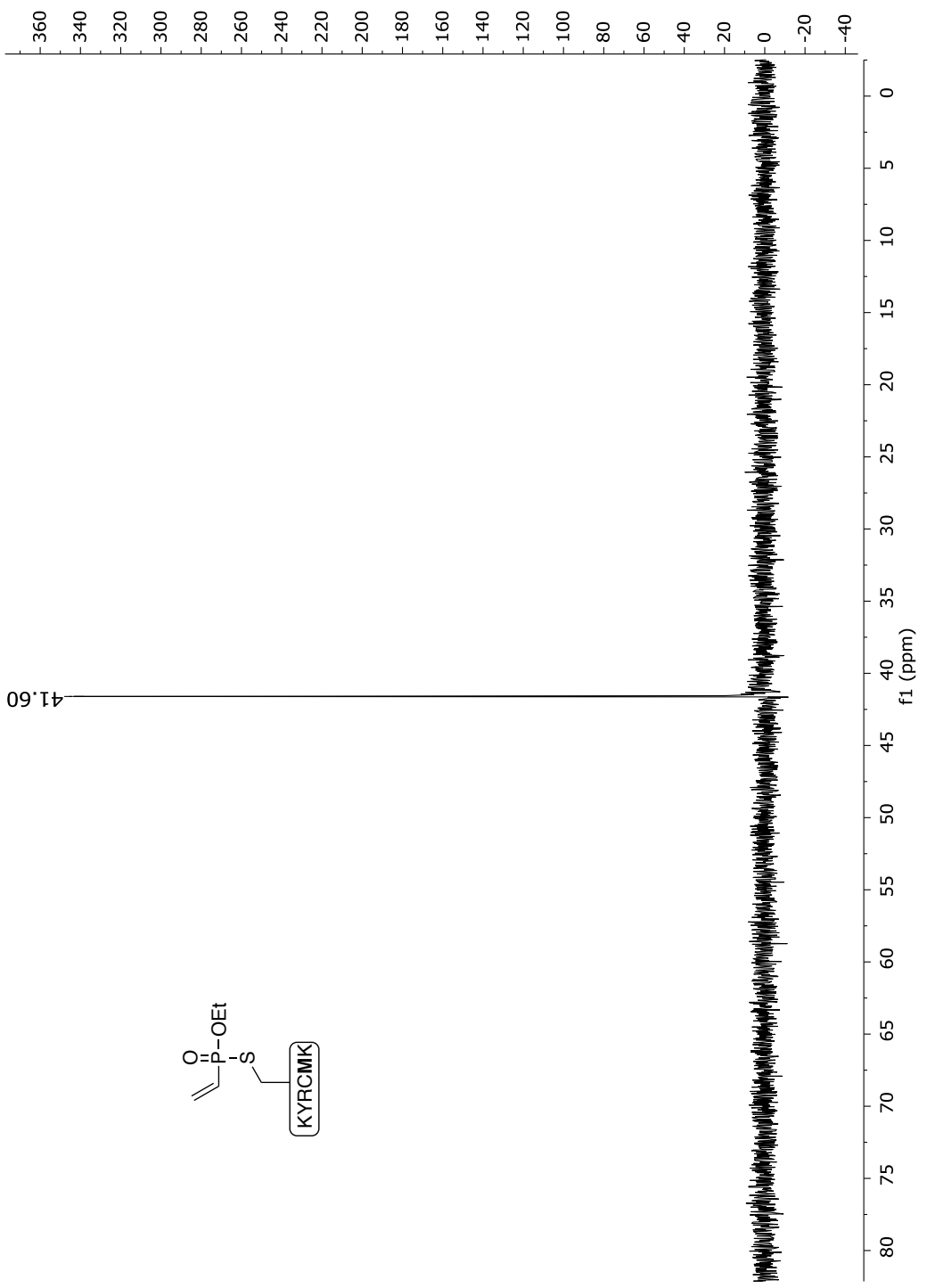

Fig. 165 ^{31}P-NMR spectrum of peptide **32** in DMSO−d_6(one diastereoisomer) (122 MHz).

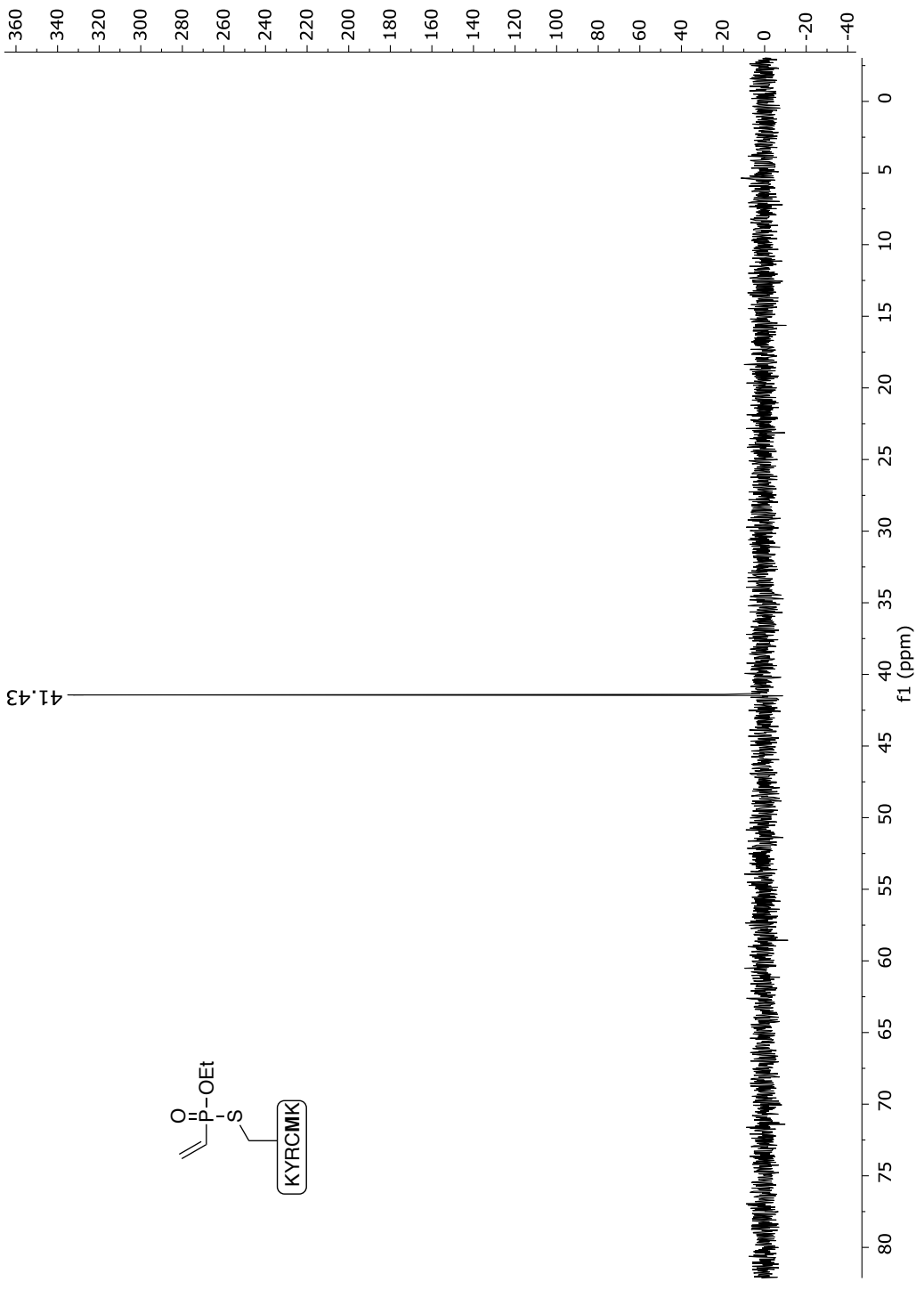

Fig. 166 ^{31}P-NMR spectrum of peptide **32** in DMSO−d_6 (one diastereoisomers) (122 MHz).

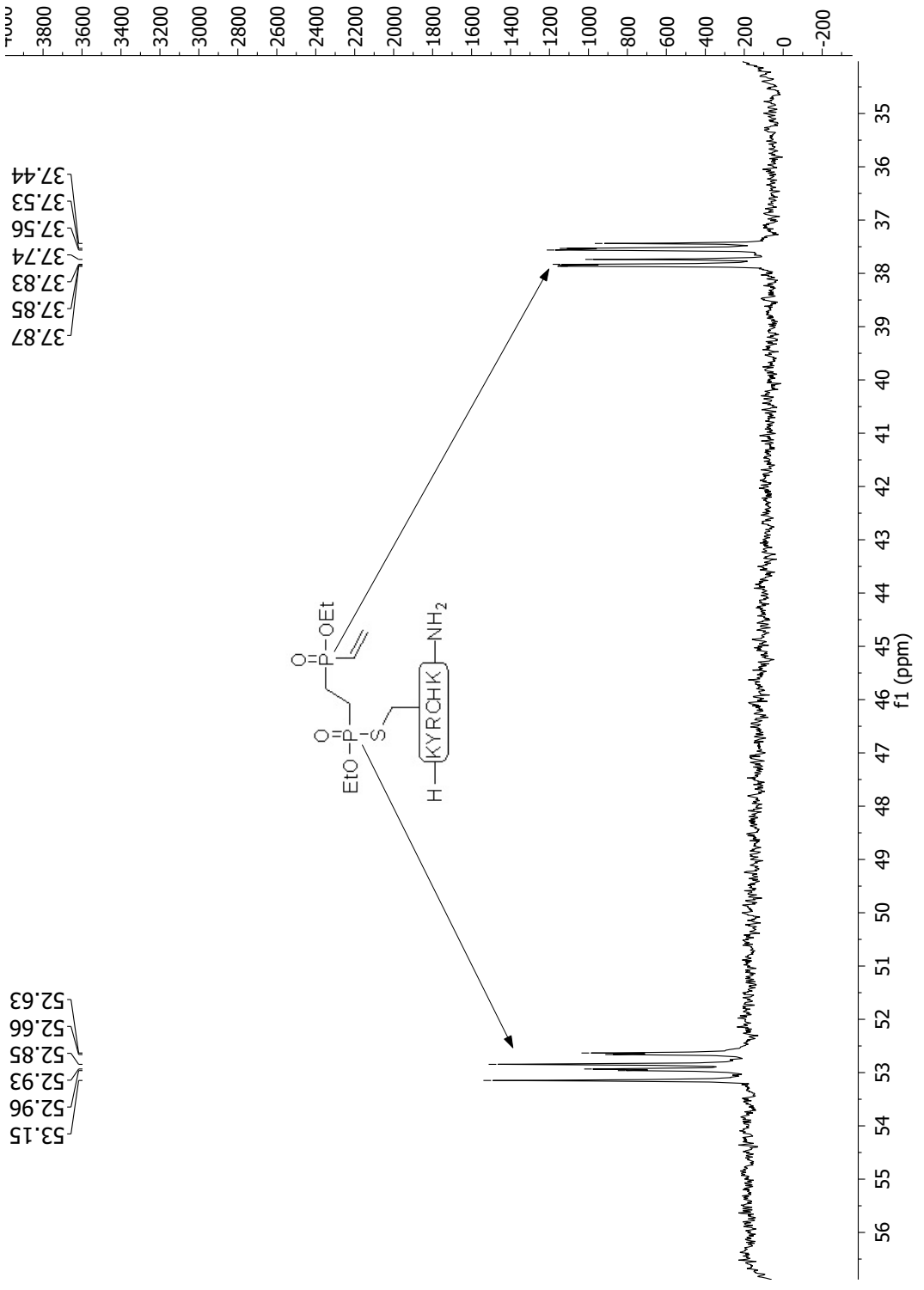

Fig. 167 ^{31}P-NMR spectrum of phosphonite-addition product to peptide **30** in DMSO−d_6 (243 MHz).

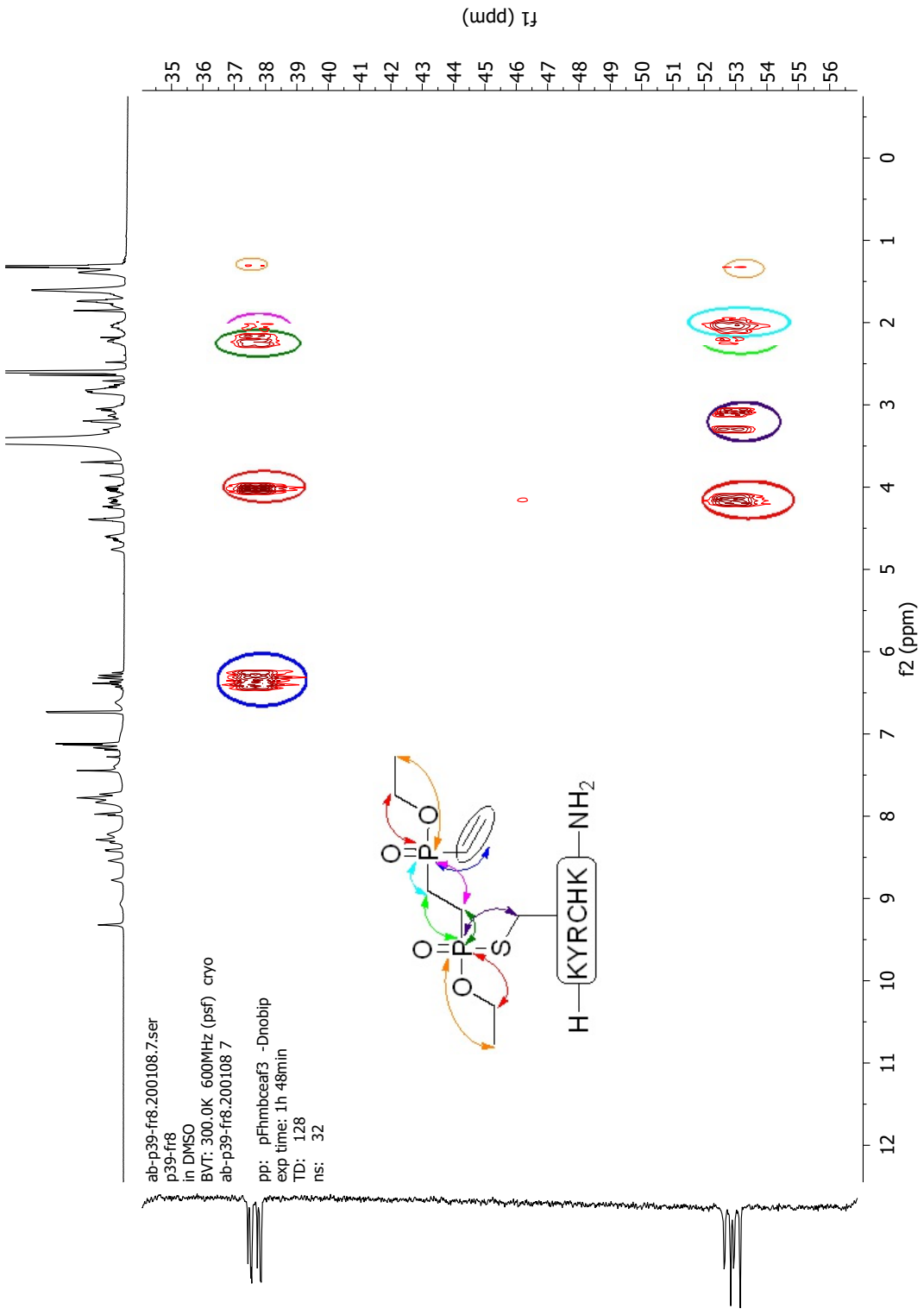

Fig. 168 ^{31}P-^{1}H-HMBC NMR spectrum of phosphonite-addition product to peptide **30** in DMSO−d_6.

1-ethoxy-1-ethynyl-*N*,*N*-diisopropylphosphanamine (33)

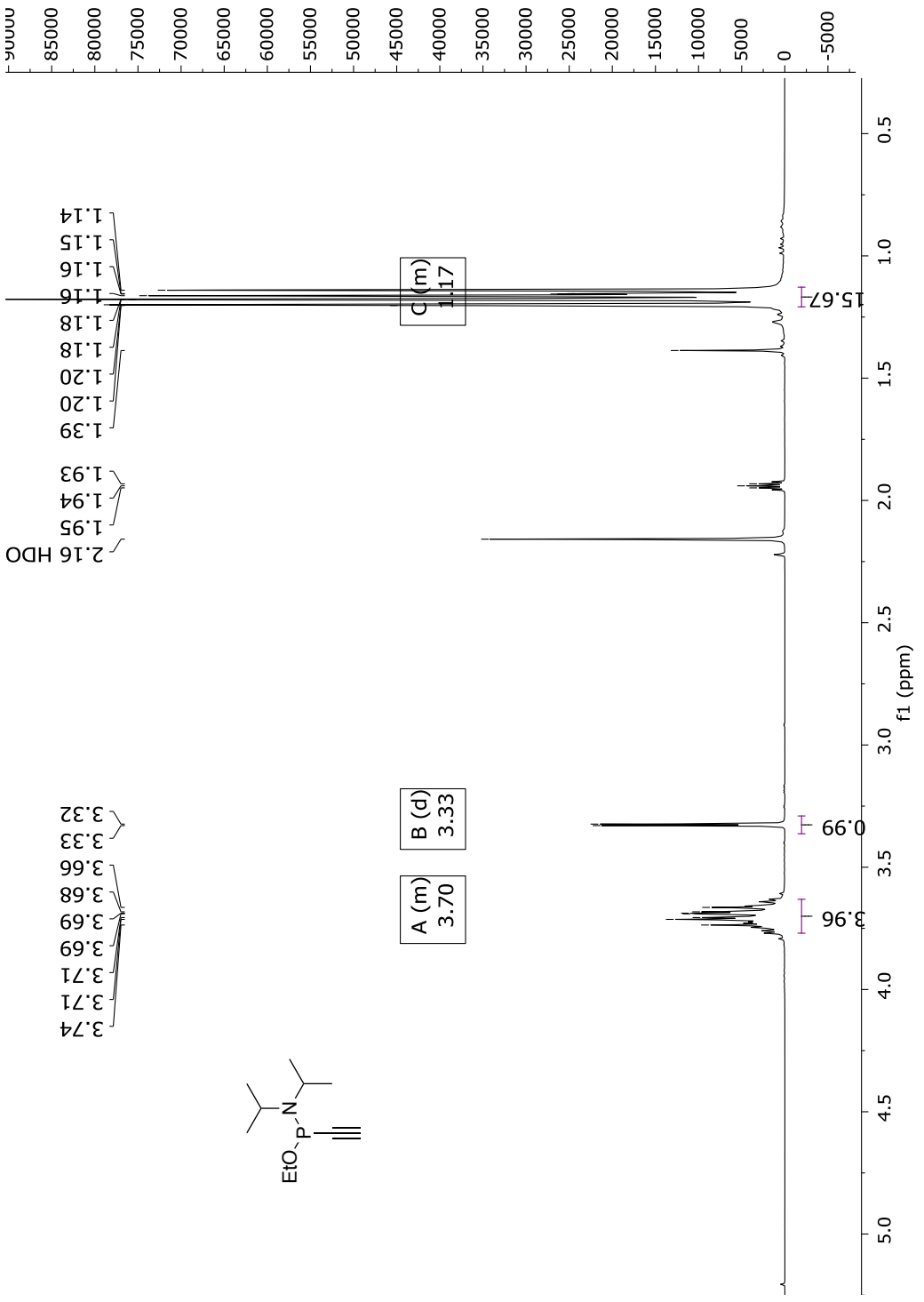

Fig. 169 ^{1}H-NMR spectrum of compound **33** in CD_3CN (300 MHz).

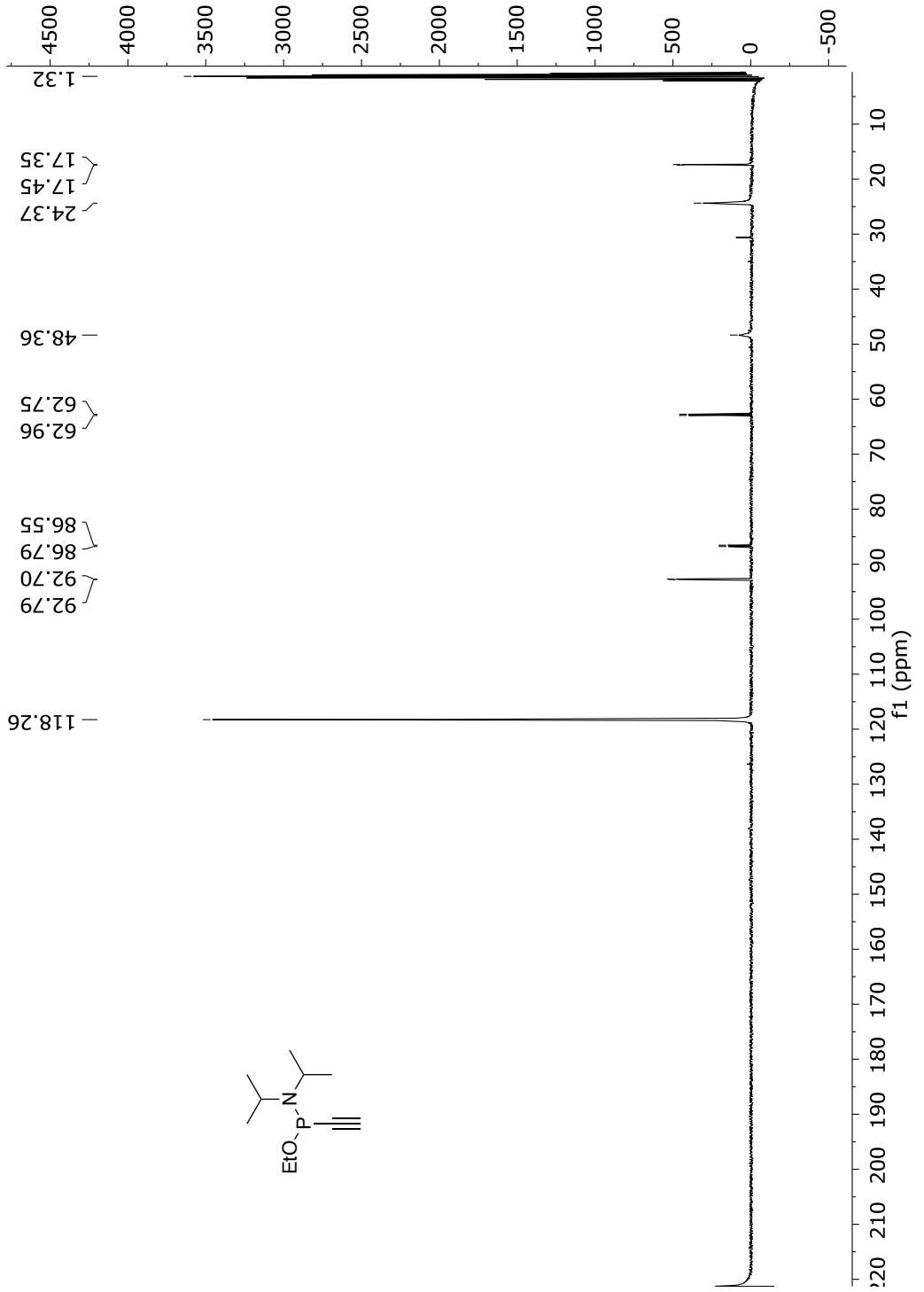

Fig. 170 ^{13}C-NMR spectrum of compound **33** in CD_3CN (75 MHz).

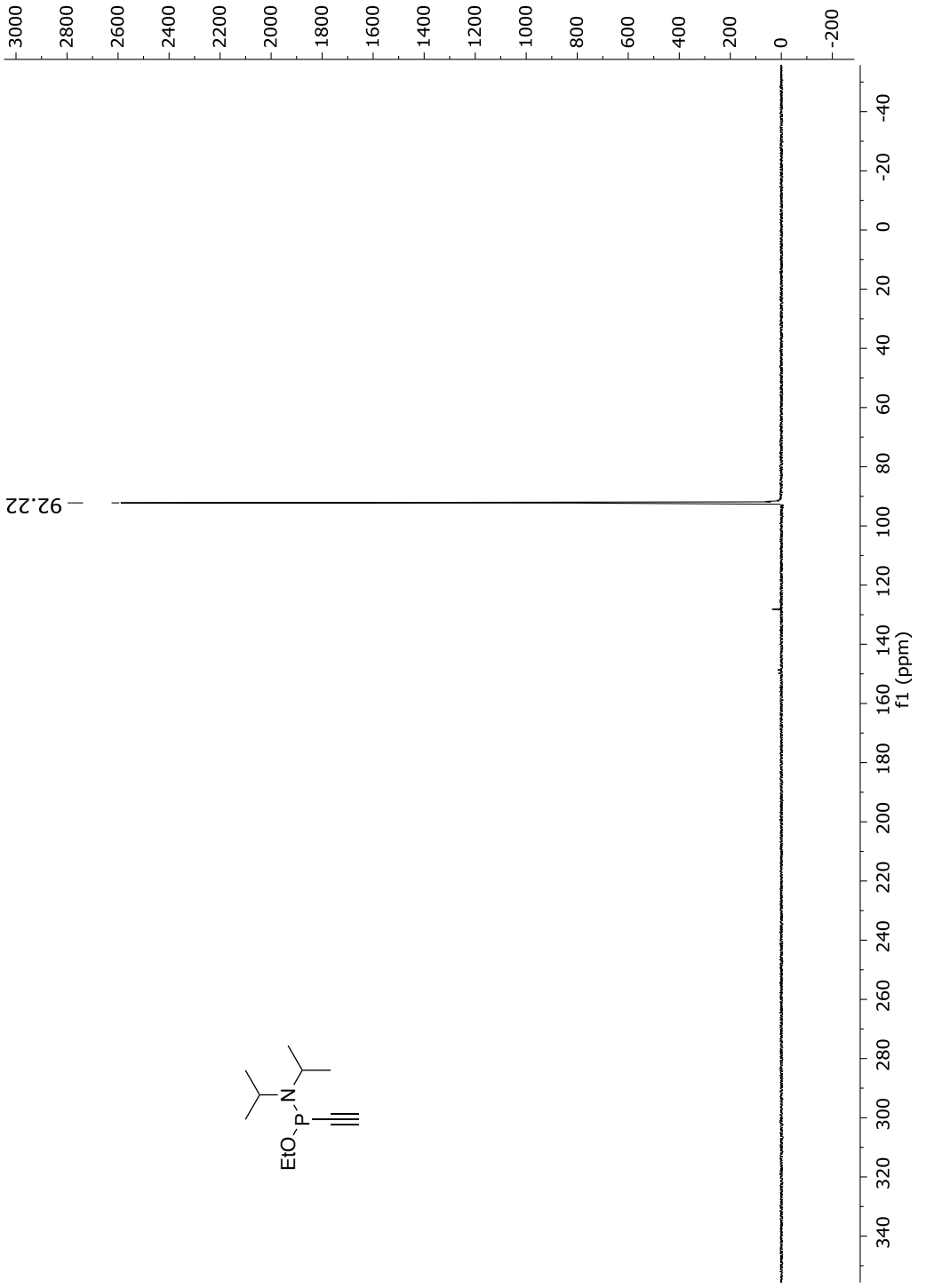

Fig. 171 ^{31}P-NMR spectrum of compound **33** in CD_3CN (122 MHz).

1-ethoxy-*N*,*N*-diisopropyl-1-vinylphosphanamine (34)

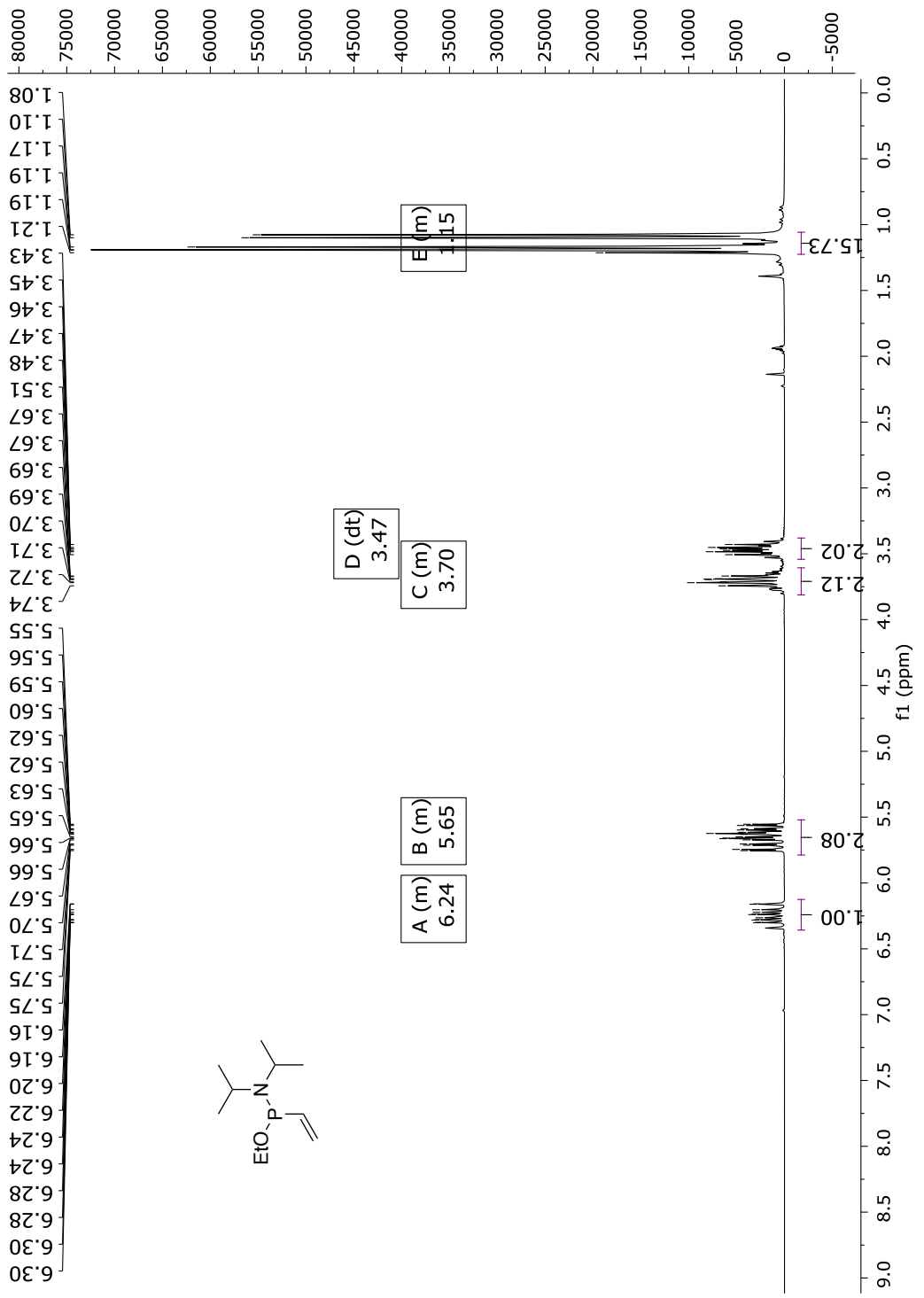

Fig. 172 ^{1}H-NMR spectrum of compound **34** in CD_3CN (300 MHz).

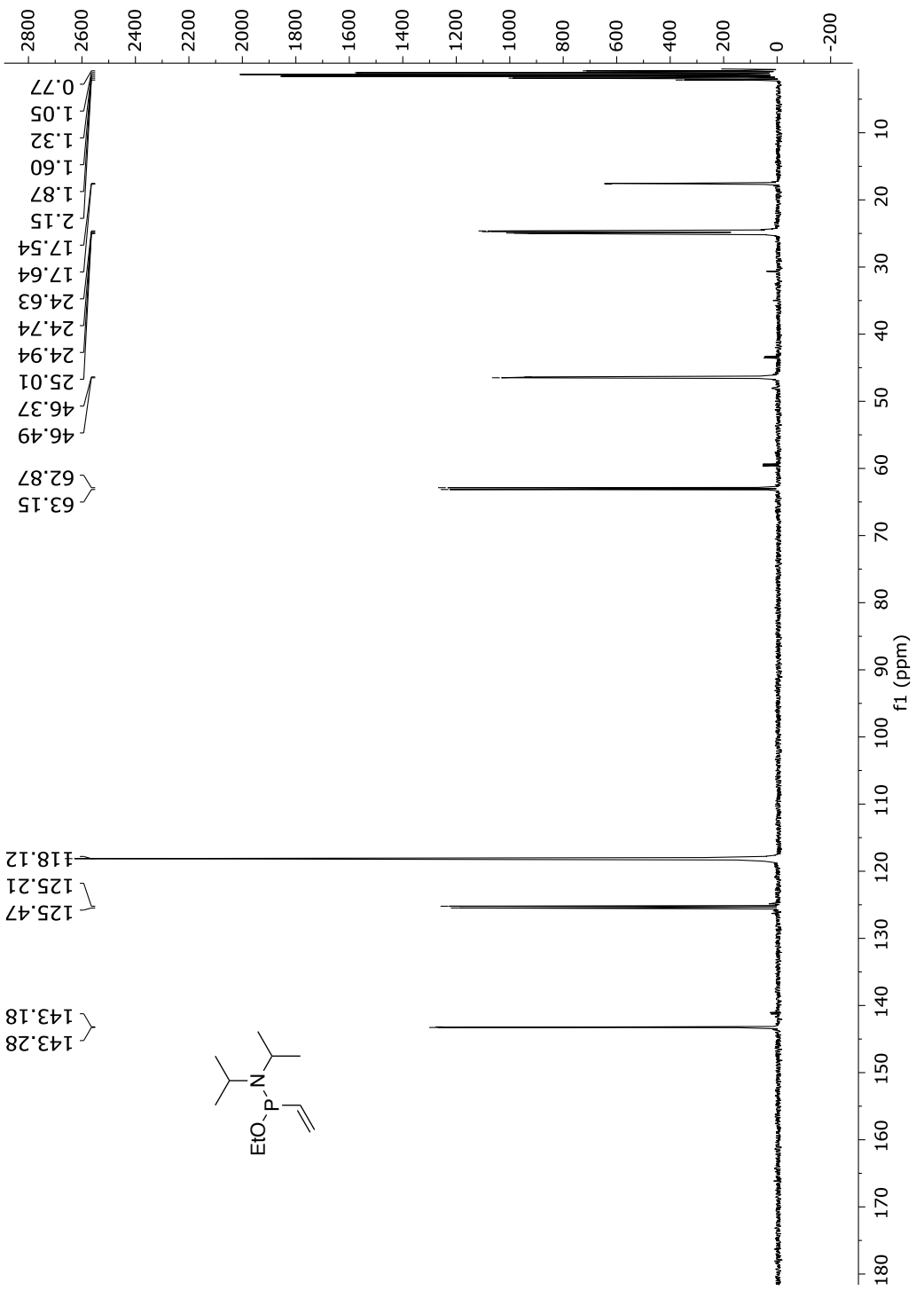

Fig. 173 ^{13}C-NMR spectrum of compound **34** in CD_3CN (75 MHz).

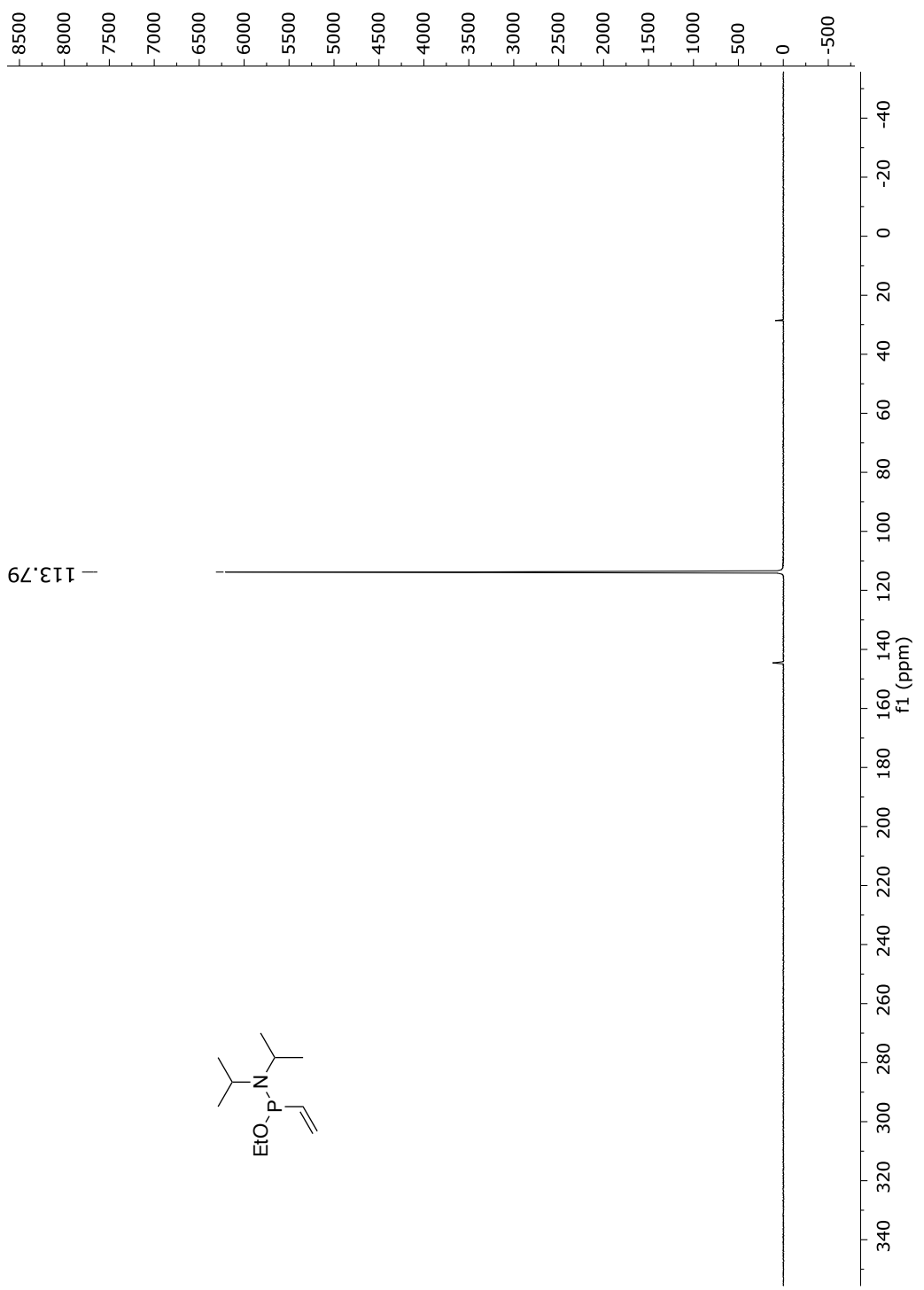

Fig. 174 ^{31}P-NMR spectrum of compound **34** in CD_3CN (122 MHz).

_S_-benzyl _O_-ethyl ethynylphosphonothiolate (35)

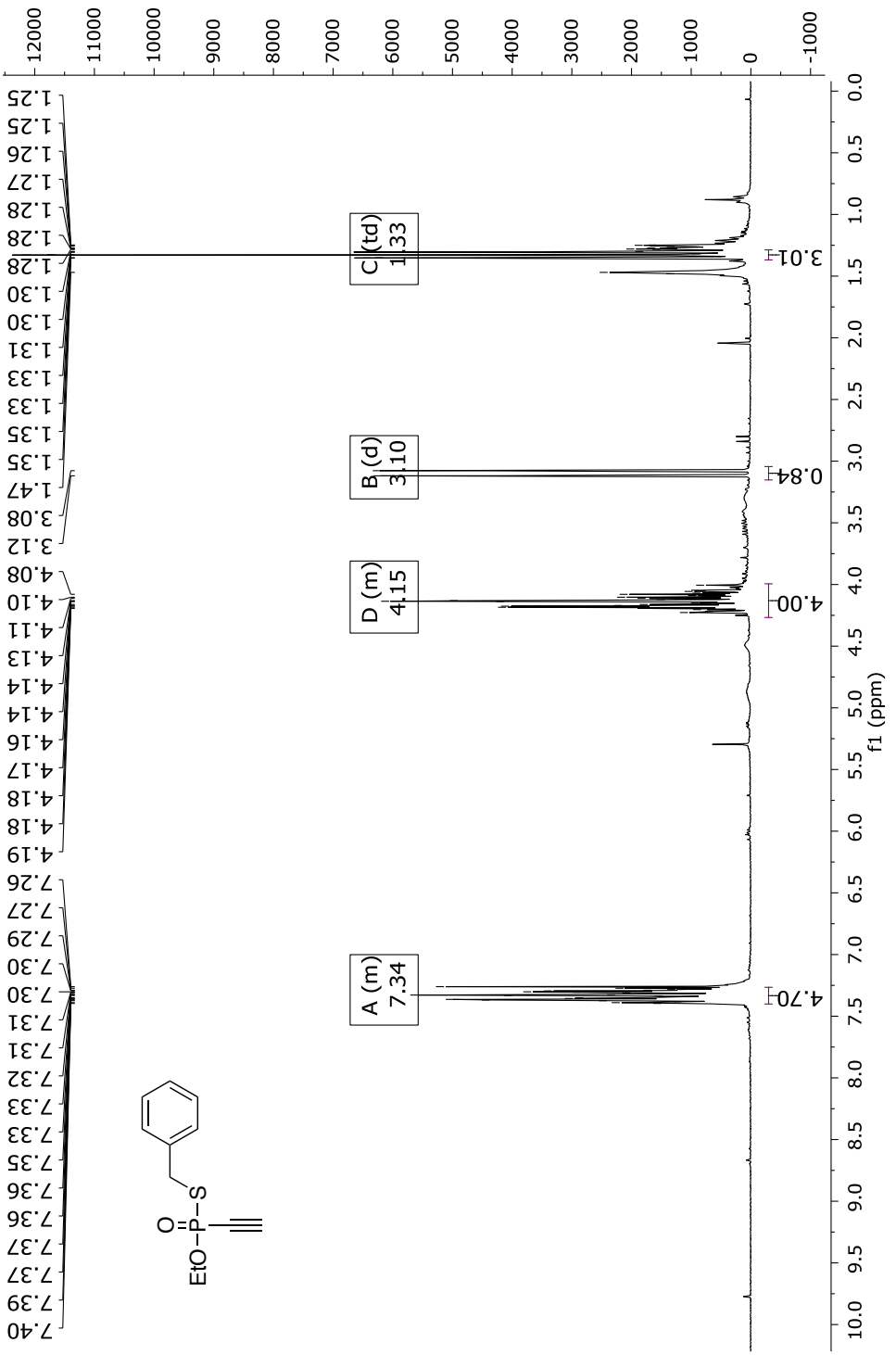

Fig. 175 ^{1}H-NMR spectrum of compound **35** in $CDCl_3$ (300 MHz).

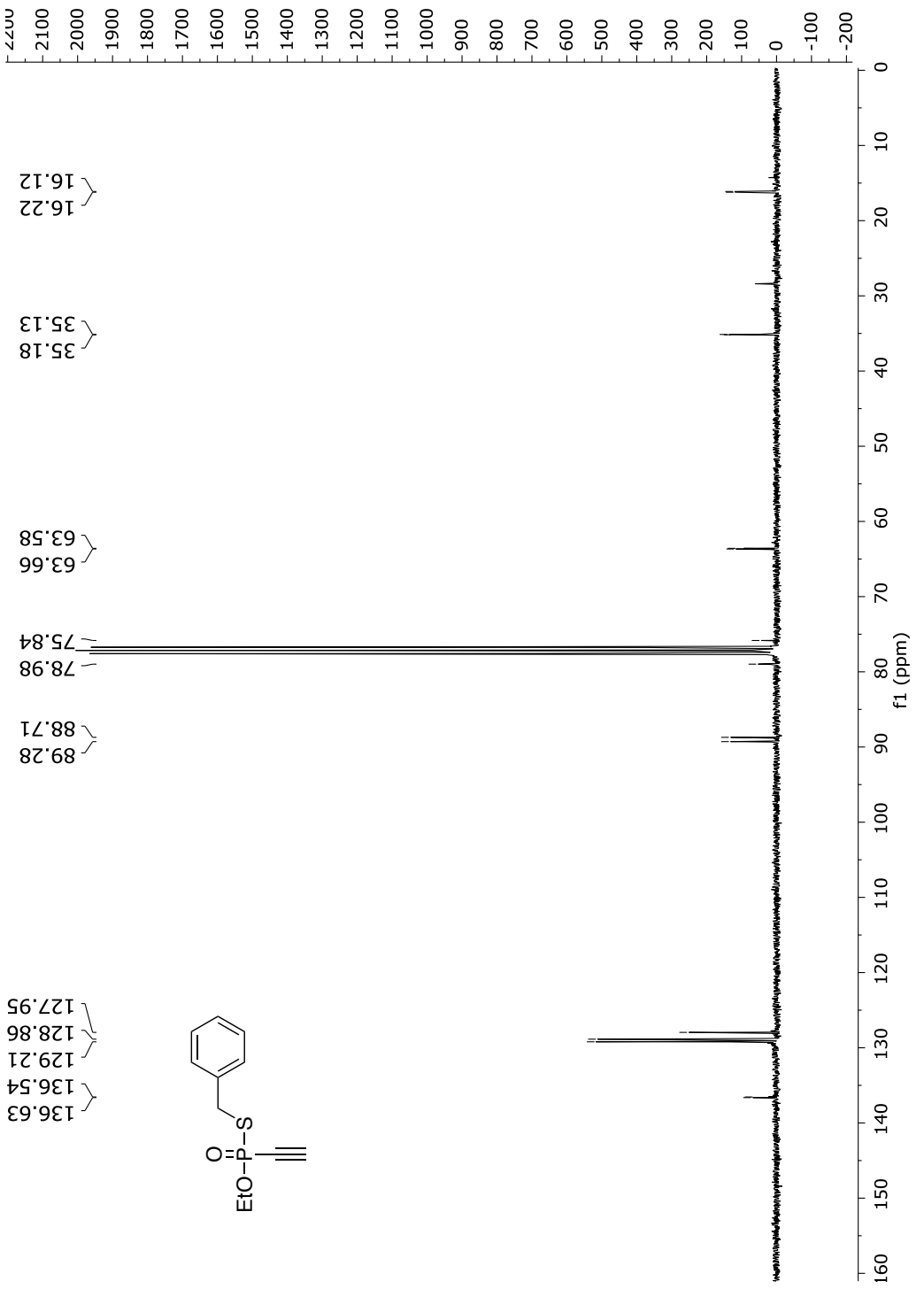

Fig. 176 ^{13}C-NMR spectrum of compound **35** in $CDCl_3$ (75 MHz).

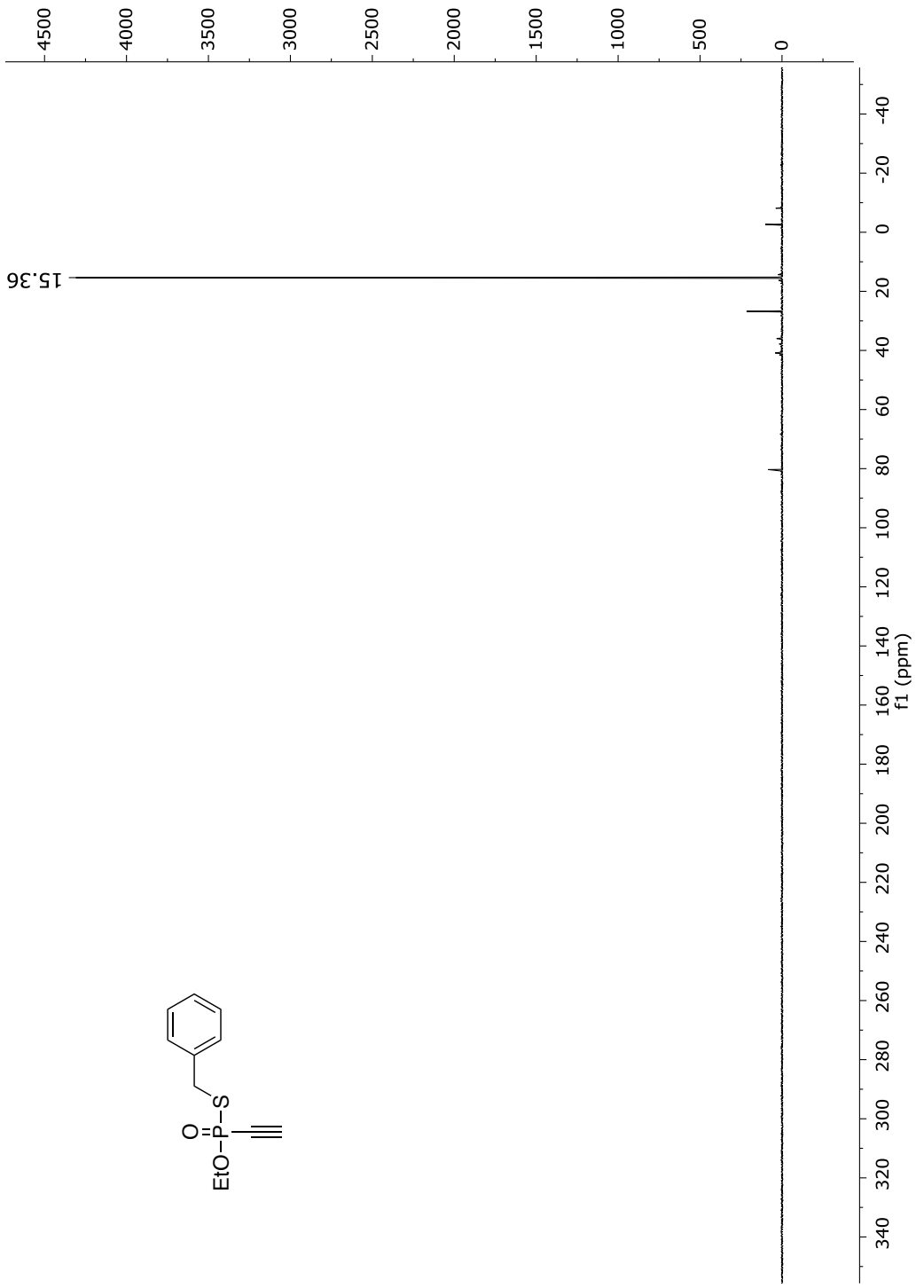

Fig. 177 ^{31}P-NMR spectrum of compound **35** in $CDCl_3$ (122 MHz).

_S_-Boc-ethylamine _O_-ethyl ethynylphosphonothiolate (36)

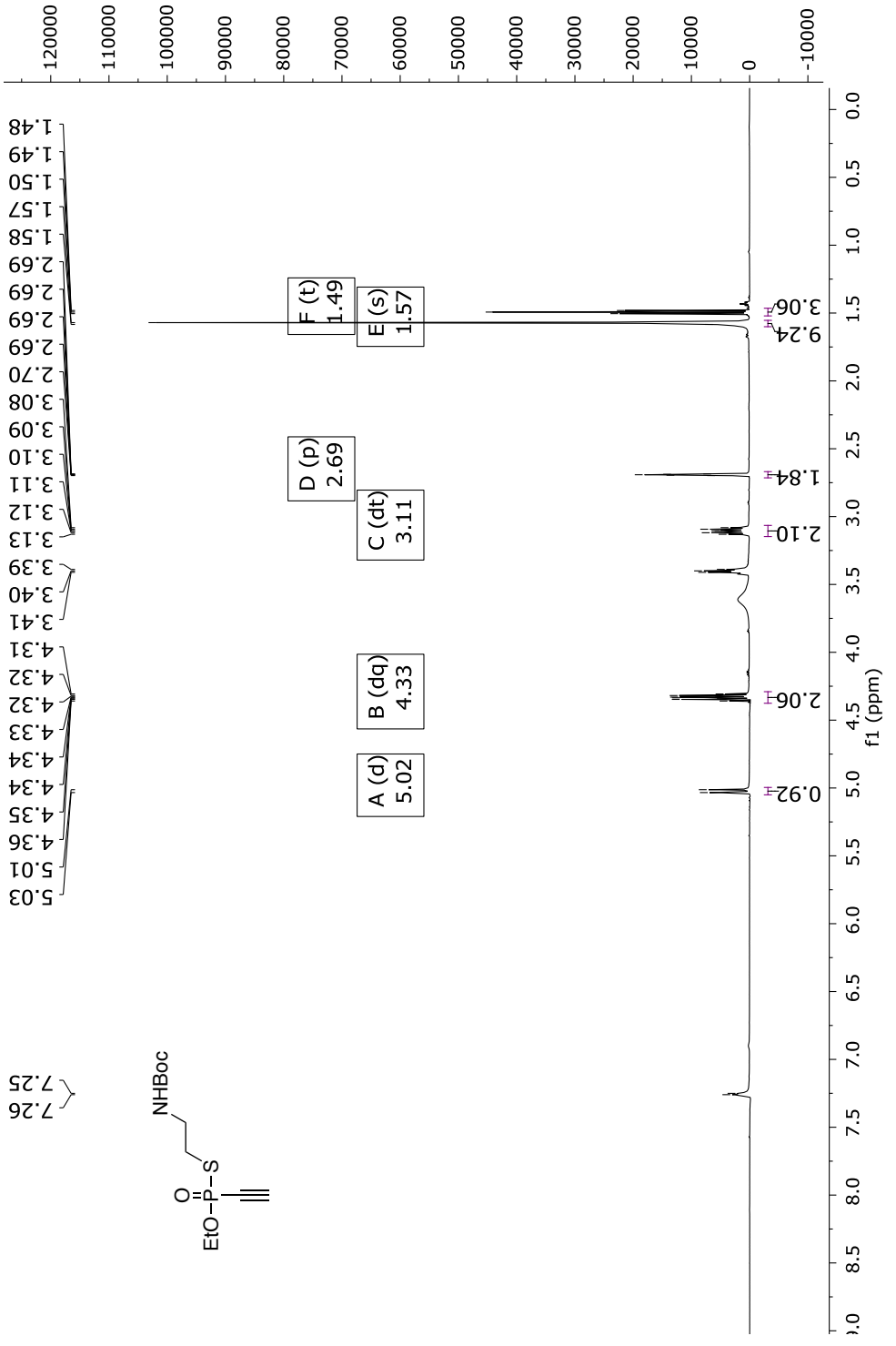

Fig. 178 ^{1}H-NMR spectrum of compound **36** in $CDCl_3$ (600 MHz).

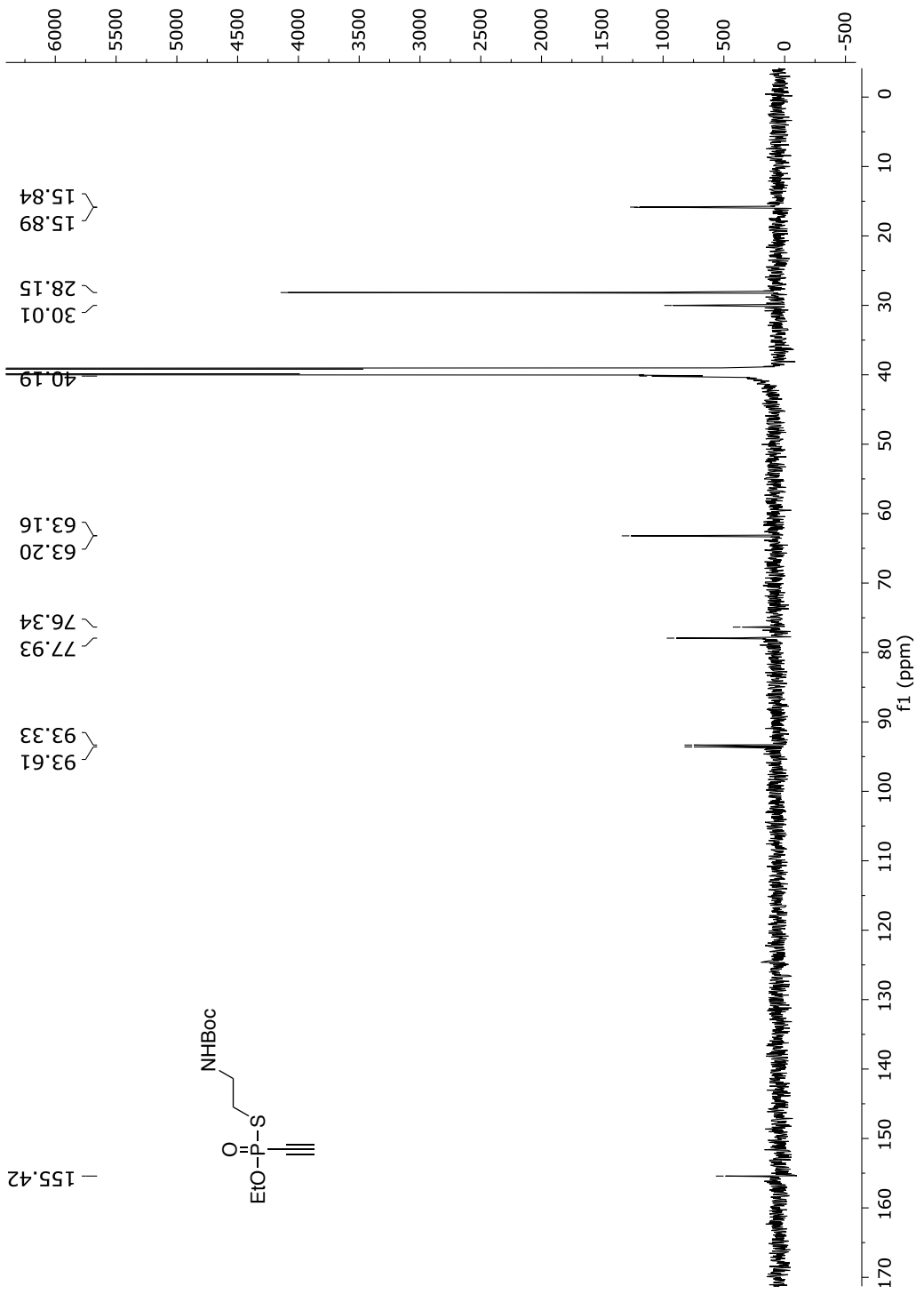

Fig. 179 ^{13}C-NMR spectrum of compound **36** in $CDCl_3$ (151 MHz).

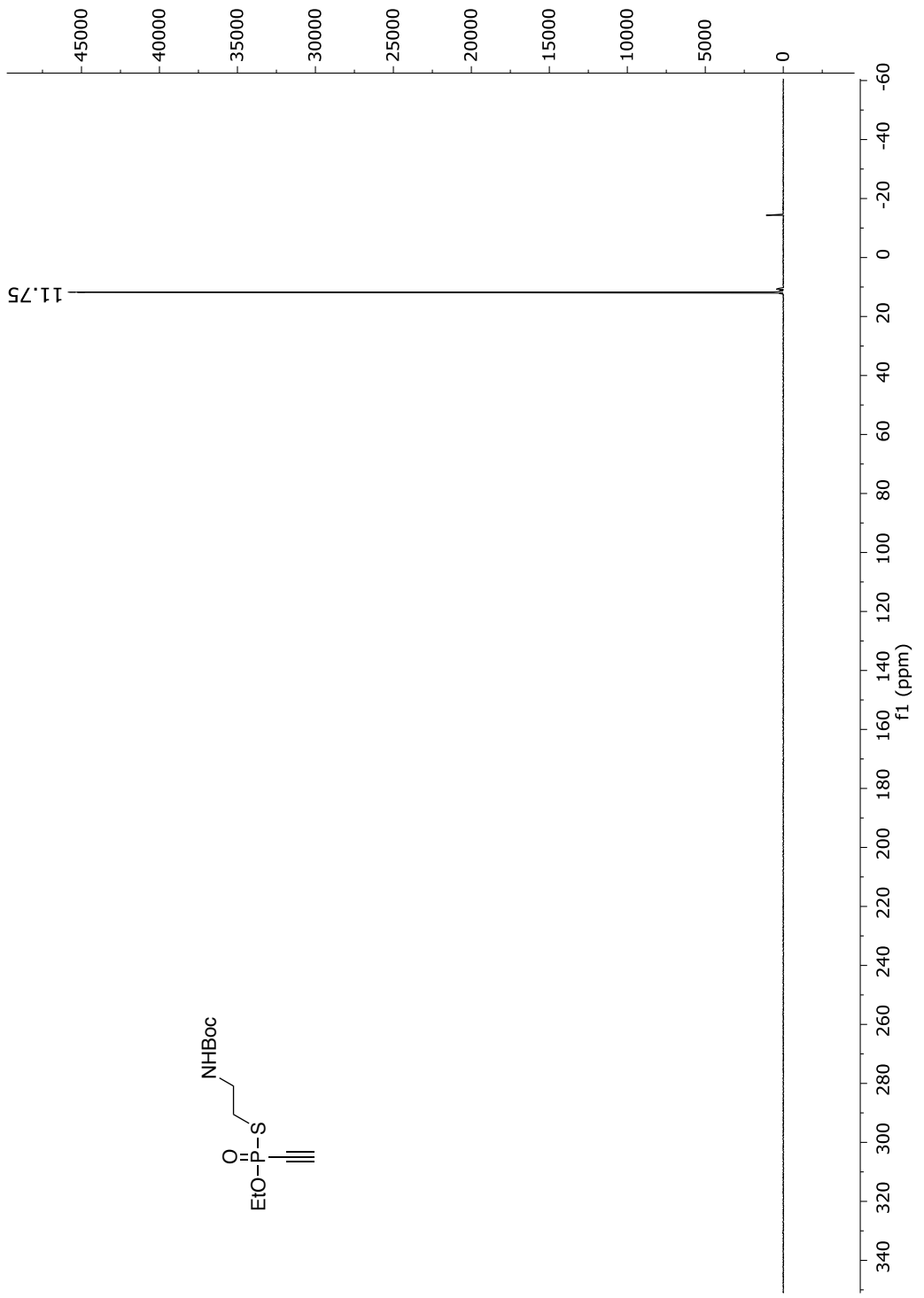

Fig. 180 ^{31}P-NMR spectrum of compound **36** in $CDCl_3$ (243 MHz).

_S_-Boc-ethylamine _O_-ethyl vinylphosphonothiolate (37)

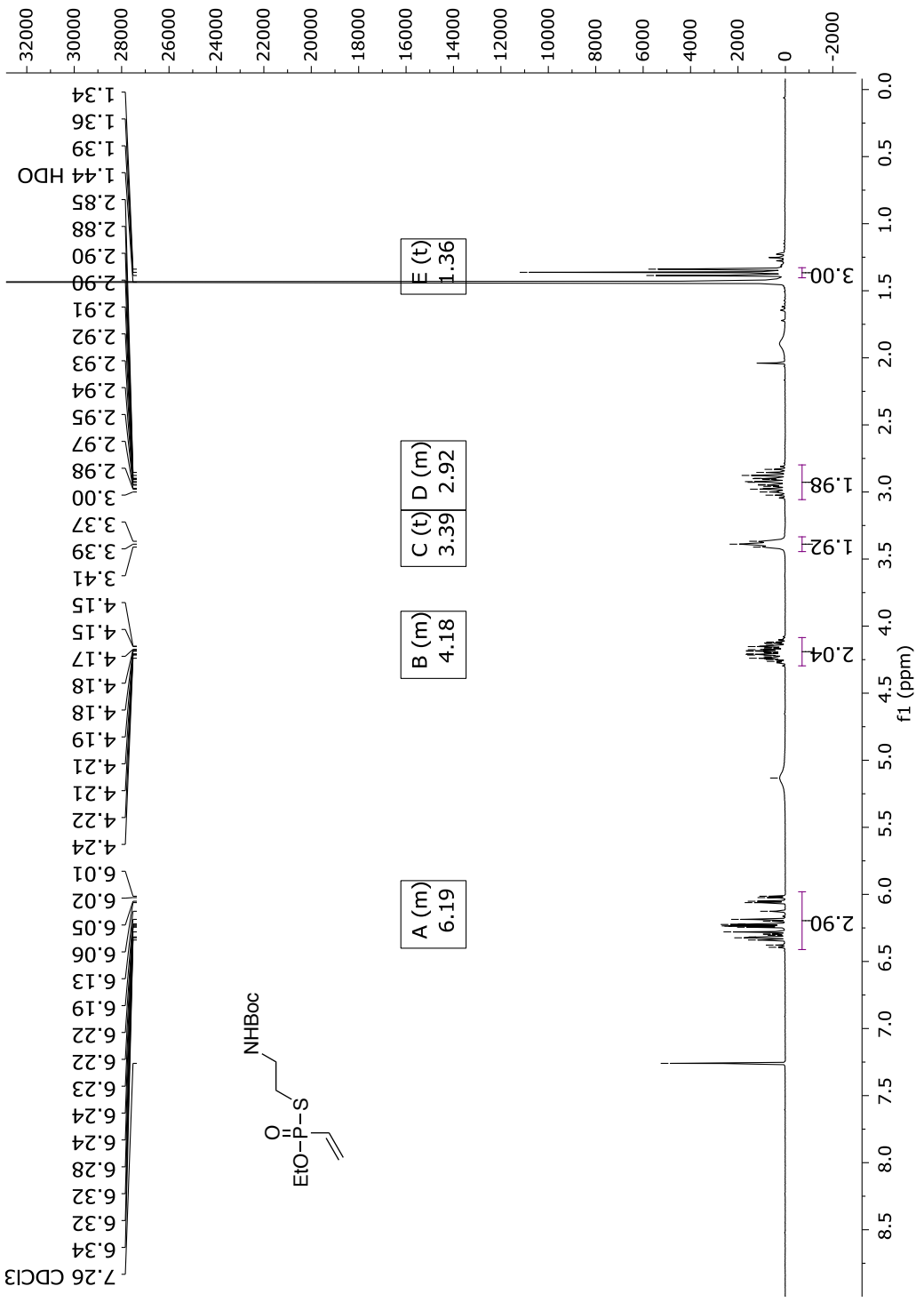

Fig. 181 ^{1}H-NMR spectrum of compound **37** in $CDCl_3$ (300 MHz).

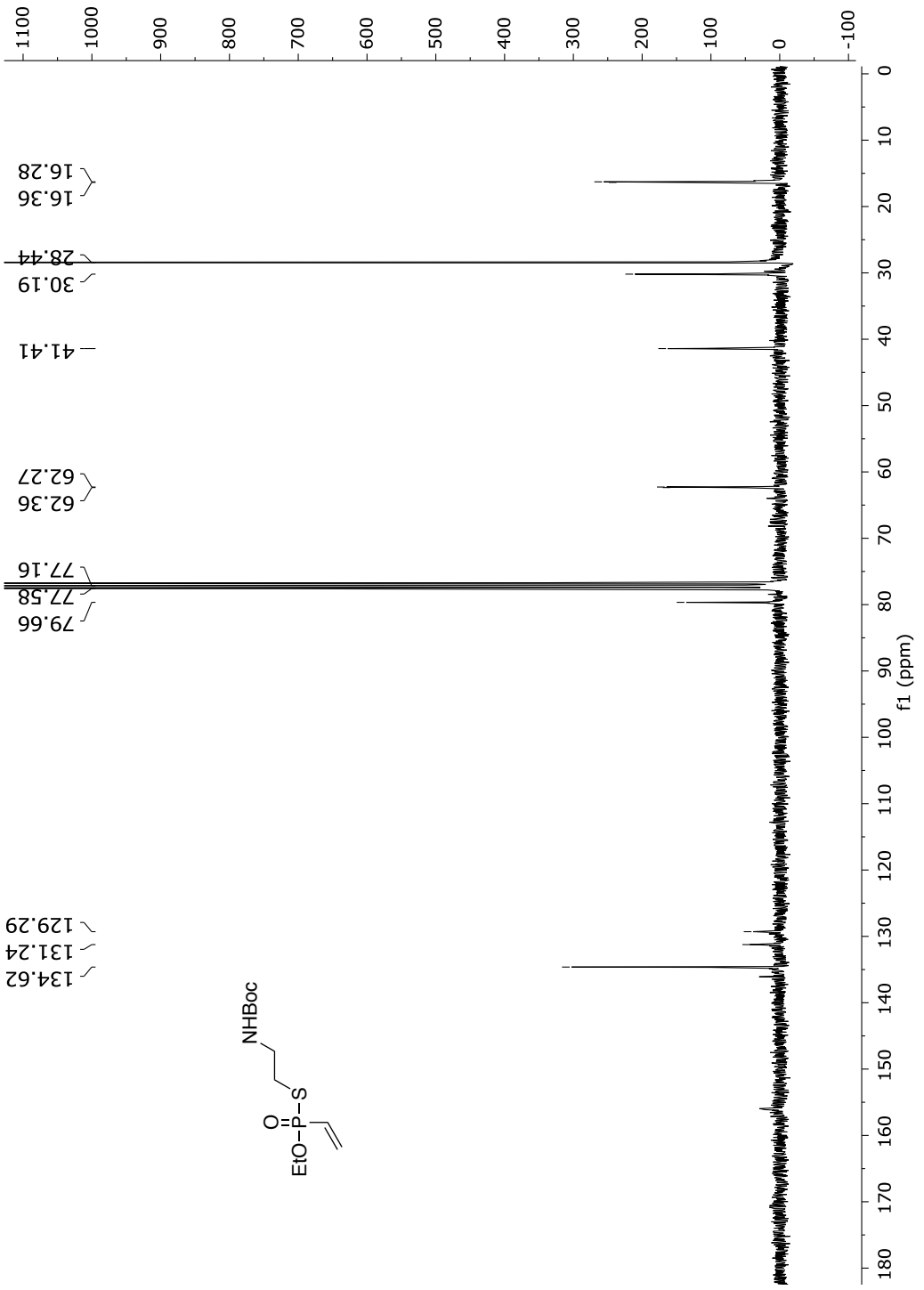

Fig. 182 ^{13}C-NMR spectrum of compound **37** in $CDCl_3$ (75 MHz).

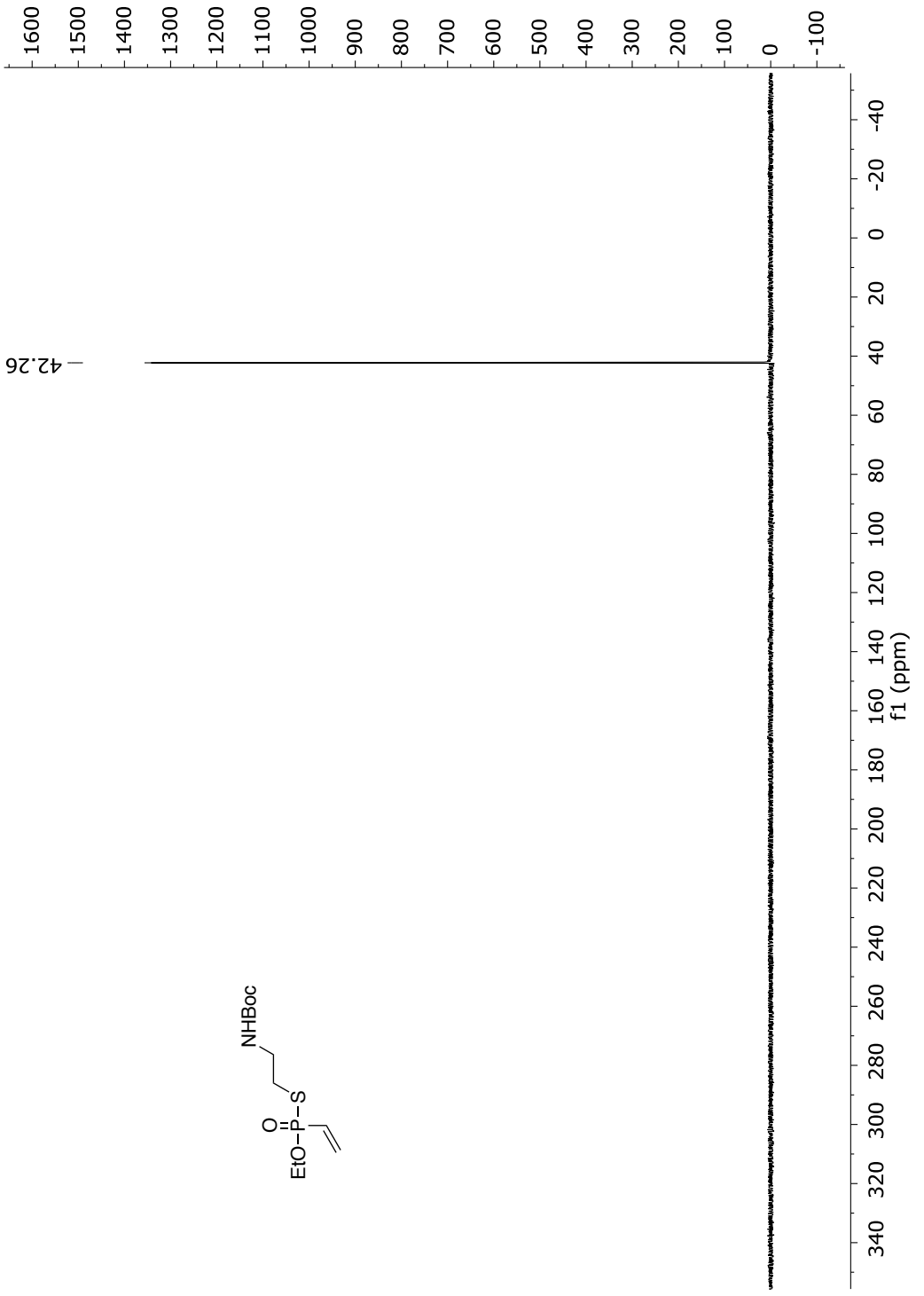

Fig. 183 ^{31}P-NMR spectrum of compound **37** in $CDCl_3$ (122 MHz).

_S_-Propanoic NHS ester _O_-ethyl vinylphosphonothiolate (38)

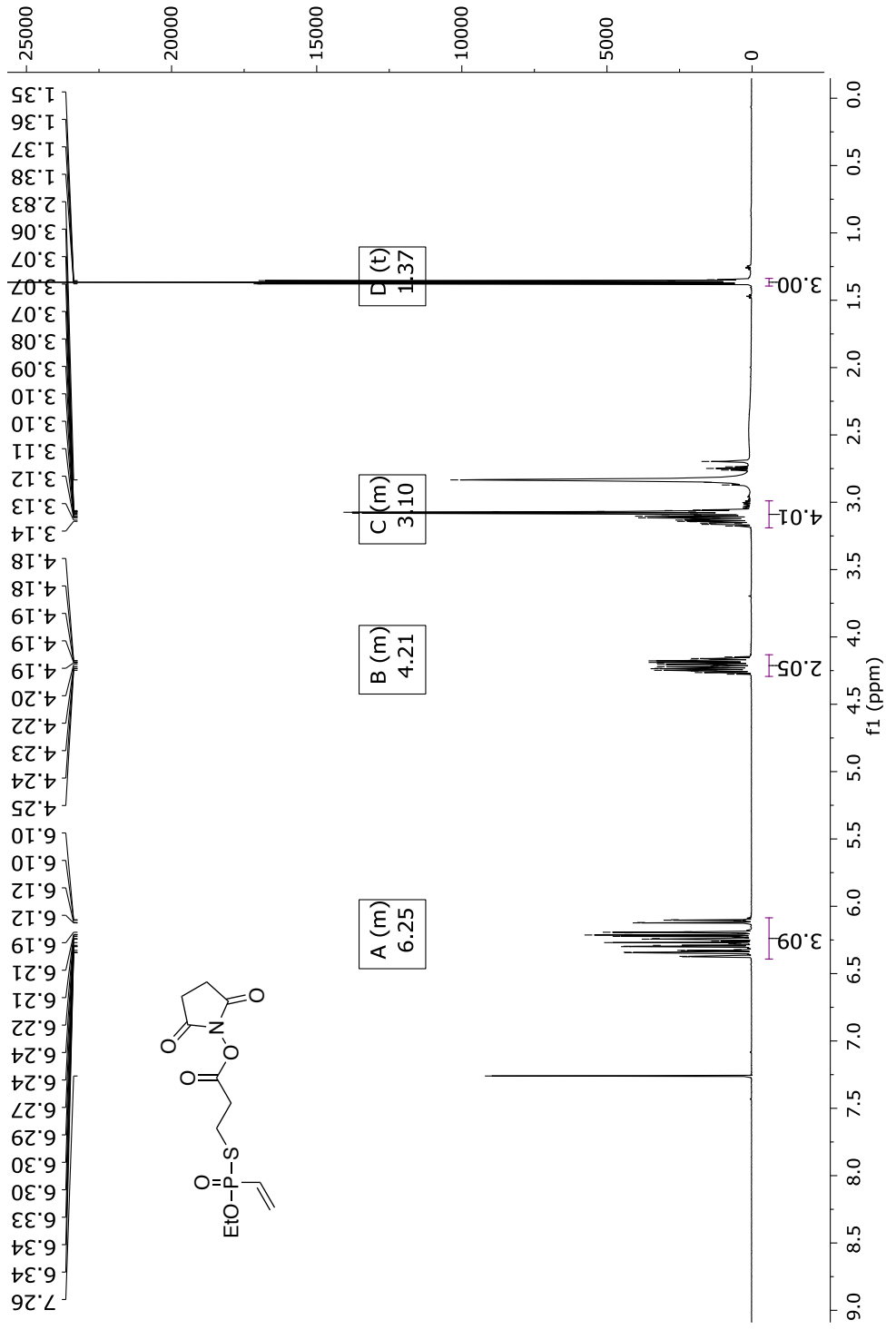

Fig. 184 ^{1}H-NMR spectrum of compound **38** in $CDCl_3$ (600 MHz).

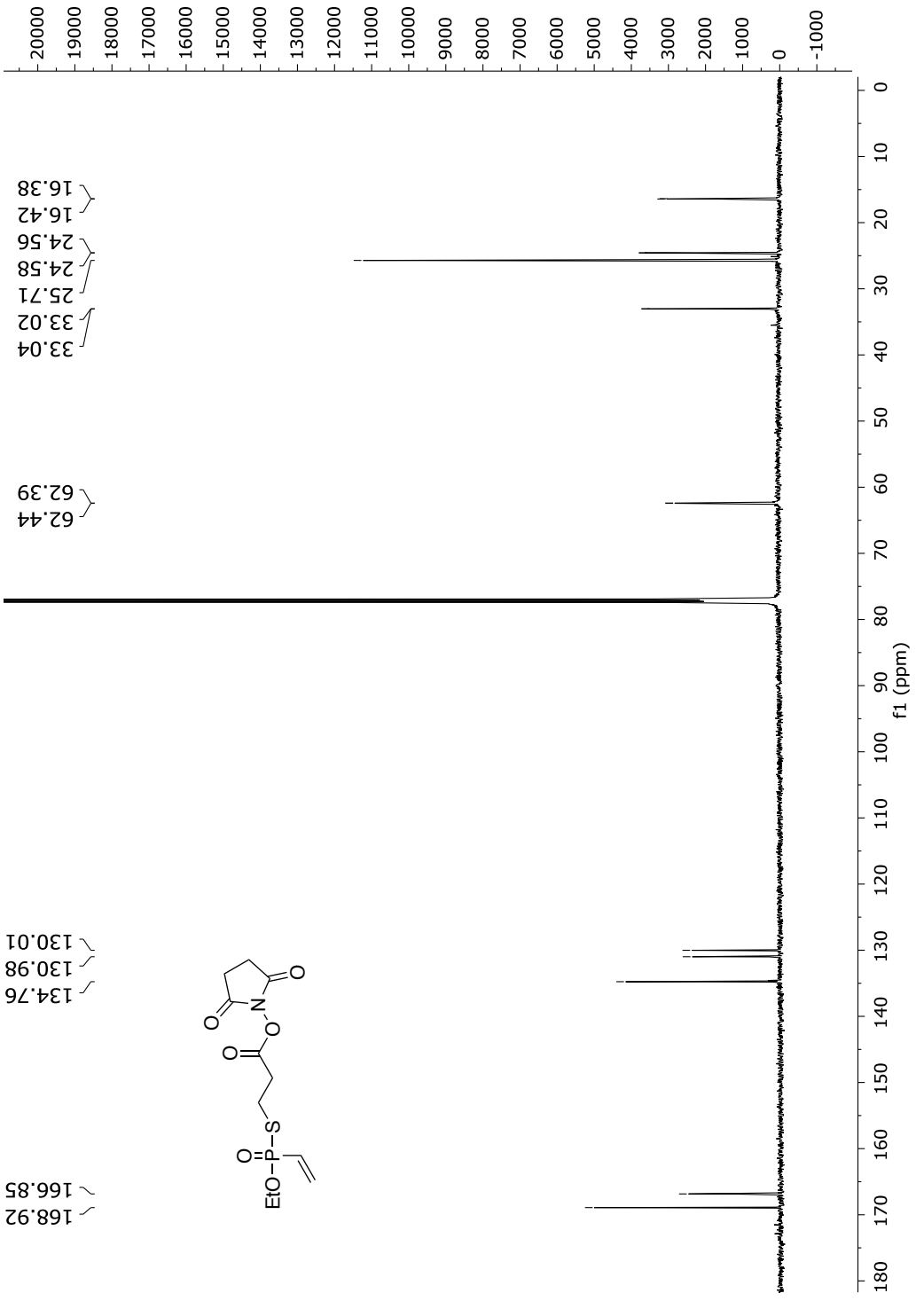

Fig. 185 ^{13}C-NMR spectrum of compound **38** in $CDCl_3$ (151 MHz).

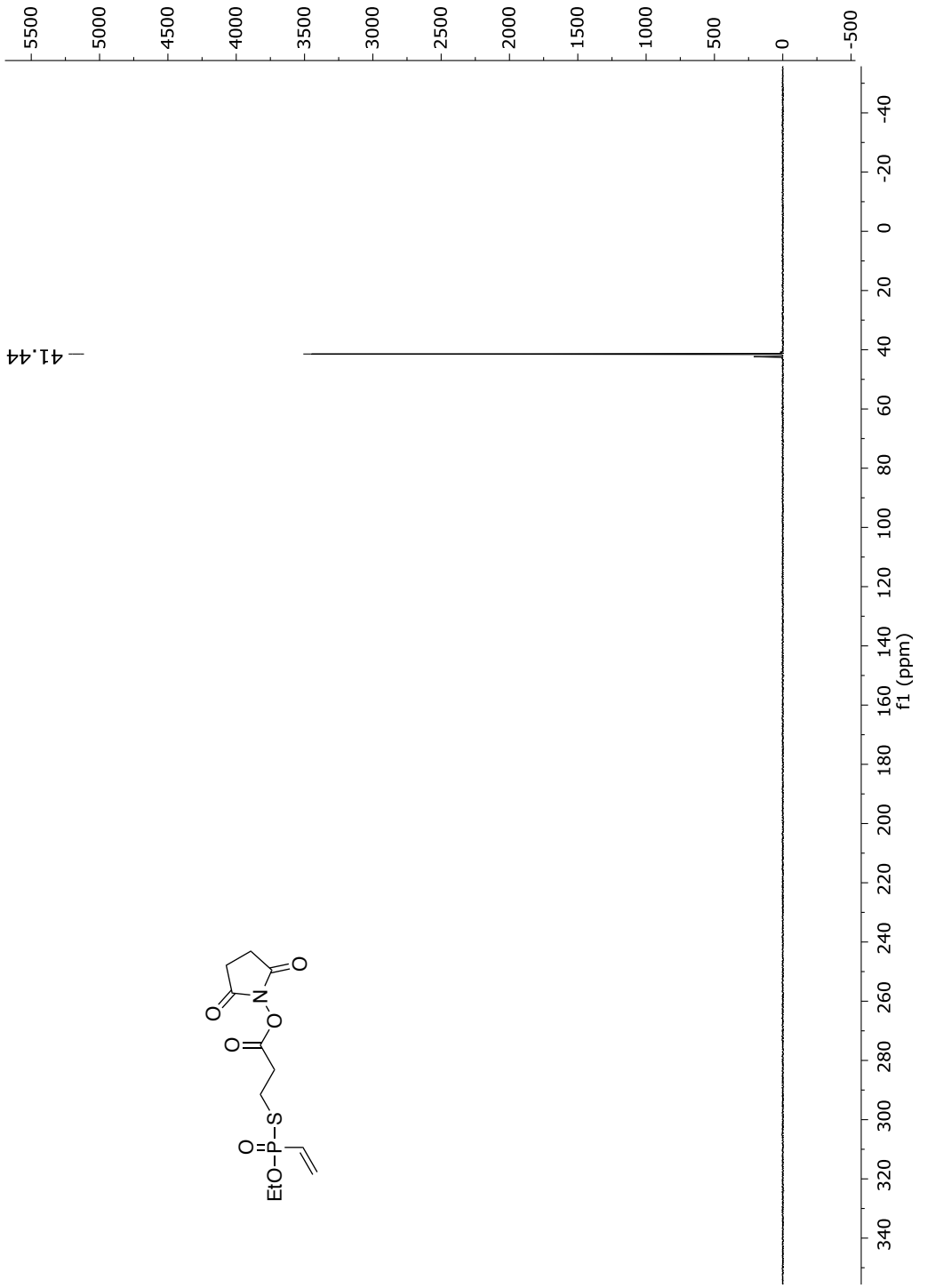

Fig. 186 ^{31}P-NMR spectrum of compound **38** in $CDCl_3$ (243 MHz).

S-EDANS O-ethyl vinylphosphonothiolate (39)

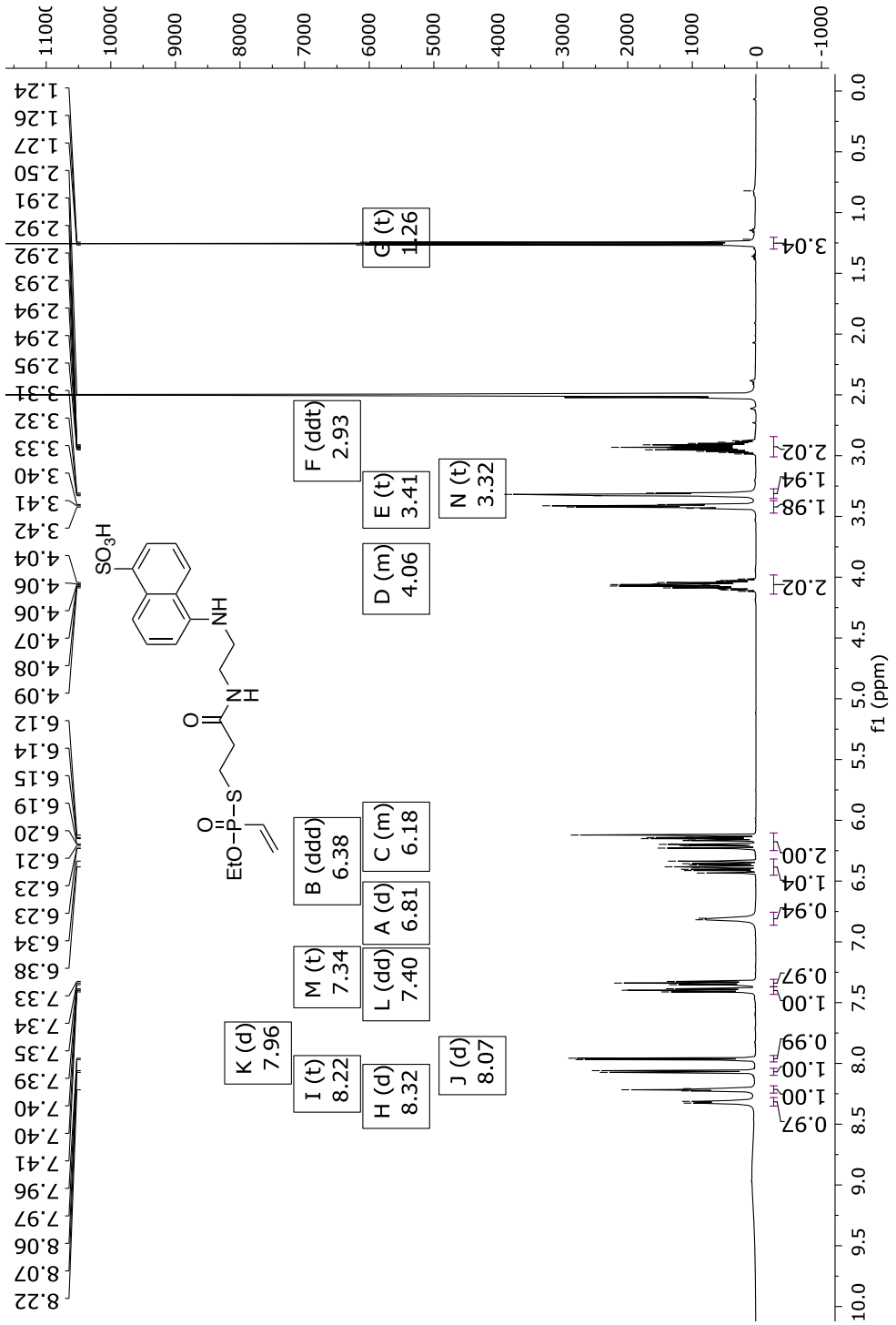

Fig. 187 ^{1}H-NMR spectrum of compound **39** in DMSO−d_6 (600 MHz).

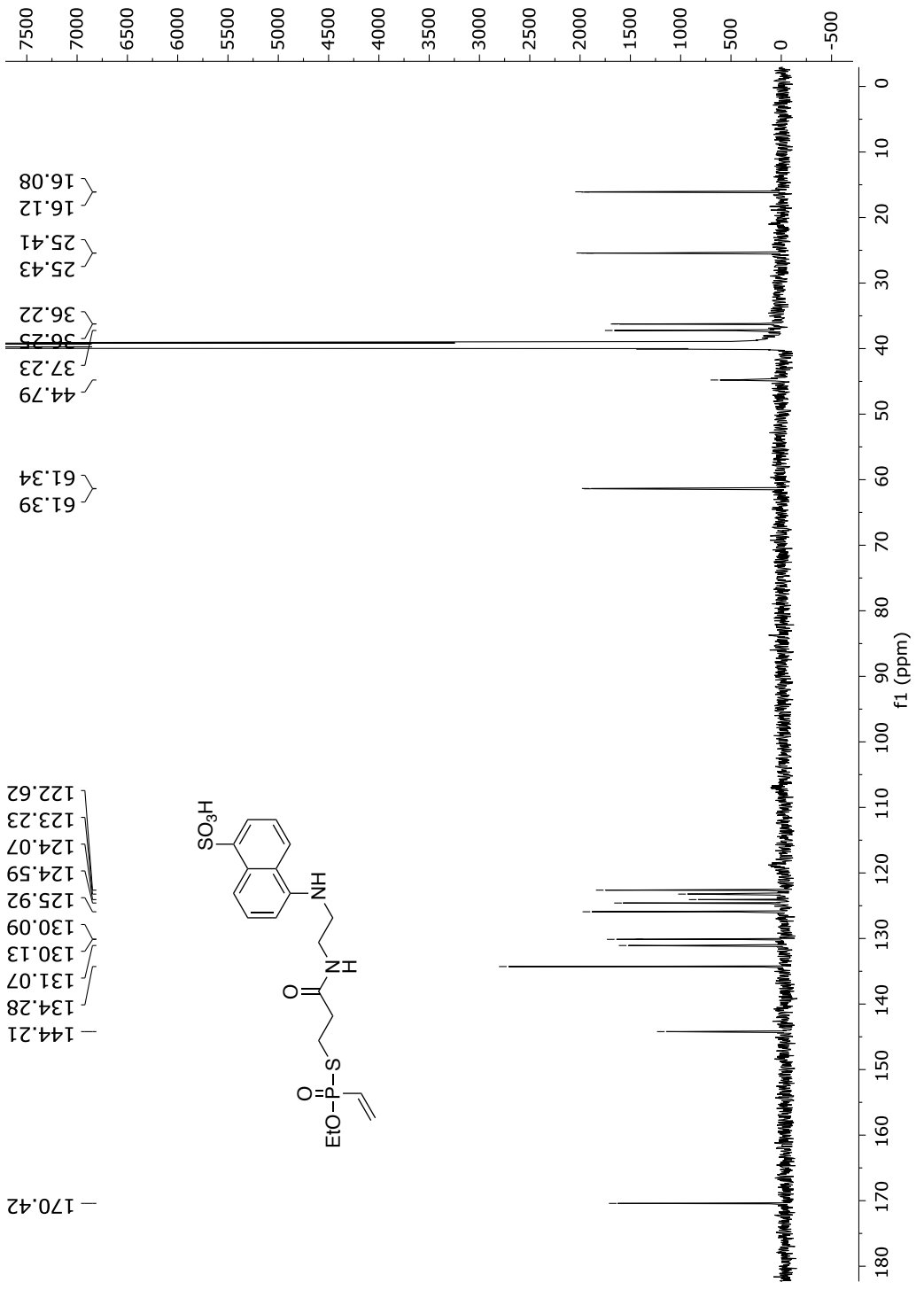

Fig. 188 ^{13}C-NMR spectrum of compound **39** in DMSO−d_6 (151 MHz).

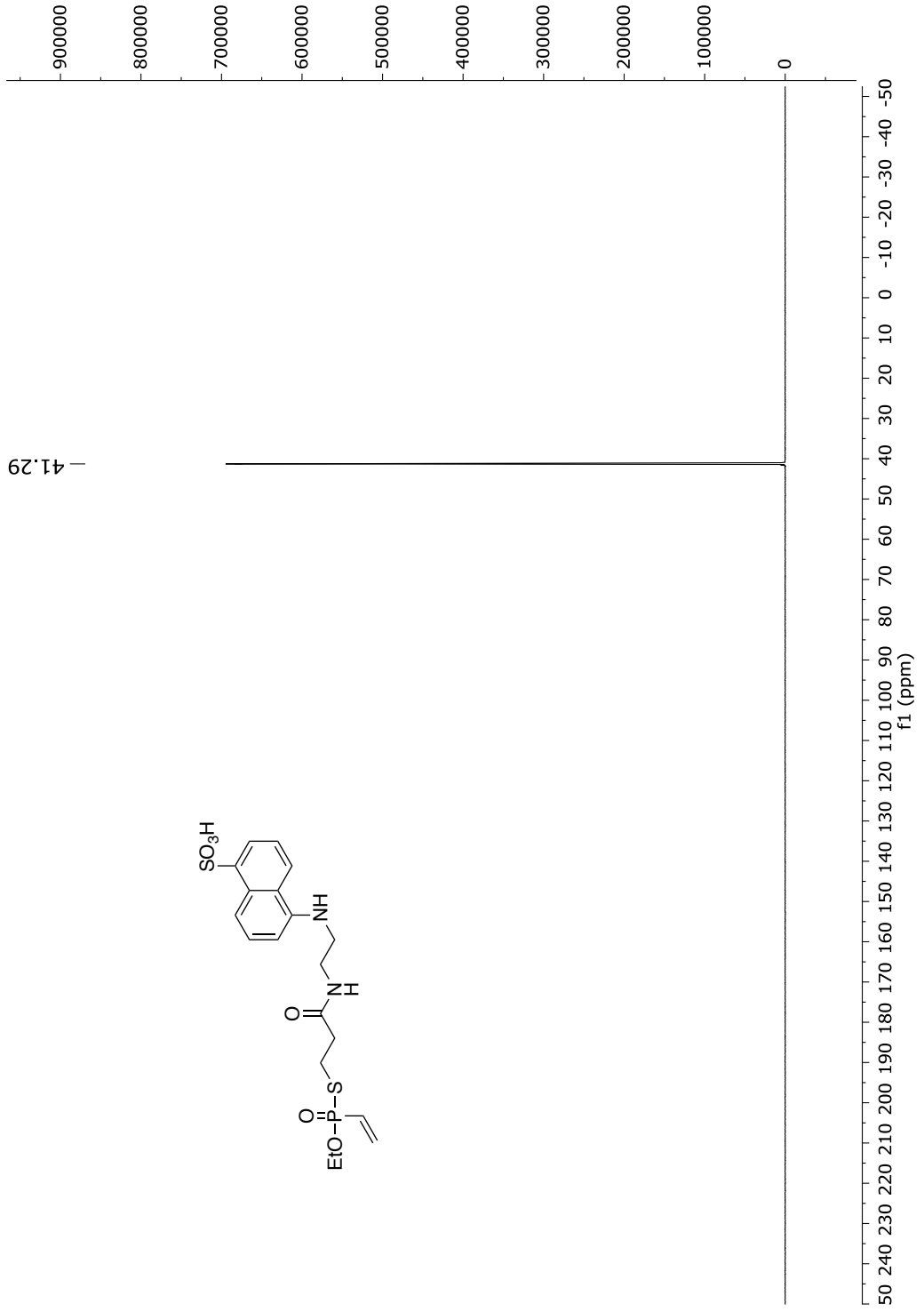

Fig. 189 ^{31}P-NMR spectrum of compound **39** in DMSO−d_6 (243 MHz).

_S_-EDANS derivative _O_-ethyl ethynylphosphonothiolate (43)

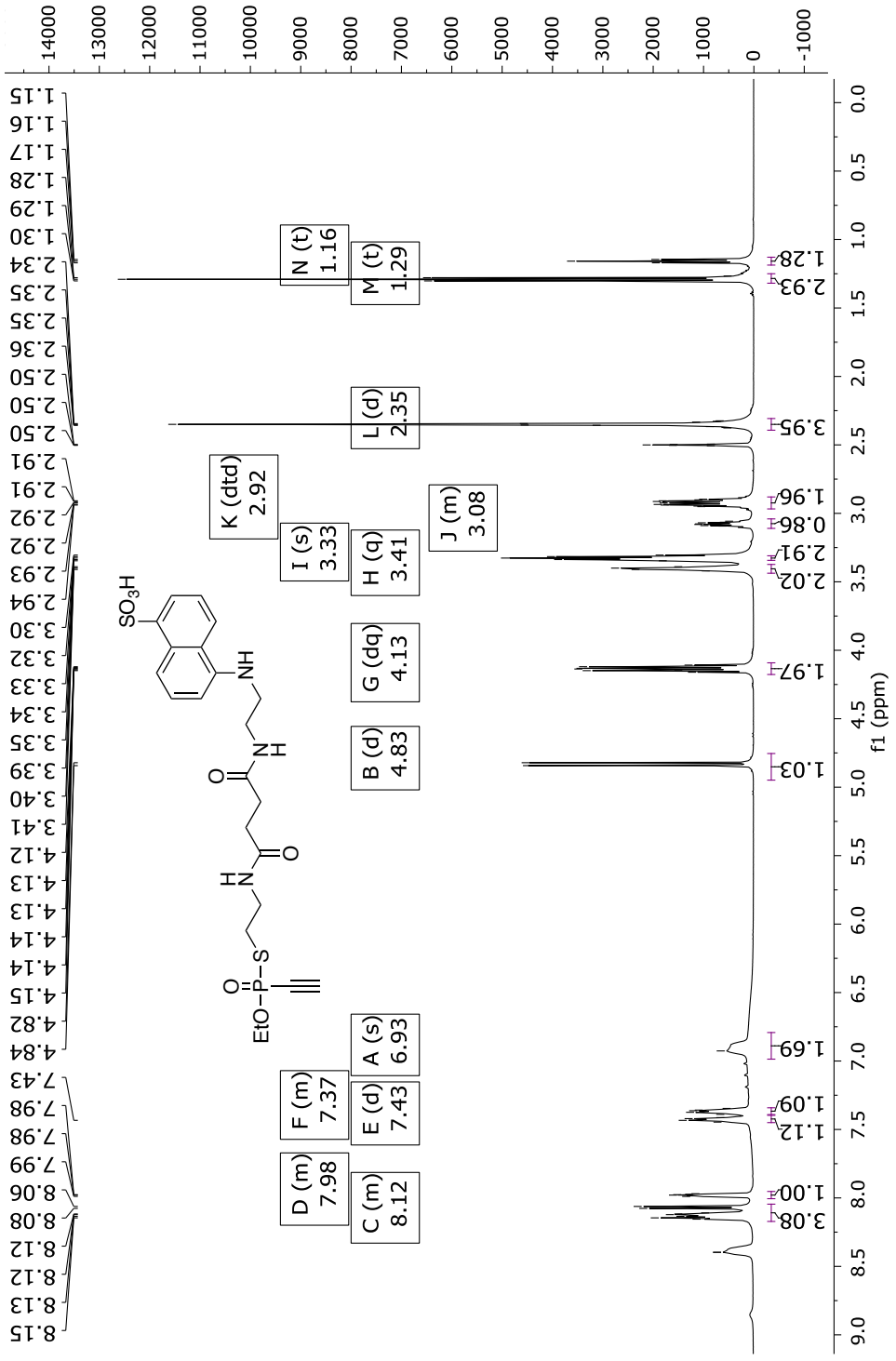

Fig. 190 ^{1}H-NMR spectrum of compound **43** in DMSO−d_6 (600 MHz).

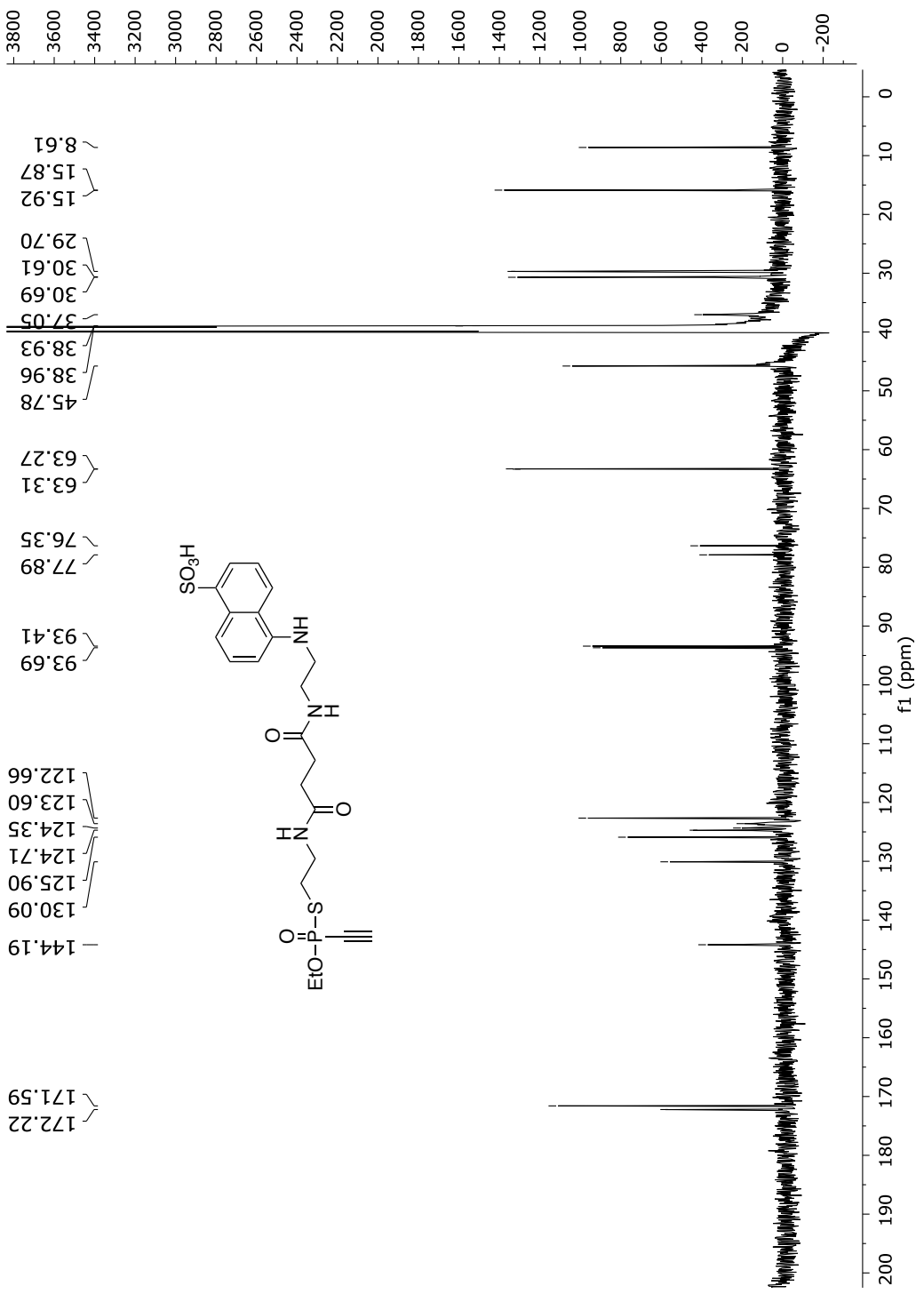

Fig. 191 ^{13}C-NMR spectrum of compound **43** in DMSO−d_6 (151 MHz).

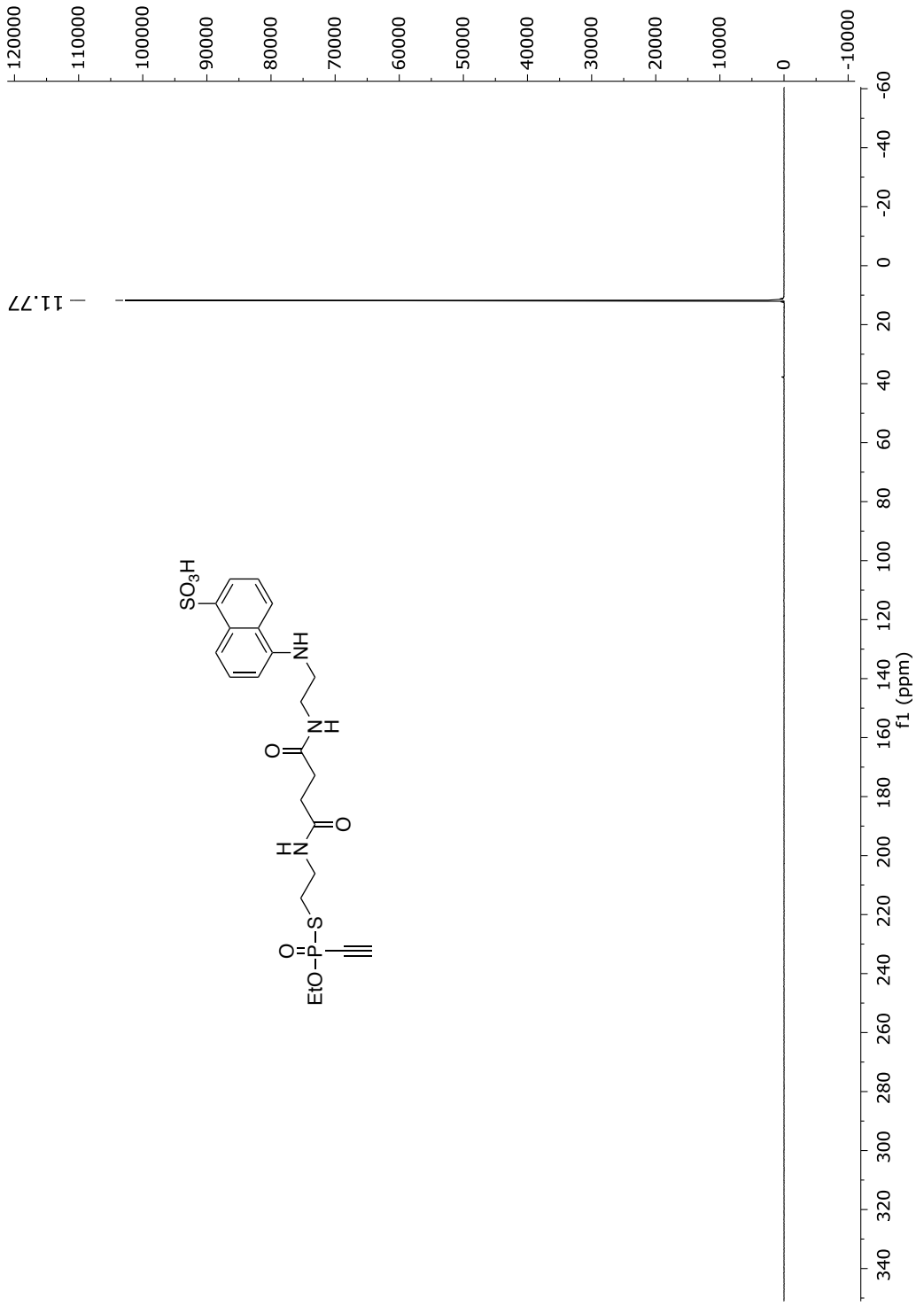

Fig. 192 ^{31}P-NMR spectrum of compound **43** in DMSO−d_6 (243 MHz).

_S_-EDANS derivative _O_-ethyl vinylphosphonothiolate (44)

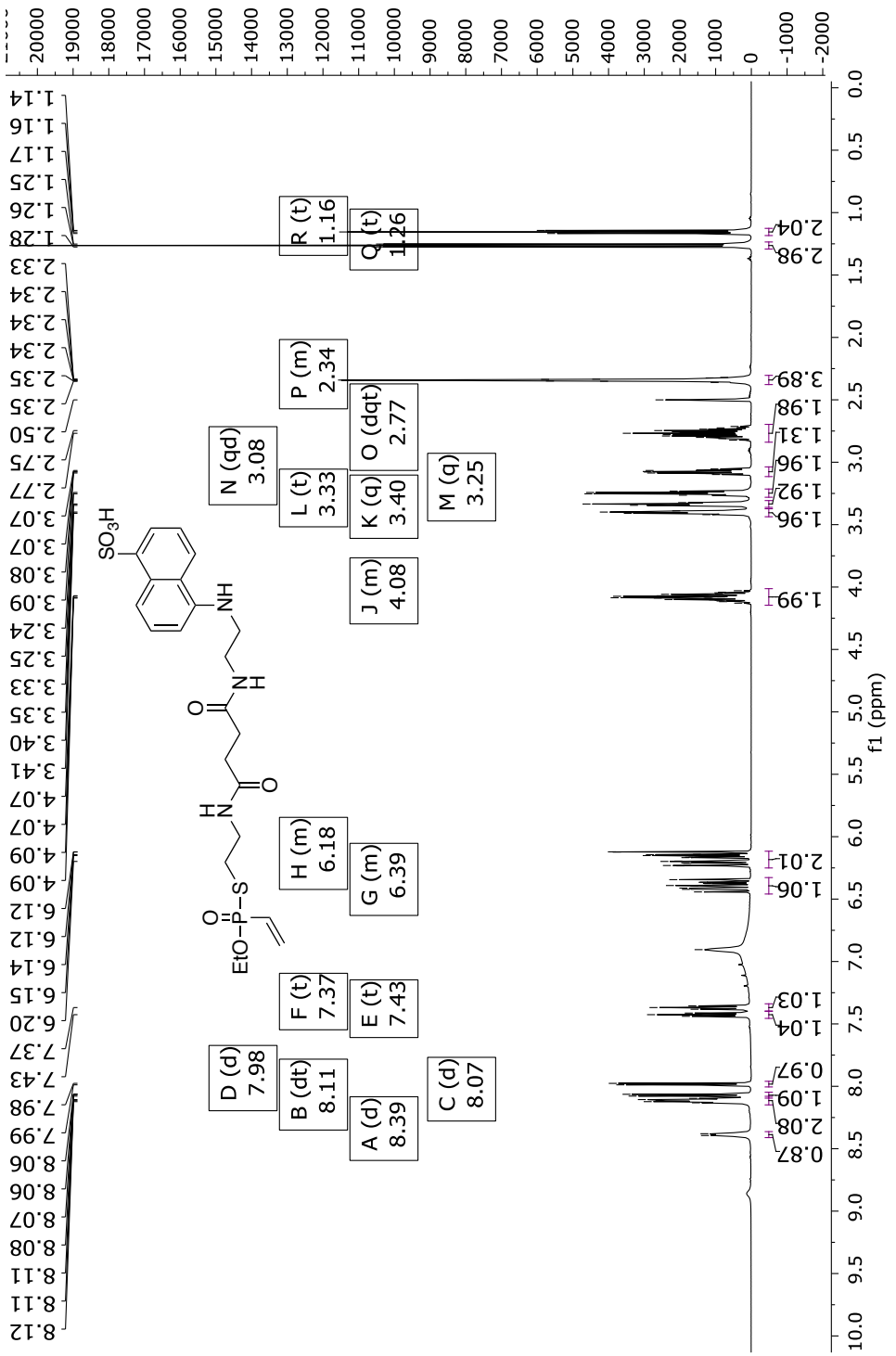

Fig. 193 ^{1}H-NMR spectrum of compound **44** in DMSO−d_6 (600 MHz).

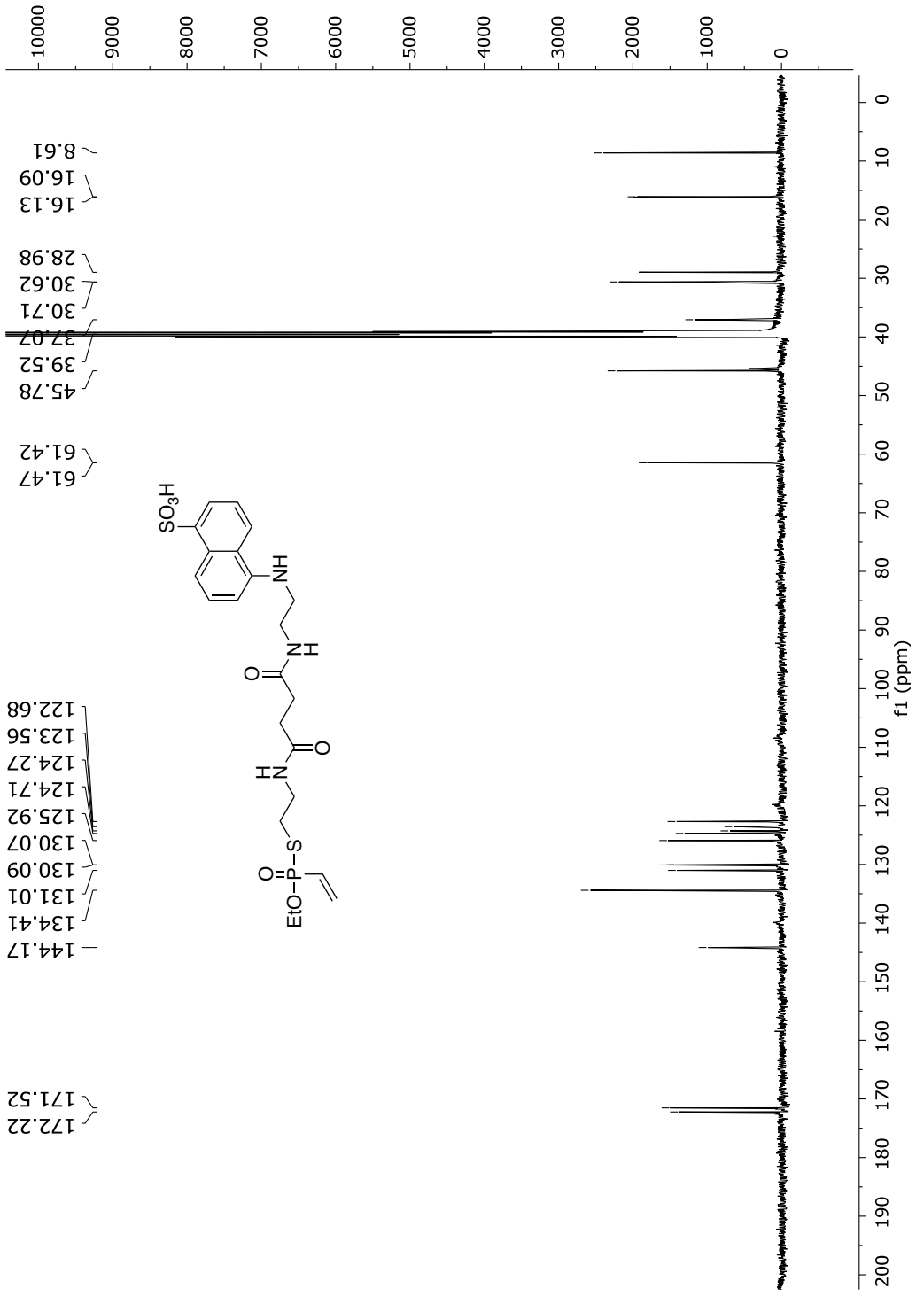

Fig. 194 ^{13}C-NMR spectrum of compound **44** in DMSO−d_6 (151 MHz).

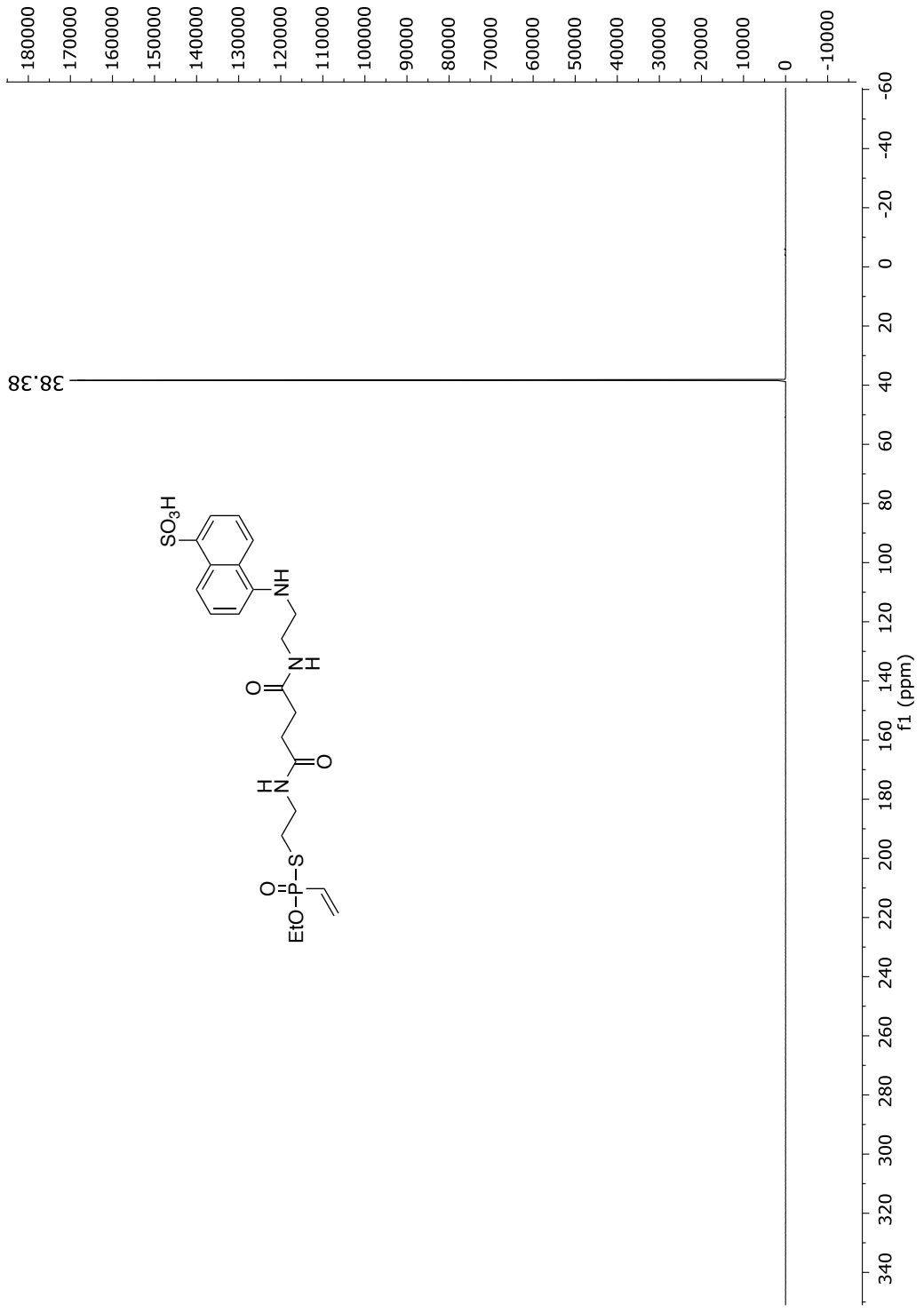

Fig. 195 ^{31}P-NMR spectrum of compound **44** in DMSO−d_6 (243 MHz).

_S_-4-(ethylamido)-4-biotin _O_-ethyl ethynylphosphonothiolate (45)

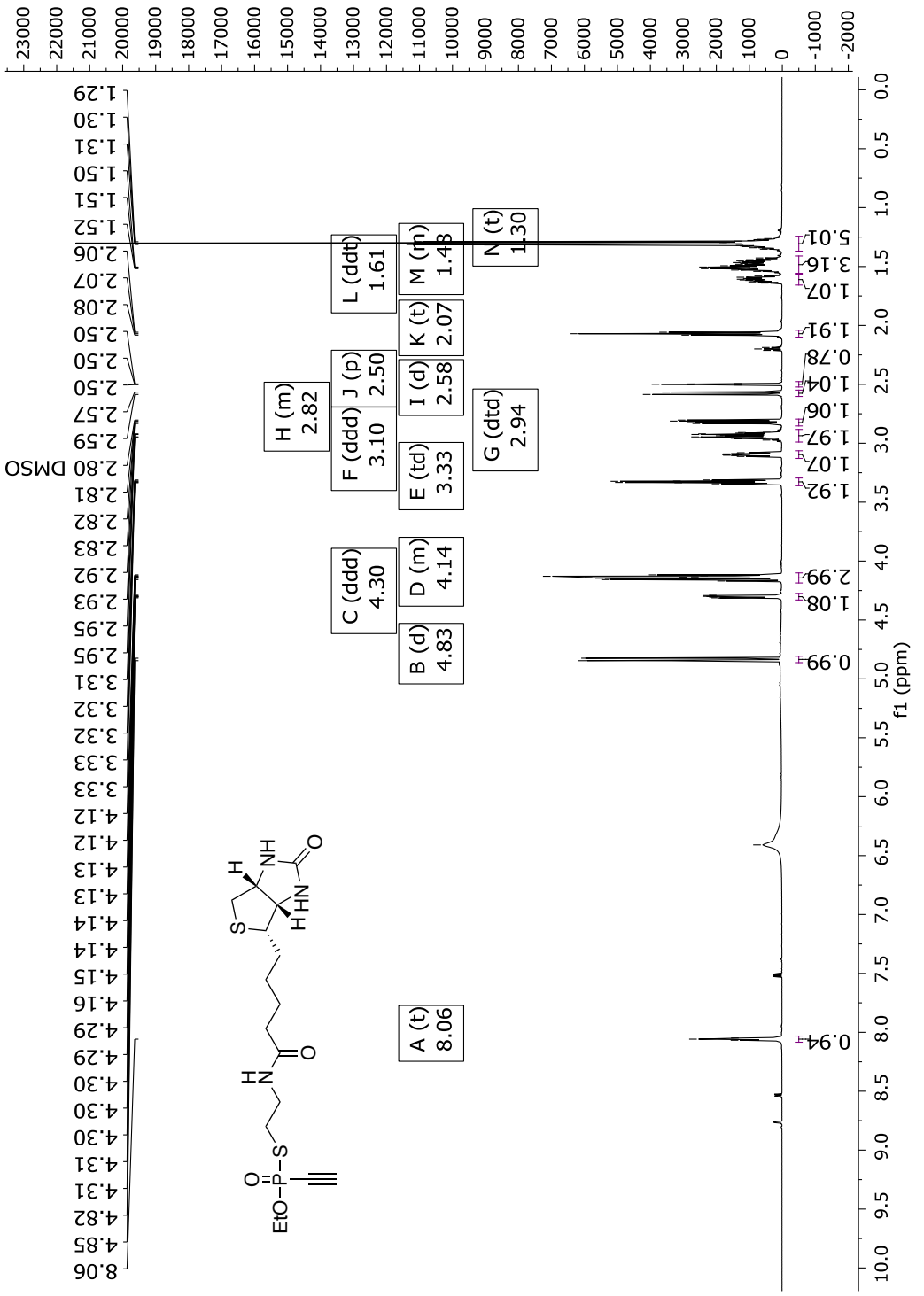

Fig. 196 ^{1}H-NMR spectrum of compound **45** in DMSO−d_6 (600 MHz).

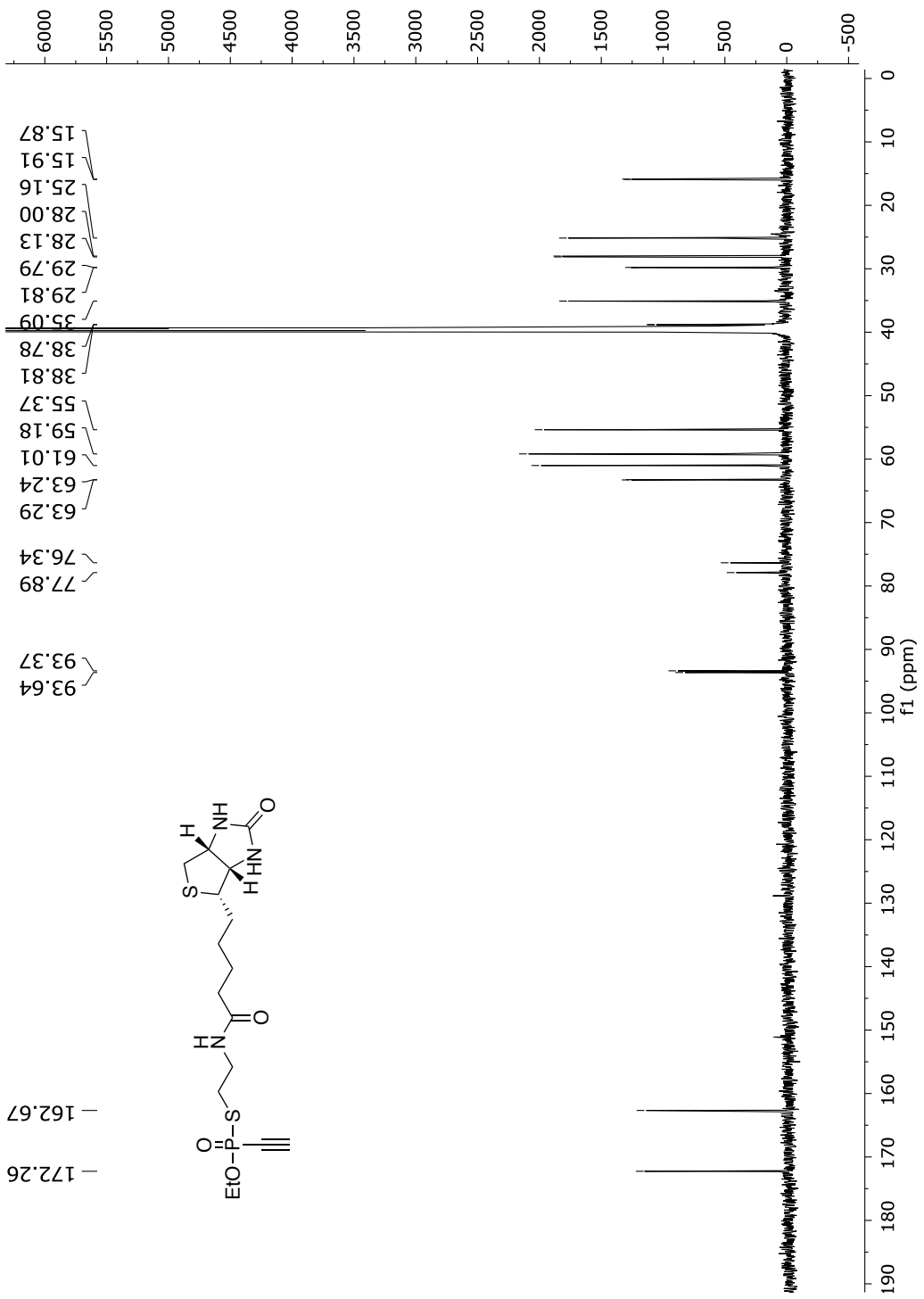

Fig. 197 ^{13}C-NMR spectrum of compound **45** in DMSO−d_6 (151 MHz).

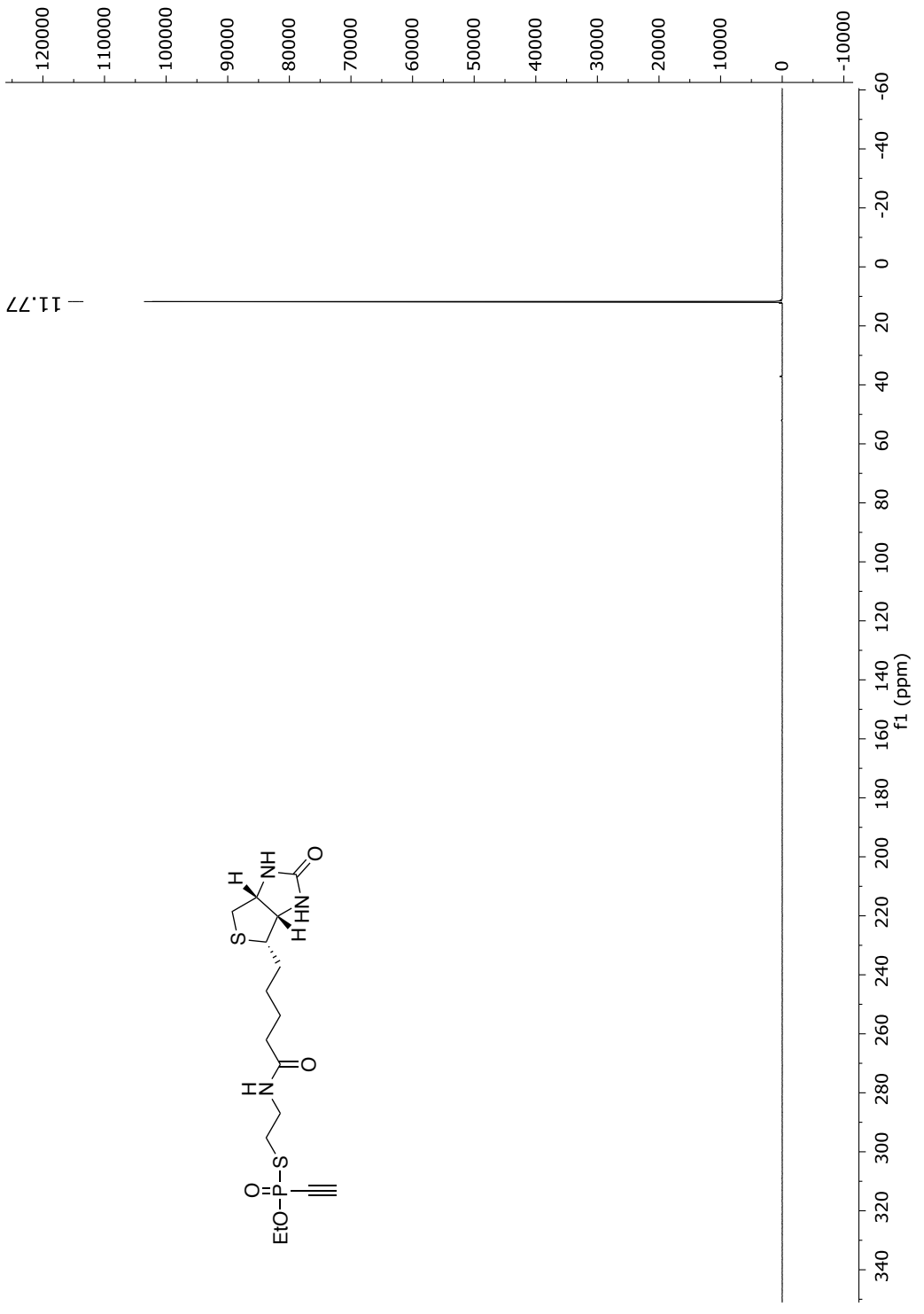

Fig. 198 ^{31}P-NMR spectrum of compound **45** in DMSO−d_6 (243 MHz).

_S_-4-(ethylamido)-4-oxobutanoic acid _O_-ethyl ethynylphosphonothiolate (47)

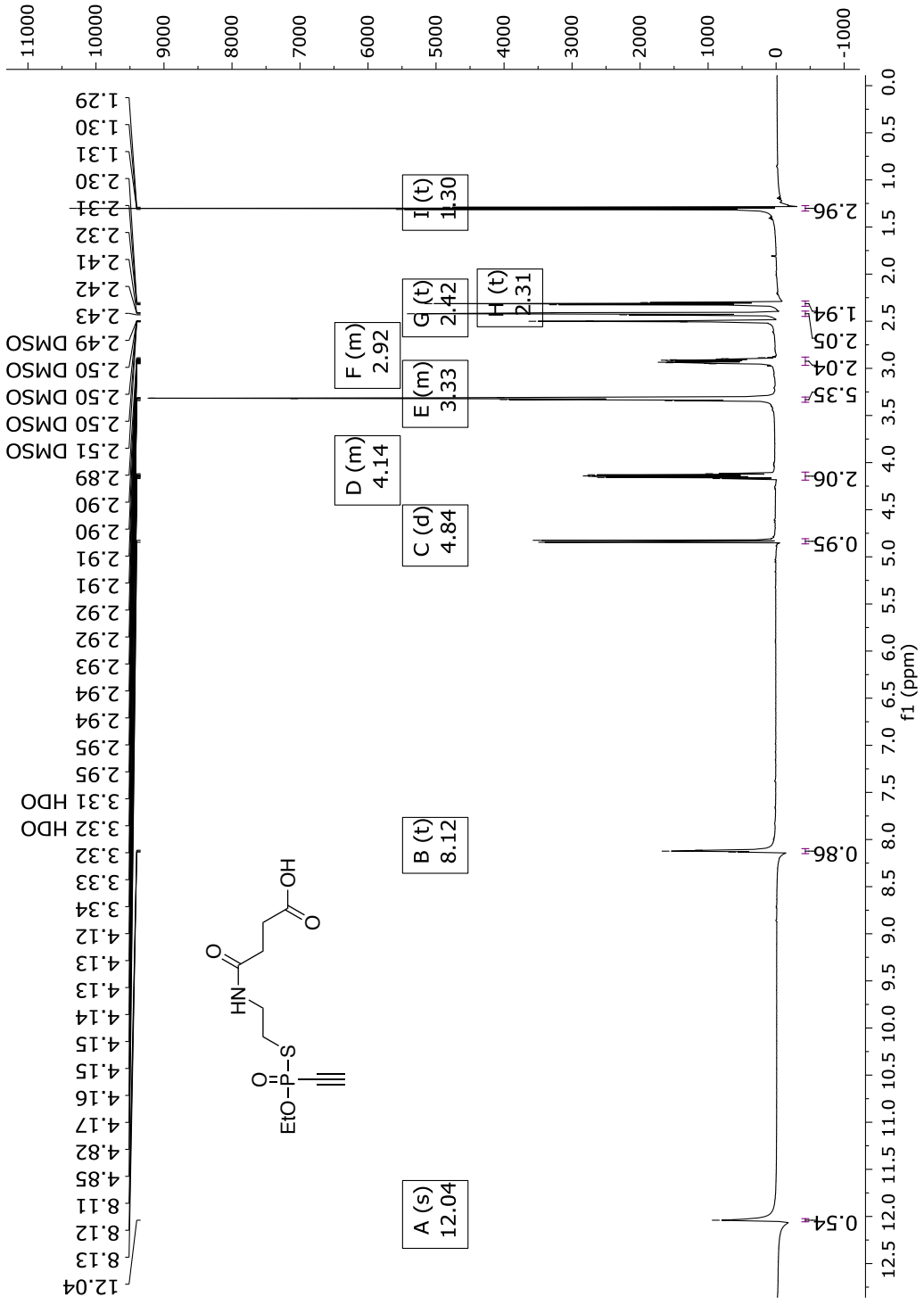

Fig. 199 ^{1}H-NMR spectrum of compound **47** in DMSO−d_6 (600 MHz).

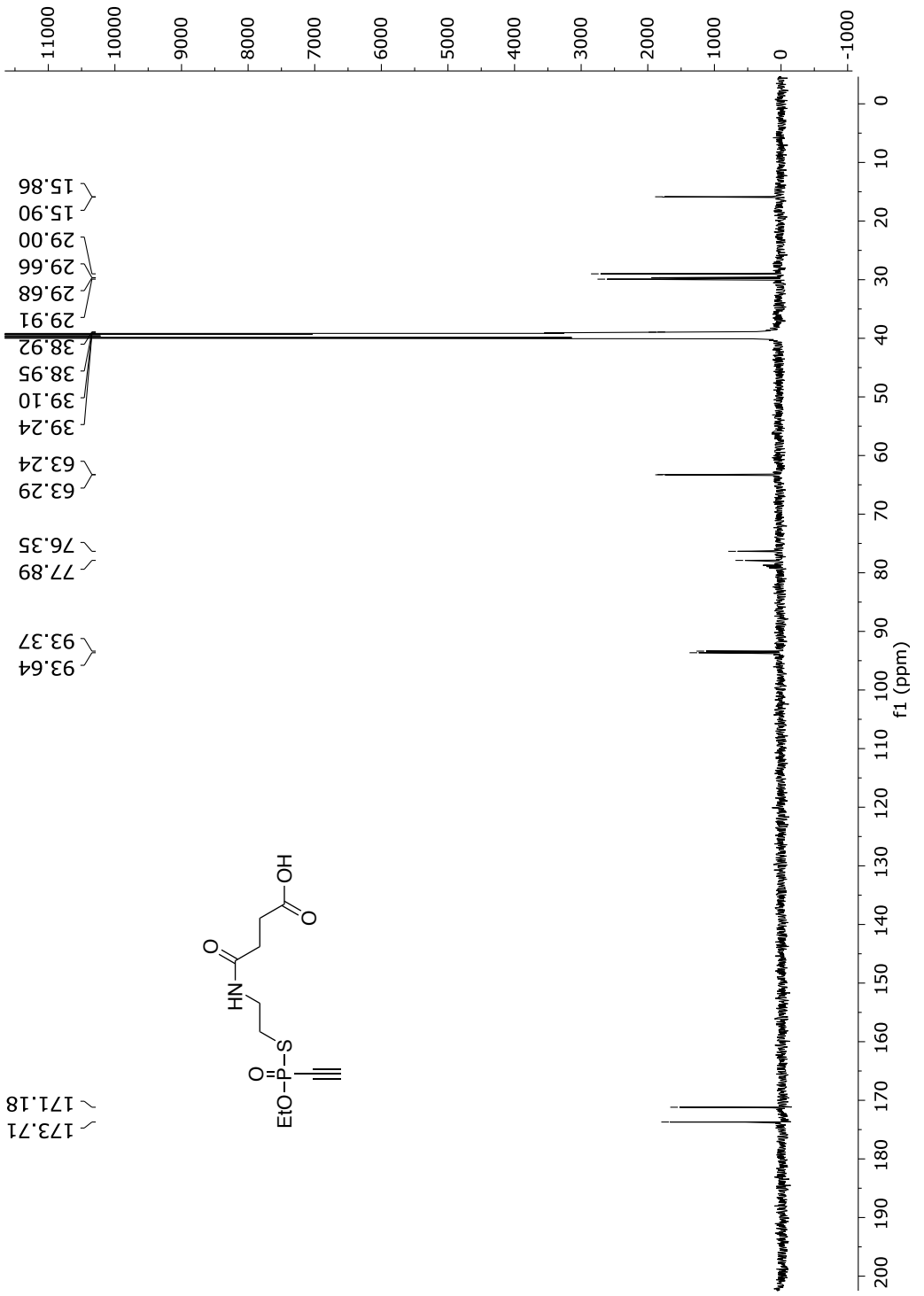

Fig. 200 ^{13}C-NMR spectrum of compound **47** in DMSO−d_6 (151 MHz).

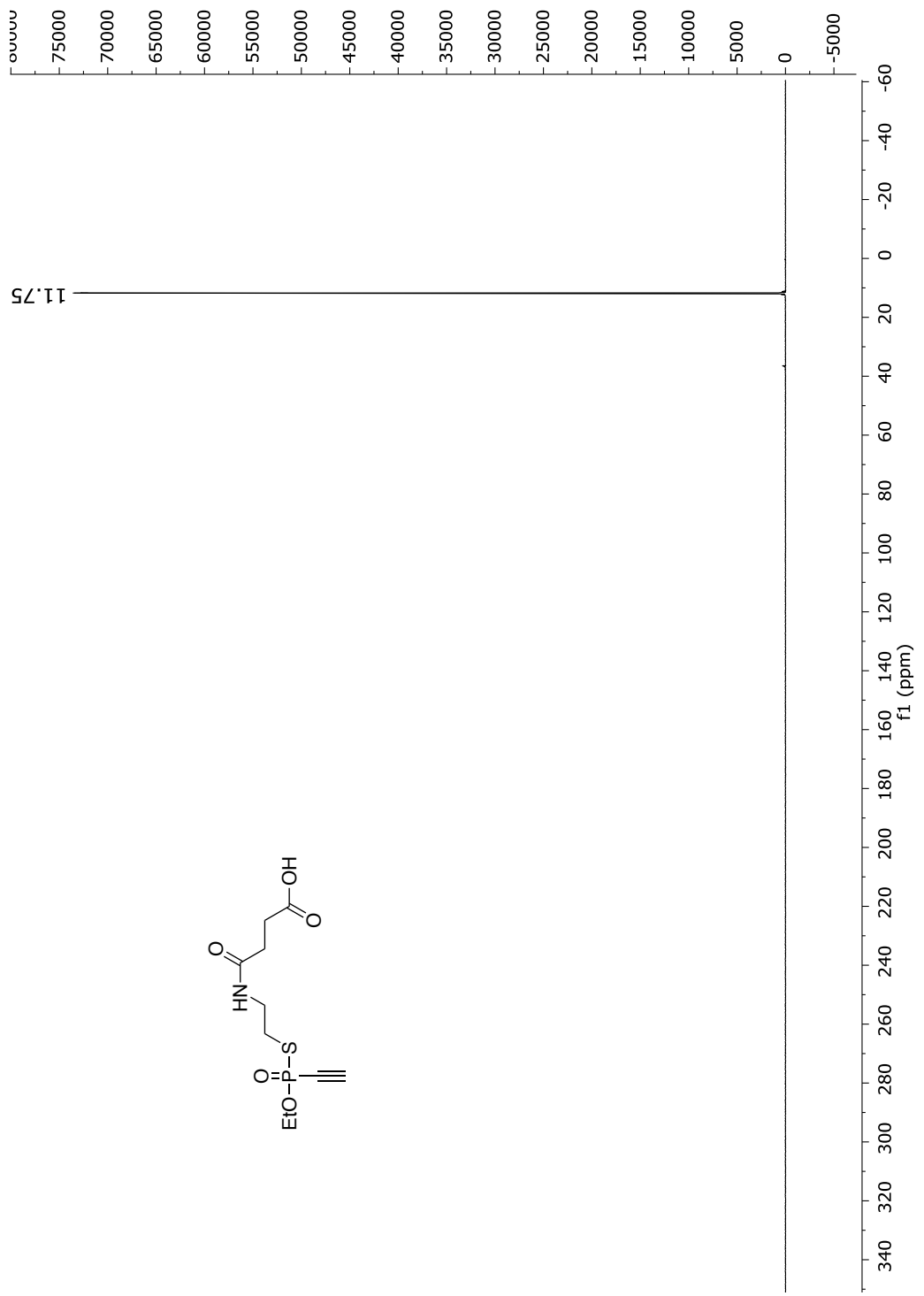

Fig. 201 ^{31}P-NMR spectrum of compound **47** in DMSO−d_6 (243 MHz).

S-4-(ethylamido)-4-oxobutanoic acid O-ethyl vinylphosphonothiolate (48)

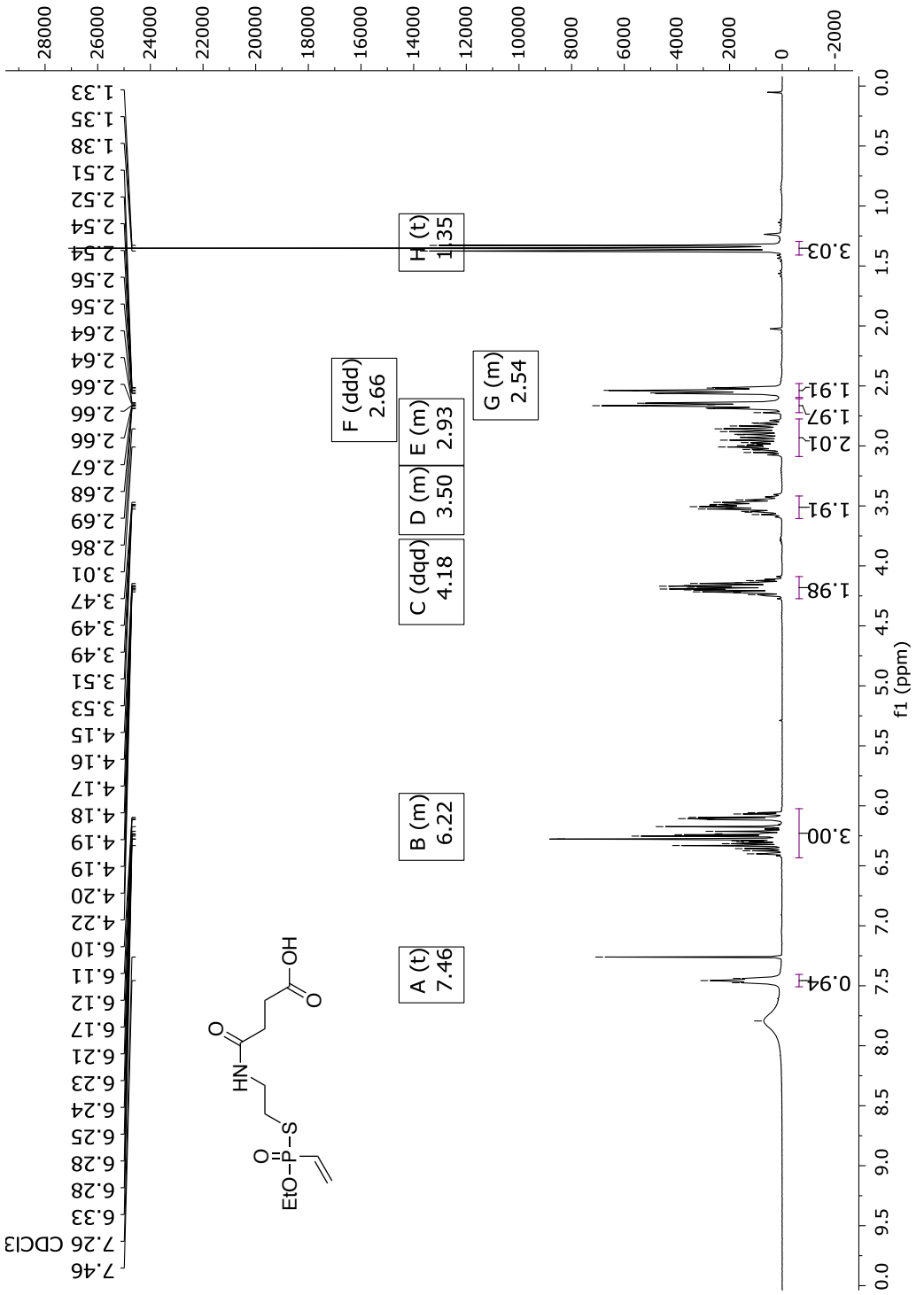

Fig. 202 ^{1}H-NMR spectrum of compound **48** in $CDCl_3$ (300 MHz).

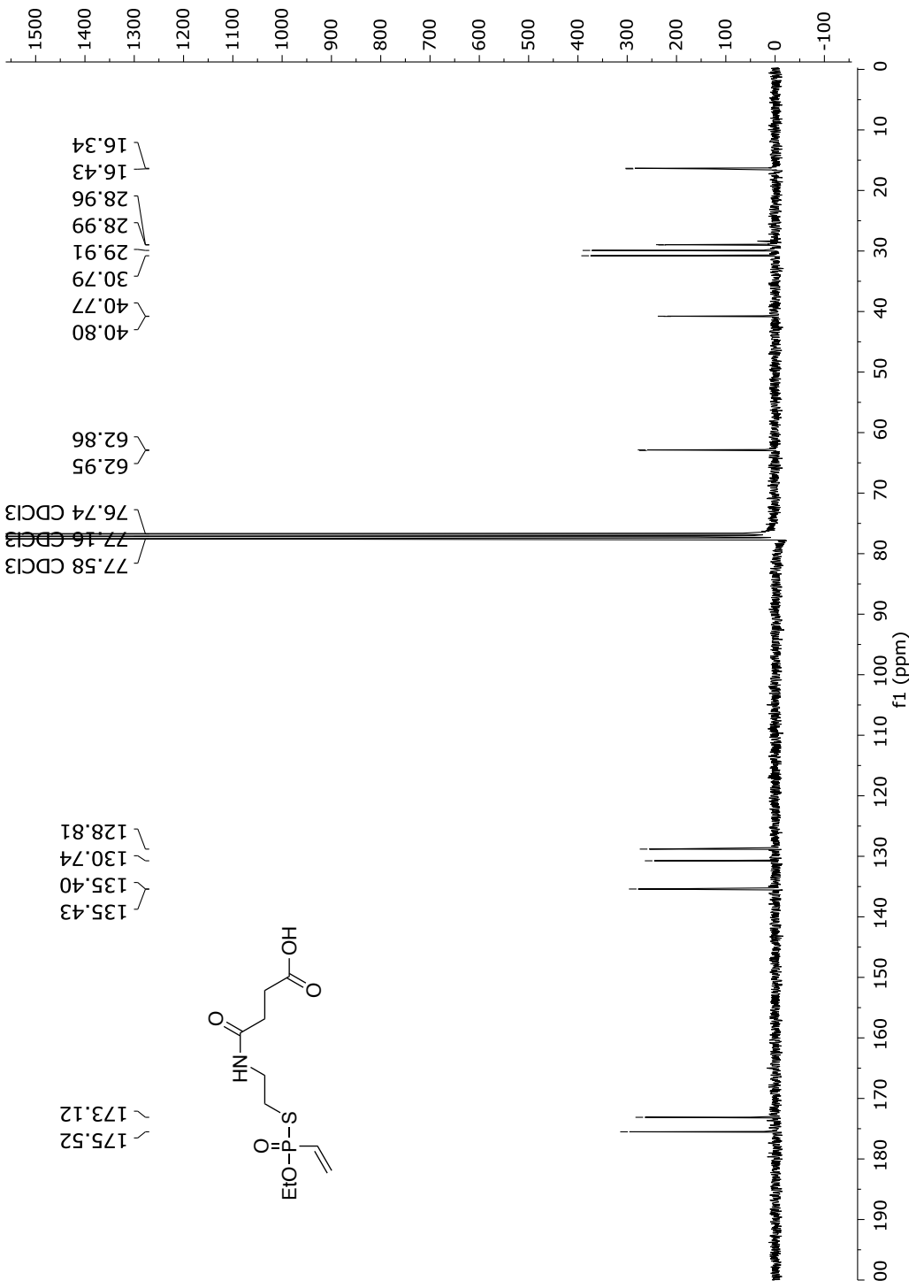

Fig. 203 ^{13}C-NMR spectrum of compound **48** in $CDCl_3$ (75 MHz).

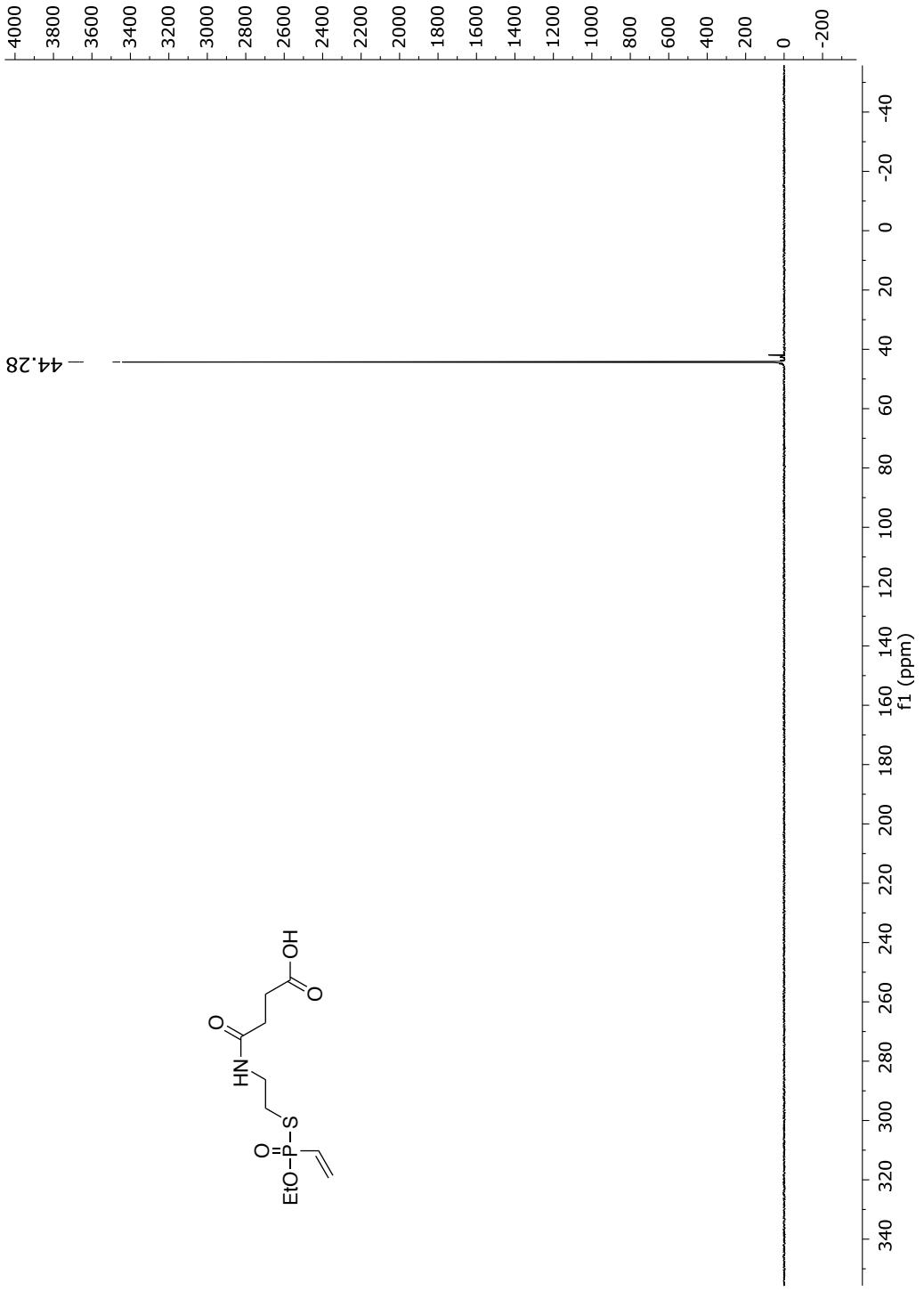

Fig. 204 ^{31}P-NMR spectrum of compound **48** in $CDCl_3$ (122 MHz).

2-(1-methyl-1H-pyrrol-2-yl)-2H-tetrazole-5-carboxylic acid (53)

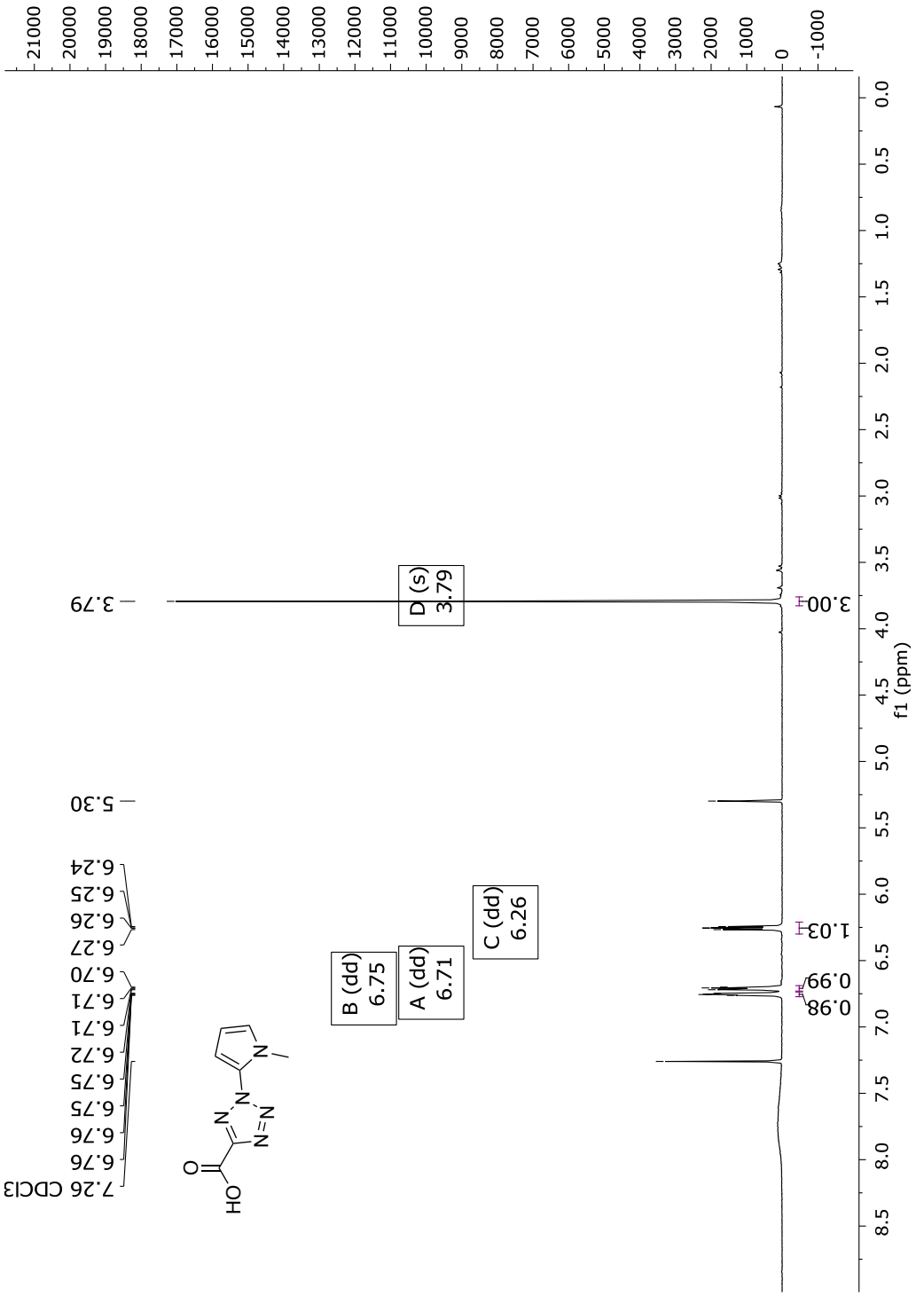

Fig. 205 ^{1}H-NMR spectrum of compound **53** in $CDCl_3$ (300 MHz).

_S_-diazirine derivative _O_-ethyl vinylphosphonothiolate (54)

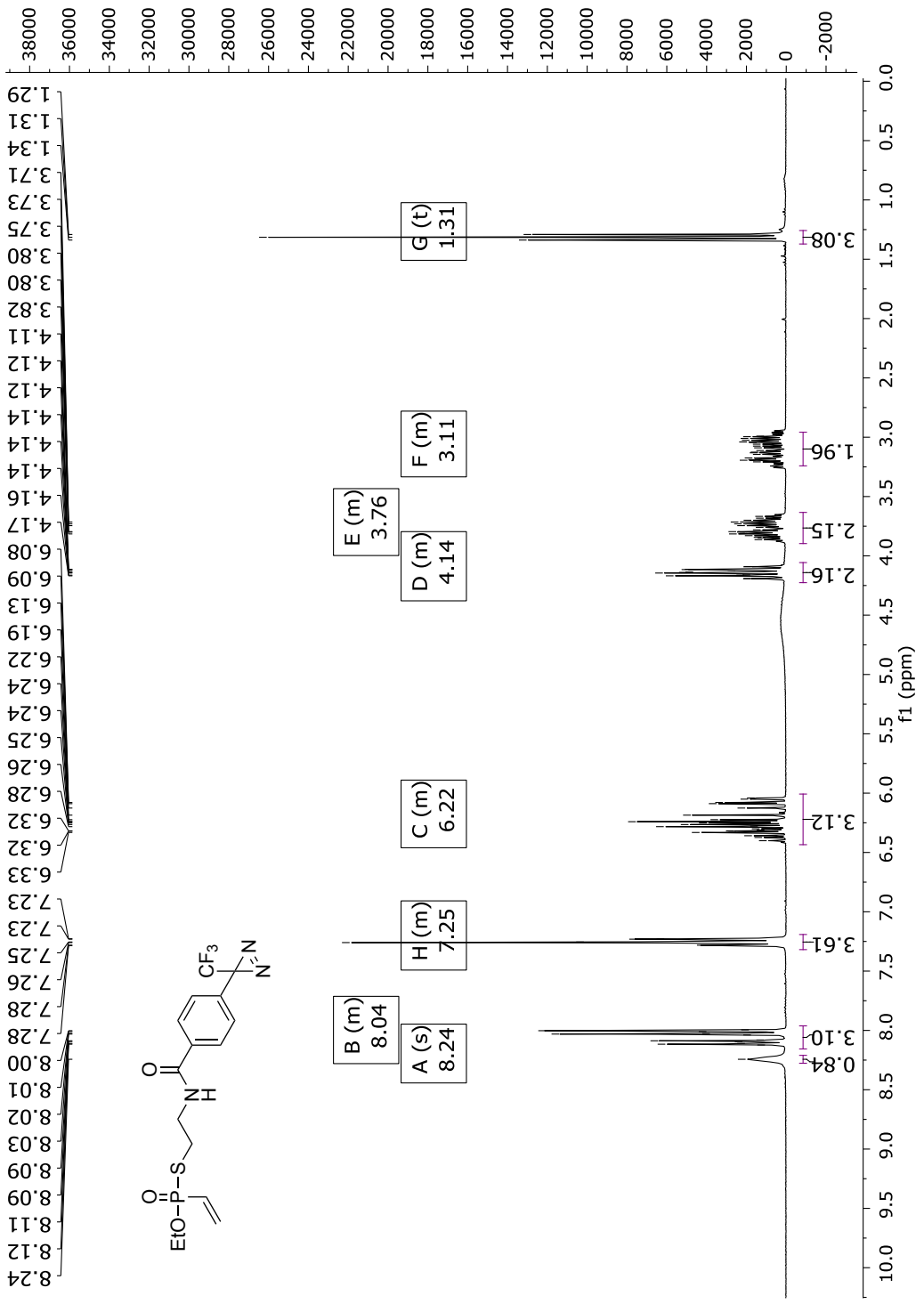

Fig. 206 ^{1}H-NMR spectrum of compound **54** in $CDCl_3$ (300 MHz).

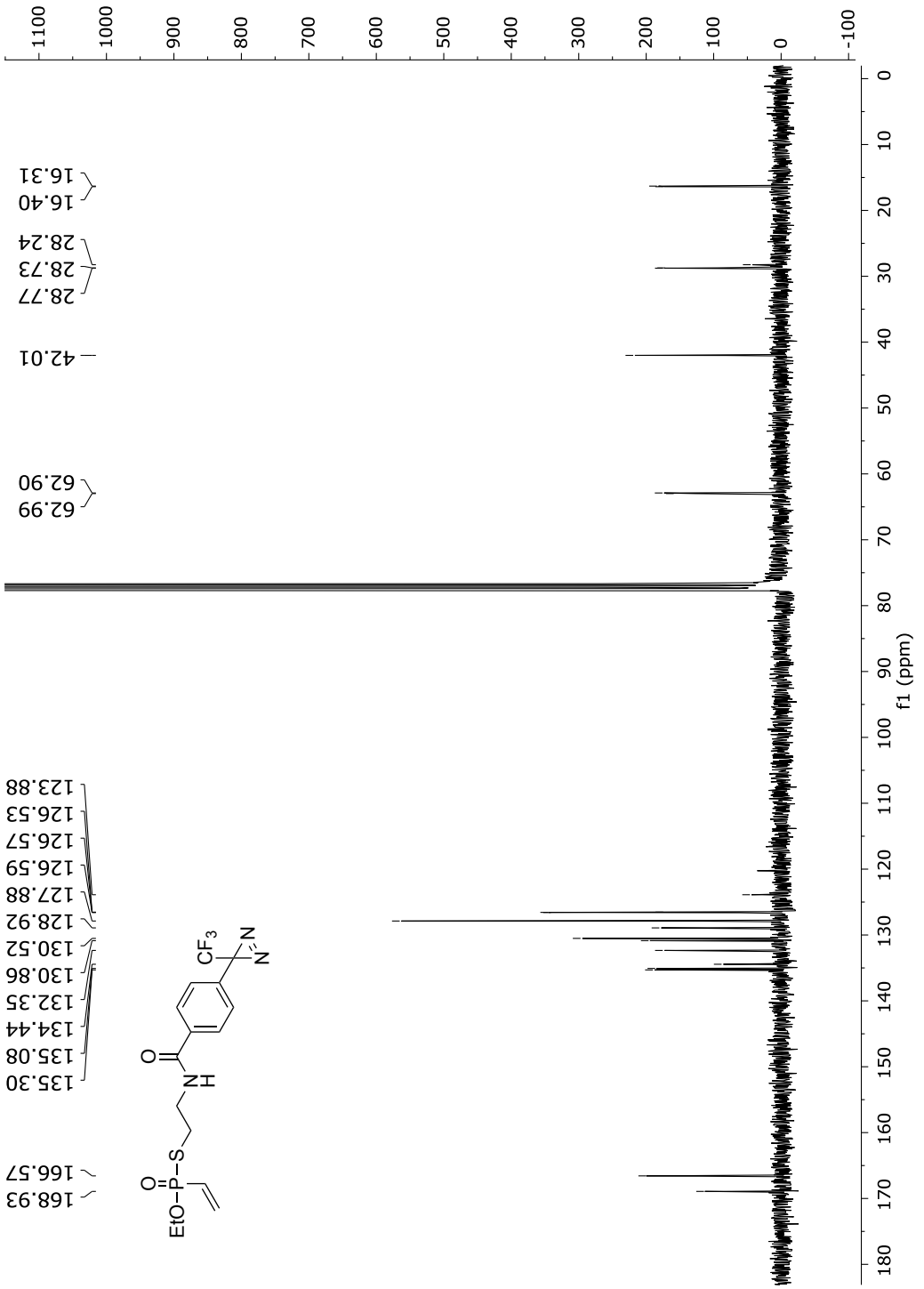

Fig. 207 ^{13}C-NMR spectrum of compound **54** in $CDCl_3$ (75 MHz).

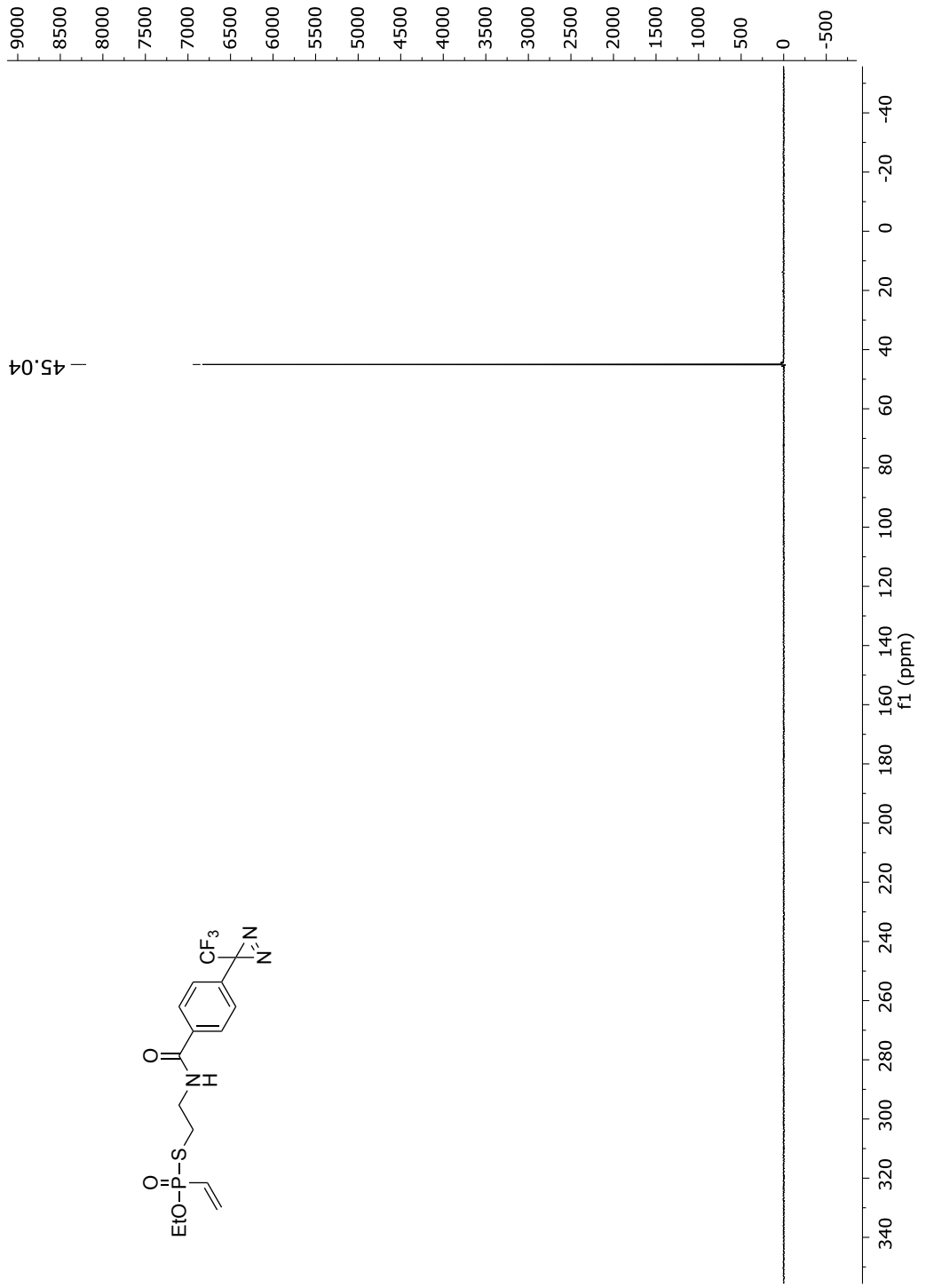

Fig. 208 ^{31}P-NMR spectrum of compound **54** in $CDCl_3$ (122 MHz).

_S_-methyl-pyrrol-tetrazole derivative _O_-ethyl vinylphosphonothiolate (55)

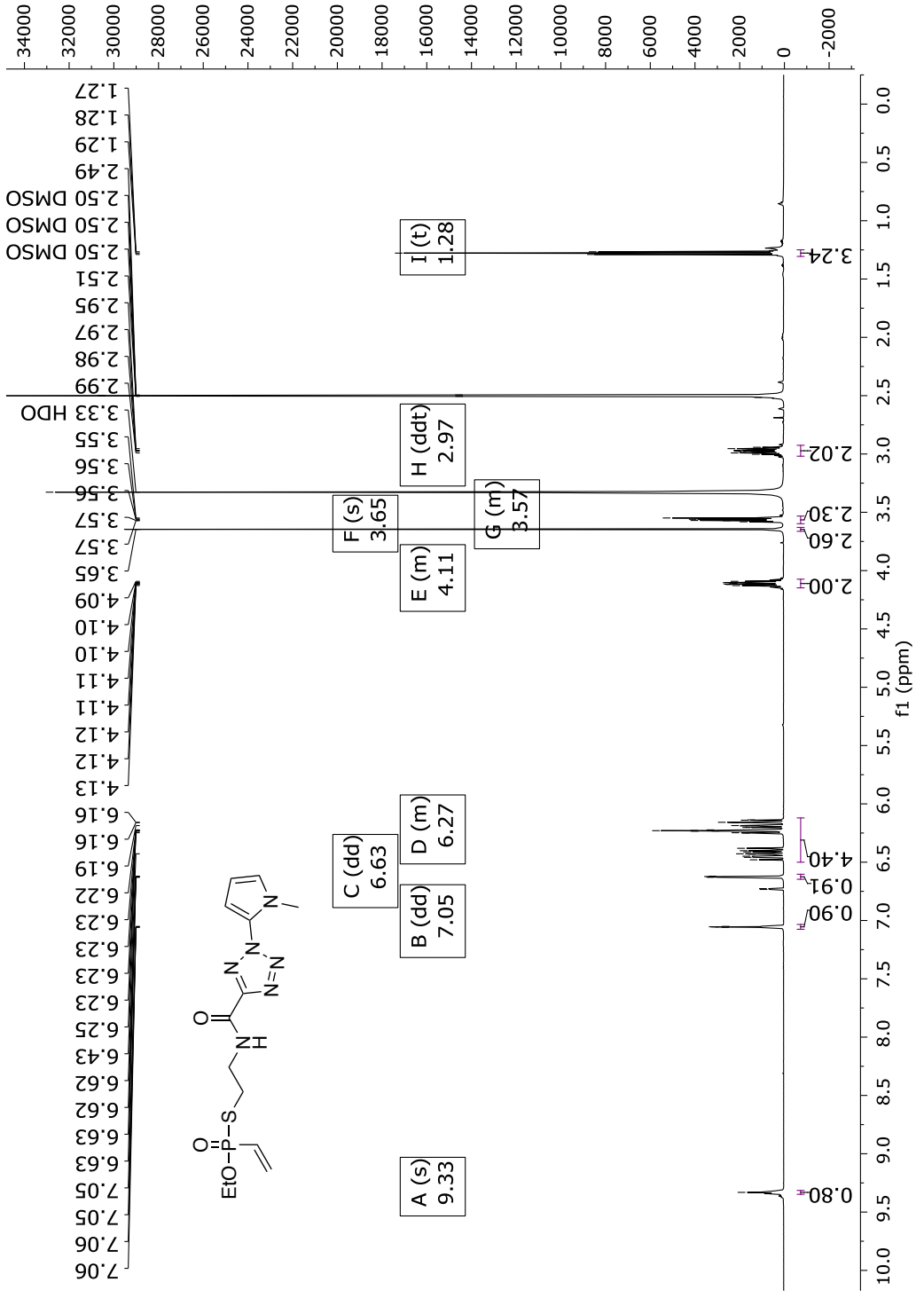

Fig. 209 ^{1}H-NMR spectrum of compound **55** in DMSO−d_6 (600 MHz).

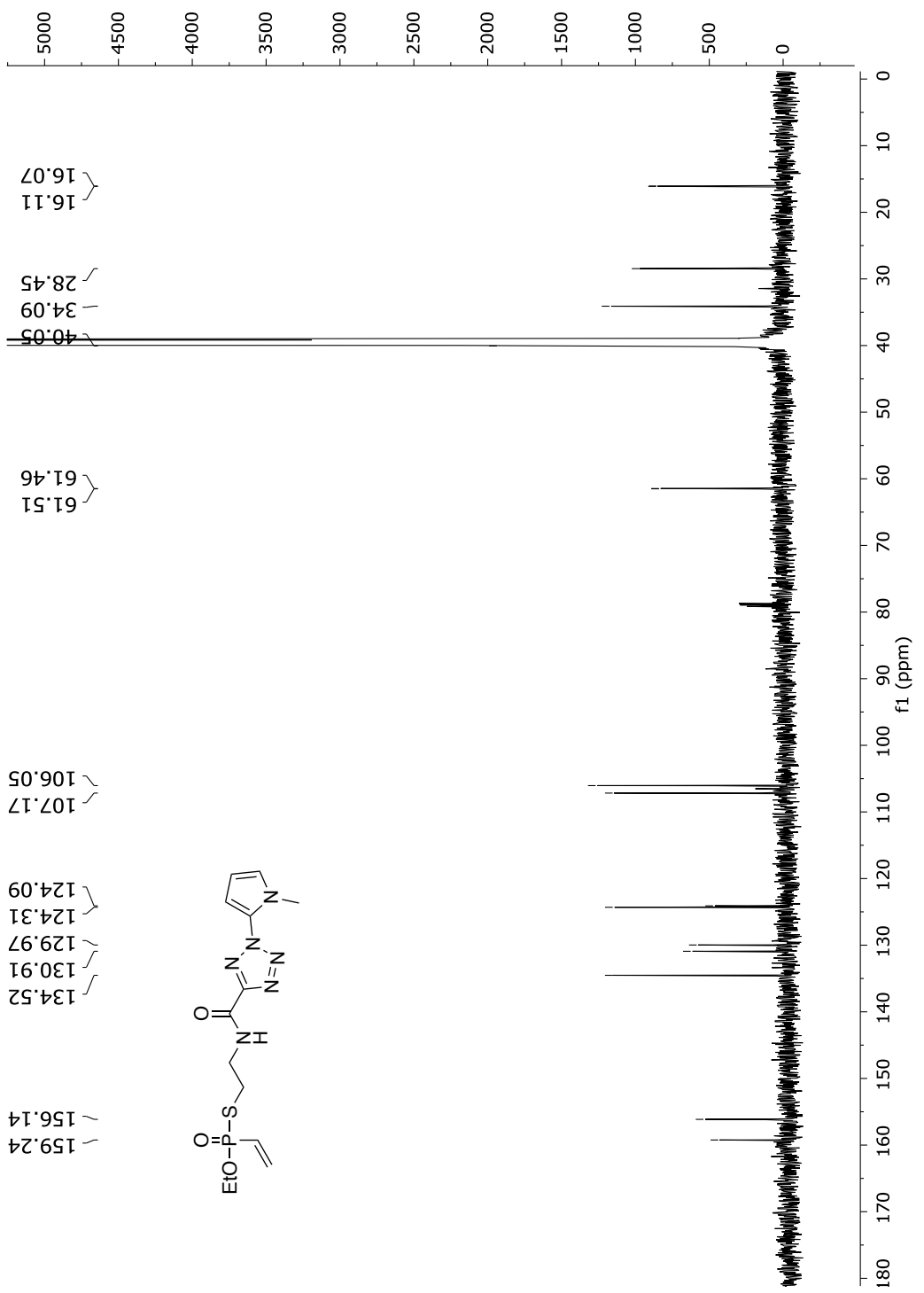

Fig. 210 ^{13}C-NMR spectrum of compound **55** in DMSO−d_6 (151 MHz).

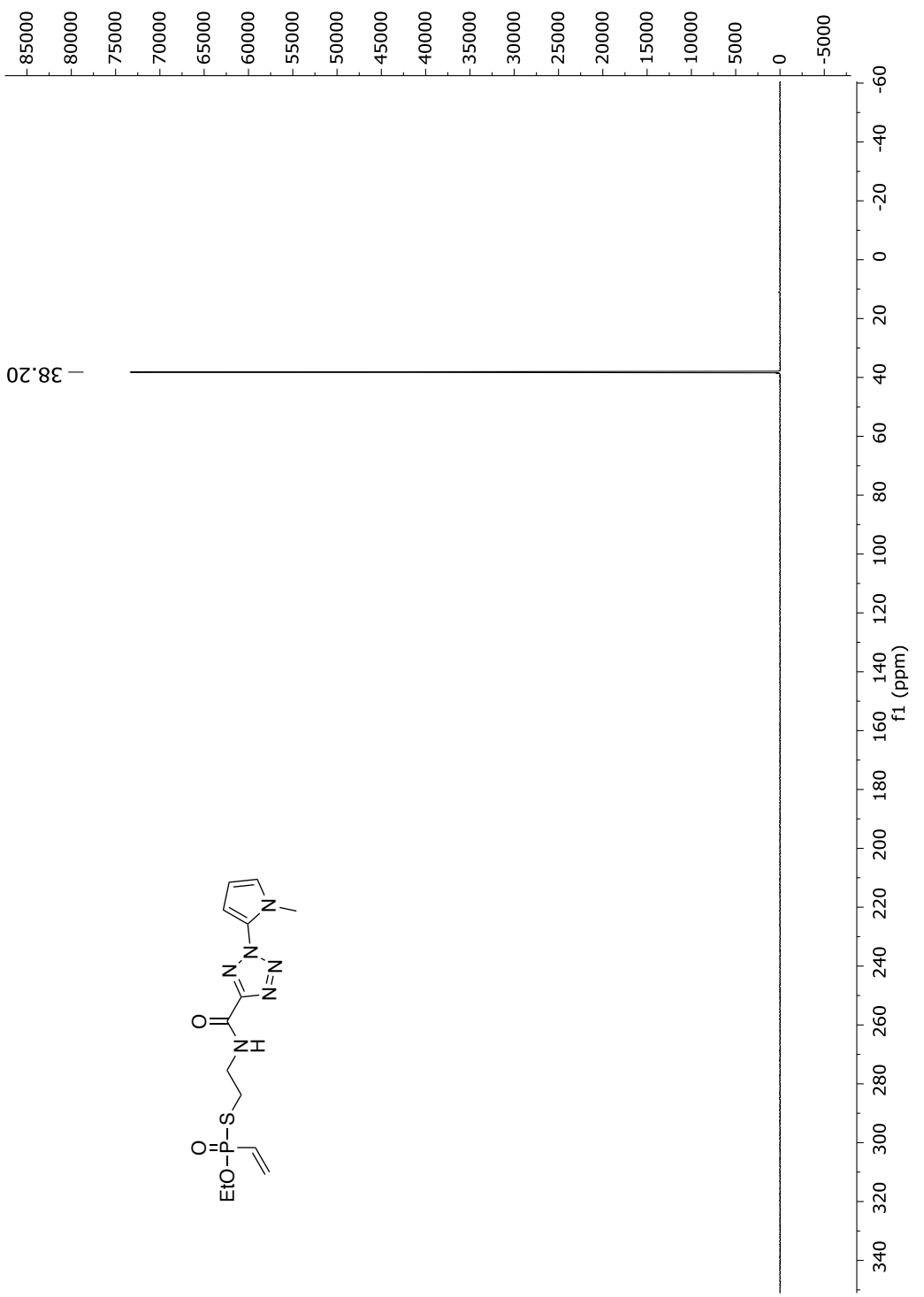

Fig. 211 ^{31}P-NMR spectrum of compound **55** in DMSO−d_6 (243 MHz).

Glutathione conjugate (56)

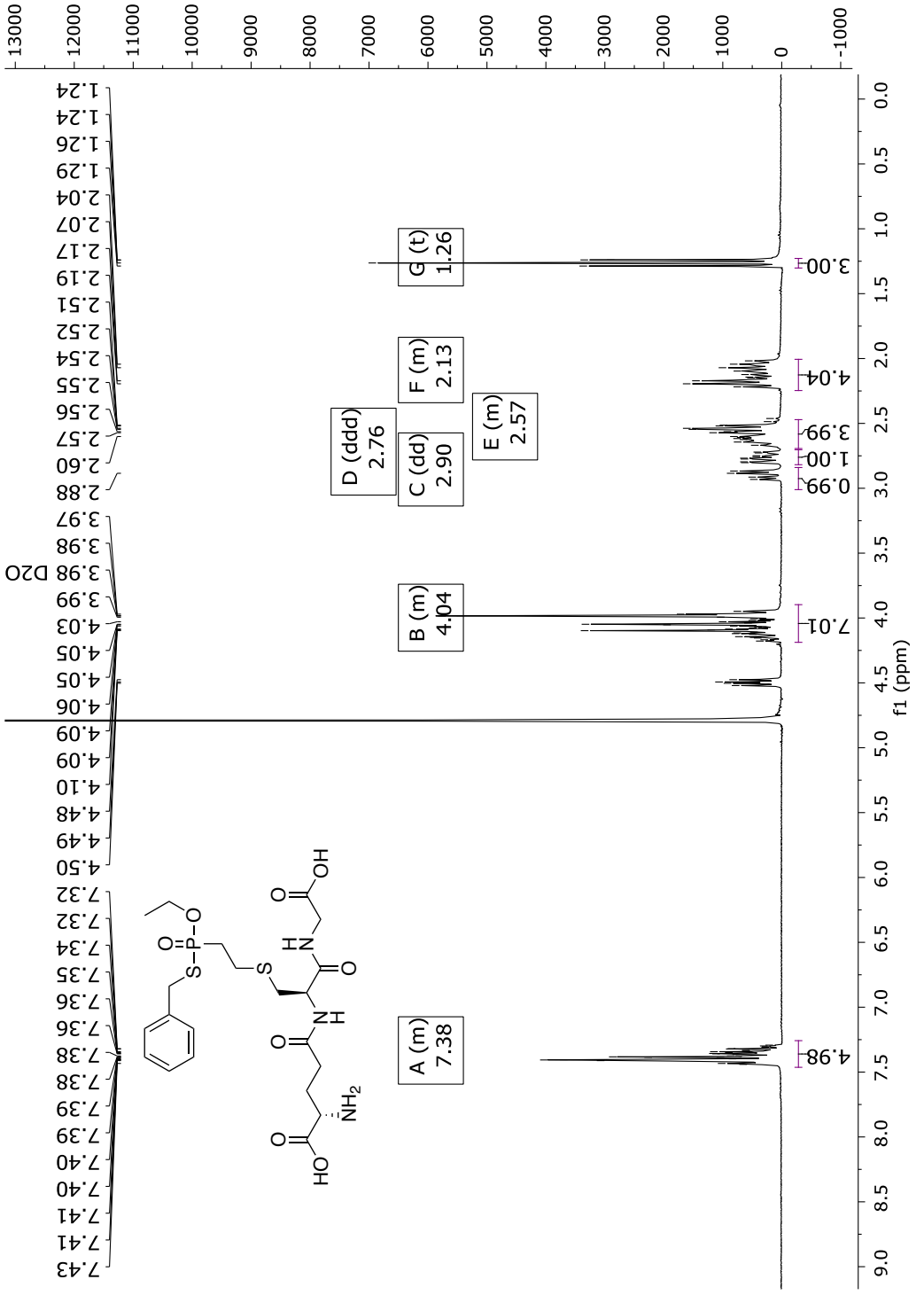

Fig. 212 ^{1}H-NMR spectrum of compound **56** in D_2O (300 MHz).

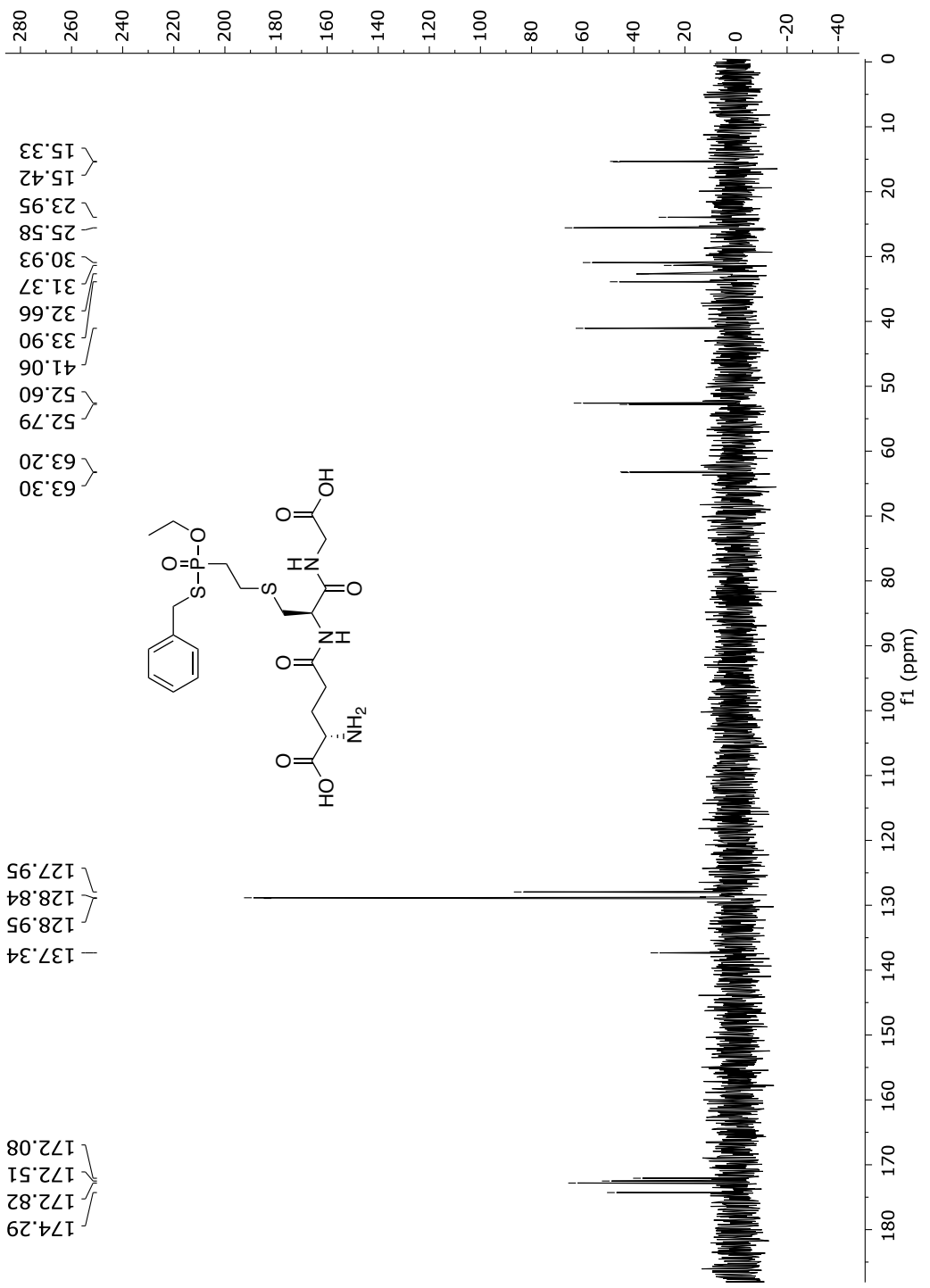

Fig. 213 ^{13}C-NMR spectrum of compound **56** in D_2O (75 MHz).

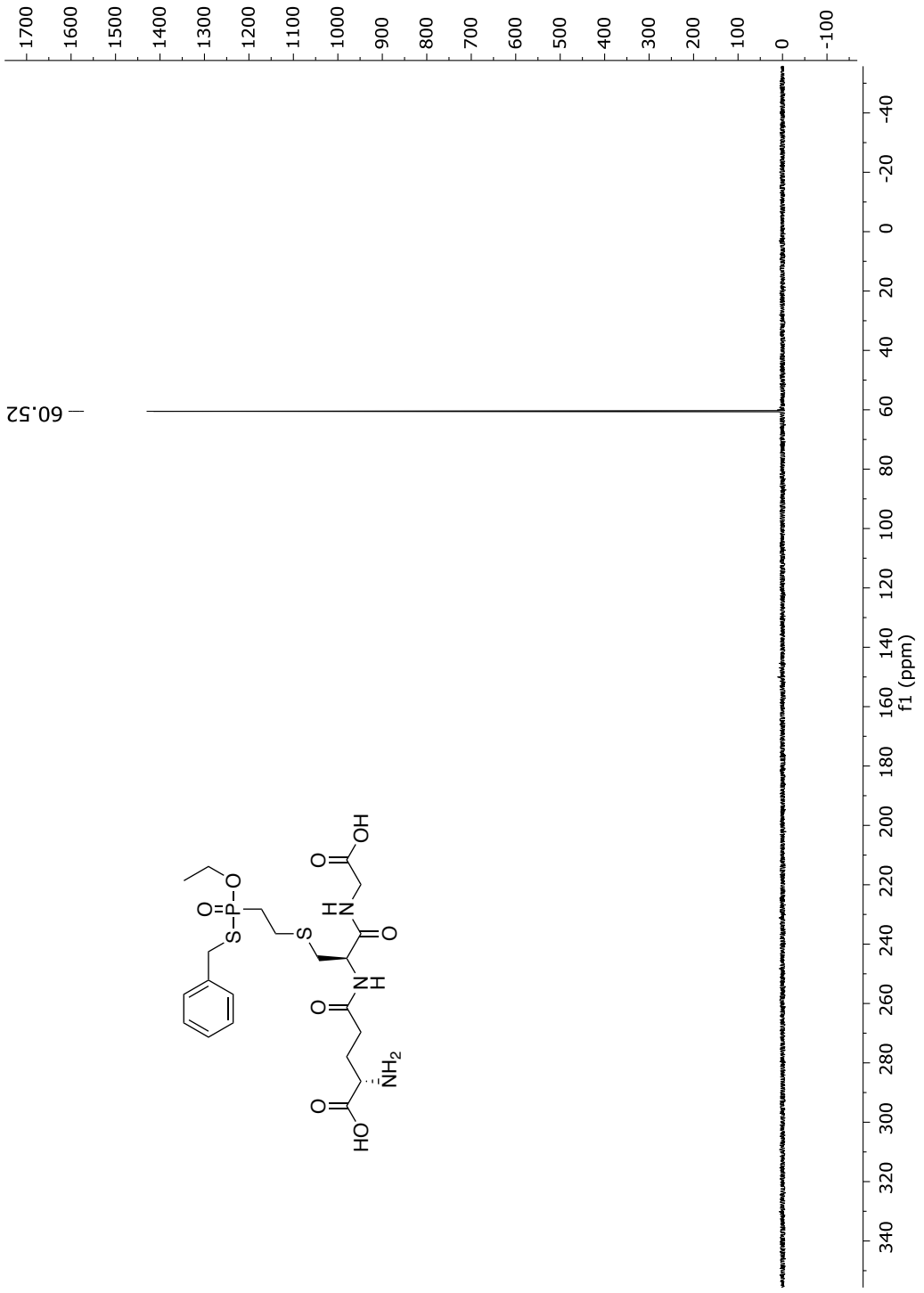

Fig. 214 ^{31}P-NMR spectrum of compound **56** in D_2O (122 MHz).

Glutathione conjugate (57), *Z*-isomer

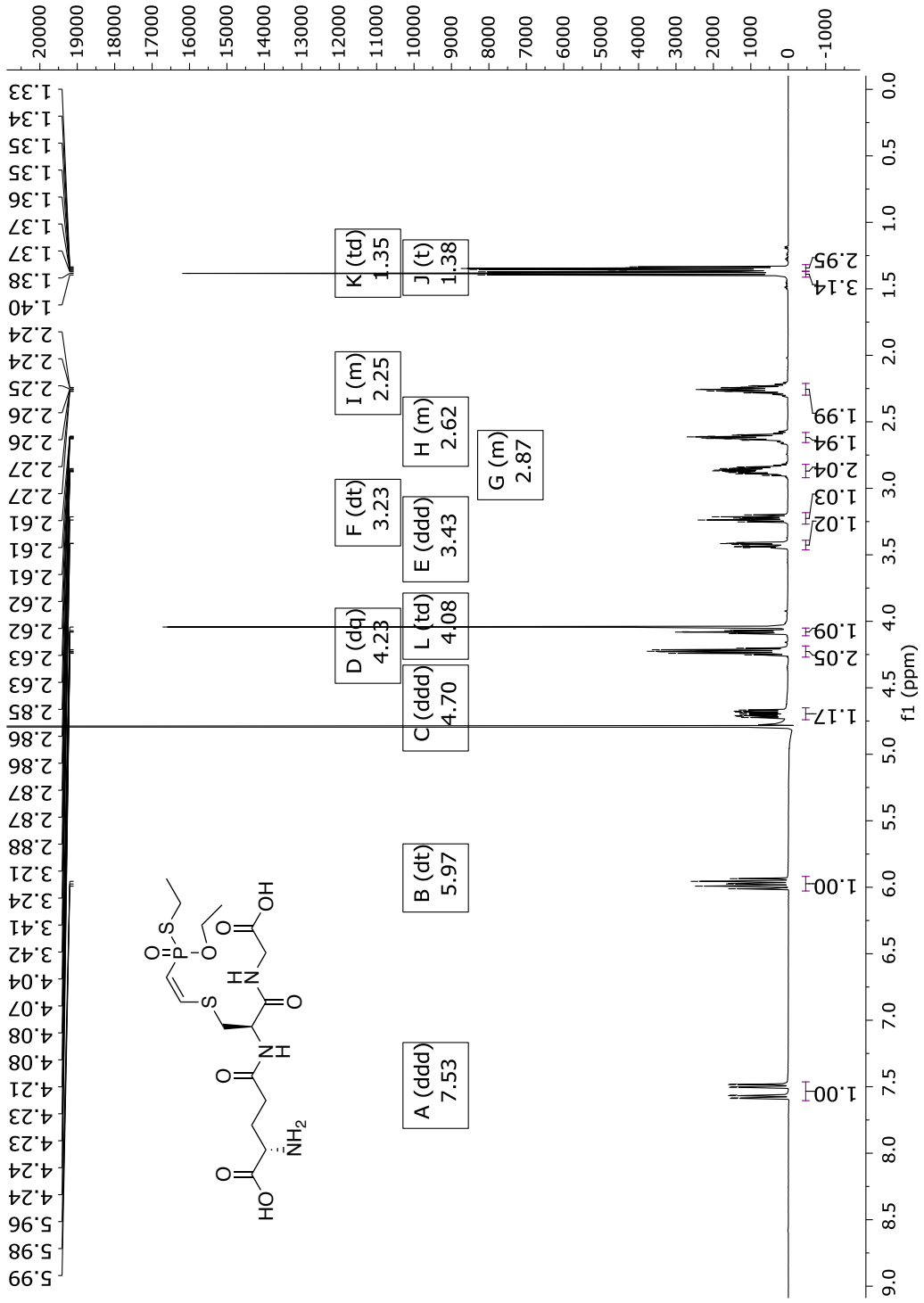

Fig. 215 ^{1}H-NMR spectrum of compound **57** (*Z*-isomer) in D_2O (600 MHz).

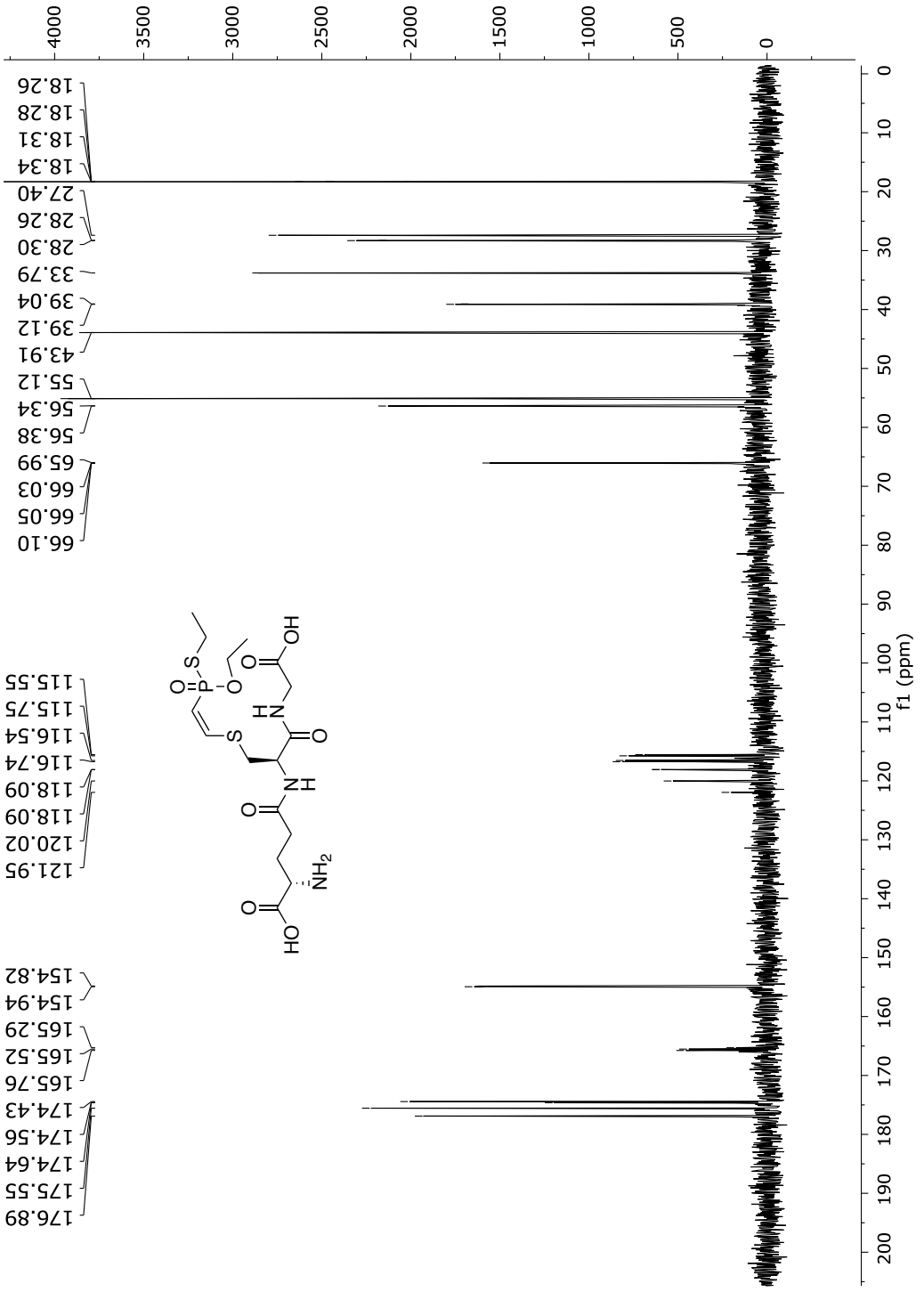

Fig. 216 ^{13}C-NMR spectrum of compound **57** (*Z*-isomer) in D_2O (151 MHz).

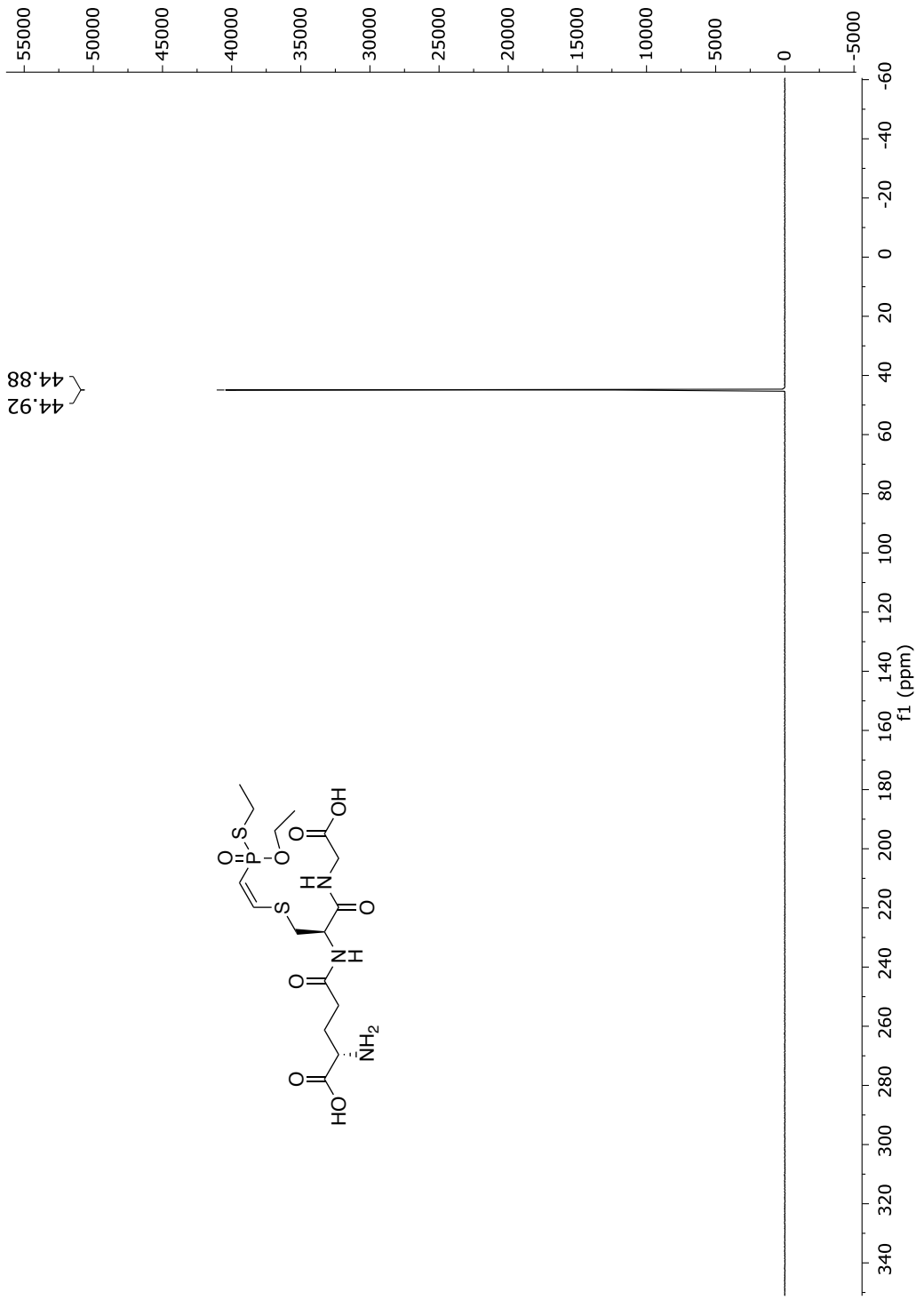

Fig. 217 ^{31}P-NMR spectrum of compound **57** (*Z*-isomer) in D_2O (243 MHz).

Glutathione conjugate (57), *E*-isomer

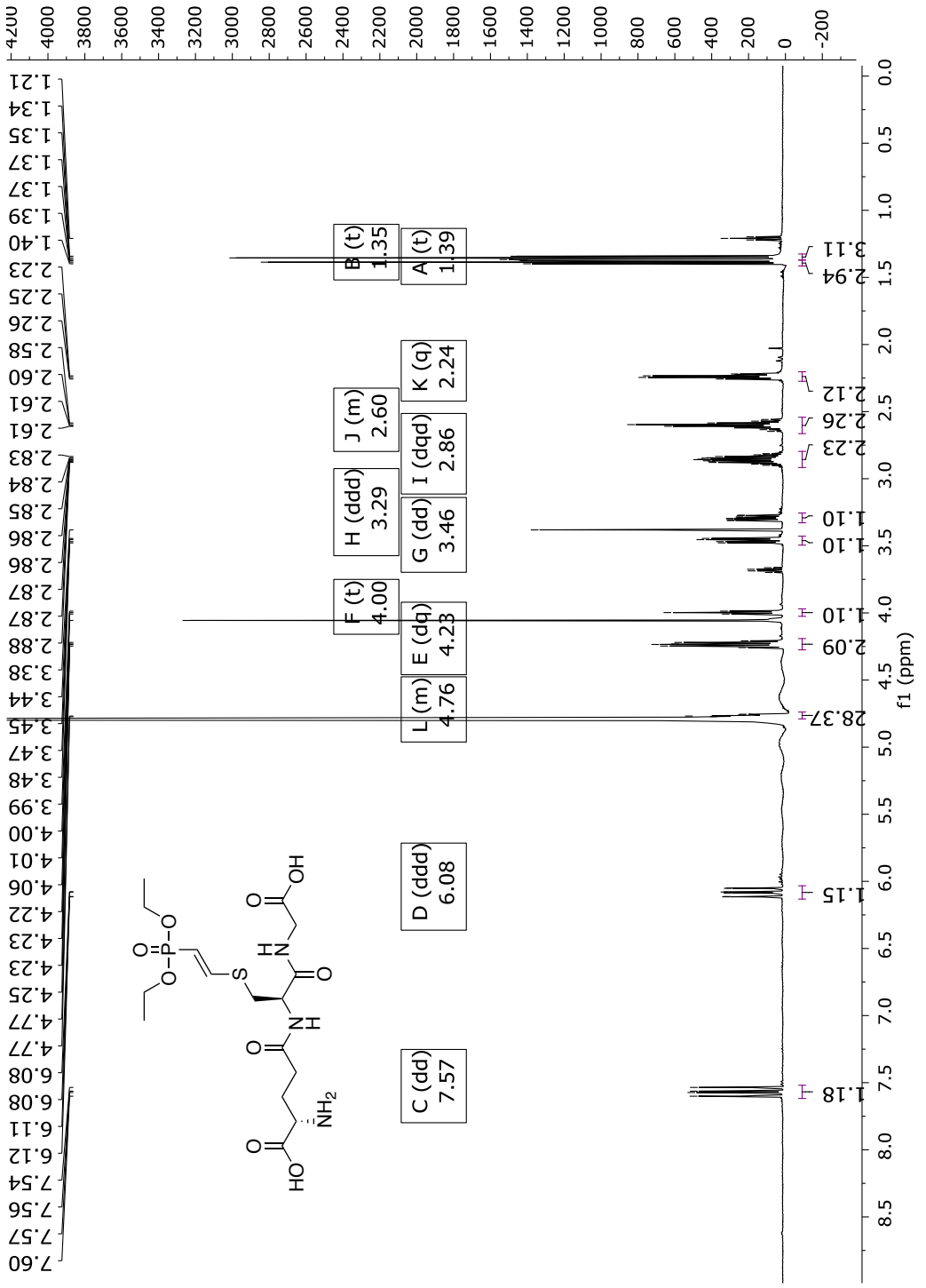

Fig. 218 ^{1}H-NMR spectrum of compound **57** (*E*-isomer) in D_2O (600 MHz).

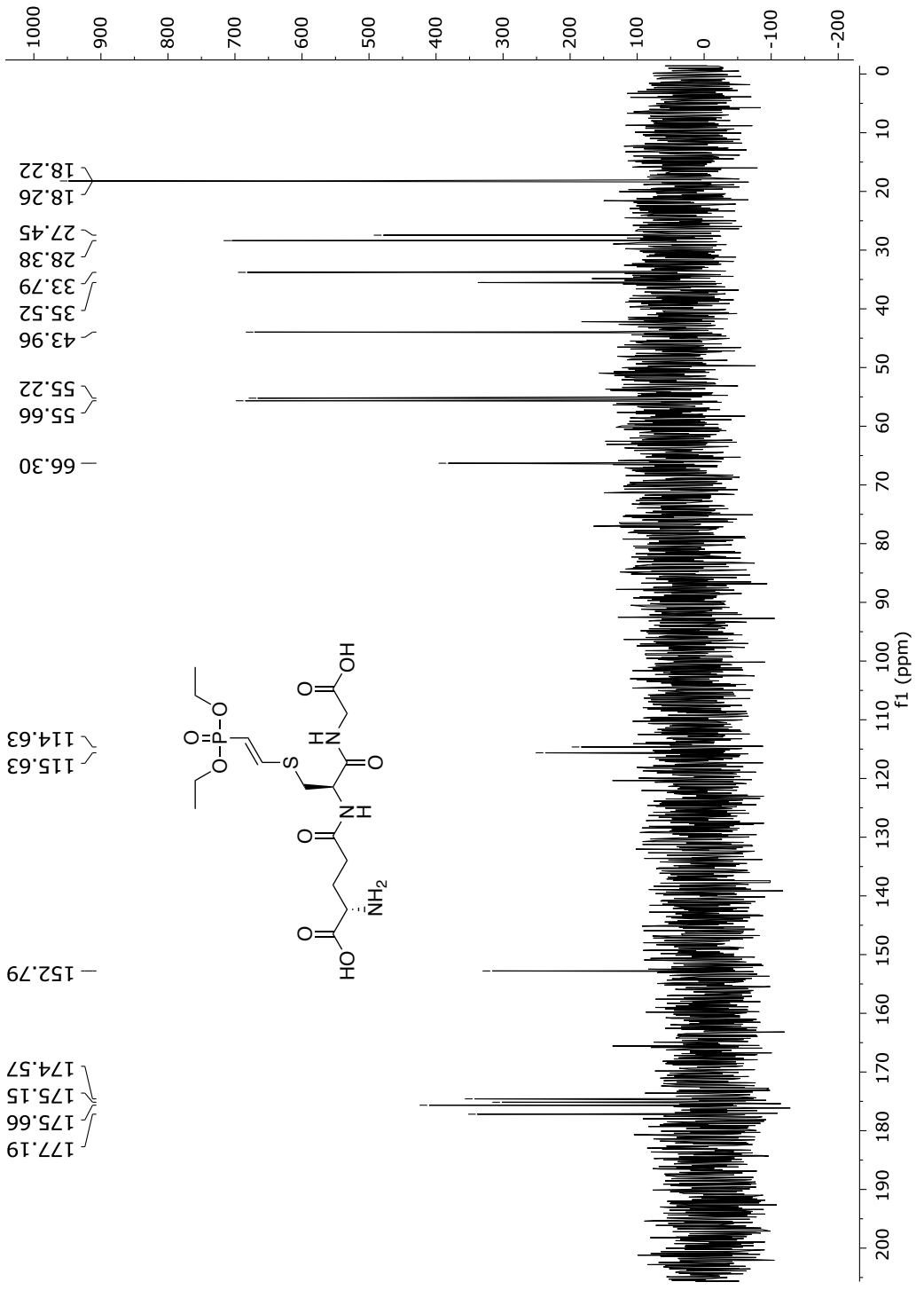

Fig. 219 ^{13}C-NMR spectrum of compound **57** (*E*-isomer) in D_2O (151 MHz).

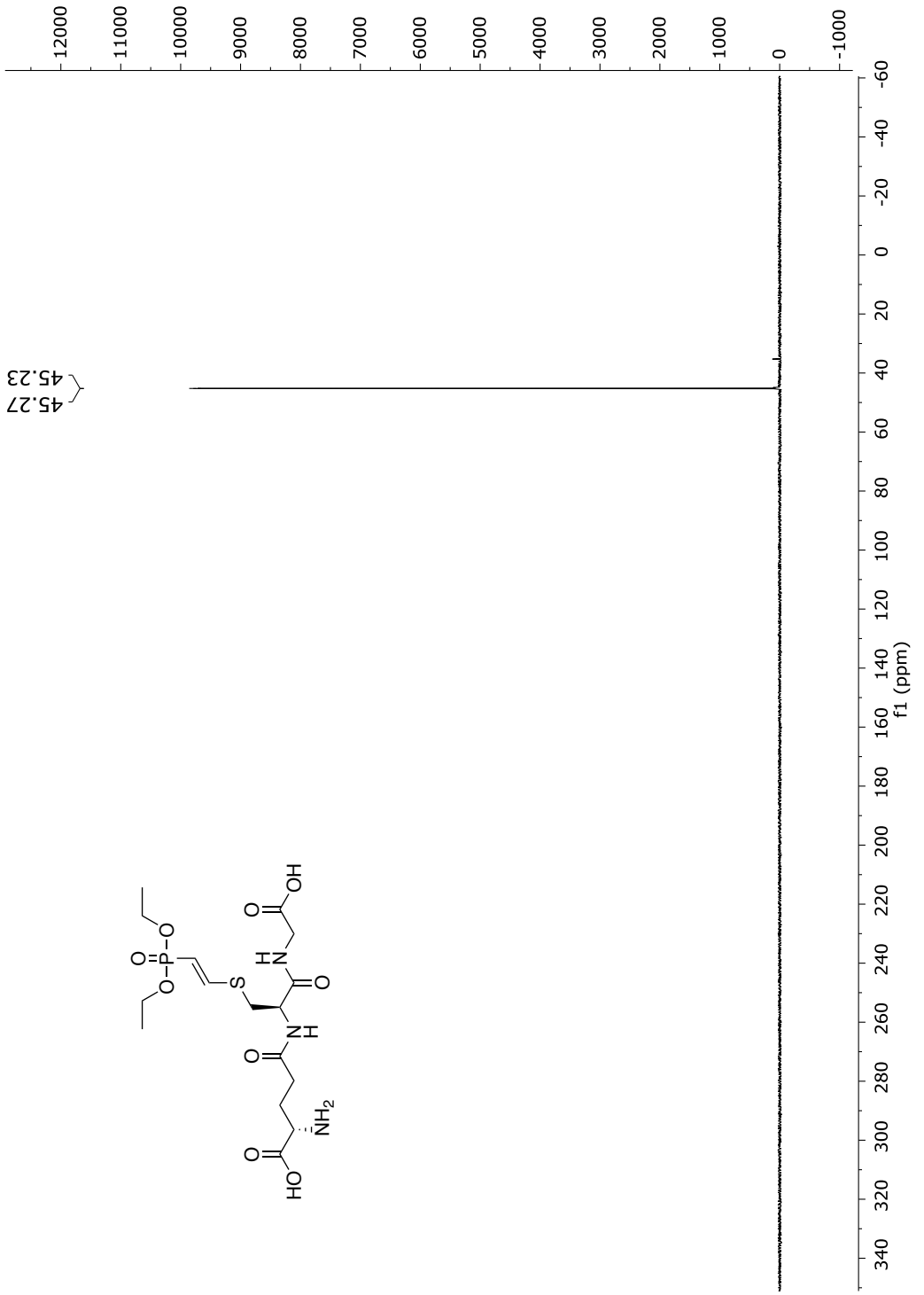

Fig. 220 ^{31}P-NMR spectrum of compound **57** (*E*-isomer) in D_2O (243 MHz).

_O_-Boc-ethylamine _O_-ethyl ethynylphosphonate (61)

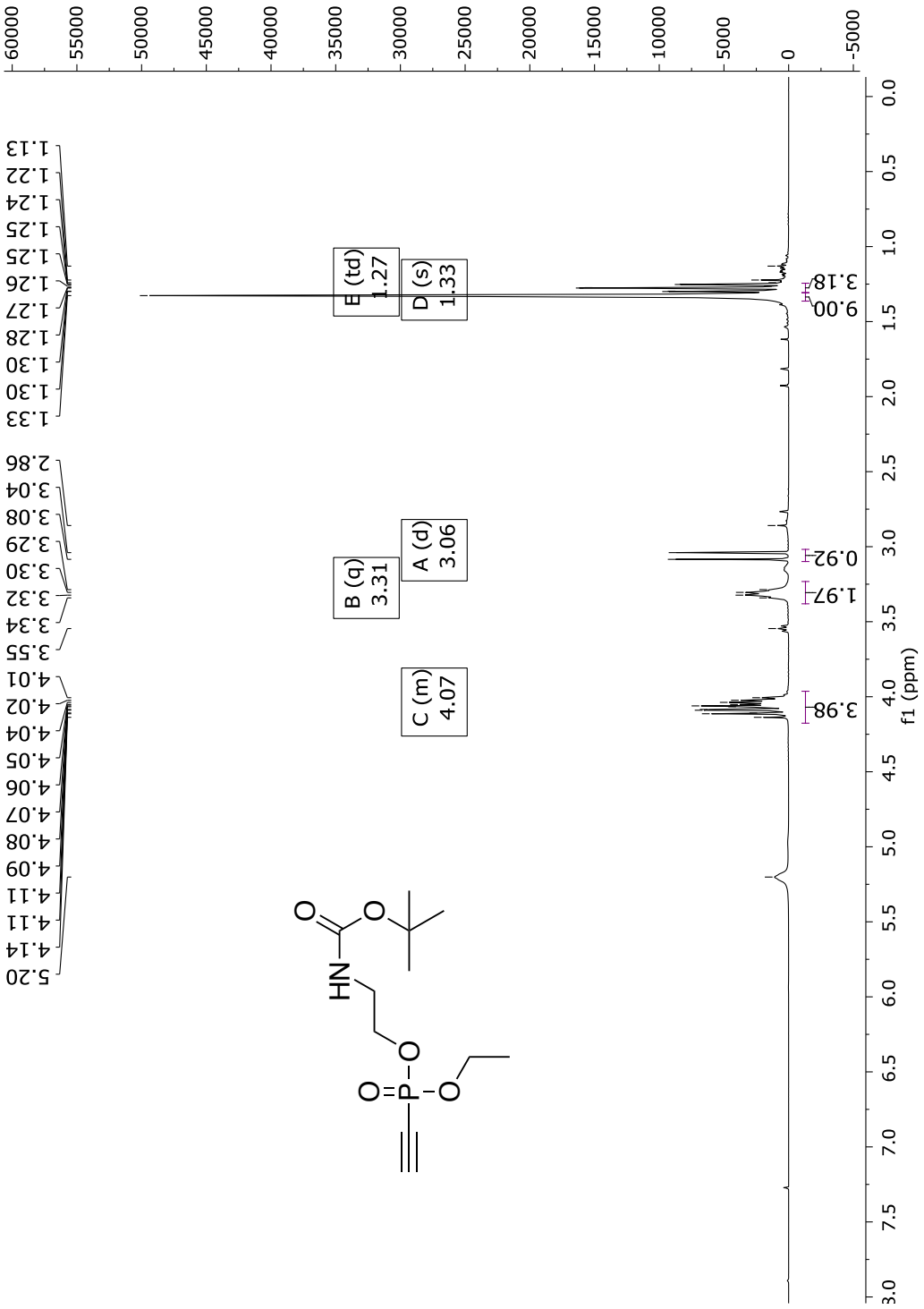

Fig. 221 ^{1}H-NMR spectrum of compound **61** in $CDCl_3$ (300 MHz).

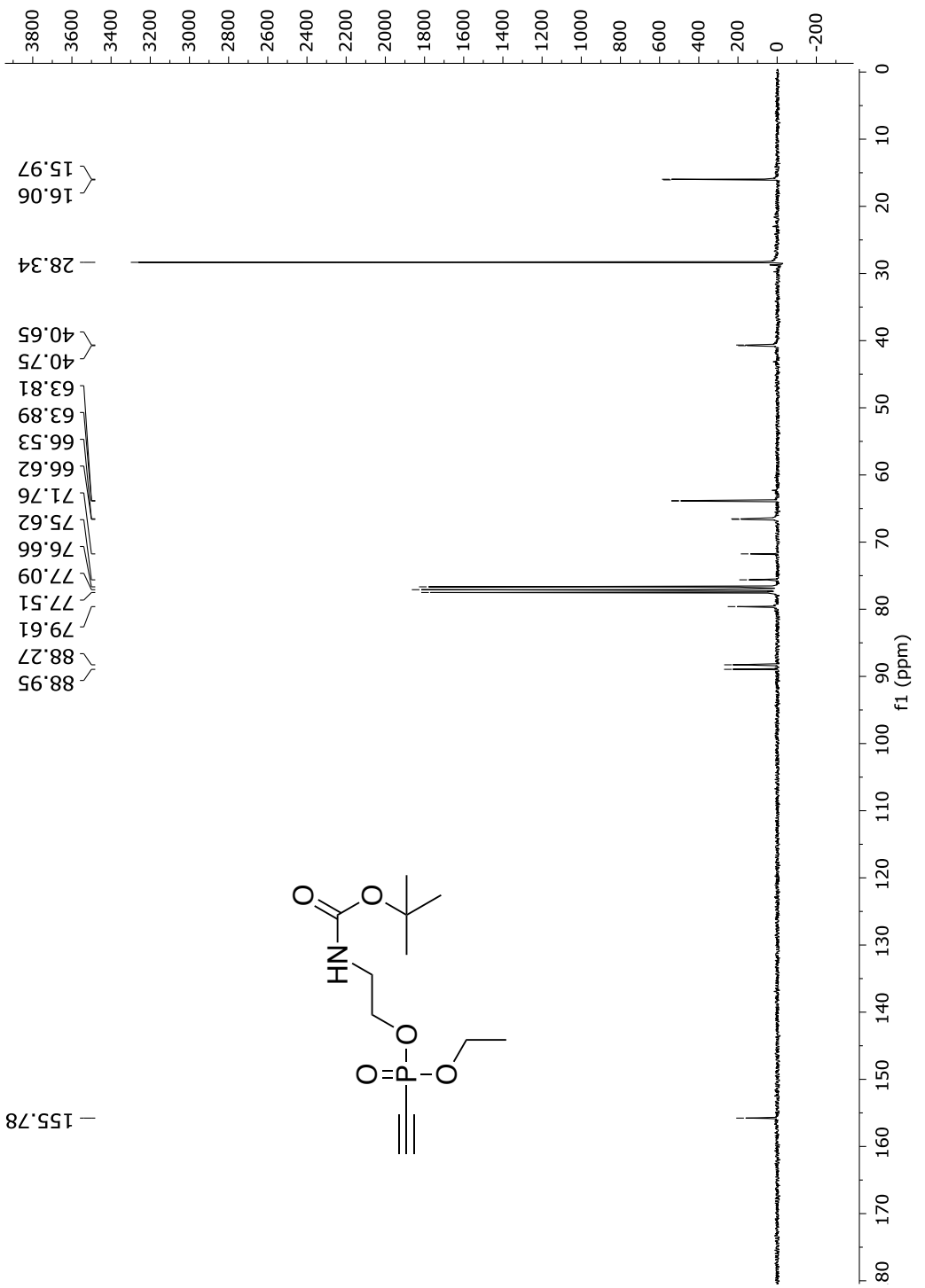

Fig. 222 ^{13}C-NMR spectrum of compound **61** in $CDCl_3$ (75 MHz).

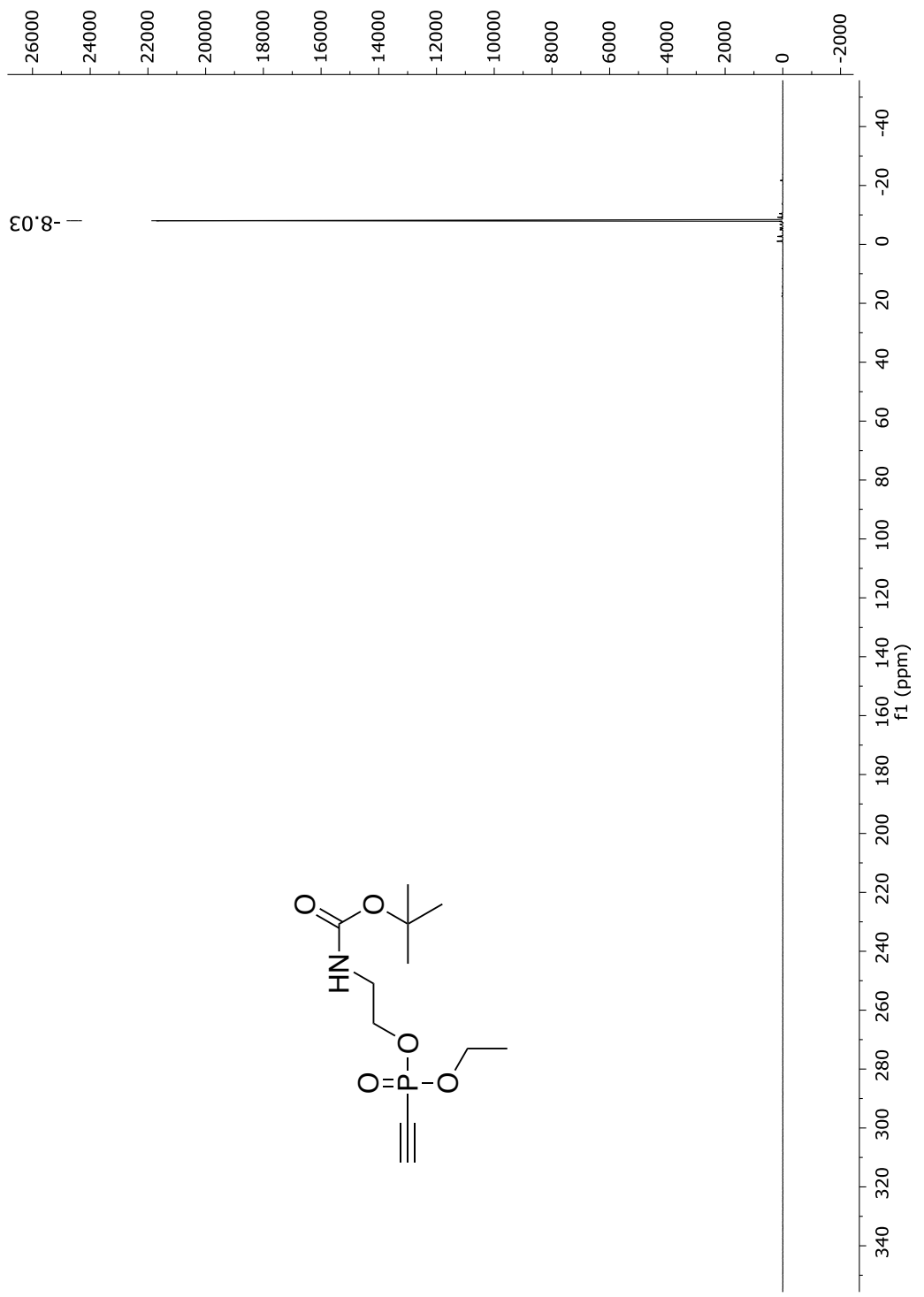

Fig. 223 ^{31}P-NMR spectrum of compound **61** in $CDCl_3$ (122 MHz).

O-Boc-ethylamine O-ethyl vinylphosphonate (62)

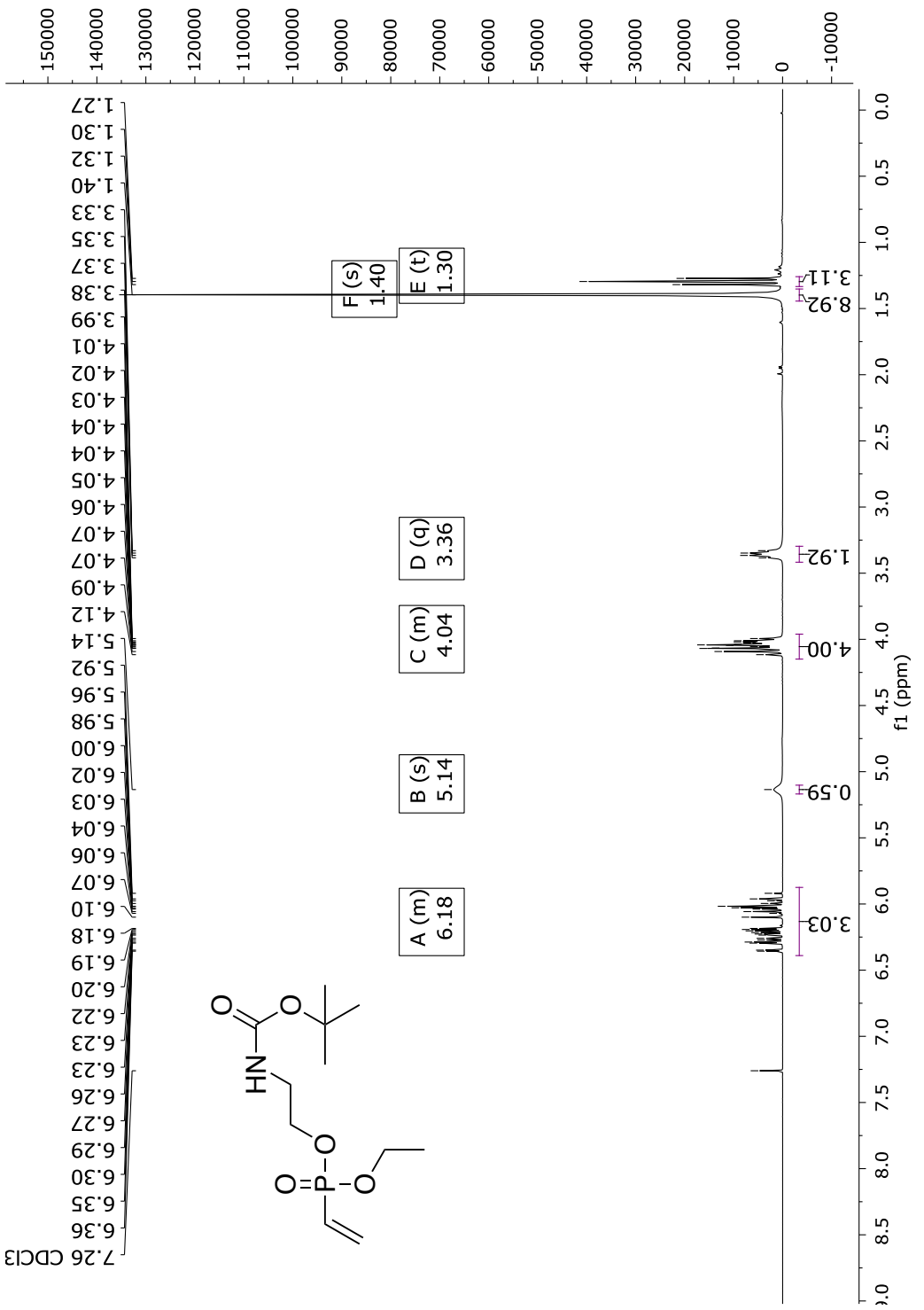

Fig. 224 ^{1}H-NMR spectrum of compound **62** in $CDCl_3$ (300 MHz).

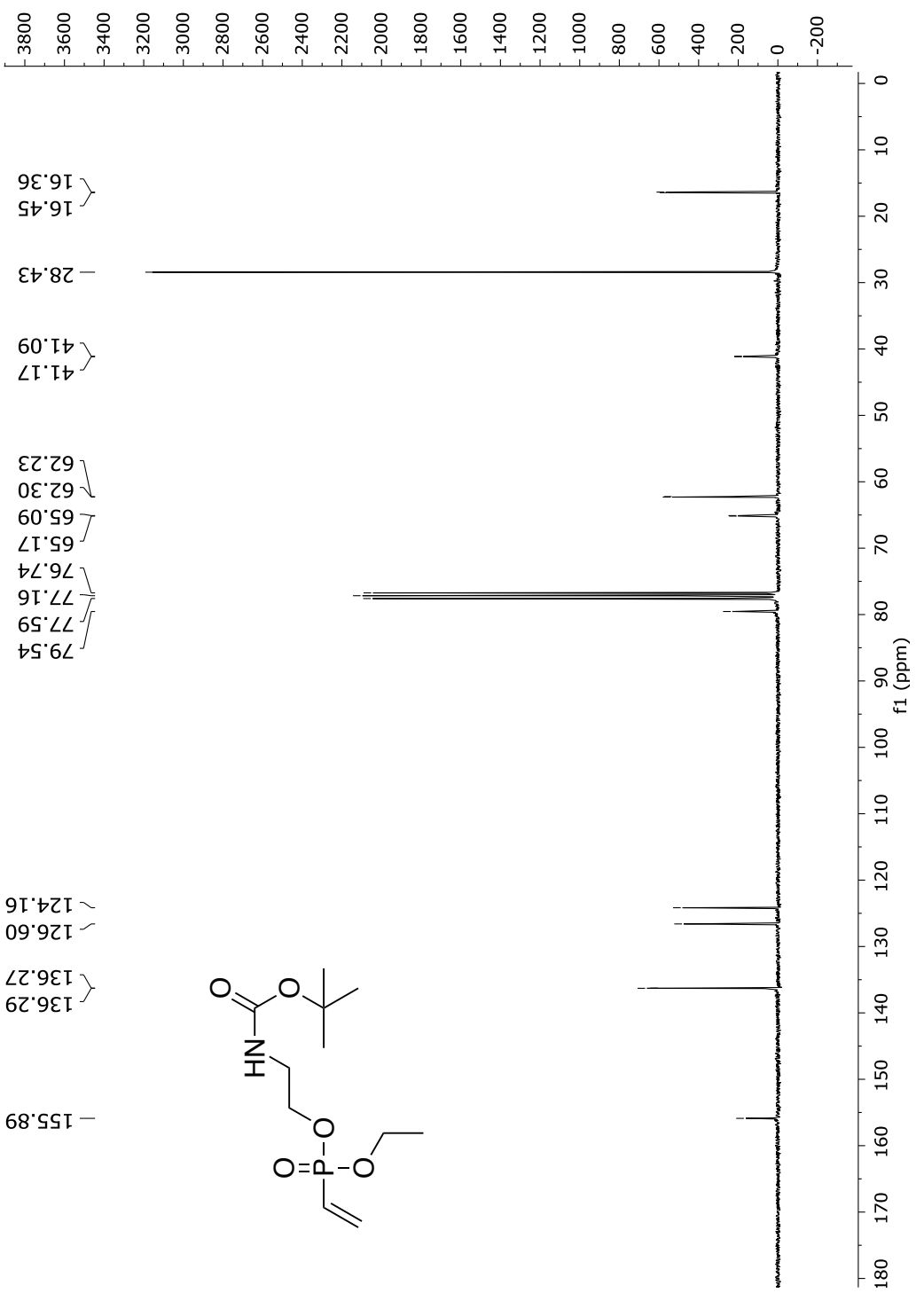

Fig. 225 ^{13}C-NMR spectrum of compound **62** in $CDCl_3$ (75 MHz).

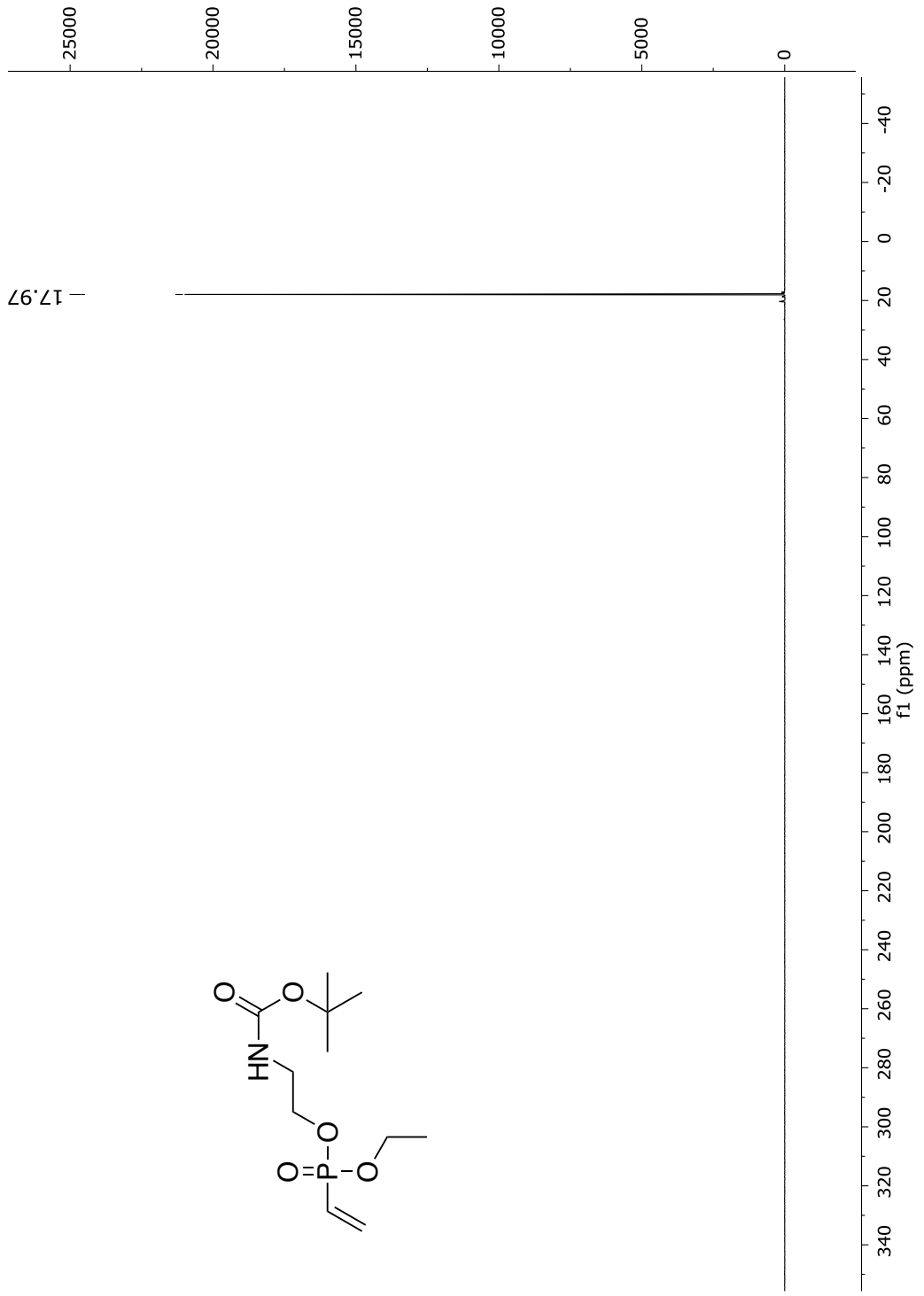

Fig. 226 ^{31}P-NMR spectrum of compound **62** in $CDCl_3$ (122 MHz).

O-EDANS derivative O-ethyl ethynylphosphonate (65)

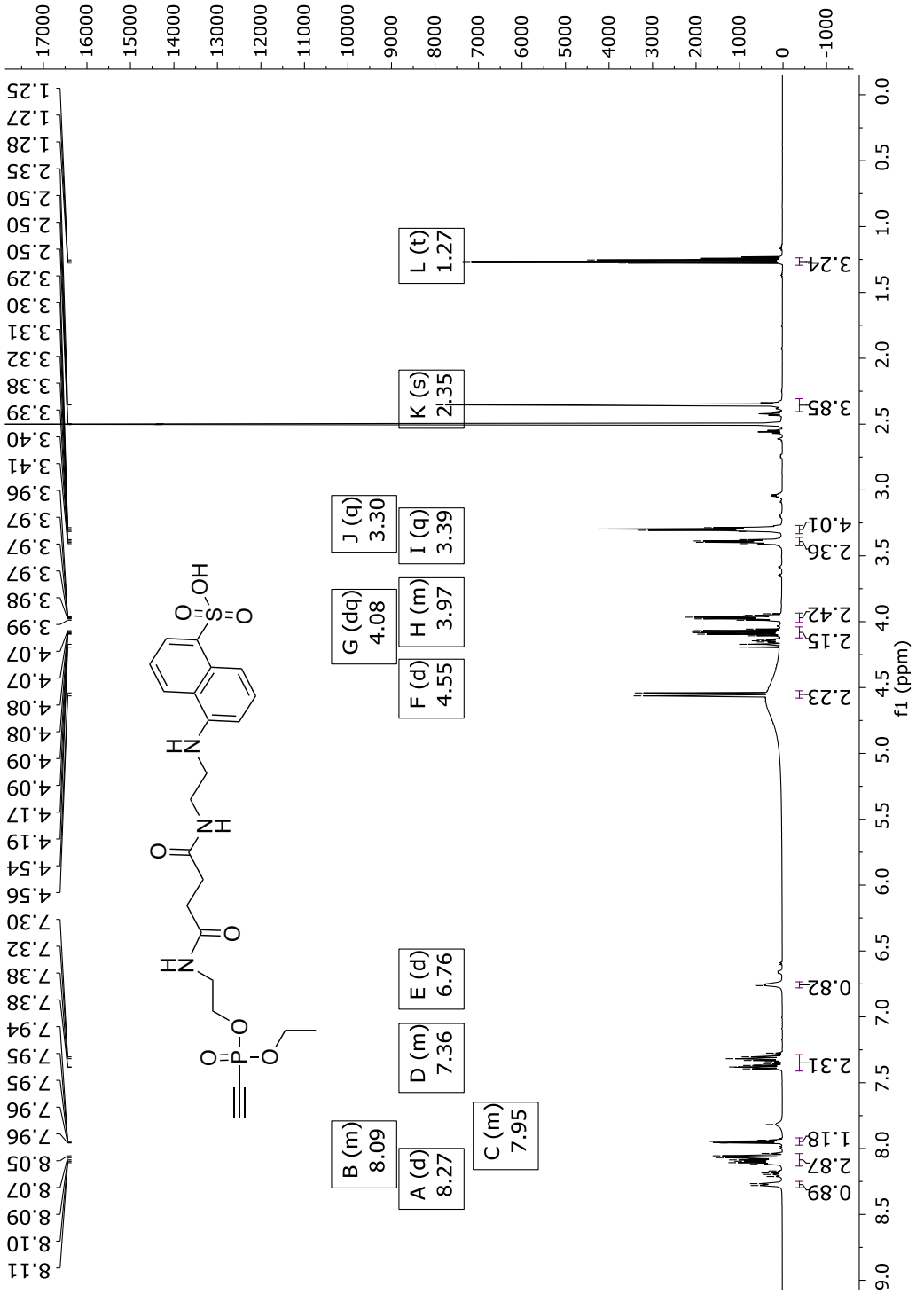

Fig. 227 ^{1}H-NMR spectrum of compound **65** in DMSO−d_6 (600 MHz).

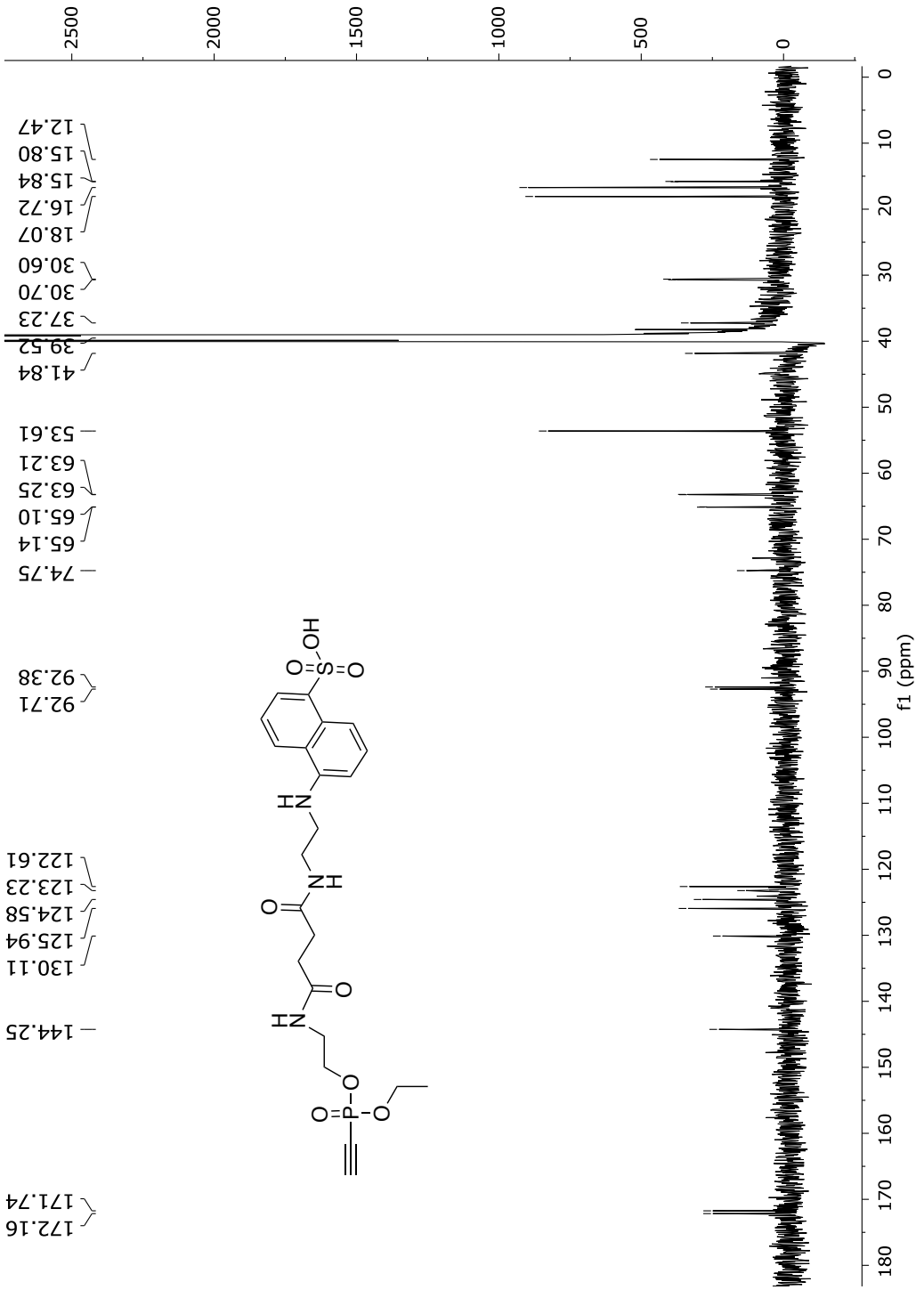

Fig. 228 ^{13}C-NMR spectrum of compound **65** in DMSO−d_6 (151 MHz).

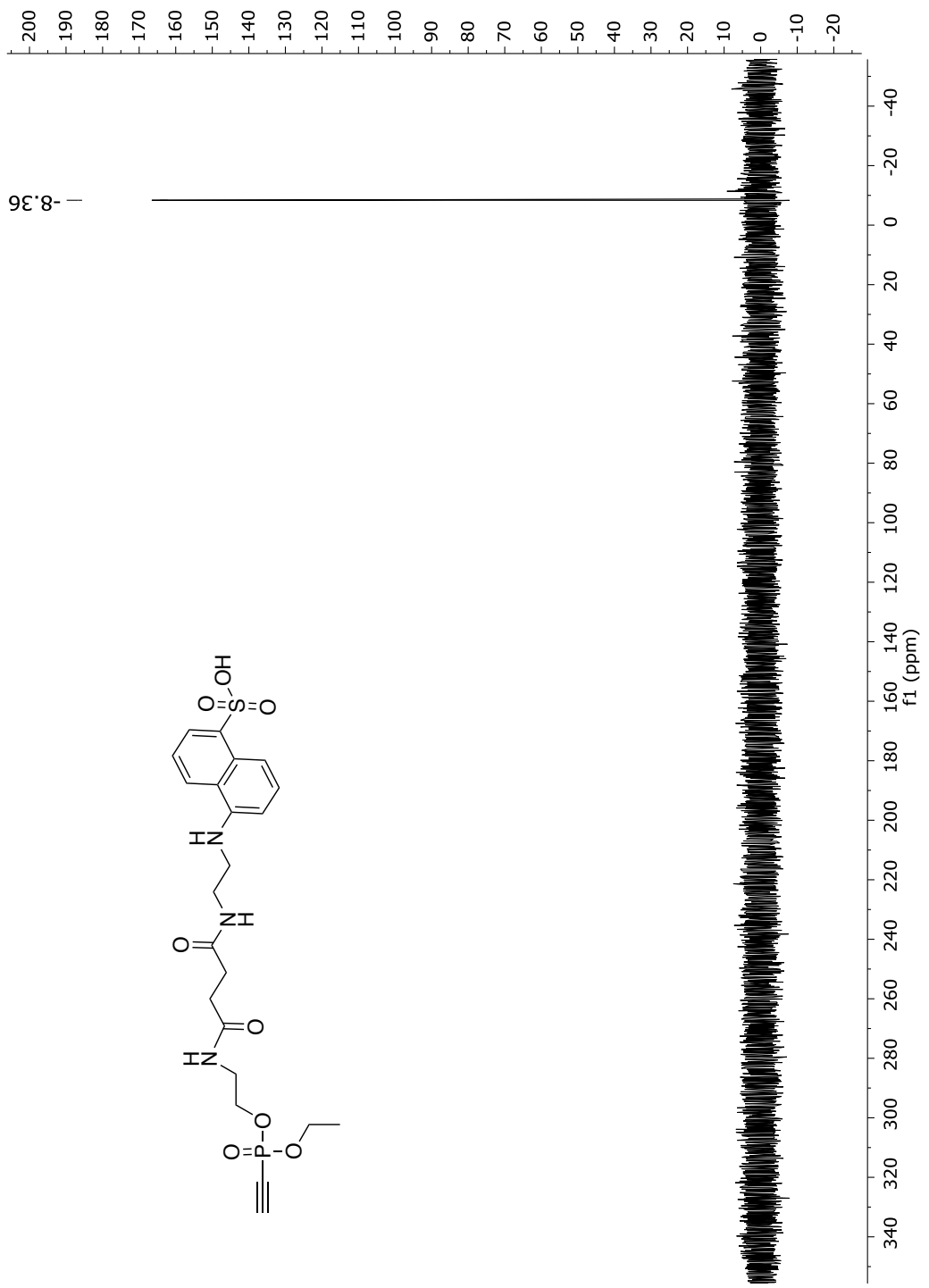

Fig. 229 ^{31}P-NMR spectrum of compound **65** in DMSO−d_6 (243 MHz).

O-EDANS derivative O-ethyl vinylphosphonate (66)

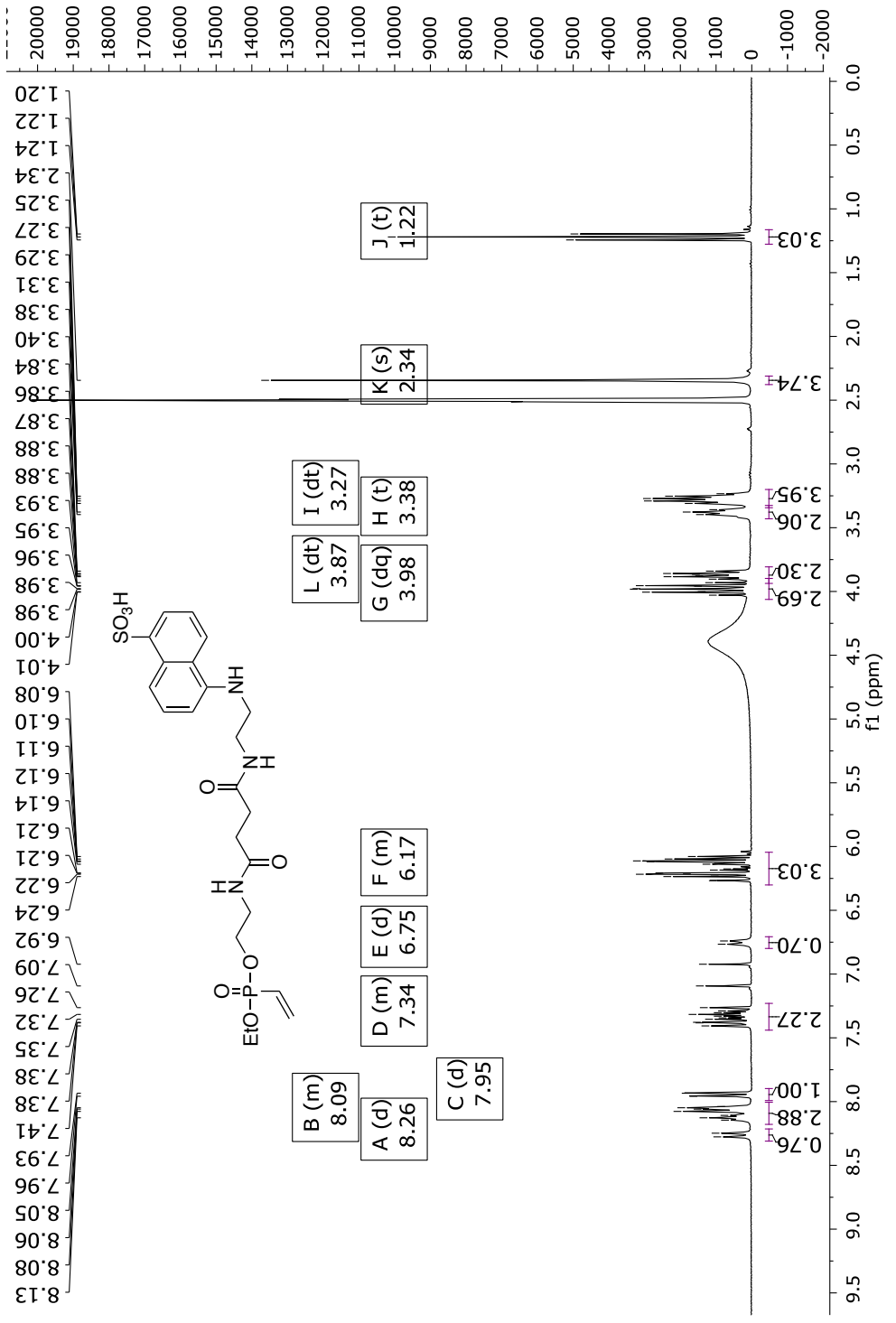

Fig. 230 ^{1}H-NMR spectrum of compound **66** in DMSO−d_6 (300 MHz).

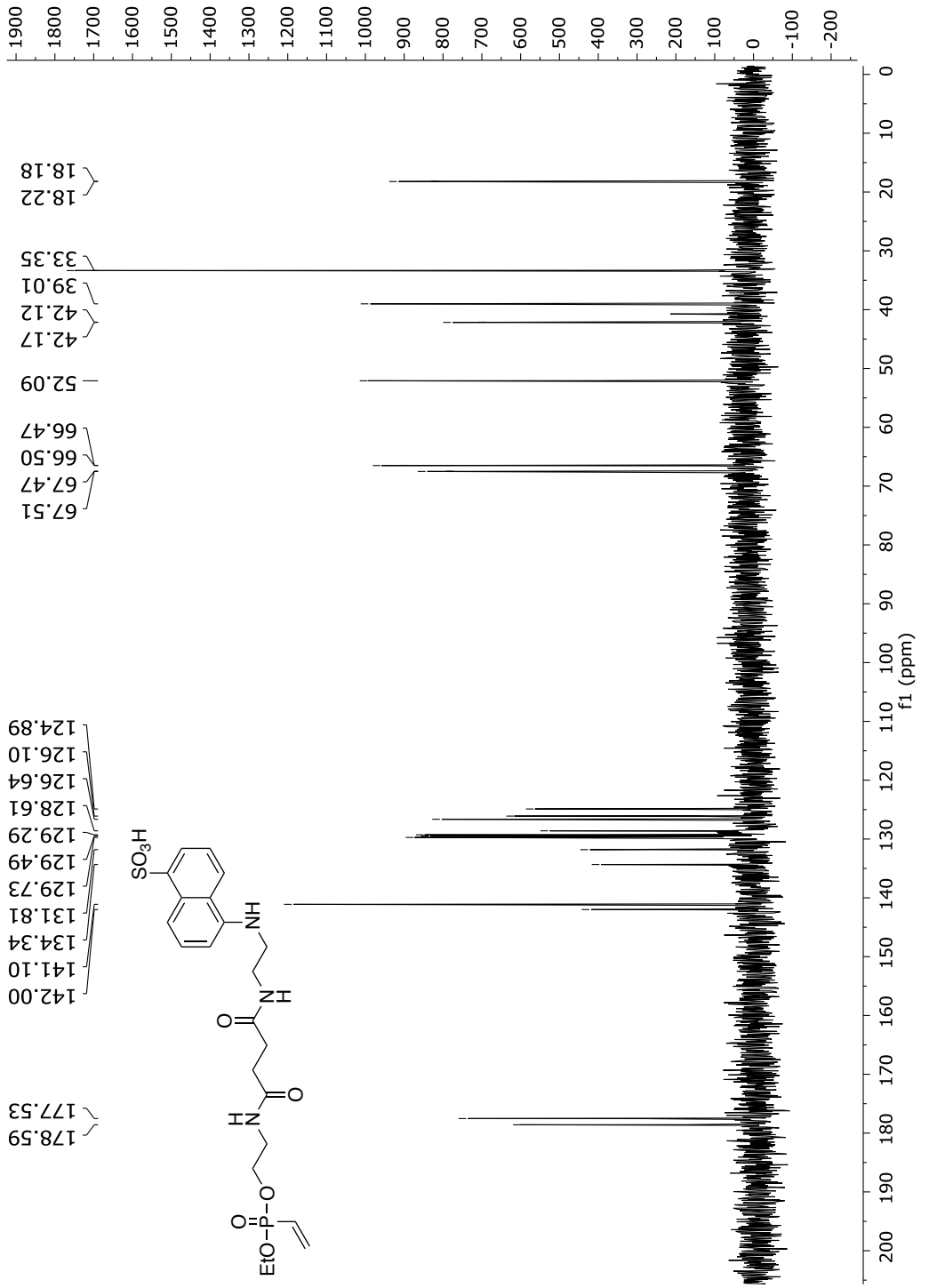

Fig. 231 ^{13}C-NMR spectrum of compound **66** in D_2O (151 MHz).

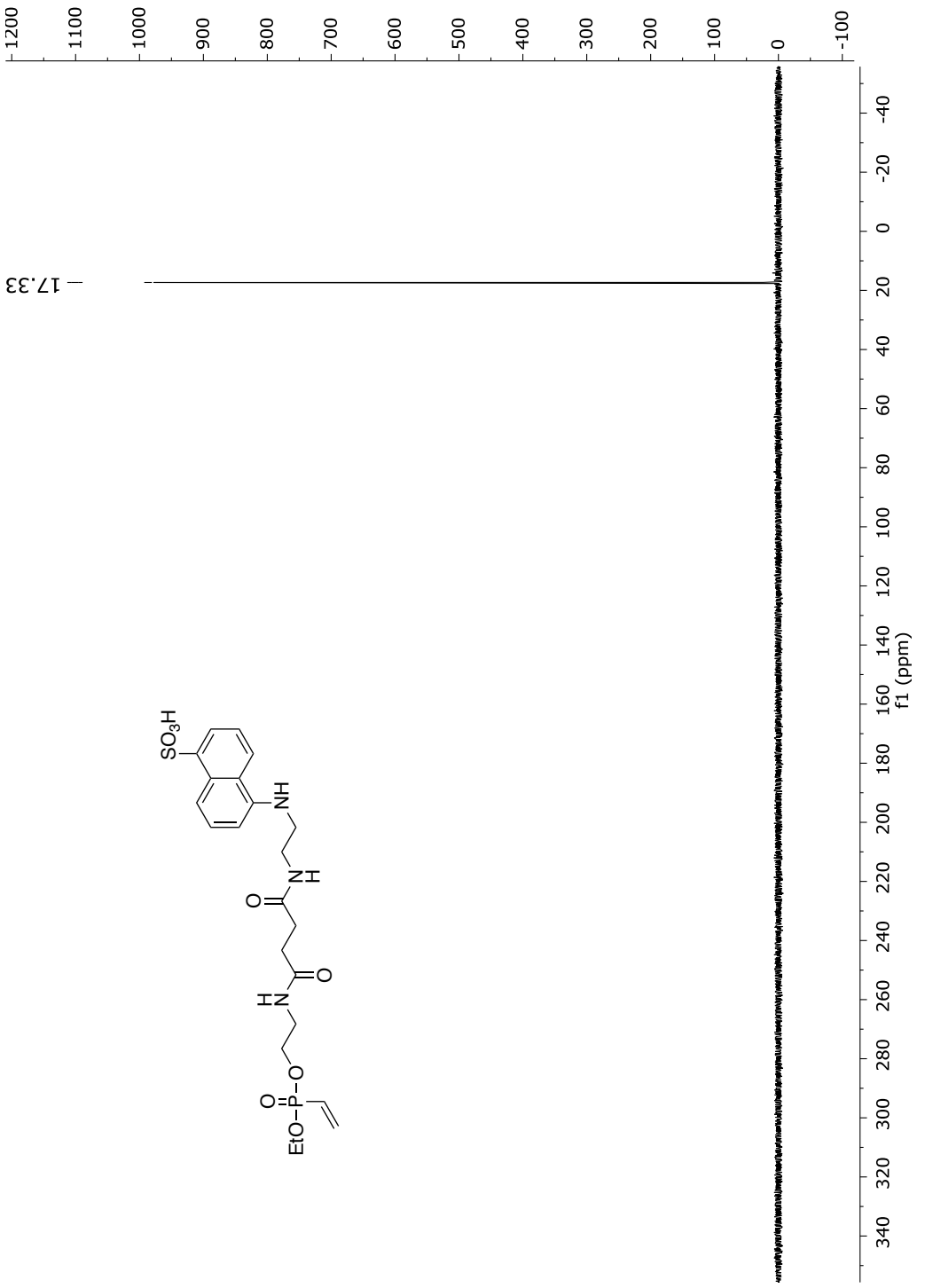

Fig. 232 ^{31}P-NMR spectrum of compound **66** in DMSO−d_6 (122 MHz).

9.2 Intact protein MS spectra

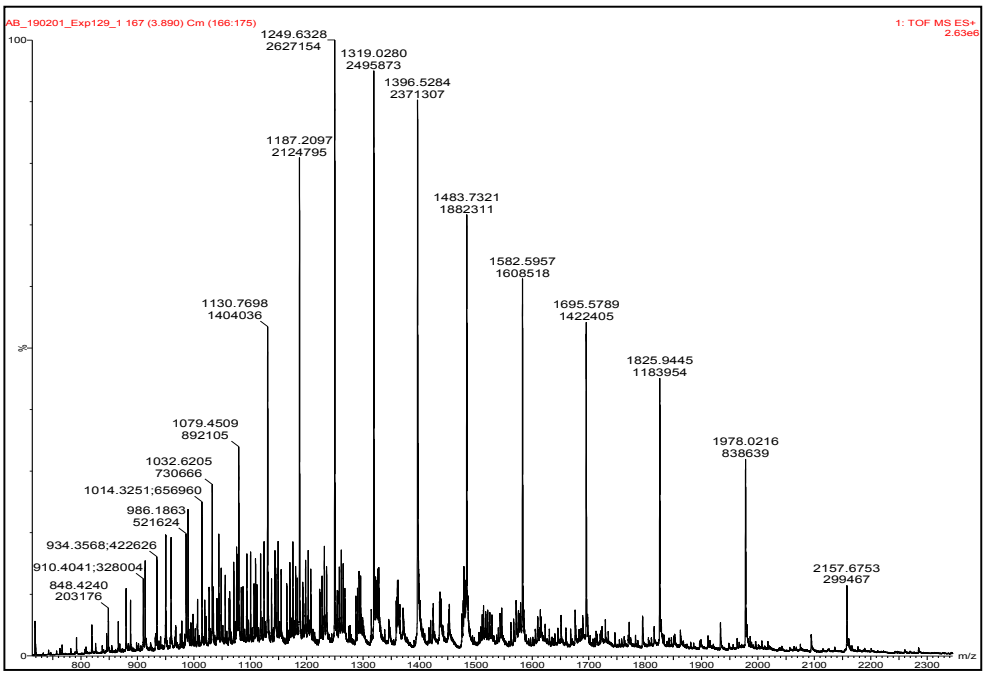

Fig. 233 Raw intact protein ESI-MS spectrum of ADC **85** (compare Fig. 42).

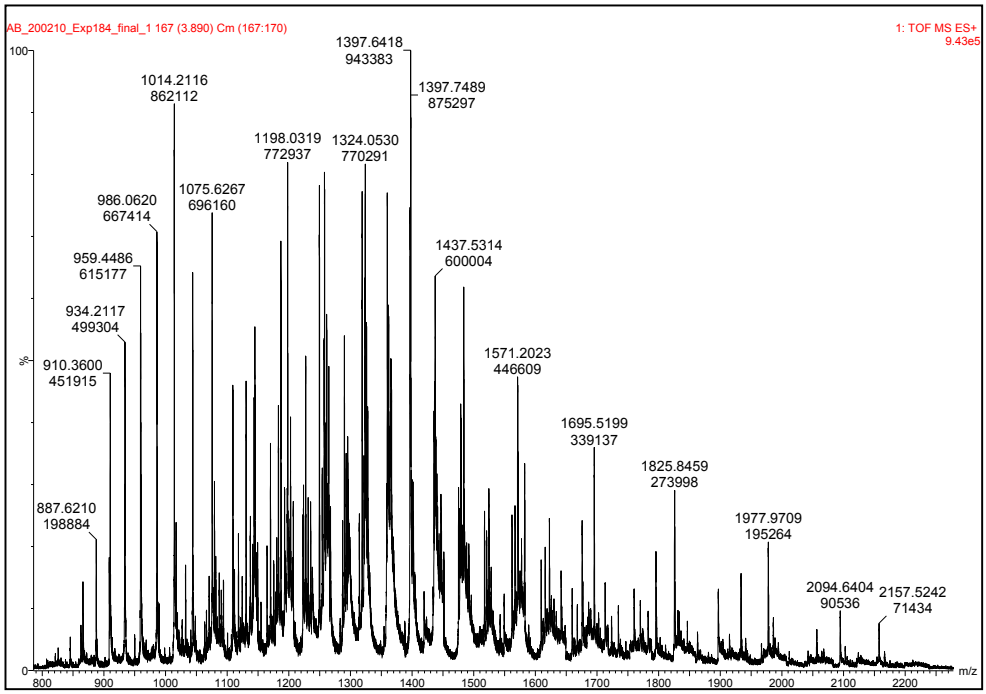

Fig. 234 Raw intact protein ESI-MS spectrum of ADC **86** (compare Fig. 44).

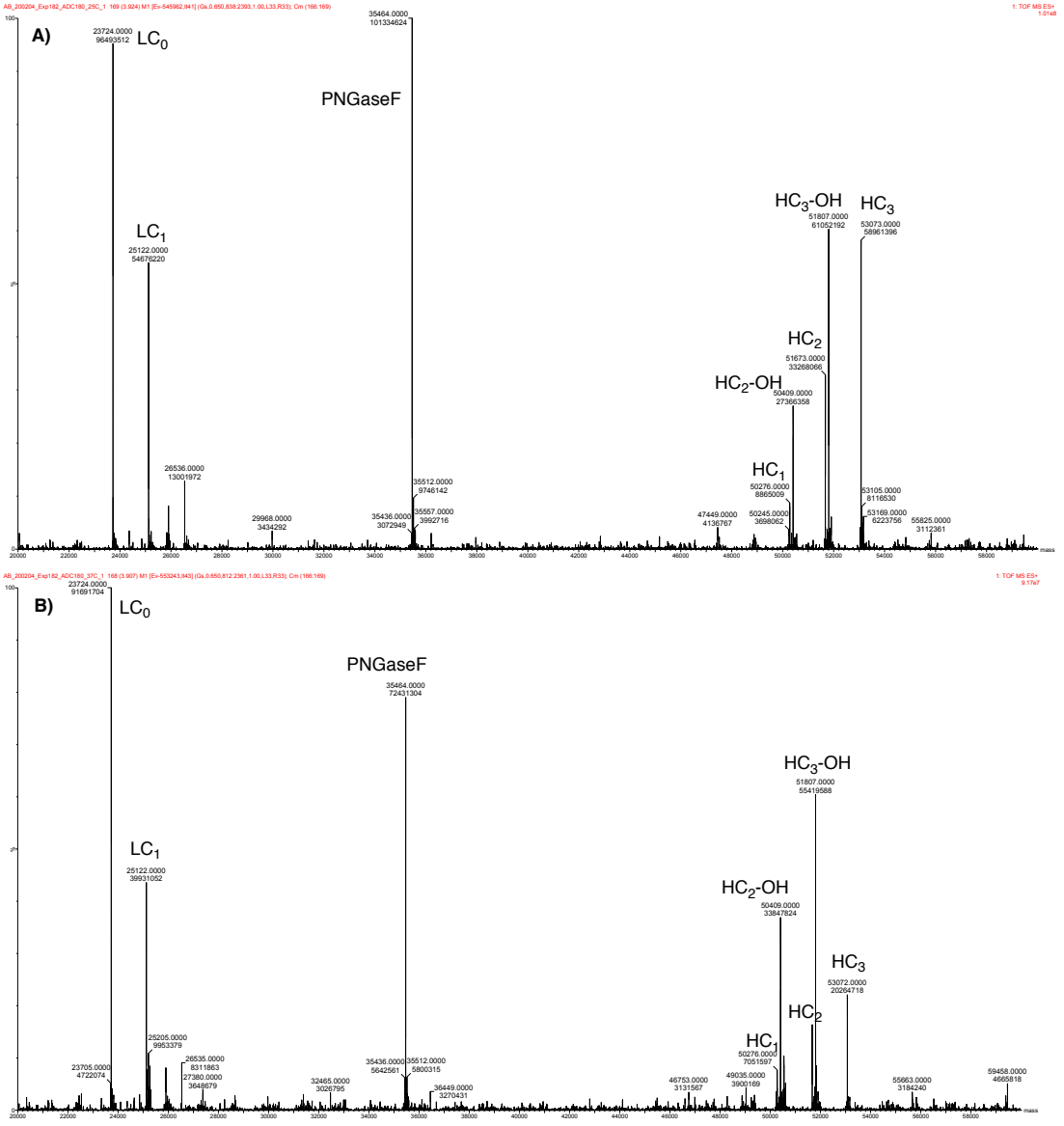

Fig. 235 Deconvoluted intact protein ESI-MS spectra of a brentuximab ADC generated with ethynylphosphonothiolate **47** with an initial DAR of 5.70. A) After incubation at 25 °C (A) and 37 °C (B) for 16 hours at pH 7.4, 25% and 35% of toxins were lost respectively as a consequence of the P-S bond cleavage in the ADC (compare scheme 52). Example: HC_2-OH is a heavy chain that initially carried two toxins, from which one was lost due to hydrolysis.

9.3 Peptide MS/MS spectra of phosphonothiolate-labeled trastuzumab

The spectra (HCD MS/MS) shown in the following belong to the trastuzumab labelling experiment shown in Fig. 47 and described in the Experimental section 8.2.9.

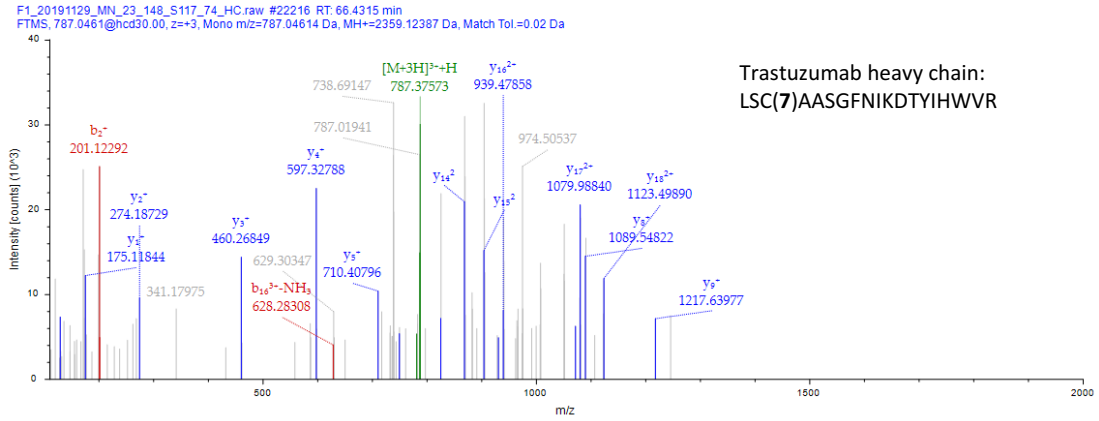

Fig. 236 Peptide spectrum match of the indicated peptide modified with ethynylphosphonothiolate **7** at position C3. Labelling conditions: pH 7.4.

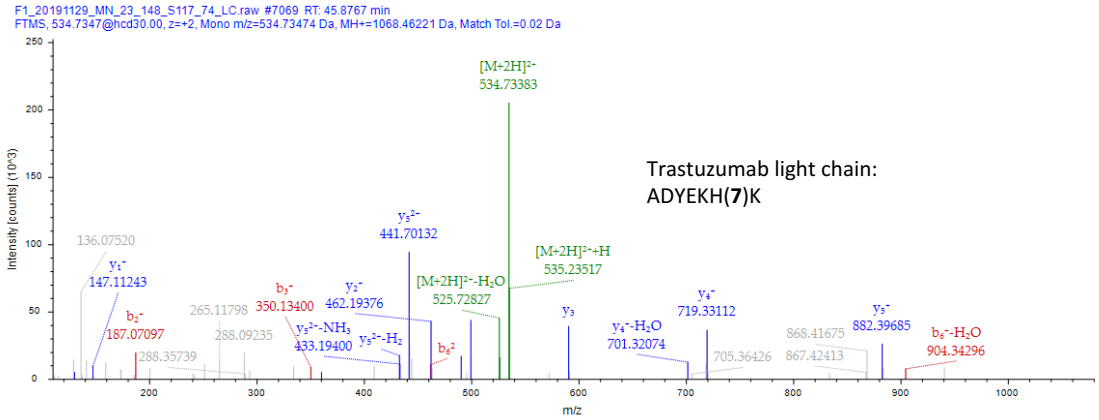

Fig. 237 Peptide spectrum match of the indicated peptide modified with ethynylphosphonothiolate **7** at position H6. Labelling conditions: pH 7.4.

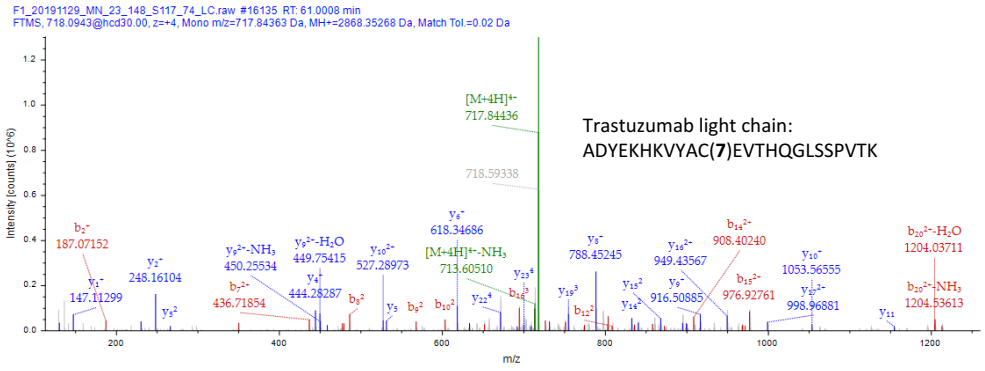

Fig. 238 Peptide spectrum match of the indicated peptide modified with ethynylphosphonothiolate **7** at position C11. Labelling conditions: pH 7.4.

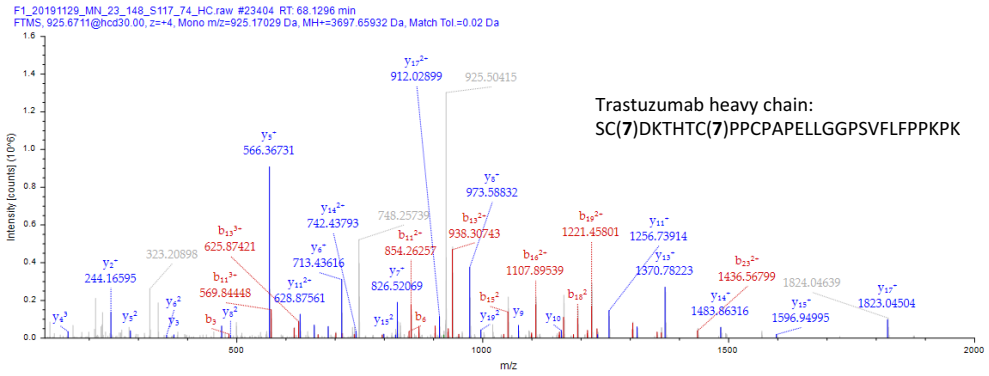

Fig. 239 Peptide spectrum match of the indicated peptide modified with ethynylphosphonothiolate **7** at the positions C2 and C8. Labelling conditions: pH 7.4.

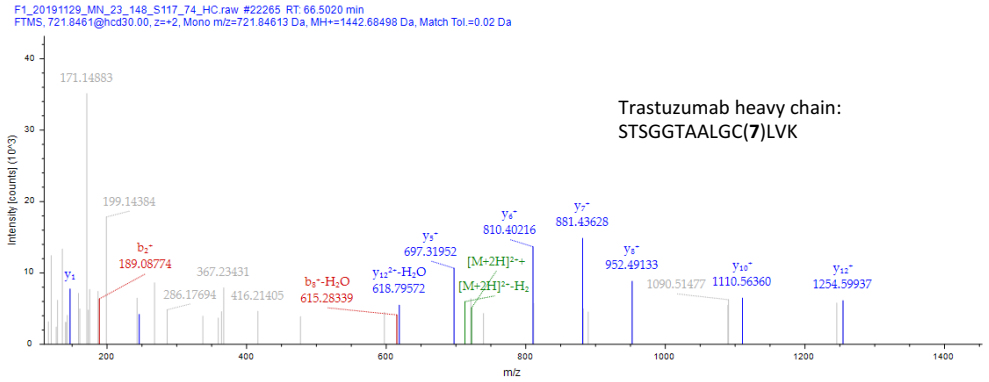

Fig. 240 Peptide spectrum match of the indicated peptide modified with ethynylphosphonothiolate **7** at position C11. Labelling conditions: pH 7.4.

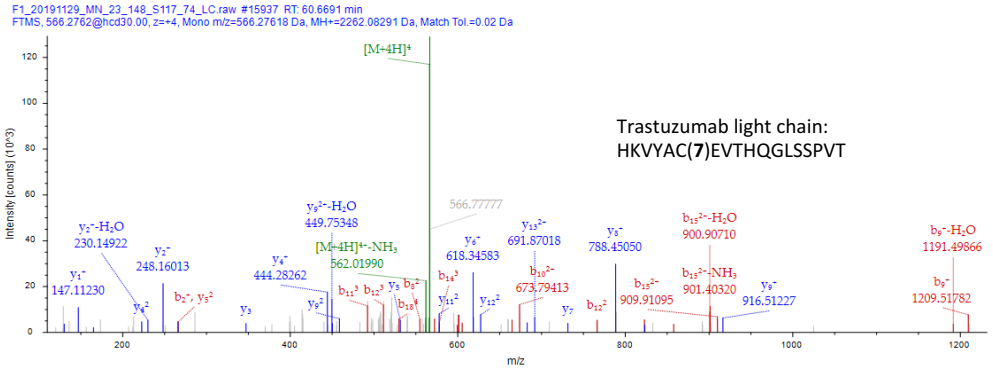

Fig. 241 Peptide spectrum match of the indicated peptide modified with ethynylphosphonothiolate **7** at position C6. Labelling conditions: pH 7.4.

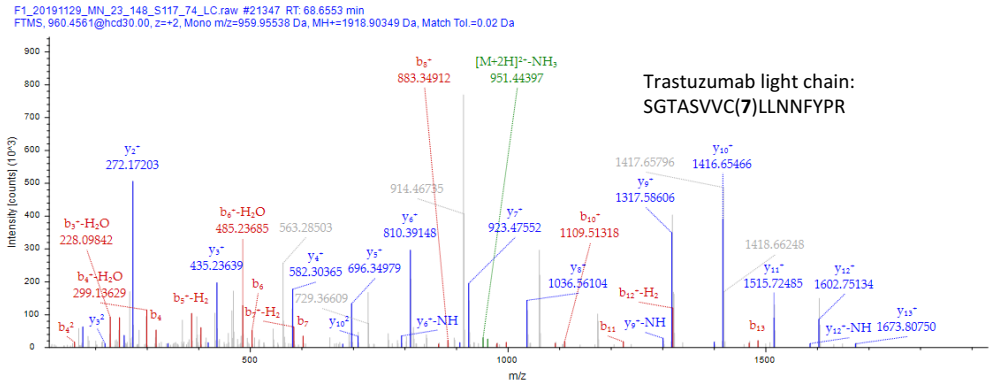

Fig. 242 Peptide spectrum match of the indicated peptide modified with ethynylphosphonothiolate **7** at position C8. Labelling conditions: pH 7.4.

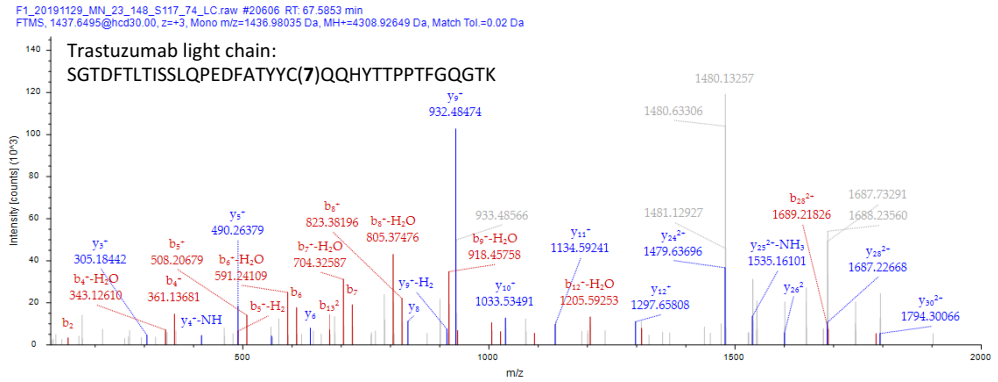

Fig. 243 Peptide spectrum match of the indicated peptide modified with ethynylphosphonothiolate **7** at position C22. Labelling conditions: pH 7.4.

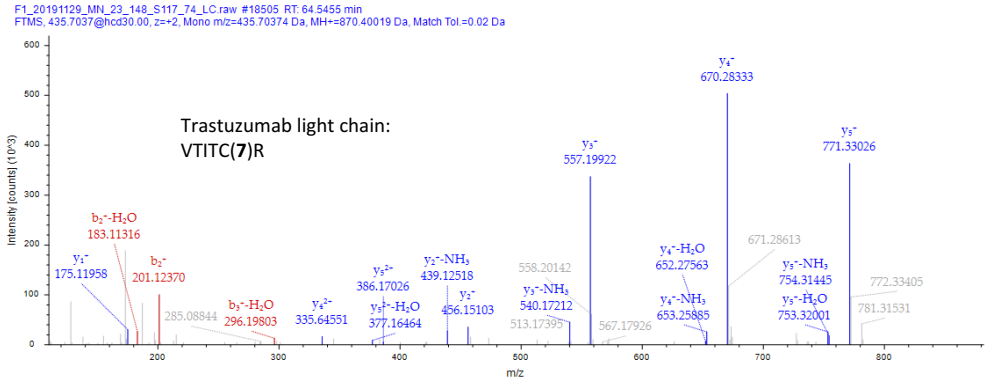

Fig. 244 Peptide spectrum match of the indicated peptide modified with ethynylphosphonothiolate **7** at position C5. Labelling conditions: pH 7.4.

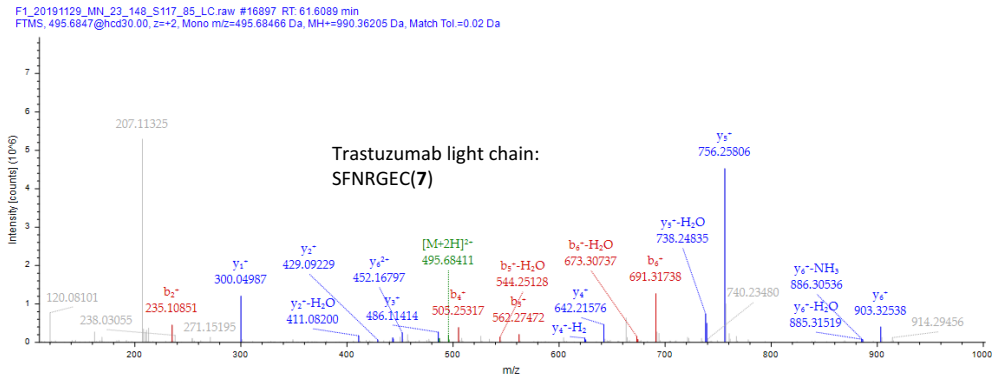

Fig. 245 Peptide spectrum match of the indicated peptide modified with ethynylphosphonothiolate **7** at position C7. Labelling conditions: pH 8.5.

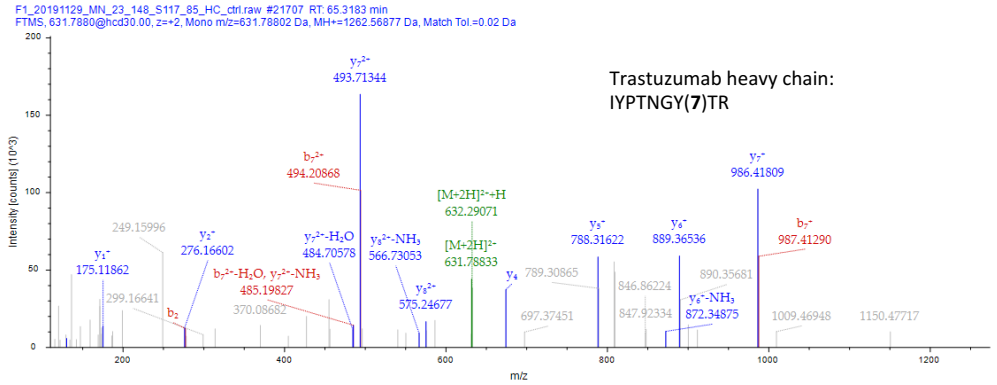

Fig. 246 Peptide spectrum match of the indicated peptide modified with ethynylphosphonothiolate **7** at position Y7. Labelling conditions: pH 8.5 (-DTT control).

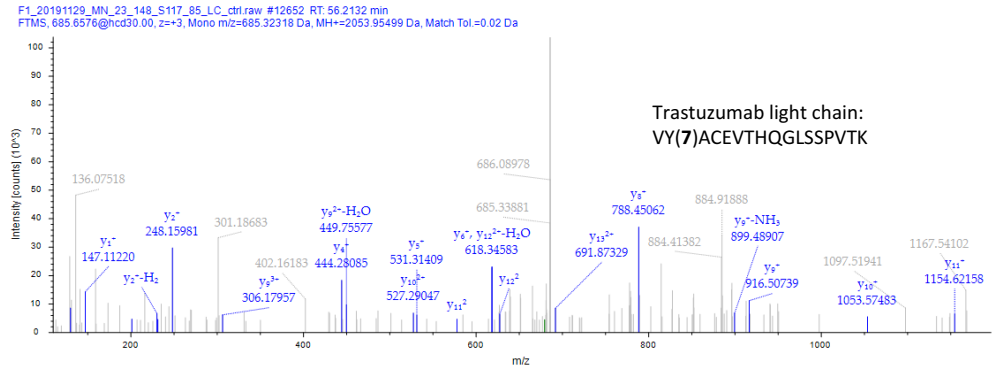

Fig. 247 Peptide spectrum match of the indicated peptide modified with ethynylphosphonothiolate **7** at position Y2. Labelling conditions: pH 8.5 (-DTT control).

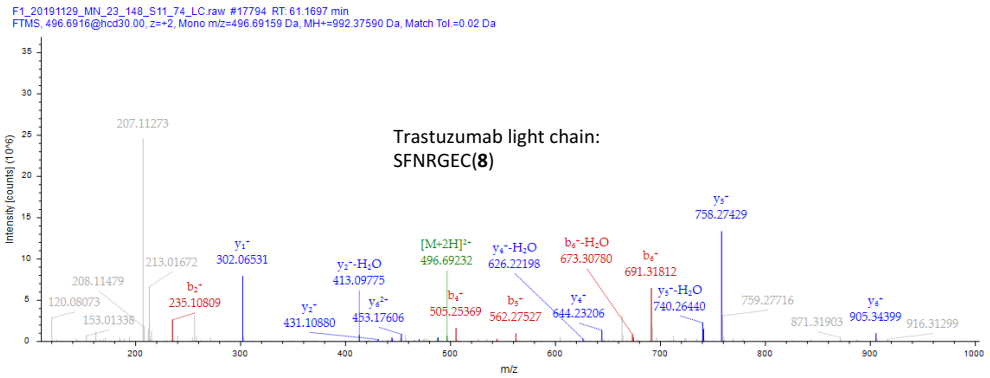

Fig. 248 Peptide spectrum match of the indicated peptide modified with vinylphosphonothiolate **8** at position C7. Labelling conditions: pH 7.4.

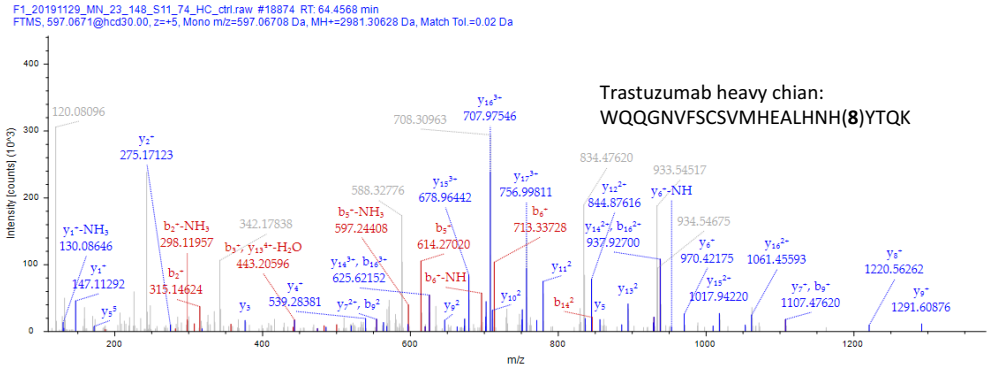

Fig. 249 Peptide spectrum match of the indicated peptide modified with vinylphosphonothiolate **8** at position H19. Labelling conditions: pH 7.4 (-DTT control).

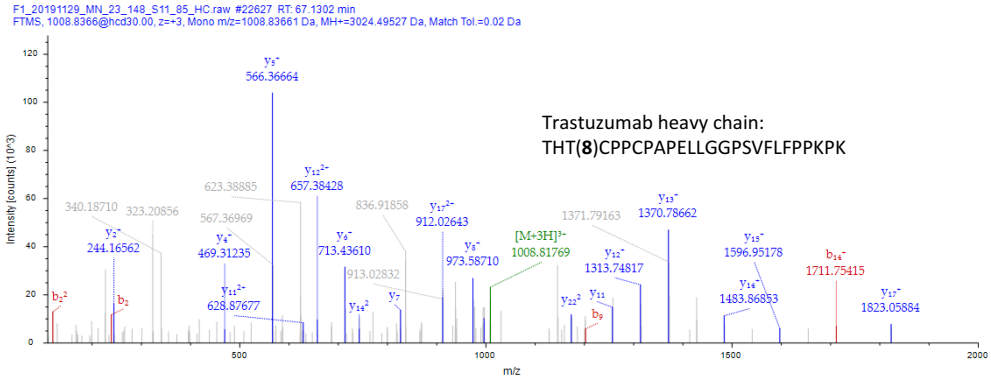

Fig. 250 Peptide spectrum match of the indicated peptide modified with vinylphosphonothiolate **8** at position T3. Labelling conditions: pH 8.5.

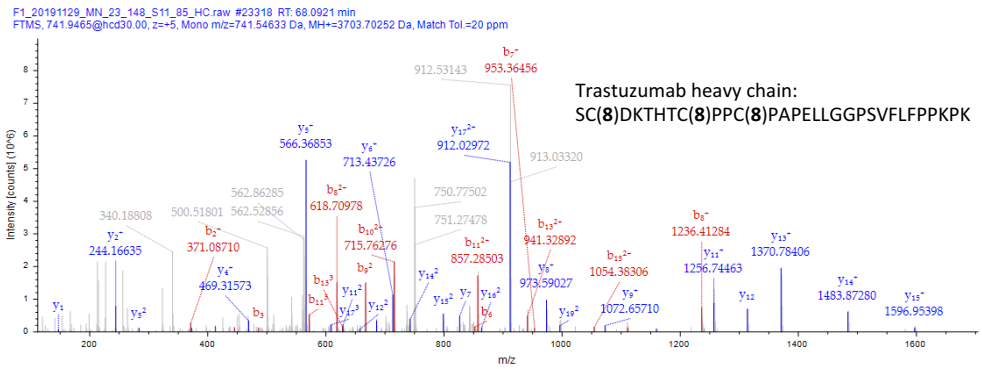

Fig. 251 Peptide spectrum match of the indicated peptide modified with vinylphosphonothiolate **8** at the positions C2, C8 and C11. Labelling conditions: pH 8.5.

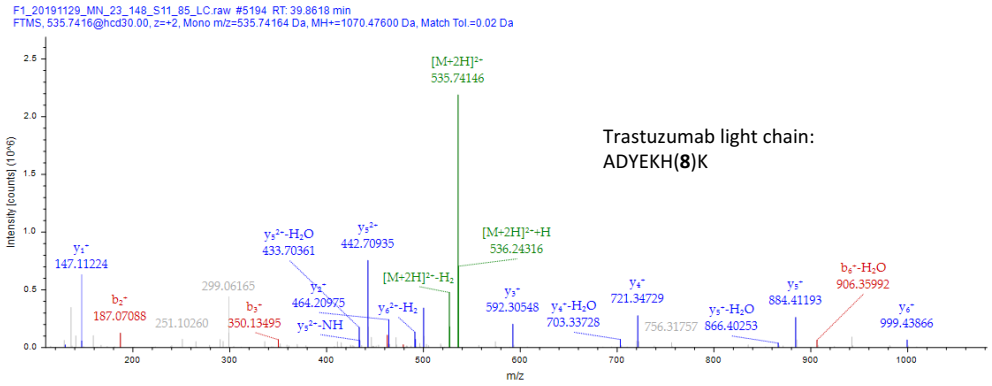

Fig. 252 Peptide spectrum match of the indicated peptide modified with vinylphosphonothiolate **8** at position H6. Labelling conditions: pH 8.5.

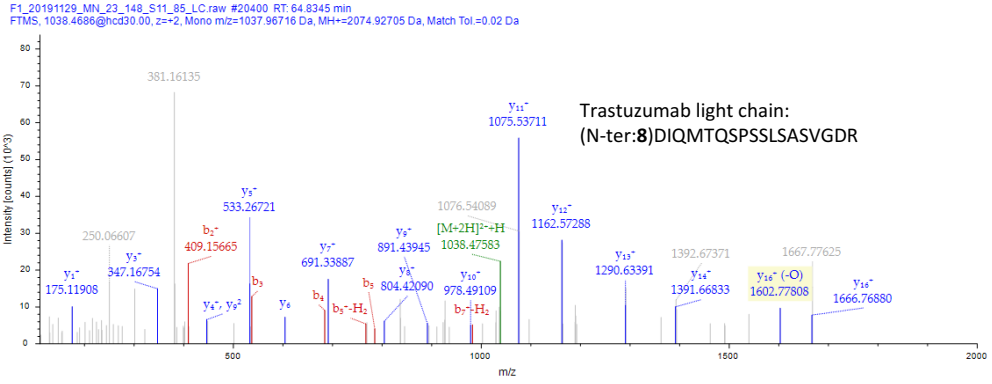

Fig. 253 Peptide spectrum match of the indicated peptide modified with vinylphosphonothiolate **8** at the N-terminus. Labelling conditions: pH 8.5.

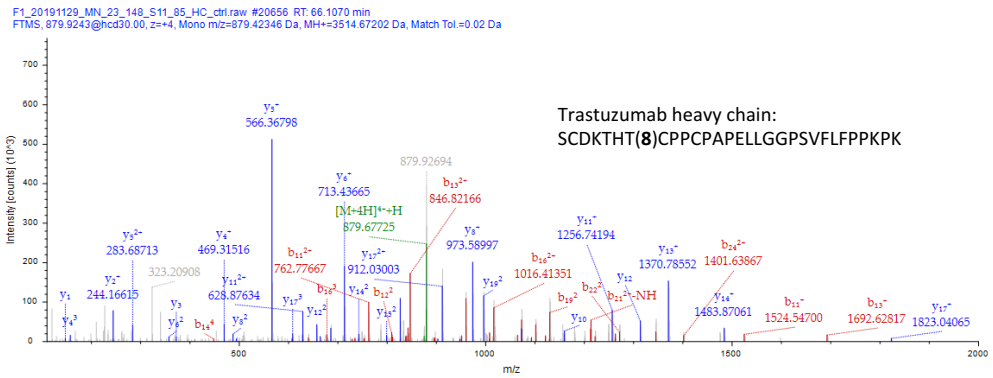

Fig. 254 Peptide spectrum match of the indicated peptide modified with vinylphosphonothiolate **8** at position T7. Labelling conditions: pH 8.5 (-DTT control).

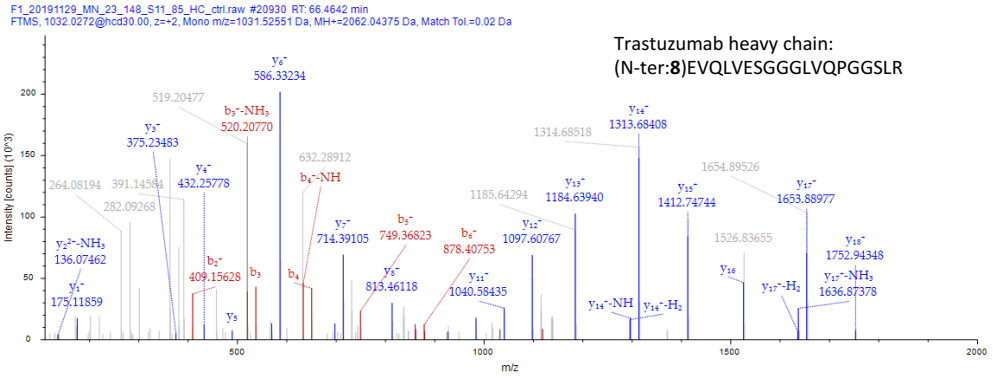

Fig. 255 Peptide spectrum match of the indicated peptide modified with vinylphosphonothiolate **8** at the N-terminus. Labelling conditions: pH 8.5 (-DTT control).

Bibliography

[1] C. P. Hackenberger and D. Schwarzer, "Chemoselective ligation and modification strategies for peptides and proteins," *Angewandte Chemie - International Edition*, vol. 47, no. 52, pp. 10030–10074, 2008.

[2] E. M. Sletten and C. R. Bertozzi, "Bioorthogonal chemistry: Fishing for selectivity in a sea of functionality," *Angewandte Chemie - International Edition*, vol. 48, no. 38, pp. 6974–6998, 2009.

[3] E. A. Hoyt, P. M. Cal, B. L. Oliveira, and G. J. Bernardes, "Contemporary approaches to site-selective protein modification," *Nature Reviews Chemistry*, vol. 3, no. 3, pp. 147–171, 2019.

[4] J. A. Shadish and C. A. DeForest, "Site-Selective Protein Modification: From Functionalized Proteins to Functional Biomaterials," *Matter*, vol. 2, no. 1, pp. 50–77, 2020.

[5] N. C. Reddy, M. Kumar, R. Molla, and V. Rai, "Chemical methods for modification of proteins," *Organic & Biomolecular Chemistry*, 2020.

[6] P. K. Mishra, C. M. Yoo, E. Hong, and H. W. Rhee, "Photo-crosslinking: An Emerging Chemical Tool for Investigating Molecular Networks in Live Cells," *ChemBioChem*, vol. 21, no. 7, pp. 924–932, 2020.

[7] G. Guidotti, L. Brambilla, and D. Rossi, "Cell-Penetrating Peptides: From Basic Research to Clinics," *Trends in Pharmacological Sciences*, vol. 38, no. 4, pp. 406–424, 2017.

[8] A. Beck, L. Goetsch, C. Dumontet, and N. Corvaïa, "Strategies and challenges for the next generation of antibody-drug conjugates," *Nature Reviews Drug Discovery*, vol. 16, no. 5, pp. 315–337, 2017.

[9] E. A. Rodriguez, R. E. Campbell, J. Y. Lin, M. Z. Lin, A. Miyawaki, A. E. Palmer, X. Shu, J. Zhang, and R. Y. Tsien, "The Growing and Glowing Toolbox of Fluorescent and Photoactive Proteins," *Trends in Biochemical Sciences*, vol. 42, no. 2, pp. 111–129, 2017.

[10] R. Y. Tsien, "The Green Fluorescent Protein (GFP)," *Annual Review of Biochemistry*, vol. 67, pp. 509–544, 1998.

[11] T. Gronemeyer, G. Godin, and K. Johnsson, "Adding value to fusion proteins through covalent labelling," *Current Opinion in Biotechnology*, vol. 16, no. 4, pp. 453–458, 2005.

[12] A. Keppler, S. Gendreizig, T. Gronemeyer, H. Pick, H. Vogel, and K. Johnsson, "A general method for the covalent labeling of fusion proteins with small molecules in vivo," *Nature Biotechnology*, vol. 21, no. 1, pp. 86–89, 2003.

[13] A. Gautier, A. Juillerat, C. Heinis, I. R. Corrêa, M. Kindermann, F. Beaufils, and K. Johnsson, "An Engineered Protein Tag for Multiprotein Labeling in Living Cells," *Chemistry and Biology*, vol. 15, no. 2, pp. 128–136, 2008.

[14] N. B. Cole, "Site-specific protein labeling with SNAP-tags," *Current Protocols in Protein Science*, vol. 2013, pp. 30.1.1–30.1.16, 2013.

[15] G. V. Los, L. P. Encell, M. G. McDougall, D. D. Hartzell, N. Karassina, C. Zimprich, M. G. Wood, R. Learish, R. F. Ohana, M. Urh, D. Simpson, J. Mendez, K. Zimmerman, P. Otto, G. Vidugiris, J. Zhu, A. Darzins, D. H. Klaubert, R. F. Bulleit, and K. V. Wood, "HaloTag: A novel protein labeling technology for cell imaging and protein analysis," *ACS Chemical Biology*, vol. 3, no. 6, pp. 373–382, 2008.

[16] C. G. England, H. Luo, and W. Cai, "HaloTag Technology: A Versatile Platform for Biomedical Applications," *Bioconjugate Chemistry*, vol. 26, no. 6, pp. 975–986, 2015.

[17] J. Lotze, U. Reinhardt, O. Seitz, and A. G. Beck-Sickinger, "Peptide-tags for site-specific protein labelling: In vitro and in vivo," *Molecular BioSystems*, vol. 12, no. 6, pp. 1731–1745, 2016.

[18] B. A. Griffin, S. R. Adams, and R. Y. Tsien, "Specific Covalent Labeling of Recombinant Protein Molecules Inside Live Cells," *Science*, vol. 281, no. 5374, pp. 269–272, 1998.

[19] S. R. Adams, R. E. Campbell, L. A. Gross, B. R. Martin, G. K. Walkup, Y. Yao, J. Llopis, and R. Y. Tsien, "New biarsenical ligands and tetracysteine motifs for protein labeling in vitro and in vivo: Synthesis and biological applications," *Journal of the American Chemical Society*, vol. 124, no. 21, pp. 6063–6076, 2002.

[20] H. Cao, B. Chen, T. C. Squier, and M. U. Mayer, "CrAsH: A biarsenical multiuse affinity probe with low non-specific fluorescence," *Chemical Communications*, no. 24, pp. 2601–2603, 2006.

[21] H. Cao, Y. Xiong, T. Wang, B. Chen, T. C. Squier, and M. U. Mayer, "A red Cy3-based biarsenical fluorescent probe targeted to a complementary binding peptide," *Journal of the American Chemical Society*, vol. 129, no. 28, pp. 8672–8673, 2007.

[22] T. L. Halo, J. Appelbaum, E. M. Hobert, D. M. Balkin, and A. Schepartz, "Selective recognition of protein tetraserine motifs with a cell-permeable, pro-fluorescent bis-boronic acid," *Journal of the American Chemical Society*, vol. 131, no. 2, pp. 438–439, 2009.

[23] C. Zhang, P. Dai, A. A. Vinogradov, Z. P. Gates, and B. L. Pentelute, "Site-Selective Cysteine-Cyclooctyne Conjugation," *Angewandte Chemie - International Edition*, vol. 57, no. 22, pp. 6459–6463, 2018.

[24] C. Zhang, M. Welborn, T. Zhu, N. J. Yang, M. S. Santos, T. Van Voorhis, and B. L. Pentelute, "π-Clamp-mediated cysteine conjugation," *Nature Chemistry*, vol. 8, no. 2, pp. 120–128, 2016.

[25] B. Tripet, L. Yu, D. L. Bautista, W. Y. Wong, R. T. Irvin, and R. S. Hodges, "Engineering a de novo designed coiled-coil heterodimerization domain for the rapid

detection, purification and characterization of recombinantly expressed peptides and proteins," *Protein Engineering*, vol. 10, no. 3, p. 299, 1997.

[26] Y. Yano, A. Yano, S. Oishi, Y. Sugimoto, G. Tsujimoto, N. Fujii, and K. Matsuzaki, "Coiled-coil tag - Probe system for quick labeling of membrane receptors in living cells," *ACS Chemical Biology*, vol. 3, no. 6, pp. 341–345, 2008.

[27] U. Reinhardt, J. Lotze, S. Zernia, K. Mörl, A. G. Beck-Sickinger, and O. Seitz, "Peptide-templated acyl transfer: A chemical method for the labeling of membrane proteins on live cells," *Angewandte Chemie - International Edition*, vol. 53, no. 38, pp. 10237–10241, 2014.

[28] A. L. Baumann and C. P. R. Hackenberger, "Modern Ligation Methods to Access Natural and Modified Proteins," *CHIMIA*, vol. 72, no. 11, pp. 802–808, 2018.

[29] L. Abrahms, J. Tom, J. Burnier, K. A. Butcher, A. Kossiakoff, and J. A. Wells, "Engineering Subtilisin and Its Substrates for Efficient Ligation of Peptide Bonds in Aqueous Solution," *Biochemistry*, vol. 30, no. 17, pp. 4151–4159, 1991.

[30] T. K. Chang, D. Y. Jackson, J. P. Burnier, and J. A. Wells, "Subtiligase: A tool for semisynthesis of proteins," *Proceedings of the National Academy of Sciences of the United States of America*, vol. 91, no. 26, pp. 12544–12548, 1994.

[31] A. M. Weeks and J. A. Wells, "Engineering peptide ligase specificity by proteomic identification of ligation sites," *Nature Chemical Biology*, vol. 14, no. 1, pp. 50–57, 2018.

[32] O. Schneewind, A. Fowler, and K. F. Faull, "Structure of the cell wall anchor of surface proteins in Staphylococcus aureus," *Science*, vol. 268, no. 5207, pp. 103–106, 1995.

[33] H. Mao, S. A. Hart, A. Schink, and B. A. Pollok, "Sortase-Mediated Protein Ligation: A New Method for Protein Engineering," *Journal of the American Chemical Society*, vol. 126, no. 9, pp. 2670–2671, 2004.

[34] L. Schmohl and D. Schwarzer, "Sortase-mediated ligations for the site-specific modification of proteins," *Current Opinion in Chemical Biology*, vol. 22, pp. 122–128, 2014.

[35] M. Fottner, A. D. Brunner, V. Bittl, D. Horn-Ghetko, A. Jussupow, V. R. Kaila, A. Bremm, and K. Lang, "Site-specific ubiquitylation and SUMOylation using genetic-code expansion and sortase," *Nature Chemical Biology*, vol. 15, no. 3, pp. 276–284, 2019.

[36] G. K. Nguyen, S. Wang, Y. Qiu, X. Hemu, Y. Lian, and J. P. Tam, "Butelase 1 is an Asx-specific ligase enabling peptide macrocyclization and synthesis," *Nature Chemical Biology*, vol. 10, no. 9, pp. 732–738, 2014.

[37] G. K. Nguyen, Y. Qiu, Y. Cao, X. Hemu, C. F. Liu, and J. P. Tam, "Butelase-mediated cyclization and ligation of peptides and proteins," *Nature Protocols*, vol. 11, no. 10, pp. 1977–1988, 2016.

[38] G. K. Nguyen, A. Kam, S. Loo, A. E. Jansson, L. X. Pan, and J. P. Tam, "Butelase 1: A Versatile Ligase for Peptide and Protein Macrocyclization," *Journal of the American Chemical Society*, vol. 137, no. 49, pp. 15398–15401, 2015.

[39] C. Janke, "The tubulin code: Molecular components, readout mechanisms, functions," *Journal of Cell Biology*, vol. 206, no. 4, pp. 461–472, 2014.

[40] D. Schumacher, J. Helma, F. A. Mann, G. Pichler, F. Natale, E. Krause, M. C. Cardoso, C. P. Hackenberger, and H. Leonhardt, "Versatile and Efficient Site-Specific Protein Functionalization by Tubulin Tyrosine Ligase," *Angewandte Chemie - International Edition*, vol. 54, no. 46, pp. 13787–13791, 2015.

[41] D. Schumacher, O. Lemke, J. Helma, L. Gerszonowicz, V. Waller, T. Stoschek, P. M. Durkin, N. Budisa, H. Leonhardt, B. G. Keller, and C. P. Hackenberger, "Broad substrate tolerance of tubulin tyrosine ligase enables one-step site-specific enzymatic protein labeling," *Chemical Science*, vol. 8, no. 5, pp. 3471–3478, 2017.

[42] R. D. Row and J. A. Prescher, "Constructing New Bioorthogonal Reagents and Reactions," *Accounts of Chemical Research*, vol. 51, no. 5, pp. 1073–1081, 2018.

[43] L. K. Mahal, K. J. Yarema, and C. R. Bertozzi, "Engineering Chemical Reactivity on Cell Surfaces Through Oligosaccharide Biosynthesis," *Science*, vol. 276, pp. 1125–1128, 1997.

[44] K. Rose, "Facile Synthesis of Homogeneous Artificial Proteins," *Journal of the American Chemical Society*, vol. 116, no. 1, pp. 30–33, 1994.

[45] J. Shao and J. P. Tam, "Unprotected Peptides as Building Blocks for the Synthesis of Peptide Dendrimers with Oxime, Hydrazone, and Thiazolidine Linkages," *Journal of the American Chemical Society*, vol. 117, no. 14, pp. 3893–3899, 1995.

[46] D. Rideout, "Self-Assembling Drugs: A New Approach to Biochemical Modulation in Cancer Chemotherapy," *Cancer Investigation*, vol. 12, no. 2, pp. 189–202, 1994.

[47] K. Lang and J. W. Chin, "Bioorthogonal reactions for labeling proteins," *ACS Chemical Biology*, vol. 9, no. 1, pp. 16–20, 2014.

[48] J. A. Prescher and C. R. Bertozzi, "Chemistry in Living Systems," *Nature Chemical Biology*, vol. 1, no. 1, pp. 13–21, 2005.

[49] A. Michael, "Ueber die Einwirkung von Diazobenzolimid auf Acetylendicarbonsaeuremethylester," *ournal fuer Praktische Chemie*, vol. 48, pp. 94–95, 1893.

[50] R. Huisgen, "1,3-Dipolar Cycloadditions Past and Future," *Angewandte Chemie - International Edition*, vol. 2, no. 10, pp. 565–632, 1963.

[51] V. V. Rostovtsev, L. G. Green, V. V. Fokin, and K. B. Sharpless, "A Stepwise Huisgen Cycloaddition Process: Copper(I)-Catalyzed Regioselective Ligation of Azides and Terminal Alkynes," *Angewandte Chemie - International Edition*, vol. 41, no. 14, pp. 2596–2599, 2002.

[52] C. W. Tornoe, C. Christensen, and M. Meldal, "Peptidotriazoles on solid phase: [1,2,3]-Triazoles by regiospecific copper(I)-catalyzed 1,3-dipolar cycloadditions of terminal alkynes to azides," *Journal of Organic Chemistry*, vol. 67, no. 9, pp. 3057–3064, 2002.

[53] Z. Chen, H. Meng, G. Xing, C. Chen, Y. Zhao, G. Jia, T. Wang, H. Yuan, C. Ye, F. Zhao, Z. Chai, C. Zhu, X. Fang, B. Ma, and L. Wan, "Acute toxicological effects of copper nanoparticles in vivo," *Toxicology Letters*, vol. 163, no. 2, pp. 109–120, 2006.

[54] G. Wittig and A. Krebs, "Zur Existenz niedergliedriger Cycloalkine, I," *Chem. Ber*, vol. 94, no. 5, pp. 3260–3275, 1961.

[55] N. J. Agard, J. A. Prescher, and C. R. Bertozzi, "A strain-promoted [3 + 2] azide-alkyne cycloaddition for covalent modification of biomolecules in living systems," *Journal of the American Chemical Society*, vol. 126, no. 46, pp. 15046–15047, 2004.

[56] H. Tian, T. P. Sakmar, and T. Huber, "Micelle-enhanced bioorthogonal labeling of genetically encoded azido groups on the lipid-embedded surface of a GPCR," *ChemBioChem*, vol. 16, no. 9, pp. 1314–1322, 2015.

[57] R. Van Geel, G. J. Pruijn, F. L. Van Delft, and W. C. Boelens, "Preventing thiol-yne addition improves the specificity of strain-promoted azide-alkyne cycloaddition," *Bioconjugate Chemistry*, vol. 23, no. 3, pp. 392–398, 2012.

[58] B. L. Oliveira, Z. Guo, and G. J. Bernardes, "Inverse electron demand Diels-Alder reactions in chemical biology," *Chemical Society Reviews*, vol. 46, no. 16, pp. 4895–4950, 2017.

[59] D. L. Boger, "Diels-Alder Reactions of Heterocyclic Azadienes: Scope and Applications," *Chemical Reviews*, vol. 86, no. 5, pp. 781–793, 1986.

[60] J. Sauer and H. Wiest, "Diels-Alder-Additionen mit inversem Elektronenbedarf," *Angewandte Chemie*, vol. 10, p. 353, 1962.

[61] M. L. Blackman, M. Royzen, and J. M. Fox, "Tetrazine ligation: Fast bioconjugation based on inverse-electron-demand Diels-Alder reactivity," *Journal of the American Chemical Society*, vol. 130, no. 41, pp. 13518–13519, 2008.

[62] N. K. Devaraj, R. Weissleder, and S. A. Hilderbrand, "Tetrazine-based cycloadditions: Application to pretargeted live cell imaging," *Bioconjugate Chemistry*, vol. 19, no. 12, pp. 2297–2299, 2008.

[63] R. Selvaraj and J. M. Fox, "trans-Cyclooctene - a stable, voracious dienophile for bioorthogonal labeling," *Current Opinion in Chemical Biology*, vol. 17, no. 5, pp. 753–760, 2013.

[64] M. T. Taylor, M. L. Blackman, O. Dmitrenko, and J. M. Fox, "Design and synthesis of highly reactive dienophiles for the tetrazine-trans-cyclooctene ligation," *Journal of the American Chemical Society*, vol. 133, no. 25, pp. 9646–9649, 2011.

[65] A. Darko, S. Wallace, O. Dmitrenko, M. M. Machovina, R. A. Mehl, J. W. Chin, and J. M. Fox, "Conformationally strained trans-cyclooctene with improved stability and excellent reactivity in tetrazine ligation," *Chemical Science*, vol. 5, no. 10, pp. 3770–3776, 2014.

[66] S. S. Kulkarni, J. Sayers, B. Premdjee, and R. J. Payne, "Rapid and efficient protein synthesis through expansion of the native chemical ligation concept," *Nature Reviews Chemistry*, vol. 2, no. 4, 2018.

[67] D. B. Cowie and G. N. Cohen, "Biosynthesis by Escherichia Coli of active altered proteins containing selenium instead of sulfur," *Biochimica et Biophysica Acta*, vol. 26, pp. 252–261, 1957.

[68] J. C. Van Hest, K. L. Kiick, and D. A. Tirrell, "Efficient incorporation of unsaturated methionine analogues into proteins in vivo," *Journal of the American Chemical Society*, vol. 122, no. 7, pp. 1282–1288, 2000.

[69] A. J. Link, M. K. Vink, and D. A. Tirrell, "Presentation and detection of azide functionality in bacterial cell surface proteins," *Journal of the American Chemical Society*, vol. 126, no. 34, pp. 10598–10602, 2004.

[70] D. Lauster, S. Klenk, K. Ludwig, S. Nojoumi, S. Behren, L. Adam, M. Stadtmüller, S. Saenger, S. Zimmler, K. Hönzke, L. Yao, U. Hoffmann, M. Bardua, A. Hamann, M. Witzenrath, L. E. Sander, T. Wolff, A. C. Hocke, S. Hippenstiel, S. De Carlo, J. Neudecker, K. Osterrieder, N. Budisa, R. R. Netz, C. Böttcher, S. Liese, A. Herrmann, and C. P. Hackenberger, "Phage capsid nanoparticles with defined ligand arrangement block influenza virus entry," *Nature Nanotechnology*, vol. 15, no. 5, pp. 373–379, 2020.

[71] J. W. Chin, "Expanding and Reprogramming the Genetic Code of Cells and Animals," *Annual Review of Biochemistry*, vol. 83, no. 1, pp. 379–408, 2014.

[72] K. Wals and H. Ovaa, "Unnatural amino acid incorporation in E. coli: Current and future applications in the design of therapeutic proteins," *Frontiers in Chemistry*, vol. 2, no. APR, pp. 1–12, 2014.

[73] A. R. Nödling, L. A. Spear, T. L. Williams, L. Y. Luk, and Y. H. Tsai, "Using genetically incorporated unnatural amino acids to control protein functions in mammalian cells," *Essays in Biochemistry*, vol. 63, no. 2, pp. 237–266, 2019.

[74] K. J. Lee, D. Kang, and H. S. Park, "Site-Specific Labeling of Proteins Using Unnatural Amino Acids," *Molecules and cells*, vol. 42, no. 5, pp. 386–396, 2019.

[75] J. W. Chin, T. A. Cropp, J. C. Anderson, M. Mukherji, Z. Zhang, and P. G. Schultz, "An expanded eukaryotic genetic code," *Science*, vol. 301, no. 5635, pp. 964–967, 2003.

[76] T. Mukai, T. Kobayashi, N. Hino, T. Yanagisawa, K. Sakamoto, and S. Yokoyama, "Adding l-lysine derivatives to the genetic code of mammalian cells with engineered pyrrolysyl-tRNA synthetases," *Biochemical and Biophysical Research Communications*, vol. 371, no. 4, pp. 818–822, 2008.

[77] S. M. Hancock, R. Uprety, A. Deiters, and J. W. Chin, "Expanding the genetic code of yeast for incorporation of diverse unnatural amino acids via a pyrrolysyl-tRNA synthetase/tRNA pair," *Journal of the American Chemical Society*, vol. 132, no. 42, pp. 14819–14824, 2010.

[78] S. Greiss and J. W. Chin, "Expanding the genetic code of an animal," *Journal of the American Chemical Society*, vol. 133, no. 36, pp. 14196–14199, 2011.

[79] A. Bianco, F. M. Townsley, S. Greiss, K. Lang, and J. W. Chin, "Expanding the genetic code of Drosophila melanogaster," *Nature Chemical Biology*, vol. 8, no. 9, pp. 748–750, 2012.

[80] R. J. Ernst, T. P. Krogager, E. S. Maywood, R. Zanchi, V. Beránek, T. S. Elliott, N. P. Barry, M. H. Hastings, and J. W. Chin, "Genetic code expansion in the mouse brain," *Nature Chemical Biology*, vol. 12, no. 10, pp. 776–778, 2016.

[81] S. Han, A. Yang, S. Lee, H. W. Lee, C. B. Park, and H. S. Park, "Expanding the genetic code of Mus musculus," *Nature Communications*, vol. 8, pp. 1–7, 2017.

[82] Y. Yang, S. Lin, W. Lin, and P. R. Chen, "Ligand-assisted dual-site click labeling of EGFR on living cells," *ChemBioChem*, vol. 15, no. 12, pp. 1738–1743, 2014.

[83] A. H. Smits, A. Borrmann, M. Roosjen, J. C. Van Hest, and M. Vermeulen, "Click-MS: Tagless Protein Enrichment Using Bioorthogonal Chemistry for Quantitative Proteomics," *ACS Chemical Biology*, vol. 11, no. 12, pp. 3245–3250, 2016.

[84] J. L. Seitchik, J. C. Peeler, M. T. Taylor, M. L. Blackman, T. W. Rhoads, R. B. Cooley, C. Refakis, J. M. Fox, and R. A. Mehl, "Genetically encoded tetrazine amino acid directs rapid site-specific in vivo bioorthogonal ligation with trans-cyclooctenes," *Journal of the American Chemical Society*, vol. 134, no. 6, pp. 2898–2901, 2012.

[85] K. Lang, L. Davis, S. Wallace, M. Mahesh, D. J. Cox, M. L. Blackman, J. M. Fox, and J. W. Chin, "Genetic encoding of bicyclononynes and trans-cyclooctenes for site-specific protein labeling in vitro and in live mammalian cells via rapid fluorogenic diels-alder reactions," *Journal of the American Chemical Society*, vol. 134, no. 25, pp. 10317–10320, 2012.

[86] T. S. Young and P. G. Schultz, "Beyond the canonical 20 amino acids: Expanding the genetic lexicon," *Journal of Biological Chemistry*, vol. 285, no. 15, pp. 11039–11044, 2010.

[87] K. Amaike, T. Tamura, and I. Hamachi, "Recognition-driven chemical labeling of endogenous proteins in multi-molecular crowding in live cells," *Chemical Communications*, vol. 53, no. 88, pp. 11972–11983, 2017.

[88] C. C. Hughes, Y. L. Yang, W. T. Liu, P. C. Dorrestein, J. J. La Clair, and W. Fenical, "Marinopyrrole A target elucidation by acyl dye transfer," *Journal of the American Chemical Society*, vol. 131, no. 34, pp. 12094–12096, 2009.

[89] S. Tsukiji, H. Wang, M. Miyagawa, T. Tamura, Y. Takaoka, and I. Hamachi, "Quenched ligand-directed tosylate reagents for one-step construction of turn-on fluorescent biosensors," *Journal of the American Chemical Society*, vol. 131, no. 25, pp. 9046–9054, 2009.

[90] S. H. Fujishima, R. Yasui, T. Miki, A. Ojida, and I. Hamachi, "Ligand-directed acyl imidazole chemistry for labeling of membrane-bound proteins on live cells," *Journal of the American Chemical Society*, vol. 134, no. 9, pp. 3961–3964, 2012.

[91] S. Tsukiji, M. Miyagawa, Y. Takaoka, T. Tamura, and I. Hamachi, "Ligand-directed tosyl chemistry for protein labeling in vivo," *Nature Chemical Biology*, vol. 5, no. 5, pp. 341–343, 2009.

[92] S. Sakamoto and I. Hamachi, "Recent progress in chemical modification of proteins," *Analytical Sciences*, vol. 35, no. 1, pp. 5–27, 2019.

[93] S. B. Gunnoo and A. Madder, "Chemical Protein Modification through Cysteine," *ChemBioChem*, vol. 17, no. 7, pp. 529–553, 2016.

[94] P. Ochtrop and C. P. R. Hackenberger, "Recent advances of thiol-selective bioconjugation reactions," *Current Opinion in Chemical Biology*, vol. 58, pp. 28–36, 2020.

[95] D. Gilis, S. Massar, N. J. Cerf, and M. Rooman, "Optimality of the genetic code with respect to protein stability and amino-acid frequencies.," *Genome biology*, vol. 2, no. 11, pp. 1–12, 2001.

[96] G. Bulaj, T. Kortemme, and D. P. Goldenberg, "Ionization-reactivity relationships for cysteine thiols in polypeptides," *Biochemistry*, vol. 37, no. 25, pp. 8965–8972, 1998.

[97] N. M. Giles, A. B. Watts, G. I. Giles, F. H. Fry, J. A. Littlechild, and C. Jacob, "Metal and redox modulation of cysteine protein function," *Chemistry and Biology*, vol. 10, pp. 677–693, 2003.

[98] H. J. Reich and R. J. Hondal, "Why Nature Chose Selenium," *ACS Chemical Biology*, vol. 11, no. 4, pp. 821–841, 2016.

[99] J. Gonzalez-Flores, S. P. Shetty, A. Dubey, and P. R. Copeland, "The Molecular Biology of Selenocysteine," *Biomol. Concepts.*, vol. 4, no. 4, pp. 349–365, 2013.

[100] B. Cordero, V. Gómez, A. E. Platero-Prats, M. Revés, J. Echeverría, E. Cremades, F. Barragán, and S. Alvarez, "Covalent radii revisited," *Journal of the Chemical Society. Dalton Transactions*, no. 21, pp. 2832–2838, 2008.

[101] R. Kundu and Z. T. Ball, "Rhodium-catalyzed cysteine modification with diazo reagents," *Chemical Communications*, vol. 49, no. 39, pp. 4166–4168, 2013.

[102] K. K. Y. Kung, H. M. Ko, J. F. Cui, H. C. Chong, Y. C. Leung, and M. K. Wong, "Cyclometalated gold(iii) complexes for chemoselective cysteine modification via ligand controlled C-S bond-forming reductive elimination," *Chemical Communications*, vol. 50, no. 80, pp. 11899–11902, 2014.

[103] E. V. Vinogradova, C. Zhang, A. M. Spokoyny, B. L. Pentelute, and S. L. Buchwald, "Organometallic palladium reagents for cysteine bioconjugation," *Nature*, vol. 526, no. 7575, pp. 687–691, 2015.

[104] N. Gupta, J. Kancharla, S. Kaushik, A. Ansari, S. Hossain, R. Goyal, M. Pandey, J. Sivaccumar, S. Hussain, A. Sarkar, A. Sengupta, S. K. Mandal, M. Roy, and S. Sengupta, "Development of a facile antibody-drug conjugate platform for increased stability and homogeneity," *Chemical Science*, vol. 8, no. 3, pp. 2387–2395, 2017.

[105] Y. Chen, K. Tsao, É. De Francesco, and J. W. Keillor, "Ring Substituent Effects on the Thiol Addition and Hydrolysis Reactions of N-Arylmaleimides," *Journal of Organic Chemistry*, vol. 80, no. 24, pp. 12182–12192, 2015.

[106] F. Saito, H. Noda, and J. W. Bode, "Critical evaluation and rate constants of chemoselective ligation reactions for stoichiometric conjugations in water," *ACS Chemical Biology*, vol. 10, no. 4, pp. 1026–1033, 2015.

[107] C. F. Brewer and J. P. Riehm, "Evidence for possible nonspecific reactions between N-ethylmaleimide and proteins," *Analytical Biochemistry*, vol. 18, no. 2, pp. 248–255, 1967.

[108] A. D. Baldwin and K. L. Kiick, "Tunable degradation of maleimide-Thiol adducts in reducing environments," *Bioconjugate Chemistry*, vol. 22, no. 10, pp. 1946–1953, 2011.

[109] B. Q. Shen, K. Xu, L. Liu, H. Raab, S. Bhakta, M. Kenrick, K. L. Parsons-Reponte, J. Tien, S. F. Yu, E. Mai, D. Li, J. Tibbitts, J. Baudys, O. M. Saad, S. J. Scales, P. J. McDonald, P. E. Hass, C. Eigenbrot, T. Nguyen, W. A. Solis, R. N. Fuji, K. M. Flagella, D. Patel, S. D. Spencer, L. A. Khawli, A. Ebens, W. L. Wong, R. Vandlen, S. Kaur, M. X. Sliwkowski, R. H. Scheller, P. Polakis, and J. R. Junutula, "Conjugation site modulates the in vivo stability and therapeutic activity of antibody-drug conjugates," *Nature Biotechnology*, vol. 30, no. 2, pp. 184–189, 2012.

[110] R. P. Lyon, J. R. Setter, T. D. Bovee, S. O. Doronina, J. H. Hunter, M. E. Anderson, C. L. Balasubramanian, S. M. Duniho, C. I. Leiske, F. Li, and P. D. Senter, "Self-hydrolyzing maleimides improve the stability and pharmacological properties of antibody-drug conjugates," *Nature Biotechnology*, vol. 32, no. 10, pp. 1059–1062, 2014.

[111] D. Kalia, P. V. Malekar, and M. Parthasarathy, "Exocyclic Olefinic Maleimides: Synthesis and Application for Stable and Thiol-Selective Bioconjugation," *Angewandte Chemie - International Edition*, vol. 55, no. 4, pp. 1432–1435, 2016.

[112] L. M. Tedaldi, M. E. Smith, R. I. Nathani, and J. R. Baker, "Bromomaleimides: New reagents for the selective and reversible modification of cysteine," *Chemical Communications*, no. 43, pp. 6583–6585, 2009.

[113] S. Ramesh, P. Cherkupally, T. Govender, H. G. Kruger, F. Albericio, and B. G. De La Torre, "Highly chemoselective ligation of thiol- and amino-peptides on a bromomaleimide core," *Chemical Communications*, vol. 52, no. 11, pp. 2334–2337, 2016.

[114] M. E. Smith, F. F. Schumacher, C. P. Ryan, L. M. Tedaldi, D. Papaioannou, G. Waksman, S. Caddick, and J. R. Baker, "Protein modification, bioconjugation, and disulfide bridging using bromomaleimides," *Journal of the American Chemical Society*, vol. 132, no. 6, pp. 1960–1965, 2010.

[115] M. Morais, J. P. Nunes, K. Karu, N. Forte, I. Benni, M. E. Smith, S. Caddick, V. Chudasama, and J. R. Baker, "Optimisation of the dibromomaleimide (DBM) platform for native antibody conjugation by accelerated post-conjugation hydrolysis," *Organic and Biomolecular Chemistry*, vol. 15, no. 14, pp. 2947–2952, 2017.

[116] C. P. Ryan, M. E. Smith, F. F. Schumacher, D. Grohmann, D. Papaioannou, G. Waksman, F. Werner, J. R. Baker, and S. Caddick, "Tunable reagents for multi-functional bioconjugation: Reversible or permanent chemical modification of proteins and peptides by control of maleimide hydrolysis," *Chemical Communications*, vol. 47, no. 19, pp. 5452–5454, 2011.

[117] F. F. Schumacher, M. Nobles, C. P. Ryan, M. E. Smith, A. Tinker, S. Caddick, and J. R. Baker, "In situ maleimide bridging of disulfides and a new approach to protein PEGylation," *Bioconjugate Chemistry*, vol. 22, no. 2, pp. 132–136, 2011.

[118] Y. Zhang, C. Zang, G. An, M. Shang, Z. Cui, G. Chen, Z. Xi, and C. Zhou, "Cysteine-specific protein multi-functionalization and disulfide bridging using 3-bromo-5-methylene pyrrolones," *Nature Communications*, vol. 11, no. 1, pp. 1–10, 2020.

[119] V. Chudasama, M. E. Smith, F. F. Schumacher, D. Papaioannou, G. Waksman, J. R. Baker, and S. Caddick, "Bromopyridazinedione-mediated protein and peptide bioconjugation," *Chemical Communications*, vol. 47, no. 31, pp. 8781–8783, 2011.

[120] M. Sortino, F. Garibotto, V. Cechinel Filho, M. Gupta, R. Enriz, and S. Zacchino, "Antifungal, cytotoxic and SAR studies of a series of N-alkyl, N-aryl and N-alkylphenyl-1,4-pyrrolediones and related compounds," *Bioorganic and Medicinal Chemistry*, vol. 19, no. 9, pp. 2823–2834, 2011.

[121] C. D. Mayer, M. Kehrel, and F. Bracher, "An improved approach to n-substituted maleimides and phthalimides by microwave-promoted mitsunobu reaction," *Organic Preparations and Procedures International*, vol. 40, no. 6, pp. 574–579, 2008.

[122] L. Castañeda, Z. V. Wright, C. Marculescu, T. M. Tran, V. Chudasama, A. Maruani, E. A. Hull, J. P. Nunes, R. J. Fitzmaurice, M. E. Smith, L. H. Jones, S. Caddick, and J. R. Baker, "A mild synthesis of N-functionalised bromomaleimides, thiomaleimides and bromopyridazinediones," *Tetrahedron Letters*, vol. 54, no. 27, pp. 3493–3495, 2013.

[123] M. A. Walker, "The Mitsunobu reaction: A novel method for the synthesis of bifunctional maleimide linkers," *Tetrahedron Letters*, vol. 35, no. 5, pp. 665–668, 1994.

[124] H. D. King, G. M. Dubowchik, and M. A. Walker, "Facile synthesis of maleimide bifunctional linkers," *Tetrahedron Letters*, vol. 43, no. 11, pp. 1987–1990, 2002.

[125] S. Marburg, A. C. Neckers, and P. R. Griffin, "Introduction of the maleimide function onto resin-bound peptides: A simple, high-yield process useful for discriminating among several lysines," *Bioconjugate Chemistry*, vol. 7, no. 5, pp. 612–616, 1996.

[126] A. Sánchez, E. Pedroso, and A. Grandas, "Maleimide-dimethylfuran exo adducts: Effective maleimide protection in the synthesis of oligonucleotide conjugates," *Organic Letters*, vol. 13, no. 16, pp. 4364–4367, 2011.

[127] D. R. Goddard and L. Michaelis, "Derivatives of Keratin," *Derivatives of Keratin*, vol. 112, no. 1, pp. 361–371, 1935.

[128] N. Lundell and T. Schreitmüller, "Sample preparation for peptide mapping - A pharmaceutical quality- control perspective," *Analytical Biochemistry*, vol. 266, no. 1, pp. 31–47, 1999.

[129] S. C. Alley, D. R. Benjamin, S. C. Jeffrey, N. M. Okeley, D. L. Meyer, R. J. Sanderson, and P. D. Senter, "Contribution of linker stability to the activities of anticancer immunoconjugates," *Bioconjugate Chemistry*, vol. 19, no. 3, pp. 759–765, 2008.

[130] H. Lindely, "A Study of the Kinetics of Reaction between Thiol Compounds and Chloroacetamide," *The Biochemical Journal*, vol. 74, no. 3, pp. 577–584, 1960.

[131] T. Müller and D. Winter, "Systematic evaluation of protein reduction and alkylation reveals massive unspecific side effects by iodine-containing reagents," *Molecular and Cellular Proteomics*, vol. 16, no. 7, pp. 1173–1187, 2017.

[132] B. S. Balaji and N. Dalal, "An expedient, chemoselective n-chloroacetylation of aminoalcohols under metal-free bio-compatible conditions," *Green Chemistry Letters and Reviews*, vol. 11, no. 4, pp. 534–543, 2018.

[133] B. A. Mendelsohn, S. D. Barnscher, J. T. Snyder, Z. An, J. M. Dodd, and J. Dugal-Tessier, "Investigation of Hydrophilic Auristatin Derivatives for Use in Antibody Drug Conjugates," *Bioconjugate Chemistry*, vol. 28, no. 2, pp. 371–381, 2017.

[134] D. T. Krist and A. V. Statsyuk, "Catalytically Important Residues of E6AP Ubiquitin Ligase Identified Using Acid-Cleavable Photo-Cross-Linkers," *Biochemistry*, vol. 54, no. 29, pp. 4411–4414, 2015.

[135] B. Bernardim, P. M. Cal, M. J. Matos, B. L. Oliveira, N. Martínez-Saéz, I. S. Albuquerque, E. Perkins, F. Corzana, A. C. Burtoloso, G. Jiménez-Osés, and G. J. Bernardes, "Stoichiometric and irreversible cysteine-selective protein modification using carbonylacrylic reagents," *Nature Communications*, vol. 7, no. May, pp. 1–9, 2016.

[136] F. Diwischek, *Development of synthesis pathways and characterization of cerulenin analogues as inhibitors of the fatty acid biosynthesis of Mycobacterium tuberculosis and of efflux pump resistant Candida albicans.* PhD thesis, 2008.

[137] S. Ariyasu, H. Hayashi, B. Xing, and S. Chiba, "Site-Specific Dual Functionalization of Cysteine Residue in Peptides and Proteins with 2-Azidoacrylates," *Bioconjugate Chemistry*, vol. 28, no. 4, pp. 897–902, 2017.

[138] H. Khalili, A. Godwin, J. W. Choi, R. Lever, and S. Brocchini, "Comparative binding of disulfide-bridged PEG-Fabs," *Bioconjugate Chemistry*, vol. 23, no. 11, pp. 2262–2277, 2012.

[139] T. Wang, A. Riegger, M. Lamla, S. Wiese, P. Oeckl, M. Otto, Y. Wu, S. Fischer, H. Barth, S. L. Kuan, and T. Weil, "Water-soluble allyl sulfones for dual site-specific labelling of proteins and cyclic peptides," *Chemical Science*, vol. 7, no. 5, pp. 3234–3239, 2016.

[140] N. J. Smith, K. Rohlfing, L. A. Sawicki, P. M. Kharkar, S. J. Boyd, A. M. Kloxin, and J. M. Fox, "Fast, irreversible modification of cysteines through strain releasing conjugate additions of cyclopropenyl ketones," *Organic and Biomolecular Chemistry*, vol. 16, no. 12, pp. 2164–2169, 2018.

[141] L. A. Fisher, N. J. Smith, and J. M. Fox, "Chiral cyclopropenyl ketones: Reactive and selective diels-alder dienophiles," *Journal of Organic Chemistry*, vol. 78, no. 7, pp. 3342–3348, 2013.

[142] Q. Luo, Y. Tao, W. Sheng, J. Lu, and H. Wang, "Dinitroimidazoles as bifunctional bioconjugation reagents for protein functionalization and peptide macrocyclization," *Nature Communications*, vol. 10, no. 1, pp. 1–9, 2019.

[143] E. Gil De Montes, E. Jiménez-Moreno, B. L. Oliveira, C. D. Navo, P. M. Cal, G. Jiménez-Osés, I. Robina, A. J. Moreno-Vargas, and G. J. Bernardes, "Azabicyclic vinyl sulfones for residue-specific dual protein labelling," *Chemical Science*, vol. 10, no. 16, pp. 4515–4522, 2019.

[144] E. Gil de Montes, A. Istrate, C. D. Navo, E. Jiménez-Moreno, E. A. Hoyt, F. Corzana, I. Robina, G. Jiménez-Osés, A. J. Moreno-Vargas, and G. J. Bernardes, "Stable Pyrrole-Linked Bioconjugates through Tetrazine-Triggered Azanorbornadiene Fragmentation," *Angewandte Chemie - International Edition*, vol. 59, no. 15, pp. 6196–6200, 2020.

[145] N. G. Khusainova, O. A. Mostovaya, E. A. Berdnikov, Y. Y. Efremov, D. R. Sharafutdinova, and R. A. Cherkasov, "Reactions of 1,2 ethanedithiol and 2 mercaptoethanol," *Russian Chemical Bulletin, International Edition*, vol. 53, no. 10, pp. 2253–2256, 2004.

[146] F. Gao, X. Yan, and K. Auclair, "Synthesis of a phosphonate-linked aminoglycoside-coenzyme a bisubstrate and use in mechanistic studies of an enzyme involved in aminoglycoside resistance," *Chemistry - A European Journal*, vol. 15, no. 9, pp. 2064–2070, 2009.

[147] P. Fourgeaud, C. Midrier, J. P. Vors, J. N. Volle, J. L. Pirat, and D. Virieux, "Oxaphospholene and oxaphosphinene heterocycles via RCM using unsymmetrical phosphonates or functional phosphinates," *Tetrahedron*, vol. 66, no. 3, pp. 758–764, 2010.

[148] V. Liautard, V. Desvergnes, K. Itoh, H. W. Liu, and O. R. Martin, "Convergent and stereoselective synthesis of iminosugar-containing Galf and UDP-Galf mimicks: Evaluation as inhibitors of UDP-Gal mutase," *Journal of Organic Chemistry*, vol. 73, no. 8, pp. 3103–3115, 2008.

[149] C. E. Hoyle and C. N. Bowman, "Thiol-ene click chemistry," *Angewandte Chemie - International Edition*, vol. 49, no. 9, pp. 1540–1573, 2010.

[150] A. B. Lowe, C. E. Hoyle, and C. N. Bowman, "Thiol-yne click chemistry: A powerful and versatile methodology for materials synthesis," *Journal of Materials Chemistry*, vol. 20, no. 23, pp. 4745–4750, 2010.

[151] N. B. Cramer, S. K. Reddy, A. K. O'Brien, and C. N. Bowman, "Thiol - Ene Photopolymerization Mechanism and Rate Limiting Step Changes for Various Vinyl Functional Group Chemistries," *Macromolecules*, vol. 36, no. 21, pp. 7964–7969, 2003.

[152] S. K. Reddy, N. B. Cramer, and C. N. Bowman, "Thiol-vinyl mechanisms. 2. Kinetic modeling of ternary thiol-vinyl photopolymerizations," *Macromolecules*, vol. 39, no. 10, pp. 3681–3687, 2006.

[153] F. Li, A. Allahverdi, R. Yang, G. B. J. Lua, X. Zhang, Y. Cao, N. Korolev, L. Nordenskiöld, and C. F. Liu, "A direct method for site-specific protein acetylation," *Angewandte Chemie - International Edition*, vol. 50, no. 41, pp. 9611–9614, 2011.

[154] A. Dondoni, A. Massi, P. Nanni, and A. Roda, "A new ligation strategy for peptide and protein glycosylation: Photoinduced thiol-ene coupling," *Chemistry - A European Journal*, vol. 15, no. 43, pp. 11444–11449, 2009.

[155] N. Floyd, B. Vijayakrishnan, J. R. Koeppe, and B. G. Davis, "Thiyl glycosylate of olefinic proteins: S-linked glycoconjugate synthesis," *Angewandte Chemie - International Edition*, vol. 48, no. 42, pp. 7798–7802, 2009.

[156] R. Hoogenboom, "Thiol-yne chemistry: A powerful tool for creating highly functional materials," *Angewandte Chemie - International Edition*, vol. 49, no. 20, pp. 3415–3417, 2010.

[157] A. Massi and D. Nanni, "Thiol-yne coupling: Revisiting old concepts as a breakthrough for up-to-date applications," *Organic and Biomolecular Chemistry*, vol. 10, no. 19, pp. 3791–3807, 2012.

[158] M. L. Conte, S. Staderini, A. Marra, M. Sanchez-Navarro, B. G. Davis, and A. Dondoni, "Multi-molecule reaction of serum albumin can occur through thiol-yne coupling," *Chemical Communications*, vol. 47, no. 39, pp. 11086–11088, 2011.

[159] D. R. Feleciano, K. Arnsburg, and J. Kirstein, "Interplay between redox and protein homeostasis," *Worm*, vol. 5, no. 2, p. e1170273, 2016.

[160] U. Brinkmann and R. E. Kontermann, "The making of bispecific antibodies," *mAbs*, vol. 9, no. 2, pp. 182–212, 2017.

[161] C. Chatterjee, R. K. McGinty, B. Fierz, and T. W. Muir, "Disulfide-directed histone ubiquitylation reveals plasticity in hDot1L activation," *Nature Chemical Biology*, vol. 6, no. 4, pp. 267–269, 2010.

[162] J. Chen, Y. Ai, J. Wang, L. Haracska, and Z. Zhuang, "Chemically ubiquitylated PCNA as a probe for eukaryotic translesion DNA synthesis," *Nature Chemical Biology*, vol. 6, no. 4, pp. 270–272, 2010.

[163] F. Meier, T. Abeywardana, A. Dhall, N. P. Marotta, J. Varkey, R. Langen, C. Chatterjee, and M. R. Pratt, "Semisynthetic, site-specific ubiquitin modification of α-synuclein reveals differential effects on aggregation," *Journal of the American Chemical Society*, vol. 134, no. 12, pp. 5468–5471, 2012.

[164] A. R. Nödling, L. A. Spear, T. L. Williams, L. Y. Luk, and Y. H. Tsai, "Using genetically incorporated unnatural amino acids to control protein functions in mammalian cells," *Essays in Biochemistry*, vol. 63, no. 2, pp. 237–266, 2019.

[165] X. H. Chen, Z. Xiang, Y. S. Hu, V. K. Lacey, H. Cang, and L. Wang, "Genetically encoding an electrophilic amino acid for protein stapling and covalent binding to native receptors," *ACS Chemical Biology*, vol. 9, no. 9, pp. 1956–1961, 2014.

[166] Y. Li, M. Yang, Y. Huang, X. Song, L. Liu, and P. R. Chen, "Genetically encoded alkenyl-pyrrolysine analogues for thiol-ene reaction mediated site-specific protein labeling," *Chemical Science*, vol. 3, no. 9, pp. 2766–2770, 2012.

[167] B. Lee, S. Sun, E. Jiménez-Moreno, A. A. Neves, and G. J. Bernardes, "Site-selective installation of an electrophilic handle on proteins for bioconjugation," *Bioorganic and Medicinal Chemistry*, vol. 26, no. 11, pp. 3060–3064, 2018.

[168] L. Holm, P. Moody, and M. Howarth, "Electrophilic affibodies forming covalent bonds to protein targets," *Journal of Biological Chemistry*, vol. 284, no. 47, pp. 32906–32913, 2009.

[169] S. K. Singh, I. Sahu, S. M. Mali, H. P. Hemantha, O. Kleifeld, M. H. Glickman, and A. Brik, "Synthetic Uncleavable Ubiquitinated Proteins Dissect Proteasome Deubiquitination and Degradation, and Highlight Distinctive Fate of Tetraubiquitin," *Journal of the American Chemical Society*, vol. 138, no. 49, pp. 16004–16015, 2016.

[170] J. E. Hudak, R. M. Barfield, G. W. Dehart, P. Grob, E. Nogales, C. R. Bertozzi, and D. Rabuka, "Synthesis of heterobifunctional protein fusions using copper-free click chemistry and the aldehyde tag," *Angewandte Chemie - International Edition*, vol. 51, no. 17, pp. 4161–4165, 2012.

[171] G. Powis and W. R. Montfort, "Properties and biological activites of thioredoxins," *Annu. Rev. Pharmacol. Toxicol.*, vol. 41, pp. 261–295, 2001.

[172] D. P. Gamblin, P. Garnier, S. Van Kasteren, N. J. Oldham, A. J. Fairbanks, and B. G. Davis, "Glyco-SeS: Selenenylsulfide-mediated protein glycoconjugation - A new strategy in post-translational modification," *Angewandte Chemie - International Edition*, vol. 43, no. 7, pp. 828–833, 2004.

[173] O. Behagel and H. Seibert, "Ueber die Einwirkung von Halogen auf Aryl-selencyanide.," *Justus Liebigs Ann. Chem.*, vol. 65, pp. 812–816, 1932.

[174] J. L. Kice and T. W. Lee, "Oxidation-Reduction Reactions of Organoselenium Compounds. 1. Mechanism of the Reaction between Seleninic Acids and Thiols," *Journal of the American Chemical Society*, vol. 100, no. 16, pp. 5094–5102, 1978.

[175] J. M. Chalker, S. B. Gunnoo, O. Boutureira, S. C. Gerstberger, M. Fernández-González, G. J. Bernardes, L. Griffin, H. Hailu, C. J. Schofield, and B. G. Davis, "Methods for converting cysteine to dehydroalanine on peptides and proteins," *Chemical Science*, vol. 2, no. 9, pp. 1666–1676, 2011.

[176] J. Dadová, S. R. Galan, and B. G. Davis, "Synthesis of modified proteins via functionalization of dehydroalanine," *Current Opinion in Chemical Biology*, vol. 46, pp. 71–81, 2018.

[177] J. M. Chalker, L. Lercher, N. R. Rose, C. J. Schofield, and B. G. Davis, "Conversion of cysteine into dehydroalanine enables access to synthetic histones bearing diverse post-translational modifications," *Angewandte Chemie - International Edition*, vol. 51, no. 8, pp. 1835–1839, 2012.

[178] Y. A. Lin, O. Boutureira, L. Lercher, B. Bhushan, R. S. Paton, and B. G. Davis, "Rapid cross-metathesis for reversible protein modifications via chemical access to se-allyl-selenocysteine in proteins," *Journal of the American Chemical Society*, vol. 135, no. 33, pp. 12156–12159, 2013.

[179] A. M. Freedy, M. J. Matos, O. Boutureira, F. Corzana, A. Guerreiro, P. Akkapeddi, V. J. Somovilla, T. Rodrigues, K. Nicholls, B. Xie, G. Jiménez-Osés, K. M. Brindle, A. A. Neves, and G. J. Bernardes, "Chemoselective Installation of Amine Bonds on Proteins through Aza-Michael Ligation," *Journal of the American Chemical Society*, vol. 139, no. 50, pp. 18365–18375, 2017.

[180] T. H. Wright, B. J. Bower, J. M. Chalker, G. J. Bernardes, R. Wiewiora, W. L. Ng, R. Raj, S. Faulkner, M. R. J. Vallée, A. Phanumartwiwath, O. D. Coleman,

M. L. Thézénas, M. Khan, S. R. Galan, L. Lercher, M. W. Schombs, S. Gerstberger, M. E. Palm-Espling, A. J. Baldwin, B. M. Kessler, T. D. Claridge, S. Mohammed, and B. G. Davis, "Posttranslational mutagenesis: A chemical strategy for exploring protein side-chain diversity," *Science*, vol. 354, no. 6312, 2016.

[181] G. J. Bernardes, J. M. Chalker, J. C. Errey, and B. G. Davis, "Facile conversion of cysteine and alkyl cysteines to dehydroalanine on protein surfaces: Versatile and switchable access to functionalized proteins," *Journal of the American Chemical Society*, vol. 130, no. 15, pp. 5052–5053, 2008.

[182] N. Metanis and D. Hilvert, "Natural and synthetic selenoproteins," *Current opinion in chemical biology*, vol. 22, pp. 27–34, 2014.

[183] S. D. Whedon, N. Markandeya, A. S. Rana, N. A. Senger, C. E. Weller, F. Tureček, E. R. Strieter, and C. Chatterjee, "Selenocysteine as a Latent Bioorthogonal Electrophilic Probe for Deubiquitylating Enzymes," *Journal of the American Chemical Society*, vol. 138, no. 42, pp. 13774–13777, 2016.

[184] J. Wang, S. M. Schiller, and P. G. Schultz, "A biosynthetic route to dehydroalanine-containing proteins," *Angewandte Chemie - International Edition*, vol. 46, no. 36, pp. 6849–6851, 2007.

[185] J. Guo, J. Wang, J. S. Lee, and P. G. Schultz, "Site-specific incorporation of methyl- and acetyl-lysine analogues into recombinant proteins," *Angewandte Chemie - International Edition*, vol. 47, no. 34, pp. 6399–6401, 2008.

[186] R. Meledin, S. M. Mali, S. K. Singh, and A. Brik, "Protein ubiquitination: Via dehydroalanine: Development and insights into the diastereoselective 1,4-addition step," *Organic and Biomolecular Chemistry*, vol. 14, no. 21, pp. 4817–4823, 2016.

[187] N. Haj-Yahya, H. P. Hemantha, R. Meledin, S. Bondalapati, M. Seenaiah, and A. Brik, "Dehydroalanine-based diubiquitin activity probes," *Organic Letters*, vol. 16, no. 2, pp. 540–543, 2014.

[188] M. Jbara, S. Laps, M. Morgan, G. Kamnesky, G. Mann, C. Wolberger, and A. Brik, "Palladium prompted on-demand cysteine chemistry for the synthesis of challenging and uniquely modified proteins," *Nature Communications*, vol. 9, no. 1, 2018.

[189] R. Meledin, S. M. Mali, O. Kleifeld, and A. Brik, "Activity-Based Probes Developed by Applying a Sequential Dehydroalanine Formation Strategy to Expressed Proteins Reveal a Potential α-Globin-Modulating Deubiquitinase," *Angewandte Chemie - International Edition*, vol. 57, no. 20, pp. 5645–5649, 2018.

[190] H. Staudinger and J. Meyer, "Über neue organische Phosphorverbindungen III. Phosphinmethylenderivate und Phosphinimine," *Helvetica Chimica Acta*, vol. 2, no. 1, pp. 635–646, 1919.

[191] M. Köhn and R. Breinbauer, "The Staudinger ligation - A gift to chemical biology," *Angewandte Chemie - International Edition*, vol. 43, no. 24, pp. 3106–3116, 2004.

[192] E. Saxon, J. I. Armstrong, and C. R. Bertozzi, "A traceless Staudinger ligation for the chemoselective synthesis of amide bonds," *Organic Letters*, vol. 2, no. 14, pp. 2141–2143, 2000.

[193] B. L. Nilsson, L. L. Kiessling, and R. T. Raines, "Staudinger ligation: A peptide from a thioester and azide," *Organic Letters*, vol. 2, no. 13, pp. 1939–1941, 2000.

[194] B. L. Nilsson, L. L. Kiessling, and R. T. Raines, "High-yielding staudinger ligation of a phosphinothioester and azide to form a peptide," *Organic Letters*, vol. 3, no. 1, pp. 9–12, 2001.

[195] N. J. Agard, J. M. Baskin, J. A. Prescher, A. Lo, and C. R. Bertozzi, "A comparative study of bioorthogonal reactions with azides.," *ACS chemical biology*, vol. 1, no. 10, pp. 644–648, 2006.

[196] B. L. Nilsson, R. J. Hondal, M. B. Soellner, and R. T. Raines, "Protein assembly by orthogonal chemical ligation methods," *Journal of the American Chemical Society*, vol. 125, no. 18, pp. 5268–5269, 2003.

[197] O. David, W. J. Meester, H. Bieräugel, H. E. Schoemaker, H. Hiemstra, and J. H. Van Maarseveen, "Intramolecular Staudinger ligation: A powerful ring-closure method to form medium-sized lactams," *Angewandte Chemie - International Edition*, vol. 42, no. 36, pp. 4373–4375, 2003.

[198] R. Kleineweischede and C. P. Hackenberger, "Chemoselective peptide cyclization by traceless staudinger ligation," *Angewandte Chemie - International Edition*, vol. 47, no. 32, pp. 5984–5988, 2008.

[199] M. I. Kabachnik and V. A. Gilyarov, "Trialkyl phosphorimidates," *Bulletin of the Academy of Sciences of the USSR, Division of chemical science*, vol. 5, pp. 809–816, 1956.

[200] C.-g. Shin, Y. Yonezawa, K. Watanabe, and J. Yoshimura, "α, β-Unsaturated carboxylic acid derivatives. XXI. A novel synthesis of α-dehydroamino acid derivatives by the Arbusov reaction of α-phosphoranylideneamino-2-alkenoates," *Bulletin of the Chemical Society of Japan*, vol. 54, pp. 3811–3814, 1981.

[201] Vaccarino, "Biosynthesis of phosphonic and phosphinic acid natural products," *Annual Review of Biochemistry*, vol. 78, pp. 65–94, 2009.

[202] B. C. Challis, J. A. Challis, and J. N. Iley, "Mechanism of the pseudomolecular rearrangement of triethyl N-phenylphosphorimidate to diethyl N-ethyl-N-phenylphosphoramidate," *Journal of the Chemical Society, Perkin Transactions 2*, p. 813.818, 1978.

[203] B. Chen and A. K. Mapp, "A Phosphorimidate Rearrangement for the Facile and Selective Preparation of Allylic Amines," *Journal of the American Chemical Society*, vol. 126, no. 17, pp. 5364–5365, 2004.

[204] B. Chen and A. K. Mapp, "Thermal and catalyzed [3,3]-phosphorimidate rearrangements," *Journal of the American Chemical Society*, vol. 127, no. 18, pp. 6712–6718, 2005.

[205] I. Wilkening, G. Del Signore, and C. P. Hackenberger, "Synthesis of N,N-disubstituted phosphoramidates via a Lewis acid-catalyzed phosphorimidate rearrangement," *Chemical Communications*, no. 25, pp. 2932–2934, 2008.

[206] I. Wilkening, G. Del Signore, W. Ahlbrecht, and C. P. Hackenberger, "Lewis acid or alkyl halide promoted rearrangements of phosphor- and phosphinimidates to N,N-disubstituted phosphor- and phosphinamidates," *Synthesis*, no. 17, pp. 2709–2720, 2011.

[207] R. Serwa, L. Wakening, G. D. Signore, M. Mühlberg, I. Claußnitzer, C. Weise, M. Gerrits, and C. P. Hackenberger, "Chemoselective staudinger-phosphite reaction of azides for the phosphorylation of proteins," *Angewandte Chemie - International Edition*, vol. 48, no. 44, pp. 8234–8239, 2009.

[208] M. A. Kasper, M. Glanz, A. Stengl, M. Penkert, S. Klenk, T. Sauer, D. Schumacher, J. Helma, E. Krause, M. C. Cardoso, H. Leonhardt, and C. P. Hackenberger, "Cysteine-Selective Phosphonamidate Electrophiles for Modular Protein Bioconjugations," *Angewandte Chemie - International Edition*, vol. 58, no. 34, pp. 11625–11630, 2019.

[209] M. A. Kasper, M. Glanz, A. Oder, P. Schmieder, J. P. Von Kries, and C. P. Hackenberger, "Vinylphosphonites for Staudinger-induced chemoselective peptide cyclization and functionalization," *Chemical Science*, vol. 10, no. 25, pp. 6322–6329, 2019.

[210] R. L. Letsinger and G. A. Heavner, "Synthesis of phosphoromonoamidate diester nucleotides via the phosphite-azide coupling method," *Tetrahedron Letters*, vol. 16, no. 2, pp. 147–150, 1975.

[211] R. L. Letsinger and M. E. Schott, "Selectivity in Binding a Phenanthridinium-Dinucleotide Derivative to Homopolynucleotides," *Journal of the American Chemical Society*, vol. 103, no. 24, pp. 7394–7396, 1981.

[212] J. Bertran-Vicente, R. A. Serwa, M. Schümann, P. Schmieder, E. Krause, and C. P. Hackenberger, "Site-specifically phosphorylated lysine peptides," *Journal of the American Chemical Society*, vol. 136, no. 39, pp. 13622–13628, 2014.

[213] R. Serwa, P. Majkut, B. Horstmann, J. M. Swiecicki, M. Gerrits, E. Krause, and C. P. Hackenberger, "Site-specific PEGylation of proteins by a Staudinger-phosphite reaction," *Chemical Science*, vol. 1, no. 5, pp. 596–602, 2010.

[214] N. Nischan, A. Chakrabarti, R. A. Serwa, P. H. Bovee-Geurts, R. Brock, and C. P. Hackenberger, "Stabilization of peptides for intracellular applications by phosphoramidate-linked polyethylene glycol chains," *Angewandte Chemie - International Edition*, vol. 52, no. 45, pp. 11920–11924, 2013.

[215] E. Hoffmann, K. Streichert, N. Nischan, C. Seitz, T. Brunner, S. Schwagerus, C. P. Hackenberger, and M. Rubini, "Stabilization of bacterially expressed erythropoietin by single site-specific introduction of short branched PEG chains at naturally occurring glycosylation sites," *Molecular BioSystems*, vol. 12, no. 6, pp. 1750–1755, 2016.

[216] D. M. Jaradat, H. Hamouda, and C. P. Hackenberger, "Solid-phase synthesis of phosphoramidate-linked glycopeptides," *European Journal of Organic Chemistry*, no. 26, pp. 5004–5009, 2010.

[217] V. Böhrsch, T. Mathew, M. Zieringer, M. R. J. Vallée, L. M. Artner, J. Dernedde, R. Haag, and C. P. Hackenberger, "Chemoselective Staudinger-phosphite reaction

of symmetrical glycosyl-phosphites with azido-peptides and polygycerols," *Organic and Biomolecular Chemistry*, vol. 10, no. 30, pp. 6211–6216, 2012.

[218] M. Mag and J. W. Engels, "Synthesis and selective cleavage of oligodeoxyribonucleotides containing non-chiral internucleotide phosphoramidate linkages," *Nucleic Acids Res.*, vol. 17, no. 15, pp. 5973–5988, 1989.

[219] V. Böhrsch, R. Serwa, P. Majkut, E. Krause, and C. P. Hackenberger, "Site-specific functionalisation of proteins by a Staudinger-type reaction using unsymmetrical phosphites," *Chemical Communications*, vol. 46, no. 18, pp. 3176–3178, 2010.

[220] N. Nischan, M. A. Kasper, T. Mathew, and C. P. Hackenberger, "Bis(arylmethyl)-substituted unsymmetrical phosphites for the synthesis of lipidated peptides: Via Staudinger-phosphite reactions," *Organic and Biomolecular Chemistry*, vol. 14, no. 31, pp. 7500–7508, 2016.

[221] W. S. Hwang and J. T. Yoke, "Autoxidation of Ethyl Phosphinite, Phosphonite, and Phosphite Esters," *Journal of Organic Chemistry*, vol. 45, no. 11, pp. 2088–2091, 1980.

[222] M. R. J. Vallée, P. Majkut, I. Wilkening, C. Weise, G. Müller, and C. P. Hackenberger, "Staudinger-phosphonite reactions for the chemoselective transformation of azido-containing peptides and proteins," *Organic Letters*, vol. 13, no. 20, pp. 5440–5443, 2011.

[223] M. R. J. Vallée, L. M. Artner, J. Dernedde, and C. P. Hackenberger, "Alkyne phosphonites for sequential azide-azide couplings," *Angewandte Chemie - International Edition*, vol. 52, no. 36, pp. 9504–9508, 2013.

[224] S. Ortial and J. L. Montchamp, "Synthesis of Z-alkenyl phosphorus compounds through hydroalumination and carbocupration of alkynyl precursors," *Organic Letters*, vol. 13, no. 12, pp. 3134–3137, 2011.

[225] M. R. J. Vallée, P. Majkut, D. Krause, M. Gerrits, and C. P. Hackenberger, "Chemoselective bioconjugation of triazole phosphonites in aqueous media," *Chemistry - A European Journal*, vol. 21, no. 3, pp. 970–974, 2015.

[226] K. D. Siebertz and C. P. Hackenberger, "Chemoselective triazole-phosphonamidate conjugates suitable for photorelease," *Chemical Communications*, vol. 54, no. 7, pp. 763–766, 2018.

[227] H. Y. Shiu, T. C. Chan, C. M. Ho, Y. Liu, M. K. Wong, and C. M. Che, "Electron-deficient alkynes as cleavable reagents for the modification of cysteine-containing peptides in aqueous medium," *Chemistry - A European Journal*, vol. 15, no. 15, pp. 3839–3850, 2009.

[228] M.-A. Kasper, A. Stengl, P. Ochtrop, M. Gerlach, T. Stoschek, D. Schumacher, J. Helma, M. Penkert, E. Krause, H. Leonhardt, and C. P. R. Hackenberger, "Ethynylphosphonamidates for the Rapid and Cysteine-Selective Generation of Efficacious Antibody-Drug Conjugates," *Angewandte Chemie International Edition*, vol. 58, pp. 11631–11636, 2019.

[229] M. A. Kasper, M. Gerlach, A. F. Schneider, C. Groneberg, P. Ochtrop, S. Boldt, D. Schumacher, J. Helma, H. Leonhardt, M. Christmann, and C. P. Hackenberger,

"N-Hydroxysuccinimide-Modified Ethynylphosphonamidates Enable the Synthesis of Configurationally Defined Protein Conjugates," *ChemBioChem*, vol. 21, no. 1-2, pp. 113–119, 2020.

[230] A. Michaelis and R. Kaehne, "Ueber das Verhalten der Jodalkyle gegen die sogen. Phosphorigsaeureester oder O-Phosphine," *Chemische Berichte*, vol. 31, pp. 1048–1055, 1898.

[231] A. E. Arbuzov, "On the structure of phosphonic acid and its derivates: Isomerization and transition of bonds from trivalent to pentavalent phosphorus," *J. Russ. Phys. Chem. Soc.*, vol. 38, p. 687, 1906.

[232] A. K. Bhattacharya and G. Thyagarajan, "The Michaelis-Arbuzov Rearrangement," *Chemical Reviews*, vol. 81, no. 4, pp. 415–430, 1981.

[233] J. Á. Bisceglia and L. R. Orelli, "Recent Progress in the Horner-Wadsworth-Emmons Reaction," no. 1113, pp. 744–775, 2015.

[234] T. C. Myers, R. G. Harvey, and E. V. Jensen, "Phosphonic Acids. II. Synthesis of γ-Ketophosphonic Acids from Methyl Ketones via Mannich Bases," *Journal of the American Chemical Society*, vol. 77, no. 11, pp. 3101–3103, 1955.

[235] T. C. Myers, S. Preis, and E. V. Jensen, "Synthesis of Phosphonic Acids from Alcohols via Sulfonate Esters," *Journal of the American Chemical Society*, vol. 76, no. 16, pp. 4172–4173, 1954.

[236] D. C. Morrison, "The Reaction of Sulfenyl Chlorides with Trialkyl Phosphites," *Journal of the American Chemical Society*, vol. 77, no. 1, pp. 181–182, 1955.

[237] H. I. Jacobson, R. G. Harvey, and E. V. Jensex, "The Reaction of Triethyl Phosphite with a Dialkyl Disulfide," *Journal of the American Chemical Society*, vol. 77, no. 22, pp. 6064–6065, 1955.

[238] A. C. Poshkus and J. E. Herweh, "The Reaction of Triaryl Phosphites with Sulfonyl Chlorides," *Journal of the American Chemical Society*, vol. 79, no. 15, p. 4245, 1957.

[239] R. G. Harvey, H. I. Jacobson, and E. V. Jensen, "Phosphonic Acids. VI. The Reaction of Trivalent Phosphorus Esters with Organic Disulfides," *Journal of the American Chemical Society*, vol. 85, no. 11, pp. 1618–1623, 1963.

[240] C. M. Timperley, M. Bird, and M. J. Waters, "Fluorinated phosphorus compounds: Part 9. The reactions of bis(fluoroalkyl) phosphorochloridates with oxygen nucleophiles," *Journal of Fluorine Chemistry*, vol. 126, no. 6, pp. 892–901, 2005.

[241] Y. Zhu, T. Chen, S. Li, S. Shimada, and L. B. Han, "Efficient Pd-Catalyzed Dehydrogenative Coupling of P(O)H with RSH: A Precise Construction of P(O)-S Bonds," *Journal of the American Chemical Society*, vol. 138, no. 18, pp. 5825–5828, 2016.

[242] R. D. Crocker, M. A. Hussein, J. Ho, and T. V. Nguyen, "NHC-Catalyzed Metathesis and Phosphorylation Reactions of Disulfides: Development and Mechanistic Insights," *Chemistry - A European Journal*, vol. 23, no. 26, pp. 6259–6263, 2017.

[243] A. P. Higson, G. K. Scott, D. J. Earnshaw, A. D. Baxter, R. A. Taylor, and R. Cosstick, "Synthesis and structure of S-nucleosidyl S-aryl disulfides and their reaction with phosphites," *Tetrahedron*, vol. 52, no. 3, pp. 1027–1034, 1996.

[244] J. Bertran-Vicente, M. Penkert, O. Nieto-Garcia, J. M. Jeckelmann, P. Schmieder, E. Krause, and C. P. Hackenberger, "Chemoselective synthesis and analysis of naturally occurring phosphorylated cysteine peptides," *Nature Communications*, vol. 7, pp. 1–9, 2016.

[245] H. H. Pas and G. T. Robillard, "S-Phosphocysteine and Phosphohistidine Are Intermediates in the Phosphoenolpyruvate-Dependent Mannitol Transport Catalyzed by Escherichia coli EIIMtl," *Biochemistry*, vol. 27, no. 16, pp. 5835–5839, 1988.

[246] H. Cho, R. Krishnara, C. T. Wals, E. Kitas, W. Bannwarth, and K. S. Anderson, "Isolation and Structural Elucidation of a Novel Phosphocysteine Intermediate in the LAR Protein Tyrosine Phosphatase Enzymatic Pathway," *Journal of the American Chemical Society*, vol. 114, no. 18, pp. 7296–7298, 1992.

[247] T. A. Brandão, A. C. Hengge, and S. J. Johnson, "Insights into the reaction of protein-tyrosine phosphatase 1B: Crystal structures for transition state analogs of both catalytic steps," *Journal of Biological Chemistry*, vol. 285, no. 21, pp. 15874–15883, 2010.

[248] Y. Kimura, M. Miyamoto, and T. Saegusa, "New Synthesis of Spiro Phosphorane by Using Diphenyl Disulfide. A Facile Route to Cyclic Acyloxyphosphoranes from α-Hydroxy Acids," *Journal of Organic Chemistry*, vol. 47, no. 6, pp. 916–919, 1982.

[249] Y. Kimura, T. Kokura, and T. Saegusa, "Reversible Reaction between Cyclic Phosphonite and Aromatic Cyclic Disulfide To Form a Spiro Dithiophosphorane. Observation of Reductive Eliminaiion of a Phosphorus(V) Compound," *Journal of Organic Chemistry*, vol. 48, no. 21, pp. 3815–3816, 1983.

[250] W. Chunxiao, C. Qian, W. Xiaofeng, Y. Guodian, H. Yanping, and Z. Kun, "Synthetic method of thiophosphate compound, CN 108774260," 2018.

[251] Y. G. Trishin, E. A. Bondarenko, I. A. Stepanov, and V. N. Chistokletov, "Chemoselectivity of reactions of dialkyl α,β-unsaturated phosphonites with p-nitrophenylsulfenyl chloride," *Zhurnal Obshchei Khimii*, vol. 59, pp. 230–231, 1989.

[252] J. D. Sadowsky, T. H. Pillow, J. Chen, F. Fan, C. He, Y. Wang, G. Yan, H. Yao, Z. Xu, S. Martin, D. Zhang, P. Chu, J. Dela Cruz-Chuh, A. O'Donohue, G. Li, G. Del Rosario, J. He, L. Liu, C. Ng, D. Su, G. D. Lewis Phillips, K. R. Kozak, S. F. Yu, K. Xu, D. Leipold, and J. Wai, "Development of Efficient Chemistry to Generate Site-Specific Disulfide-Linked Protein- and Peptide-Payload Conjugates: Application to THIOMAB Antibody-Drug Conjugates," *Bioconjugate Chemistry*, vol. 28, no. 8, pp. 2086–2098, 2017.

[253] P. Ribière, K. Bravo-Altamirano, M. I. Antczak, J. D. Hawkins, and J. L. Montchamp, "NiCl2-catalyzed hydrophosphinylation," *Journal of Organic Chemistry*, vol. 70, no. 10, pp. 4064–4072, 2005.

[254] F. G. Bordwell, "Equilibrium Acidities in Dimethyl Sulfoxide Solution," *Accounts of Chemical Research*, vol. 21, no. 12, pp. 456–463, 1988.

[255] R. B. King and P. M. Sundaram, "Bis(dialkylamino)phosphines," *Journal of Organic Chemistry*, vol. 49, no. 10, pp. 1784–1789, 1984.

[256] M. S. Timmer, H. Ovaa, D. V. Filippov, G. A. Van der Marel, and J. H. Van Boom, "An expeditious route to phosphorus heterocycles based on ring-closing metathesis," *Tetrahedron Letters*, vol. 41, no. 44, pp. 8635–8638, 2000.

[257] G. J. Bernardes, G. Casi, S. Trüssel, I. Hartmann, K. Schwager, J. Scheuermann, and D. Neri, "A traceless vascular-targeting antibody-drug conjugate for cancer therapy," *Angewandte Chemie - International Edition*, vol. 51, no. 4, pp. 941–944, 2012.

[258] G. J. Bernardes, M. Steiner, I. Hartmann, D. Neri, and G. Casi, "Site-specific chemical modification of antibody fragments using traceless cleavable linkers," *Nature Protocols*, vol. 8, no. 11, pp. 2079–2089, 2013.

[259] J. M. Ravasco, H. Faustino, A. Trindade, and P. M. Gois, "Bioconjugation with Maleimides: A Useful Tool for Chemical Biology," *Chemistry - A European Journal*, vol. 25, no. 1, pp. 43–59, 2019.

[260] Walsh G, "Biopharmaceutical benchmarks 2010," *Nature Biotechnology*, vol. 28, no. 9, pp. 917–924, 2010.

[261] D. Komander and M. Rape, "The Ubiquitin Code," *Annual Review of Biochemistry*, vol. 81, no. 1, pp. 203–229, 2012.

[262] T. Nonaka, T. Iwatsubo, and M. Hasegawa, "Ubiquitination of α-synuclein," *Biochemistry*, vol. 44, no. 1, pp. 361–368, 2005.

[263] M. Isasa, E. J. Katz, W. Kim, V. Yugo, S. González, D. S. Kirkpatrick, T. M. Thomson, D. Finley, S. P. Gygi, and B. Crosas, "Monoubiquitination of RPN10 Regulates Substrate Recruitment to the Proteasome," *Molecular Cell*, vol. 38, no. 5, pp. 733–745, 2010.

[264] R. Baker, S. M. Lewis, A. T. Sasaki, E. M. Wilkerson, J. W. Locasale, L. C. Cantley, B. Kuhlman, H. G. Dohlman, and S. L. Campbell, "Site-specific monoubiquitination activates Ras by impeding GTPase-activating protein function," *Nature Structural and Molecular Biology*, vol. 20, no. 1, pp. 46–52, 2013.

[265] M. Haj-Yahya, B. Fauvet, Y. Herman-Bachinsky, M. Hejjaoui, S. N. Bavikar, S. V. Karthikeyan, A. Ciechanover, H. A. Lashuel, and A. Brik, "Synthetic polyubiquitinated α-Synuclein reveals important insights into the roles of the ubiquitin chain in regulating its pathophysiology," *Proceedings of the National Academy of Sciences of the United States of America*, vol. 110, no. 44, pp. 17726–17731, 2013.

[266] H. P. Hemantha, S. N. Bavikar, Y. Herman-Bachinsky, N. Haj-Yahya, S. Bondalapati, A. Ciechanover, and A. Brik, "Nonenzymatic polyubiquitination of expressed proteins," *Journal of the American Chemical Society*, vol. 136, no. 6, pp. 2665–2673, 2014.

[267] S. K. Singh, I. Sahu, S. M. Mali, H. P. Hemantha, O. Kleifeld, M. H. Glickman, and A. Brik, "Synthetic Uncleavable Ubiquitinated Proteins Dissect Proteasome Deubiquitination and Degradation, and Highlight Distinctive Fate of Tetraubiquitin," *Journal of the American Chemical Society*, vol. 138, no. 49, pp. 16004–16015, 2016.

[268] R. Meledin, S. M. Mali, S. K. Singh, and A. Brik, "Protein ubiquitination: Via dehydroalanine: Development and insights into the diastereoselective 1,4-addition step," *Organic and Biomolecular Chemistry*, vol. 14, no. 21, pp. 4817–4823, 2016.

[269] T. Schneider, D. Schneider, D. Rösner, S. Malhotra, F. Mortensen, T. U. Mayer, M. Scheffner, and A. Marx, "Dissecting Ubiquitin Signaling with Linkage-Defined and Protease Resistant Ubiquitin Chains," *Angewandte Chemie - International Edition*, vol. 53, no. 47, pp. 12925–12929, 2014.

[270] F. Meier, T. Abeywardana, A. Dhall, N. P. Marotta, J. Varkey, R. Langen, C. Chatterjee, and M. R. Pratt, "Semisynthetic, site-specific ubiquitin modification of α-synuclein reveals differential effects on aggregation," *Journal of the American Chemical Society*, vol. 134, no. 12, pp. 5468–5471, 2012.

[271] E. M. Valkevich, R. G. Guenette, N. A. Sanchez, Y. C. Chen, Y. Ge, and E. R. Strieter, "Forging isopeptide bonds using thiol-ene chemistry: Site-specific coupling of ubiquitin molecules for studying the activity of isopeptidases," *Journal of the American Chemical Society*, vol. 134, no. 16, pp. 6916–6919, 2012.

[272] V. H. Trang, M. L. Rodgers, K. J. Boyle, A. A. Hoskins, and E. R. Strieter, "Chemoenzymatic synthesis of bifunctional polyubiquitin substrates for monitoring ubiquitin chain remodeling," *ChemBioChem*, vol. 15, no. 11, pp. 1563–1568, 2014.

[273] Q. Zheng, T. Wang, G.-C. Chu, C. Zuo, R. Zhao, X. Sui, L. Ye, Y. Yu, J. Chen, X. Wu, W. Zhang, H. Deng, J. Shi, M. Pan, Y.-M. Li, and L. Liu, "Isopeptide-N-ethylated deubiquitylase-resistant ubiquitin probes made through an E1-catalyzed chemoenzymatic strategy," *Angewandte Chemie International Edition*, 2020.

[274] P. Gopinath, S. Ohayon, M. Nawatha, and A. Brik, "Chemical and semisynthetic approaches to study and target deubiquitinases," *Chemical Society Reviews*, vol. 45, no. 15, pp. 4171–4198, 2016.

[275] M. C. Rodrigo-Brenni, S. A. Foster, and D. O. Morgan, "Catalysis of Lysine 48-Specific Ubiquitin Chain Assembly by Residues in E2 and Ubiquitin," *Molecular Cell*, vol. 39, no. 4, pp. 548–559, 2010.

[276] M. T. Haldeman, G. Xia, E. M. Kasperek, and C. M. Pickart, "Structure and function of ubiquitin conjugating enzyme E2-25K: The tail is a core-dependent activity element," *Biochemistry*, vol. 36, no. 34, pp. 10526–10537, 1997.

[277] P. D. Senter and E. L. Sievers, "The discovery and development of brentuximab vedotin for use in relapsed Hodgkin lymphoma and systemic anaplastic large cell lymphoma," *Nature Biotechnology*, vol. 30, no. 7, pp. 631–637, 2012.

[278] I. Seattle Genetics, "A Pivotal Study of SGN-35 in Treatment of Patients With Relapsed or Refractory Hodgkin Lymphoma (HL)," tech. rep., Seattle Genetics, Inc., 2011.

[279] I. Seattle Genetics, "A Phase 2 Study of Brentuximab Vedotin in Relapsed or Refractory Non-Hodgkin Lymphoma (NHL)," tech. rep., Seattle Genetics, Inc., 2016.

[280] C. Bahou, E. A. Love, S. Leonard, R. J. Spears, A. Maruani, K. Armour, J. R. Baker, and V. Chudasama, "Disulfide Modified IgG1: An Investigation of Biophysical Profile and Clinically Relevant Fc Interactions," *Bioconjugate Chemistry*, vol. 30, no. 4, pp. 1048–1054, 2019.

[281] F. Chiti and C. M. Dobson, "Protein Misfolding, Functional Amyloid, and Human Disease," *Annual Review of Biochemistry*, vol. 75, no. 1, pp. 333–366, 2006.

[282] R. I. Morimoto, "Proteotoxic stress and inducible chaperone networks in neurodegenerative disease and aging," *Genes and Development*, vol. 22, no. 11, pp. 1427–1438, 2008.

[283] I. Amm, T. Sommer, and D. H. Wolf, "Protein quality control and elimination of protein waste: The role of the ubiquitin-proteasome system," *Biochimica et Biophysica Acta - Molecular Cell Research*, vol. 1843, no. 1, pp. 182–196, 2014.

[284] H. Rampelt, J. Kirstein-Miles, N. B. Nillegoda, K. Chi, S. R. Scholz, R. I. Morimoto, and B. Bukau, "Metazoan Hsp70 machines use Hsp110 to power protein disaggregation," *EMBO Journal*, vol. 31, no. 21, pp. 4221–4235, 2012.

[285] N. B. Nillegoda, J. Kirstein, A. Szlachcic, M. Berynskyy, A. Stank, F. Stengel, K. Arnsburg, X. Gao, A. Scior, R. Aebersold, D. L. Guilbride, R. C. Wade, R. I. Morimoto, M. P. Mayer, and B. Bukau, "Crucial HSP70 co-chaperone complex unlocks metazoan protein disaggregation," *Nature*, vol. 524, pp. 247–251, 2015.

[286] A. Scior, A. Buntru, K. Arnsburg, A. Ast, M. Iburg, K. Juenemann, M. L. Pigazzini, B. Mlody, D. Puchkov, J. Priller, E. E. Wanker, A. Prigione, and J. Kirstein, "Complete suppression of Htt fibrilization and disaggregation of Htt fibrils by a trimeric chaperone complex," *The EMBO Journal*, vol. 37, no. 2, pp. 282–299, 2018.

[287] D. P. Murale, S. C. Hong, M. M. Haque, and J. S. Lee, "Photo-affinity labeling (PAL) in chemical proteomics: A handy tool to investigate protein-protein interactions (PPIs)," *Proteome Science*, vol. 15, no. 1, pp. 1–34, 2017.

[288] J. Brunner, "New Photolabeling and Crosslinking Methods," *Annual Review of Biochemistry*, vol. 62, no. 1, pp. 483–514, 1993.

[289] A. Herner, J. Marjanovic, T. M. Lewandowski, V. Marin, M. Patterson, L. Miesbauer, D. Ready, J. Williams, A. Vasudevan, and Q. Lin, "2-Aryl-5-carboxytetrazole as a New Photoaffinity Label for Drug Target Identification," *Journal of the American Chemical Society*, vol. 138, no. 44, pp. 14609–14615, 2016.

[290] L. Dubinsky, B. P. Krom, and M. M. Meijler, "Diazirine based photoaffinity labeling," *Bioorganic and Medicinal Chemistry*, vol. 20, no. 2, pp. 554–570, 2012.

[291] J. Wang, J. Kubicki, H. Peng, and M. S. Platz, "Influence of solvent on carbene intersystem crossing rates," *Journal of the American Chemical Society*, vol. 130, no. 20, pp. 6604–6609, 2008.

[292] Y. Wang and Q. Lin, "Synthesis and evaluation of photoreactive tetrazole amino acids," *Organic Letters*, vol. 11, no. 16, pp. 3570–3573, 2009.

[293] J. A. Zahra, A. A. Thaher, M. M. El-abadelah, and R. Boese, "3-Mercaptopropionic acid-nitrile imine adducts. An unprecedented cyclization into 1,3,4-thiadiazol-2(3H)-ones and -2(3H)-thiones," *Organic and Biomolecular Chemistry*, vol. 3, pp. 2599–2603, 2005.

[294] A. Kao, C.-l. Chiu, D. Vellucci, Y. Yang, V. R. Patel, S. Guan, A. Randall, P. Baldi, S. D. Rychnovsky, and L. Huang, "Development of a Novel Cross-linking Strategy for Fast and Accurate Identification of Cross-linked Peptides of Protein Complexes," *Molecular & Cellular Proteomics*, vol. 10, no. 1, p. M110.002212, 2011.

[295] Y. T. Kwon and A. Ciechanover, "The Ubiquitin Code in the Ubiquitin-Proteasome System and Autophagy," *Trends in Biochemical Sciences*, vol. 42, no. 11, pp. 873–886, 2017.

[296] N. Nakamura, "Ubiquitin system," *International Journal of Molecular Sciences*, vol. 19, no. 4, pp. 1–5, 2018.

[297] M. J. Clague, S. Urbé, and D. Komander, "Breaking the chains: deubiquitylating enzyme specificity begets function," *Nature Reviews Molecular Cell Biology*, vol. 20, no. 6, pp. 338–352, 2019.

[298] K. N. Swatek and D. Komander, "Ubiquitin modifications," *Cell Research*, vol. 26, no. 4, pp. 399–422, 2016.

[299] A. Y. Amerik and M. Hochstrasser, "Mechanism and function of deubiquitinating enzymes," *Biochimica et Biophysica Acta - Molecular Cell Research*, vol. 1695, no. 1-3, pp. 189–207, 2004.

[300] J. A. Fischer, "Deubiquitinating enzymes: Their roles in development, differentiation, and disease," *International Review of Cytology*, vol. 229, pp. 43–72, 2003.

[301] Y. H. Jiang and A. L. Beaudet, "Human disorders of ubiquitination and proteasomal degradation," *Current Opinion in Pediatrics*, vol. 16, no. 4, pp. 419–426, 2004.

[302] J. Ma, J. D. Martin, Y. Xue, L. A. Lor, K. M. Kennedy-Wilson, R. H. Sinnamon, T. F. Ho, G. Zhang, B. Schwartz, P. J. Tummino, and Z. Lai, "C-terminal region of USP7/HAUSP is critical for deubiquitination activity and contains a second mdm2/p53 binding site," *Archives of Biochemistry and Biophysics*, vol. 503, no. 2, pp. 207–212, 2010.

[303] A. Bremm, S. M. Freund, and D. Komander, "Lys11-linked ubiquitin chains adopt compact conformations and are preferentially hydrolyzed by the deubiquitinase Cezanne," *Nature Structural and Molecular Biology*, vol. 17, no. 8, pp. 939–947, 2010.

[304] D. Flierman, G. J. Van Der Heden Van Noort, R. Ekkebus, P. P. Geurink, T. E. Mevissen, M. K. Hospenthal, D. Komander, and H. Ovaa, "Non-hydrolyzable Diubiquitin Probes Reveal Linkage-Specific Reactivity of Deubiquitylating Enzymes Mediated by S2 Pockets," *Cell Chemical Biology*, vol. 23, no. 4, pp. 472–482, 2016.

[305] D. S. Hewings, J. A. Flygare, M. Bogyo, and I. E. Wertz, "Activity-based probes for the ubiquitin conjugation-deconjugation machinery: new chemistries, new tools, and new insights," *FEBS Journal*, vol. 284, no. 10, pp. 1555–1576, 2017.

[306] A. C. Faesen, M. P. Luna-Vargas, P. P. Geurink, M. Clerici, R. Merkx, W. J. Van Dijk, D. S. Hameed, F. El Oualid, H. Ovaa, and T. K. Sixma, "The differential modulation of USP activity by internal regulatory domains, interactors and eight ubiquitin chain types," *Chemistry and Biology*, vol. 18, no. 12, pp. 1550–1561, 2011.

[307] X. Zhang, A. H. Smits, G. B. van Tilburg, P. W. Jansen, M. M. Makowski, H. Ovaa, and M. Vermeulen, "An Interaction Landscape of Ubiquitin Signaling," *Molecular Cell*, vol. 65, no. 5, pp. 941–955.e8, 2017.

[308] Y. Tian, M. P. Jacinto, Y. Zeng, Z. Yu, J. Qu, W. R. Liu, and Q. Lin, "Genetically Encoded 2-Aryl-5-carboxytetrazoles for Site-Selective Protein Photo-Cross-Linking," *Journal of the American Chemical Society*, vol. 139, no. 17, pp. 6078–6081, 2017.

[309] T. Hata and M. Sekine, "Silyl Phosphites. I. The Reaction of Silyl Phosphites with Diphenyl Disulfide. Synthesis of S-Phenyl Nucleoside Phosphorothioates," *Journal of the American Chemical Society*, vol. 96, no. 23, pp. 7363–7364, 1974.

[310] O. Roling, C. Wendeln, U. Kauscher, P. Seelheim, H. J. Galla, and B. J. Ravoo, "Layer-by-layer deposition of vesicles mediated by supramolecular interactions," *Langmuir*, vol. 29, no. 32, pp. 10174–10182, 2013.

[311] S. Ortial, D. A. Thompson, and J. L. Montchamp, "Mixed 1,1-bisphosphorus compounds: Synthesis, alkylation, and Horner-Wadsworth-emmons olefination reactions," *Journal of Organic Chemistry*, vol. 75, no. 23, pp. 8166–8179, 2010.

[312] V. Dorfer, P. Pichler, T. Stranzl, J. Stadlmann, T. Taus, S. Winkler, and K. Mechtler, "MS Amanda, a universal identification algorithm optimized for high accuracy tandem mass spectra," *Journal of Proteome Research*, vol. 13, no. 8, pp. 3679–3684, 2014.

[313] R. Dennington, T. A. Keith, and J. M. Millam, "GaussView," 2016.

[314] G. Scalmani and M. J. Frisch, "Continuous surface charge polarizable continuum models of solvation. I. General formalism," *Journal of Chemical Physics*, vol. 132, no. 11, 2010.

[315] J. Hasegawa and E. al., "Gaussian 16," 2016.

[316] A. L. Baumann, S. Schwagerus, K. Broi, K. Kemnitz-Hassanin, C. E. Stieger, N. Trieloff, P. Schmieder, and C. P. Hackenberger, "Chemically induced vinylphosphonothiolate electrophiles for thiol-thiol bioconjugations," *Journal of the American Chemical Society*, vol. 142, pp. 9544–9552, 2020.

[317] W. Hoyer, T. Antony, D. Cherny, G. Heim, T. M. Jovin, and V. Subramaniam, "Dependence of α-synuclein aggregate morphology on solution conditions," *Journal of Molecular Biology*, vol. 322, no. 2, pp. 383–393, 2002.

[318] Z. L. Chen, J. M. Meng, Y. Cao, J. L. Yin, R. Q. Fang, S. B. Fan, C. Liu, W. F. Zeng, Y. H. Ding, D. Tan, L. Wu, W. J. Zhou, H. Chi, R. X. Sun, M. Q. Dong, and S. M. He, "A high-speed search engine pLink 2 with systematic evaluation for proteome-scale identification of cross-linked peptides," *Nature Communications*, vol. 10, no. 1, 2019.

[319] L. Kolbowski, C. Combe, and J. Rappsilber, "XiSPEC: Web-based visualization, analysis and sharing of proteomics data," *Nucleic Acids Research*, vol. 46, no. W1, pp. W473–W478, 2018.

[320] Y. Wang and Q. Lin, "Synthesis and evaluation of photoreactive tetrazole amino acids," *Organic Letters*, vol. 11, no. 16, pp. 3570–3573, 2009.